TABLE OF CONTENTS

Page

INTRODUCTION 1

CHAPTER 1 BITUMINOUS MIXTURES USED IN PAVEMENT STRUCTURE AND RECYCLING 7
1.1 Pavement structure 7
1.1.1 Flexible pavements 9
1.2 Asphalt mixtures 9
1.2.1 Aggregate skeleton 9
1.2.2 Asphalt binder 10
1.2.3 HMA volumetric properties 12
1.2.4 Benefit of recycling asphalt pavement 16
1.2.5 Asphalt recycling methods 16
1.3 Recycled mixtures 19
1.4 Composition of recycled mixtures containing RAP- definition 19
1.5 Recycling rate of recycled asphalt mixtures 19
1.5.1 Low level recycling 20
1.5.2 Recycling rate higher than 10% - 20% 20
1.6 Designing HMA with high percentage of RAP 21
1.7 Extraction and recovery of asphalt binder 24
1.8 Determining RAP aggregate properties 25
1.8.1 RAP aggregate gradation 26
1.8.2 RAP aggregate specific gravity 27
1.8.3 Coarse aggregate angularity (CAA) 28
1.8.4 Fine aggregate angularity (FAA) 29
1.8.5 Flat and elongated particles 29
1.8.6 Hardness/wear 30
1.8.7 Cleanliness 30
1.9 Binder test and aging 31
1.10 Aging methods of HMA 32
1.11 Production of hot mix asphalt 33
1.11.1 Recycling at drum mix plants with parallel-flow or counter-flow drying (cold addition) 33
1.11.2 Recycling at a batch plant 35
1.11.3 Special plants 36

CHAPTER 2 MECHANICAL PROPERTIES OF ASPHALT MIXTURES: BEHAVIOUR AT SMALL DEFORMATION 39
2.1 Introduction 39
2.2 Solicitation on bituminous roadways 39
2.2.1 Traffic effect 39
2.2.2 Temperature effect 40

2.3 Bituminous materials behaviour classification 41
2.4 Application to the pavement structure design 43
2.5 Linear viscoelastic behaviour 43
2.6 Measurement of the modulus of asphalt mixtures in the frequency domain: complex modulus 45
2.6.1 Definition and measurement's principle 45
2.6.2 Complex modulus tests 49
2.6.2.1 Tension-compression test on cylindrical sample 50
2.6.3 Alternative methods of analyzing complex modulus test results 51
2.6.3.1 Isothermal and isochronal curves 51
2.6.3.2 Cole - Cole plane (complex plane) 52
2.6.3.3 Black space 53
2.6.3.4 Time temperature superposing principles and shift factor 55
2.6.4 Mechanical models used in linear viscoelastic 57
2.6.4.1 Presentation of the 2S2P1D model 58
2.7 Fatigue phenomenon of bituminous mixtures 60
2.7.1 Introduction 60
2.7.2 Hot mix asphalt fatigue 60
2.7.3 Laboratory fatigue test 63
2.7.4 Fatigue test analysis methods 65
2.7.4.1 Criterion based on the evolution of the stiffness modulus (classical method) 65
2.7.4.2 End of phase II criterion 66
2.7.5 Determination of the initial modulus $E0*$ 68
2.7.6 Approaches used to predict failure in fatigue 70
2.7.6.1 Fatigue curve or Wöhler curve 70
2.7.6.2 Fatigue cracking prediction modelling 74
2.7.7 Method of analysis in terms of damage (the DGCB approach) 80
2.7.8 Performance of RAP mixtures in laboratory: complex modulus tests 82
2.7.9 Fatigue performance of RAP mixtures in laboratory 91
2.8 Chapter conclusion 99

CHAPTER 3 RESEARCH METHODOLOGY AND EXPERIMENTAL WORK 101
3.1 Introduction 101
3.1.1 Research Methodology 102
3.1.2 Task 1 – literature review 102
3.1.3 Task 2 – Materials and Mix design and Preparation 103
3.1.3.1 Design of mixture with no RAP 104
3.1.3.2 Design of mixture with RAP 104
3.1.4 Task 3 – Laboratory experimental testing 105
3.1.4.1 Complex modulus test 105
3.1.4.2 Fatigue resistance test 106
3.1.5 Task 4: Improvement of the basic fatigue model 107

3.1.6 Task 5: Fatigue life prediction performance of RAP mixtures using the new models 111
3.2 Experimental work 111
3.2.1 RAP sampling 115
3.2.2 Volumetric properties of the mixtures 115
3.2.3 RAP insertion in mixes 115
3.2.3.1 Hot recycling with cold RAP 116
3.2.3.2 Hot recycling with reheated RAP 117
3.2.4 Mixing temperature 118
3.2.5 Mix selection 122

CHAPTER 4 MATERIALS CHARACTERIZATION FOR MIX DESIGNS AND LABORATORY TESTING 125
4.1 Introduction 125
4.2 RAP material characterization 126
4.2.1 RAP material preparation 127
4.2.2 Sieve analysis before extraction 130
4.2.3 RAP aggregate specific gravity 130
4.2.4 RAP binder content by ignition oven 132
4.2.5 RAP binder content from solvent extraction 136
4.2.6 Comparison between the ignition oven test results and solvent extraction test 138
4.2.6.1 Gradation analysis 138
4.2.6.2 Asphalt binder content analysis 139
4.2.7 Recovered RAP binder (RRB) 140
4.2.8 Virgin aggregate properties 145
4.2.9 Properties of virgin binder 147
4.3 Recycled mix design 147
4.3.1 Reference mix design 148
4.3.1.1 Mixing procedure 149
4.3.2 Mix specification 153
4.4 Slab preparation 154
4.4.1 Manufacturing 154
4.4.2 Coring 155
4.4.3 Sawing and resurfacing 155
4.4.4 Compact of tested specimens 157
4.5 Tension-compression test: complex modulus and fatigue 158
4.5.1 Principle of tension-compression test on cylindrical sample 158
4.5.2 Implementation of tension-compression test 160
4.5.2.1 Gluing the specimen to the testing platens 160
4.5.3 Procedure for complex modulus 162
4.5.4 Procedure for fatigue test 163
4.5.5 Data Acquisition and measured parameters 164
4.5.6 Data processing 166
4.5.7 Quality of the mechanical test 167

CHAPTER 5 ANALYSIS OF COMPLEX MODULUS RESULTS AND LVE MODELLING USING 2S2P1D MODEL 169
5.1 Introduction 169
5.2 Complex modulus test results 169
5.2.1 Isothermal and isochronal curves 172
5.2.2 Cole-Cole plane and Black space diagram 172
5.2.3 Master curves 173
5.3 Modelling the behaviour of asphalt mixtures using 2S2P1D model 176
5.3.1 LVE Simulation results for the virgin mixture (RAP028) 176
5.4 Statistical analysis 180
5.5 Complex modulus results' repeatability 181
5.6 Analysis and Discussion 185
5.6.1 Effect of RAP content on complex modulus 186
5.6.2 Effect of other parameters on complex modulus 189
5.7 Shift factors 191
5.8 RAP coefficient of evolution $\boldsymbol{CRCE}*$ 192
5.8.1 Variation coefficient evolution between replicates of complex modulus specimen's ($\boldsymbol{CVCE}*$) 193
5.8.1.1 Comparison between $\boldsymbol{CVCE}*$ obtained from experimental data or using 2S2P1D model 194
5.8.1.2 Summary of the results corresponding to the repeatability of complex modulus 198
5.8.2 Effect of RAP content 200
5.8.3 Influence of binder grade 204
5.8.4 Effect of RAP aging 207
5.8.4.1 Sensitivity of RAP conditioning evolution values ($\boldsymbol{CRCE - 2S2P1D}*$) of mixes made with 25% RAP 213
5.9 Normalized curves 214
5.10 Chapter conclusion 222

CHAPTER 6 ANALYSIS OF FATIGUE TEST RESULTS 225
6.1 Introduction 225
6.2 Tested mixes 225
6.3 Experimental campaign 227
6.4 Results and analysis 229
6.4.1 Interpretation of fatigue test results 230
6.4.1.1 Evolution of temperature 231
6.4.1.2 Evolution of the heating on the surface of the specimen 232
6.4.1.3 Curves of the quality index 233
6.4.1.4 Evolution of the norm of complex modulus 234
6.4.1.5 Evolution of axial deformation 235
6.4.1.6 Axial Strain's signal centered value 237
6.4.1.7 Stress amplitude 239
6.4.1.8 Center of stress's signal 240
6.4.1.9 Phase angle evolution 241

6.4.1.10 Presentation in the black space 242
6.4.1.11 Dissipated energy evolution..... 243
6.4.1.12 Fatigue test validation 245
6.5 Correction of the test results based on air voids of the specimens 245
6.6 Comparison of fatigue test results.....246
6.6.1 Comparison of initial values of the dynamic modulus 246
6.6.2 Comparison of fatigue tests results performed on the same asphalt mixtures at different levels of deformation..... 247
6.6.3 Comparison of fatigue tests at the same imposed strain level for different recycled mixtures..... 248
6.7 Evaluation of the fatigue life.....251
6.7.1 Relationship between the fatigue life and the amplitude of deformation: fatigue lines 254
6.7.1.1 Relationship between the fatigue line parameters and RAP content of a mix..... 258
6.7.2 Measurement of the correlation between the N_f predicted by the basic model and the measured N_f..... 261
6.8 Effect of the addition of RAP 262
6.8.1 Comparison between recycled asphalt mixtures..... 262
6.8.2 Summary of the results 266
6.9 Prediction of the fatigue life according to the DGCB method.....268
6.9.1 Calculation of the corrected damage at the end of phase II: D_{IIIc} 269
6.9.2 Level of damage leading to rupture (***DIII***) 272
6.9.3 Evolution of the corrected damage leading to rupture (D_{IIIc}) 273
6.9.4 Effect of air voids content on the critical damage (***DIIIc***) 274
6.10 Predicting the number of cycles to failure when considering only the 300 000 first cycles ($N_{fII/III}^{DGCB}$).....276
6.11 Summary of the results 280

CHAPTER 7 PROPOSED MODIFICATIONS TO THE BASIC FATIGUE MODEL TO TAKE INTO ACCOUNT THE EFFECT OF RAP CONTENT ON THE FATIGUE CRACKING RESISTANCE OF HMA MIXTURES.....281
7.1 Introduction.....281
7.2 Statistical approach: goodness-of-fit.....283
7.3 Modification of the basic fatigue model based on phenomenological approach 284
7.3.1 Evaluation of the Accuracy of the newly developed model by the phenomenological approach 288
7.3.2 Determination of the ***A*** parameter value acting in the slope by the optimization process 292
7.3.3 Specific validation of the general fatigue model 296
7.3.4 Conclusion 297
7.4 Statistical fatigue model.....298
7.5 Prediction of fatigue life at the pavement structure level 302

7.5.1 Determination of the fatigue lives values at the pavement level 307
7.5.2 Comparisons between the predicted pavement fatigue lives (structure level) and the predicted fatigue lives of recycled asphalt mixtures (material level)..... 321
7.6 Chapter conclusion.....328

SUMMARY AND CONCLUSION 331

APPENDIX I CHARACTERIZATION OF RAP PROPERTIES AND FORMULATION OF RECYCLED MIXTURES.....339

APPENDIX II COMPLEX MODULUS MEASUREMENT RESULTS OBTAINED BY THE AUTHORS ON RECYCLED MATERIALS.....375

APPENDIX III PRESENTATION OF FATIGUE TEST RESULTS.....415

APPENDIX IV DATA OF THE BASIC FATIGUE MODEL IMPROVEMENT 475

LIST OF REFERENCES.....491

LIST OF TABLES

Page

Table 2.1 The value of the initial modulus according to the literature review 69

Table 2.2 Major fatigue model for hot mix asphalt 79

Table 2.3 Beam fatigue average life cycles of various mixtures 93

Table 2.4 Overall Summary of the laboratory evaluation of RAP containing mixtures.....95

Table 2.5 Required virgin binders grades for the various RAP sources and contents 97

Table 3.1 Properties of bituminous bound graded aggregate.....109

Table 3.2 Characteristics of GB-20 mixture developed under the LC method 113

Table 3.3 The possible laboratory-produced mixtures.....123

Table 3.4 Summary of asphalt mixtures 124

Table 4.1 Data from sieve analysis test of the RAP material before extraction 131

Table 4.2 RAP asphalt content by ignition method 132

Table 4.3 Data from sieve analysis test of the RAP material from ignition 133

Table 4.4 Average RAP gradations before and after ignition test 135

Table 4.5 Percent of asphalt binder of the RAP obtained by extraction (by weight).....137

Table 4.6 RAP gradation after solvent extraction.....137

Table 4.7 Asphalt binder content test results 139

Table 4.8 DSR Test Results of recovery bitumen binder of as-received RAP.....141

Table 4.9 DSR Test Results of recovery bitumen binder of heated microwave RAP (HM).....142

Table 4.10 DSR Test Results of recovery bitumen binder of the aged RAP 142

Table 4.11 BBR Test Results of recovery bitumen binder of as received RAP 143

Table 4.12 BBR Test Results of recovery bitumen binder of heated microwave RAP (HM) 143

Table 4.13 BBR Test Results of recovery bitumen binder of the aged RAP 144

Table 4.14 Summary table of estimation of mixing and compaction temperatures for asphalt mixtures and PG grade predicted of the different bitumen binders 145

Table 4.15 Gradation of virgin aggregate (Reported by Supplier) 146

Table 4.16 Characteristics of the PG 64-28 and PG 58–34 asphalt binder 148

Table 4.17 Summary of GB-20 asphalt mixtures produced in the laboratory 152

Table 4.18 Number of applied cycles according to the frequency 162

Table 4.19 Acquisition number according to the number of applied cycles applied 163

Table 5.1 Characteristics of cylindrical samples used for the complex modulus test 171

Table 5.2 Constants of the 2S2P1D model gauged for the tested materials 179

Table 5.3 Goodness of fit statistical analysis for the recycled mixture 181

Table 5.4 Average complex dynamic modulus of mixtures that have repeatability and CV 185

Table 5.5 Summary of max and min $CVCE*$ value calculated from the ratio of modulus values obtained from 2S2P1D model for two repetitions of different mixes 195

Table 6.1 Characteristics of specimens for the four mixes 226

Table 6.2 Summary table of the performed fatigue tests 229

Table 6.3 Presentation of the obtained fatigue test results 252

Table 6.4 Characteristics of the fatigue lines for different performed tests 257

Table 6.5	Characteristics of the fatigue lines for the corrected tests results for a specific air void of 5,1%	258
Table 6.6	Comparison between the estimated laboratory fatigue life values of the two failure criteria using the corrected fatigue test results for a specific air void of 5,1%	265
Table 6.7	Damage values at the transition between phases II and phases III for the four recycled mixtures: $DIII$ no correction; $DIIIc$ correction from artefact effects	271
Table 7.1	Subjective criterion for goodness-of-fit statistical parameters for modelling	284
Table 7.2	Fatigue parameters of the general fatigue model established from $Nf50\%\ and\ NfII/III$ using the corrected fatigue test results for a specific air void of 5,1%	287
Table 7.3	Summary of A values based on an optimum process used to minimize the error between the predicted and measured fatigue life values ($k4 = k40/40$)	293
Table 7.4	Summary of A values based on an optimum process used to minimize the error between the predicted and measured fatigue life values ($k4 = k40/25$)	294
Table 7.5	Parameters used in the proposed general fatigue model for RAP mixtures listed in this research program	298
Table 7.6	Statistical fatigue model regression coefficients for all the recycled mixes combined up to 40%	300
Table 7.7	Statistical fatigue model regression coefficients for all the recycled mixes combined up to 25% RAP	301
Table 7.8	Summary of all the models newly developed in this study	303
Table 7.9	Modulus of the mixtures predicted by	306
Table 7.10	Resulted strain at the bottom of the bituminous layer of Alizé software	308
Table 7.11	Comparison between the fatigue life values predicted from the basic and the general fatigue models according to the criteria $N_{f50\%}$ based on the structure level ($k3 = k2^{a}/2$): modelling up to 40%	311

Table 7.12 Comparison between the estimated fatigue life values of the basic and the general fatigue models according to the criteria $Nf II/III$ based on the structure level ($k3 = k2/2$): (modelling up to 40%) 312

Table 7.13 Comparison between the estimated fatigue life values determined based on the structure level at 10°C – 10Hz and based on the material level determined at an equivalent deformation ε_t = 97,7 μm/m determined according to the N$f50\%$using the basic model (modelling up to 40%) 322

Table 7.14 Comparison between the estimated fatigue life values determined based on the structure level at 10°C – 10Hz and based on the material level determined at an equivalent deformation ε_t = 97,7 μm/m determined according to the NfII/III using the basic model (modelling up to 40%) 323

LIST OF FIGURES

Page

Figure 1.1 Typical stress distribution in a flexible pavement structure 8

Figure 1.2 Behaviour classes of asphalt cement according to the strain amplitude (|Ɛ|) and the temperature (T) 11

Figure 1.3 Volumetric representation of a compacted mixture.....14

Figure 1.4 Schematic of pavement recycling operation in central plant 17

Figure 1.5 Presentation of the technical possibilities of recycling of bituminous pavements Adapted from Navaro (2011).....18

Figure 1.6 Composition of a recycled asphalt mixtures.....20

Figure 1.7 RAP mix design procedure – Step 1 22

Figure 1.8 RAP mix design procedure – Step 2 and 3 23

Figure 1.9 Recycling technique at drum plants with parallel-flow drying.....34

Figure 1.10 Recycling technique at drum mix plants with counter-flow drying 34

Figure 1.11 Example of the mobile parallel drum plant of AAPPIA Grands Travaux a) overall view & b) closer view of the two parallel drum dryers (the first one for virgin aggregates, the second one for recycled aggregate) 35

Figure 1.12 Recycling at a batch plant 36

Figure 1.13 Schematic of the CYCLEAN process.....37

Figure 2.1 Schematic of the traffic induced solicitations.....40

Figure 2.2 Schematic of the temperature induced solicitations.....41

Figure 2.3 Typical bituminous mix behaviour domain, (|Ɛ| strain amplitude – N number of cycles).....42

Figure 2.4 Sinusoidal load (F) and displacement (Δh) applied and resulting sinusoidal stress (σ) and strain (ε) response at a given point of the sample.....46

Figure 2.5 The vector representation of the real part and the imaginary part of the complex modulus....49

Figure 2.6 Uniaxial tension-compression complex modulus test setup....50

Figure 2.7 Example of isothermal curves of the complex modulus....51

Figure 2.8 Example of isochronal curves of the complex modulus....52

Figure 2.9 Example of the complex modulus curve in the Cole-Cole plane....53

Figure 2.10 Example of the complex modulus curve in the Black plane....54

Figure 2.11 Example of materials referring to TTSP or not from the complex modulus Black plane curve....55

Figure 2.12 Example of master curve at 10°C....56

Figure 2.13 Examples of mechanical models used for characterization of bituminous materials....58

Figure 2.14 Influence of parameters of the 2S2P1D model on the complex modulus represented in the Cole-Cole plan....59

Figure 2.15 Fatigue cracking types: (a) Bottom-up (b) Top-down....61

Figure 2.16 Severity levels of fatigue cracking....62

Figure 2.17 Schematic of fatigue test....63

Figure 2.18 Definition of the traditional criterion for determining the fatigue life (N_{f50})....66

Figure 2.19 Wöhler curve (fatigue curve) and determination of ε_6....71

Figure 2.20 Determination of E_{00i} and a_T from the dissipate energy curve....81

Figure 2.21 Determination of W_{00i} and a_w from the dissipated energy curve....82

Figure 2.22 Effect of RAP on complex modulus at 21ºC and 0,1 Hz....84

Figure 2.23 Complex modulus master curves at 4 ºC for 4 replicates of the 0% RAP mix....84

Figure 2.24 Complex modulus master curves at 4ºC for 4 replicates of the 20% RAP mix....85

Figure 2.25 Complex modulus master curves at 4ºC for 4 replicates of the 40% RAP mix 85

Figure 2.26 Average dynamic modulus test data for 4 replicates at 25 Hz 86

Figure 2.27 Dynamic modulus master curves in compression for all mixtures 88

Figure 2.28 Dynamic modulus master curves in tension for all mixtures 88

Figure 2.29 Master Curve for Complex Modulus for R028 and R034, T_{ref} = 4ºC 89

Figure 2.30 Master curves for Complex modulus for R2034 and M2034, T_{ref} = 4ºC 90

Figure 2.31 Master curves for Complex modulus for R4034 and M4034, T_{ref} = 4ºC 90

Figure 2.32 Complex modulus changes with temperature at 0,1 Hz 91

Figure 2.33 Complex modulus changes with frequency at 21ºC 91

Figure 2.34 Beam Fatigue, Cycles vs. Stiffness High Strain, PG 52-34 93

Figure 2.35 Beam Fatigue, Cycles vs. Stiffness High Strain, PG 64-22 94

Figure 2.36 Beam Fatigue Cycles to Failure vs. Stiffness, PG 64-22, Low Strain 94

Figure 2.37 SCB Fatigue test results 96

Figure 2.38 Indirect Tensile Test (IDT) 98

Figure 2.39 Effect of RAP percentage to IDT stress and strain curves 99

Figure 3.1 Summary of research approach 103

Figure 3.2 Relation between strain and number of repetitions to failure 108

Figure 3.3 Experimental design flow chart 114

Figure 3.4 Evolution of virgin aggregate temperature when adding cold RAP with different percentages to reach to the target mixing temperature of 160°C 120

Figure 3.5 Evolution of virgin aggregate temperature when adding RAP heated in a microwave at 110°C with different percentages to reach to the target mixing temperature of 160°C 120

Figure 3.6 Evolution of the calculated mix temperature when adding different percentages of cold RAP to overheated (300°C) virgin aggregate compared to the targeted mix temperature 121

Figure 3.7 Evolution of the calculated mix temperature when adding microwave heated RAP (110°C) to heated virgin aggregate (180°C) compared to the targeted mix temperature.....122

Figure 4.1 RAP material preparation 128

Figure 4.2 Top view buckets pattern of RAP materials capable of holding approximately 30kg 129

Figure 4.3 A riffle splitter used for RAP sample splitting 129

Figure 4.4 Random RAP gradation before extraction.....130

Figure 4.5 Gradation of four samples of the RAP after extraction using ignition oven 134

Figure 4.6 Gradation of average samples of the RAP before and after extraction using ignition oven.....135

Figure 4.7 Gradation of two samples of the RAP after solvent extraction 138

Figure 4.8 Gradation of average samples of the RAP before and after extraction using ignition oven & solvent.....139

Figure 4.9 Recovered bitumen binder penetration values.....140

Figure 4.10 Viscosity of the unaged RAP and the aged RAP recovered asphalt binders 141

Figure 4.11 DSR test results of recovery bitumen binders of unaged and aged RAP at 76°C and 82°C 142

Figure 4.12 Viscosity versus temperature for the as-received recovered bitumen binder 145

Figure 4.13 Gradation of virgin aggregate materials 147

Figure 4.14 Gradation of three trials for 0% RAP mixture.....149

Figure 4.15 Gradation for all mixtures.....153

Figure 4.16 Notation of the specimens for the complex modulus test 154

Figure 4.17 Compactor of plates of LCPC.....155

Figure 4.18 Five Cored cylindrical specimens of 75 mm diameter 156

Figure 4.19 Specimen resurfacing.....156

Figure 4.20 Representation of the coring plan and the numeration of the specimen: (a) side view, (b) top view (P refers to the plate number and A refers to the specimen number).....157

Figure 4.21 Overview of the experimental device 159

Figure 4.22 Test setup for complex modulus and fatigue 159

Figure 4.23 Principle of tension-compression test on cylindrical sample.....160

Figure 4.24 Apparatus for gluing 161

Figure 4.25 Sample after gluing.....162

Figure 4.26 Axial stress and strains measured by the extensometers (fatigue test -15RAP-(P2-A3)-D130, 2 cycles around cycle N = 22).....166

Figure 5.1 Air void of tests specimens.....170

Figure 5.2 Isothermal curves (a) and isochrones (b) of the norm of the complex modulus versus the frequency and the temperature, respectively (mix RAP028: sample P1-A4).....172

Figure 5.3 Curves of the complex modulus: a) in a Cole-Cole plane; and b) in the Black space (mix RAP028: sample P1-A4).....173

Figure 5.4 Construction of the master curves at $T_{ref} = 5{,}4°C$ with the shifting procedures for the virgin mix (RAP028), (a) master curve of |E*|, (b) the master curve of the phase angle of E*.....174

Figure 5.5 Master curves of all 'Experimental' results that obtained for this study at $T_{ref} = 10°C$ 176

Figure 5.6 Master curves of the virgin mix (RAP028): Simulation with the model 2S2P1D (T_{ref} = 5,4 °C), (a) Master curves of the norm of the complex modulus |E*|, (b) Master curve of ϕ of the complex modulus.....177

Figure 5.7 Complex modulus of the virgin mix (RAP028) in the Cole-Cole plane and in the Black space, Simulation with the model 2S2P1D, (a) Cole-Cole plane, (b) Black space.....177

Figure 5.8 E_{00} and E_0 values for the tested specimens of different mixes 180

Figure 5.9 Master curves & Cole-Cole plane of different asphalt mixtures according to complex modulus repeatability. Simulation with the model 2S2P1D 183

Figure 5.10 Following Master curves & Cole-Cole plane of different asphalt mixtures according to complex modulus repeatability. Simulation with the model 2S2P1D.....184

Figure 5.11 Master curves of the norm of the complex modulus at 10°C for mixes with binder grade PG 64-28, Cold RAP addition, and different percentages of RAP, 2S2P1D model of a single test (a) Cold RAP addition (b) Hot RAP addition.....187

Figure 5.12 Cole-Cole diagram for the four RAP mixes prepared with different RAP content (0%, 15%, 25%, and 40%), 2S2P1D model of a single test (a) Cold RAP addition (b) Hot RAP addition.....188

Figure 5.13 E_0 stiffness ratios of the recycled mixtures made with RAP added cold and RAP added hot relative to the virgin mix 189

Figure 5.14 Master curves of the norm of the complex modulus (T_{ref} = 10°C) and Cole-Cole diagram different mixes with different conditioning.....190

Figure 5.15 Shift factors of the tested materials made with different RAP dosage and RAP added cold or hot (a) Cold RAP addition (b) Hot RAP addition.....191

Figure 5.16 $CVCE - data*$ and $CVCE - 2S2P1D*$ vs. equivalent frequency (T_{ref} = 5°C).....197

Figure 5.17 Coefficient of damage ($CRCE*$, ϕRCE) vs. equivalent frequency of mixtures made of PG64-28 bitumen and cold added RAP (unaged), at different RAP content: 0%, 15%, 25%, 40%, RAP028 mix (mix No.1) is the reference. T_{ref}=10°C 201

Figure 5.18 Coefficient of damage ($CRCE - 2S2P1D*$) vs. equivalent frequency of mixtures made of PG64-28 bitumen and RAP is added hot, at different RAP content: 0%, 15%, 25%, 40%, RAP028 mix (mix No.1) is the reference. T_{ref}=10 °C.....203

Figure 5.19 Norm and Phase angle of the complex RAP coefficient of evolution vs. equivalent frequency for mixtures composed

	of PG 64-28 bitumen or PG 58-34 bitumen and made with different RAP contents. T_{ref}=10°C	206
Figure 5.20	Complex aging coefficient (norm and phase angle) of 40% recycled asphalt mixtures made with PG 64-28 (RAP is added cold). T_{ref}=10°C	208
Figure 5.21	Evolution of $CRCE - 2S2P1D *$ and $\phi RCE - 2S2P1D$ vs. equivalent frequency of mixtures made of PG 64-28 bitumen (RAP is added cold or hot), at RAP contents: 15%, 25%, and 40%. T_{ref}=10°C, RAP1528CU (mix No.2) is the reference	212
Figure 5.22	$CRCE - 2S2P1D *$ vs. equivalent frequency of mixtures made of PG 64-28 bitumen and cold adding RAP or hot adding RAP, at different RAP content: 25%. T_{ref}=10°C	214
Figure 5.23	Normalized complex modulus curves in Cole-Cole diagram of the mixes with two repetitions	217
Figure 5.24	Following Normalized complex modulus curves in Cole-Cole diagram of the mixes with two repetitions	218
Figure 5.25	Normalized complex modulus curves in Cole-Cole diagram of the mixtures made with different percentages of RAP (the RAP at the room temperature was added to the mix)	220
Figure 5.26	Normalized complex modulus curves in Cole-Cole diagram of the mixtures made with different percentages of RAP (the heated RAP to 110°C was added to the mix)	221
Figure 6.1	Air voids content for the specimens of the four mixtures	227
Figure 6.2	Notation of the name of the fatigue test	228
Figure 6.3	Evolution of the temperature at the surface of the specimen according to the number of cycles for the test 25RAP-(P1-A1)-D110 (ε_A = 108,8 µm/m; T = 10°C)	231
Figure 6.4	Evolution of the heating on the surface of the specimen of the test 25RAP-(P1-A1)-D110 (ε_A = 108,8 µm/m; T = 10°C)	232
Figure 6.5	Evolution of quality indices according to the number cycles for the test 25RAP-(P1-A1)-D110 (ε_A = 108,8 µm/m; T = 10°C)	234
Figure 6.6	Evolution of the modulus according to the number of cycles for the test 25RAP-(P1-A1)-D110 (ε_A = 108,8 µm/m; T = 10°C)	235

Figure 6.7 Evolution of the amplitude of the deformation as a function of the number of cycles for the test 0RAP-(P2-A4)-D130 (ε_A = 124,7 µm/m; T = 10°C) 236

Figure 6.8 Differences relative to the mean of the deformation (average deviations of deformation) depending on the number of cycles for the test 25RAP-(P1-A1)-D110 (εA = 108,8 µm/m; T = 10°C) 237

Figure 6.9 Changes in the center of the deformation as a function of the number cycles for the test 25RAP-(P4-A5)-D130 (ε_A = 128,5 µm/m; T = 10°C) 238

Figure 6.10 Changes in the center of the deformation as a function of the number cycles for the test 25RAP-(P1-A1)-D110 (ε_A = 108,8 µm/m; T = 10°C) 239

Figure 6.11 Evolution of the signal of the stress according to the number of cycles for the test 25RAP-(P1-A1)-D110 (ε_A = 110 µm/m; T = 10°C) 240

Figure 6.12 Evolution of the stress signal according to the number of cycles for the test 25RAP-(P1-A1)-D110 (ε_A = 110 µm/m; T = 10°C) 241

Figure 6.13 Evolution of the phase angle of the complex modulus according to the number of cycles for the test 242

Figure 6.14 Presentation for the black space for the tests 243

Figure 6.15 Evolution of the dissipated energy according to the number of cycles for the test 25RAP-(P1-A1)-D110 (ε_A = 110 µm/m; T = 10°C) 244

Figure 6.16 Initial complex modulus and phase angle for the four tested mixtures 247

Figure 6.17 Comparison of ($E*/E0$), - log (N)) for six different strain level tests for the virgin mix (0RAP28) 248

Figure 6.18 Comparison of a fatigue test at 130 µm/m strain level, real strain values range from 125 to 133 µm/m, for 4 recycled mixtures in the axes $E*/E0$) - log (N) (0% RAP, 15% RAP, 25% RAP, and 40% RAP) 249

Figure 6.19 Comparison of a fatigue test at test at 140 µm/m strain level, values of real strain range from 133 to 145 µm/m, for 4

recycled mixtures in the axes $E*/E0$) - log (N)
(0% RAP, 15% RAP, 25% RAP, and 40% RAP).....250

Figure 6.20 Comparison of a fatigue test at test at 150 µm/m strain level, real strain values lie in the range of 145 to 157 µm/m, for 4 recycled mixtures in the axes $E*/E0$) - log (N) (0% RAP, 15% RAP, 25% RAP, and 40% RAP).....250

Figure 6.21 Wöhler curve in the domain log N_f vs log ε_0 (m/m) 255

Figure 6.22 Wöhler curves for the four mixes (0% RAP, 15% RAP, 25% RAP, 40% RAP) determined with the classical criteria (left) and with the criterion of the end of phase II (right) and the corresponding regression lines in the logarithmic axis log N_f-log ε.....256

Figure 6.23 Wöhler curves for the four mixes after corrected to air void of 5,1% determined with the classical criteria (left) and with the criterion of the end of phase II (right) and the corresponding regression lines in the logarithmic axis log N_f-log ε 256

Figure 6.24 Relation between %RAP and $logk1$ before and after correction for a specific air void of 5,1% according to the classical criterion ($N_{f50\%}$) and the criterion of the end of phase II ($N_{fII/III}$).....260

Figure 6.25 Relation between %RAP and $k2$ before and after correction for a specific air void of 5,1% according to the classical criterion ($N_{f50\%}$) and the criterion of the end of phase II ($N_{fII/III}$).....260

Figure 6.26 Basic predicted model versus measured N_f using the fatigue parameters $k1$, and $k2$ defined for each mix 262

Figure 6.27 ε_6 values of the four tested mixes determined with the criteria of 50% decrease of the initial modulus and the criteria of transition between II and III.....263

Figure 6.28 Damage values at the transition between phases II and phases III (beginning of macro-crack propagation) for Tension/ compression strain control tests: $DIII$ no correction; $DIIIc$ correction from artefact effects Di Benedetto et al. (2004) 270

Figure 6.29 Level of damage leading to rupture ($DIII$) for all tested specimens (group), tested at +10°C and 10 Hz, depending on the corrected deformation amplitude 272

Figure 6.30 Level of damage leading to fracture the specimens group of each mix separately, tested at +10°C and 10 Hz, in function of the amplitude of corrected deformation and voids content 273

Figure 6.31 Evolution of damage leading to failure, corrected for artefact effects, depending on the corrected deformation amplitude for all the data at +10°C and 10Hz 274

Figure 6.32 Evolution of damage leading to failure, corrected for artefact effects, depending on the magnitude of corrected deformation and voids content for each mix separately (group of the specimens of the same mix) at +10°C and 10Hz 274

Figure 6.33 Evolution of damage leading to failure, corrected for artefact effects, depending on the air void content for all the data at +10°C and 10Hz.....275

Figure 6.34 Prediction of the fatigue life according to the DGCB method.....277

Figure 6.35 The Nf for the 4 recycled mixtures: (a to d) Wöhler curves determined using the failure criterion ($N_{fII/III}$) and the DGCB Nfpred, (e to h) Correlation between the DGCB Nfpred and the $N_{fII/III}$ 279

Figure 7.1 Relationship between $logk\%RAP1, \theta test$ and %RAP for the two studied criteria.....286

Figure 7.2 Predicted N_f in accordance with equation 7.3 versus observed N_f in accordance to the two criterion $Nf50\%$ and $NfII/III$ using the parameters of Table 7.2 as defined in § 7.3.....288

Figure 7.3 Relationship between $k2\%RAP$ and %RAP for the two studied criteria dotted line: dotted line: $k40/25$extrapolated form data for 0 to 25% RAP.....289

Figure 7.4 Predicted versus observed N_f using the two criterion $Nf50\%$ and $NfII/III$ using the testing data up to 40% with the value of the parameter $A0/40$ (Table 7.2) fixed from the $k2\%RAP - \%RAP$ relationship ($k20/40$ versus %RAP) 291

Figure 7.5 Predicted versus observed N_f using the two criterion $N_{f50\%}$ and $N_{fII/III}$ using the testing data up to 25% with the value of the parameter $A0/25$ (Table 7.2) fixed from the $k2\%RAP - \%RAP$ relationship ($k20/25$ versus RAP %) 292

Figure 7.6 Predicted versus measured N_f using testing data by assuming variable slopes of the fatigue lines by considering A as the average of the three results obtained for each mix (15, 25, 40% of RAP) with both failure criteria 294

Figure 7.7 Predicted versus measured N_f using testing data by assuming the slope of the fatigue line is variant and by considering the A value determined from the optimization process as an average of $A15$ and $A25$ 295

Figure 7.8 Predicted versus measured N_f using testing data by assuming the slope of the fatigue line as variant and using the optimum values of A for each mix (those values are shown in Table 7.3) 297

Figure 7.9 Statistical fatigue model versus measured N_f using the statistical fatigue parameters $k1stat-0/40$, and $k2stat-0/40$ and the $SFstat-0/40$ defined for all the mixes combined up to 40% 300

Figure 7.10 Statistical fatigue model versus measured N_f using the statistical fatigue parameters $k1stat-0/25$, and $k2stat-0/25$ and the $SFstat-0/25$ defined for the mixes combined up to 25% RAP 302

Figure 7.11 Studied pavement structure 305

Figure 7.12 Location of the calculation of the strain considered in Alizé software 307

Figure 7.13 Relations between the computation strains at the bottom of the bituminous layer, between the dual tire of standard 18,000-lb single axle with (an ESAL), and the temperatures for the mixtures containing different percentages of RAP at 10 Hz and 3 Hz 308

Figure 7.14 $Ncalculated0-40\%$ relative to $N0\%RAP0/40$ determined based on the structure level at different temperatures and at 10 Hz according to the $Nf50\%0/40$ using three different models 314

Figure 7.15 $Ncalculated0/40$ relative to $N0\%RAP0/40$ determined based on the structure level at three different temperatures and at 10 Hz according to the $NfII/III0/40$ using three different models. 315

Figure 7.16 Basic predicted model values versus the new predicted models values using the suitable coefficients fatigue factors established from $Nf50\%$ criterion based on the structure level point of view (top: the general model, and down: the statistical model) 318

Figure 7.17 Basic predicted model values versus the new predicted models values using the suitable coefficients fatigue factors established from $NfII/III$ criterion based on the structure level point of view (top: the general model, and down: the statistical model) 319

Figure 7.18 $N_{f\text{-}calculated}$ relative to $N_{f\text{-}0\%RAP}$ determined based on the material level and the structure level at 10°C and 10 Hz according to the $Nf50\%$ using the basic model and the general model.....324

Figure 7.19 $N_{f\text{-}calculated}$ relative to $N_{f\text{-}0\%RAP}$ determined based on the material level and the structure level at 10°C and 10 Hz according to the $NfII/III$ using the basic model and the general model.....325

LIST OF ABREVIATIONS

AASHTO	American Association of State Highway and Transportation
ARRA	Asphalt Recycling and Reclaimed Association
BBR	Bending Beam Rheometer
DGCB	Département de génie civil et bâtiment
HMA	Hot Mix Asphalt
IDOT	Illinois Department of Transportation
IDS	Indirect tensile Strength
IDT	Indirect Tensile Test
MEDG	Mechanistic Empirical Design Guide
NAPA	National Asphalt Pavement Association
NCHRP	National Cooperative Highway Research Program
PAV	Pressure Aging Vessel
RAP	Reclaimed Asphalt Pavement
RHM	Recycled Hot Mix
RTC	Regional Transportation Commission
RTFO	Rolling Thin Film Oven
SCB	Semi-Circular Bending
TTSP	Time Temperature Superposition Principle
UT	University of Tennessee
LVE	Linear Viscoelastic behaviour
WLF	Williams, Landell and Ferry
ENTPE	École Nationale des Travaux Publics de l'État
ÉTS	École de Technologie Supérieure
LC	Laboratoire des Chaussées du MTQ
LCPC	Laboratoire Central des Ponts et Chaussées
LCMB	Laboratoire sur les Chaussées et les Matériaux Bitumineux
MTQ	Ministère des Transports du Québec
MTS	Materials Testing System
SGC	Superpave Gyratory Compactor

SETRA	Service d'Études sur les Transports, les Routes et leurs Aménagements
SHRP	Strategic Highway Research Program

LIST OF SYMBOLS AND UNITS OF MEASUREMENTS

§	Section
°C	Degree Celsius
C_1, C_2	WLF constants
A	Amplitude of signal
$a_{(m)}$	Slope of the m-value-temperature curve
$a_{(S)}$	Slope of the stiffness-temperature curve
a_F	Slope of fatigue
a_T	Shift factor in the complex modulus test
a_T	Slope of the modulus of the test
a_w	Slope of the dissipated energy of the test
b	Slope of fatigue line
C_i	Coefficient of correction
ΔE_a	Apparent activation energy characterizing the material, typically 250 kJ/mol
k_1	Coefficient corresponding to the life duration of the material for an imposed strain amplitude of 1 m/m, at a temperature and frequency data
k_2	Coefficient related to the slope of the fatigue right for a given material
cm	Centimeter
D	Diameter
D	Damage
D_{III}	Damage at the beginning of phase III
D_{IIIc}	Corrected damage at the beginning of phase III
G_{mm}	Aggregate's maximum theoretical specific gravity
G_{mb}	Bulk density of the mixture
G_{sa}	Apparent specific gravity of the aggregate
G*(W)	Shear modulus
E	Elastic modulus due to loading
E*	Complex modulus
E_0	Initial modulus

E_{00i}	Initial modulus of the chosen interval extrapolated at the first cycle
E_{III}	Modulus at the beginning of phase III
E_F	Modulus of fatigue
E_r	Relative error
E_N	Norm of complex modulus of material at cycle N
Fr	Frequency
$G_{mesured}$	Grandeur of measured signal
$G_{calculated}$	Grandeur of calculated signal
g	Gram
H	Hight
Hz	Hertz
IQ	Quality index
$K^*(\omega)$	Complex bulk modulus
kg	Kilogram
km	Kilometer
kN	Kilo Newton
MPa	Mega Pascal
m	Meter
mm	Millimeter
N	Number of cycles
N	Number of gyration
N_f	Number of cycle at the rupture
$N_{f50\%}$	Number of cycle at the half of the initial modulus
$N_{fII/III}$	Number of cycle at the point of transition between phases II and III
N_{fDGCB}	Number of cycle at the rupture corrected by the DGCB method
P_{aged}	The stiffness value measured on an aged asphalt specimen
P_{unaged}	The value on an unaged asphalt specimen
P_{ba}	The mass of asphalt absorbed by the aggregate
P_{bi}	Mass of initial asphalt expressed as a percentage of the pavement mixture

Pa	Pascal
PG	Performance grade
p.	Page
R	Universal gas constant = 8,314 J K^{-1} mol^{-1}
R^2	Coefficient of determination
S_N	Standard deviation
STD	Standard
s	Second
T°	Temperature
T_o	Reference temperature
T_g	Transition temperature
t	Time of solicitation
V_{be}	Volume of effective asphalt binder
VAM	Volume of voids in the mineral aggregate in the compacted mixture
VFA	Percent of voids in the mineral aggregate occupied by the volume of effective asphalt binder
W_i	Dissipated energy at load cycle
ε_t	Tensile strain
ε	Deformation
ε_0	Initial Deformation
ε_6	Deformation at 1 million of cycles
ε_A	Amplitude of signal of deformation
ε_{i0}	Average value of the deformation
ε_{iA}	Amplitude of signals of deformation for the three extensometers
θ	Temperature
σ	Stress
σ_0	Initial stress
σ_A	Amplitude of signal of stress
υ	Coefficient of Poisson (usually assumed)
ϕ_E	Phase angle

μdef	Micro deformation
μm	Micron
ω	Angular frequency
S_e	Standard error
S_y	Standard deviation

BASE UNITS

Length

km	kilometer
m	meter
cm	centimeter
mm	mm
µm	micrometer

Area

m^2	square meter

Volume

m^3	cubic meter
cm^3	cubic centimeter
mm^3	cubic millimeter

UNITS OF MASS

Mass

kg	kilogram
g	gram

Density

g/cm^3	grams per cubic centimeter

HEATING UNITS

Temperature

°C	degree Celsius
K	Kelvin
°F	degree Fahrenheit

XL

MECHANICAL UNITS

Plase angle

°	degree

UNITS OF TIME

Time

H	hour
Min	minute
s	second
d	day
wk	week

Energy, work, quantity of heat

J	Joule

Power

kW	kilowatt

Stress, pressure

MPa	megapascal
kPa	kilopascal
Pa	pascal

Frequency

MHz	megahertz
Hz	hertz

Force

kN	kilonewton
N	newton

INTRODUCTION

Pavement recycling is one of the options available to pavement engineers for the rehabilitation of the roads. Reclaimed Asphalt Pavement (RAP) can be inserted in new mixes with various techniques, including hot in-plant recycling. As of now, it is common to add 20% of RAP in new mixes (West, 2008).

The basic concept of recycling of pavement lies in the conservation of the energy necessary to rehabilitate the damaged road, conservation of materials thanks to the re-use of the old roadway and the reduction of the use of new materials, and the safeguarding of the environment by eliminating the need for disposing old materials. Asphalt pavement recycling is not a novel concept; cold recycling dates back to the early 1900's. The first hot in-place recycling was reported in the literature in the 1930's. Modern asphalt recycling technologies that are used today evolved in the 1970s (Recycled Materials Resource Center, consulted on march 2014). The concept of recycling was regarded as ideal in the 1970s, but seldom carried out owing to the fact that the recycling of the pavement was more expensive than traditional re-construction. Nowadays, because of improvements in recycling techniques and also because of an increase in the price of raw materials, mostly bitumen, pavement recycling has become a viable option. Moreover, recent progress in technology available for the characterization and analysis of materials and mixtures improved the reliability of the design of the recycled mixture. Fatigue, associated with repetitive traffic loading, is considered to be one of the most significant distresses in flexible pavements. The fatigue life of an asphalt pavement is related to the various aspects of hot mix asphalt (HMA). Previous studies have been conducted to understand how fatigue cracking occurs and how to increase the fatigue resistance of bituminous materials under repetitive traffic loading (Daniel et Kim 2001; Di Benedetto, Ashayer Soltani et Chaverot, 1996; Anderson *et al.* 2001).

Accurate prediction of the fatigue life of asphalt mixtures is a difficult task due to the complex nature of fatigue phenomenon under various loading and environmental conditions. For the past several decades, significant research efforts have focused on developing reliable

fatigue prediction models. However these models do not take into account the effect of RAP percentages. Therefore, it is important to develop a specific model to predict the fatigue life of asphalt concrete mixture containing RAP.

Understanding the ability of an asphalt pavement to resist fracture from repeated loads is essential for the design of HMA pavement. However, reaching a better understanding of this fatigue behaviour of asphalt pavements continues to challenge researchers all over the world, particularly as newer materials with complex properties are being used in HMA pavements. It is important to obtain behaviour of these RAP mixtures in the laboratory, so that the fatigue performance can be predicted in the field. In addition, the utilization of these materials will enable engineers to find an environmentally friendly method to deal with these materials while saving money and energy.

Objectives of this study

The time and money required to conduct sufficient fatigue tests to develop a satisfactory model discourage the development of a model for individual mixture. For this reason, a model that could easily measure properties of an asphalt concrete mixture containing RAP is needed. Therefore, this study is conducted to evaluate the fatigue resistance of recycled asphalt mixtures, and also to develop a model that takes into account the addition of different percentage of RAP.

The specific objectives of this study are:

1. To conduct a literature review on the impact of the use of RAP in laboratory on fatigue cracking behaviour and on tests performed on mix containing RAP;
2. To evaluate RAP properties that are of particular interest when RAP is added to hot mix asphalt. This includes gradation, specific gravity, asphalt content, and the penetration and the viscosity of asphalt binder;

3. To examine how the addition of RAP to an asphalt mixture will change the properties of asphalt mixtures such as stiffness;
4. To evaluate fatigue resistance properties of recycled and conventional mixtures; and
5. To adjust the usual fatigue predictive models for RAP mixtures.

Thesis layout

The work is organized in seven chapters plus the general introduction, the summary and a conclusion. The introduction outlines the problem statement and the objectives of the research work as well as a layout of the thesis.

CHAPTER 1 provides an extensive literature review beginning with a brief summary regarding to bituminous mixtures used in pavement structure and recycling. An overview is given for various techniques of recycling and laboratory procedures recommended for the mix design of hot mix asphalt (HMA) with RAP.

CHAPTER 2 is also a literature review, but its presents the basics on rheology, thermo-mechanical properties of asphalt mixtures and the phenomenon of fatigue. It allows establishing the general frame work of this study.

The chosen methodology to achieve the desired objectives is discussed in CHAPTER 3. The layout of the laboratory testing program is also presented in the third chapter.

CHAPTER 4 describes in detail the laboratory procedure adopted for the design of recycled asphalt mixtures. The materials used in this study and experimental design including specimen fabrication are presented in this chapter. Some examples of typical results of experimental campaign are also presented.

CHAPTER 5 describes the results of complex modulus tests on bituminous mixtures. The analysis of the obtained results is also presented here.

CHAPTER 6 presents a study of the fatigue behaviour of different mixtures tested in the experimental campaign. After presentation of the fatigue test results, a study on the various criteria of fatigue and the method of DGCB is conducted.

CHAPTER 7, which is the last part of the thesis, deals with modelling and the improvement of the basic fatigue model in the form $N_f = k_1 \times \varepsilon_0^{-k_2}$ for the recycled mixtures by applying shift factors to this model to take into account the effect of RAP added content. Conventional statistical fatigue prediction models were created in CHAPTER 7.

Finally, a list of conclusion as results of the research work as well as recommendations that are needed for future studies and research were discussed. Also, at the end of thesis, the list of references is provided. All the supporting test data and additional graphical plots are included in the appendices.

Problem statement

For over a century, paved roadways have been constructed using asphalt concrete mixtures in Canada and elsewhere in the world. However, a major problem still exists in asphalt pavement involving premature distresses and failures, e.g., permanent deformation, fatigue cracking, and low temperature cracking. Since the early 1970s, many highway agencies have recycled old pavements in overlays or in major reconstruction of highways. Recently, the use of Recycled Asphalt Pavement (RAP) has significantly increased due to the protection of the environment, economy of construction/rehabilitation procedures, and to preserve non-renewable materials. However, the evaluation of RAP mixes performance has not been properly established.

Moreover, the quantity of RAP that is used in mixes depends on the type of roads, the traffic and the position of the HMA layer in the pavement structure. As of now, it's common to put, in Canada, up to 50% of RAP in binder layer but no more than 20% in the top layer.

Unfortunately, those limits are based more on past experience than on scientific studies. The impact of the addition of RAP in HMA is not well known.

The work done in this thesis revolves around two questions. First, what the effect of RAP content, binder type, added aged RAP, and RAP conditioning on the stiffness of the HMA mixtures with RAP is. The answer of this question is very important since it was shown in past studies that RAP has some potential drawbacks in term of performance. The second part of this work is concentrated on fatigue modelling of the HMA mixtures containing RAP. Can we predict fatigue life of HMA containing different percentages of RAP based on the fatigue results of the virgin mixture? Also can we predict fatigue life of road based on laboratory investigation? This research provides some answers and a novel approach to predict fatigue life of RAP mixes.

Statement of originality

There are three main contributions in this project. First, we proposed a modified fatigue model for predicting the fatigue life of asphalt mixtures. The model is based on the phenomenological approach that enables us to test only the virgin mixture. We have modified the basic fatigue model (equation 6.4) to the general fatigue model (equation 7.7) to take into account the addition of different percentages of RAP. We also added a shift factors into the fatigue parameters (k_1 and k_2), which means that we consider the slopes of the fatigue line to vary according to the amount of RAP. This differs than the assumptions in the literature review of keeping the slopes of the fatigue lines constant.

Second, we have tested eleven recycled mixtures that covered different conditions and different factors to study the impact on the mixture's stiffness. Our finding allowed for a better understanding of the effect of RAP on mixture stiffness. We found little or no effect of adding RAP. This is not surprising as the number of common studies showed that recycled mixtures can have similar performance to virgin mixtures.

Third, four of these mixtures were selected to study the fatigue behaviour of RAP mixtures. Our results showed that the inclusion of less than 25% of RAP in HMA mix had very limited influence on the fatigue performance of the mix. The results also showed that the inclusion of 40% of RAP in the HMA mixtures in this study improved its resistance to fatigue.

CHAPTER 1

BITUMINOUS MIXTURES USED IN PAVEMENT STRUCTURE AND RECYCLING

1.1 Pavement structure

The basic function of a pavement is to reduce the stresses induced by traffic at the subgrade level. The latter would indeed be unable to bear the stresses by the repeated traffic loading (see Figure 1.1).

The basic parts of a flexible pavement structure are:

- **Surface layer**: It is the top layer that comes in contact with traffic loads. It may be composed of one or several different HMA sublayers (Pavement interactive, 2010). It can be divided into three layers: the HMA wearing course, the HMA binder course and the HMA base course. The HMA wearing course is in direct contact with the tires and it ensures the security and the comfort of the users because it helps to provide a well bonded surface free from loose particles which might endanger people. The HMA base course protects the granular layer underneath by providing mechanical protection (load transfer), thermal (attenuation of the temperature variations), and hydrous (water proofing). The composition of the HMA mix in the binder or base course can be modified by including RAP to up to 40%. Between those two course, a binder course is often used for ease of construction;

- **Base course:** The base course is the lowest asphalt layers and it's composed of granular materials, treated or not. It is subdivided in two layers: base and subbase, its essential function is to distribute the loads induced by traffic to be compatible with the subgrade (Laveissiere, 2002). The subbase layer is used in areas where the subgrade soil is extremely weak. The subbase course functions like the base course. The material requirements for the subbase are not as strict as those for the base course since the

subbase is subjected to lower load stresses. The subbase consists of stabilized or properly compacted granular material (The constructor, 2015). The binder course is located between the surface layer and the base course and its use for its bearing capacity;

- **Subgrade**: The subgrade is the natural soil under the pavement. Usually, the top of the subgrade is graded and compacted to rectify heterogeneities and to increase the bearing capacity.

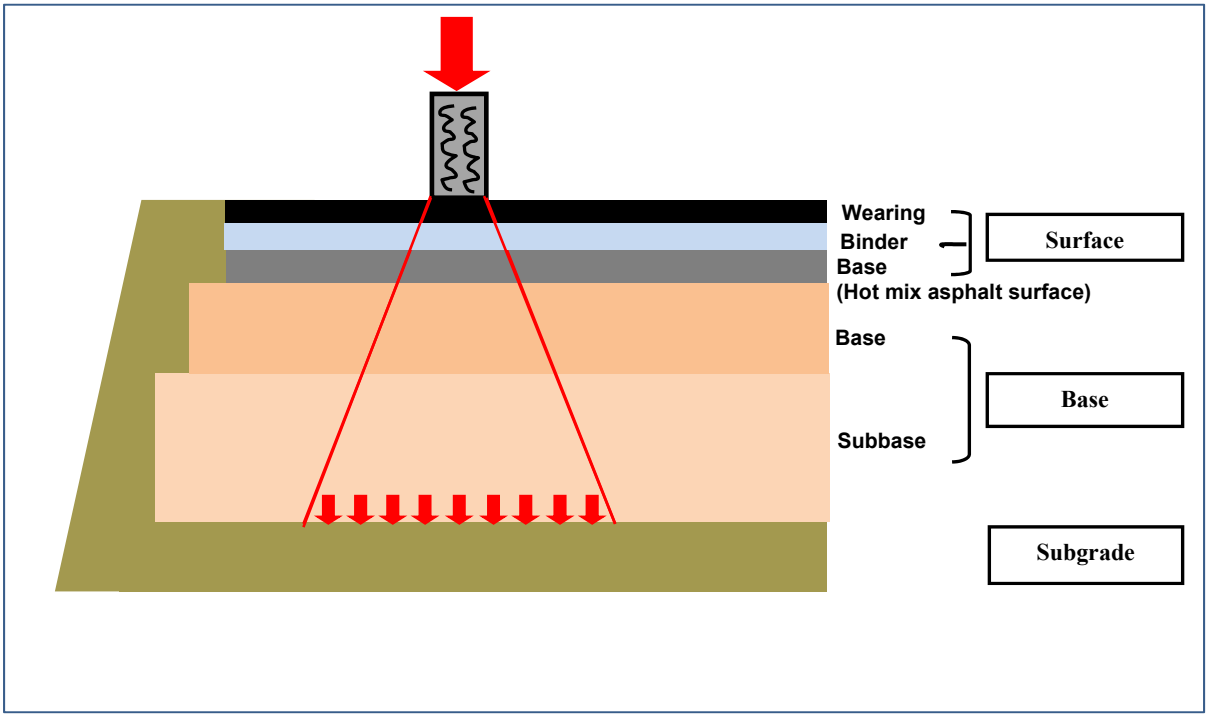

Figure 1.1 Typical stress distribution in a flexible pavement structure
Adapted from Laveissiere (2002)

There are three types of pavement structures depending on the materials used. Flexible pavements are made with bituminous materials, rigid pavements are made with concrete, and semi rigid pavement contains both concrete and bituminous materials. Only flexible pavements are studied this thesis.

1.1.1 Flexible pavements

Flexible pavements are composed of bituminous materials over granular materials. The thickness of these structures is designed according to the volume of traffic over a given period of time. In the case of low traffic pavement, the surface layer can be made of a single layer (Laveissiere, 2002).

1.2 Asphalt mixtures

The asphalt mixtures are composed of various selected aggregates (around 95% by mass) bound together into a cohesive mass with asphalt cement (around 5% by mass). According to Di Benedetto and Corté (2004), there are different compositions of asphalt mixtures that can be used according to their function and location within the pavement structure. Nevertheless, it is always the aggregate skeleton and the asphalt that will determine their mechanical and functional characteristics (Di Benedetto et Corté, 2004). Asphalt cement binds the aggregate particles together, enhancing the stability of the mixture and providing resistance to deformation under induced tensile, compressive and shear stresses. Bitumen materials are viscoelastic and their mechanical behaviour is dependent on both the temperature and rate of loading. At low temperatures and short loading times, asphalt cements behave as elastic solids, while at high temperatures and long loading times they behave as simple viscous liquids. At intermediate temperatures and loading times, the behaviour is more complex. A medium temperature range from 15 to 30°C is most suitable for fatigue cracking analysis and pavement fatigue life prediction (Deacon *et al.*, 1994).

1.2.1 Aggregate skeleton

The skeleton of the asphalt concrete is provided by the aggregates which carry most of the load (Sefimazgi, Tashman et Bahia, 2012). This structure is called aggregate internal structure. The connectivity of this structure is represented by the number of aggregate contacts in the asphalt mixture. Increasing the number of contact points can lead to a better stress distribution with less stress concentration. The effective parts of the aggregate internal structure are those that are in

the aggregate skeleton, which is composed of connected aggregate in loading direction. Examination of the literature reveals that mixes with different aggregate structure are expected to have different performance by keeping all other parameters constant (i.e., density, aggregate type, binder type, VFA, VMA, etc). However, Coenen, Kutay and Bahia (2011) have also shown that mixes with the same density can have different performance parameters.

The filler, which represents the aggregate portion passing the 80μm sieve, is added to dense-graded HMA to partly fill the voids in the aggregate skeleton. When asphalt binder is mixed with aggregate, the fines mix with the asphalt binder to form a mastic or bituminous mortar (Harris et Stuart, 1995). The filler will increase the compactness of the bituminous mix and will improve cohesion of the bituminous mortar (Tremblay, 2001).

1.2.2 Asphalt binder

Asphalt binder, or asphalt cement, is defined by the American Society for Testing and Materials as a ‘dark or black cementitious material occurring in nature or obtained by crude oil refining’ (ASTM, 1998). Atmospheric and vacuum distillations are the basic operation to produce asphalt binder. However, blending, air blowing, solvent of asphalting, solvent extraction, emulsification and modification are available to produce various grades of asphalt depending on the crude sources (Pumphrey, 2003).

The components of asphalt can be separated into two chemical groups, called asphaltenes and maltenes (Di Benedetto et Corté, 2004). Maltenes can be sub divided into three groups: saturates, aromatics and resins. The proportion of each group will affect the rheological properties of the asphalt.

Asphalt is a thermo-rheological material which means that its characteristics are directly related to temperatures. At high temperature, asphalt behaves like a viscous Newtonian liquids, while at cold freezing temperatures, it undergoes failure like an elastic solid. In between, it passes through the areas of linear and nonlinear viscoelasticity (Figure 1.2) (Di

Benedetto et Corté, 2004). Asphalt binders are also sensitive to the rate of loading. This kinetic susceptibility is due to its viscous nature.

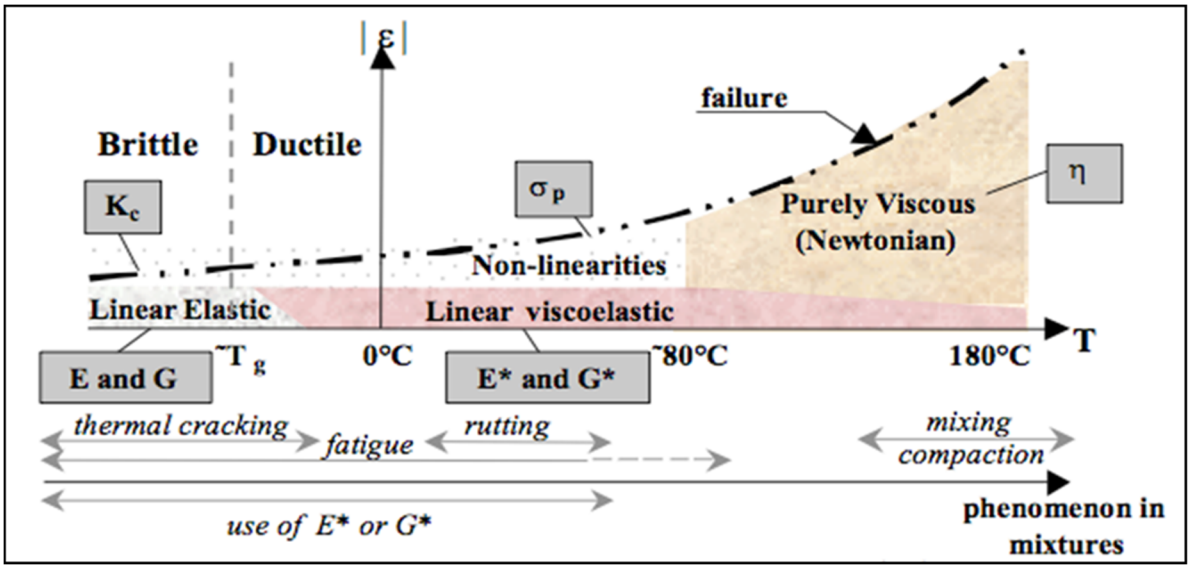

Figure 1.2 Behaviour classes of asphalt cement according to the strain amplitude (|Ɛ|) and the temperature (T)
Taken from Olard and Di Benedetto (2003)

In France, the classification of the asphalt binder intended for road industry is done according to their penetration NF EN 1426 (AFNOR, 1999) and to the temperature of ring and ball test, Softening point test NF EN 1427 (AFNOR, 2000). The penetration test is carried out at 25ºC and measures (in 0,1 mm) the depth of penetration of a 100 g needle. A bitumen classified 20/30 (penetration between 20mm and 30mm) is harder than another one classified 35/50 (penetration between 35 mm and 50 mm).

The softening point's test measures the softening point by ring and ball method. This test makes it possible to determine the temperature at which asphalt cement filling a brass ring and placed in a heated bath cannot support the weight of steel ball. An asphalt 55-63 whose softening point is between 55ºC and 63ºC is harder than an asphalt 50-58 whose softening point is between 50ºC and 58ºC (Gaonach, 2012).

In Quebec, asphalt cement is classified according to its performance grade (PG). The PG defines the temperature range for good performance of the asphalt binder. For example, the asphalt cement classified PG 58-28 is not considered sensitive to rutting at temperatures below 58ºC and becomes prone to thermal cracking below -28ºC. A bituminous mix made up of an asphalt cement of grade PG 64-28 offers better resistance to rutting than another bituminous mix made up of bitumen of PG 58-28 but will not provide any additional protection at low temperature (Gaonach, 2012).

It is possible to modify the rheology of bitumen by adding polymers to improve the performances during asphalt service life. The addition of polymers allows, for example, extending the performance range of the PG. In road construction, it is common to add between 3% and 7% by weight of styrene-butadiene-styrene (SBS) polymer (Di Benedetto et Corté, 2004).

1.2.3 HMA volumetric properties

The behaviour of an asphalt mixture is largely affected by the volumetric proportions of asphalt binder and aggregate components. The principle volumetric properties are:

- Air voids (V_a);
- Voids in the mineral aggregate (VMA);
- Voids filled with asphalt (VFA); and
- Volume of effective asphalt binder (V_{be}).

Hot mix asphalt pavement is comprised of asphalt binder, aggregate and air in specific volumetric proportions. These individual components are presented schematically in Figure 1.3 as an attempt to assist in visualization of the volumetric and mass relationships used in the analysis of hot mix asphalt pavement.

The definition of the volumetric properties helps to understand the principle behind the use of volumetric method in the formulation of asphalt mixture. Thus, the brief definitions of the key elements involved in asphalt volumetric are defined as follows (Jaffee, 2001):

V_a Air voids, the total volume of the small pockets of air between the coated aggregate particles within a compacted asphalt mixture expressed as a percentage of the bulk volume of compacted mixture (V_{mb}).

VMA Voids in mineral aggregates is the volume of intergranular space between aggregate particles in a compacted mix, including the air voids (V_a) and the volume of effective asphalt binder, expressed as a percentage of bulk volume of compacted mixture (V_{mb}).

V_{be} Total volume of asphalt cement in the mixture minus the volume of asphalt cement absorbed by the aggregate (V_{ba}), expressed as a percentage of the voidless volume of compacted mixture (V_{mm}).

VFA Voids filled with asphalt is the volume of voids in the mineral aggregate (VMA) occupied by the volume of effective asphalt cement (V_{be}) expressed as percentage of the voids in the mineral aggregate (VMA).

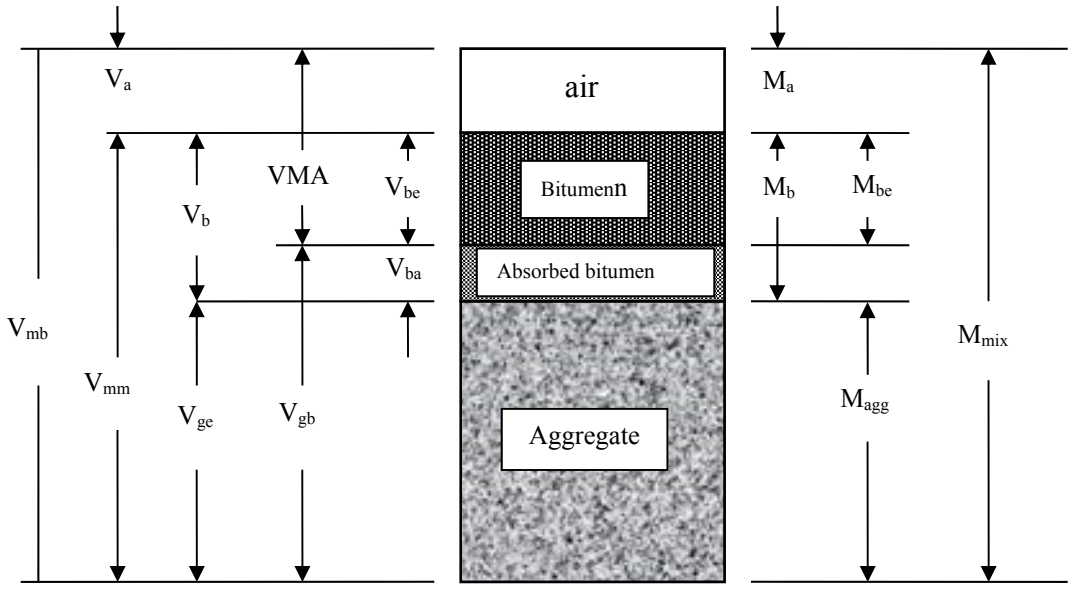

VMA = Volume of voids in mineral aggregate; M_{mix} = Total mass of asphalt mixture;

V_a = Volume of air voids; M_b = Mass of asphalt binder;

V_b = Volume of asphalt binder; M_{be} = Mass of effective asphalt binder;

V_{mb} = Bulk volume of compacted mixture; M_{agg} = Mass of aggregate;

V_{mm} = Voidless volume of compacted mixture; M_a = Mass of air = 0

V_{be} = Volume of effective asphalt binder (corresponds to volume of voids filled with asphalt);

V_{ba} = Volume of absorbed asphalt binder;

V_{ge} = Bulk volume aggregate;

V_{ge} = Effective volume aggregate;

Figure 1.3 Volumetric representation of a compacted mixture
Taken from Jafee (2001)

The first mention of recycling dates back to 1915 (Gannon *et al.*, 1980). A number of recycling techniques have been patented during 1930's to 1950's (Abdul-Rahman, 1985). Recycling of hot mix asphalt (HMA) has increased in popularity and became a common rehabilitation and maintenance process in the mid-1970s (Castedo-Franco, 1985). The first report on recycling appears in the proceedings of the Association of Asphalt Paving Technologists (AAPT) in 1975. These last years, a large number of reports on pavement

recycling have emerged (McDaniel et Anderson, 2001; Kennedy, Tam et Solaimanian, 1998; Roberts *et al.*, 1996). The state of the art of design and construction of pavements composed of recycled materials has advanced to a point where recycling is regarded as an alternative to conventional procedures for the majority of the projects of paving (Castedo-Franco, 1985).

Many different reasons led to the increased interest in recycling. Probably the greatest single factor was the oil embargo in the beginning of 1970s and the subsequent increase in the price of asphalt cement. Before the oil embargo, the price of asphalt cement was so low that it was more economical to build a new pavement than to remove, stockpile and recycle an old pavement (Roberts *et al.*, 1996).

The development of the milling machine is the second item that had a great impact on recycling. Before the development of the milling machine, old asphalt pavement had to be ripped from the roadway, then crushed in plant before being reused (Roberts *et al.*, 1996). This process required full depth removal of the HMA and required the roadway to be closed for long periods of time. Another process which was used before the milling machine was the heater planer. This process did require a great quantity of energy to heat the pavement, resulting in pollution, and it damaged the removed HMA by overheating (Roberts *et al.*, 1996).

The milling machine solved all the problems observed with heater planers. With milling machines, asphalt can be removed at desired depth and does not produce appreciable pollution since heat is not required (Roberts *et al.*, 1996). The material removed with a milling machine does not always need to be crushed since it is rather fine immediately after being removed to be recycled. A milled surface can also be opened to traffic temporarily until the overlay has been completed. In the 1970's, the milling machine became an integral part of many programs of asphalt rehabilitation and millions of tons of RAP was produced each year.

The term Reclaimed asphalt pavement (RAP) is given to removed and/or reprocessed pavement materials which contain asphalt and aggregates. These materials are generated when asphalt pavements are removed for rebuilding, resurfacing, or to obtain access to the public services underneath. When it is correctly milled, RAP is composed of high-quality, well-graded aggregates coated by asphalt cement (FHWA, 2011). Thus, the addition of RAP in new HMA mixes has become increasingly widespread (Daniel et Lachance, 2005).

1.2.4 Benefit of recycling asphalt pavement

Asphalt recycling has become a key component of the Canadian paving industry (Federation of Canadian Municipalities et National Research Council, 2005). Recycling can reduce disposal of the materials removed from a road surface. Before recycling came about, this removed asphalt had to be taken to a dumping site for disposal. The discarded material and cost of trucking represented a waste of money.

The use of RAP offers majors benefits as (Navaro, 2011):

- Conservation of natural resources of aggregates and binders;
- Preservation of the environment by reducing the emissions of greenhouse and toxic gases;
- Conservation of energy;
- Reduced construction cost;
- Reduction in transportation cost.

1.2.5 Asphalt recycling methods

Different types of pavement recycling exist, which could be hot or cold and in-place or in plant. Those are characterized by the temperature at which the bituminous mixture can be produced. The bituminous mixtures can be produced hot; at temperature ranging between 160°C and 180°C, or cold, at room temperature (Navaro, 2011). They are also different by

displacement of the material taken from the pavement to be reused (reuse in central plant or in-place).

Recycling of pavement material can be done like an in-place process or as a plant process. The in-place process combines heating (for hot process), scarifying, rejuvenating, mixing, lay down, and compaction into a single paving train in the field. The central plant process involves processing RAP to a desired gradation using a screener and sometimes a crusher. Then, it is stockpiled at the asphalt plant. This product is mixed with new aggregates and asphalt binder in a hot mix plant. Finally, it is trucked to the construction for laydown and compaction (Daniel et Lachance, 2003). The complete operation is shown schematically in Figure 1.4.

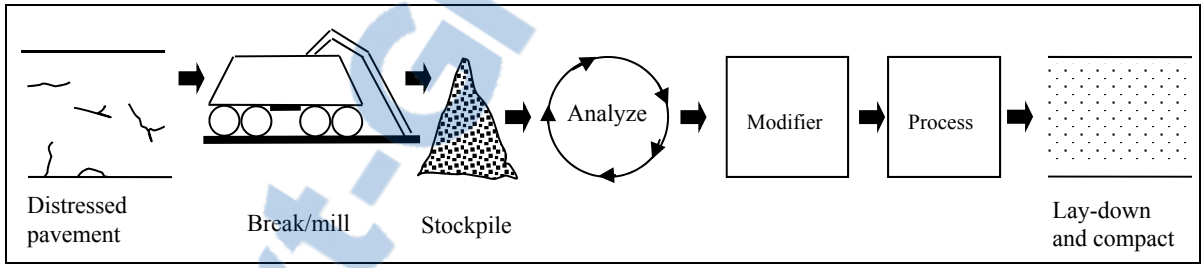

Figure 1.4 Schematic of pavement recycling operation in central plant
Adapted from Abdul-Rahman (1985)

The availability of various techniques of recycling makes it possible to choose the technique based on the desired performance of the produced mixtures and the development of the techniques at each country. These techniques are illustrated in Figure 1.5. It is important to note that the techniques of cold recycling are similar to the hot recycling except that the RAP material is reused without any use of heat.

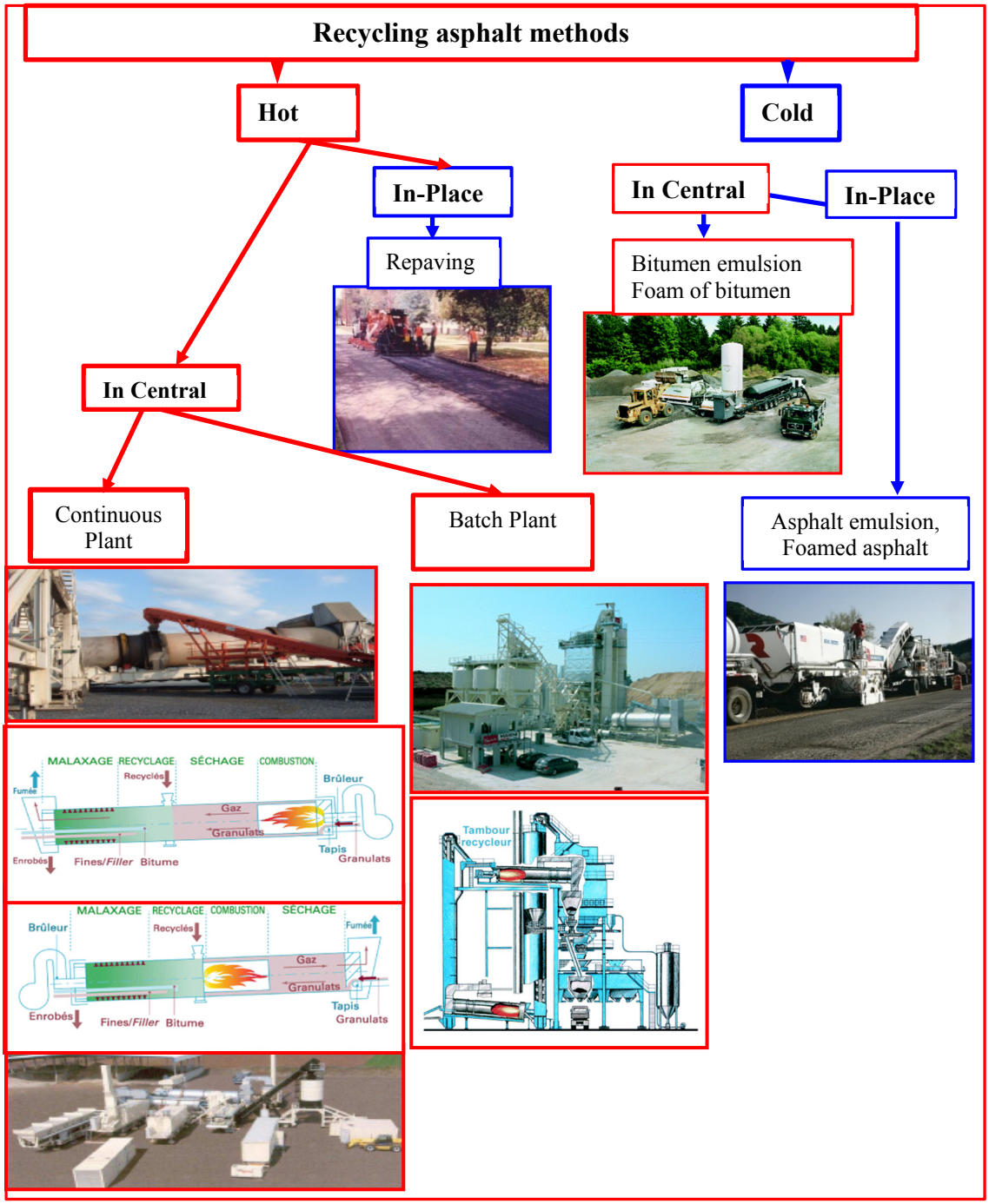

Figure 1.5 Presentation of the technical possibilities of recycling of bituminous pavements
Adapted from Navaro (2011)

1.3 Recycled mixtures

The recycling of asphalt mixtures is carried out by incorporating recycled asphalt mixtures in the production cycle of new bituminous mixtures. The RAP is used in HMA mixes at varying percentages. We will see later that the addition of low rate of RAP is easier than the addition of high rate of RAP.

1.4 Composition of recycled mixtures containing RAP- definition

Recycled asphalt mixtures containing RAP is made up of a mixture of 'new' or 'virgin' materials (Virgin Aggregates, VA, and Virgin Binder, VB) and RAP. This RAP is made up of RAP Aggregates (RAP A) and RAP Binder (RAP B). Therefore, the recycled asphalt mixtures consist of aggregates of recycled asphalt mixture, RAM A (mixture of VA and RAP A), and recycled asphalt mixture binder, RAM B (mixture of VB and RAP B). The denomination of the components of the recycled asphalt mixtures is presented in Figure 1.6.

1.5 Recycling rate of recycled asphalt mixtures

The recycled asphalt mixture is mainly defined by the mass of RAP that they comprise. This mass is commonly called "percentage of RAP". Recycled mixtures containing up to 20% of RAP are said to be "low rate of recycling". This denomination is opposed to the asphalt mixtures containing between 40% and 65% of RAP which are then indicated by the term "high rate of recycling". This arbitrary division does not preclude of recycling at intermediate rates (Berthier, 1982). Since there is no strict definition of low and high rate, we will present the following proposed definition which is taken from the French experiment of recycling at high rate.

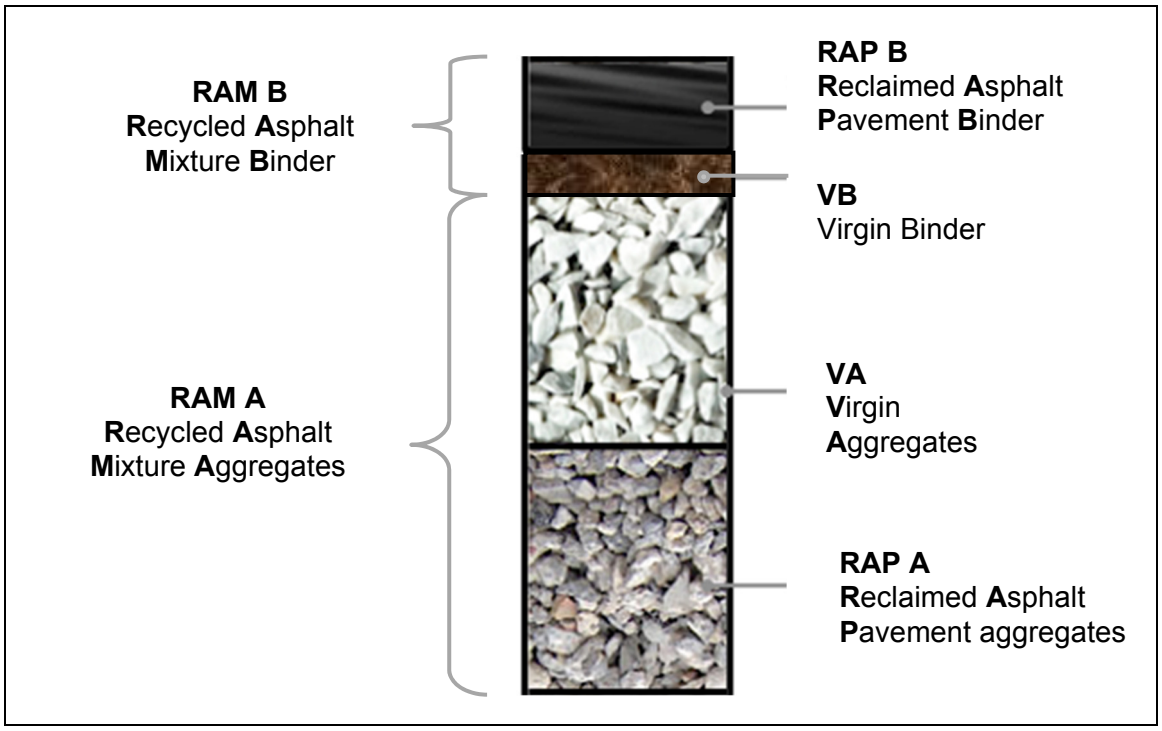

Figure 1.6 Composition of a recycled asphalt mixtures
Adapted from Navaro (2011)

1.5.1 Low level recycling

At low level of recycling, the properties of a bituminous mix are barely influenced by the composition (gradation, binder content and binder grade) of the RAP (Moneron et Measson, 2004; Li *et al.*, 2008). Therefore, on a regulatory level, it is not necessary to take into account the composition of RAP and its influence on the produced recycled mixture manufactured when less than 10% of RAP is used (Gandil et Vesseron, 2001). This rate is increased to 20% in the case of binder courses. This provision of law specified in circular 2001-39 of June 18, 2001 aims to encourage using RAP to reduce the volume of waste from road industry.

1.5.2 Recycling rate higher than 10% - 20%

At higher rates of recycling, the composition of RAP must be taken into account because of the presence of stiffer (aged) binder in the RAP material and its influence on hot mix asphalt.

Hence, because of the influence of aging, the HMA mixture with RAP may become vulnerable to durability cracking and premature failure. The composition of RAP is then studied in order to determine the characteristics of the RAP aggregate skeleton and the RAP asphalt cement (Daniel et Lachance, 2005).

1.6 Designing HMA with high percentage of RAP

In the middle of 1990s, the implementation of the Superpave method of mix design started. The original specifications for Superpave did not include guidance on how to include RAP into the new mix design system. Interim recommendations were developed through the FHWA Asphalt Mixture Expert Task Group (FHWA Superpave Mixture Expert Task group, 1997) based on experience and performances of Marshall mixes with RAP. The specifications were changed in 2002 after the results of an NCHRP research project (Incorporation of Reclaimed Asphalt Pavement in the Superpave System) became available (Mc Daniel *et al.*, 2000). AASHTO Standards MP2 (now M323) (AASHTO, 1999), Standard Specification for Superpave Volumetric Mix Design for Hot Mix Asphalt, describe how to design HMA with RAP.

The guiding principle of the AASHTO standard is that mixtures with and without RAP should satisfy the same requirements. The aggregates provided by the RAP are included in the determination of the gradation of the mixture and in the consensus properties (coarse aggregate angularity (CAA), fine aggregate angularity (FAA), flat and elongated particles (F&E particles) and the sand equivalent value which is waived because of the inability to test. The bitumen contained in the RAP is regarded as part of the total binder content of the mixture.

The Federal Highway Administration (FHWA) and its Superpave Expert Task Groups developed a guide (draft) for RAPs usage based on past experience. These guidelines established a tiered approach for the use of RAP. Under those guidelines, up to 15% of RAP can be used without changing the virgin binder grade (McDaniel *et al.*, 2000). When between

15 and 25% RAP is added, the high and low temperature grades of the virgin binder are both reduced by one grade. For more than 25% RAP, blending charts are used (McDaniel *et al.*, 2000).

According to McDaniel and Anderson (2001), in Superpave mix design, when RAP is used in amount greater than 20%, it is suggested to test both the RAP and virgin binder, and a blending chart should be used. Figures 1.7 and 1.8 present flow charts to design mixes with RAP.

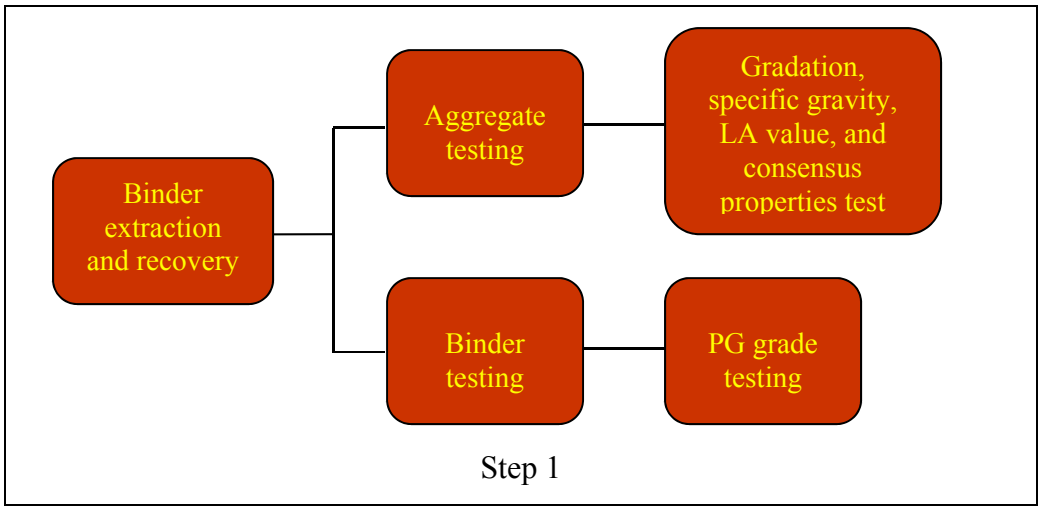

Figure 1.7 RAP mix design procedure – Step 1
Taken from Newcomb *et al.* (2007)

As shown in Figures 1.7 and 1.8, there are three main steps that should be followed when RAP is used in new HMA. The purpose of step 1 is to characterize RAP aggregates and asphalt when a high percentage of RAP is used in a new HMA. Gradation, specific gravity, consensus properties, and LA abrasion properties of aggregates should be checked. It is also important to determine PG grade of the RAP binder because asphalt stiffens due to aging.

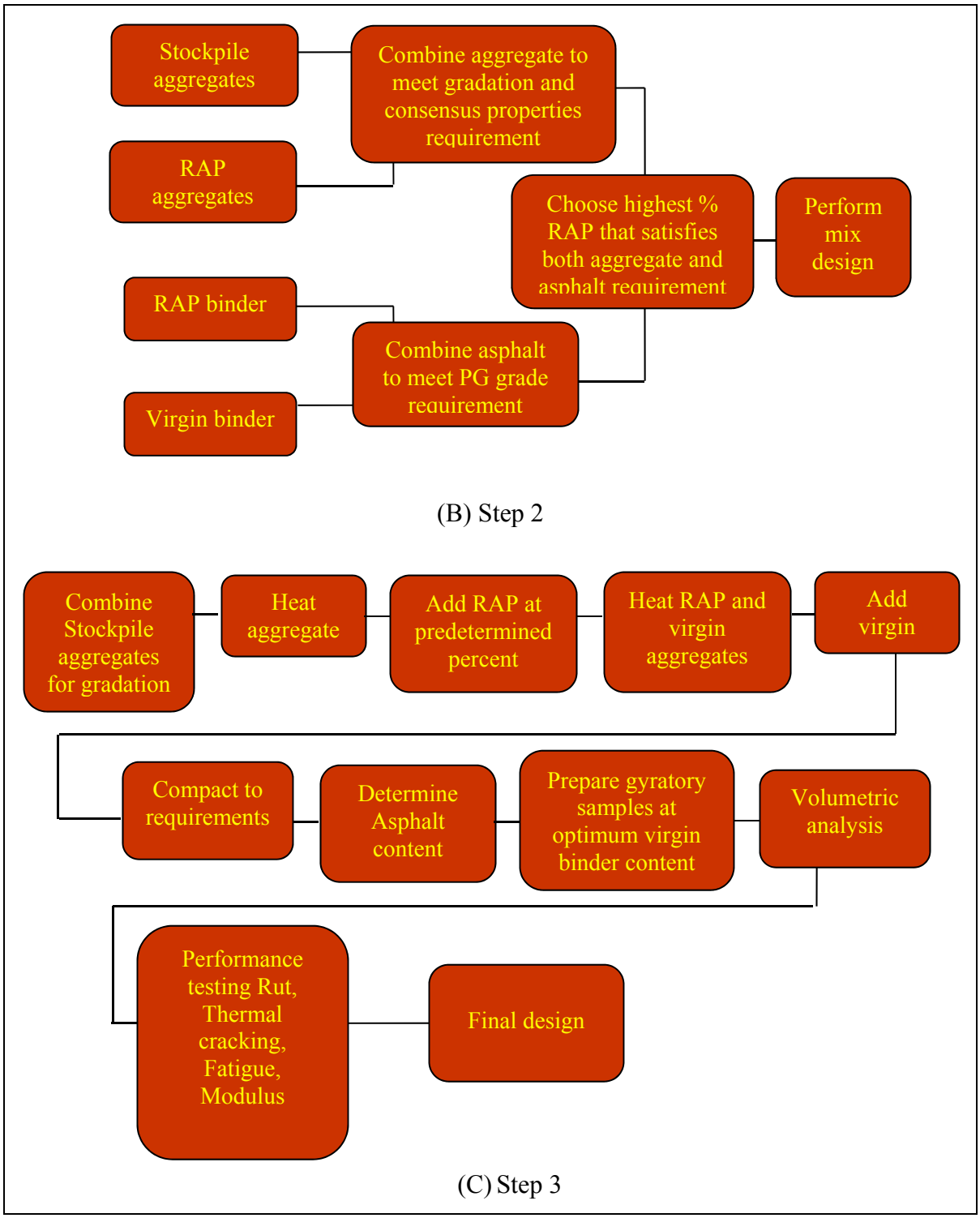

Figure 1.8 RAP mix design procedure – Step 2 and 3
Taken from Newcomb *et al.* (2007)

Once the RAP aggregate and asphalt have been characterized, the combined aggregate and the combined asphalt cement should meet the following requirements: the gradation, consensus properties, and the PG grade for the combined binder using blending charts as shown in step 2. Finally, step 3 presents an overview of how to incorporate RAP in mix design. This process is quite similar to the mix design of virgin HMA. The only difference is the handling of RAP material. Specimens are prepared at the desired asphalt content following mix designs with RAP that were recommended and adapted in AASHTO MP2 (AASHTO, 1999) as follow:

- A blend of RAP and virgin aggregate is prepared using one of the following two heating scenarios which are used in this work:

    1) Virgin aggregate is heated in an oven at 180°C (356°F) for 3 hours, and the RAP is heated in an oven at 110°C (230°F) for 2 to 2,5 hours;
    2) Virgin aggregate is superheated to 300°C (572°F) for 15 minutes, and the RAP is left unheated at ambient laboratory temperature. These scenarios are intended to simulate the effect of RAP heating conditions on the mixture properties.

- Virgin bitumen is heated to approximately 150°C then added at the desired amount, and mixed thoroughly with the blend of virgin aggregate and RAP materials;
- All the materials are mixed and compacted using a gyratory compactor for volumetric evaluation;
- Specimens are prepared at different asphalt contents;
- Select RAP mix samples that meet volumetric requirements;
- Samples prepared at the optimum asphalt content are tested for performance.

1.7 Extraction and recovery of asphalt binder

It is important to determine asphalt content, properties of RAP binder, and aggregate gradation, in the design of mixtures containing RAP. The only way to get the above

information is to separate the asphalt cement from RAP. The most widely used methods are solvent extraction and ignition oven, which can determine both binder content and aggregate gradation (Pavement interactive, 2015).

In the solvent extraction method, a solvent such as trichloroethylene or ethylene chloride is used to dissolve and separate the binder from the aggregate. Asphalt cement is then calculated from the mass difference before and after extraction. In the ignition method, the mix sample is heated to around 540°C for about 45 minutes until all the asphalt is burned off. The difference in mass before and after ignition is determined as the asphalt content. There are some disadvantages of the solvent extraction method such as it has a high standard deviation of test results (Brown et Murphy, 1994). Peterson *et al.* (1999) showed that the amount of binder content extracted differs by 0,3% to 9,5% when comparing different extraction methods using solvent. However, the solvent extraction method is banned in many countries because Trichloroethylene is hazardous to both man and environment. According to Kandhal et al (1995), the ignition method is accurate and precise. However, the ignition extraction method causes degradation of aggregate because of combustion of RAP in the oven which changed the properties of the aggregate (Prowell et Carter, 2000). This degradation can also lead to erroneous estimates of the binder content with some aggregates, especially for RAP sources with unknown correction factors. Therefore, ignition oven should be allowed only if it is calibrated with clean aggregate. Abson recovery method (ASTM D1856-09, Standard Practice for recovery of asphalt from solution by Abson method (ASTM. 2009)) and Rotavapor method (ASTM D5404/D5404M – 12 (ASTM. 2012)) can be used for recovery of asphalt cement from solvent.

1.8 Determining RAP aggregate properties

The two main critical properties that need to be evaluated in the case of RAP aggregates are gradation and specific gravity. Additionally, the RAP aggregates may also be tested to determine its consensus properties depending on the amount of RAP to be used in the mix.

After extraction test, the RAP aggregates are used to determine the aggregates gradation and certain physical properties as it is done with virgin aggregates.

1.8.1 RAP aggregate gradation

The gradation analysis is used to determine particle size distribution. The aggregate gradation is one of the most important HMA mixes properties associated with its control. Roberts *et al.* (1996) found that gradation affects every influential HMA property including stiffness, stability, workability, durability, permeability, fatigue resistance, and resistance to moisture damage. The rutting characteristics of pavements are also controlled by asphalt cement and aggregate gradation. The standard gradation and sieve analysis can be conducted according to LC 26-350 (MTQ, 2002) or AASHTO T 27 (AASHTO, 2011) and ASTM C 136 (ASTM, 2001) 'Sieve analysis for fine and coarse aggregate'.

The aggregate gradation of the processed RAP in HMA mixes is usually finer and denser than virgin aggregate because of mechanical degradation that has occurred during milling or crushing during pavement removal and processing. Milling is a term referred to describe the material that is produced by removing the existing pavement material using the milling plant. Generally, both milling and crushing processes can cause degradation of RAP's aggregate. However, RAP obtained from milling is finer than the RAP obtained from crushing. It has been found that RAP aggregate generally meets the ASTM requirements based on ASTM D692 (ASTM, 2004) 'Coarse aggregate for bituminous pavement mixtures' and ASTM D1073 (ASTM, 2007) 'Fine aggregate for bituminous pavement mixtures' (FHWA, 1998).

Studies on pavements conducted elsewhere have shown that before and after milling, the material fraction passing the 2,36 mm (No. 8) sieve increased from a pre-milled range of 41 to 69% to a post-milled range of 52 to 72%. The fraction passing the 0,075 mm (No. 200) sieve increased from approximately 6 to 10% to 8 to 10% (Kallas, 1984).

1.8.2 RAP aggregate specific gravity

The specific gravity of the combined gradation of RAP and stockpiled aggregates is required to determine the voids in mineral aggregate (VMA), or to use the LC design method developed by MTQ (*Ministère des Transport du Quebec*). For example, for estimating the binder content of a mixture, the bulk specific gravity of each aggregate component (stockpile) including RAP aggregate is needed for the calculation of the combined bulk specific gravity. The extracted RAP aggregate is sieved into coarse and fine fractions, and the specific gravity is determined for each fraction. The disadvantage of this procedure is that the extraction procedure can change the aggregate properties and may result in a change in the amount of fine materials which could also change the specific gravity of the aggregate (McDaniel et Michael Anderson, 2001).

According to NCHRP research results No. 452 (McDaniel et Michael Anderson, 2001), there are two approaches to avoid this problem. In the past, some used the effective specific gravity (G_{se}) of the RAP aggregate in lieu of its bulk specific gravity (G_{sb}). The effective specific gravity can be calculated based on the maximum theoretical specific gravity of the RAP mixture, which can easily be determined by conducting LC 26-045 "*Détermination de la densité maximale*" (MTQ, 2008). Once the binder content of RAP is determined, the G_{se} of the RAP aggregate can be calculated as follow:

$$G_{se} = \frac{100 - P_b}{\frac{100}{G_{mm}} - \frac{P_b}{G_b}} \tag{1.1}$$

Where:

G_{se} Effective specific gravity of RAP aggregate;

G_{mm} Theoretical maximum specific gravity of asphalt mixtures from the LC 26-045 test;

P_b RAP binder content at which the LC 26-045 test was performed, percent by total mass of mixture; and

G_b Specific gravity of RAP binder.

However, substituting the G_{se} for the G_{sb} of the RAP aggregate will result in overestimating for both the combined aggregate bulk specific gravity and the VMA since G_{sb} is always smaller than G_{se} for a given aggregate.

The second approach discussed in NCHRP 452, 2001 (McDaniel et Michael Anderson, 2001), consists of assuming a value for the absorption of the RAP aggregate (based on the past experience on the same virgin aggregate) and on the calculation of the maximum theoretical specific gravity of the RAP mixture. The G_{se} of the RAP aggregate can be calculated as explained before in equation 1.1. This G_{se} is used to calculate G_{sb} as follows:

$$G_{sb} = \frac{G_{se}}{\left(\frac{P_{ba} * G_{se}}{100 * G_b}\right) + 1} \tag{1.2}$$

Where:

P_{ba} Absorbed binder, percent by G_{sb} weight of aggregate.

The disadvantage of this method is that the absorbed binder is assumed and not measured, which could lead to wrong G_{sb}.

1.8.3 Coarse aggregate angularity (CAA)

Coarse aggregate angularity (CAA) is determined manually by the visual inspecting of a small sample of coarse aggregates, separating the sample into the aggregates with or without fracture faces, and counting the number of aggregates with fractured faces in the sample. Then, the percentage of particles having fractured faces is compared to the specification requirements. The fractured face of each rock particle must meet a minimum cross-sectional area requirement to be counted. Typically, specifications contain requirements for percentage

of fractured aggregate particles in order to maximize shear strength in HMA mixtures. Angular particles are important in the design of HMA mix because they tend to lock together and resist rutting after initial compaction. Rounded particle may not produce sufficient inter-particle interlocking to prevent rutting. The test can be conducted by following the test procedure described in AASHTO TP 61 (AASHTO, 2004) or ASTM D 5821 (ASTM, 2006).

1.8.4 Fine aggregate angularity (FAA)

Fine aggregate angularity (FAA) is as important as CAA. A greater amount of rounded fine particles can lead to a decrease of the rut resistance of the HMA. FAA is quantified by measuring loose un-compacted void content of a fine aggregate sample (Thakur, 2010). On a sample of known gradation, the loose un-compacted void content is indicative of the relative angularity and surface texture of the sample. In general, the higher the void content, the higher the assumed angularity and rougher the surface. This test ensures that a blend of fine aggregates has adequate angularity and texture to resist rutting. Angular particles tend to lock up and offer resistance to compaction; however, the rounded particles are easy to compact (Thakur, 2010). FAA test can be conducted using ASTM C1252 (ASTM, 2006) (AASHTO T304 – (AASHTO, 2011)).

1.8.5 Flat and elongated particles

Particle shape is usually as the number of flat and elongated particles and is determined according to the test ASTM D 4791 ‘Flat particles, elongated particles, or flat and elongated particles in coarse aggregate’ (ASTM, 2010). The aspect ratio of the coarse aggregate particles (greatest dimension to smallest) is measured and the percent mass of flat and elongated coarse aggregate is calculated (Pratheepan, 2008). The existing of an excessive amount of flat and elongated particles in the HMA mixtures can cause different problems in production, placement, and in compactions. Current superpave mix design allows maximum 10% flat and elongated particles for the aggregate coarser than 4,75 mm when using the flat and elongated ratio 5,1 (Thakur, 2010).

1.8.6 Hardness/wear

The standard Los Angeles abrasion test, LA test, (LC 21-400 (MTQ, 2001), AASHTO T96 (AASHTO, 2002), ASTM C131 (ASTM, 2001)) has been used to evaluate the resistance of aggregate to degradation that may occur during production, placement, or even during its service life. An interesting study was conducted in 2004 by Ahmad et al. (Ahmad *et al*, 2004) in Malaysia to evaluate the degradation and abrasion of RAP aggregate. This study focused on aggregates extracted from RAP from both milling and full depth recovery. The results of this study show that, the aggregate clearly degraded by further refinement of aggregate size but still have resistance to wear and abrasion. Also, this research concluded that the milling process and scraping caused degradation of aggregate which made the RAP finer than a virgin aggregate. Finally, it was also concluded that the milling process caused degradation of aggregate more than the full depth recovery.

1.8.7 Cleanliness

The percentage of fine clay particles contained in the fine aggregate compared with the amount of sand in the aggregate is determined in accordance with the sand equivalent test (ASTM D2419 – (ASTM, 2002)). The percentage is an indication of how clean the fine aggregate is and how well the binder can coat the fine aggregate. Since the fine aggregate is already used in HMA and is already coated with asphalt, then this test is not required for the RAP aggregate. Also, because of extraction process, fine may be washed away during solvent extraction or additional fines can be created by aggregate degradation during extraction. This test is probably not meaningful for extracted aggregate (McDaniel et Michael Anderson, 2001). The adhesion between the asphalt binder and aggregate can be prevented by the presence of dust and clay coating on the coarse and/or fine aggregate, which results in stripping of HMA mixture. In some cases where there may be a presence of water, some very fine clayey material may cause stripping by weakling the asphalt binder (Kandhal et F. Parker, 1998).

1.9 Binder test and aging

The performance of the mixture containing RAP is known to be dependent on the change in the properties of binder and RAP due to aging. The aging is reflected in the change in the rheological properties of asphalt.

The following factors are reported to contribute to age hardening of asphalt during mixing and/or during the service life (Robert *et al.*, 1996):

- Oxidation through diffusive reaction of oxygen in the air with asphalt binder;
- Volatilization through evaporation of the lighter components from asphalt binder. It usually does not contribute to long-term aging in the pavement and is primarily a function of temperature;
- Polymerization through chemical reaction of molecular component;
- Thixotropy due to the formation of a structure within the asphalt binder over a period of time;
- Syneresis due to the exudation of lighter constituents of the binder; and
- Separation through the removal of oil constituents and resins by absorptive aggregates.

The rheological behaviour of aged binder will differ from virgin materials as asphalt binder reacts and loses some of its components during the aging process which effects on the PG grade. Thus, designing a mix with RAP should be done with care. If the old binder is too stiff, the blending of old and virgin binders can't function as envisaged. With small percentages (up to 20%), an aged binder does not influence the properties of the blend of virgin and RAP binder significantly (Kennedy, Tam et Solaimanian, 1998).

It was found that as the amount of RAP binder increases, the stiffness of the mix increases (Souparth, 1998). Lee, Terrell and Mahoney (1983) conducted a study on the evaluation of the mechanical and rheological properties of asphalt binders containing binders from RAP. In their study, two virgin binders (PG 58-28 and PG 64-22) were blended with 0, 10, 20, 30, 40,

50, 75, and 100% reclaimed asphalt binders obtained from two different stockpiles. RAP and virgin binders were tested using dynamic shear rheometer (DSR) according to AASHTO TP5-98 (AASHTO, 1998). It was observed that the RAP binder is stiffer than the virgin binder for about 10 times more. Also, it was found in the same study that the RAP binder obtained from one asphalt plant RAP stockpile were 10 times stiffer than those for a RAP binder obtained from a different RAP stockpile located in the same region. Moreover, there was variability in stiffness of a RAP binder from the same source but with different magnitude.

1.10 Aging methods of HMA

Different methods are used to simulate long term aging of HMA specimens. One method was observed by conducting an aging process known as 'SHRP long term oven aging' (Wu, 2006). This process involves placing specimens in a force draft oven for 120 hours at 85°C. Experience has shown that this is a good simulation of 15 years of field aging in a wet, no-freeze climate. The aging of the asphalt specimens was expressed by means of an aging index, equation (1.3).

$$\text{Aging index} = P_{aged}/P_{unaged} \tag{1.3}$$

Where:

P_{aged} The stiffness value measured on an aged asphalt specimen; and

P_{unaged} The value on an unaged asphalt specimen.

Another method is a test developed by Carter and Stoup-Gardiner (2007) to also measure the effect of aging on the complete HMA mix, some samples are compacted using a gyratory compactor at 100 gyrations, and then stored at 22ºC in a dark storage room for 1 year. The samples are then removed from storage and these aged samples are tested to study the effect of aging. There is also other method they used by placing samples on a flat pan, stored in a

55°C oven for three months. Then it can be tested to take into consideration the effect of hardening associated to aging.

Walubita *et al.* (2006) investigated the effects of aging on HMA mixture fatigue properties and N_f by using the three conditions of laboratory aging exposure (0, 3, and 6 months) at 60ºC that simulate up to 12 years of HMA in the field at critical pavement service temperature. In this aging process, the compacted HMA specimens are placed in a temperature-controlled room at 60ºC and air circulates freely around the specimens. It is important to note that all the loose HMA mixtures are subjected to the standard AASHTO PP2 4 hrs short-oven aging process at 135ºC prior to 60ºC aging of the compacted HMA specimens (AASHTO, 1994).

1.11 Production of hot mix asphalt

The majority of HMA with or without RAP are produced by one of the two big families of hot mix asphalt plants which dominate the market nowadays (Olard *et al.*, 2008):

- Dryer drum mixers working on the continuous principle; and
- Batch plants working on the discontinuous cycle principle.

Each type includes some variants. Almost all can recycle if equipped or designed specifically to do so. RAP adding conditions differ according to the type of plant.

1.11.1 Recycling at drum mix plants with parallel-flow or counter-flow drying (cold addition)

In this setup, all virgin aggregates are added at the high side of the drum and are superheated when they pass close to the flame (Robert *et al.*, 1996). The cold recycled materials are added to the drum close the midpoint by a recycling ring, which is generally present at these drum mix plants, followed by the new asphalt (Olard *et al.*, 2008). Figure 1.9 and Figure 1.10

illustrate configurations of plants often encountered in most countries. Drum plants are sometimes equipped with a separate pugmill mixer.

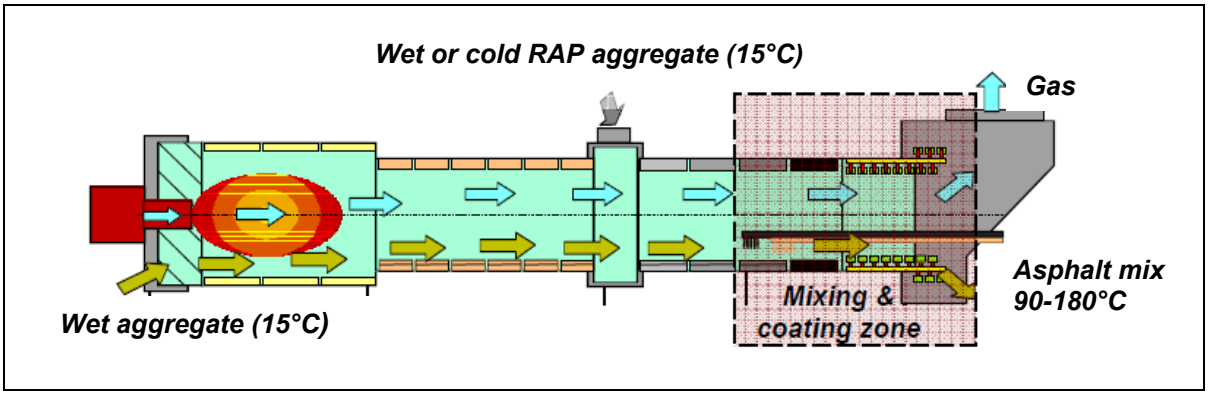

Figure 1.9 Recycling technique at drum plants with parallel-flow drying
Taken from Olard *et al.* (2008)

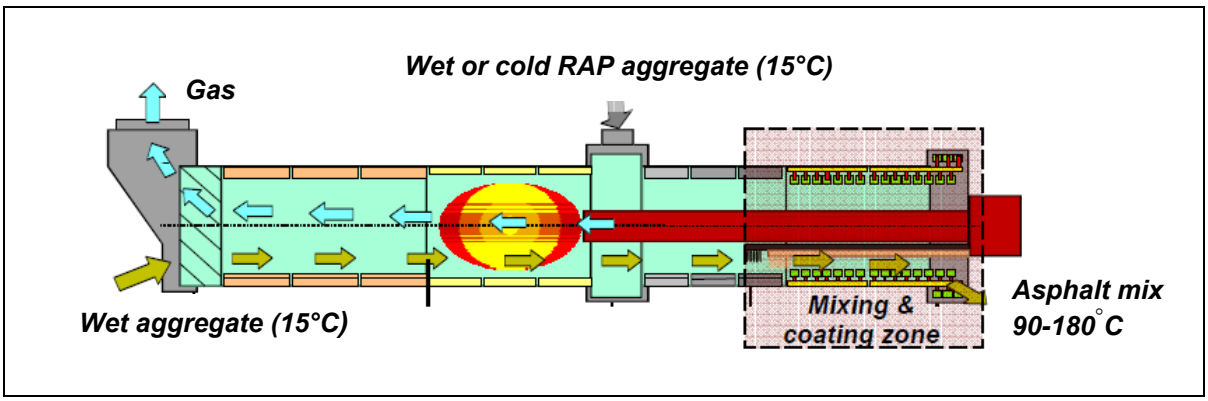

Figure 1.10 Recycling technique at drum mix plants with counter-flow drying
Taken from Olard *et al.* (2008)

Since 2004, APPIA Grands Travaux (subsidiary of EIFFAGE Travaux Publics) has developed its own parallel drum batch mix plant working on a continuous principle, by heating reclaimed materials (RAP at 110-150°C) separately from the virgin aggregates (150-190°C) before being combined into a continuous mixer where the new heated bitumen is introduced. This new type of plants is well suited for high rates of recycling, up to 100%. This plant is illustrated in Figure 1.11.

Figure 1.11 Example of the mobile parallel drum plant of AAPPIA Grands Travaux a) overall view & b) closer view of the two parallel drum dryers (the first one for virgin aggregates, the second one for recycled aggregate) Taken from Olard *et al.* (2008)

1.11.2 Recycling at a batch plant

For batch plants, an hopper is added to store the RAP into the weigh bin, and additional controls in the plant control room are needed to control the quantity of RAP added to each batch (Etonray, 1983). In these plants, the aggregate is superheated as high as 260-315 °C in the dryer and diverted from the bucket elevator directly to a pug mill mixer. The cold, wet RAP is fed directly into the pug mill where the liquid asphalt is injected and where the three components are mixed. The synopsis of asphalt manufacture with RAP at a batch plant appears in Figure 1.12.

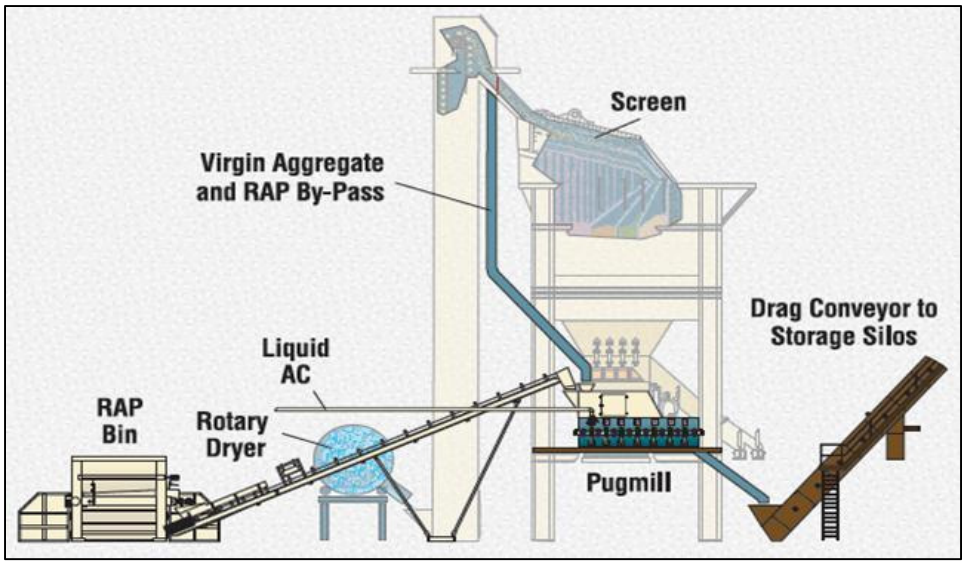

Figure 1.12 Recycling at a batch plant
Taken from Brock and Richmond (2007)

1.11.3 Special plants

Special plants have been developed in USA in order to increase the amount of RAP, it recycles with the help of the process called CYCLEAN by using microwave technology (limit gaseous emissions - blue smoke) combined with high velocity warm air in a fluidized bed (Howard et Reed, 1989). Microwave generates heat by producing high vibration in the molecules of the aggregates which create intermolecular friction to heat the aggregate (Shoenberger, Rollings et Graham, 1995). Because of differences in molecular structure, the microwave energy does not directly heat the asphalt content in a very appreciable way, but the asphalt is heated quickly by heat transfer from the aggregate to the necessary recycling temperature of about 150°C (300°F) without being burned (Jeppson, 1986). Then, a recycling agent is added to restore the asphalt to its original state. Finally, the rejuvenator, the asphalt, and the aggregates are re-mixed, and the result blend is a hot mixture (Howard et Reed, 1989). Schematic of the CYCLEANE process is shown in Figure 1.13.

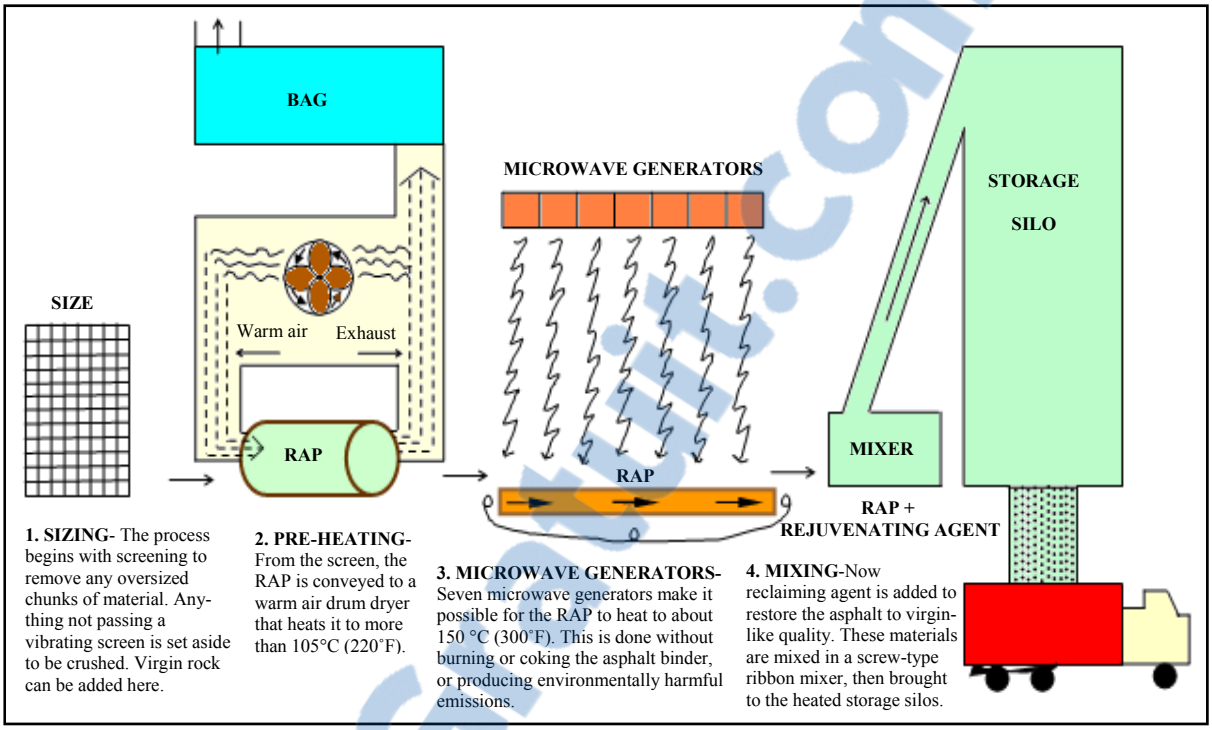

Figure 1.13 Schematic of the CYCLEAN process
Taken from Howard and Reed (1989)

CHAPTER 2

MECHANICAL PROPERTIES OF ASPHALT MIXTURES: BEHAVIOUR AT SMALL DEFORMATION

2.1 Introduction

Under the effect of external solicitation, roadway structures are subjected to complex phenomena. Mechanical, thermal, physical and chemical phenomena often appear in a coupled manner. In this chapter, the external solicitations to which pavement structure are subjected to will be presented first. From the analysis of these solicitations, different aspects of the thermo-mechanical behaviour of asphalt mixtures are considered. The description of these different types of bituminous materials behaviour is presented in the following paragraphs. As part of this thesis, we focus on two principal types of behaviour: linear viscoelastic (LVE) and fatigue cracking which are detailed in sections 2.5 to 2.7. Finally, this chapter provides a literature review on the performance of asphalt mixtures using RAP regarding two main properties:

- The effect of the addition of RAP on the mixture modulus; and
- The fatigue resistance of mixes containing RAP.

2.2 Solicitation on bituminous roadways

The main external solicitations imposed on the asphalt mixtures are related to mechanical stresses imposed by the vehicles (traffic effect) and imposed by the environment, mainly because of the temperature changes (thermal effects).

2.2.1 Traffic effect

The traffic creates a loading on the surface of the pavement in the form of repeated, cyclic surface loadings (Olard et Di Benedetto, 2005). The strain amplitudes of cyclic loadings are

low, producing deformation usually below 10^{-4}m/m. The calculation of the stresses and the strains in the flexible pavement is made by considering an isotropic linear elastic multi-layer model which gives a good approximation of the real behaviour (Figure 2.1) (Olard et Di Benedetto, 2005).

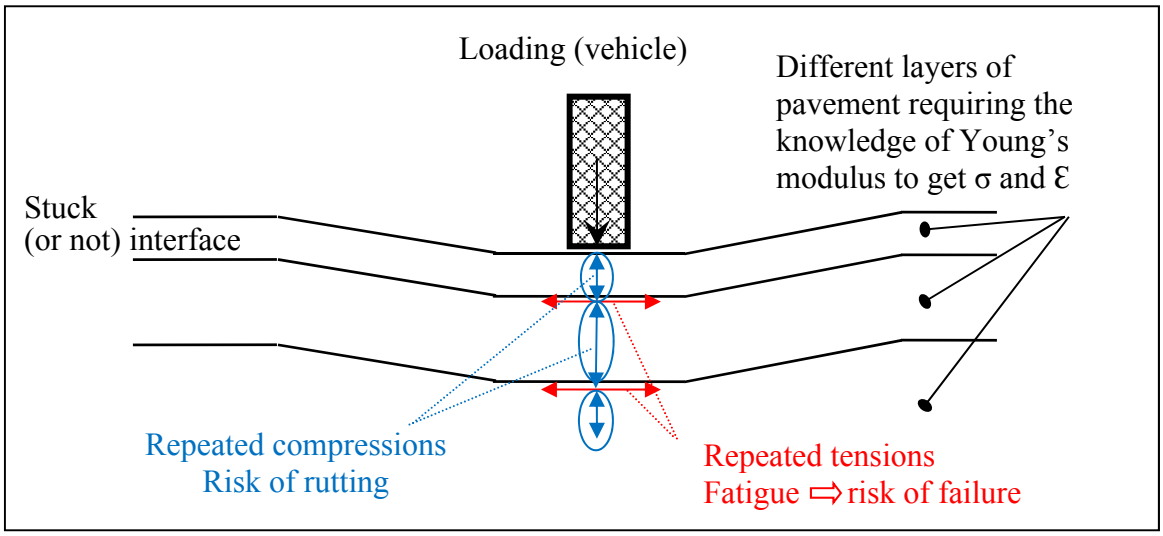

Figure 2.1 Schematic of the traffic induced solicitations
Taken form Olard and Di Benedetto (2005)

Under cyclic solicitations, the base of the structural layers undergoes a repeated tension which can create micro degradations and cause the ruin of the layers by bottom up fatigue cracking. This phenomenon of fatigue causes cracks in the pavement. At the same time, the upper part of each layer is subjected to the repeated vertical compressive forces which can cause permanent deformations inducing rutting on the surface of the pavement (Nguyen, 2009).

2.2.2 Temperature effect

In addition to the mechanical loadings, the pavement undergoes consecutive loadings from temperature variations. These thermal variations lead to changes of the stiffness of the mixtures: at low temperature, the bituminous mixture is rigid and brittle while at high

temperature, the rigidity of the mixture decreases and the mixture become softer (Olard et Di Benedetto, 2005).

On the other hand, the change of temperatures can cause stresses and deformations within material due to thermal dilatations and contractions during temperature changes (Figure 2.2). This phenomena is particularly important because when low temperature are applied, cracks may appear and propagate with thermal cycling (daily or otherwise) or it can cause degradations at the interfaces between layers (Di Benedetto et Corté, 2004).

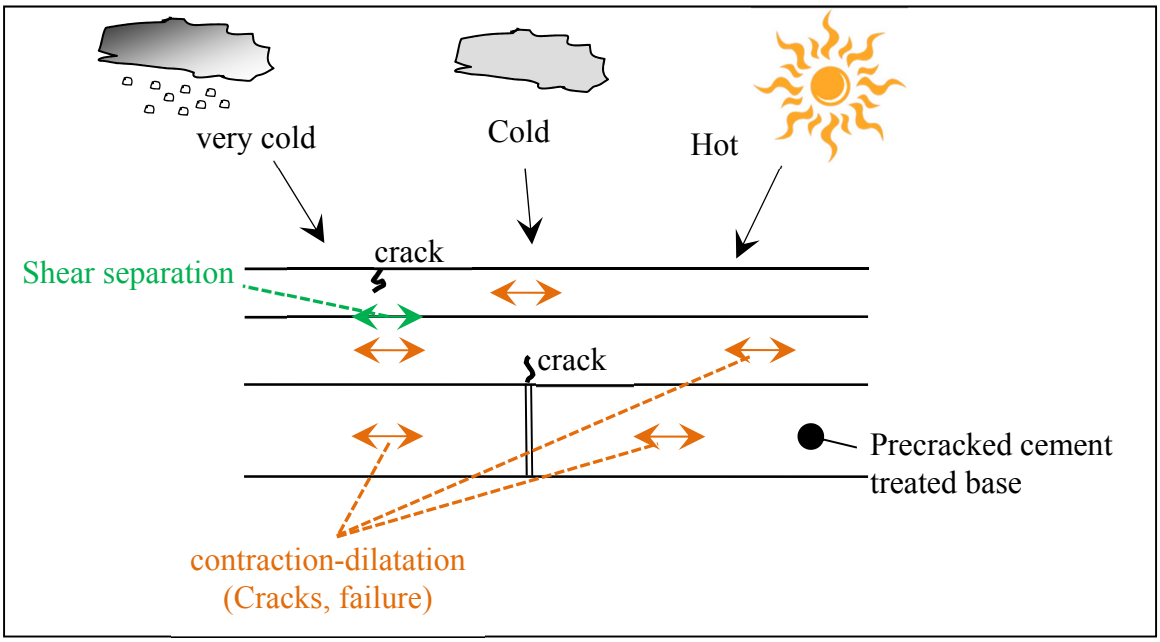

Figure 2.2 Schematic of the temperature induced solicitations
Taken from Olard and Di Benedetto (2005)

2.3 Bituminous materials behaviour classification

Asphalt mixtures have complex behaviour. However, it is possible to identify different kinds of bituminous mixtures behaviour by considering the amplitude of the strain ($|\varepsilon|$) and the number of loading cycles (N) as shown in Figure 2.3 (Di Benedetto et Corté, 2004).

- For load consisting of few hundred cycles and small amplitude of strains (<10^{-4} m/m), behaviour is seen, in first approximation, as linear viscoelastic (LVE);
- For a small number of loading cycles and deformations of a few percent, behaviour is highly non-linear;
- For several thousand loading cycles at small strain, fatigue phenomena occurs;
- When non-linear cycles load are applied from a zero stress, significant irreversible deformations occur for amplitude of deformation near the failure limit. Their accumulations create rutting which is the fourth type of behaviour.

Figure 2.3 highlights the different behaviour of bituminous mixes as a function of the strain amplitude and the number of cyclic loads (Olard et Di Benedetto, 2005) as explained before. The boundaries shown for the different behaviours are orders of magnitude which may vary significantly depending on the material, temperature and the direction of loading path (compression, shear, etc.).

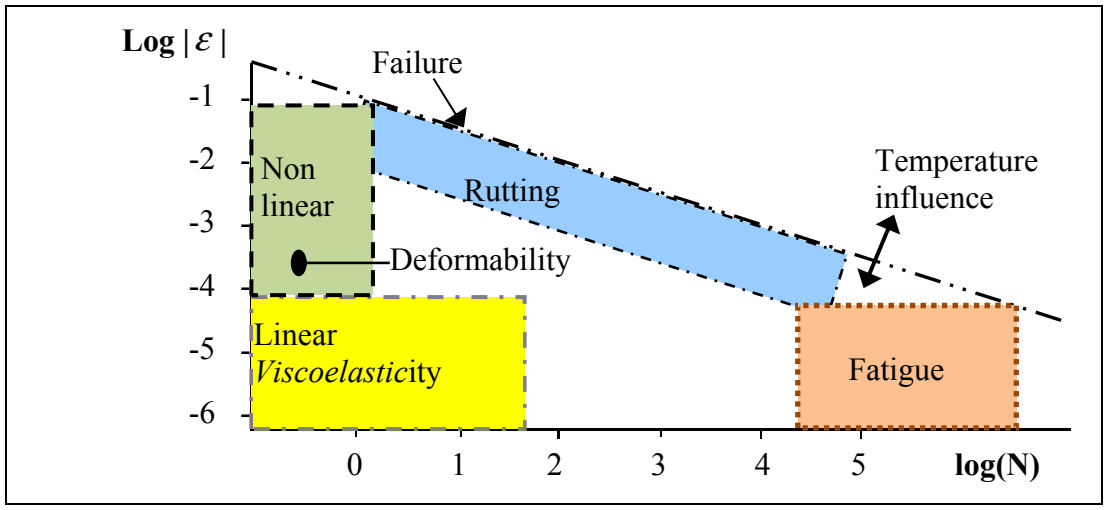

Figure 2.3 Typical bituminous mix behaviour domain, (|Ɛ| strain amplitude – N number of cycles)
Taken from Olard and Di Benedetto (2005)

2.4 Application to the pavement structure design

According to Di Benedetto and Corté (2005), in pavement design, it is advisable to take into account and to characterize four thermomechanical properties:

- The dependence of the stiffness modulus to the temperature and the mode of loading. At small deformation, it's described by the linear viscoelasticity (discussed in section 2.5);
- The characterisation of fatigue that describes the degradation of material when it is subjected to a great number of "small" strain amplitudes (presented in the section 2.7);
- Resistance to rutting which are permanent deformations accumulated with the number of loadings;
- Resistance to the propagation of the cracks especially at low temperatures.

In this thesis, only the linear viscoelastic behaviour and the fatigue characterisation will be presented.

2.5 Linear viscoelastic behaviour

'An elastic material is a material that, when unloaded, returns to its initial geometry with the unloading curve corresponding exactly with the loading curve in the stress-strain space. It means that the forces acting under the process are instantaneous, conservative, and, consequently, no dissipation of energy occurs' (Lundstrom, 2002). The mechanical behaviour of a linear elastic material can be described by Hook's law as follow (Pellinen, 2001):

$$\varepsilon = \sigma/\mathrm{E} \tag{2.1}$$

Where:

ε is the strain, σ is the stress and E is the modulus of elasticity.

In a similar manner, the mechanical behaviour of viscous material is usually described by Newton's law. Newton's law says that the applied shear stress (τ) is directly proportional to the strain rate ($\dot{\gamma}$) and the constant of proportionality (η) is called the viscosity (Lundstrom, 2002):

$$\tau = \eta \frac{d\gamma}{dt} = \eta\dot{\gamma} \tag{2.2}$$

Analogous to Hooke's law at low rates of strain, a linear relationship is obtained, but at higher strain rates deviations are predicted to occur. In purely Newtonian viscous fluids, strain increases continuously and linearly with time as energy is dissipated in flow, giving permanent deformation. If the viscosity does not depend on strain rate, the behaviour is called Newtonian (Lundstrom, 2002; Young, 1998).

However, many materials exhibit behaviour neither purely elastic nor purely viscous, but behaviour in between. This so-called viscoelastic behaviour means that the current stress is a function of the current strain and strain rate and/or past values of strain and strain rate, that is: (Lundstrom, 2002).

$$\sigma = \sigma\{\varepsilon\} \tag{2.3}$$

The assumption of linear viscoelastic behaviour of asphalt mixtures assumed that the response of a material to a solicitation composed of some of elementary solicitations is the sum of the responses of a material to each elementary solicitation. Then, we can say that the behaviour of material obeys the Boltzmann superposition principle. There are several ways for measuring the stiffness of asphalt mixtures. The most common methods are in time mode that applies a quasi-static loading and in frequency mode that applies a cyclic loading (Baaj, 2002).

2.6 Measurement of the modulus of asphalt mixtures in the frequency domain: complex modulus

2.6.1 Definition and measurement's principle

This type of test consists in subjecting the material to tension-compression cyclic loading, usually sinusoidal at various frequencies and temperatures. These measurements are made at small deformations and low number of solicitations at which the bituminous mix behaves mainly like a linear viscoelastic material (see Figure 2.3). Complex modulus tests can be performed in stress or strain control modes which are defined by:

$$\sigma(t) = \sigma_0 \sin(\omega t) \; or \; \varepsilon(t) = \varepsilon_0 \sin(\omega t) \tag{2.4}$$

Where:

$\sigma(t)$	The amplitude of sinusoidal stress;
σ_0	Peak (maximum) stress;
$\varepsilon(t)$	The amplitude of sinusoidal strain;
ε_0	Peak (maximum) strain;
ϕ	Phase angle, degrees;
ω	Angular velocity; and
t	Time, seconds.

The response to those solicitations will be also sinusoidal with the same angular frequency (Baaj, 2002). In a steady state, we obtain:

$$\sigma(t) = \sigma_0 \sin(\omega t) \; or \; \varepsilon(t) = \varepsilon_0 \sin(\omega t - \phi) \tag{2.5}$$

Due to the viscoelastic character of the materials, in the case of a solicitation at constant temperature, the strain lags behind the stress resulting in a phase angle, ϕ, between the two signals (Figure 2.4) (Di Benedetto et al., 2001).

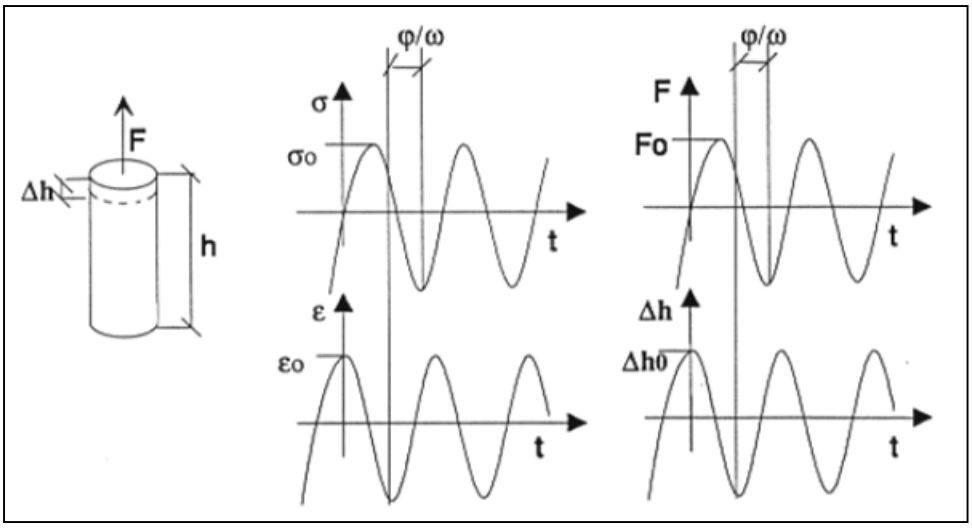

Figure 2.4 Sinusoidal load (F) and displacement (Δh) applied and resulting sinusoidal stress (σ) and strain (ε) response at a given point of the sample
Taken from Baaj (2002)

Therefore, to evaluate the complex modulus, the amplitude of the sinusoidal stress $\sigma(t) = \sigma_0 \sin(\omega t)$ at any given time, t, as well as the angular load frequency, ω=2π× frequency, and the amplitude of the sinusoidal strain $\varepsilon(t) = \varepsilon_0 \sin(\omega t - \phi)$, at the same frequency is needed and the phase shift is also needed.

Assuming that:

$$\sigma^*(t) = \sigma_0 e^{i\omega t} \tag{2.6}$$

$$\varepsilon^*(t) = \varepsilon_0 e^{i(\omega t - \phi)} \tag{2.7}$$

We can write that:

$$\sigma(t) = \mathrm{Im}[\sigma^*(t)] and\ \varepsilon(t) = \mathrm{Im}[\varepsilon^*(t)] \tag{2.8}$$

And by using Euler Identify:

$$\sigma^*(t) = \sigma_0 e^{i\omega t} = \sigma_0(\cos \omega t + i \sin \omega t) \quad (2.9)$$

Also,

$$\varepsilon^*(t) = \varepsilon_0 e^{i(\omega t - \phi)} = \varepsilon_0(\cos(\omega t - \phi) + i \sin(\omega t - \phi)) \quad (2.10)$$

By definition, the complex modulus, E^*, is the ratio between the complex amplitude of the sinusoidal stress of angular frequency ω applied to the material and the complex amplitude of sinusoidal strain (Di Benedetto et al, 2001). We can write:

$$E^*(t) = \frac{\sigma^*(t)}{\varepsilon^*(t)} \quad (2.11)$$

And

$$E^*(\omega) = \frac{\sigma_0 e^{i\omega t}}{\varepsilon_0 e^{i(\omega t - \phi)}} \quad (2.12)$$

Where:

$$E^*(\omega) = |E^*| e^{i\phi} \quad (2.13)$$

Where $|E^*|$ is the norm of the complex modulus and ϕ is the phase angle of the material.

Mathematically, the norm of the complex ("dynamic" modulus) is defined as the absolute value of the complex modulus, i.e. $|E^*| = \frac{\sigma_0}{\varepsilon_0}$ (Sebaaly, 2007).

The term "complex" modulus $|E^*|$ is based on the fact that E^* is a complex number consisting of both real and imaginary components (see Figure 2.5).

$$\mathrm{E}^* = E_1 + iE_2 \tag{2.14}$$

Figure 2.5Where:

E^*	Complex modulus;
E_1	Storage modulus $= \lvert E^* \rvert \cos\phi$;
E_2	Loss modulus $= \lvert E^* \rvert \sin\phi$; and
i	Imaginary part ($i^2 = (-1)$).

The "dynamic" modulus E^*, as defined in the United State, represents the magnitude of E^*, noted $|E^*|$:

$$|E^*| = (E_1^2 + E_2^2)^{\frac{1}{2}} \tag{2.15}$$

It is important to note that the real component, the storage modulus, and the elastic part are all the same thing. Similarly, imaginary component, loss modulus, and viscous part are also equivalent.

The complex bulk modulus $\mathrm{K}^*(\omega)$ and the shear modulus $\mathrm{G}^*(\omega)$ can also be defined in a similar manner. By supposing a linear viscoelastic and isotropic behaviour, the relations between these rheological parameters are the following (Di Benedetto et al., 2001):

$$\mathrm{K}^* = \frac{E^*}{3(1-2\nu^*)} \tag{2.16}$$

$$\mathrm{G}^* = \frac{E^*}{2(1+\nu^*)} \tag{2.17}$$

Where:

ν^*	The Poisson's ratio.

ν^* is defined as the ratio of transverse contraction strain to longitudinal extension strain in the direction of stretching force. In the two previous relations given above, ν^* is a priori, a complex number. However, direct measurements of ν^* based on strain measurements in tension-compression during a complex modulus tests, with or without a confinement pressure, tend to show that its imaginary part is very small. Hence, for tested bituminous materials, it can be treated as real; its value varies between 0,2 and 0,5 according to temperature and frequency (Di Benedetto et al., 2001).

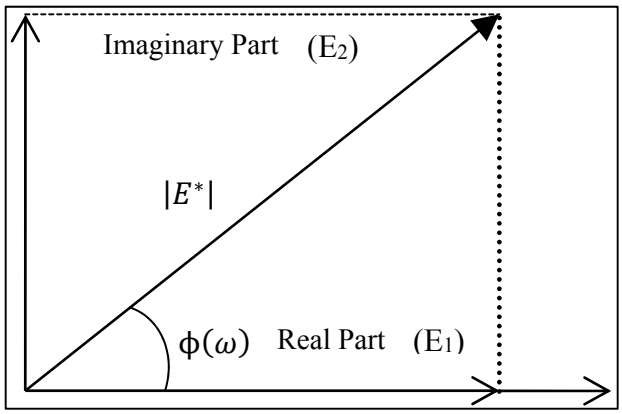

Figure 2.5 The vector representation of the real part and
the imaginary part of the complex modulus
Taken from Pellinen (2001)

2.6.2 Complex modulus tests

For complex modulus tests, the standard specimens are subjected to repeated solicitation under sinusoidal loading centered at zero. As stated before, the complex modulus is measured at various frequencies and temperatures. These two parameters are set for each elementary measure. The tested frequencies and temperatures usually depend on capabilities of test equipment and tested materials, and vary between 0,01 and 40 Hz for the frequency, and between -30°C and 60°C for the temperature. Tests are usually performed at strain level of 50×10^{-6} m/m based on experience and to make sure it is well below the 10^{-4}m/m limit to avoid fatigue damage.

There are different tests to characterize bituminous mixtures or geo-materials. They can be classified into two main categories: homogeneous and non-homogenous tests (Di Benedetto et al., 2001).

Homogenous tests provide direct access to the stresses and strains, and therefore to the behaviour law. For non-homogenous tests, a constitutive law should be postulate first (linear viscoelastic as an example). Then, the geometry of the specimen needs to be taken into account for the calculations of the parameters of the constitutive law, which is often complicated, (complex modulus for example). In this study, the complex modulus is observed in homogenous tension-compression tests.

2.6.2.1 Tension-compression test on cylindrical sample

This homogenous test was developed at laboratory DGCB of the ENTPE (Baaj, 2002). The cylindrical specimen is subjected to axial alternating stresses of tension and compression centered at zero. It can be carried out in stress or strain controlled conditions. Figure 2.6 presents this test setup, which was used in this research.

Figure 2.6 Uniaxial tension-compression
complex modulus test setup

2.6.3 Alternative methods of analyzing complex modulus test results

As per Di Benedetto and De la Roche (1998), complex modulus test results can be presented using several classical representations: isothermal curves, isochronal curves, Cole-Cole plane (complex plane) and Black space.

The different components of the complex modulus differ with temperature and frequency of loading, which are fixed for each elementary test. The following sections show examples of the complex modulus test results $(|E^*|)$,(ϕ), (E_1), (E_2) presented in the above mentioned ways. These results were taken from Di Benedetto and De la Roche (1998).

2.6.3.1 Isothermal and isochronal curves

Isothermal curves are obtained by plotting the dynamic complex modulus according to the frequency for each test temperature T in log-log coordinates. Figure 2.7 shows an example of this representation.

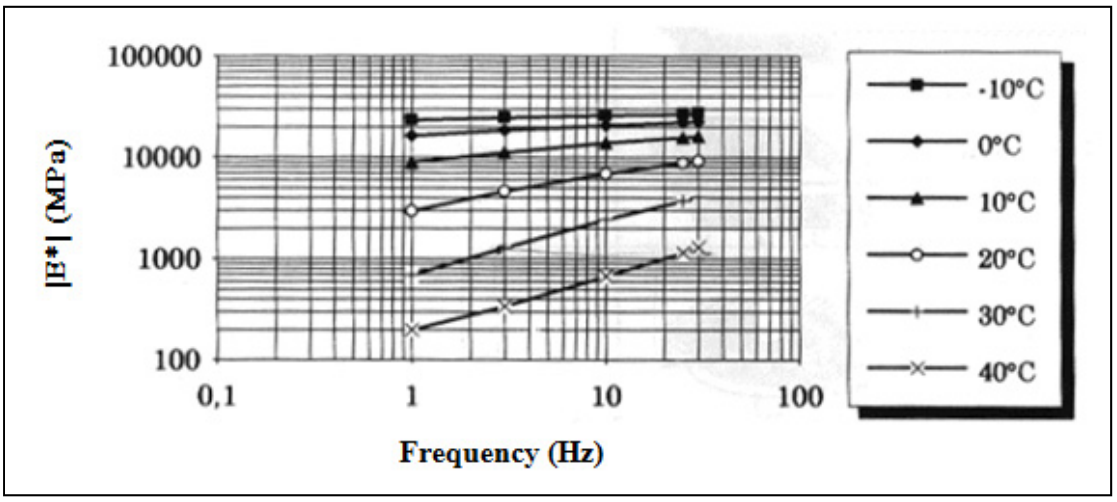

Figure 2.7 Example of isothermal curves of the complex modulus
Taken from Di Benedetto and De la Roche (1998)

Isochronal curves are the same type of presentation as the isothermal curves by inverting the frequency and temperature parameters but expressed in a semi-logarithmic coordinates. Figure 2.8 shows an example of isochronal curves. Isothermal and isochronal curves indicate if there are obvious errors in the measured experimental modulus values. Since each set of data measurements come from testing at one specific temperature for various frequencies, the results should form one smooth curve. If this curve is not a smooth, it means there are errors.

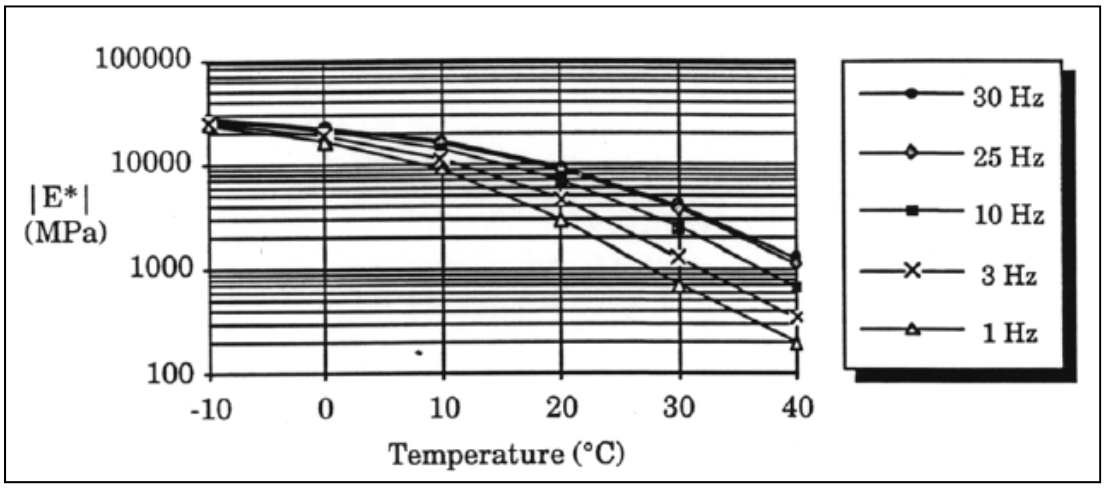

Figure 2.8 Example of isochronal curves of the complex modulus
Taken from Di Benedetto and De la Roche (1998)

2.6.3.2 Cole - Cole plane (complex plane)

Figure 2.9 presents the complex modulus test results in Cole-Cole plane or in the complex plane. The storage modulus (E_1) is plotted on the real axis (x-axis), and the loss modulus (E_2) is plotted on the imaginary axis (y-axis). Therefore, the plotted modulus value ($|E^*|$) should form a single curve, which is independent of temperature or frequency (Pellinen, 2001). The property of the time temperature equivalence appears directly in this plane. This property will be described in paragraph 2.6.3.4.

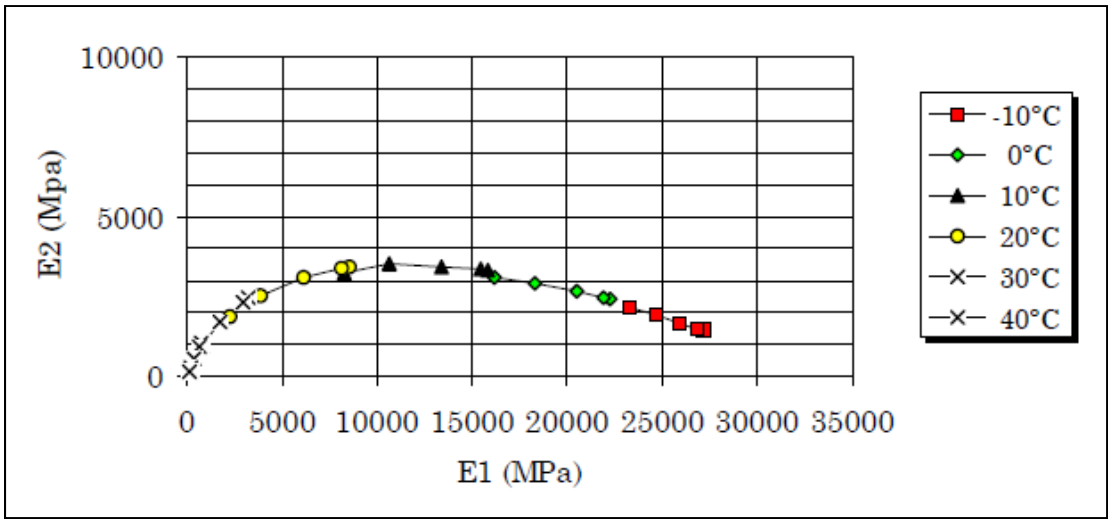

Figure 2.9 Example of the complex modulus curve in the Cole-Cole plane
Taken from Di Benedetto and De la Roche (1998)

In Cole-Cole Plane, the curve is a characteristic of the studied material. Huet (1963) has shown that this representation gives a single curve shaped like a circular arc. It can be used to calibrate a model of rheological behaviour. This representation allows assessment of the quality of the test data at intermediate and low temperatures. However, it is not very accurate for the modulus at low values at high temperatures (Pellinen, 2001). The representation in the black space (|E*| versus ϕ) allows to better compare experimental values and values obtained from the model for low modulus values at high temperatures.

In Cole-Cole Plane, the curve is a characteristic of the studied material. Huet (1963) has shown that this representation gives a single curve shaped like a circular arc. It can be used to calibrate a model of rheological behaviour. However, it is not very accurate for the modulus at low values. The representation in the Black space (|E*| versus ϕ) allows to better compare experimental values and values obtained from the model for low modulus values.

2.6.3.3 Black space

In the Black space, the dynamic modulus is usually plotted on a logarithmic scale as a function of the phase angle (x axis, arithmetic scale) as shown in Figure 2.10.

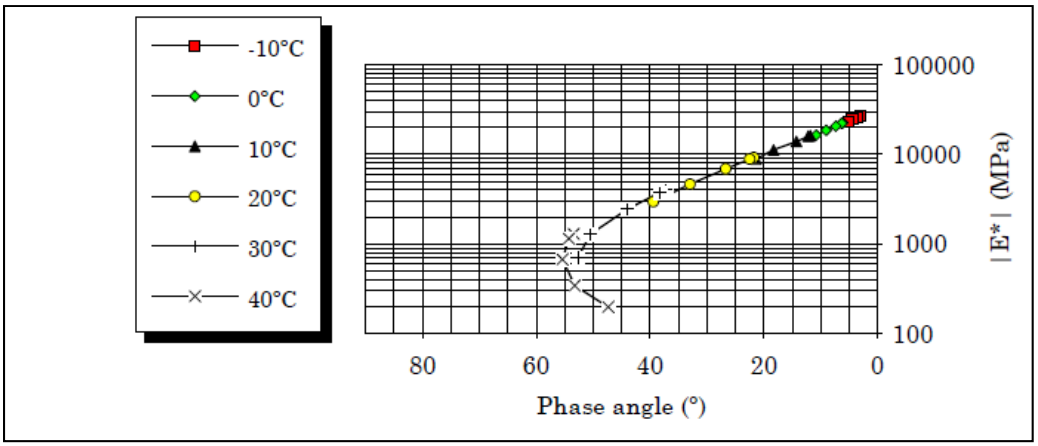

Figure 2.10 Example of the complex modulus curve in the Black plane
Taken from Di Benedetto and De la Roche (1998)

The obtained curve is different for every tested material. As in the Cole-Cole plane representation, when the material obeys the principle of time-temperature equivalence, as it will be shown later, all the experimental points fall into a single curve.

This curve allows visualizing the zone of the modulus with small values and in particular the decrease of phase angle for the high temperatures. This phenomenon of elastic return is related to the presence of the aggregates in the mixture. Indeed, the aggregates have an elastic behaviour (Baaj, 2002).

One should bear in mind that some mixes do not conform to the Time-temperature superposition principle (TTSP) as their Black curves are not unique as we shall see hereafter. This property is called 'Partial Time-Temperature Superposition Principle' (PTTSP) as the shifting procedure gives a unique and continuous master curve only for the norm of the modulus (|E*|) (Olard et Di Benedetto, 2003).

In the example shown on Figure 2.11, it can be seen that most mixes do follow the TTSP. But the PMB2 and PMB3 mixes do not conform the TTSP, since all points are not on a single line that means that their black curves are not unique.

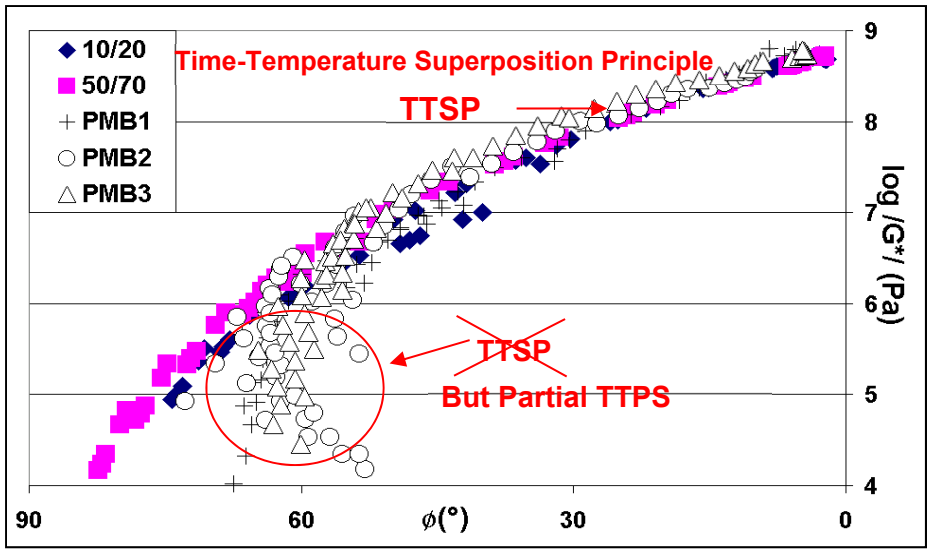

Figure 2.11 Example of materials referring to TTSP or not from the complex modulus Black plane curve
Taken from Olard and Di Benedetto (2003)

2.6.3.4 Time temperature superposing principles and shift factor

It is necessary to consider both the temperature and time (or frequency) dependence of the material to describe linear viscoelastic behaviour. It is noticed, with the examination of the isothermal curves, that the same modulus value for a material can be obtained from various (frequency, temperature) couples. This property is called Time-Temperature Superposition Principle (TTSP) or time temperature equivalence (Di Benedetto et De la Roche, 1998). It is used to describe viscoelastic materials (Pellinen, 2001). With this principle, E*(ω, T) can be transformed into E*(ω. fr(T)).

It is possible by using this property, to construct a single curve (log|E*|, log fr) for an arbitrarily chosen reference temperature (T_o). This curve is obtained by translating, parallel to the frequency axis, each isotherm, with respect to the isotherm corresponding to the reference temperature, until superposition of points having the same modulus value is achieved. The obtained curve is called 'master curve'. Figure 2.12 presents an example of master curve at 10°C obtained for a bituminous mixture (Di Benedetto et De la Roche, 1998).

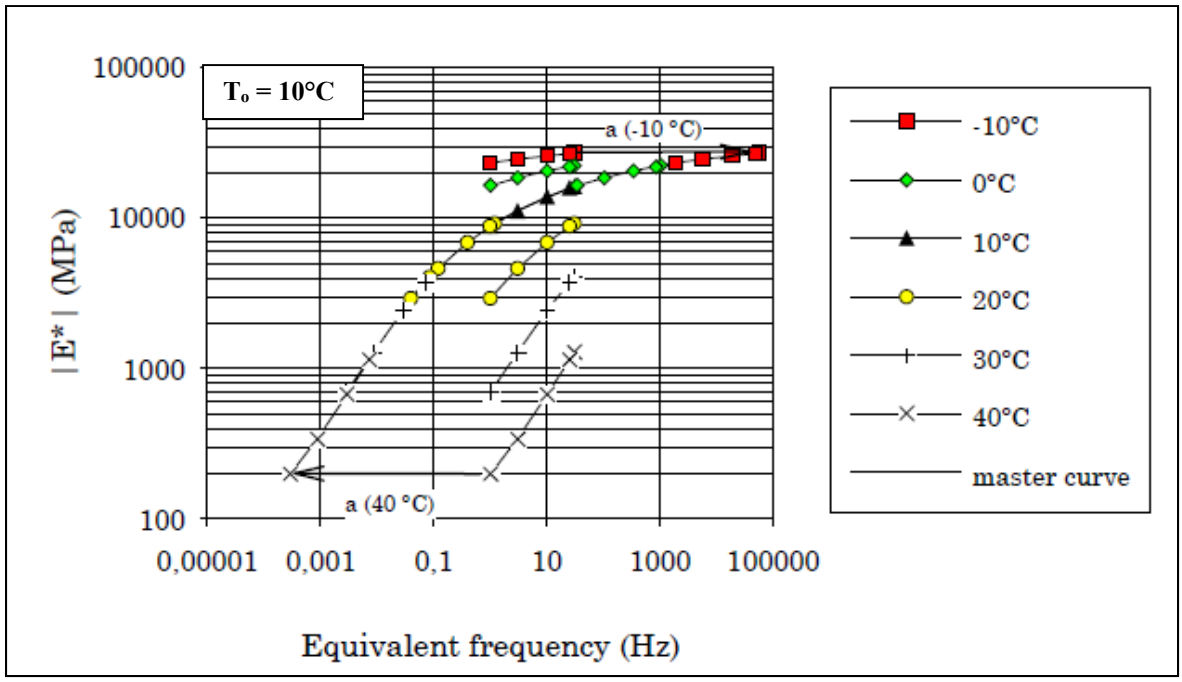

Figure 2.12 Example of master curve at 10°C
Taken from Di Benedetto and De la Roche (1998)

A master curve allows the comparison of asphalt mixes that were tested at different frequencies and different temperatures (Pellinen, 2001). Also, it allows the calculation of modulus values for frequencies inaccessible by experimentation.

Several different equations were used to describe the time temperature superposition relationship to obtain shift factors in the viscoelastic materials, a_T , but the most frequently used is the Williams, Landell and Ferry (WLF) equation.

Williams, Landell and Ferry (WLF) equation is (William, Landel et Ferry, 1955):

$$\log a_T = \frac{-C_1(T - T_0)}{C_2 + (T - T_0)} \tag{2.18}$$

Where:

a_T Horizontal shift factor;

C_1 and C_2	Material constants;
T	Temperature of curve to be shifted in ºC; and
T_o	Reference temperature in ºC.

The WLF equation has been found to adjust observed data for a broad range of binders from temperature of -20 to 60 ºC. An analysis of the shift factors for the aged and unaged SHRP asphalts showed that all the primarily constants had the same values: -19 for C_1, and 92 for C_2 (Anderson, Christense et Bahia, 1991).

2.6.4 Mechanical models used in linear viscoelastic

Mechanical models are relating stress to strain or vice-versa based on linear differential equations which allows expression of viscoelastic behaviour (Lundstrom, 2002). Mechanical model consists of combinations of basic elements like elastic springs and viscous dashpots, which obey Hooke's law and Newton's law, respectively. The simplest models are the Maxwell and the Kelvin models that consist of a single spring and a single dashpot, either in series or parallel. From a practical standpoint, these two models cannot describe correctly the complex linear viscoelastic behaviour of bituminous materials (Orald et Di Benedetto, 2003). Therefore, more appropriate models are frequently used to describe real viscoelastic behaviour of bituminous mixtures, like Burger or Huet or Huet-Sayegh or 2S2P1D models. Figure 2.13 shows examples of mechanical models used to characterize bituminous mixtures.

In this study, the 2S2P1D model was used. Therefore, other models will not be further discussed. 2S2P1D model was selected for this study because it was found that it translates correctly the linear viscoelastic behaviour for any bituminous materials: binders, mastic or mix for any range of frequencies and temperatures in the small strain domains (Olard et di Benedetto, 2003; Delaporte et al., 2007).

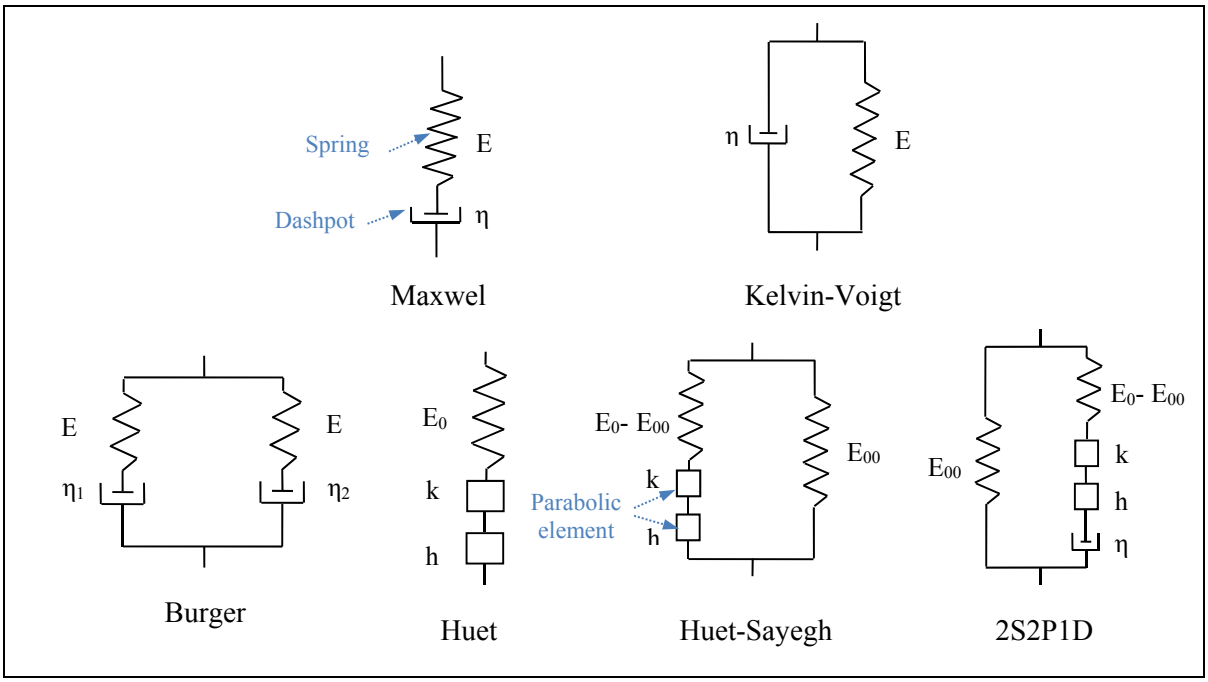

Figure 2.13 Examples of mechanical models used for characterization of bituminous materials

2.6.4.1 Presentation of the 2S2P1D model

The model 2S2P1D is based on a simple combination of these three physical elements (spring, dashpot and parabolic element) (Olard et Di Benedetto, 2003). To obtain the model 2S2P1D, the Huet-Sayegh model has been adapted by adding a linear dashpot in series with the two parabolic elements and the spring of rigidity $E_0 - E_{00}$ as shown in Figure 2.14.

At a given temperature, the introduced 2S2P1D model has 7 constants and its complex modulus is given by the following expression (Olard et Di Benedetto, 2003):

$$E^*(i\omega\tau) = E_{00} + \frac{E_0 - E_{00}}{1 + \delta(i\omega\tau)^{-k} + (i\omega\tau)^{-h} + (i\omega\beta\tau)^{-1}} \quad (2.19)$$

It has to be emphasized that only 7 constants ($\delta, k, h, E_0, E_{00}, \beta$ and τ_0) are needed to entirely determine the linear viscoelastic behaviour of the considered material, at a given temperature.

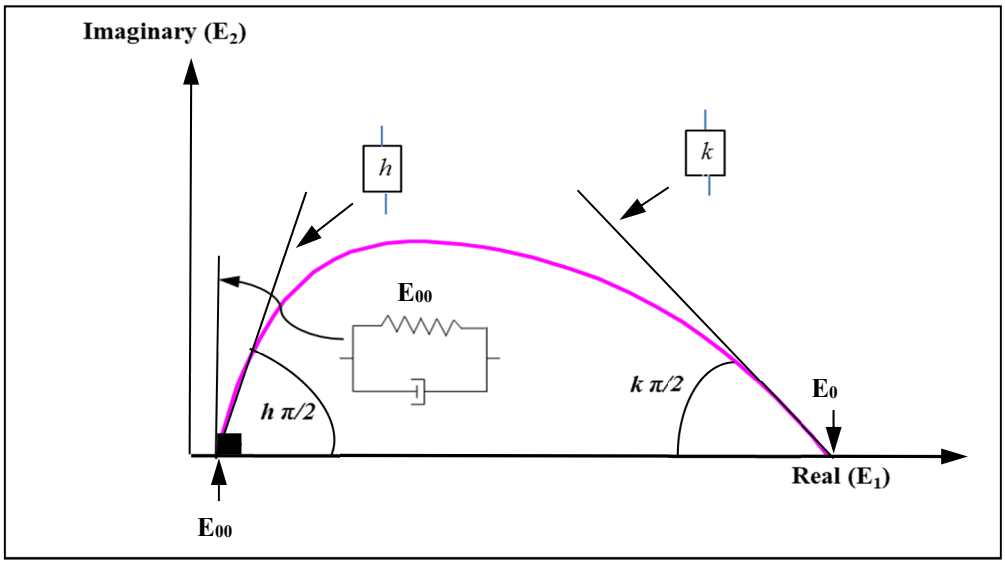

Figure 2.14 Influence of parameters of the 2S2P1D model on the complex modulus represented in the Cole-Cole plan

With:

h, k Exponents such as 0<k <h<1;

E_{00} The static modulus obtained when $\omega\tau \to 0$ (at low frequencies and high temperatures) with ω=2π× frequency;

E_0 The glassy modulus when $\omega\tau \to \infty$ (at high frequencies and low temperatures),

δ Dimensionless constant;

β Dimensionless constant;

τ Characteristic time, which value varies only with temperature; account for the Time-Temperature Superposition Principle (TTSP); and

η Newtonian viscosity, $\eta = (E_0 - E_{00})\beta\tau$, when $\omega \to 0$, the $E^*(i\omega t) \to E_{00} + i\omega(E_0 - E_{00})\beta\tau \times \beta$.

At a given temperature T, the 7 constants $\delta, k, h, E_0, E_{00}, \beta$ and τ_0 of the 2S2P1D model (equation 2.19) can be determined so that the complex modulus calculated by the model is as

close as possible to the experimental data. Then, the effect of temperature is taken into account using the parameter τ. This parameter is the only one which varies according to the temperature.

2.7 Fatigue phenomenon of bituminous mixtures

2.7.1 Introduction

Pavement distresses are different in both type and shape based on their causes and surrounding conditions. The prevailing asphalt pavement distresses types can be classified as cracking, permanent deformation, and disintegration such as raveling and stripping. Cracking is a major cause of distress in asphalt concrete pavement layers. Among these cracking, comes one major type: fatigue cracking, which is traffic related. This major type of distress will be reviewed in this thesis.

2.7.2 Hot mix asphalt fatigue

Fatigue cracking or alligator cracking is a load-related pavement distress that occurs only in areas under the wheel paths of HMA pavement (Robert et al., 1996). Fatigue cracking can be considered as one of the primary asphalt pavement distress which reduces the performance of the asphalt layer (Paris, Pereira et Picado-Santos, 2002). There are predominantly two types of fatigue cracks that occur in flexible pavements that are defined based on the direction of crack propagation: bottom-up cracking and top-down cracking (Figure 2.15). It is difficult to identify where the fatigue cracks initiate without taking cores or excavating test pits to visually observe the direction of crack propagation. Top-down cracking is considered to be more critical, because once the crack occurs it is visible and allows water and air to readily infiltrate deeper into the HMA mixture. Conversely, fatigue cracks that initiate at the bottom of the HMA layer must propagate to the surface before they become visible and allow water infiltration (Witczak et al., 2013).

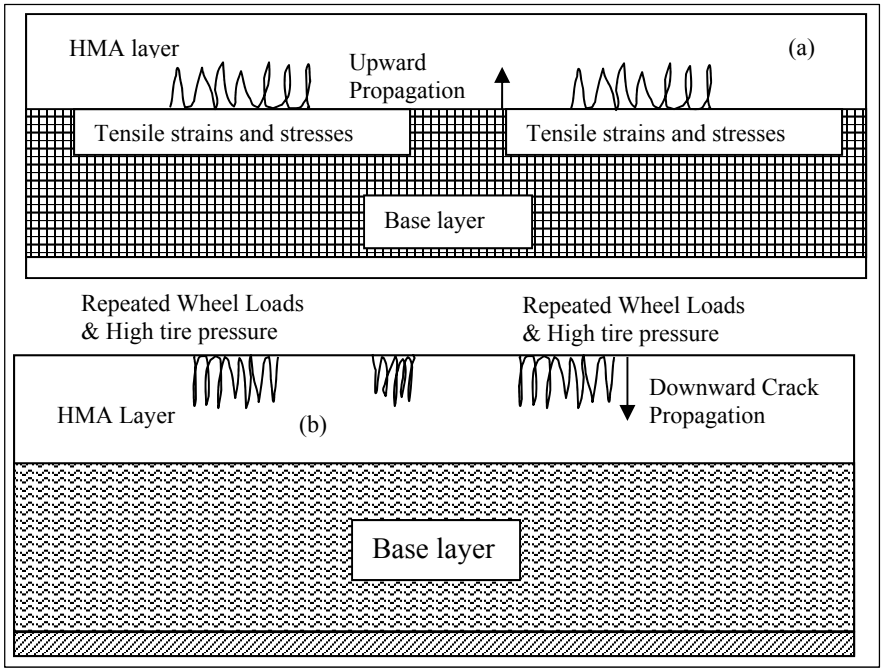

Figure 2.15 Fatigue cracking types: (a) Bottom-up (b) Top-down
Taken from Abdel-Hameed (2006)

According to the LTPP Distress Identification Manual (LTPP, 1993), fatigue cracks that initiate at the bottom of the HMA layer and propagate to the surface are what is classically defined as alligator cracks. This type of fatigue cracking first shows up as short longitudinal cracks in the wheel path that quickly spread and become interconnected to form a cracking pattern generally defined as alligator cracks.

The severity of fatigue cracking can be rated in three main levels (Lavin, 2003):

- Low severity: fine, longitudinal cracks are running parallel to each other with none or only a few interconnecting cracks. The cracks are not spalled. Initially, there may only be a single crack in the wheel path or pavement loading area (see Figure 2.16a);
- Medium severity: further development of light alligator cracks into pattern or network of cracks (many sided, sharp-angled pieces, usually less than 0,3m). The cracks may also be slightly spalled (see Figure 2.16b);

- High severity: the pattern of cracks has progressed so that the individual pieces of HMA physically separate from the adjacent material. Some of the pieces may move under traffic or loading. Pieces may begin to disintegrate, forming potholes. Pumping of the pavement may also exist (see Figure 2.16c).

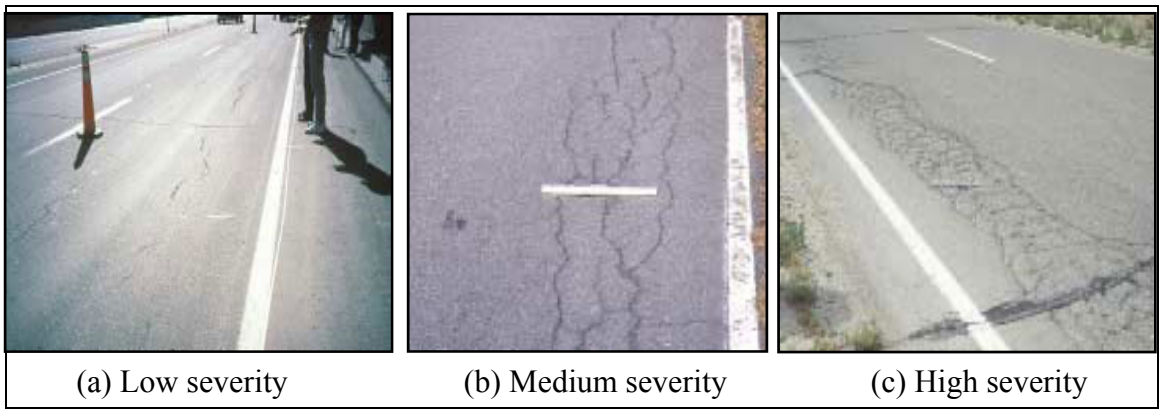

(a) Low severity (b) Medium severity (c) High severity

Figure 2.16 Severity levels of fatigue cracking
Taken from Xiao (2006)

Although fatigue cracking is caused by repeated traffic loading, the fatigue response of flexible pavements is governed by several additional factors that include (Abojaradeh, 2003):

1) Mix variables such as asphalt type and source, aggregate gradation, type and source, air voids content, asphalt content, etc.;
2) Environmental variables such as temperature, temperature gradient, moisture, etc.;
3) Traffic loading magnitude and type, type and level of loading strain control or stress control, frequency, and whether there is rest period or not;
4) Specimen fabrication and preparation procedure and compaction method;
5) Test equipment; and
6) Long term oven aging of asphalt binder.

An analysis of the influence of each of these parameters is tricky as they may be interdependent. For more information about the effects of these results, see Di Benedetto and De la Roche (1998).

2.7.3 Laboratory fatigue test

The fatigue tests performed in the laboratory try to simulate the behaviour of bituminous materials under actual loads (traffic, thermal loads). Those fatigue tests are performed on specimens fabricated either from material collected in situ or reconstructed in the laboratory. Generally, the applied sinusoidal load corresponds to a displacement (or deformations in the case of homogeneous tests) or force (or stress in the case of homogeneous tests) of constant amplitude. Thus, fatigue test can be done using two different loading modes (stress controlled or strain controlled) as shown in Figure 2.17.

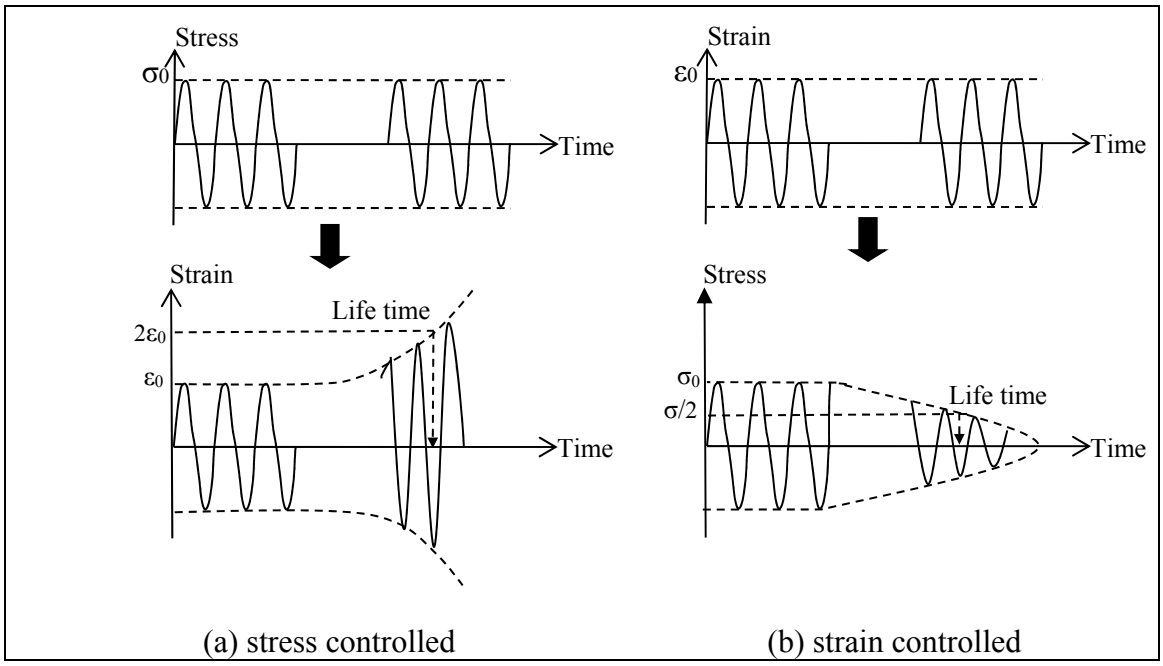

Figure 2.17 Schematic of fatigue test
Taken from Bonnaure, Huibers and Boonders (1982)

- In the stress controlled test, the test is controlled by force which is kept constant during the test, but the strain increases with the number of repetitions (Figure 2.17a). Failure is usually defined as specimen rupture. One advantage of the constant stress mode of loading is the fact that failure occurs suddenly and no judgment is needed in determining failure;

- In the strain controlled test, the strain is applied on the specimen with constant amplitude and at constant frequency and the load or stress decreases with respect of load applications (Figure 2.17b). Failure occurs when the load decreases to some predetermined percentage of the initial load, usually 50 percent (Artamendi et Khalid, 2004).

Regarding the test temperature, in France, the tests are usually done at 10°C, which is the temperature at which the lowest fatigue performance of asphalt mixtures can be obtained (Nguyen, 2009).

There are several types of tests to simulate the mechanical behaviour in order to study the resistance in fatigue of bituminous mixtures in the laboratory. Three different types of test can be distinguished (Di Benedetto et De la Roche, 1998):

- Bending tests (2-, 3-, 4-points);
- Tension-compression tests (direct and indirect);
- Shear tests.

Basically we focus our attention on giving a detailed description of the tension-compression test as it is used in this study to measure the dynamic modulus and the fatigue properties in the HMA mixtures.

Tension-Compression tests are performed on cylindrical samples (height 120mm, diameter 75mm) (Perraton et al., 2003). It is the same test that is used for the measurement of the complex modulus (presented in paragraph 2.6.2.1), but with an increase in the number of cycles of applied solicitation (to several thousands of cycles). The advantage of this test is that it can be carried out in strain or stress control, which is rarely the case in other fatigue tests. Another advantage of this test is that there is a homogenous state of stress and strain inside the sample. The stiffness, the Poisson's ratio and other mechanical characteristics can be drawn from the experiment.

The picture of the tested sample and measurements system was shown previously in Figure 2.16. The values of axial strain are obtained using three extensometers. The analysis of the differences among the three measurements given by these transducers provides clear information about the strain homogeneity within the sample. In a perfect homogenous test, these values are identical. Due to the non-homogeneity of the bituminous sample, and eventually a small eccentricity of the applied load, these values are usually different.

2.7.4 Fatigue test analysis methods

According to Baaj (2002), several criteria are proposed in the literature to characterize the fatigue failure of bituminous mixes. Some methods aim at determining the fatigue life of the specimen, while others propose values determining the state of damage in the specimen. Those criteria are explained hereafter.

2.7.4.1 Criterion based on the evolution of the stiffness modulus (classical method)

In a typical fatigue test result, where the solicitation is imposed, three different phases can be identified as a function of number of cycles to failure as shown in Figure 2.20 (Di Benedetto, Ashayer Soltani et Chaverot, 1996).

- **Phase I or adaptation phase:** This phase is marked by a rapid drop of the stiffness of the sample due to both fatigue damage and the temperature increase (Di Benedetto, Ashayer Soltani et Chaverot, 1996). The effect of heating is very difficult to separate from the fatigue damage during Phase I and therefore it is difficult to analyze. So heating and thixotropy play an important role. Generally, this phase is dominated by the influence of bias effect (thermal variations and thixotropy) in addition to fatigue damage;
- **Phase II or fatigue phase:** this phase is characterized by a moderate decline of the modulus values and the establishment of a steady and quasi-linear evolution of damage. The role of fatigue is predominant on stiffness decrease (Baaj *et al.*, 2002). Although the

influence of bias effects (thermal variations and thixotropy) is less important during this phase comparing to phase I, they must be considered;

- **Phase III or failure phase:** during this phase, there is rapid drop in the modulus. It corresponds to the macro cracks which appear progressively in the sample and propagate until the failure at the end of this phase.

The classical failure criterion is one of the most widely known fatigue criteria (Baaj, 2002). By definition, the sample is considered ruptured if its modulus reaches half of its initial value measured with the first cycle of loading under the same test conditions (temperature and frequency). Therefore, the fatigue life N_f is defined as the number of repetitions that cause a 50% drop in the calculated stiffness (Tayebali, Rowe et Sousa, 1992) (Figure 2.18). The fatigue life N_f, determined from this criterion is used for pavement design in France (Baaj, 2002).

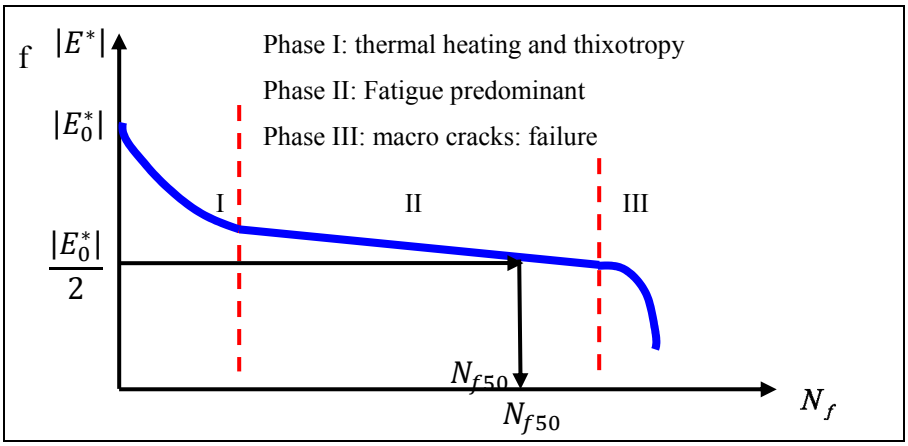

Figure 2.18 Definition of the traditional criterion for determining the fatigue life (N_{f50})

2.7.4.2 End of phase II criterion

This criterion proposes to identify when the mode of damage changes and marks the start of phase III. The corresponding fatigue life is annotated $N_{fII/III}$ and corresponds to the number of

cycles associated with the point of transition between phase II and phase III of the test. The value of $N_{fII/III}$ is not influenced by different phenomena unrelated to fatigue, and is not affected by the phase of rupture related to the macro crack propagation in the specimen.

To identify the value of $N_{fII/III}$, two elements are analyzed: 1) the evolution curves of the differentials of extensometers ($N_{f\Delta ext}$) and 2) the results of the test presented in the Black space ($N_{f\phi}$).

Fatigue life based on the curves of the extensometers ($N_{f\Delta\varepsilon ax}$)

For a homogeneous fatigue test on cylindrical specimen, the value of the fatigue life $N_{fII/III}$ is determined by examining the state of homogeneity of the deformation field within the specimen during the test. Indeed, the transition from the phase II to phase III is marked by the spread of micro cracks in the specimen and therefore the strain field becomes non-homogeneous. The value of $N_{fII/III}$ is determined by comparing the curves of differences deformation amplitudes relative to the average calculated deformation value of three extensometers distributed uniformly around the cylindrical specimen. Then, three relative axial strain amplitude differences are obtained from the following equation:

$$\Delta\varepsilon_{axi} = \frac{\varepsilon_{Aiax} - \varepsilon_{Aax}}{\varepsilon_{Aax}} \times 100\% \tag{2.20}$$

Where:

ε_{Aiax}, and ε_{Aax} are the amplitude, and the mean value for the three axial deformations: i = 1, 2 or 3.

According to Baaj (2002), a difference of more than 25% between the deformations of one of the extensometers to the average value indicates a non-homogeneous deformation field in the specimen. The number of cycles obtained corresponds to $N_{f\Delta ext}$.

Fatigue life from the Black space (maximum phase angle criterion ($N_{f\phi}$)

Di Benedetto and Corté (2004) have shown that it can use the Black space or the evolution of the stiffness curve as a function of the phase angle to determine the transition point between the phase II and III as you will see later in Figure 6.14b. This analysis proposes that the beginning of the phase III ($N_{f\phi}$) correspond to the number of cycles at the point where the value of the phase angle begins to decrease. This criterion is used in the analysis. $N_{f\phi}$ is the number of cycles corresponding to the highest value of phase angle.

The value of the fatigue life at the point of transition between phase II and III ($N_{fII/III}$) will be considered in this research as the average of the two estimates above, which is: life determined relative to differences in strain gauges ($N_{f\Delta ext}$) curves and the value identified by the Black space ($N_{f\phi}$) as shown in equation (2.21).

$$N_{fII/III} = \frac{N_{f\Delta\varepsilon ax} + N_{f\phi}}{2} \tag{2.21}$$

Other methods for determining N_f have been used in the literature based on the evolution of the dissipated energy or the evolution of the homogeneity of the strain field (Tapsoba, Sauzéat et Di Benedetto, 2013). More details about fatigue criteria can be found at a literature review of publication of Tapsoba (Tapsoba, Sauzéat et Di Benedetto, 2013).

2.7.5 Determination of the initial modulus $|E_0^*|$

To properly analyze a fatigue test, you must know the value of the stiffness of the material in the first cycle (sometimes dynamic modulus), which is designated as initial stiffness and annotated $|E_0^*|$. The value of $|E_0^*|$ is not easy to identify. Indeed, at the beginning of the test, the achievement of stabilization of imposed solicitation (strain or stress) requires a number of cycles. Several authors have defined specific criteria for determining the value of $|E_0^*|$. Table 2.1 shows the different approaches to identify the value of $|E_0^*|$.

As shown in Table 2.1, the concept of the initial modulus $|E_0^*|$ is not unique and differs from one author to another. It is clear that regardless of the type of test, it is quite necessary to remove the first cycles of loading, because the achievement of the solicitation policy is not stable: it takes a few cycles to reach the desired value (stress or strain) due to the adaptation time of the hydraulic press when the test is started. Regarding the tests performed in this work, $|E_0^*|$ is defined as the value of the y-coordinate of origin of the first 50 cycles for the fatigue test in the LCMB (*le **L**aboratoire sur les **C**haussées et **M**atériaux **B**itumineux de l'ÉTS*).

Table 2.1 The value of the initial modulus according to the literature review
Taken from Touhara (2012)

Determination of $\|E_0^*\|$	**Reference**
• The value of the initial modulus is related to the value of the stiffness in a logarithmic extrapolation of the first 100 cycles;	Di Benedetto et al., 2001
• The value of the initial modulus corresponds to the stiffness measured at the first cycle of solicitation;	Baaj, 2002
• The value of the module at the 100th cycle;	Di Benedetto et al., 2004
• The value of the initial modulus is related to the value of the stiffness extrapolated linearly by considering the values of the modulus of 50 to 300 cycles;	Nguyen, 2019
• The value of the initial modulus is related to the mean value of the stiffness measured during the first 100 cycles of solicitation,	Noël, 2011
• Linear extrapolation considering the modulus values measured between the 50^{th} and the 250^{th} cycle is retained to determine the value of the initial modulus;	Tapsoba, 2012
• In this study, the imposed deformation stabilizes after 100 cycles biasing. A linear extrapolation of the values of modulus of 200 to 300 cycles is retained to determine the value of the initial modulus.	Lamothe, 2014

2.7.6 Approaches used to predict failure in fatigue

The fatigue characteristics of asphalt materials are usually expressed as relationships between the initial stress or strain and the number of load repetition to failure determined (Xiao, 2006). The slope and the relative level of stress or strain versus the number of load repetitions to failure are usually used to characterize the fatigue behaviour of a specific mixture.

Many researchers developed equations to quantify the number of load repetitions that asphalt materials can tolerate until failure. The early developments quantified the number of cycles to failure (N_f) as a function of the repeated tensile strain at the bottom of the asphalt layer (ε_t) or the relative level of stress alone. Later on, the equations have been improved by including other related variables such as mixture stiffness and volume of bitumen in the mix. The equations are empirical in nature, applicable only for fatigue cracks at the bottom of asphalt layer and must be used with caution since they were developed based on specific materials and testing conditions and may not be widely applicable. They must be carefully calibrated to local conditions to provide for a reliable estimation of pavement fatigue life.

2.7.6.1 Fatigue curve or Wöhler curve

The first fundamental studies of the phenomenon of fatigue in the laboratory were undertaken in 1852 by Wöhler on metals (Baaj, 2002). However, the study of fatigue of concrete, road materials and a large number of composite materials are also the subject of many studies (De La Roche, 1996).

The classical test to characterize the fatigue phenomenon consists in subjecting a specimen to repeated loading and recording the number of cycle to failure. The graphical representation of the fatigue test results is usually given by the fatigue curve or Wöhler curve (Figure 2.19). This curve shows the relation between the fatigue life (N_f) and the level of loading expressed by the initial strain amplitude in a bi-logarithmic scale (Tayebali, Tsai et

Monismith, 1994). Also, with this curve, a particular value of strain called, ε_6, can be determined. It corresponds to the value of the strain level that leads to a fatigue life of 1 000 000 cycles. This value is very commonly used to characterize the fatigue resistance of bituminous mixes (Di Benedetto et de la Roche, 1998). Wöhler curve is often characterized by the following relationship:

$$S = aN^{-b} \tag{2.22}$$

Or

$$\log(S) = \alpha - \beta.\log(N) \tag{2.23}$$

Where:

S The imposed solicitation (imposed stress or strain);

N The corresponding fatigue life; and

a, b (α, β) The constants of the equation.

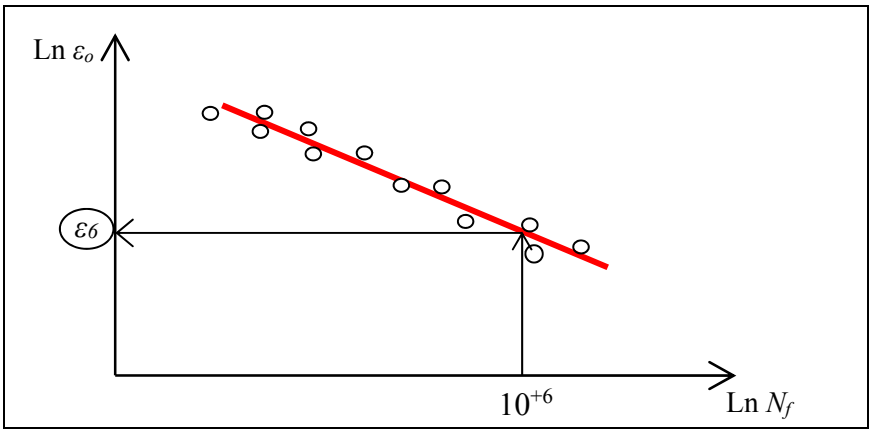

Figure 2.19 Wöhler curve (fatigue curve) and determination of ε_6
Taken from Baaj, Di Benedetto and Chaverot (2005)

Based on laboratory test data presented in the form of equation 2.21 numerous models forms can be found in the literature and have been proposed to predict fatigue lives of pavements.

Basically, all these forms are based on the Wöhler law expressed in the referred equation as it will be presented hereafter.

The most commonly used model form to predict the number of load repetitions to fatigue cracking is a function of the tensile strain or stress (Pellinen, 2001):

$$N_f = k_1(\varepsilon_t)^{-k_2} \; or \; N_f = k_1(\sigma)^{-k_2} \tag{2.24}$$

Where:

N_f The allowable number of load repetitions to fatigue failure;

ε_t The tensile strain at the bottom of the asphalt layer (m/m);

σ The initial stress (MPa); and

k_1 and k_2 Experimentally determined constants.

Various highways agencies and researchers use the dynamic modulus of asphalt layer (E) and the maximum horizontal tensile strain at the bottom of the asphalt layer (ε_t) or the relative level of stress alone to predict the allowable number of load repetitions for a specific fatigue failure criterion (N_f) and can be defined as follow (Luo, Chou et Yu, 2006):

$$N_f = k_1(\varepsilon_t)^{-k_2}(E)^{-k_3} \; or \; N_f = k_1(\sigma)^{-k_2}(E)^{-k_3} \tag{2.25}$$

The argument $(E)^{-k_3}$ in the equation 2.25 translates the effect of temperature on the fatigue life of the material.

Another similar way of analyzing fatigue characteristic is to relate fatigue life, N_f, to the total dissipated energy to failure during the test (Di Benedetto et De la Roche, 1998). A major advantage of this approach, compared with the classical model, is that predicting the fatigue behaviour of a certain mix type over a wide range of conditions, from the results of a few simple fatigue tests, is possible. Other researchers (Di Benedetto et De la Roche 1998,

Tayebali, Deacon et Monismith, 1995) have used an energy approach for describing the fatigue behaviour and have shown that the total, or cumulative, dissipated energy to failure is related to fatigue life as follows:

$$W_N = A\left(N_f\right)^z \tag{2.26}$$

Where:

N_f Fatigue life;

W_N Cumulative dissipated energy to failure; and

A, Z Coefficients determined experimentally.

In equation 2.24 and 2.25, fatigue life is related to the initial test conditions namely, the initial strain and initial mix stiffness. In equation 2.26, fatigue life is related to terminal test condition, namely the cumulative dissipated energy to failure. Neither approach directly recognizes how damage to the mix actually develops as loading proceeds from the beginning to the end. The cumulative dissipated energy to failure, W_N, is related to the energy dissipated during i^{th} load cycle, w_i, as follows:

$$W_N = \sum_{i}^{N_f} w_i \tag{2.27}$$

For a sinusoidal loading condition, the dissipated energy per load cycle, W_i, is a function of the current stress, strain and phase angle, and is given by the following equation (Di Benedetto et De la Roche, 1998).

$$W_i = \pi \sigma_i \varepsilon_i \sin(\phi_i) \tag{2.28}$$

Where:

W_i Dissipated energy at load cycle i (J/m^3);

σ_i Stress amplitude at load cycle i (MPa);

ε_i Strain amplitude at load cycle i (m/m); and

ϕ_i Phase shift between stress and strain at load cycle i (°).

2.7.6.2 Fatigue cracking prediction modelling

There are three methodologies or types of models that were used to calculate fatigue life. These models are as listed below (Abojaradeh, 2003).

1) Basic pavement response; tensile strain, stress, deflection – the methodology commonly used by most of the design procedures in existence to-date;
2) Fracture mechanisms – the methodology commonly used for predicting thermal cracks;
3) Energy or dissipated energy – the least used methodology, but believed to be the most accurate.

The fracture mechanics and dissipated energy approaches have been used to much smaller extent than the basic pavement response approach, but it's believed to more accurately represent the fatigue estimation. Here are more details about the most existing models (Abojaradeh, 2003)**.**

Shell international model

Shell International developed a fatigue-cracking model similar to that of the Asphalt Institute. The Shell equation is shown below:

$$N_f = 0{,}0685(\varepsilon_t)^{-5{,}671}(E)^{-2{,}3633} \quad (2.29)$$

Shell developed separate equations for determining the tensile strain for both constant stress and constant strain test conditions (Shell, 1978). The constant stress and constant strain test equations, based on 146 fatigue curves covering a wide range of mixtures, asphalts, and testing conditions, are shown in equations 2.30 and 2.32, respectively.

Constant stress:

$$\varepsilon_t = (4{,}102PI - 0{,}205V_{beff}[PI] + 1{,}094V_{beff} - 2{,}7807)(E_{Mix})^{-0{,}36}(N)^{-0{,}2} \quad (2.30)$$

or,

$$N_f = A_f[0{,}0252PI - 0{,}00126PI(V_b) + 0{,}00673V_b - 0{,}0167]^5 {\varepsilon_t}^{-5} E^{-1{,}4} \quad (2.31)$$

Constant strain:

$$\varepsilon_t = (0{,}300PI - 0{,}015V_{beff}[PI] + 0{,}080V_{beff} - 0{,}198)(E_{Mix})^{-0{,}28}(N)^{-0{,}2} \quad (2.32)$$

or,

$$N_f = A_f[0{,}17PI - 0{,}0085PI(V_b) + 0{,}0454V_b - 0{,}112]^5 {\varepsilon_t}^{-5} E^{-1{,}8} \quad (2.33)$$

Where:

N	Number of equivalent single axle loads;
ε_t	Allowable or permissible tensile strain, mm/mm;
PI	Penetration index;
V_{beff}:	Percentage of bitumen volume in the mix; and
E_{mix}	Stiffness modulus of the mix, N/m^2.

Asphalt institute model

The Asphalt Institute developed fatigue-cracking prediction models based on the constant stress criterion. The equation used in the 1981 MS-1 Asphalt Institute Thickness Design Manual accounted for air voids percentages (V_a), percentage volume of asphalt (V_b), stiffness of the mixture (E) in N/m^2:

$$N_f = 10^M(18{,}4)(0{,}00432)(\varepsilon_t)^{-3{,}291}(E)^{-0{,}854} \quad (2.34)$$

Where:

$\mathrm{M} = 4{,}84\left(\frac{V_b}{V_a + V_b} - 0{,}69\right)$.

For a standard HMA mix with air voids of 5 percent, and an asphalt volume of 11 percent, M is equal to 0. The number of load repetitions to failure in equation 2.34 is multiplied by a shift factor of 18,4 to adjust the fatigue curves measured in the laboratory to fatigue cracking observations made along the roadway. Thus, the number of load repetitions to failure to be used in design becomes (Yang, 2004):

$$N_f = 0{,}0796 \times (\varepsilon_t)^{-3{,}291} \times (E)^{-0{,}854} \quad (2.35)$$

UCB surrogate fatigue models

A series of surrogate statistical predictive models were developed from the study conducted at University of California Berkeley (UCB) by Tayebali *et al.* (SHRP-A404, 1994; Tayebali, Deacon et Monismith, 1995) to estimate fatigue response for conventional dense graded asphalt mixes.

These surrogate models were based on the data from the study of 8 asphalt types and 2 aggregate gradations at controlled strain testing. These mixtures are considered to be

representative of a range of conventional paving mixture being used in the United States. The models developed are (Tayebali et al., 1993):

a. Strain dependent model:

$$N_f = 466{,}4 \times exp^{0{,}052VFA} \times (\varepsilon_0)^{-3{,}948} \times (S_0 \times \sin\phi)^{-2{,}270} \quad (2.36)$$

b. Energy dependent model:

$$N_f = 6{,}72 \times exp^{0{,}049VFA} \times (w_0)^{-2{,}047} \quad (2.37)$$

Where:

$S_0 . \sin\phi$ Initial loss-stiffness in psi;

w_0 Initial dissipated energy per cycle taken at N=50th cycle (psi); and

VFA Percent voids with asphalt.

The latest surrogate models (SHRP-A404, 1994; Tayebali, Deacon et Monismith, 1995) were based on the test results of 44 mixes (196 beam specimens) at controlled strain fatigue conditions containing a range of asphalt binders and aggregates. In their study, it was concluded that the fatigue behaviour of any conventional asphalt mix can be explained by two mix properties: loss-stiffness, which is the product of the flexural stiffness and the phase angle, and the VFA (voids filled with asphalt), which is the proportion of voids filled with asphalt binder.

The recommended models for fatigue mix design and analysis based on least square analysis of the test results are (SHRP-A404, 1994; Tayebali, Deacon et Monismith, 1995):

a. Strain dependent model:

$$N_f = 2{,}738 \times 10^5 \times exp^{0{,}077VFA} \times (\varepsilon_0)^{-3{,}624} \times (S_0 \times \sin\phi)^{-2{,}270} \quad (2.38)$$

b. Energy dependent model:

$$N_f = 2{,}365 \times exp^{0{,}069VFA} \times (w_0)^{-1{,}882} \quad (2.39)$$

Where:

$S_0 . \sin \phi$ Initial loss-stiffness in psi;

w_0 Initial dissipated energy per cycle taken at N=50th cycle (psi); and

VFA Percent voids filled with asphalt.

The primary advantage of surrogate models is the elimination of the need for more extensive fatigue testing. These surrogate models are very useful for evaluating asphalt dense graded mixes with conventional binders. However, surrogate models are approximate models that lack precision.

It was also concluded that laboratory measurements of mix fatigue life always yield more accurate estimate of design fatigue life for conventional mixes than surrogate models if the test program is designed properly with sufficient numbers of test specimens and consequently a sufficient number of lab test results. On the other hand, in the case of minimal laboratory test program, four specimens were designed to be tested within 24 hours; the surrogate yield more accurate results. It is recommended that laboratory fatigue testing be used whenever high level of reliability is needed for conventional mixes and for modified binder mixes or other than dense aggregate mixes (Tayebali, Deacon et Monismith, 1995).

Prediction of fatigue life in the 2002 design guide

Within the 2002 Design Gide, the fatigue life is governed by a combination of the constant stress and constant strain loading conditions. Table 2.2 contains summary of the review of the major fatigue models formulas.

Table 2.2 Major fatigue model for hot mix asphalt

Fatigue models

1. **General fatigue model** $N_f = k_1(\varepsilon_t)^{-k_2}(E)^{-k_3}$

2. **Shell fatigue equation**

2.1 Constant stress

$N_f = A_f[0{,}0252PI - 0{,}00126PI(V_b) + 0{,}00673V_b - 0{,}0167]^5 {\varepsilon_t}^{-5} E^{-1{,}4}$

2.2 Constant strain

$N_f = A_f[0{,}17PI - 0{,}0085PI(V_b) + 0{,}0454V_b - 0{,}112]^5 {\varepsilon_t}^{-5} E^{-1{,}8}$

where:

$$\mathrm{PI} = \frac{20 - 500\mathrm{A}}{1 + 50A}$$

$$\mathrm{A} = \frac{\log(pen\ at\ T) - \log 800}{T - T_{R\&B}}$$

3. **Asphalt Institute MS-1**

3.1 MS-1

$N_f = 10^M(18{,}4)(0{,}00432)(\varepsilon_t)^{-3{,}291}(E)^{-0{,}854}$

Where: $\mathrm{M} = 4{,}84\left(\frac{V_b}{V_a+V_b} - 0{,}69\right)$

1.2 MS-11

$$N_f = 4{,}024 \times 10^{11} \times (\varepsilon_t)^{-4{,}995}(E)^{-4{,}306}$$

4. **University of California at Berkeley Surrogate model**

4.1 Strain dependent model

$$2{,}738 \times 10^5 \times exp^{0{,}077VFA} \times (\varepsilon_0)^{-3{,}624} \times (S_0 \times \sin\phi)^{-2{,}270}$$

4.2 Energy dependent model

$$N_f = 2{,}365 \times exp^{0{,}069VFA} \times (w_0)^{-1{,}882}$$

5. **2002 Design guide fatigue equation**

(2002 Design Guide)

$$N_f = (1/\beta_1) \times 0{,}004325 \times 10^M \times (\varepsilon_t)^{-3{,}9492}(S_0)^{-1{,}281}$$

Where

$\beta_1 = 0{,}0001587 + (0{,}007 - 0{,}001587)/(1 + e^{17{,}3676 - 3{,}49 \times h})$

$$\mathrm{M} = 4{,}84\left(\frac{V_b}{V_a+V_b} - 0{,}69\right)$$

Where:

No	: Fatigue life (cycles);
ε_t	: Initial strain in/in;
E&So	: Initial stiffness at N=50 cycles (psi);
LS	: S_o*sin ϕ: loss stiffness (psi);
ϕ	: Phase angle between stress and strain at N=50 cycles (degree);
w_o	: Initial dissipated energy at N=50 cycles (psi);
VFB	: Voids filled with asphalt (%)
Va	: Air voids (%);
PI	: Penetration Index;
Pb	: Binder content %;
V_b	: Percentage of bitumen volume in the mix;
β_1	: Laboratory to field adjustment factor;
A_f	: Laboratory to field adjustment factor;
H	: Pavement thickness (inch).

2.7.7 Method of analysis in terms of damage (the DGCB approach)

This method of analysis based on the evolution of the material damage during a tension-compression fatigue test on a cylindrical specimen (homogenous test) has been developed at the laboratory "DGCB" of ENTPE (Baaj 2002; Di Benedetto et al. 2004). This method provides a procedure for calculating the rate of damage by loading cycle. This calculation takes into account non-linearity of the damage with the number of cycles and corrects the influence of parasites phenomena that appear during fatigue tests.

According to Baaj (2002), the application of this methodology on the tension–compression fatigue test on a cylindrical specimen has demonstrated that the fatigue behaviour of asphalt mixtures is independent of the mode of solicitation. Therefore, it is possible to realize the tests in control stress or strain and to compare results between the two modes.

The procedure of the DGCB approach considers three particular intervals of cycles during the phase II (see paragraph 2.7.4) of the test. The interval i = 0 from 40,000 to 80,000, the interval i = 1 from 50,000 to 150,000 cycles and interval i = 2 from 150,000 to 300,000 cycles. For each of these intervals and from experimental results, several parameters need to be calculated to determine the rate of damage by loading cycle on the interval considered. Figure 2.20 and Figure 2.21 show the parameters calculated for the interval i (i = 0, 1 or 2). N_{1i} and N_{2i} represent the number of cycles at the beginning and the end of the interval i.

(E_0) Initial modulus of the sample (at the beginning of the test): this is calculated from the values of the modulus between 50 and 300 cycles using a linear extrapolation (Figure 2.20);

(E_{00i}) Initial stiffness of the interval i (i = 0, 1 or 2) obtained by linear extrapolation to the first cycle of loading (Figure 2.20);

(a_{Ti}) The slope of the regression straight line $|E^*|$ values in the interval i divided by the value E_{00i} obtained for the same interval i (Figure 2.20);

(a_{Wi}) The slope of the linear regression, in the dissipated energy values, in the considered interval, normalised by the value W_{00i} of the dissipated energy obtained from a linear extrapolation to the first cycle of loading (see Figure 2.21);

(a_{Fi}) The true fatigue slope for the considered interval obtained after correction of the nonlinearity of damage. It is calculated by the following equation:

$$a_F = a_T + a_W \frac{C_i.(E_0 - E_{00i})}{E_{00i}} \tag{2.40}$$

C_i is a coefficient that takes into account the non-linear damage evolution mainly during the phase I. The values of C_1, C_2, and C_3 are respectively 4/5, 3/4 and 2/3 for i = 0, 1 and 2 (Di Benedetto et al., 2004);

(W_{00i}) Energy dissipated initial interval i (i = 0, 1 or 2) is obtained by linear extrapolation of the dissipated energy at the first cycle of loading (Figure 2.21).

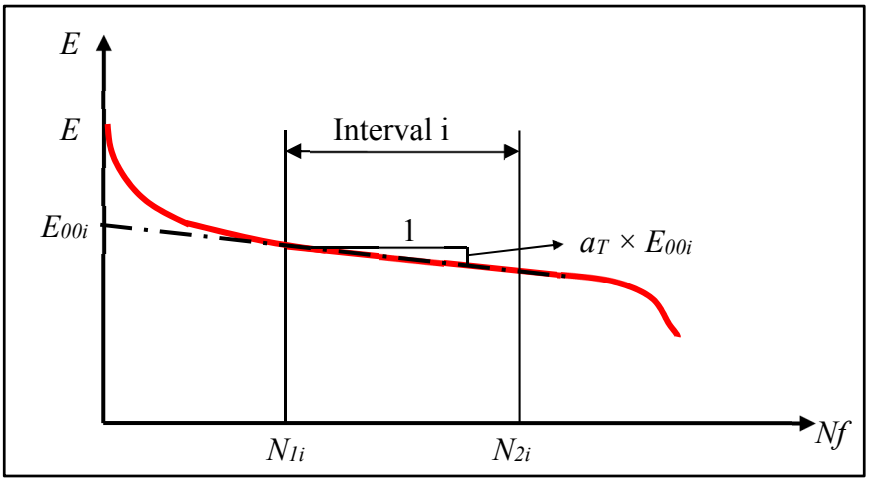

Figure 2.20 Determination of E_{00i} and a_T from the dissipate energy curve
Taken from Baaj (2002)

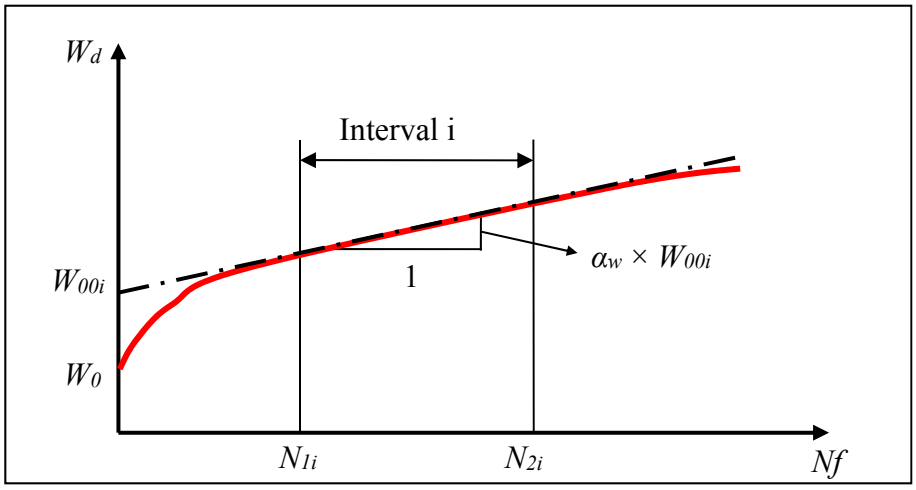

Figure 2.21 Determination of W_{00i} and a_w from the dissipated energy curve
Taken from Baaj (2002)

2.7.8 Performance of RAP mixtures in laboratory: complex modulus tests

Li et al. (2004) investigated the effect of RAP type and percentage on the final mixture properties using complex modulus as proposed by the new AASHTO 2002 design guide. Ten mixtures consisting of three RAP percentages (0%, 20%, and 40%), two virgin asphalt binders (PG 58-28 and PG 58-34), and two RAP sources (RAP and millings), were studied. The RAP sources were provided by a local contractor and were identified as follow:

- Milling–RAP from a single source, milled up from I-492 in Maple grove. The RAP has a binder content of 4,3% and an extracted binder grade of PG 76-22;
- RAP – RAP combined from a number of sources and crushed at the HMA plant. The RAP has a binder content of 5,4% and an extracted binder grade of PG 70-22.

The RAP material was blended with virgin aggregate such that all samples tested had approximately the same gradation. The Superpave mix design process was used to determine the optimum asphalt content for the mixtures. It should be noted that the mix design was performed only for the PG 58-28 asphalt binders and the same optimum binder content was used for the mixes with the PG 58-34 asphalt binders.

All ten mixtures were subjected to complex modulus testing. The limited data obtained in this project shown that the addition of RAP increased the complex modulus for all ten mixtures and that the asphalt binder grade and RAP source had a significant effect on the mixture modulus. However, this effect was reduced at low temperatures and high frequencies.

Also it is concluded that the complex modulus is not controlled only by the stiffness of the binder but also many other factors including the gradation and angularity of the aggregate. For mixtures with more RAP material, more fine aggregates were used. Older pavement may contain aggregate with less angularity, which may also be a contributor to lower complex modulus. Therefore, the increased stiffness brought about by the addition of RAP may be offset by the use of finer and round aggregates. These results are also in agreement with Daniel and Lachance (2003).

Figure 2.22 illustrates the effect of RAP content on complex modulus for all ten mixtures used in this study at 21ºC and 0,1 Hz. For the mixture with PG 58-28 asphalt binder, it is noted that the complex modulus increased by 23% with 20% addition of RAP, and adding 40% RAP resulted in a 62% increase. And for the mixture with PG 58-34 asphalt binder, it is found that the complex modulus increased by 97% with 20% addition of milling, and adding 40% milling resulted in a 133% increase in complex modulus. Finally, it was concluded that the mixtures containing RAP exhibited higher variability than virgin mixtures (i.e., 0%RAP) as it is shown in Figure 2.23, and that the variability increased with the increase in RAP content as shown by the separation of the curves in Figure 2.24 and Figure 2.25.

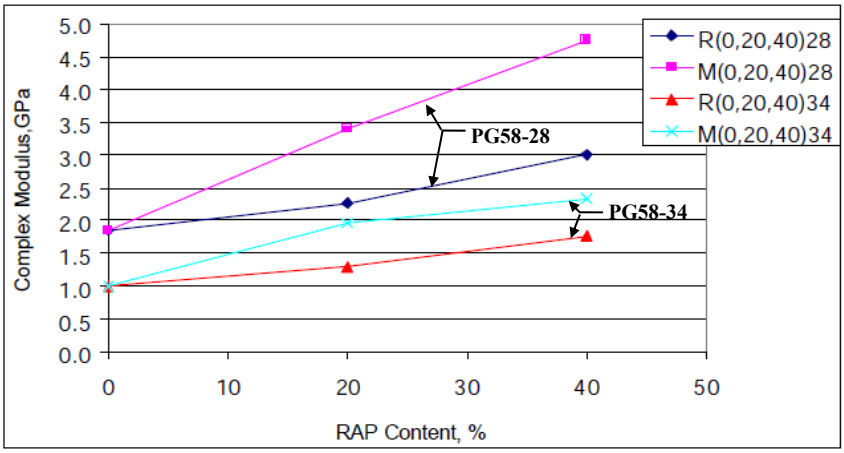

Figure 2.22 Effect of RAP on complex modulus at 21ºC and 0,1 Hz
Taken from Li, Clyne and Marasteanu (2004)

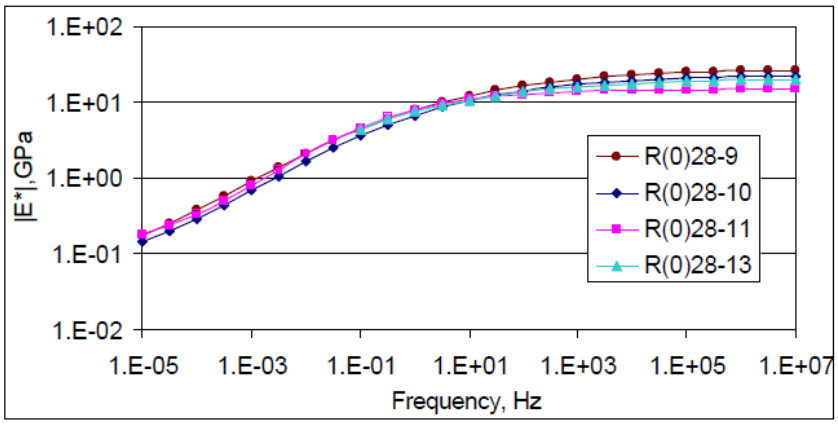

Figure 2.23 Complex modulus master curves at 4 ºC for 4 replicates of the 0% RAP mix
Taken from Li, Clyne and Marasteanu (2004)

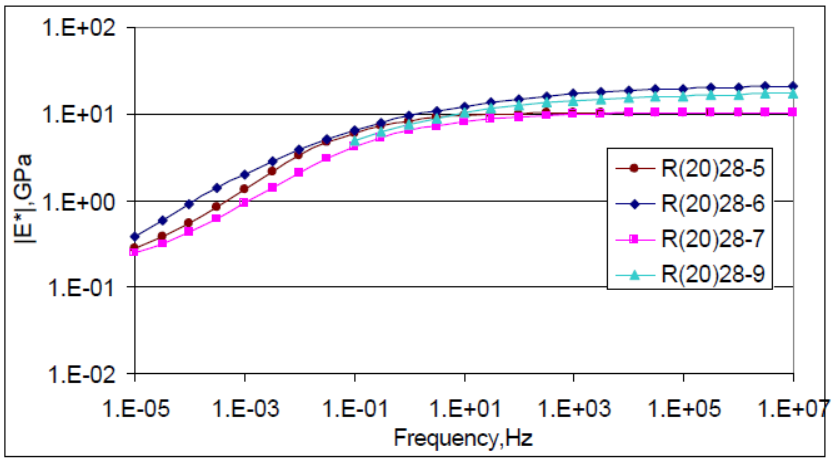

Figure 2.24 Complex modulus master curves at 4ºC for 4 replicates of the 20% RAP mix
Taken from Li, Clyne and Marasteanu (2004)

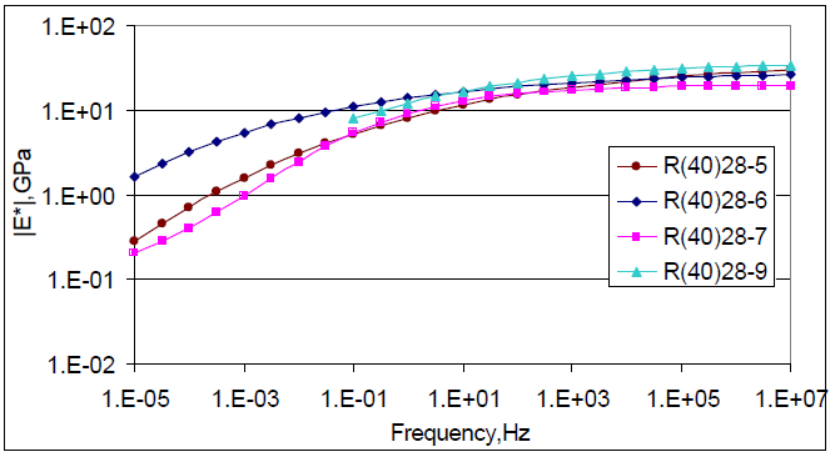

Figure 2.25 Complex modulus master curves at 4ºC for 4 replicates of the 40% RAP mix
Taken from Li, Clyne and Marasteanu (2004)

In 2006, the North Central Superpave Center conducted a pooled fund study to investigate the laboratory performance of Superpave asphalt mixtures incorporating RAP (McDaniel *et al.*, 2007). In this study, McDaniel *et al.* evaluated the influence of RAP content on the mixture of plant-produced hot mix asphalt by studying the complex modulus of RAP mixtures. RAP was added at 15%, 25% and 40% levels to HMA with PG 64-22 and at 25%

and 40% levels to HMA with PG 58-28 binder. The samples of each RAP mixture were collected at the plant and transferred to the Heritage Research Group laboratory for reheating to compaction temperature, compaction, specimen fabrication, and determination of volumetric properties. In addition, control mixture samples with PG 64-22 and no RAP were also collected and tested for comparison. Compacted specimens were tested to determine the complex modulus (|E*|) at three temperatures (20, 38, 7, and 54,4°C).

Figure 2.26 shows the test results for the dynamic modulus. Statistical analyses indicated that there were no significant differences in |E*| between the control mixture and mixtures with 15% and 25% RAP. Some differences between the control mixture and the 40% RAP mixtures were found only at the higher test temperatures. Also it was found that the complex moduli of mixes with 25% RAP but different binder appeared to be similar (Mixes C and E). Finally, it is concluded that the mixes with PG 64-22 shows higher modulus values than the mixes with PG 58-28 at the same RAP content and that this result was expected to obtain because of the stiffer virgin binder, PG 64-22.

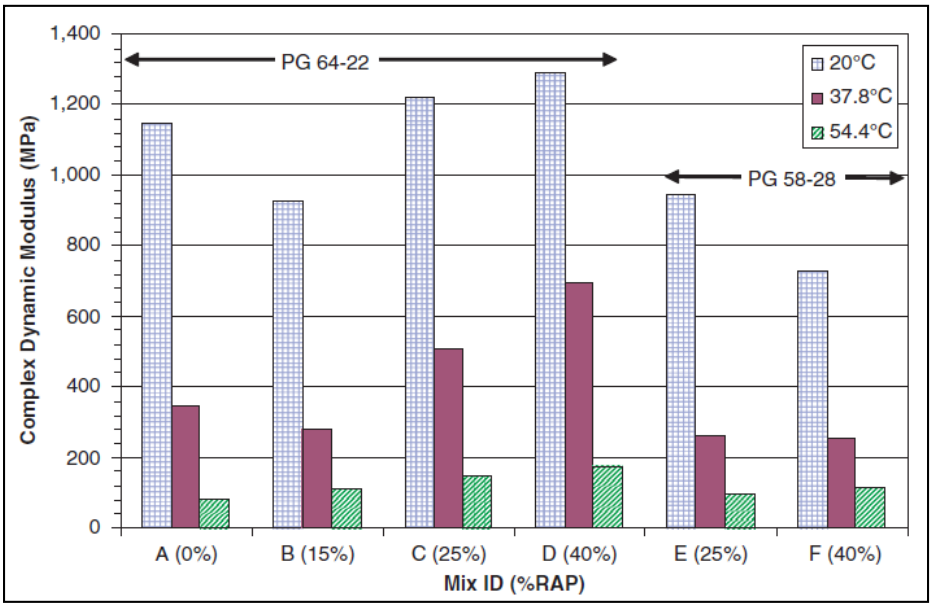

Figure 2.26 Average dynamic modulus test data for 4 replicates at 25 Hz
Taken from McDaniel et al. (2007)

Daniel and Lachance (2005) evaluated the effect of RAP and its component on the volumetric and mechanic properties of HMA mixes. The 0% RAP mix was used as the control for evaluating the properties of mixes containing 15%, 25%, and 40% RAP. A 19 mm Superpave gradation designed for low volume roads was used with an unmodified PG 58-28 binder. Two types of RAP were evaluated: a processed RAP and unprocessed RAP or grindings. The processed RAP contains a mix of recycled asphalt pavement and Portland cement concrete. The extracted processed RAP binder had a grade of PG 94-14. The samples that fabricated using the processed RAP only were tested for complex modulus by means of both tension and compression. The results shows that when samples were tested for complex modulus under compression, the variability of the results increased with increasing RAP content, but when samples were tested in tension the variability of all mixtures were lower than that of the control mixture.

The complex modulus master curves in compression and in tension are as shown in Figure 2.27 and Figure 2.28, respectively. The data shows that the 15% RAP mix had a higher stiffness than the control mixture in both tension and compression, as would be expected. This indicates that the mixture containing RAP would be less resistant to fatigue according to Lachance (2006) and this doesn't agree with Huang *et al.* (2004). The 25% and 40% RAP mixtures show similar stiffness as the control mixture in both tension and compression, though these were expected to have higher stiffness than the 15% RAP mixture. The stiffness reduction of the 25% and 40% RAP mixtures was attributed to the finer gradations and higher VMA and FVA values.

Li, Clyne and Marasteanu (2004) also found that the complex modulus of the mixture increases with increasing the stiffness of the asphalt binder. This was observed for all mixtures tested. For example as it is shown in Figure 2.29, the complex modulus master curve for R028 mixture was higher than R034 for all frequency ranges (or temperatures ranges), which means the asphalt binder grade has a significant effect on complex modulus for the entire temperature and frequency ranges.

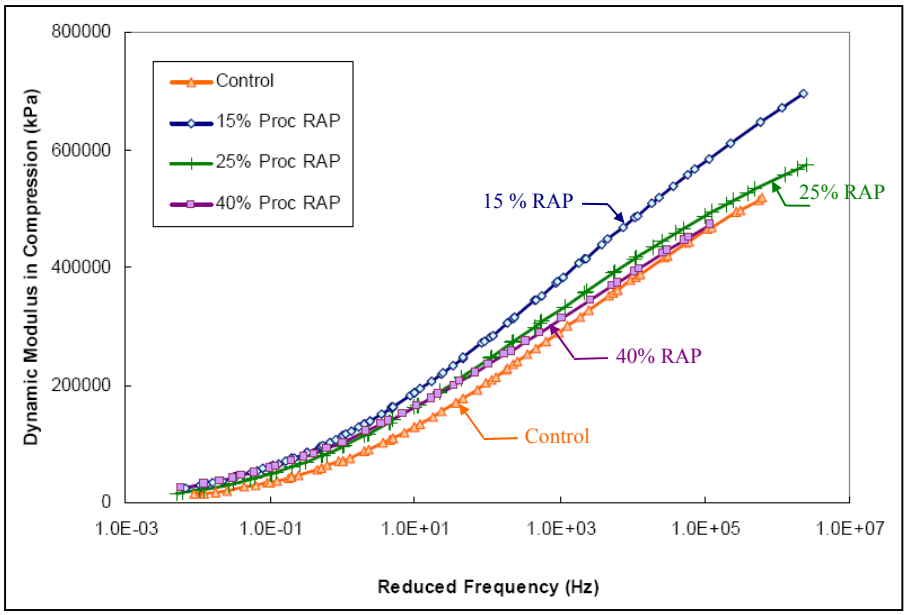

Figure 2.27 Dynamic modulus master curves in compression for all mixtures
Taken from Daniel and Lachance (2005)

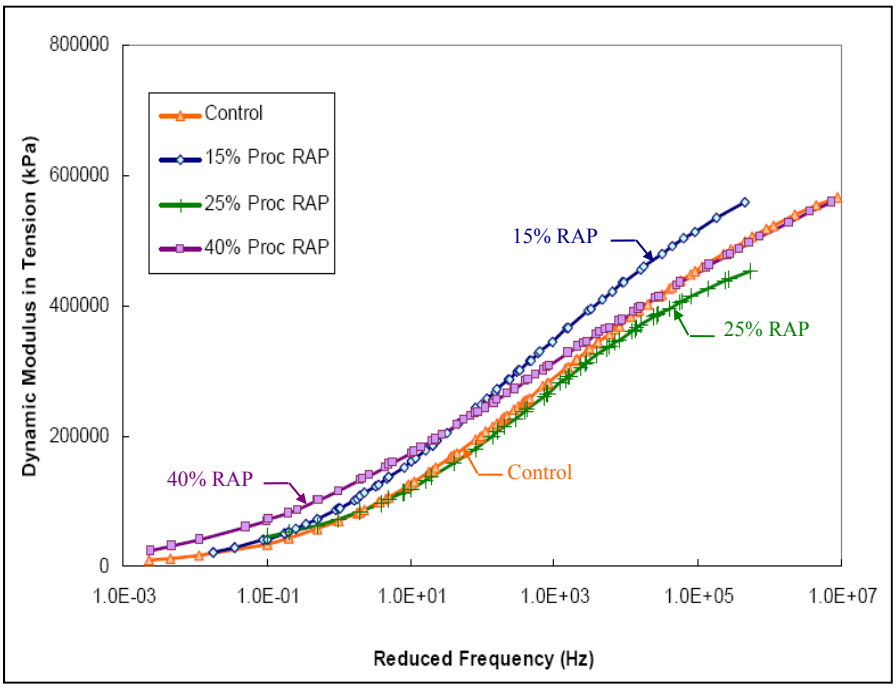

Figure 2.28 Dynamic modulus master curves in tension for all mixtures
Taken from Daniel and Lachance (2005)

Also it is noted that the complex modulus was 50% higher for the mixture incorporating the stiffer PG 58-28 asphalt binder as compared to PG 58-34 at 4ºC and 10 Hz (Figure 2.29).

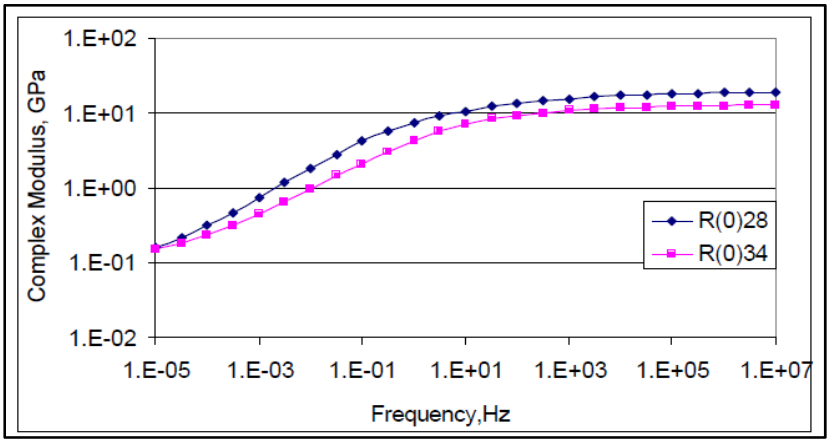

Figure 2.29 Master Curve for Complex Modulus for R028 and R034, T_{ref} = 4ºC
Taken from Li, Clyne and Marasteanu (2004)

Their results showed that RAP source has an effect on complex modulus. They found that the mixture with 20% RAP and PG 58-34 asphalt binder has a slightly higher complex modulus than the mixture with 20% milling, at high testing frequency or low temperature. However, at low frequency or high temperature, the mixture with 20% milling showed much higher complex modulus than the mixture with 20% RAP as it is shown in Figure 2.30. Also it is concluded that the mixture with 40% milling had higher complex modulus than that with 40% RAP, although the difference is not significant (Figure 2.31). A similar relationship was observed for the mixtures with PG 58-28.

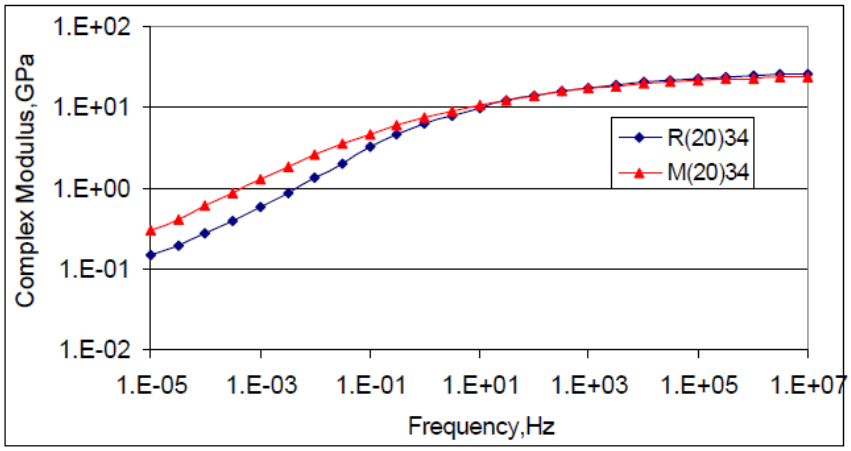

Figure 2.30 Master curves for Complex modulus for R2034 and M2034, T_{ref} = 4ºC
Taken from Li, Clyne and Marasteanu (2004)

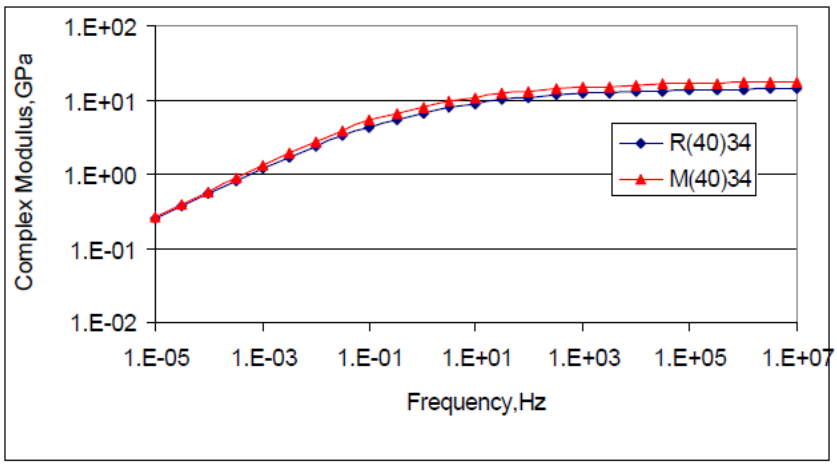

Figure 2.31 Master curves for Complex modulus for R4034 and M4034, T_{ref} = 4ºC
Taken from Li, Clyne and Marasteanu (2004)

Finally, it is observed for all the mixtures that the complex modulus increased as the test temperature decreased or test frequency increased. This result is also in agreement with Di Benedetto and De la Roche (1998). The typical behaviour of complex modulus with temperature at a frequency of 0,1 Hz is shown in Figure 2.32. Also, the typical relationship between the complex modulus and the loading frequency at 21ºC is shown in Figure 2.33.

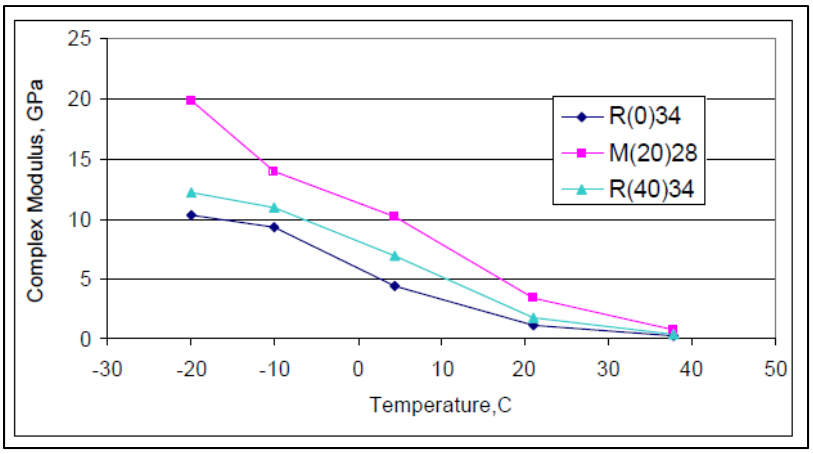

Figure 2.32 Complex modulus changes with temperature at 0,1 Hz
Taken from Li, Clyne and Marasteanu (2004)

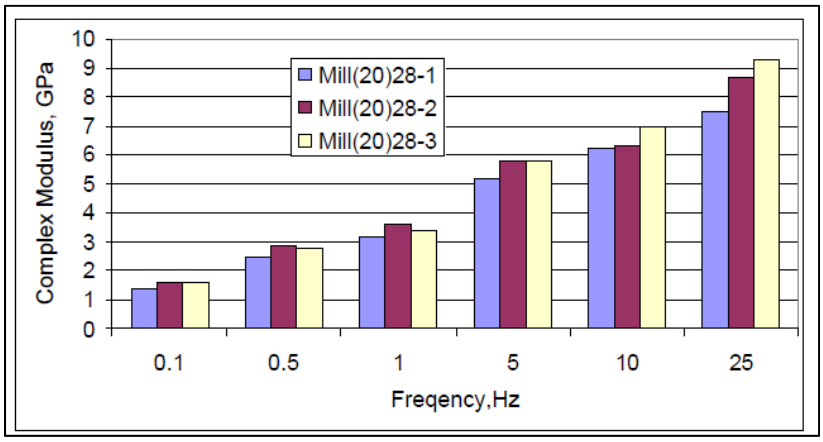

Figure 2.33 Complex modulus changes with frequency at 21ºC
Taken from Li, Clyne and Marasteanu (2004)

2.7.9 Fatigue performance of RAP mixtures in laboratory

In 1997, in an effort to incorporate the usage of RAP in Superpave HMA mixtures, the National Cooperative Highway Research Program (NCHRP) funded a three years research study to evaluate the effects of RAP on Superpave mixtures (McDaniel *et al.*, 2000).

The research used three sources of RAP, two virgin binders and one virgin aggregate. All mixtures were produced following the Superpave specification for the 12,5 mm nominal maximum size.

This study evaluated the impact of adding 0%, 10%, 20%, and 40% RAP on the properties of the final mix. All combinations of the three RAP sources and two virgin binders were evaluated. The virgin binder was not changed according to blending chart calculations. The flexural beam fatigue test in four-point loading was used to assess the mixture resistance to fatigue cracking. Beam fatigue testing was performed in accordance with AASHTO TP8 Standard Test Method for Determining the Fatigue Life of Compacted Hot Mix Asphalt (HMA) Subjected to Repeated Flexural Bending. AASHTO TP8 requires a beam of asphalt with dimensions of 380 mm-length, 50 mm-height and 63 mm-width. Smooth saw cut sides are necessary for clamping and attachment of the LVDT. The beam is placed in four-point loading with an LVDT mounted 98 in the center of the beam at mid-height to measure the deflection. Testing is conducted at 20°C, with the beam conditioned at this temperature for two hours prior to testing. Loading is applied in a sinusoidal waveform in strain-controlled mode. At specified cycles the data acquisition system uses the deflection and the applied load applied to calculate and record the maximum tensile stress, maximum tensile strain, phase angle, stiffness and dissipated energy. Full description of this test is presented in the NCHRP 9-12 report (McDaniel *et al.*, 2000).

The results of the flexural beam fatigue (Table 2.3) showed that the fatigue life of the mix decreased with the addition of the RAP if the grade of the virgin binder was not adjusted to account for the inclusion of the RAP. Also Figures 2.34 and 2.35 illustrate the relationship between cycles to failure and the initial stiffness (initial stiffness is defined as the measured stiffness after 50 cycles) of the beams at different RAP ratios for the Connecticut (CT) and Arizona (AZ) RAP. It is found from Figure 2.34 that as the stiffness increases the cycles to failure decreases and the curves on the PG 52-34 showed that the virgin binder determines the relationship of cycles to failure vs. stiffness. It should be noted that the failure criteria used in this study is defined as the number of cycles until the stiffness drops to 50 percent of

initial stiffness. The results also showed that the number of cycles vs. stiffness is determined by the stiffness of the RAP. But in Figure 2.35, cycles to failure vs. initial stiffness did not show the same relationship. The researchers were not certain of the cause of this discontinuity, but theorized that the binder is the source. Finally the results presented in Figure 2.36 shows the cycles to failure vs. stiffness for the low strain follows the same trend as the cycles vs. initial stiffness for high strain. This trend is only shown for PG 64-22 mixture with Arizona RAP since it took the stiffest of all combinations for the failure criteria to be reached before the 500,000-cycle cut off.

Table 2.3 Beam fatigue average life cycles of various mixtures
Taken from McDaniel *et al.* (2000)

RAP Source	**RAP Content (%)**	**Average fatigue life (cycles)**			
		PG 52-34		**PG 64-22**	
		Low strain level (400 με)	**High strain level (800 με)**	**Low strain level (400 με)**	**High strain level (800 με)**
Virgin	0	500 000+	129 106	500 000+	12 589
Connecticut	10	500 000+	131 121	428 842	18 164
	20	500 000*	73 767	500 000	12 822
	40	421 909*	33 533	330 424*	19 042
Arizona	10	500 000+	150 530	352 578	13 332
	20	500 000+	41 259	233 199	6 526
	40	278 816	16 892	87 090	6 608

+ Beam did not reach half stiffness even after 500 000 cycles
* One beam failed at or below 500 000 cycles and other beam did not fail after 500 000 cycles

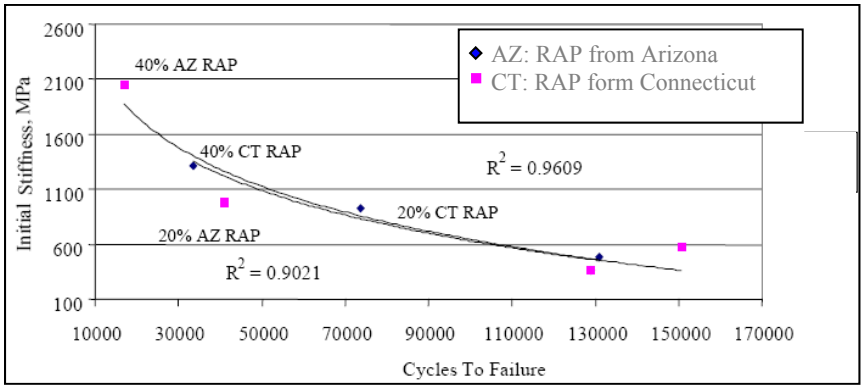

Figure 2.34 Beam Fatigue, Cycles vs. Stiffness High Strain, PG 52-34
Taken from McDaniel and Anderson (2001)

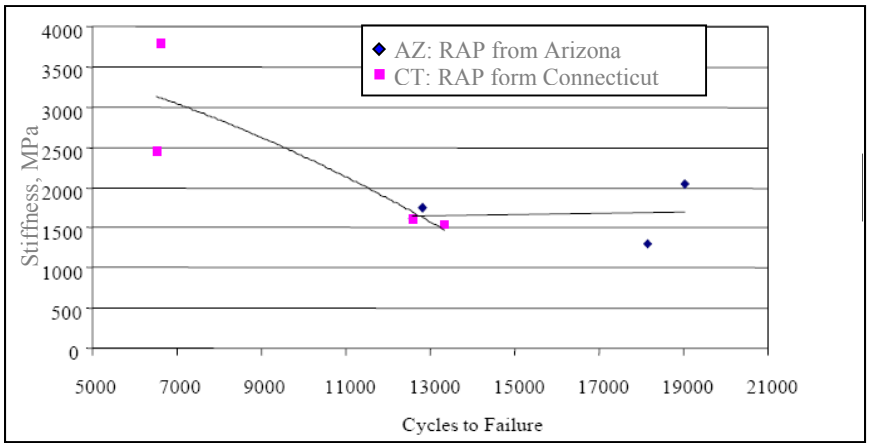

Figure 2.35 Beam Fatigue, Cycles vs. Stiffness High Strain, PG 64-22
Taken from McDaniel and Anderson (2001)

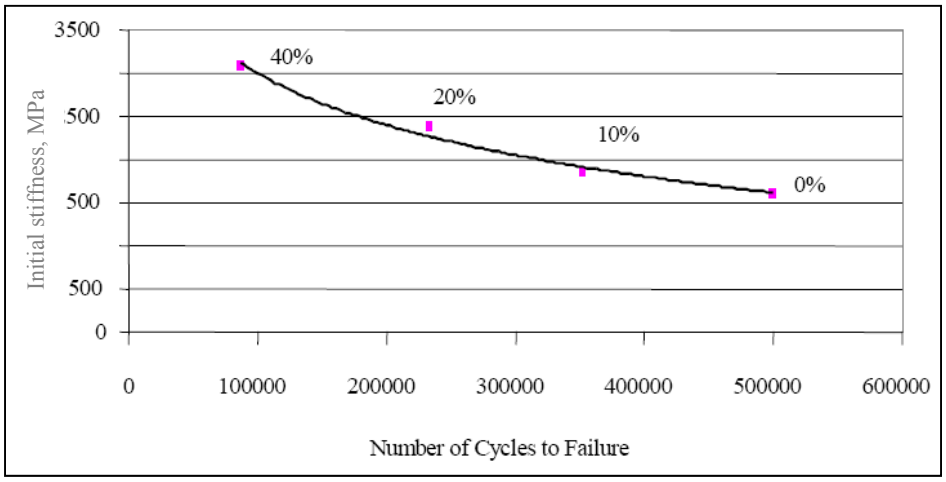

Figure 2.36 Beam Fatigue Cycles to Failure vs. Stiffness, PG 64-22, Low Strain
Taken from McDaniel and Anderson (2001)

On the other hand, in 2007 (Hajj, Sebaaly et Shrestha, 2007), an evaluation study was done to investigate the laboratory performance of the control and RAP mixtures in terms of their resistance to fatigue by conducting flexural beam fatigue test, the results showed that for PG 64-22 mixtures:

- The addition of 15% RAP to a mixture resulted in either a better or equivalent resistance to fatigue than the virgin mix regardless of the source of the RAP;
- The addition of 30% RAP to a mixture resulted in a better resistance to fatigue than the virgin mix only in the case of RAP from a 20-year old HMA pavement.

But for PG 64-28 mixtures (polymer modified asphalt binder):

- The addition of 15% or 30% RAP to a mixture resulted in a significant reduction in fatigue resistance regardless of the source of the RAP.

Table 2.4 compares the properties of the mixtures containing RAP to the properties of the control mixture (i.e., 0%RAP).

Table 2.4 Overall Summary of the laboratory evaluation of RAP containing mixtures
Taken from Hajj, Sebaaly and Shrestha (2007)

Target binder grade	RAP source	RAP %	Impact of RAP on resistance to fatigue
PG 64-22	I	15	Better --
		30	-- Worse
	II	15	Same --
		30	-- Worse
	III	15	Better --
		30	Better --
PG 64-28	I	15	-- Worse
		30	-- Worse
	II	15	-- Worse
		30	-- Worse
	III	15	-- Worse
		30	-- Worse

These results are also nearly in agreement with the study of the University of Tennessee (UT) (Huang et al., 2004) conducted to investigate the fatigue resistance of wearing course mixtures with RAP. The results of the semi-circular bending (SCB) fatigue tests showed that the addition of RAP also increased the fatigue life for both unaged and long-term aged mixtures, at load levels above 500 lbs as it is shown in Figure 2.37. But, significant changes

in fatigue cracking characteristics were noted at 30% RAP level. It was noted that the slopes of fatigue life versus applied load for mixtures with 30% RAP of fatigue life were significantly steeper than the slope for the other mixtures. This indicated that at lower stress levels which are considered close to real highway situation, the fatigue life of mixtures with 30% RAP might be lower than the other mixtures. Therefore, the authors caution the use of RAP at this quantity. This research further supports the theory that RAP may minimally, and possibly positively, influence mixture behaviour when added up to a certain threshold.

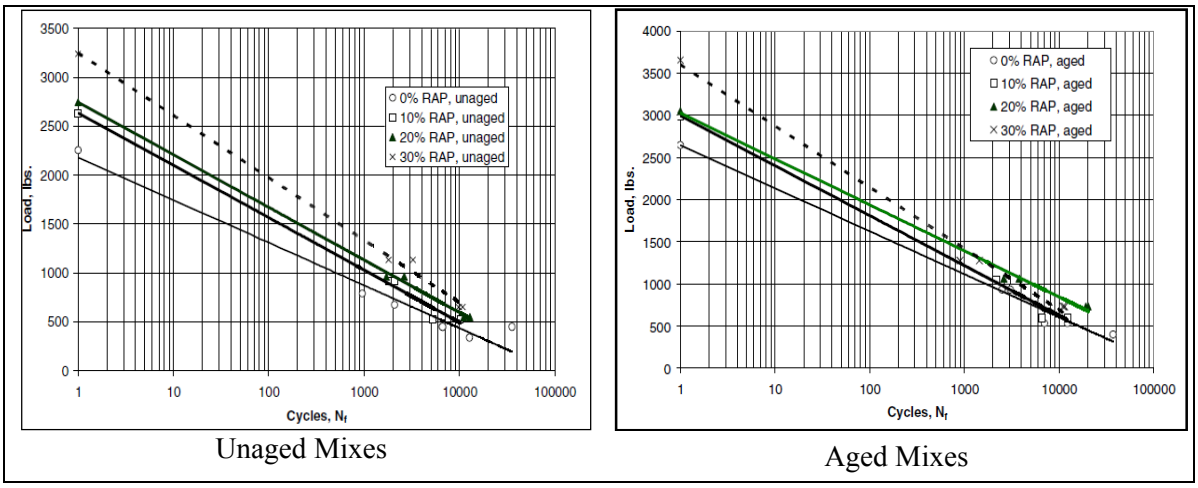

Figure 2.37 SCB Fatigue test results
Taken from Huang et al. (2004)

Currently, Hajj, Sebaaly and Shrestha (2007) use in their research study the Marshall mix design method to design HMA mixtures and specifies two binder grades for all HMA mixtures: PG 64-22 and PG 64-28. The PG 64-22 is a neat asphalt binder mostly used in bottom and middle lifts of the HMA layer. The PG 64-28 is a polymer-modified binder mostly used in the top lift of the HMA layer. The three RAPs used in this study were selected from three different local sources.

Based on the data generated by this study, the following conclusions were made. While reviewing the findings and conclusions, it should be well recognized that in most cases the addition of RAP materials necessitated a change in the virgin binder grade from the target

binder grade as shown in Table 2.5. This change in the virgin binder grade had impact on the measured performance properties of the final mix.

The Marshall Mix Design method as outlined in the Asphalt Institute's Mix Design Methods Manual MS-II and implemented by the Washoe RTC can be used to design HMA mixtures with 15 and 30% RAP.

Table 2.5 Required virgin binders grades for the various RAP sources and contents
Taken from Hajj, Sebaaly and Shrestha (2007)

RAP	**Recovered RAP binder grade**	**Required virgin binder grade (based on blending chart)**			
		Target binder: PG 64-22		**Target binder: PG 64-28NV**	
		15% RAP	30% RAP	15% RAP	30% RAP
Source I	PG 82-16	PG 64-22	PG 58-28	PG 64-34	PG 58-34
Source II	PG 82-16	PG 64-28	PG 58-28	PG 64-34	PG 58-34
Source III	PG 82-16	PG 64-28	PG 58-28	PG 64-34	PG 58-34

Blending chart process was used to identify the required grades of the virgin binders to achieve the target binder grades. The blending chart method was found to be conservative and not highly reliable in identifying the appropriate grade of the virgin binder for the various RAP sources and RAP contents.

University of Tennessee (UT) (Huang *et al.*, 2004) performed series of tests to evaluate the fatigue resistance of wearing course mixtures using RAP in varying percentages in which tests were performed not only using semi-circular bending (SCB) but also including indirect tensile (IDT).

The UT study utilized one type of aggregate (limestone), a natural sand material, and different percentages of No.4 sieve screened RAP materials (0, 10, 20, and 30 percent of RAP content), and an SBS polymer modified asphalt binder meeting Superpave specification for PG 76-22. Two types of mixtures were evaluated in this study; unaged and long term aged mixtures. The 3-days oven aging at 100ºC for mixtures was selected as the aging

protocol in this study. Results showed that the inclusion of RAP increased mixture stiffness. Figure 2.38 presents the results from IDT test. It is found that long term aged mixtures had higher indirect tensile strength (ITS) than those experienced short-term aging (referred to as "unaged" hereafter). Also results showed that there was a noticeable increase in ITS for both unaged and aged mixes between the 0% RAP control mixture and the 20% RAP mixtures. This indicates that with 20% of RAP, mixture exhibited higher tensile strength, lower post-failure tenacity, but the pre-failure maximum tensile strains remains at the similar level as shown in Figure 2.39.

It is important to note that the indirect tensile test does not make it possible to characterize the properties of fatigue correctly. Indeed, during this test, the material is subjected to load cycles which are only in tension according to the diametrical plan (Perraton et al., 2003). This test produces an accumulation of irreversible strain (deformation) and the collapse generally occurs too rapidly. The rupture is not essentially obtained by fatigue. This invalidates the use of indirect tensile test (IDT) for fatigue characterization (Di Benedetto, Ashayer Soltani et Chaverot, 1996).

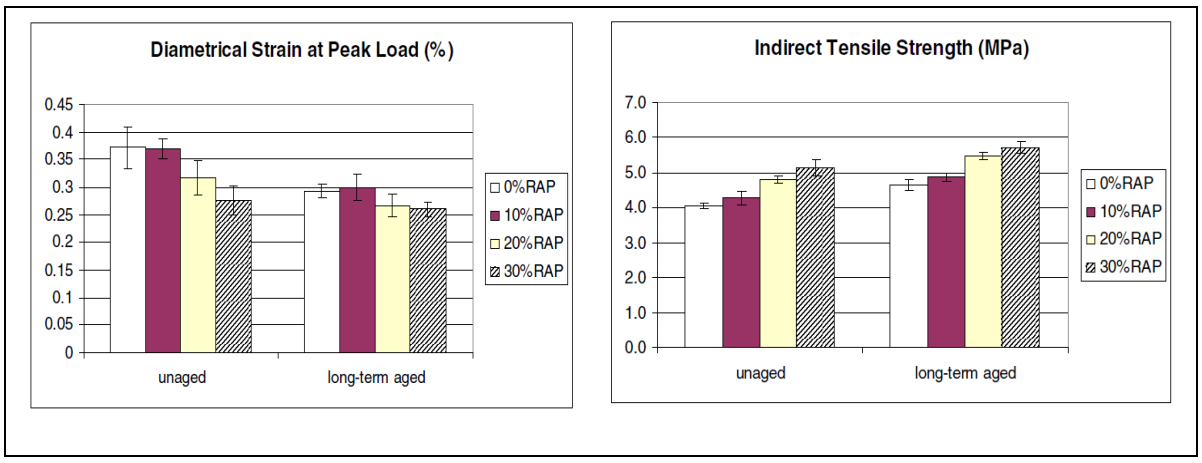

Figure 2.38 Indirect Tensile Test (IDT)
Taken from Huang et al. (2004)

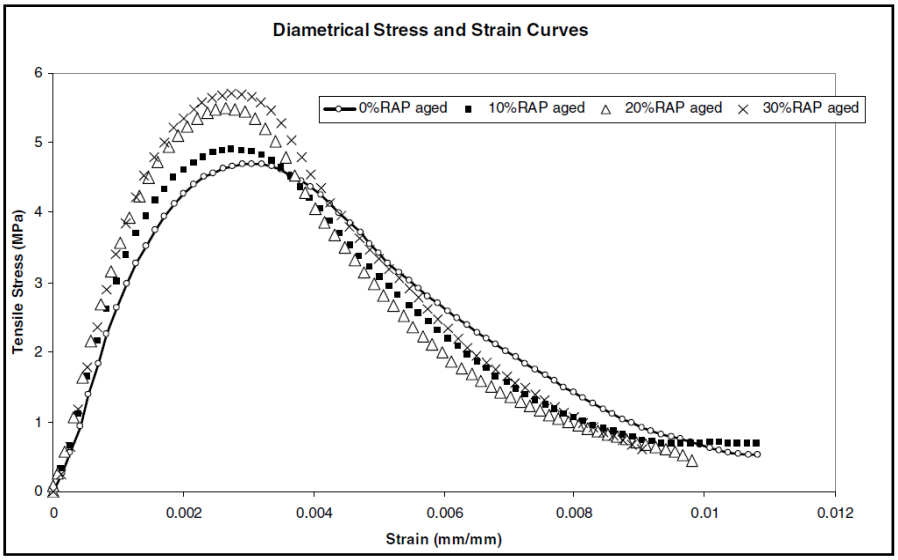

Figure 2.39 Effect of RAP percentage to IDT stress and strain curves
Taken from Huang et al. (2004)

2.8 Chapter conclusion

Even if the results have been widely mixed and no clear conclusion can be drawn from past research projects, the following general conclusions that can be drawn from the finding in the literature are:

- In general, most studies on laboratory-produced mixtures concluded that the effect of RAP on mixtures' properties is negligible at low contents of 15-20%. The low RAP content did not significantly affect the stiffness and the strength of the mixtures at low and high temperatures. However, the increase in RAP content beyond 20% increases the mixture stiffness and strength resulting in an increase in the resistance to rutting. However, other studies showed that adding up to 40% RAP to the virgin mixture did not show any significant difference in its stiffness compared to the virgin mixture. It is concluded that high quality HMA with up to 40% RAP can be designed and can attain the desired performance, i.e. fatigue resistance.

- Various researchers have investigated the proper methods of utilizing RAP and the associated performance of HMA incorporating recycled materials. Results of research studies are not the same and no clear conclusion can be drawn about the effect of addition of RAP on the fatigue performance of asphalt mix. While some researchers have found that HMA mixtures containing RAP provide poor fatigue life when compared with virgin mixes, others have reported that the use of RAP in HMA improves the fatigue cracking resistance. This conclusion appears to contradict the common belief which states that more RAPs equals a more brittle mixture, thus, a lower fatigue resistance.

- Recycled HMA which is designed and produced to verify mix design assumptions to reasonable limits, can be expected to perform comparably to virgin HMA.

CHAPTER 3

RESEARCH METHODOLOGY AND EXPERIMENTAL WORK

3.1 Introduction

Several studies showed that asphalt mixtures containing RAP can have equivalent performance to virgin mixtures. Everywhere in the world, various agencies and contractors have made a broad use of RAP in highway pavements. The state of the art of designing and constructing pavement incorporating recycled materials is now advanced to a point where recycling is considered as an alternative interesting to conventional procedures for the majority of the projects of paving.

According to Daniel, Bisirri and Richard (2004), and Robert et al. (1996) fatigue is one of the most important distresses which governs the service life of asphalt concrete pavements. Di Benedetto and Corté (2004) explain that fatigue is one of the principle modes of failure of pavement structures, which results in degradation of the materials of the pavement and the structure of pavement. For many years, significant research efforts have focused on developing reliable fatigue prediction models as presented in section 2.7.6.2. It should be noted that these models were developed for asphalt mixture without RAP. These models are usually phenomenological; namely, they relate the initial response (such as tensile strain or dissipated energy) of asphalt mixture to their fatigue life.

In asphalt concrete pavements design, it is important to have a measurement of the fatigue characteristics of specific mixtures over a range of traffic and environmental conditions so that fatigue consideration can be incorporated in the design process (Tayebali, Tsai et Monismith, 1994). Pavement design methods using mechanistic approach take into account the fatigue behaviour of asphalt material. For the Mechanistic Empirical Pavement Design Guide (MEPDG), the designer chooses a pavement structure and then analyses the design in details in order to ensure that it meets the criteria of the design, such as roughness, rutting and fatigue cracking. This method predicts the extent of the degradations such as fatigue

cracking, during the selected period of the design. Nevertheless, the basic fatigue model as presented in equation 2.23 does not take into account the addition of RAP. Moreover, no research studies in the area of developing prediction fatigue model for mixtures containing reclaimed asphalt pavement were found in the literature review.

To contribute to knowledge and to promote the usage of RAP in pavement, a specific model to predict the fatigue life of asphalt concrete mixture incorporating RAP based on the basic equation for fatigue life will be investigated.

Moreover, based on a summary of what the literature review implied, we found that there are some weakness needed to be well understood to clarify the confusion found in chapter 2 regarding to last research studies of the performance of recycled mixes in terms of stiffness and fatigue. As we presented in chapter 2, we found that the performance of recycled mixes in terms of stiffness, fatigue, could be better, worse, or similar to that of the corresponding virgin mix. Therefore, it becomes a priority to study and determine the effects that various RAP percentages and RAP introduction process have on asphalt mixtures containing RAP. Hence, this evaluation is of interest for owner and agencies seeking better performance.

3.1.1 Research Methodology

The objectives of this research will be accomplished through the completion of the tasks described below. Figure 3.1 provides the work plan of this research.

3.1.2 Task 1 – literature review

The main objective of this task is to establish the limits of actual state of good understanding RAP use and its effect on asphalt mix characteristic. A comprehensive literature review was conducted to review the following topics:

1) Reclaimed asphalt pavement characteristics;
2) Asphalt recycling methods;

3) Mix design of asphalt mixtures containing RAP;
4) Effect of addition of RAP on complex modulus and fatigue cracking based on last studies; and
5) The most important aspect under the behaviour of visco-elastic material, Fatigue cracking behaviour and characteristic, factors influence resistance to fatigue, and approaches used to predict fatigue failure.

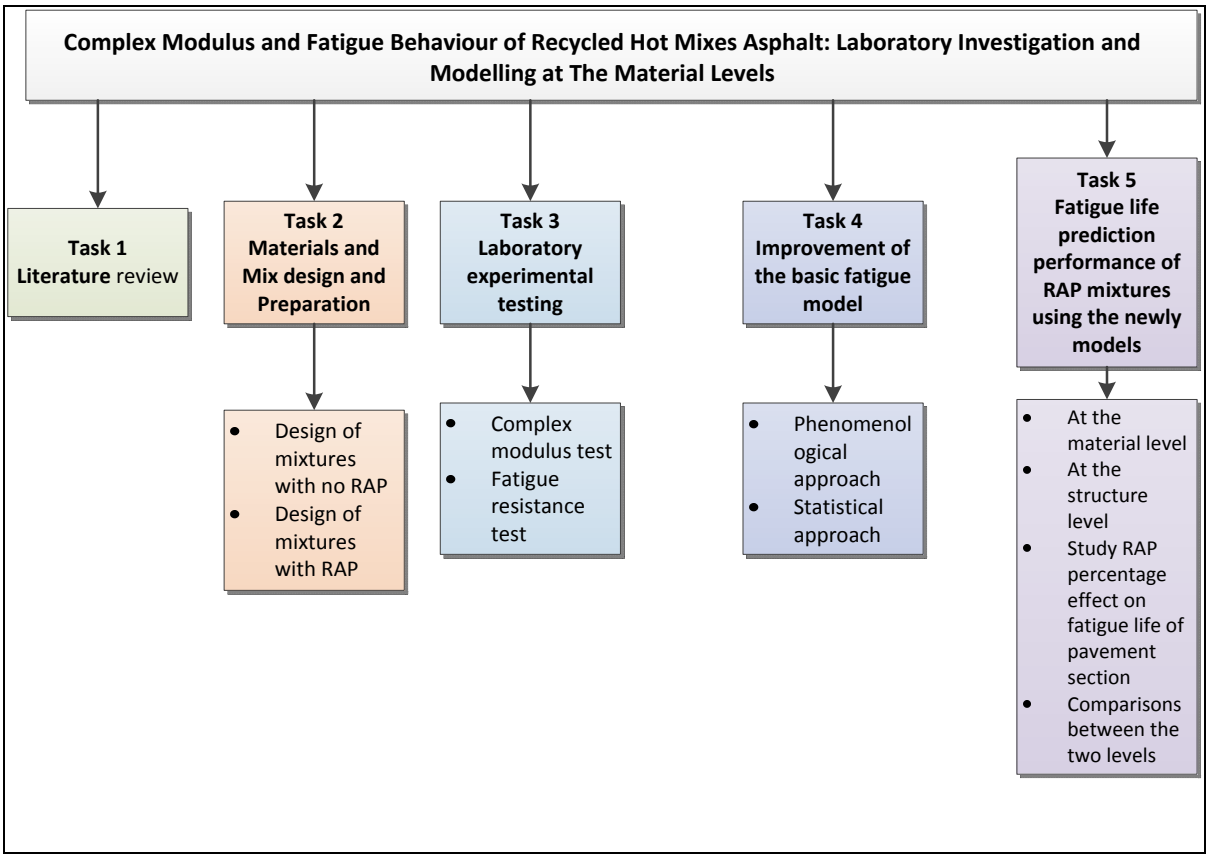

Figure 3.1 Summary of research approach

3.1.3 Task 2 – Materials and Mix design and Preparation

All the eleven mixtures evaluated in this study consisted of the same mix design, prepared based on LC method of Mix Design that was developed by the Minister of Transport of Quebec. The summary of the mixtures will be shown in Table 3.4. Laboratory mixtures use

one aggregate source; two asphalt binder types (PG 64-28 and PG 58-34); one type of RAP source. The Superpave gyratory compactor is used to compact the specimens prepared in this task. For the design, prepared compacted HMA slabs 180-mm by 500-mm by 100-mm to manufacture 75-mm diameter cylindrical specimens for stiffness characterization and fatigue testing. Specimens will be sawed for axial stiffness. More details about the preparation of specimens of each mix are discussed in the subsequent chapter. Designs of mixtures with no RAP and with RAP are described as follows:

3.1.3.1 Design of mixture with no RAP

In the LC design method, the aggregate gradation, the optimum asphalt content, the bulk specific gravity, the maximum theoretical specific gravity, the air voids, voids in mineral aggregate, and voids filled with asphalt of the specimens will be estimated. The LC design method determines all these parameters so we just follow the procedures.

3.1.3.2 Design of mixture with RAP

The main objective of this task was to fabricate RAP mixtures containing different percentages of RAP, and the other factors described before to be used in the mixture characterization testing and analysis in Task 3.2.3. After the design of mixtures for the appropriate aggregate gradation and asphalt content, two processes are used for adding RAP in mixtures in this study: unheated RAP (Cold RAP addition) and RAP heated at 110°C in a microwave. Also the process of aging RAP materials before mixing will be conducted in this task in order to give good simulation of numbers of years of field aging. The performance of the mixtures containing RAP will be compared to mixtures containing 100% virgin material. For this comparison to be reasonably valid, the only difference between the virgin material mixtures and those containing RAP should be the addition of RAP material itself.

3.1.4 Task 3 – Laboratory experimental testing

Recycled HMA mixtures were evaluated according to the complex modulus test and the fatigue resistance test as follows:

3.1.4.1 Complex modulus test

The dynamic complex modulus (E*) was commonly used in the literature to characterize the visco-elastic behaviour of HMA mixtures. In the early 1970s, the asphalt institute selected the dynamic modulus as one of the choice for the modulus test. Roberts et al. (1996) noted that the dynamic modulus is used to determine the stress-strain relationship for a flexible pavement under loading traffic. Dynamic modulus is a key material input required for computing the pavement response that is used in transfer functions for asphalt pavement in the new AASHTO Design Guide for design of New and Rehabilitated Pavement Structures. The modulus of asphalt concrete is dependent on temperature and time frequency of loading; thus the dynamic modulus E* represents time-temperature dependency of asphalt concrete.

We presented in the literature review to the reader that mixture variables such as binder PG grade, RAP source, and RAP content had an effect on the dynamic modulus. However, for some studies in RAP mixture properties, it did not seem to have a significant effect on dynamic modulus. We should bear in mind that we're trying to clarify and explain these important points to produce better understating of RAP mixture's stiffness in this described task.

The oxidative aging of asphalt binders that occurred during the service life (over 15 years) has been proven to affect the mixture stiffness. Because of the presence of the hardened RAP binder (aged) in the RAP, RAP mixes have shown higher in the mixture stiffness. Hence again aged RAP was used to simulate the field aging in this research. This effect of oxidative aging must also contribute to failure by repeated loading (fatigue cracking) through its effect on HMA mixtures' stiffness that governs material response to loading. It also explains why

producing binder that have higher high-temperature superpave grades (and thus provide stiffer mixtures at rutting temperatures) may be prone to premature fatigue cracking, particularly if the binder is very susceptible to oxidative aging under changing environmental and traffic loading conditions.

Basueny, Perraton and Carter (2014) were one of the first to present that the RAP conditioned before adding and mixing with the new virgin aggregates may have an effect on HMA mixture's stiffness. Therefore, because of the importance of mentioned variables mixtures, the effects of RAP laboratory conditioning and the effect of added aged RAP materials on dynamic modulus were studied for different RAP mixes.

Dynamic complex modulus tests will be performed at eight temperatures (-35, -25, -15, -5, 5, 15, 25 and 35ºC) and eight frequencies (0,01, 0,03, 0,1, 0,3, 1,0, 3, 10, and 20 Hz). The construction of master curves was done using the 2S2P1D sigmoidal Model.

3.1.4.2 Fatigue resistance test

The main objective of this research task is to study the impact of RAP content by comparing the laboratory performance of the RAP added mixtures with the performances of the target virgin mixture in terms of fatigue resistance. The modulus studied is based on the whole available RAP mixtures produced in this research. However, the scope of this task (fatigue testing) is limited to evaluate the four mixtures with RAP which are made with binder PG grade 64-28 and RAP added cold at ambient temperature. Cold RAP addition is commonly used in the field pavement projects.

Fatigue cracking tests were conducted on four selected mixtures containing different percentages of RAP made with the same type of binder and by adding cold RAP. Many samples (5 to 8) of the same mixture will be tested in order to measure the fatigue life. Tension-compression test was used for this purpose. All fatigue tests were conducted at 10°C

and 10 Hz, and under strain controlled. The tests will be conducted under different levels of strain.

The graphical representation of the fatigue test results were done by Wöhler curve. This curve will show the relationship between the fatigue life (N_f) (average of the number of cycle at which a decrease of 50% of the initial stiffness and the number of cycle at the end of phase II is achieved) and the level of loading expressed by the strain amplitude in a bi-logarithmic scale.

It is important to note that this study did not examine the repeatability of the fatigue test because of time constraints. However, it has been shown that tension-compression fatigue tests have good repeatability compared to other types of fatigue tests (Baaj, 2002).

The method developed at the laboratory "DGCB" of ENTPE (Di Benedetto, Ashayer Soltani et Chaverot, 1996; Baaj, 2002; Di Benedetto et al., 2004) is used to characterize the damage at the end of phase II. The DGCB method aims at taking into account artefact effects occurring mainly (but not only) during phase I to correct the reversible part due to artefact effects. From the previous finding, a method proposed by Di Benedetto (Tapsoba, Sauzéat et Di Benedetto, 2013) is proposed to predict fatigue life, when considering only the 300 000 first cycles of any test.

3.1.5 Task 4: Improvement of the basic fatigue model

The fatigue behaviour of a specific mixture can be characterized by the slope and relative level of the stress or strain versus the number of load repetitions to failure and can be defined by a relationship in the basic fatigue model form (Perraton, Di Benedetto et Carter 2011) :

$$N_f = k_{1,\theta_{test}}(\varepsilon_t)^{-k_2}\left[\frac{|E^*_{\theta_i}|}{|E^*_{\theta_{test}}|}\right]^{-k_3} \quad (3.1)$$

With $k_{1,\theta_{test}}$ corresponding to the life duration of the mix for the applied deformation equal to 1 μm/m at the fatigue test temperature (θ_{test}) (10°C), and $|E^*_{\theta_i}|$ and $|E^*_{\theta_{test}}|$ correspond respectively to the norm of the complex modulus at the considered temperature (θ_i) and at the test temperature. Generally, tests are done at (10°C). The coefficient k_3 represents the slope of the relationship $k_{1,\theta_{test}}$ versus $log|E^*_{\theta_i}|$.

It is notable that the ratio of the stiffness at θ_i to the stiffness at θ_{test} will be then equal to 1,0. It means that the stiffness has no effect on the fatigue life prediction and the basic fatigue model will be in the form:

$$N_f = k_{1,\theta_{test}}(\varepsilon_t)^{-k_2} \tag{3.2}$$

Often, fatigue tests results show that the fatigue lines, expressed by Wöhler curves, for different mixtures are assumed to be parallel, or close to be, as shown in Figure 3.2. Moreover, according to French Design Manual for Pavement Structure (Setra-LCPC, 1994) ε_6, the value of strain level that leads to a fatigue life of 1 000 000 cycles, is different for different mixes, but the slope of Wöhler curve is kept constant as shown in Table 3.1.

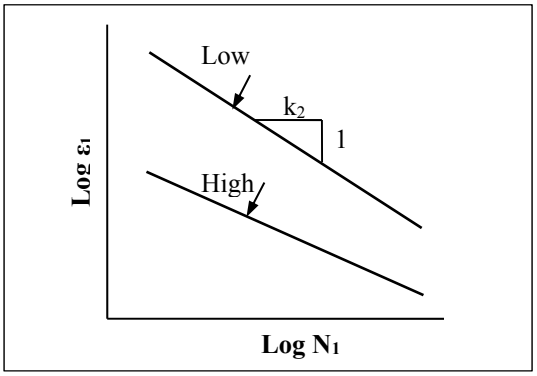

Figure 3.2 Relation between strain and number of repetitions to failure
Taken from Yang (2004)

Table 3.1 Properties of bituminous bound graded aggregate
Taken from Setra-LCPC (1994)

Class	Bituminous bound graded aggregate 1	Bituminous bound graded aggregate 2	Bituminous bound graded aggregate 3
Modulus (MPa)	7 000*	9 000	9 000
$\varepsilon_6(10^{-6})$	70*	80	90
$-1/k_2$	5	5	5

* indicate values, not specified by the standard for class 1 road base asphalt concrete

Consequently, based on the literature review, it is often assumed that the slopes of fatigue curves are constant. Here, the phenomenological approach was used in this study to improve the basic fatigue model to predict fatigue performance of RAP mixtures. To do this, two scenarios, in this research, will be presented:

Scenario 1 assumes the fatigue slope lines are parallel and presents, as a first approximation, the RAP effect on the fatigue behaviour of asphalt material with a single shift factor, denoted here as *SF*, applied on the k_1 factor (equation 3.3). The k_2 factors will be directly defined by the specific type of the control asphalt material without RAP.

$$N_f = SF \times k_{1,\theta_{test}}(\varepsilon_t)^{-k_2}\left[\frac{|E^*_{\theta_i}|}{|E^*_{\theta_{test}}|}\right]^{-k_3} \tag{3.3}$$

Where:

SF Shift factor of %RAP

Scenario 2 is proposed to correct the slope of the fatigue line (k_2) by adding a shift factor to k_2 to take into account the variation of the fatigue slope lines and the effect of RAP content. Secondly, we propose to use the statistical approach to develop statistical fatigue prediction equations that comes from the fitting of all our data measurements to fit the experimental

data. Stat graphics program was used to perform data analysis. The primary advantage of these equations or models is to eliminate the need for producing the recycled mixture to be tested for fatigue resistance for our source of RAP. However, in order to overcome the limitations of those existing models, there is need to implement and to use this approach in further studies for other RHMA mixes.

It is worth to mention that the use of high percentages of RAP (high RAP) in the mixtures reduces the amount of new asphalt binder based on the amount of binder contributed by the RAP. It is therefore questionable to use in our model the coefficients of the fatigue law (k_1 and k_2) of the virgin mix without change. This is because the characteristics of the asphalt blend may not represent the specific values of k_1 and k_2 for the virgin mix.

Also, our model can't be used for mixtures containing 100% RAP without virgin binder since its behaviour can't be linked to a virgin mix._Based on that, our attempts for improvement process will concentrate and conduct on two RAP content cases to see if it is possible to improve the model to embrace the incorporation of RAP. Particularly, they are actually made using high percentage and/or intermediate contents of RAP materials. These two cases are:

- If the amount of RAP in the mix is less than or equal to 25%;
- If the amount of RAP in the mix is less than or equal to 40%.

As we presented earlier, we studied only four RHMA mixtures to predict fatigue cracking. However, we know that mix preparation and components can have some influences on the level of improvement in the fatigue properties because of mix stiffness estimated and viscoelastic properties of the mix. However, to use the model to predict the fatigue life at different temperatures rather than our testing temperature (10°C), we have to consider the value of the stiffness ratio in the basic fatigue model shown in equation 3.2. To do this, we assume to use the results of complex modulus for other samples of the same mixes that have been tested for fatigue to determine the modulus values at different required temperatures. By doing this, we are able to predict the fatigue life of our mixtures at any other temperature

than the testing temperature (10°C). In this case, their N_f values have been obtained from a limited amount of data, based on the fatigue experimental coefficients of the conventional asphalt mix, and the most important factors adjusted or shifted to account for the RAP content, are believed to be realistic. However, the applicability of this assumption in the fatigue prediction may be incorrect in some cases, especially for some specific types of RAP source. Further studies are needed to confirm or to validate this model's assumptions.

It is to be noted that in that case, we do not need to use the stiffness values at fatigue test temperature (10°C) because the stiffness values in the ratio are the same. Of course, there is value for stiffness ratio only when the test temperature is not equal to 10°C.

3.1.6 Task 5: Fatigue life prediction performance of RAP mixtures using the new models

The mixtures were evaluated for their resistance to fatigue performances and dealt with at two different levels. At the material level, the fatigue predictions of the materials are defined at different suggested temperatures by the help of the incorporation of mix stiffness in the newly fatigue life prediction model. At the level of structure behaviour, model applications will be mention for fatigue prediction and hence a study of the effect of RAP percentage on pavement fatigue life was evaluated.

3.2 Experimental work

The most common type of asphalt recycling across Canada is the use of processed RAP in batch, drum, and drum-batch hot-mix plants to produce recycled hot mix (RHM), and is now considered standard asphalt technology (Emery, 1993). In Canada, the maximum amount of RAP permitted in hot mix asphalt (HMA) varies from province to province. Most provinces permit RAP to be used in HMA, provided testing ensures that the RHM meets all specification requirements for asphalt concrete. For example, Ontario limits the amount of RAP in surface course HMA to 15% maximum with 30% in conventional binder course mixes and up to 50% in certain situation subject to confirmatory testing, whereas Quebec

accepts up to 15% RAP in RHM (National Research Council of Canada, 2005). However, we went up to 40% RAP because of the persuasive combination of environmental, financial and technical advantage when the concentration of RAP in today's new road constructions and road preservation projects will be increased. Researches need to ensue within the industry and conclusions need to become readily available to increase RAP content in the mixture

It is being reviewed that asphalt's fatigue characteristics play an important role in pavement design. Ultimately they govern the required thickness of asphalt to structurally carry heavy traffic. The thickness of the asphalt layer is a major contributor to the cost of pavement construction. Fatigue behaviour of asphalt mixtures is regarded as one of the most important modes of distress in a pavement subjected to repeated traffic loading and stress (Xiao, 2006). With respect to the complexity of an asphalt mixture, fatigue is related to the properties of aggregate, asphalt, and asphalt aggregate interaction. Fatigue predictive models were developed to predict the fatigue life of asphalt mixtures in the laboratory and even in the field. They are often used in research and industry area.

The fatigue study of HMA containing RAP is essential to properly characterize the behaviour of those mixes. Because no specific fatigue models for mixes with RAP can be found in the literature, the past basic fatigue predictive model will be utilized to make this fatigue study possible.

For this research program, two different virgin asphalt binders (PG 64-28, and PG 58-34), one virgin aggregate, one RAP source, four RAP dosage percentages (0, 15%, 25%, and 40%) will be used to improve the fatigue predictive model. The RAP materials are provided by commercial asphalt company. Moreover, to deal with RAP materials for pavement design, it is also important to evaluate the effect of RAP on the stiffness of the material. A total of eleven different asphalt mixtures incorporating RAP in GB-20 will be fabricated to perform complex modulus and four mixes were selected to evaluate the impact of RAP content on the fatigue cracking behaviour. It is important to note that the GB-20 hot mix asphalt is one of

the most commonly mix used in Quebec for base course. Figure 3.3 shows the proposed experimental design flowchart which will be used in this research.

LC mix design will be used for preparation of complex modulus and fatigue testing specimens. Cored specimens will be used for this purpose which includes at least five specimens for each fatigue test. Based on the results, the predictive improvement to the basic model will be conducted.

A nominal maximum size 20 mm LC mixture will be used for the mix design in this study. The GB-20 LC criteria and compaction specifications is shown in Table 3.2.

Table 3.2 Characteristics of GB-20 mixture developed under the LC method
Taken from Langlois (2006)

Sieve	28 mm	**% Passing**	100
	20 mm		95-100
	14 mm		67-90
	10 mm		52-75
	5 mm		35-50
	2,5 mm×		-
	1,25 mm×		-
	630 µm×		-
	315 µm×		-
	160 µm		-
	80 µm		4,0-8,0
Percentage of fibres (%)		-	
Volume of effective asphalt (V_{be}, %)		10,2	
Voids at 10 gyrations (N_{ini})		11%	
Voids at 120 gyrations (N_{des})		4-7%	
Voids at 200 gyrations (N_{max})		≥ 2%	

× Recommended restricted zone

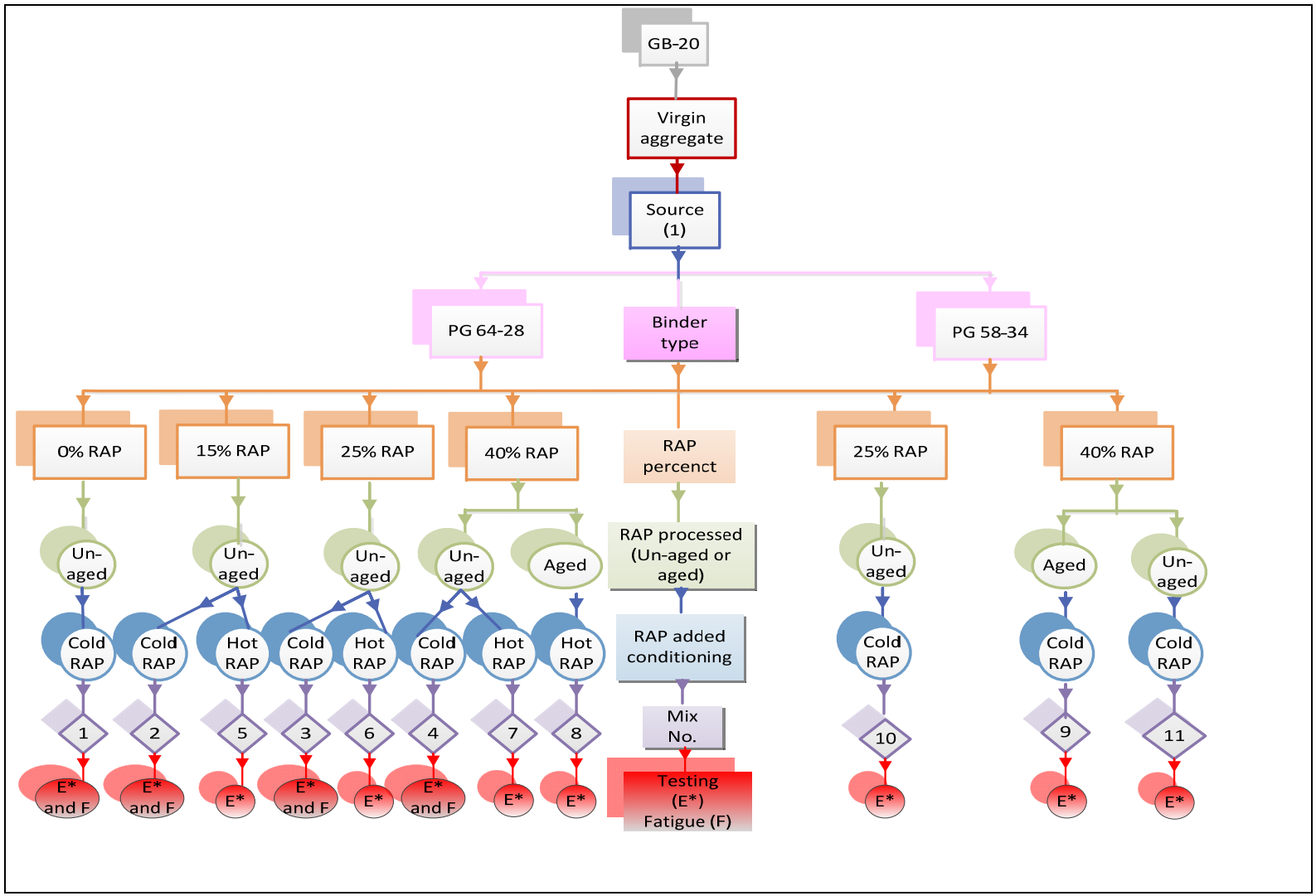

Figure 3.3 Experimental design flow chart

3.2.1 RAP sampling

To reduce RAP variability that results in a loss of quality control for a recycling project, proper RAP sampling is mandatory. Sampling of RAP can be done from the roadway (by coring before the pavement is milled), or from a stockpile. For laboratory RAP testing, it is necessary to obtain samples that accurately reflect the material which is available for use. It is necessary to sample from several locations when sampling a pile to avoid taking the entire sample from a segregated area (McDaniel et Michael Anderson, 2001). The purpose of sampling plays an important role to indicate the size of sample needed. LC specimens are like Superpave specimens which are much larger than Marshall or Hveem specimens, so more materials will be needed when doing LC mix design.

3.2.2 Volumetric properties of the mixtures

The volumetric proportion of asphalt mixture that plays a key role in LC mix design method and affect the asphalt mixture behaviour. However, these volumetric properties are only verified for the virgin binder and the aggregates (Xiao, 2006). The LC mix design system does not address the volumetric analysis of RAP, and no guidelines on such analysis are available at that time. But recently, certain researchers have conducted several studies to give some recommendations and guidelines for these materials (NCHRP 2001, FHWA 1997). The basic information about the principle volumetric properties relationship for asphalt mixture is presented in the literature (Langlois, 2006).

3.2.3 RAP insertion in mixes

The mixtures were prepared using two different RAP conditioning processes. RAP materials were added according to the following two processes: 1) Hot recycling with cold RAP addition, and 2) Hot recycling with reheated RAP addition.

The duration of the mixing process and the temperature at which it is done are two very important aspects that were controlled in this study. More details are giving in the next section.

Before the blending process, an artificial aging procedure was performed on a specific amount of RAP materials to be more representative of on-site properties. Age hardening of bitumen is a major factor that causes embrittlement of the asphalt material. Past research has determined that oxidation is the main aging factor (Wu, 2006). This occurs during both the mixing of the hot asphalt, and during the field life of the pavement.

Short term aging that occurs during mixing did not need to be simulated on this project as the specimens undergo a hot mix process anyway. To simulate long term aging of the RAP materials, the RAP went through an aging process known as long term oven aging. The aging process is conducted using the test developed by Carter and Stroup-Gardiner (2007) to simulate long term aging of the RAP materials. This method is conducted by placing samples on a flat pan, stored in a 55°C oven for three months. Afterwards, it can be used for RAP mixtures that take into consideration the effect of hardening. Experience has shown that this is a good simulation of to six years of field HMA at critical pavement temperature.

3.2.3.1 Hot recycling with cold RAP

In the first process, the new aggregate is superheated to 300°C in the oven prior to mixing with the RAP for about 5 minutes. The cold RAP materials is added to the superheated aggregate and mixed until the specified mixing temperature is reached. Then, the virgin binder is added, and the mixing continues until the aggregate is thoroughly coated by the binder. For all the mixes made with cold RAP, the RAP and virgin aggregate blending time is needed to be reached the desired mixing temperature and therefore it varied with the amount of RAP added. In this study, the time needed for each mix to reach to the mixing temperature (the blending time) is different because of the temperature difference between the superheated aggregates and the RAP. It took about 1 minute to reach to the mixing

temperature when 40% RAP was added and it actually took about 3 minutes and half when 15% RAP was added. It should be noted that the required time will increase if the moisture content of the RAP increases.

Maximum duration of the mechanical mixing of the components during the manufacture of the bituminous mix in laboratory is specified in standard EN 12697-35 (AFNOR, 2007). If the studied formula does not contain recycled mixtures, the maximum duration of mixing of the components is 3 minutes. This duration is extended to 5 minutes when recycled materials are used. The minimum duration of mixing is left to the appreciation of the operator with the condition that the aggregates are completely coated with binder and which the mixture is visually homogeneous. More information on the mixing temperature is given in section 3.2.4.

Finally, the resulted blend is heated for two hours, as short term aging, prior to compaction. It should be noted that this process is referred to, in the literature as presented in section 1.12.2, as hot recycling using batch plants without a separate heating drum.

3.2.3.2 Hot recycling with reheated RAP

In the second process (hot recycling with reheated RAP), the RAP materials are preheated in a microwave to 110+5ºC. Heating time is depending on RAP amount. By increasing the amount of RAP, a longer heating time is needed. Afterwards the RAP is mixed with overheated virgin aggregate (180°C). Then, the virgin binder that had been preheated to 155ºC is added to the mixture so that the end temperature is about 160ºC. When adding preheated RAP mixture, the amount of blue smoke emission that can occurred during mixing is reduced. This process is referred to, in the literature, as hot recycling using drum mix plants with parallel flow as presented in section 1.12.1. This practice is specified in the standard NF EN 12697-35 (AFNOR, 2007) with the difference that our RAP was heated in a microwave rather than heated it in the oven.

3.2.4 Mixing temperature

According to the Europe standard NF EN 12697-35 (AFNOR, 2007), the temperature of the virgin aggregate should be increased with the increased amount of cold RAP added. This note thus specifies that it is necessary to calculate the temperature of virgin aggregate. Thus, by mixing the components, the recycled manufactured mixture is at the desired temperature.

In the case of adiabatic heat exchange between solid components, as in the case of cold RAP added to hot aggregates, it's possible to use thermodynamics' equation to evaluate the temperature of the overheated virgin aggregates (T_{VA}) in order to have the desired resulting mix temperature (T_M) as shown here (Navaro, 2011):

$$T_{VA} = T_m + \frac{Cp_B \times \left[C_{VB}^{Rac} \times (T_m - T_{VB}) + C_{RapB}^{Rac} \times (T_m - T_{Rap})\right] + Cp_A \times C_{RapA}^{Rac} \times (T_m - T_{Rap})}{Cp_A \times C_{VA}^{Rac}} \quad (3.4)$$

$$C_{VB}^{Rac} = \frac{1}{Y} \times \left(\frac{1 - C_{RapB}^{Rap}}{C_{RapA}^{RacA}} \times \frac{C_{RacB}^{Rac}}{1 - C_{RacB}^{Rac}} - C_{RapB}^{Rap} \right) \quad (3.5)$$

$$C_{VA}^{Rac} = \frac{1}{Y} \times \left(1 - C_{RapA}^{RacA}\right) \times \frac{1 - C_{RapB}^{Rap}}{C_{RapA}^{RacA}} \quad (3.6)$$

$$C_{RapA}^{Rac} = \frac{1}{Y} \times \left(1 - C_{RapB}^{Rap}\right) \quad (3.7)$$

$$C_{Rapb}^{Rac} = \frac{1}{Y} \times C_{RapB}^{Rap} \quad (3.8)$$

$$Y = C_{RapB}^{Rap} + \left(1 - C_{RapB}^{Rap}\right) + \left(1 - C_{RapA}^{RacA}\right) \times \frac{1 - C_{RapB}^{Rap}}{C_{RapA}^{RacA}} + \left(\frac{1 - C_{RapB}^{Rap}}{C_{RapA}^{RacA}} \times \frac{C_{RacB}^{Rac}}{1 - C_{RacB}^{Rac}} - C_{RapB}^{Rap} \right) \quad (3.9)$$

Where:

Cp_A Heat capacity of Aggregate (800 $J.kg^{-1}.K^{-1}$);

Cp_B Heat capacity of Binder (1992 $J.kg^{-1}.K^{-1}$);

C_{VB}^{Rac} Mass fraction, the concentration, of virgin binder (VB) on the total reclaimed asphalt mixture (Rac);

C_{VA}^{Rac} Mass fraction, the concentration, of virgin aggregate (VA) on the total reclaimed asphalt mixture (Rac);

C_{RapA}^{Rac} Mass fraction, the concentration, of RapA reclaimed aggregate on the total reclaimed asphalt mixture (Rac);

C_{RapB}^{Rac} Mass fraction, the concentration, of RapB reclaimed binder on the total reclaimed asphalt mixture (Rac); and

C_{RapA}^{RacA} Mass fraction, the concentration, of RapA reclaimed aggregate in the Rac aggregates.

The calculations for the T_{VA} corresponding to the various studied mixtures to reach to the manufacture temperature (160°C) for the two processes discussed before are presented graphically in Figures 3.4 and 3.5. However, in our work, for the first process, the virgin aggregate was superheated to about 300°C where RAP is typically added cold. This temperature was kept constant for various mixtures of different percentages of RAP. As it can be seen on Figure 3.6, a waiting period was needed before adding the virgin binder since the resulting temperature was over the desired mixing temperature even for the mixes with 40% cold RAP, It is important to note that we continued mixing the mixture for a few minutes during the waiting time until reaching the desired temperature.

It should be noted that the mixing durations are about 200 sec for the mix with 15% RAP, 150 sec for the mix with 25% RAP, and 50 sec for the mix with 40% RAP. For our case, the duration is defined as the time required reaching the manufacture temperature (160°C) from the point where RAP was added to the virgin aggregate prior to the point where the binder is added to that mix. This method is experienced based but it seems to work according to

NCAT (National Center for Asphalt Technology). Basically, that method is more used for hot mix recycling in central plants (Prithvi et Rajib, 1997), but in the other plants, the virgin aggregate must be heated based on the amount of RAP and the desired temperature of the final mix (Brock et Richmond, 2007).

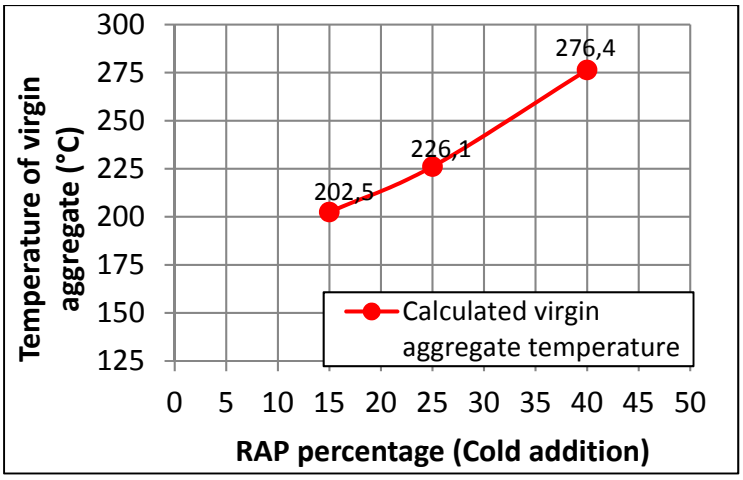

Figure 3.4 Evolution of virgin aggregate temperature when adding cold RAP with different percentages to reach to the target mixing temperature of 160°C

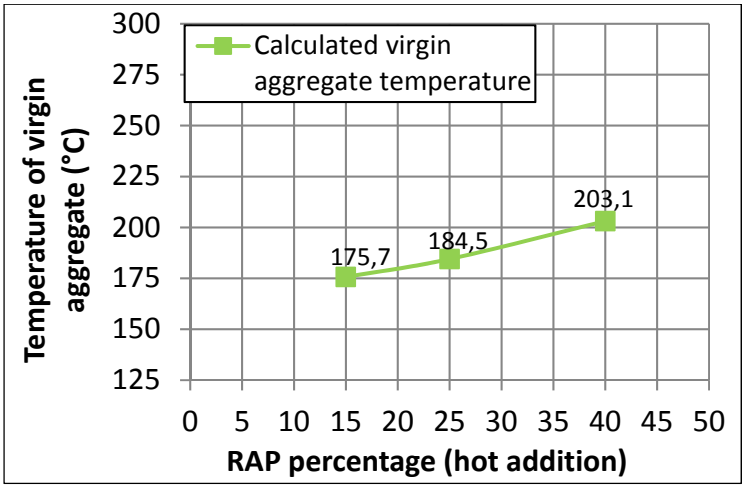

Figure 3.5 Evolution of virgin aggregate temperature when adding RAP heated in a microwave at 110°C with different percentages to reach to the target mixing temperature of 160°C

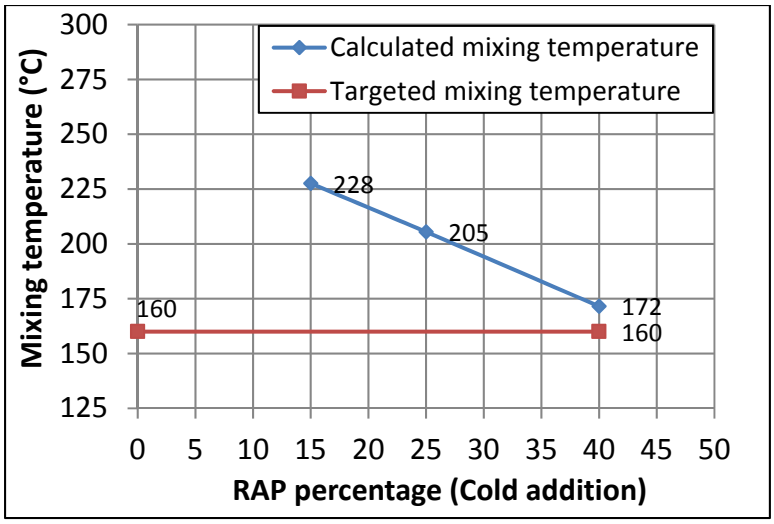

Figure 3.6 Evolution of the calculated mix temperature when adding different percentages of cold RAP to overheated (300°C) virgin aggregate compared to the targeted mix temperature

It is worthy to note that to avoid increasing the temperature of virgin aggregate in a plant, the amount of RAP was limited to 50% as a way to avoid the increasing possibility of the dryer and other component from the higher temperatures (Brown, 1983). For the mixes with microwave heated RAP a similar conclusion can be drawn (Figure 3.7). A very short blending time is needed for the mix to reach the targeted temperature. However, for mixes with 25% or 40% RAP, the calculated mixing temperature is below the target. For the 40% RAP, the actual mixing temperature measured in the laboratory was about 140°C instead of 160°C and in the 25% RAP it was not so far from the target (150°C).

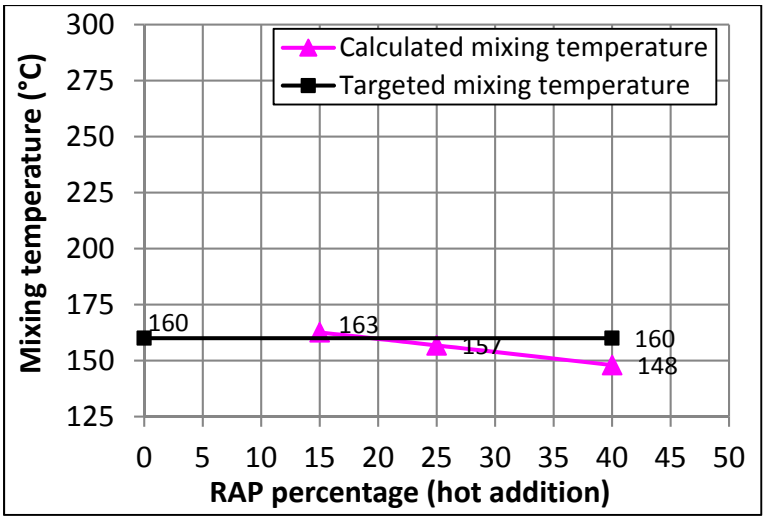

Figure 3.7 Evolution of the calculated mix temperature when adding microwave heated RAP (110°C) to heated virgin aggregate (180°C) compared to the targeted mix temperature

3.2.5 Mix selection

In this research, the impact of different factors such as the RAP content, the binder grade, the RAP conditioning process and the aging of RAP on the mixture's stiffness are studied. If a full factorial study was conducted, 26 different mixes would be tested (Table 3.3). In order to facilitate our work and to reduce time, this study investigates eleven laboratory-produced mixtures that were selected for testing for complex modulus in a way that it considers all factors to provide a wide variation in the different mixtures. These mixtures have the series number as follow: 1; 3; 4; 11; 12; 15; 19; 20; 21; 23; 24 (see Table 3.3).

Because of the very high amounts of time needed to do fatigue test, only four mixes out of those eleven were selected for that part of the study. Those mixes are the ones with the PG 64-28 binder with 0%, 15%, 25% and 40% of RAP added cold to the mix. The experimental design flow chart, as shown in Figure 3.3, was used for this study. Also, the summary of the mixtures used in this study is shown in Table 3.4. The mix designations given in the last column of the table is used throughout the thesis to identify the eleven mixtures. It is better to give an example of the designation (ID- sample) of each mixture to give good understanding

of these mixtures. For example, RAP1528CU means that the mixture is prepared with a PG 64-28 binder and 15% unaged RAP, typically added cold to the HMA.

Table 3.3 The possible laboratory-produced mixtures

Mixture series	RAP %	Type of binder	RAP process	RAP added conditioning		RAP aging	
		PG 64-28	PG 58-34	Cold	Hot	Unaged	Aged
1	0	x					
2			x				
3	15	x		x		x	
4		x			x	x	
5		x		x			x
6		x			x		x
7			x	x		x	
8			x		x	x	
9			x	x			x
10			x		x		x
11	25	x		x		x	
12		x			x	x	
13		x		x			x
14		x			x		x
15			x	x		x	
16			x		x	x	
17			x	x			x
18			x		x		x
19	40	x		x		x	
20		x			x	x	
21		x		x			x
22		x			x		x
23			x	x		x	
24			x		x	x	
25			x	x			x
26			x		x		x

Table 3.4 Summary of asphalt mixtures

Mix No.*	Binder	RAP source	% RAP	Process	Aging	Designation
1	PG 64-28	(1)	0		Not applicable	RAP028
2	PG 64-28	(1)	15	Cold RAP	Unaged	RAP1528CU
3	PG 64-28	(1)	25	Cold RAP	Unaged	RAP2528CU
4	PG 64-28	(1)	40	Cold RAP	Unaged	RAP4028CU
5	PG 64-28	(1)	15	Hot RAP	Unaged	RAP1528HU
6	PG 64-28	(1)	25	Hot RAP	Unaged	RAP2528HU
7	PG 64-28	(1)	40	Hot RAP	Unaged	RAP4028HU
8	PG 64-28	(1)	40	Cold RAP	Aged	RAP4028CA
9	PG 58-34	(1)	40	Cold RAP	Aged	RAP4034CA
10	PG 58-34	(1)	25	Cold RAP	Unaged	RAP2534CU
11	PG 58-34	(1)	40	Cold RAP	Unaged	RAP4034CU

* It is important to note that laboratory fatigue test were performed on the first four asphalt mixtures and complex modulus tests were performed at all.

CHAPTER 4

MATERIALS CHARACTERIZATION FOR MIX DESIGNS AND LABORATORY TESTING

4.1 Introduction

The various stages of material characterization were divided into multiple tasks in chronological order which were carried out in laboratory at the time of research operation. These various tasks are briefly discussed in the following paragraphs.

The tests' descriptions in this chapter are divided into four sections: 1) RAP materials characterization, and virgin materials (binder & aggregates) characterization, 2) Asphalt mixtures design, 3) Specimens fabrication, and 4) Laboratory testing. In the first section, the properties of the materials used in this study are presented and analyzed. RAP samples were evaluated in terms of aggregate gradation before and after extraction, aggregate specific gravity, and RAP binder content (by ignition and by solvent). The binder was recovered from RAP and the rheological properties were evaluated using a dynamic shear rheometer and a bending beam rheometer in accordance with the procedure AASHTO TP5-98 (AASHTO. 1998), and AASHTO test method T 313 (AASHTO. 2008). Likewise, the properties of the virgin aggregates and asphalt binders used in this study are presented and explained. All the information on materials characterization is provided below in section 4.2.

The design of asphalt mixtures consisting entirely of virgin materials and various percentages of RAP are presented in section 4.3. The goal of the mix design is to design mixtures that meet specific criteria for the performance evaluation portion of this research. The LC mix design procedure and specifications were used for this purpose. 11 different recycled mixes were considered in this study (20 mm nominal maximum aggregate size). These mixtures were designed at 4 different RAP contents; 0% RAP (100% virgin materials), 15% RAP, 25% RAP, and 40% RAP. One type of aggregate with different fractions and two types of binder (PG64-28, PG58-34) were used for the mixtures. Inclusion of RAP into the hot mix

asphalt was Cold or Hot. There are two kinds of RAPs that were used for the asphalt mixtures (unaged and aged RAP). As shown previously in Figure 3.3, some RAP materials are artificially aged in the laboratory in order to simulate the performance of paving mixtures containing RAP using traditional laboratory aging technique provided by Carter and Stoup-Gardiner (2006).

Section 4.4 presents specimens fabrication. The rectangular slab specimens of asphalt mixtures were fabricated with the rolling wheel compacts (LCPC wheel tracker). The slab specimens were compacted using a slab compactor to 5% air void. The size of the slab samples was 500 mm in length, 180 mm in width, and 100 mm in thickness. Compacted cylindrical specimens were cored in the thickness of the slab with a diameter of 75 mm and a height of 120 mm (ϕ 75mm x H 120mm) for mechanical testing. In addition the specimens were sawed. This meant that a flat smooth surface was achieved.

Section 4.5 incorporates laboratory setup and a basic testing overview. Two mixture tests were investigated and were successfully used in this study including complex modulus and fatigue test. In this part of this study, a brief presentation of the test methods is presented. After that, some details about data analysis are given.

4.2 RAP material characterization

The tests in this section are:

1) RAP material preparation;
2) Sieve analysis of the RAP aggregate before extraction;
3) Measurement of specific gravity of RAP;
4) RAP extraction tests;
5) Sieve analysis of the recovered aggregate from RAP after extraction;
6) Extraction and recovery of asphalt binder;
7) Physical properties of the recovered binder;

8) Physical properties of virgin aggregate; and
9) Properties of virgin binder.

It is notable that the preparation of the RAP material in the laboratory for different tests is an important task.

4.2.1 RAP material preparation

Around 700 to 800 kg of RAP materials were used in this project. RAP was sampled at an asphalt plant near Montreal. The sampling was done in accordance with testing method LC 21-010 (MTQ, 2006): *Échantillonnage*. Afterwards, the RAP was stored in 30 kg buckets in the lab.

In the laboratory, 2 buckets of 30 kg each were homogenized by mixing with the aid of a concrete mixer (Figure 4.1). The two buckets of RAP were then deposited on a clean, non-absorbent surface. The material was homogenized manually with a square head shovel before being divided by quartering (Figure 4.1). After that, the material was divided into four equal quarters (quarters: 1, 2, 3, and 4) before being recombined (quarter 1 with the 3rd quarter, and the second quarter with the 4th). The separated samples (30 kg each) were placed in sealed plastic buckets for storage until needed for different laboratory tests. The material in the buckets was separated mechanically on when needed.

In order to be sure that we always have the same material, we checked the gradation for a certain number of samples as seen in the paragraph below. It should be noted that the sample size is based on the test for which the material is needed. For the gradation analysis, a 1,0 kg sub sample was split from the sample, and for the mix design testing, RAP materials from each storage bucket were split into 8 equal portions using the riffle splitting.

Figure 4.1 RAP material preparation

As illustrated in Figure 4.2, we selected 2 buckets ‘A and B’ from the whole set of buckets available, and we did the blending as explained previously to obtain the recommended representative samples. The homogenous bucket ‘A’ was then passed through a sample splitter several times by the use of open bin riffle splitter (Figure 4.3). At the beginning, it was splitted into 8 equal portions (3750 grams). We repeated the previous process with the other bucket ‘B’. These small splits were further used for sieve analysis test. Two random selected samples were obtained from the previous blend for using in the gradation test. It means that we randomly select one sample from the first homogenous bucket (bucket A) and one sample from the second bucket. To obtain other 2 samples for the sieve analysis test, we did the previous process in buckets ‘C’ and ‘D’ to obtain 2 other samples. We repeated again the procedure in buckets ‘E’ and ‘F’ to obtain 2 more samples. We continued this process randomly until we obtain the proper number of samples of given size. Those samples were used for quality control (QC.) and our gradation test results showed that our random sampling is appropriate, which means that all the materials are homogenous. The rest of the

materials were placed in small plastic bags (3,75 kg) for doing our testing program and to continue our research work.

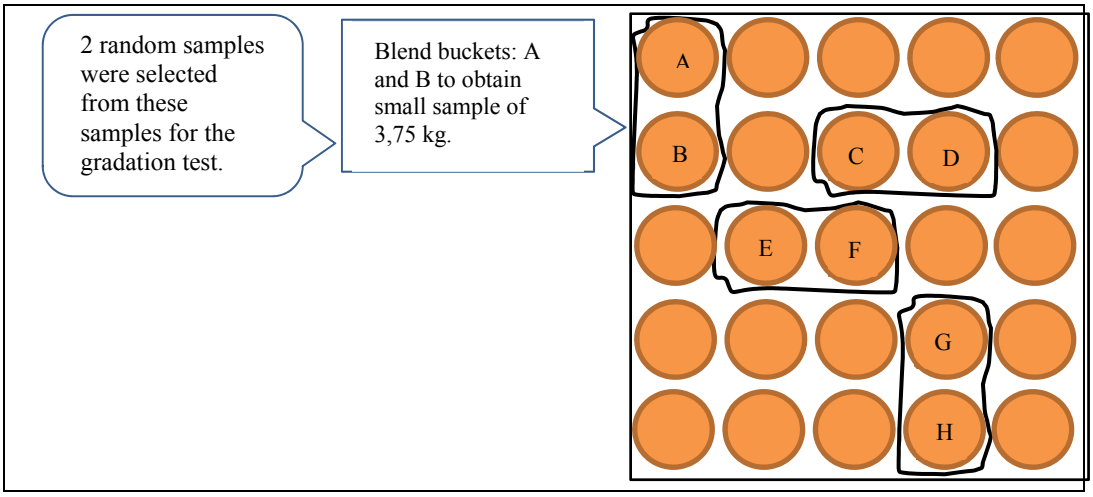

Figure 4.2 Top view buckets pattern of RAP materials capable of holding approximately 30kg

Figure 4.3 A riffle splitter used for RAP sample splitting

4.2.2 Sieve analysis before extraction

The gradation of the RAP, as received, hereafter called black curve, was determined with the LC 21-040 method (MTQ, 2003). As explained previously, RAP was batched to obtain 8 samples of 1000 grams each of oven dried samples (110°C). Wet sieve was not done because RAP has a lot of fines. This test was used to determine the particle distribution of the black curve of the RAP material. Black curves are plotted in Figure 4.4 and reported in Table 4.1. Results showed that the RAP as received contained 43% of coarse aggregate, retained on the 5-mm sieve and, 89% was retained on the 0,630 mm before extraction. The nominal maximum size (NMSA) of the RAP is 10 mm.

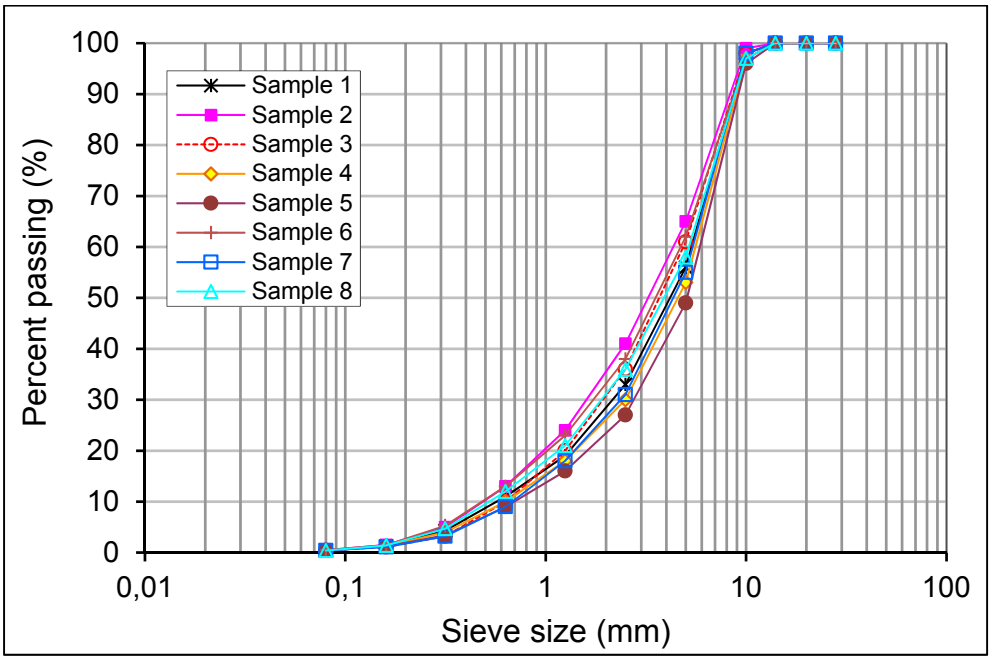

Figure 4.4 Random RAP gradation before extraction

4.2.3 RAP aggregate specific gravity

It is important to obtain the bulk specific gravity (G_{sb}) of the combined aggregates because it is one of the inputs for calculating voids in mineral aggregate (VMA). The G_{sb} of the combined aggregates is determined from specific gravities tests conducted on samples from

each component in the mixture. The G_{sb} of the RAP aggregate was estimated using the recommended methodology in NCHRP Report 452 (McDaniel et Michael Anderson, 2001). The estimated G_{sb} values were calculated from a maximum specific gravity (G_{mm}) tests on the RAP samples (the G_{mm} method).

Table 4.1 Data from sieve analysis test of the RAP material before extraction

Sample no.	**1**	**2**	**3**	**4**	**5**	**6**	**7**	**8**	**Average**	**Std. Dev.**
RAP blend sample buckets	**A and B**		**C and D**		**E and F**		**G and H**			
Homogenous bucket	**A**	**B**	**C**	**D**	**E**	**F**	**G**	**H**		
Sieve size (mm)	Percent passing									
28	100	100	100	100	100	100	100	100	100	0,00
20	100	100	100	100	100	100	100	100	100	0,00
14	100	100	100	100	100	100	100	100	100	0,00
10	98	99	98	97	96	97	98	97	98	0,87
5	56	65	61	53	49	62	55	58	57	4,87
2,5	33	41	36	30	27	38	31	36	34	4,60
1,25	19	24	20	18	16	23	18	21	20	2,52
0,630	11	13	10	10	9	13	9	12	11	1,54
0,315	4,3	5,0	4,0	4,0	3,4	5,3	3,2	4,7	4,1	0,77
0,160	1,3	1,5	1,3	1,3	1,2	1,5	1,1	1,4	1,3	0,15
0,080	0,4	0,5	0,5	0,5	0,4	0,5	0,4	0,4	0,4	0,05

In the G_{mm} method, the RAP G_{mm} and the asphalt content of the RAP were used to estimate G_{sb}. The effective specific gravity of the RAP aggregate (G_{se}) can be calculated based on the G_{mm} and asphalt content values. We used the two equations 1.1 and 1.2 to compute the G_{se} value. It is important to note that the value of specific gravity of RAP binder (G_b) was assumed to be 1,020, and the value of absorbed binder (P_{ba}), to be 1,4% in this study. This fits with what was found in the literature, where 1,5% is assumed (McDaniel et Michael Anderson, 2001).

The RAP maximum specific gravity (G_{mm}) was measured by performing the G_{mm} test (LC 26-045 – MTQ, 2008) and it was found to be 2,602. Then, the estimated G_{sb} of the RAP aggregate can be calculated to be 2,679.

4.2.4 RAP binder content by ignition oven

The amount of asphalt binder present in the RAP samples was determined by LC 26-006 method (MTQ, 2010): ''*Détermination de la teneur en bitume par ignition*''. Three random samples of RAP were assigned a number and that number was randomly selected for testing in order to reduce any procedural bias in the results of the test. In this test procedure, a RAP sample (1000 grams) is heated to approximately 540°C for 45 minutes and the asphalt binder is burned from the sample by ignition. After that, the aggregate is cooled down to room temperature. The asphalt content is determined from the difference in the initial and final sample masses. In addition to the binder content of the asphalt mixture sample, the ignition method produces a clean aggregate sample that can be used to determine a mixture's aggregate gradation, here after called white curve. The Bitumen content of the RAP is given in Table 4.2. Results show that the RAPs have an average asphalt content of about 3,9% by weight of the total mix. The detailed results of this tests replicates are shown in appendix I in Table-A I-1.

Table 4.2 RAP asphalt content by ignition method

RAP Source	**Sample number – Asphalt binder content % by weight (corrected)**			**Average content**	**Standard deviation**
	1	**2**	**3**		
(1)	3,90	3,89	3,90	3,90	0,005

The gradations of the aggregate recovered from RAP samples submitted to ignition tests are reported in Table 4.3 and shown in Figure 4.5. The amount of particles that passing 80um sieve (filler) in each RAP aggregate sample cleaned was determined by washing each aggregate size fraction with water. Results show that the RAP from ignition contained 29%

coarse aggregate retained on the 5-mm sieve and 68% was retained on the 0,630-mm. The RAP source also appears to have a nominal maximum size aggregate (NMSA) of 10 mm as the as received RAP.

Table 4.3 Data from sieve analysis test of the RAP material from ignition

Sample no.	**1**	**2**	**3**	**4***	**Averages**	**Std. Dev.**
Sieve size (mm)	**Percent passing**					
28	100	100	100	100	100	0,00
20	100	100	100	100	100	0,00
14	100	100	100	100	100	0,00
10	99	98	98	98	98	0,43
5	70	71	67	74	71	2,50
2,5	52	52	48	55	52	2,49
1,25	41	41	38	42	41	1,50
0,630	32	32	31	33	32	0,71
0,315	23	24	22	24	23	0,83
0,160	15	16	15	16	16	0,50
0,080	9,5	9,8	9,7	10	10	0,18

* There is no asphalt content for sample No.4 because of the missing data and results in this test

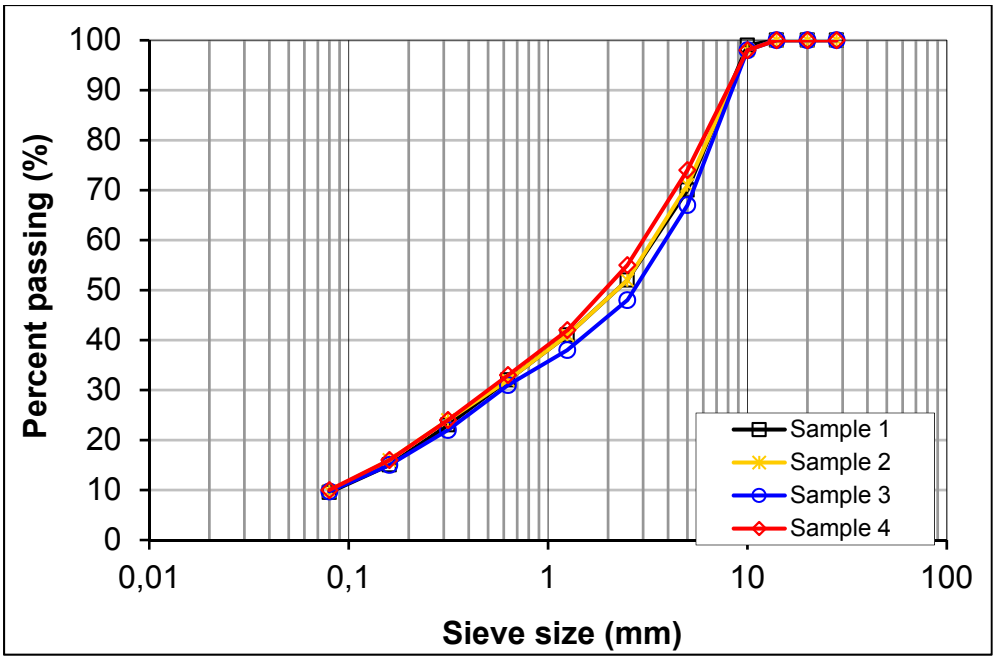

Figure 4.5 Gradation of four samples of the RAP after extraction using ignition oven

The differences between a sieve analysis of RAP before and after extraction are shown in Table 4.4 and presented graphically in Figure 4.6. The purpose of the comparison is to identify how the asphalt cement present in the RAP material could affect the gradation of recycled asphalt mixtures. It is assumed that as RAP is added to hot mix asphalt, the asphalt binder of the RAP will tend to separate and disperse in the mix because of the heat. Consequently, the added virgin aggregate will receive some coating, and basically, the added RAP reduces the virgin asphalt needed for the mixtures. As the extracted asphalt binder leaves the RAP aggregates, the gradation curve tends to shift to a smaller size (to the left). The shape of the gradation curve remains the same since the asphalt binder itself has no gradation, and the components of the RAP which could constitute a gradation are left behind after extraction. The only difference is that the particles are no longer coated, and are thus smaller by approximately one sieve size (Potyondy, 1996). In addition, it can be stated that those before and after extraction curves represent the extremes that will occur when the RAP material is added to a hot mix asphalt.

Table 4.4 Average RAP gradations before and after ignition test

Sieve size	RAP As Received	Recovered Aggregate from ignition
	Percent passing	
28 mm	100	100
20 mm	100	100
14 mm	100	100
10 mm	98	98
5 mm	57	71
2,5 mm	34	52
1,25 mm	20	41
630 um	11	32
315 um	4,1	23
160 um	1,3	16
80 um	0,4	10

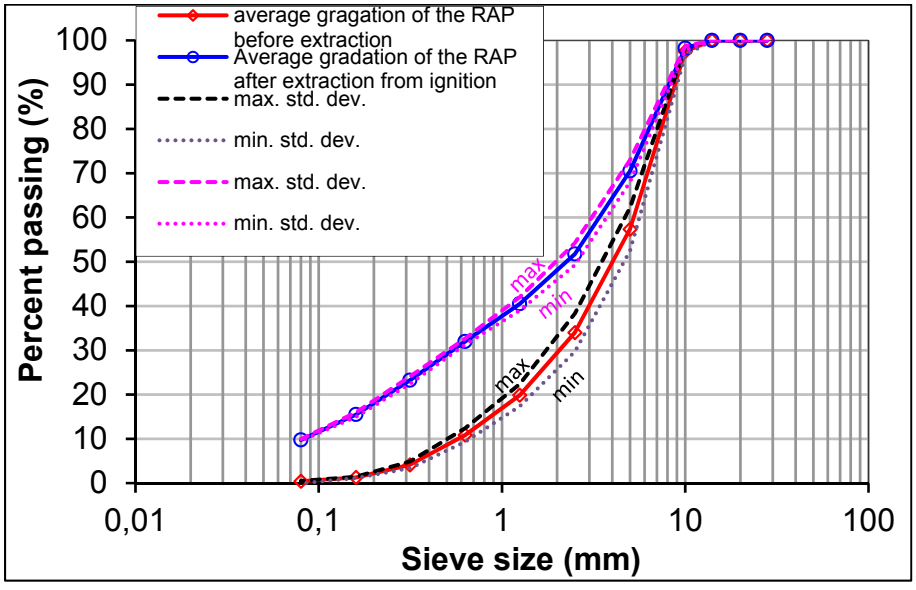

Figure 4.6 Gradation of average samples of the RAP before and after extraction using ignition oven

Finally, according to the McDaniel et al. (2001) report, it is indicated that ignition ovens may cause degradation of some aggregates after ignition test. Therefore, care should be taken when analyzing the gradation of aggregates after the ignition oven. It is recommended for any ignition of asphalt binder to perform ignition of asphalt mixture that its aggregate type shall be the same as it was used in the asphalt concrete mixture. Unfortunately, we don't have the information on the original compositions of the RAP, especially the filler content, as well as aggregate size and type. Calibration factor needs to be determined. For this reason, we proposed to correct our asphalt binder by fabricating asphalt mixture of type EB-10s because its gradation was found to be closer to the gradation of our kind of RAP source. EB-10s is one of the mixtures that are commonly used in Quebec for road construction. We believed that the results can be accurate but it is not a precise number. All results for the ignition test to find the corrected factor are presented in Appendix I in Table-A I-2 and Table-A I-3.

4.2.5 RAP binder content from solvent extraction

Solvent extraction of asphalt binder from RAP mixtures is achieved by means of dissolving the RAP asphalt binder with reagents and then separating the solution from the aggregate and filler components of the RAP asphalt mixtures.

The solvent extraction used in this study involves a centrifuge extraction apparatus. This method follows the procedures recommended in LC 26-100 (MTQ, 2015): *''Détermination de la teneur en bitume''*. For the extraction, trichloroethylene was used as a solvent. Results are presented in Table 4.5. The average asphalt content in the RAP from solvent is about 3,7% by weight of the total mix. The detailed test method is shown in Appendix I in Tables-A from I-4 to I-8.

After extraction, the analysis of the aggregate gradation was performed and results are shown in Table 4.6. Results show a typical breakdown of the residual aggregate by weight and the results are presented graphically in Figure 4.7.

Table 4.5 Percent of asphalt binder of the RAP obtained by extraction (by weight)
(Using 0,25 as correction factor: refer to Table-A I-8)

Sample No.	Sample 1	Sample 2
Correction factor	-0,25	-0,25
% Asphalt binder (corrected)	3,78%	3,53%
Standard deviation	0,125	
Average % Asphalt binder (corrected)	3,66 %	

Table 4.6 RAP gradation after solvent extraction

Sample no.	1	2	Averages	Std. Dev.
Sieve size	**Percent passing**			
28 mm	100	100	100	0,00
20 mm	100	100	100	0,00
14 mm	100	100	100	0,00
10 mm	99	98	99	0,50
5 mm	65	73	69	4,00
2,5 mm	46	55	51	4,50
1,25 mm	36	43	40	3,50
630 um	29	33	31	2,00
315 um	21	24	23	1,50
160 um	14	15	15	0,50
80 um	9,9	10,1	10	0,60

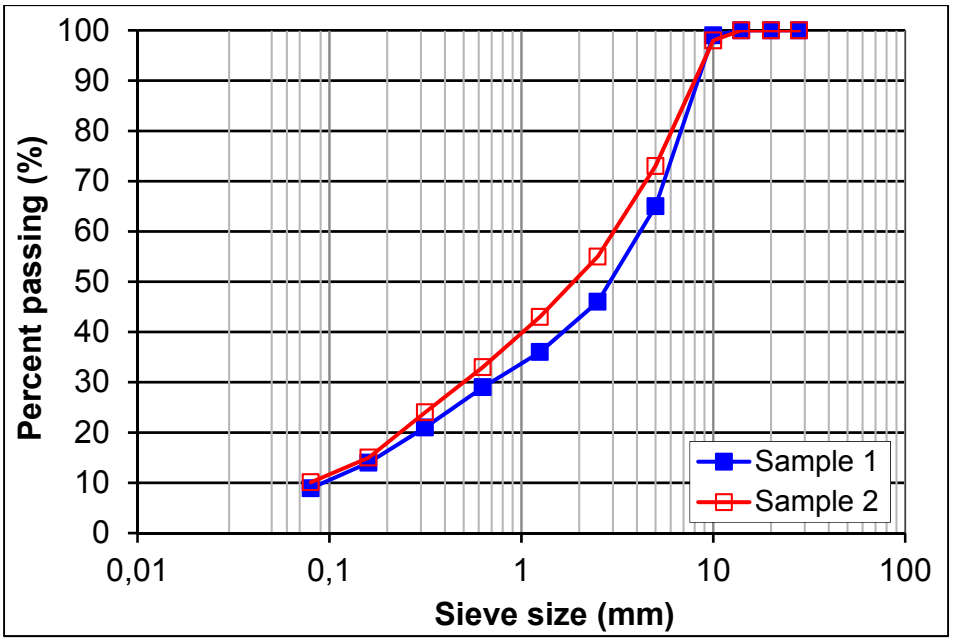

Figure 4.7 Gradation of two samples of the RAP after solvent extraction

4.2.6 Comparison between the ignition oven test results and solvent extraction test

Results from ignition test and those from the solvent extraction are here compared in order to evaluate the test methods. These results are used to determine the asphalt binder content and aggregate gradation.

4.2.6.1 Gradation analysis

Considering the overall gradation as reflected by the mean of percent passing on the individual sieves, the results show that the aggregate gradation obtained from the ignition and the solvent extraction are very close to each other (see Figure 4.8). By comparing the standard deviations of the two methods, there appears to be no pronounced differences in the variability on the individual sieves. The results also support two tendencies in gradation: a) the intermediate sieve sizes (5, 2,5, 1,25, 0,630, 0,315 mm) have more variability than other sieves, and b) there is a higher amount of fines aggregate after extraction than before. The results shown here are in agreement with what is found in the literature. Since our results

showed that the gradation of the ignition test was very similar to the gradation of the solvent test, we can select one of them. For this study, the after extraction gradation obtained from the ignition method was selected to be used in the mix design.

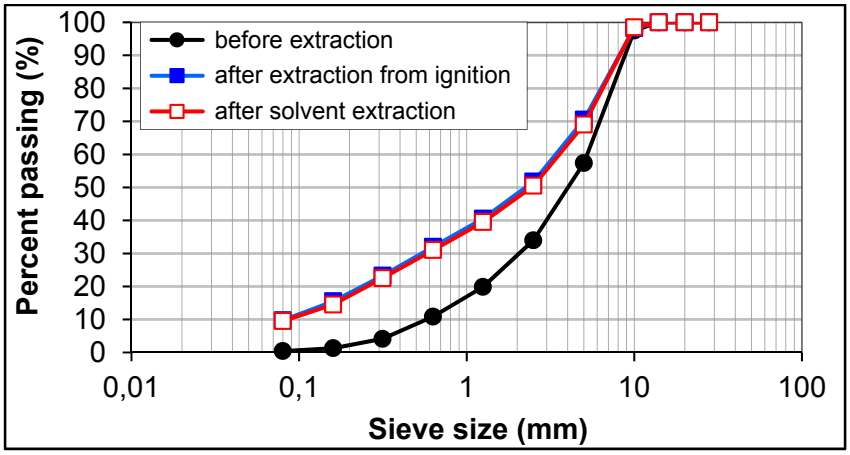

Figure 4.8 Gradation of average samples of the RAP before and after extraction using ignition oven & solvent

4.2.6.2 Asphalt binder content analysis

The asphalt binder content test results are shown in the following Table:

Table 4.7 Asphalt binder content test results

Method	Mean	St. Deviation	%*
Ignition extraction	3,90	0,005	0,1
Solvent extraction	3,66	0,125	3,4

*Difference between the design asphalt content (4%) and asphalt content determined by extraction methods

This table shows that the mean values for the asphalt binder content which resulted from the ignition extraction and solvent extraction are rather close to the supplier's binder content (4%), with ignition asphalt being closer to the predicted target asphalt content. Because of that, the asphalt content obtained from the ignition oven test will be used for the mix design.

4.2.7 Recovered RAP binder (RRB)

As noted in chapter 3, there are three RAPs in this study: the as-received RAP, RAP heated in a microwave and laboratory aged RAP (artificial RAP). Samples of each RAP were taken after applying the conditioning process for recovering binder using trichloroethylene to separate bitumen from mineral aggregate according to LC 25-001 (MTQ, 2014).

The properties of the RAP binder were evaluated using selected Superpave binder test procedures including penetration test (ASTM test methods ASTM D 5/D5M-(ASTM, 2013)), the viscosity test (ASTM test methods D4402-06 – (ASTM, 2006)), the dynamic shear rheometer (DSR) test (AASHTO TP5-98, (AASHTO. 1998)), and the bending beam rheometer (BBR) test (AASHTO test method T 313 – (AASHTO, 2008)). The results of the penetration test are shown in Figure 4.9.

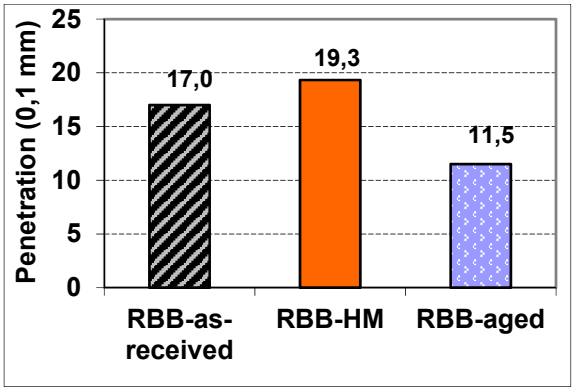

Figure 4.9 Recovered bitumen binder penetration values

In this study, the DSR test was performed at 76°C and 82°C, in an attempt to estimate the SUPERPAVE performance grade of the RAP binder. Test temperatures used for the bending beam rheometer (BBR) test were -18°C, and -24°C.

The rotational viscometer test results, presented in Tables-A I-9 and I-10 in Appendix I, shows that the as-received and aged RAP binders have a viscosity of 2586 and 2965,3 Pa.s at

135°C and 471 and 650 Pa.s 165°C, respectively. As shown in Figure 4.10, For the RAP binders tested, the relative increase in viscosity is dependent on the RAP kind. The results in this figure indicate that the viscosity ratio between the unaged RAP recovered asphalt and the aged RAP recovered asphalt raises by 1,14 times at 135°C.

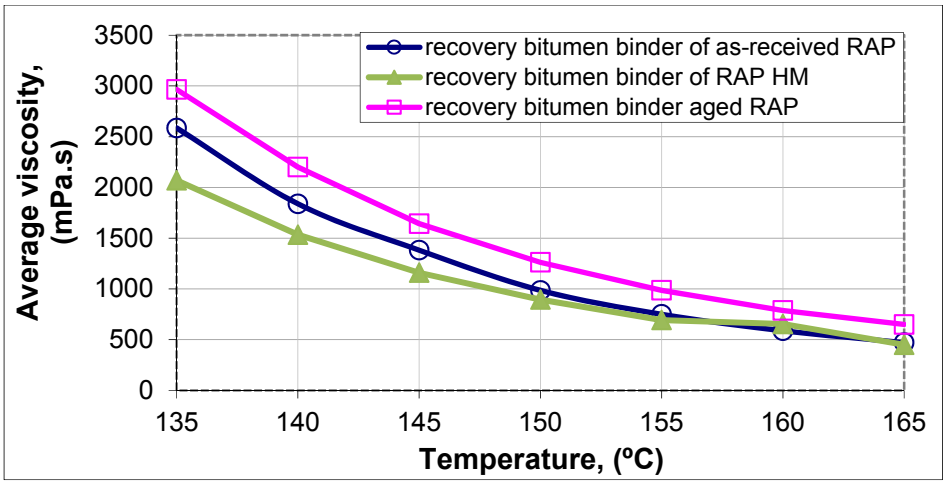

Figure 4.10 Viscosity of the unaged RAP and the aged RAP recovered asphalt binders

The results of the DSR test are given in Tables 4.8 to 4.10 and in Figure 4.11. The G*/sin δ value measured using DSR at 76°C was found to be 4,0 kPa for the unaged RAP and 3,051 kPa for the aged RAP at 82°C. The unaged RAP binder would have an estimated high temperature grade of PG82 as the binder meet the requirements of G*/sin δ > 2,2 kPa at the temperature 76°C while the aged RAP binder would have an estimated high temperature grade of PG88 as the binder meet the requirements of G*/sin δ > 2,2 kPa at the temperature 82°C.

Table 4.8 DSR Test Results of recovery bitumen binder of as-received RAP

Replicate Number	Temp. (°C)	G*/sin δ (kPa)	Phase Angle, δ, (degree)	Min Allow G*/sin δ	Test status
1	76	4,1	71,3	2,2	Passed
2	82	2,1	73,8	2,2	Failed

Table 4.9 DSR Test Results of recovery bitumen binder of heated microwave RAP (HM)

Replicate Number	Temp. (ºC)	G*/sin δ (kPa)	Phase Angle, δ, (degree)	Min Allow G*/sin δ	Test status
1	70	6,0	70,55	2,2	Passed
2	76	3,1	73,12	2,2	Passed
3	82	1,6	75,85	2,2	Failed

Table 4.10 DSR Test Results of recovery bitumen binder of the aged RAP

Replicate Number	Temp. (ºC)	G*/sin δ (kPa)	Phase Angle, δ, (Degree)	Min Allow G*/sin δ	Test status
1	70	12,7	72,15	2,2	Passed
2	76	6,2	75,22	2,2	Passed
3	82	3,1	78,00	2,2	Passed

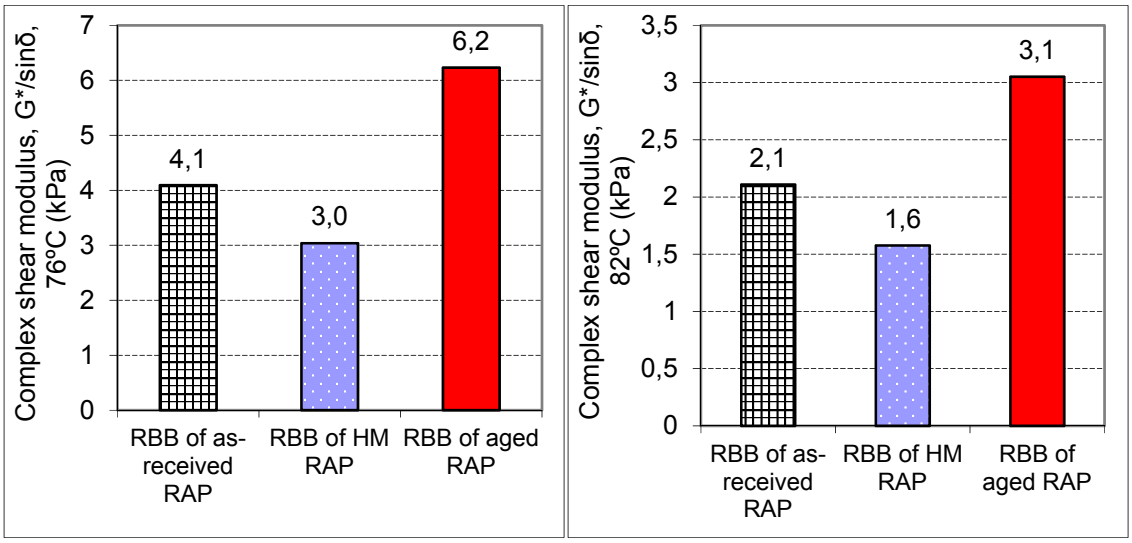

Figure 4.11 DSR test results of recovery bitumen binders of unaged and aged RAP at 76°C and 82°C

Tables 4.11-4.13 show the results of the BBR tests. From those tables, it can be seen that the stiffness value for the unaged RAP and aged RAP binders are 141 and 201,3MPa. The measured creep stiffness value (S) meet the 300MPa maximum requirement of AASHTO

MP1 (Standard specification for performance graded asphalt binder) for the as-received RAP and aged RAP binders to satisfy a low temperature grade of -18°C and -24°C, respectively.

Table 4.11 BBR Test Results of recovery bitumen binder of as received RAP

Replicate Number	Temp. * (ºC)	Creep Stiffness, S(60) (MPa)	m-value m(60)	Average S(60) (std. deviation)	Average m(60) (std. deviation)	Min Allow	m(60) Test results
1	-18	133	0,320	141 (8)	0,326 (0)	0,300	Passed
2	-18	149	0,331			0,300	Passed
1	-24	313	0,292	277 (25)	0,290 (0)	0,300	Passed
2	-24	259	0,291			0,300	Passed
3	-24	260	0,287			0,300	Passed
* Fluid bath temperature at 60 seconds; Target test temperature = -18 ºC and -24 ºC							

Table 4.12 BBR Test Results of recovery bitumen binder of heated microwave RAP (HM)

Replicate Number	Temp. *(ºC)	Creep Stiffness, S(60) (MPa)	m-value m(60)	Average S(60) (std. deviation)	Average m(60) (std. deviation)	Min Allow	m(60) Test results
1	-18	129	0,339	141 (9)	0,339 (0)	0,300	Passed
2	-18	142	0,347			0,300	Passed
3	-18	151	0,331			0,300	Passed
1	-24	243	0,297	263 (15)	0,290 (0)	0,300	Passed
2	-24	277	0,290			0,300	Passed
3	-24	270	0,284			0,300	Passed
* Fluid bath temperature at 60 seconds; Target test temperature = -18 ºC and -24 ºC							

Table 4.13 BBR Test Results of recovery bitumen binder of the aged RAP

Replicate Number	Temp. *(ºC)	Creep Stiffness, S(60) (MPa)	m-value m(60)	Average S(60) (std. deviation)	Average m(60) (std. deviation)	Min Allow	m(60) Test results
1	-24	215	0,308	201 (11)	0,304 (0,0)	0,300	Passed
2	-24	202	0,299			0,300	Passed
3	-24	187	0,304			0,300	Passed
1	-30	414	0,267	396 (43)	0,268 (0,0)	0,300	Failed
2	-30	390	0,272			0,300	Failed
3	-30	384	0,266			0,300	Failed
* Fluid bath temperature at 60 seconds; Target test temperature = -24 ºC and -30 ºC							

Also, the measured m-values are lower than the 0,300 minimum established to fulfill the same grade requirement. In terms of the m-value, all recycled binders satisfied the minimum limit set for forth by Superpave (i.e., 0,300). Similar to the DSR test results at 76°C and 82°C, the stiffness values from the BBR tests showed a similar trend regardless of the binder type.

It appears that the viscosity, the G*/sinδ values, and the stiffness values from the BBR tests of the aged binder show general trend of the highest values, whereas the HM binder show general trend of the lowest values.

Estimation of mixing and compaction temperature ranges for asphalt mixtures is determined at evaluated temperatures from plain asphalt viscosity–temperature charts at 0,170+0,02 Pa.s and 0,280+0,03 Pa.s (Anderson, 1987) (see Figure 4.12). Predicted superpave performance grading is reported using the two numbers, the first being high temperature characterization (T_e) and the second being the low temperature characterization (T_b). The results of DSR test on the recovered bitumen binder were used to calculate the T_e value. T_b was determined by calculating the parameters measures S(60) and m(60) obtained from the sample submitted to the BBR tests.

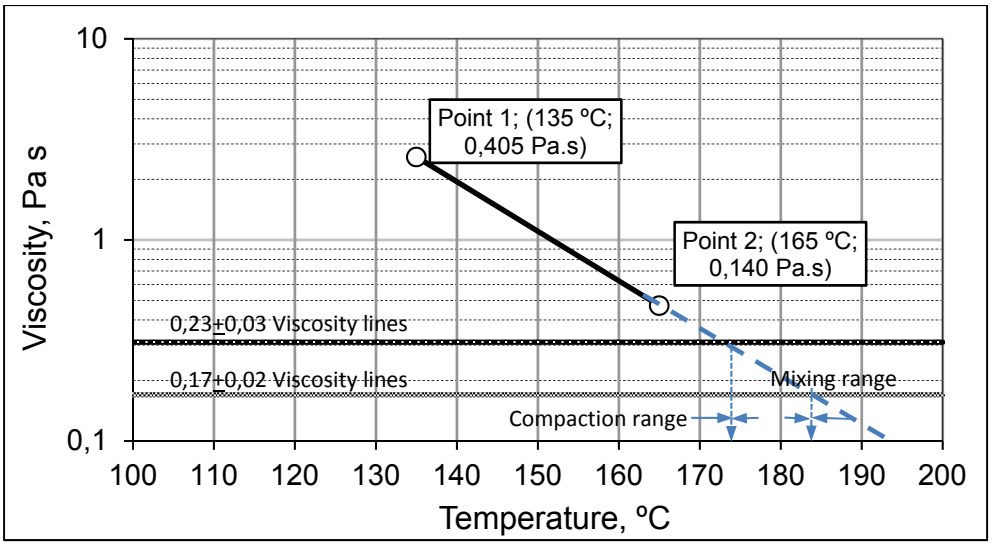

Figure 4.12 Viscosity versus temperature for the as-received recovered bitumen binder

Table 4.14 shows a summary of the recovered binder test results

Table 4.14 Summary table of estimation of mixing and compaction temperatures for asphalt mixtures and PG grade predicted of the different bitumen binders

Recovered bitumen binder	Mix design		PG		Predicted PG grade
	Mixing temperature, °C	Compaction temperature, °C	High temperature, °C	Low temperature, °C	
Recovered bitumen binder from as received RAP	177	184	85,3	27,4	82-22
Recovered bitumen binder from RAP heated in a microwave	174	184	84,4	33,2	82-28
Recovered bitumen binder from aged RAP	184	189	86,1	34,6	82-34

4.2.8 Virgin aggregate properties

Seven different stockpiles of virgin aggregate were used in this research: 10-20 mm, 5-10 mm, two different 0-5 mm, 2,5-5 mm, 0-1,25 mm, and Filler. The aggregates were loaded,

transported, and stored in closed barrels for the duration of the project to prevent contamination. All these materials require no additional mechanical processing to create the desired gradation.

One main reason for selecting those particular aggregates was based on past experience. These aggregates have been found to exhibit very consistent physical properties with regard to specific gravity, gradation and particle shape to produce asphalt mixes. Table 4.15 lists the gradation of these materials, and Figure 4.13 graphically represents this data. It can be seen from the table that the stockpiles have different gradations.

Table 4.15 Gradation of virgin aggregate (Reported by Supplier)

Aggregate's stockpiles	**Aggregate 1**	**Aggregate 2**	**Aggregate 3**	**Aggregate 4**	**Aggregate 5**	**Aggregate 6**	**Aggregate 7**
Identification	**10-20mm**	**5-10mm**	**0-5mm**	**0-1,25mm**	**Filler**	**0-5mm**	**2,5-5mm**
Sieve size	**Percent passing**						
28 mm	100	100	100	100	100	100	100
20 mm	96	100	100	100	100	100	100
14 mm	49	100	100	100	100	100	100
10 mm	12	92	100	100	100	100	100
5 mm	2,0	9,0	96	100	100	94	90
2,5 mm	1,0	3,0	61	100	100	58	2,0
1,25 mm	0,0	2,0	39	98	100	29	1,0
630 um	0,0	2,0	26	91	100	14	1,0
315 um	0,0	2,0	18	66	100	10	1,0
160 um	0,0	1,0	13	29	100	8,0	1,0
80 um	0,8	0,7	9,1	6,0	98	7,0	0,4

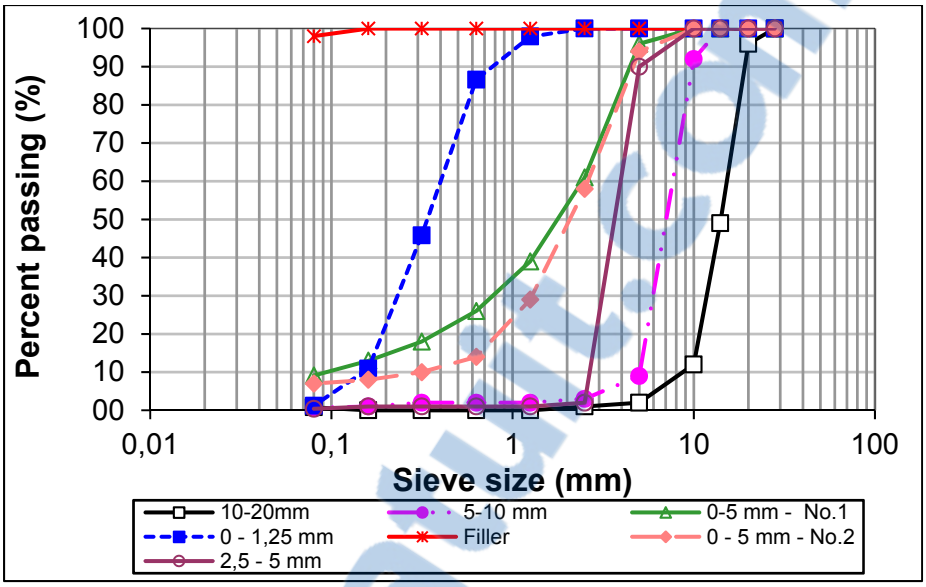

Figure 4.13 Gradation of virgin aggregate materials

4.2.9 Properties of virgin binder

Two grades of virgin asphalt binders (PG 64-28 and PG 58–34) were used in this research. The selected asphalt binders are widely used in many provinces all over Canada. Characteristics of both asphalt binders are reported in Table 4.16. The two virgin binders selected represent medium grade asphalt binders that could be blended in warm climates. PG 64-28 asphalt binder used on high traffic passing lanes and PG 58-34 asphalt binder typically used for new construction. In order to reduce the effects of asphalt binder source, only one source for each type of binder (PG 64-28 and PG 58–34) were utilized for all mix designs.

4.3 Recycled mix design

The mix design for the eleven asphalt mixtures, as discussed in chapter 3, is essentially based on the LC mix design procedure. A control mixture was designed first, which served as a baseline to compare with the other mixtures. The subsequent mixtures including RAP were prepared using an aggregate gradation as close as possible to the control mixture in an effort to minimize additional factors that can affect the results. Generally, failure to meet LC

requirements is an indication that improper asphalt cement is used, improper aggregate is used, or mix design is improperly conducted.

Table 4.16 Characteristics of the PG 64-28 and PG 58–34 asphalt binder Reported by Supplier (Bitumar Inc. for PG 64-28 and the Industries McAsphalt Ltee for PG 58–34)

Properties	PG 64-28	PG 58–34
Density (g/cm^3), at 25 °C, AASHTO T228	1,026	1,014
Density (g/cm^3), at 15 °C, AASHTO T228	1,033	1,021
Storage stability (°C), LC 25-003	0,4	1,4
Viscosity Brookfield (Pa.s), at 135 °C, AASHTO T 316	0,455	0,405
Viscosity Brookfield (Pa.s), at 165 °C, AASHTO T 316	0,132	0,140
High temperature for characterization T_e(°C)	65,1	60,7
Low temperature for characterization T_b(°C)	-28,8	-34,4
Modulus of rigidity S_o (60) (MPa) from BBR test	90,2	107
Slope of m_o (60) from BBR test	0,437	0,439
Minimum recommended mixing temperature for using (°C)	151	152
Maximum recommended mixing temperature for using (°C)	165	166

4.3.1 Reference mix design

A 100 percent virgin mix of a GB20 was prepared as the control mixture with a PG 64-28 asphalt binder. The gradation for the mixture was adjusted by controlling the percentage of the different virgin aggregates. A total of five virgin aggregate stockpiles were used in the virgin mixture. A minimum of three trial blends are specified for this purpose. The combinations of aggregates are shown in Table-A I-11 in Appendix I. In order to achieve the volumetric requirements of the mixtures, these gradation curves were adjusted several times prior to selecting the optimal gradation.

The gradation curves of the three trials of virgin mixture created in this study is shown in Figure 4.14. The goal in designing each mixture containing RAP after that was to achieve the

desired quantity of RAP for each condition such that the required gradation would match the gradation of the control mixture as closely as possible. As shown in Figure 4.14, the design gradation for the selected virgin mixture (Trial 3) passes through the Superpave control points which the LC method recommends to use. For the 0% RAP mix design, the optimum asphalt binder content was found to be 4,5% by weight (9,7% by volume) for a V_{be} of 10,2%. Table-A I-12 in Appendix I shows the characteristics of the selected virgin mixture. The volumetric properties of the mix are as will be shown in Table 4.17 here after. The voids filled with asphalt (VFA) were approximately 74,4%. The VMA of the mix, which is the volume of voids between aggregate particles, is 13,9%. The bulk specific gravity of the mix, G_{sb}, is 2,530. The mix was compacted to the minimum density of 2,641 to verify the compact ability of the mix in the laboratory.

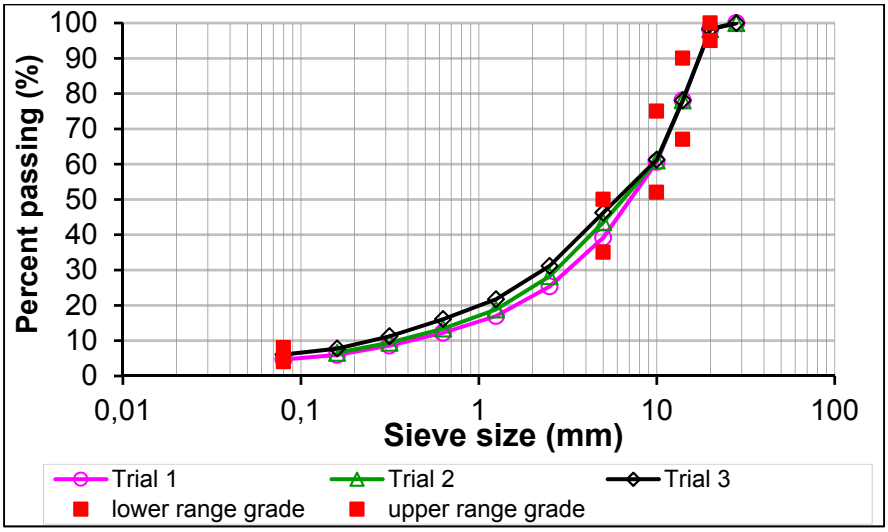

Figure 4.14 Gradation of three trials for 0% RAP mixture

4.3.1.1 Mixing procedure

Individual batch of different aggregates stockpile for each test specimen was prepared. Those aggregates were heated to a temperature 25ºC higher than mixing temperature before mixing. The heated virgin binder, at the mixing temperature, was added to the preheated virgin aggregates. For asphalt mixture incorporating RAP, the total binder content used in the virgin

mix was kept constant for all trials of mixtures. Before mixing a RAP with virgin aggregates, the RAP was heated in a microwave to 110 $\pm$ 5°C for about 7 minutes before mixing with the heated virgin aggregates. It is important to note that the time of heating in a microwave depends on the amount of RAP material that needs to be heated.

As noted earlier, our testing program was planned to test the effect of adding cold RAP in the mix. For those cases, the RAP dried at ambient temperature (23°C) is simply added to the virgin aggregate after being overheated in an oven at 300°C in the mixer and blend for few minutes prior to the addition to the preheated virgin binder at the specified (target) mixing temperature. The blending duration of RAP/virgin binder is dependent on the amount of RAP inserted to the mix and it should be long enough for all the aggregates particles to be thoroughly coated by the binder. Also, based on our testing program, we aimed to examine the effect of adding aged RAP materials on the resulting mixture properties. This reflects the influence of aging asphalt binder in the RAP material on the performance of recycled asphalt mixture. In this case, the aged RAP is added cold to the heated virgin aggregate and both are blended together before mixing with the preheated virgin bitumen.

For mixes with RAP, the mixture of virgin aggregates and RAP material was blended with a mechanical mixer for few minutes. The mixing time is different and was calculated or fixed based upon the proportion of RAP that is added to the virgin aggregate. The total asphalt binder dosage was kept constant at 4,5%. The use of RAP typically reduces the amount of virgin binder because RAP binder is contributing binder into the mix, which would be deducted from the total binder required for the mixture, and then combining the preheated virgin binder with the blending of virgin aggregates and RAP materials.

Immediately after mixing, the mix was transferred into a clean pan and placed (covered) in a 153°C draft oven for a minimum 2 hours for conditioning at the compaction temperature in a closed draft oven in order to simulate short term aging, prior to maximum theoretical specific gravity test or before the compaction with the Superpave gyratory compactor (SGC). This time is to permit time for the aggregates to absorb asphalt. All samples should be cured the

same amount of time. Keep in mind that the procedure used for design in the laboratory will need to closely match the field conditions at the time of construction. Failure to consistently test the materials at the same time interval will result in highly erratic maximum specific gravity values and possibly failure to achieve the required VMA.

After conditioning, maximum theoretical specific gravity (G_{mm}) was evaluated according to the LC 26-045 (MTQ, 2008). After this test, it is followed by compacting samples using the Superpave Gyratory Compactor (SGC). Mixtures were sampled to compact specimens according to the LC 26-045 (MTQ, 2008). The values of the G_{mm} were used for the calculation of the mass of the SGC test sample. The N_{in}, N_{des}, and N_{max} values used for this study were 10, 120, 200; respectively. After the necessary testing has been accomplished, the calculation of the volumetric parameters can begin. Calculation of these volumetric parameters is an iterative process. It is very important to use numeric values that correctly correspond to the sample being tested. Use of a carefully constructed, accurate, computer spreadsheet is highly recommended. We select the mixes that satisfy air void content and the specified volumetric criteria.

The resulting volumetric properties of the compacted specimens tested in our study are presented in Table 4.17. It should be noted that the same procedure was followed to prepare slabs for all the detailed mixtures. See section 4.4 for information regarding preparing laboratory-asphalt slabs for study.

Table 4.17 summarizes the properties for each mix design. It can be seen that the effective volumetric asphalt content (V_{be}) is kept constant as part of the mix design hypothesis and process for all the mixtures and consequently the VFA and VMA values of all the mixtures are close. Higher VMA values are indicative of compacted mixtures with higher voids between the aggregate particles (including voids filled with asphalt binder). The higher the VMA, the less direct aggregate interaction it will have, and therefore the more the mixture will rely on the asphalt binder for strength.

Table 4.17 Summary of GB-20 asphalt mixtures produced in the laboratory

Mix No.		1	2	3	4	5	6	7	8	9	10	11
Mixture Description		RAP 0% RAP028	RAP 15% RAP1528 CUN	RAP 25% RAP2528 CUN	RAP 40% RAP4028 CUN	RAP 15% RAP1528 HUN	RAP 25% RAP2528 HUN	RAP 40% RAP4028 HUN	RAP 40% RAP4028 CA	RAP 40% RAP4034 CA	RAP 25% RAP2534 CUN	RAP 40% RAP4034 CUN
Percent of RAP (%)		0	15	25	40	15	25	40	40	40	25	40
Binder grade (PG)		PG 64-28								PG 58-34		
Passing (%)	28 mm	100	100	100	100	100	100	100	100	100	100	100
	20 mm	98,3	98,4	98,6	98,4	98,4	98,4	98,4	98,4	98,4	98,4	98,4
	14 mm	78,1	79,6	81,6	79,6	79,6	79,6	79,6	79,6	79,6	79,6	79,6
	10 mm	61,3	63,6	66,4	63,2	63,6	63,2	63,2	63,2	63,2	63,2	63,2
	5 mm	46,3	45,1	39,9	39,6	45,1	39,6	39,6	39,6	39,6	39,6	39,6
	2,5 mm	31,2	29,1	25,2	27,0	29,1	27,0	27,0	27,0	27,0	27,0	27,0
	1,25 mm	21,7	20,2	17,6	20,7	20,2	20,7	20,7	20,7	20,7	20,7	20,7
	630 um	16,1	14,9	13,3	16,4	14,9	16,4	16,4	16,4	16,4	16,4	16,4
	315 um	11,3	11,1	10,5	12,4	11,1	12,4	12,4	12,4	12,4	12,4	12,4
	180 um	7,7	8,5	8,3	9,2	8,5	9,2	9,2	9,2	9,2	9,2	9,2
	80 um	6,1	6,6	6,8	6,8	6,6	6,8	6,8	6,8	6,8	6,8	6,8
Mixture	Stone 10-20 (%)	43%	40%	36%	40%	40%	36%	40%	40%	40%	40%	40%
	Stone 5-10 (%) – No,1	11%	11%	18%	10%	11%	18%	10%	10%	10%	10%	10%
	Stone 0-5 (%)	40%	30%	0%	5%	30%	0%	5%	5%	5%	5%	5%
	Sand 0-1,25 (%)	4%	0%	0%	0%	0%	0%	0%	0%	0%	0%	0%
	Filler (%)	2%	2%	3%	2%	2%	3%	2%	2%	2%	2%	2%
	Stone 2,5 - 5 (%)	0%	2%	5%	3%	2%	5%	3%	3%	3%	3%	3%
	Stone 0-5 (%) – No,2	0%	0%	13%	0%	0%	13%	0%	0%	0%	0%	0%
	RAP 0-40 (%)	0%	15%	25%	40%	15%	25%	40%	40%	40%	40%	40%
	Asphalt binder (%)	4,5	4,5	4,5	4,5	4,5	4,5	4,5	4,5	4,5	4,5	4,5
	V_i (%)	4,2	4,01	4,01	3,7	4,01	4,8	5,3	2,0	2,2	3,8	3,6
	V_{be} (%)	10,2	10,2	10,2	10,2	10,2	10,2	10,2	10,2	10,2	10,2	10,2
	VMA (%)	13,9	12,6	13,9	13,5	13,1	14,5	14,9	12,0	12,2	13,7	13,2
	VFA (%)	70,4	78,6	70,5	72,7	75,3	66,9	64,7	83	81,7	71,8	74,4
	G_{mb}	2,530	2,535	2,517	2,521	2,519	2,492	2,488	2,548	2,540	2,524	2,527
	G_{mm}	2,641	2,602	2,622	2,618	2,612	2,617	2,627	2,600	2,597	2,624	2,621
Gyratory compactor (SGC) (LC 26-003)	10 N (target ≥ 11%)	14,1	13,8	16,7	15,1	14,75	16,7	16	12,4	13,11	14,9	14,55
	120 N (target 4%-7%)	5,5	4,0	5,7	5,1	5,05	6,4	6,7	3,4	3,6	5,3	4,95
	200 N (target ≥ 2%)	4,2	2,60	4,01	3,7	3,55	4,8	5,3	2,0	2,2	3,8	3,6
RAP aging process		-	Unaged	Unaged	Unaged	Unaged	Unaged	Unaged	Aged	Aged	Unaged	Unaged
RAP conditioning		-	Cold	Cold	Cold	Hot	Hot	Hot	Cold	Cold	Cold	Cold

A graphical comparison of the gradation for the four basic mixtures used in this study (RAP of 0, 15, 25, and 40%) is presented in Figure 4.15. It can be seen that the gradations are very

similar at the 10mm sieve and larger, and also at sieves smaller than 1,25mm. In between those two sieve sizes, the gradation of the different mixes are different but within the limits.

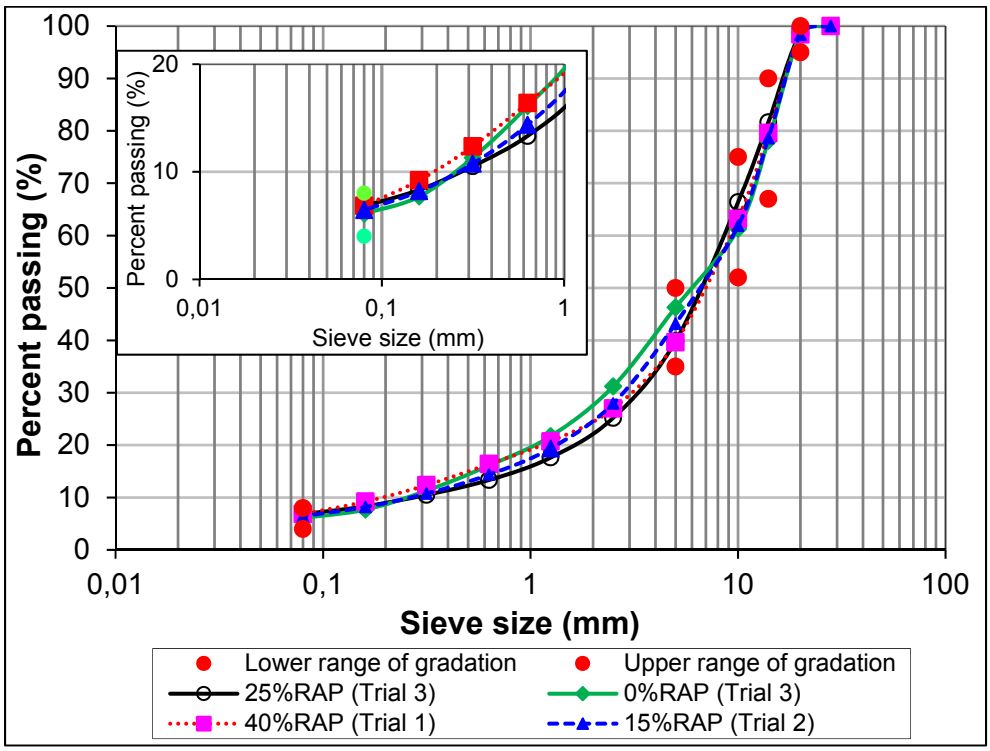

Figure 4.15 Gradation for all mixtures

A summary of the mixture properties determined for the eleven mixtures used in this research is found in Appendix A-I (Tables-A I-9 to I.32). It is interesting to note that a spread sheet was developed for the ease of the calculation of the actual amount of each material to add in each mix, as shown in appendix in Table-A I.33.

4.3.2 Mix specification

We proposed a simple nomenclature to name our mixtures which can provide information about the important tested parameters (see Figure 4.16). Thus, the name is composed of four parts. The first part is the percentage of RAP used in the mix (0, 15, 25, 40%). The second is the type of binder. They are identified as:

- 28 - PG 64-28 was used to prepare the asphalt mixture.
- 34 - PG 58-34 was used to prepare the asphalt mixture.

The third represents the RAP conditions when it is introduced in the mix (Cold RAP addition, or Hot RAP addition). And the last number refers to the RAP source. It means using of artificial aged RAP in the mix or not.

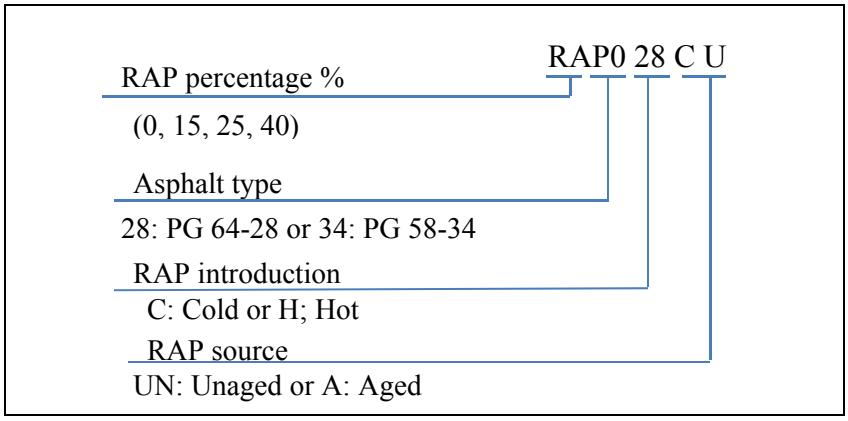

Figure 4.16 Notation of the specimens for the complex modulus test

4.4 Slab preparation

4.4.1 Manufacturing

To produce asphalt mixture samples that are representative of the field, slabs were compacted using LCPC plate compactor (Central laboratory for bridges and roads) at the LCMB laboratory, in compliance with European Standard NF EN 12697-33 (AFNOR, 2007). The asphalt slabs produced by the LCPC compactor can be easily cut apart for subsequent test. Slabs dimensions are typically 500mm wide by 180mm long by 100mm thick (minimum 1 slab/mixture). Slabs of all mixtures were produced in the LCMB laboratory. The compactor plates MLPC consist of a half axle (two small tires) rolling back on forth at constant velocity and constant pressure parallel to the axis of the mould (Figure 4.17). Following compaction of a plate, a curing period of 2 weeks at room temperature before coring is recommended and

respected in order to ensure an adequate curing of the asphalt mixtures. Good homogeneity of the sample is required and the compaction process must be perfectly controlled.

Figure 4.17 Compactor of plates of LCPC

4.4.2 Coring

Coring of cylindrical specimens from the long side of the slabs was performed at the laboratory as illustrated in Figure 4.18. It is important to note that the coring was done in the direction perpendicular to the direction of compaction. The coring machine consists of an electrical drill with hollow drill bits and a water cooling system. Five cylindrical specimens are cored from each asphalt mixture slab. First, the slabs are cored from the center and approximately 1 cm far from each edge. The following are four specimens cored with the least possible deviation compared to that of the center (to make the most of the most homogeneous area). The Test specimens are approximately 75 mm in diameter. The Figure 4.18 illustrates the cored samples.

4.4.3 Sawing and resurfacing

The cutting of sample ends is necessary to create uniform specimens in term of density and also to adjust the specimen's length. To ensure the flatness of the surfaces for gluing of the

platens at the ends of the specimen, a resurfacing machine was used. Resurfacing of the ends allows having smooth surfaces (Figure 4.19), which ensures good gluing of the platens. It also helps to ensure proper alignment after the specimens were glued (fixed) to the loading platens. Samples were stored overnight in a room temperature under a fan and allowed to dry to constant mass before the voids content was determined. The bulk specific gravity (G_{mb}) of the sample is measured using the dimensional measurement by incorporating the weight measurement of the specimen and the formula for the volume of the specimen [$V = \pi \times (radius)^2 \times (height)$] as presented below. The specimen height is approximately 120 mm.

Figure 4.18 Five Cored cylindrical specimens of 75 mm diameter

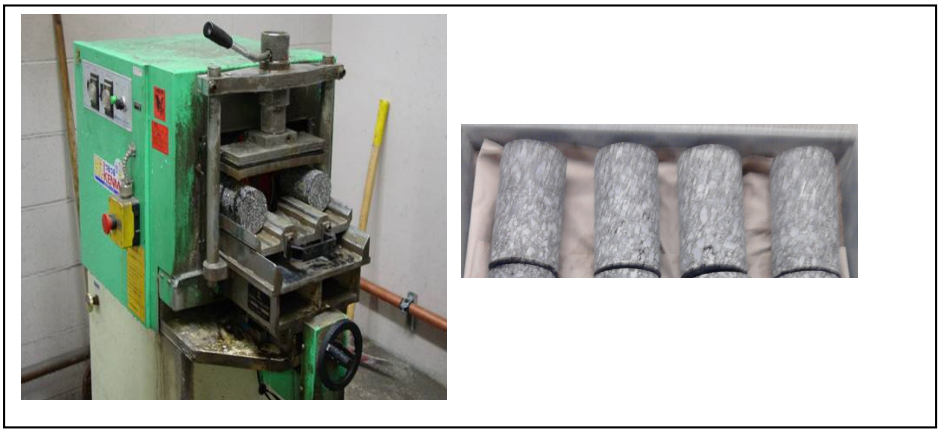

Figure 4.19 Specimen resurfacing

Figure 4.20 shows the plan for cutting plate and the numeration of the specimen.

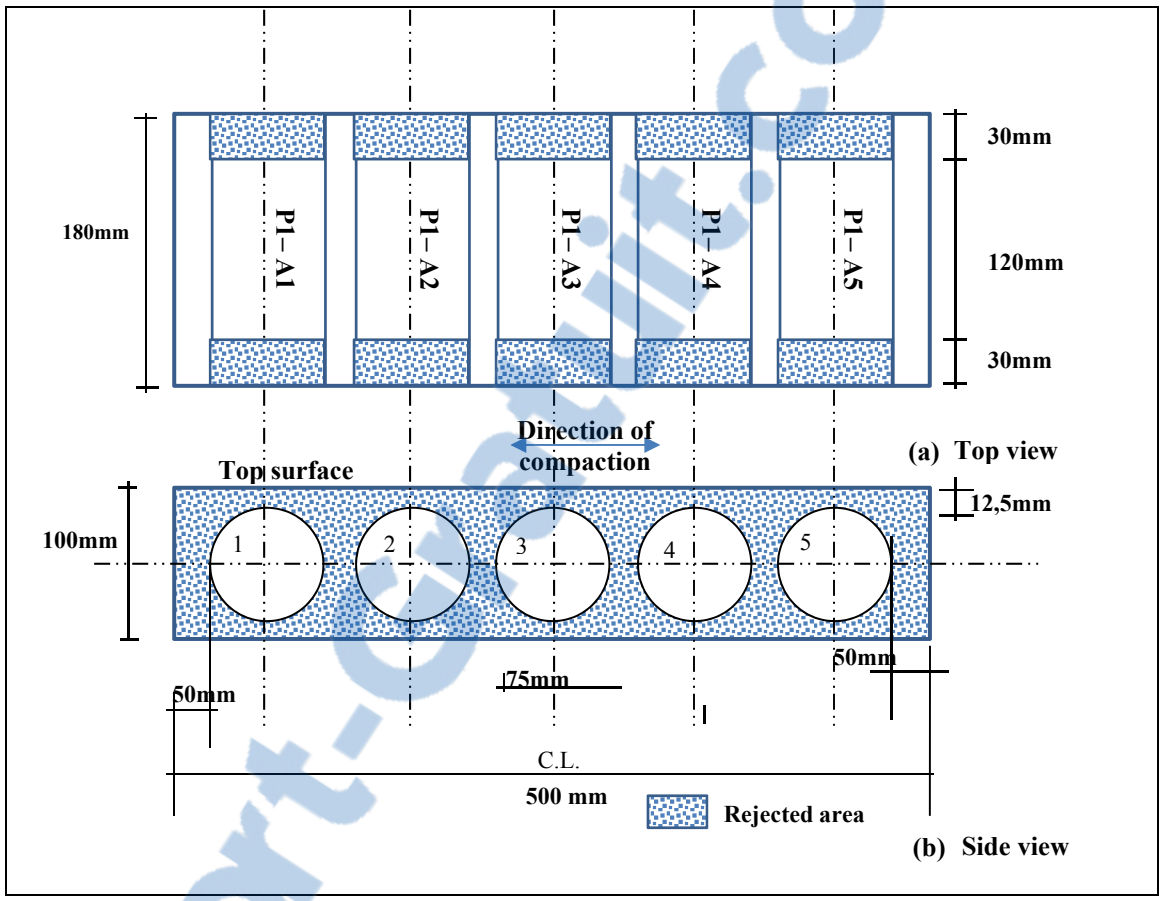

Figure 4.20 Representation of the coring plan and the numeration of the specimen: (a) side view, (b) top view (P refers to the plate number and A refers to the specimen number)

4.4.4 Compact of tested specimens

The LC test method 26-320 (MTQ, 2014) is used to determine the percentage of voids and compactness in the compacted hot mix asphalt. Voids content (V_i) was determined using the volumetric method (see appendix I). After the determination of the bulk density of asphalt mixture (G_{mb}) from the volumetric method and with considering the maximum density (G_{mm}) of the mix, the percentage of voids, of each sample, is calculated using the following equation:

$$V_i(\%) = \left(1 - \frac{G_{mb}}{G_{mm}}\right) \times 100 \quad (4.1)$$

Where:

G_{mb} Bulk density of compacted asphalt mixtures; and

G_{mm} Maximum density of the mix.

The compacity is calculated by the equation below:

$$\text{Compacity (\%)} = 100 - \text{percentage of voids (\%)} \quad (4.2)$$

The values for voids content (V_i) for all samples obtained for all the samples tested for complex modulus and fatigue tests are as it will be presented in chapters 5 and 6.

4.5 Tension-compression test: complex modulus and fatigue

This section is devoted to the presentation of the tests used in this research to characterize the effect of the addition of RAP on the thermomechanical properties of asphalt mixtures. The chosen experiment is the classical tension-compression test on cylindrical samples, (height 120mm, diameter 75mm). This kind of test makes it possible to study the behaviour of linear viscoelastic (LVE) and/or to determine the fatigue damage of bituminous mixtures. This test is considered homogenous as the values of stress and strain are the same in each point within the sample.

4.5.1 Principle of tension-compression test on cylindrical sample

The test setup (Figure 4.21, and Figure 4.22) is the same for both complex modulus and fatigue tests and consisted of servo-hydraulic press MTS (Material Testing System) available at LCMB laboratory (***L**aboratoire sur les **C**haussées et **M**atériaux **B**itumineux*) of ÉTS, controlled by an electronic system, 8800 series, with a nominal operating pressure of 210 bar, and a load cell of 50 KN.

Figure 4.21 Overview of the experimental device

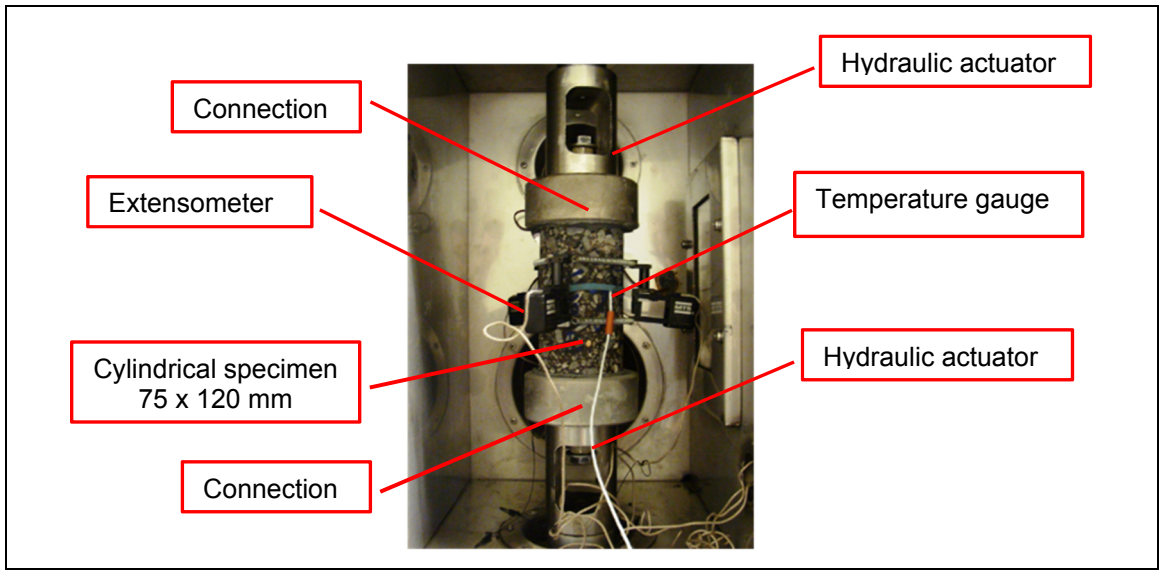

Figure 4.22 Test setup for complex modulus and fatigue

The axial deformations were measured using three on-sample MTS extensometers spaced 120° apart and connected springs around the middle of the sample (Figure 4.22). The gauge length was chosen to 50 mm to avoid end effects close to the end-caps due to gluing.

During all complex modulus testing, the specimen is subjected to a sinusoidal oscillating axial load in both tension and compression (through zero) (see Figure 4.23). The test is carried out with a small number of cycles (as you will see in Table 4.18) at different frequencies (from 0,01 Hz to 20 Hz). The complex modulus tests were considered to be non-destructive, which allows subsequent fatigue testing.

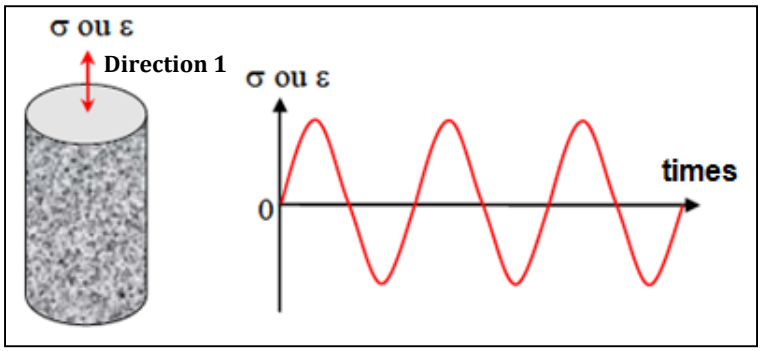

Figure 4.23 Principle of tension-compression test on cylindrical sample
Taken from Nguyen (2009)

In a fatigue test, a large number of cycles are performed. The temperature of a test is also dependent on the type of test. The complex modulus is measured on a wide temperature range and frequency, while the fatigue test is performed at a single temperature at constant frequency.

4.5.2 Implementation of tension-compression test

The different steps to establish the tensile–compression test are presented in the following paragraph.

4.5.2.1 Gluing the specimen to the testing platens

To test samples in tension-compression, it is necessary to use appropriate testing platens glued to the samples. Vertical alignment of the specimen is an important factor to avoid side

loading or bending moment created in the specimen and to achieve the homogeneity in axial tension and compression. The gluing operation takes place as follows: first, to ensure good adhesion between the platen and the specimen, aluminum platen are cleaned with acetone and then a thin uniform layer of epoxy is applied to the flat surfaces of the specimen and those platens. After that both the top and the bottom platens are held in place through a system of fixing rings and screws (the bench bonding device available at LCMB), and then are diameter adjustable (Figure 4.24). This machine is capable of accommodating specimens of various heights and diameters. Then, the specimen is placed between the two platens and the platens are pressed against the test sample forcing the assembly together while the epoxy cures. The gluing apparatus, pictured in Figure 4.24, holds the sample in-line with the testing platens, preventing undesirable eccentric or non-axial loading of the sample during testing. The specimen is removed after gluing is completed (4 hours minimum). Figure 4.25 shows the shape of the sample after gluing.

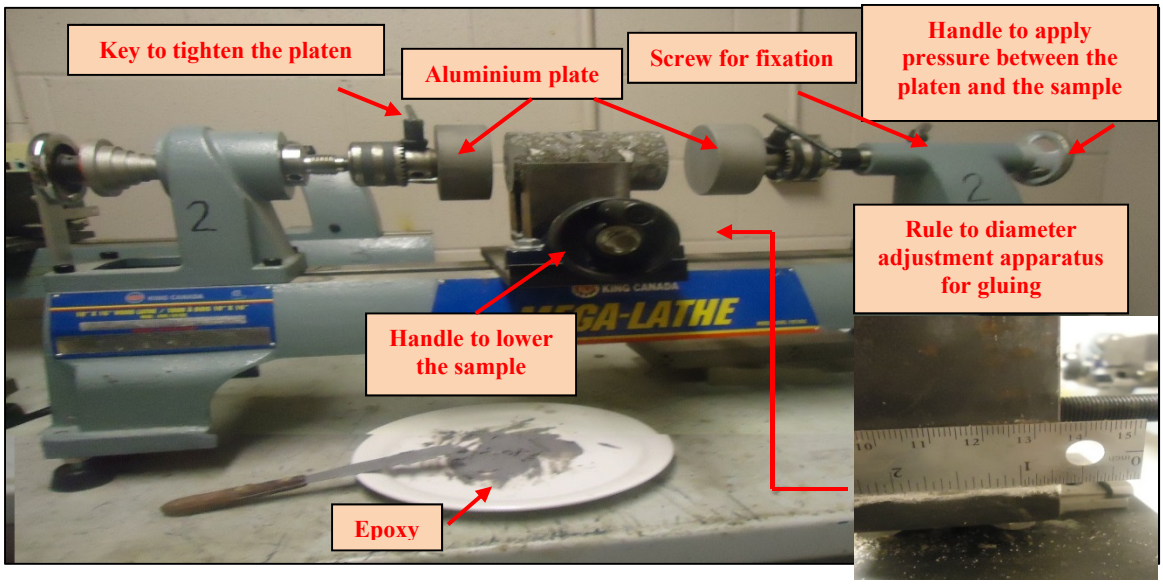

Figure 4.24 Apparatus for gluing

Figure 4.25 Sample after gluing

4.5.3 Procedure for complex modulus

As mentioned before, the complex modulus tests are performed at different temperatures and frequencies. All tests are performed at eight temperatures (-35, -25, -15, -5, 5, 15, 25, 35 °C), and at each temperature, a frequency sweep consisting of eight frequencies (0,01, 0,03, 0,1, 0,3, 1, 3, 10, 20 Hz) was performed. A conditioning time of 4 hours is imposed to achieve a uniform temperature in the test specimen whenever the testing temperature is changed. The sequence of the temperature stages is applied from the lowest to the highest. Moreover, for each level of temperature, stress is applied to reach constant strain variation to the different target frequencies from the fastest to slowest. At each frequency, a limited number of cycles are performed (Table 4.18). Rest period (about 2 minutes) is taken into account at each change of frequency.

Table 4.18 Number of applied cycles according to the frequency

Frequency (Hz)	Number of applied cycles
0,01	20
0,03	20
0,1	20
0,3	40
1	40
3	80
10	80
20	80

4.5.4 Procedure for fatigue test

During fatigue test, the specimens are subjected to sinusoidal oscillating axial load in both tension and compression. The fatigue test is also performed using controlled strain mode. All tests are performed were performed at a single temperature of 10 °C and at a single frequency of 10 Hz. A large number of cycles are applied to reach the 'failure' of the specimen. To characterize an asphalt mixture for fatigue resistance, at least five specimens must be tested at different strain levels (Baaj, 2002). The imposed strain level should be suitable to obtain sufficient fatigue life to assess the fatigue performance. More details on the chosen imposed strain level will be presented in section 6.4.1.12

Due to a large number of cycles of solicitation, it is not possible to record data for every cycle and with a very high frequency. The acquisition frequency is fixed at 1 kHz (100 point recorded by a cycle). In order to observe the best variations in the complex modulus values during the test, the time between the acquisition cycles (which is fixed before the test) varies during the test (Table 4.19). This time is very short at the beginning of the test where the modulus evolves quickly. Thus, it is necessary to record a great number of cycles at the beginning of the test. The first 100 cycles are recorded, and then at the end of the test, the interval between two acquisitions increases.

Table 4.19 Acquisition number according to the number of applied cycles applied
Taken from Baaj (2002, p. 101)

Number of cycles	**The acquisition frequency**	**Number of measuring points**
cycle 1 to 120	all the cycles	60
cycle 120 to 1000	a measurement every 15 cycles	60
cycle 1000 to 10000	a measurement every 150 cycles	60
cycle 10000 to 100000	a measurement every 1000 cycles	90
cycle 100000 to 300000	a measurement every 2500 cycles	100
cycle 300000 to the end of the test	a measurement every 5000 cycles	Dependent from the end of the test

4.5.5 Data Acquisition and measured parameters

The data collected during the test are used to obtain characteristics of the tested samples. The force, the values given by the three extensometers, and the temperatures measured by the probe are registered at each data acquisition. Each acquisition consists of registration of two consecutive cycles on 200 points. The time interval is adapted to have 100 points per cycle. The choice of two cycles allows obtaining a more accurate calculation of the stress, the strain and the phase angle at each cycle. In addition, the system and acquisition software (test ware MTS) allow recording the following data:

- The time (t);
- The force (F) for calculating the stress (σ_1) by considering the surface of the specimen determined by measuring the diameter of the specimen (D):

$$\sigma_1 = \frac{F}{\pi(D/2)^2} \tag{4.3}$$

We have noted that our calculations for the stress and the strain were done in only one direction (we'll call it the vertical direction or the direction 1) (see Figure 4.23).

- The axial displacement Δh_i of three extensometers (i = 1, 2 or 3) allows to calculate the axial deformations ε_{axi} of the specimen by considering the distance of measurement of extensometers. For our case, h_0 is equal to 50mm for the extensometers of 50mm. Axial strain is calculated as:

$$\varepsilon_{axi} = \frac{\Delta h_i}{h_0} \tag{4.4}$$

- Average axial strain ε_{1ext} of the specimen is measured by the extensometers calculated using the average of the three extensometers

$$\varepsilon_{1ext} = \frac{\varepsilon_{ax1} + \varepsilon_{ax2} + \varepsilon_{ax3}}{3} \quad (4.5)$$

- The temperatures measured by the probe PT100 and / or thermocouple;
- The number of cycle.

For a linear viscoelastic material, the application of a solicitation in sinusoidal stress in the direction 1 results in:

$$\sigma_1(t) = \sigma_{01} \sin(\omega t) \quad (4.6)$$

And strain response in this direction is sinusoidal in steady state:

$$\varepsilon_1(t) = \varepsilon_{01} \sin(\omega t - \phi_E) \quad (4.7)$$

The phase angle ϕ_E is related to the phase shift between the signal of stress and that of the average strain of the three axial measures.

$$\emptyset_E = \phi_\sigma - \phi_{\varepsilon ax} \quad (4.8)$$

It is possible to link the deformation ε_1 to the stress σ_1 by the following relationship:

$$E^* = \frac{\sigma_1^*}{\varepsilon_1^*} \quad (4.9)$$

The complex modulus E* is the ratio between the amplitudes of σ_1^* and ε_1^*. In complex notation, it is written:

$$E^* = \frac{\sigma_{01}^* \times e^{i\omega t}}{\varepsilon_{01}^* \times e^{i(\omega t - \phi_E)}} = |E^*| \times e^{i\phi t} \quad (4.10)$$

The components of the complex modulus: the storage modulus E_1 and the loss modulus E_2 are calculated by the equations (4.11) and (4.12):

$$E_1 = |E^*| \times \cos \phi_E \tag{4.11}$$

$$E_2 = |E^*| \times \sin \phi_E \tag{4.12}$$

The dissipated energy per cycle is calculated the using the equation (4.13). This parameter is used for the study of fatigue tests:

$$W_d = \pi \times \varepsilon_A \times \sigma_A \times \sin \phi_E \tag{4.13}$$

Figure 4.26 illustrates an example of experimental signals from a fatigue test. The axial stress and the strains measured by the extensometers are centered on zero and plotted against time.

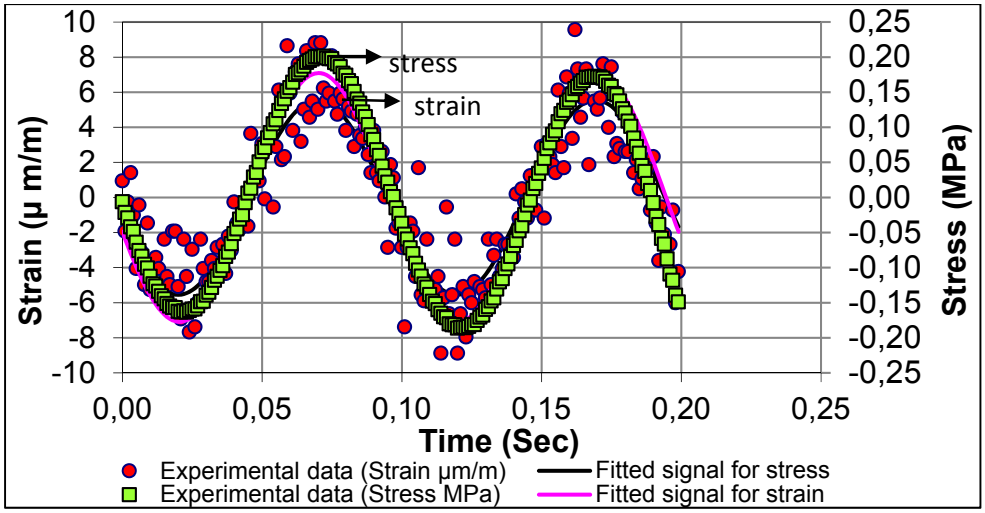

Figure 4.26 Axial stress and strains measured by the extensometers (fatigue test - 15RAP-(P2-A3)-D130, 2 cycles around cycle N = 22)

4.5.6 Data processing

The data is processed using macros with VBA component (Visual Basic for Applications) Microsoft Excel software. The data is recorded to include two successive cycles sampled

over 200 points. These data items are not located exactly on a sinusoidal curve due to experimental imperfections and low non-linearity behaviour. The experimental acquisition data are then treated as approximate sinusoidal curves defined by the following equation:

$$y = y_0 + y_A \times \sin(\omega t + \phi) \tag{4.14}$$

Thus, the part of frequency is constant, and the other parameters of the equation are calculated by the least squares method. In the treatment file, the signal of the stress (σ_A) in the material is calculated by relationship between the measured force (F) applied directly by the force sensor on the specimen and the cross section area of the specimen using the equation (4.3). Moreover, the axial strain (ε_A) is calculated using the equation (4.4).

ln the processing file, we systematically determined the following parameters:

- for the stress signal: σ_A, σ_0, ϕ_σ (amplitude, centered value and phase angle);
- for the axial deformation signals: ε_{Aaxi}, ε_{0axi}, $\phi_{\varepsilon axi}$ (amplitude, the centered value and phase angle to the two or three axial deformations: i = 1, 2 or 3) and ε_{Aax}, ε_{0ax}, $\phi_{\varepsilon ax}$ (amplitude, the centered value, the phase angle of the mean deformation of the two or three previous measures).

4.5.7 Quality of the mechanical test

It is also necessary to check the quality of the mechanical test. For each parameter Y (stress or strain) calculated on two cycles, the K_Y criterion evaluates the gap between the experimental points and the sinusoidal function approximated by the least squares method. This criterion is the quality index (*QI*) test. Expression of K_y (in percent) is calculated by considering 200 acquisition points (2 cycles) and is given by equation (4.15). Y_k^m denotes the value measured at the point of acquisition k (1, 2, 3, ... to 200) and Y_k^c denotes the magnitude calculated by the sinusoidal function. *n* denotes number of the analyzed point (200 points) and Y_A denotes the amplitude of the signal.

$$K_Y(100\%) = QI(\%) = \left(\frac{1}{n} \sum_{K=1}^{n} \frac{\left| Y_k^m - Y_k^c \right|}{Y_A} \right) \times 100 \tag{4.15}$$

A test is considered good or acceptable when all QI values less than 10% or 15% respectively. This applies in particular to signals of stress and strains measured by the equipment controlling the test (in our case, the extensometers). Example of the curve of the quality indices according to the number of cycles for a fatigue test will be as presented later in chapter 6 in Figure 6.5. Note that the limit was set at 15%. Beyond this limit, the test is canceled and subsequent cycles are no longer considered valid.

In addition, the difference of strain amplitude of an extensometer (i = 1, 2 or 3) with respect to the average of the three must be lower than 25% (the $\Delta\varepsilon_{exi}$ value can be determined according to the equation 2.20). This last criterion ensures that the level of deformation in the specimen is uniform and that the test may be considered homogeneous. Then, the test results are accepted if the QI $\leq$ 15% the set of signals and $\Delta\varepsilon_{exti} \leq 25\%$ (strain measured by the extensometers).

CHAPTER 5

ANALYSIS OF COMPLEX MODULUS RESULTS AND LVE MODELLING USING 2S2P1D MODEL

5.1 Introduction

This chapter includes nine main sections: the first section presents the complex modulus test results of the reference mix (the mixture with no RAP). Complex modulus test results are presented using isothermal curves, isochronal curves, Cole-Cole plane (complex plane) and Black space. The next two sections (5.2 and 5.3) contain the 2S2P1D rheological model used to fit the experimental results for the tested mixtures. Section 5.4 covers correlations between the parameters of the model and the constituents of the tested materials are underlined as well. Section 5.5 describes a test repeatability study, and section 5.6 discusses the complex modulus measurements of different mixes. Section 5.7 shows the plots of complex modulus shift factors of the mixes. We introduce the newly RAP coefficient of evolution, C^*_{RCE} used to quantitatively compare the results of complex modulus of mixes with RAP in section 5.8. Finally, we present the normalized curves which allow comparisons for different bituminous materials by plotting Cole-Cole (or Black) curves in section 5.9.

5.2 Complex modulus test results

For complex modulus, Tension-Compression (T-C) test on cylindrical specimen was performed. The results obtained from this test make it possible to reflect the linear viscoelastic behaviour of these materials. Complex modulus testing was performed in general on one sample for each mix. However, we did repetitions by testing two samples for some selected mixes to study the variation in the results. The characteristics of the tested samples are presented in Table 5.1. Figure 5.1 shows the air voids of specimens RAP mixtures. The range for air void content between samples can be higher than the current acceptable range of $\pm$0,5%.

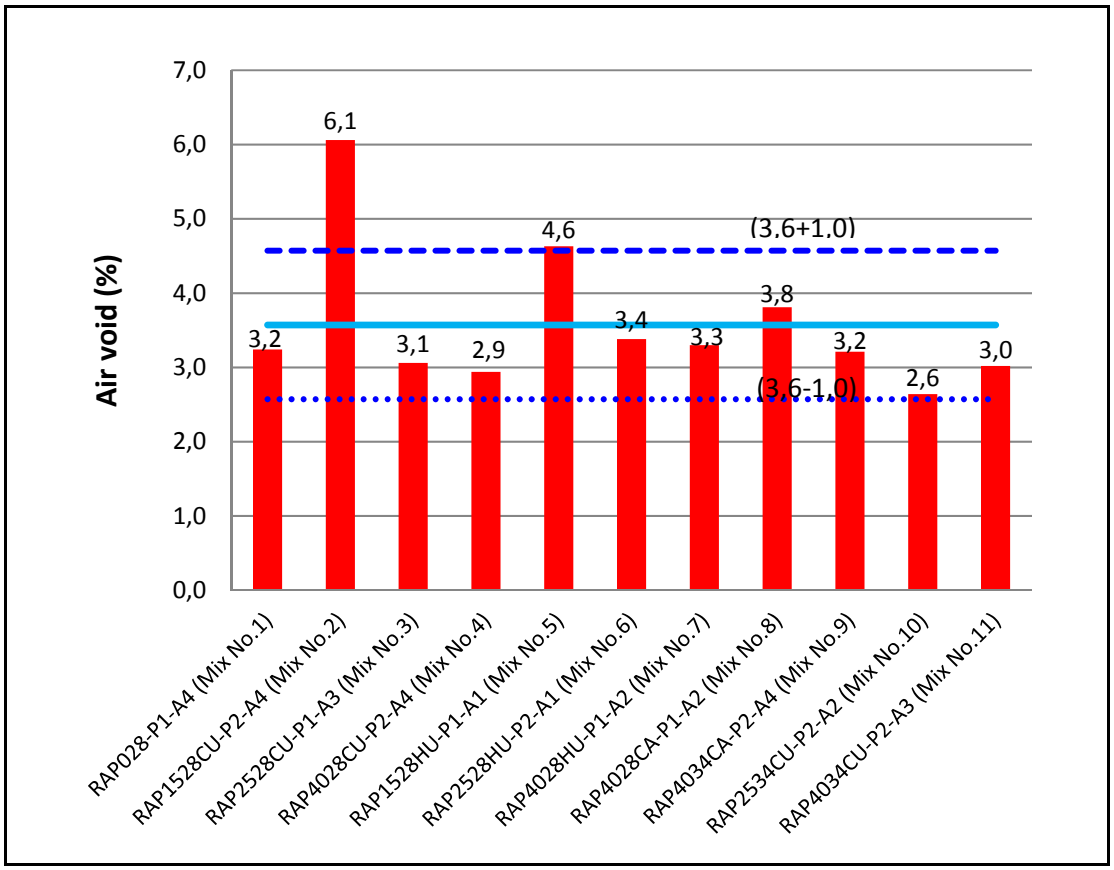

Figure 5.1 Air void of tests specimens

The air voids content of all the specimens tested is in the range of 3,6±1,0% except the one of mix #2 which had a higher air void. We select the P2-A4 sample for mix #2 for comparisons between mixes even if it show more higher level in the air void because there is an absence of the measurements data at 35°C in the other replicate sample (P1-A5).

In order to compare the mixtures, it is possible to deal with the average of two samples for the mixes, if they are close for air voids content, or to refer to one-to-one sample results. Here, we picked the second choice and for the comparison, we cautiously selected the samples that have similar air voids as possible. In Table 5.1, we added a fuchsia thick box on samples used in our comparison. In some cases, we saw a visual difference between the repetitions. In this case, we will present the results for comparisons two times. In the first time we will use one selected sample of a specific mix to compare with the two repetitions of

the other mix and in the second time we will use the other sample of the same mix to compare with the two repetitions of the other mix.

Table 5.1 Characteristics of cylindrical samples used for the complex modulus test

Mix No.	Mix ID	Specimen	Dimension (cm)		Weight (kg)	Bulk density (g/cm^3)	Maximum density (g/cm^3)	Air voids %
			Diameter	Height				
1	**RAP028**	P1-A4	7,39 [A]	12,1 [A]	1,329	2,555	2,641	3,2
2	**RAP1528CU**	P2-A4	7,39	12,1	1,273	2,443	2,601	6, 1
		P1-A5	7,4	12,3	1,295	2,459	2,601	5,5
3	**RAP2528CU**	P1-A3	7,35	12,6	1,358	2,542	2,622	3,1
		P2-A2	7,40	12,4	1,339	2,503	2,622	4,5
4	**RAP4028CU**	P2-A4	7,39	12,5	1,367	2,541	2,618	2, 9
5	**RAP1528HU**	P1-A1	7,39	12,3	1,317	2,491	2,612	4,6
6	**RAP2528HU**	P1-A1	7,36	12,6	1,354	2,518	2,617	3,8
		P2-A1	7,35	12,4	1,317	2,529	2,617	3,4
7	**RAP4028HU**	P1-A2	7,39	12,5	1,359	2,507	2,627	3, 3
		P2-A4	7,38	12,4	1,337	2,528	2,627	3,9
8	**RAP4028CA**	P1-A1	7,40	12,2	1,301	2,481	2,601	4,6
		P1-A2	7,40	12,5	1,344	2,502	2,601	3,8
9	**RAP4034CA**	P2-A4	7,39	12,5	1,351	2,514	2,597	3,2
		P2-A3	7,39	12,4	1,340	2,513	2,597	3,2
10	**RAP2534CU**	P2-A2	7,36	12,3	1,335	2,555	2,624	2, 6
11	**RAP4034CU**	P2-A3	7,39	12,3	1,339	2,542	2,621	3, 0

[A] mean of 3 measurements

Only results that were obtained with good quality index, QI, (less than 15%) are shown and used in the analysis, except for the results at low temperature, where the QI value can be higher than 15%. We found that it can go a bit higher because the stiffness of the asphalt mix is great and it can reduce the level of strain. Other results that didn't respect the conditions of acceptance were rejected from the analysis.

5.2.1 Isothermal and isochronal curves

The Figures 5.2a and 5.2b present respectively the isothermal and isochronal curves of the norm of complex modulus according to the frequency and the temperature for the mix RAP028: sample P1-A4.

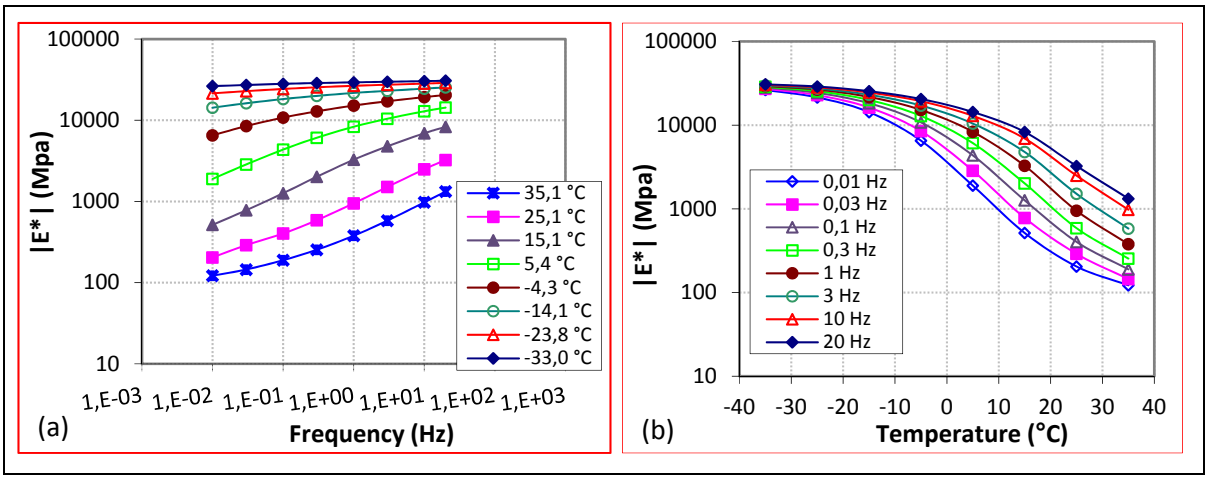

Figure 5.2 Isothermal curves (a) and isochrones (b) of the norm of the complex modulus versus the frequency and the temperature, respectively (mix RAP028: sample P1-A4)

It can be observed that the norm of complex modulus increases when the frequency increases, and decreases when the temperature increases as implied in the literature.

5.2.2 Cole-Cole plane and Black space diagram

Examples of curves of the complex modulus in the Cole-Cole plane and Black space diagram are presented in Figure 5.3a and Figure 5.3b, respectively. The single curve obtained in the Cole-Cole plane shows that the principle of time-temperature superposition (TTSP) in the domain of LVE of the tested bituminous is verified.

For Black curve shown in Figure 5.3b, some scattered results can be observed, which means that its Black curve is not unique. It could be related to the bitumen type. Bitumen containing polymer sometimes shows scattering result in the Black space diagram, which means that

they don't conform entirely to the Time-Temperature Superposition Principle (TTSP). This observation can also be seen for a few curves shown in Figures in Appendix II. It's in accordance with the literature review (Delaporte *et al.*, 2007).

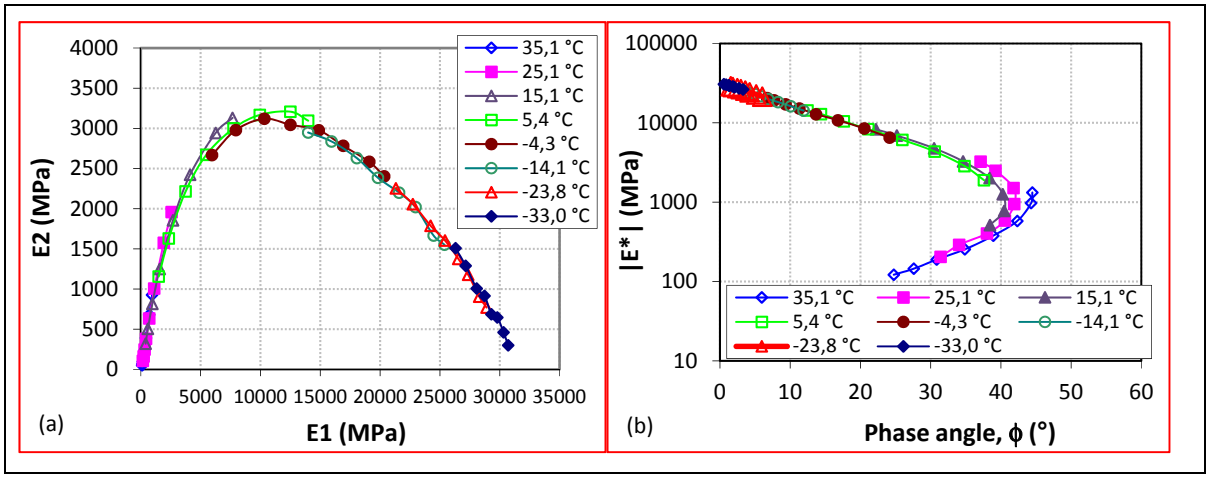

Figure 5.3 Curves of the complex modulus: a) in a Cole-Cole plane; and b) in the Black space (mix RAP028: sample P1-A4)

This is in agreement with Olard and Di Benedetto (2003) who found that some mixes do not follow the TTSP since all points are not on a single line. A unique complex modulus master curves of |E*| can be plotted at a reference temperature using a Partial Time-Temperature Superposition Principle (PTTSP) since the shifting procedure gives a unique and continuous master curve only for the norm of the modulus.

5.2.3 Master curves

The complex modulus can be represented by the master curves (norm of the complex modulus and phase angle). It can be constructed as a function of the equivalent frequency f_e utilizing the TTSP, which describes viscoelastic behaviour of asphalt binder and mixtures. Data collected at different temperatures can be 'shifted' relative to the time of loading (or frequency), so that the various curves can be aligned to form a single master curve, as discussed in section 2.6.3.4. The expression of f_e is given by the following equation:

$$f_e = a_T(T, T_{ref}) \times f_r \quad (5.1)$$

Where:

a_T	The shift factor at temperature T ;
T	The test temperature (°C);
T_{ref}	The reference temperature (°C): $a_T(T, T_{ref}) = 1$; and
f_r	The real frequency of solicitation (Hz).

For example, the construction of the master curve of the virgin mix (test RAP028) by the shifting procedure at $T_{ref} = 5{,}4°C$ is illustrated in Figures 5.4a (norm of E*) and b (phase angle of |E*|).

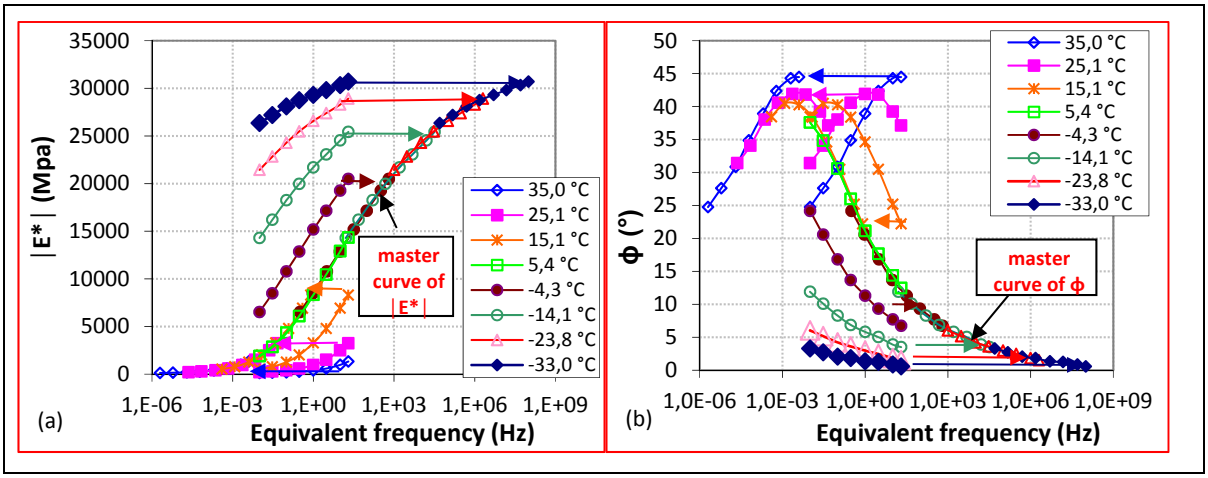

Figure 5.4 Construction of the master curves at $T_{ref} = 5{,}4°C$ with the shifting procedures for the virgin mix (RAP028), (a) master curve of |E*|, (b) the master curve of the phase angle of E*

The complex modulus test results for the RAP tested mixtures are presented in tabular form in Appendix II for all the tests.

Master curves obtained from the complex modulus tests results of various HMA mixes were considered at a reference temperature set at 10°C (T_{ref}) for comparison between mixtures. To

plot master curves, shift factors, called a_{TE_mix}, were determined for each mix at a chosen mix reference temperature (T_{mix_ref}) with respect to one of those used for each mix under testing. As differences on chosen T_{mix_ref} do exist between mixtures, new a_{TE} must be considered to plot master curves at T_{ref} = 10°C. The new a_{TE} values are obtained from the following equation:

$$a_{TE}(T) = \frac{a_{TE\_mix}\,(T)}{a_{TE\_mix}\,(10°C)} \tag{5.2}$$

Where:
$a_{TE\_mix}\,(10°C)$ corresponds to the a_{TE_mix} value at 10°C as extrapolated from the experimental data from each mix.

We can also determine the new WLF constants C_1^{ref} *and* C_2^{ref} with respect to T_{ref} = 10°C using the following formula:

$$C_2^{ref} = C_2^{ref`} + T_{ref} - T_{ref`} \tag{5.3}$$

$$C_1^{ref} = \frac{C_1^{ref`} . C_2^{ref`}}{C_2^{ref}} \tag{5.4}$$

Where:

$C_1^{ref`}$ and $C_2^{ref`}$ Constants with respect to the chosen reference temperature $T_{ref`}$; and

$T_{ref`}$ The chosen reference temperature in °K (T_{mix_ref}).

To better compare the results, it's interesting to show all the master curves obtained from raw results for all tested samples as shown in Figure 5.5. The reference temperature in Figure 5.5 is 10°C.

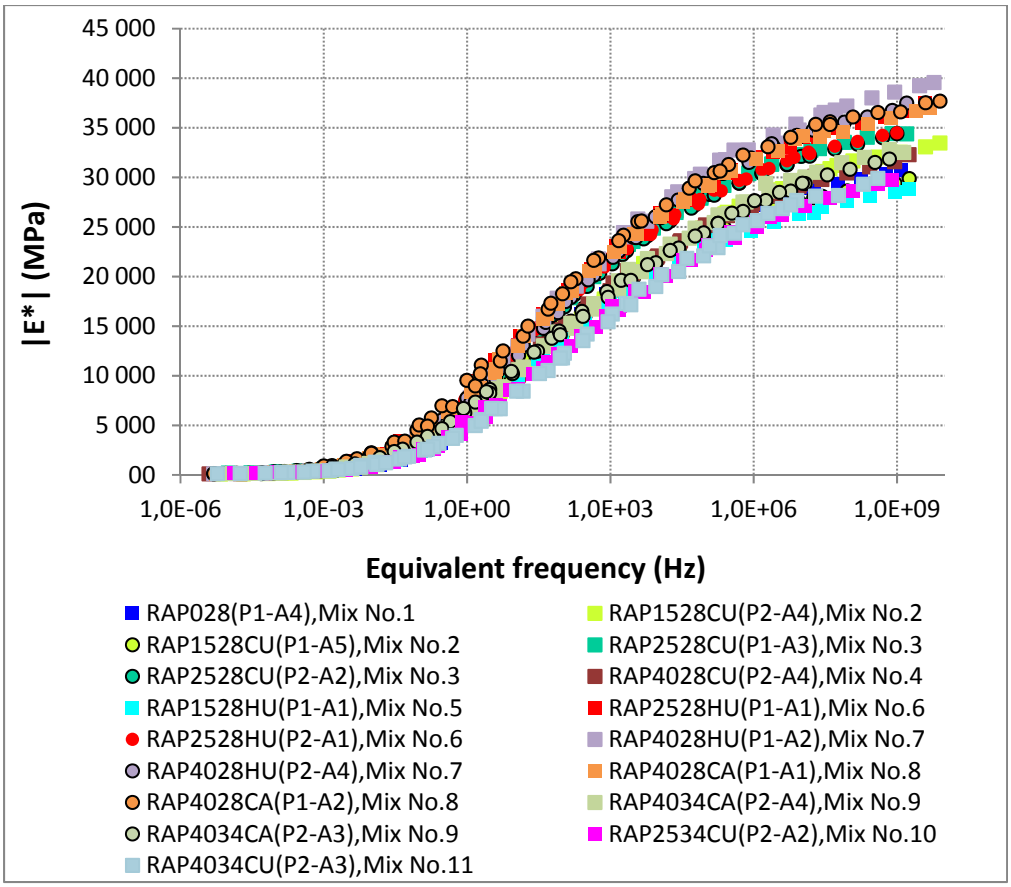

Figure 5.5 Master curves of all 'Experimental' results that obtained for this study at T_{ref} = 10°C

5.3 Modelling the behaviour of asphalt mixtures using 2S2P1D model

5.3.1 LVE Simulation results for the virgin mixture (RAP028)

Simulations of the LVE behaviour (complex modulus) using the 2S2P1D model of the virgin mix (RAP028) is compared with the experimental results presented in the previous section. Information regarding the modelling of the behaviour of asphalt mixtures using 2S2P1D model is presented in section 2.6.4.1.

The simulations of the norm of the complex modulus and the phase angle of the complex modulus are presented using the following 4 types of representation:

- Master curve of |E*| with T_{ref} = 5,4°C in the Figure 5.6a;
- Master curve of ϕ of the complex modulus with T_{ref} = 5,4°C in the Figure 5.6b;
- Cole-Cole plane in the Figure 5.7a; and
- Black space in the Figure 5.7b.

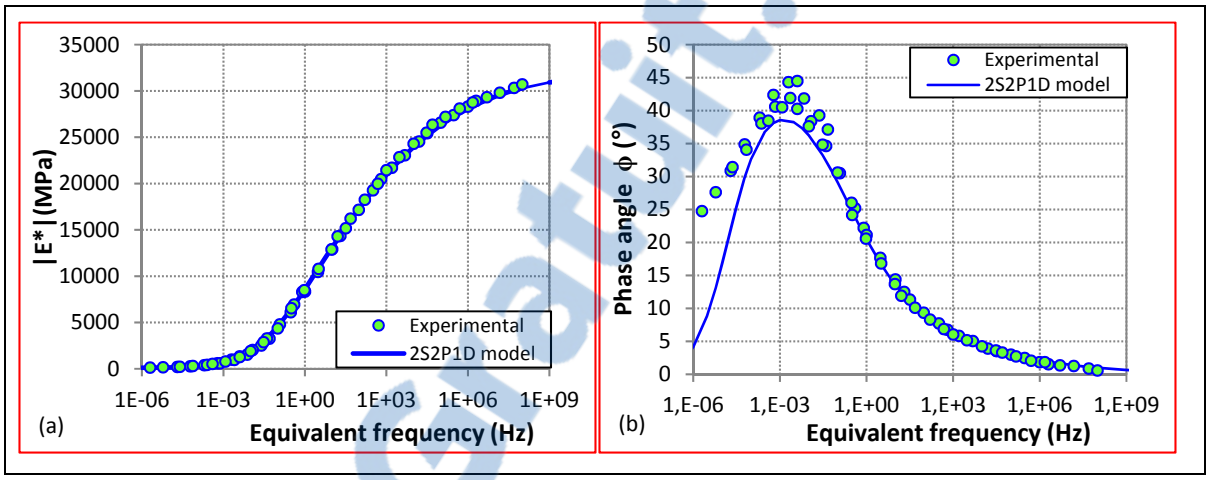

Figure 5.6 Master curves of the virgin mix (RAP028): Simulation with the model 2S2P1D (T_{ref} = 5,4 °C), (a) Master curves of the norm of the complex modulus |E*|, (b) Master curve of ϕ of the complex modulus

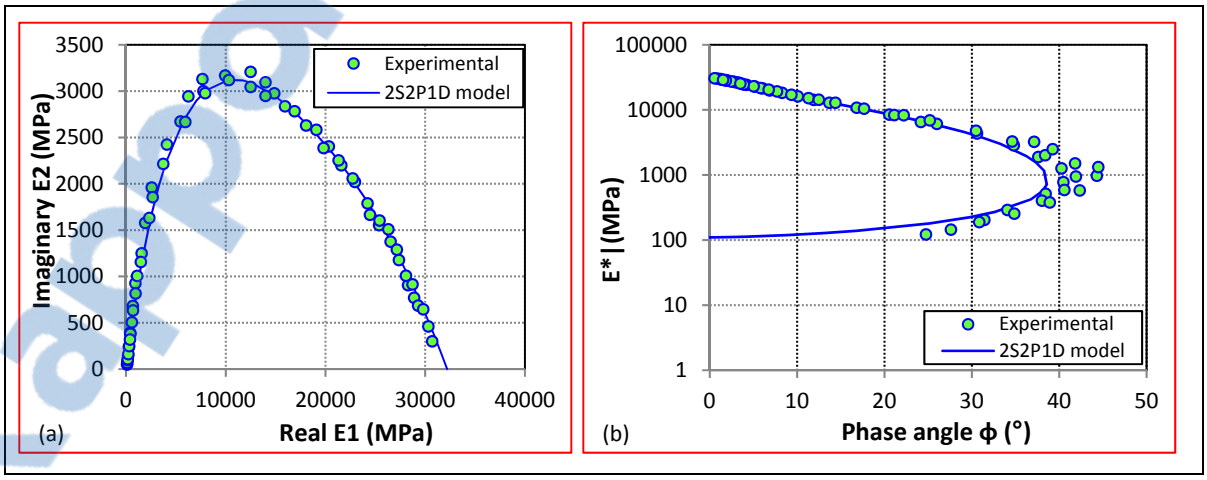

Figure 5.7 Complex modulus of the virgin mix (RAP028) in the Cole-Cole plane and in the Black space, Simulation with the model 2S2P1D, (a) Cole-Cole plane, (b) Black space

These figures highlight the good performance of the 2S2P1D model to simulate the viscoelastic behaviour of the virgin mix (RAP028) on the wide range of tested temperatures and frequencies. In particular, the norm of E* is very well modelled on all the range of temperatures and/or frequencies. Regarding the phase angle, the model provides good results at low temperature. At high temperature, we observe variations reaching up to 7° between the measured phase angle and the one that is being modelled (Figure 5.6b). Moreover, the Cole-Cole plane highlights very good quality of modelling on all the tested temperatures and frequencies band (Figure 5.7a). Finally, since the model fits the experimental points well, it can be concluded that our sample has been prepared and tested very well, and that the model's parameters have been adjusted properly.

The 2S2P1D model parameters are determined by hand to ensure the best fit possible between measured and modelled data. Table 5.2 presents the model parameters calibrated to each mix (corresponding to its samples) evaluated in this thesis, for the virgin mix (RAP028) and for the other tested materials, T_{Ref} = 10°C. The constants C_1 and C_2 of the WLF law (William, Landel and Ferry) (equation (2.18)) are also listed in this table. C_1 and C_2 are calculated from the reference temperature.

The figures in Apendix II were constructed to show the fitting of laboratory data according to the master curves, Cole-Cole, and Black diagrams for all the tested recycled materials. Table 5.2 highlights that the two repetitions of the same mix have the same value for the parameters δ, k, h, and β. The parameters of the considered mixes could appear as different, but they might have identical linear viscoelastic properties when considered at different temperatures. That's why we will go deeper in our analysis by presenting more details of comparisons in the next section and in the sections that comes afterwards. Figure 5.8 shows the static and glassy moduli for all the tested bituminous samples (E_{00} and E_0). The static moduli (resp. glassy) the tested mixes range from 60 to 127MPa (resp. from 32 000 to 40 700MPa). Generally, the slight heterogeneity among the tested samples could explain the variation of the static modulus from one mix to another. Indeed, in overall the different mixture samples may have slightly different aggregate grading and/or air voids (3,6±0,93%) and it was

reviewed that the static modulus probably depends likewise on the aggregate skeleton and void content (Delaporte et al., 2007).

Table 5.2 Constants of the 2S2P1D model gauged for the tested materials (7 constants of E*, and 2 constants of WLF law) (T_{ref} = 10°C)

Mix No	Mix ID	Sample ID	E*							WLF	
			E_0 (MPa)	E_{00} (MPa)	δ	k	β	h	τ_0 (sec)	C_1	C_2
1	RAP028	P1-A4	32 200	100	1,82	0,182	500	0,530	0,03	20,33	152,69
2	RAP1528CU	P2-A4	34 900	60	2,30	0,177	500	0,544	0,03	26,63	183,00
		P1-A5	31 300	80	2,30	0,177	500	0,544	0,11	154,21	982,51
3	RAP2528CU	P1-A3	36 350	127	1,81	0,177	500	0,544	0,04	25,49	184,02
		P2-A2	35 950	107	1,90	0,177	500	0,544	0,04	27,79	189,69
4	RAP4028CU	P2-A4	33 700	110	2,15	0,177	500	0,544	0,04	21,57	154,96
5	RAP1528HU	P1-A1	30 700	110	2,15	0,177	500	0,544	0,04	21,73	154,94
6	RAP2528HU	P1-A1	38 600	80	2,30	0,177	500	0,540	0,09	28,74	213,42
		P2-A1	36 300	82	1,85	0,177	500	0,544	0,04	25,61	180,13
7	RAP4028HU	P1-A2	40 700	80	2,15	0,177	500	0,544	0,04	25,09	174,57
		P2-A4	39 200	75	2,30	0,180	500	0,544	0,04	21,26	162,02
8	RAP4028CA	P1-A1	38 900	100	2,20	0,168	500	0,544	0,09	33,22	237,61
		P1-A2	38 900	100	2,15	0,177	500	0,544	0,09	33,75	234,43
9	RAP4034CA	P2-A4	35 200	80	2,20	0,175	2000	0,510	0,03	36,01	135,26
		P2-A3	33 900	120	2,30	0,177	2000	0,544	0,04	21,95	155,94
10	RAP2534CU	P2-A2	32 000	115	2,70	0,182	2000	0,560	0,05	20,05	154,83
11	RAP4034CU	P2-A3	32 300	110	2,40	0,177	2000	0,544	0,02	21,88	156,44

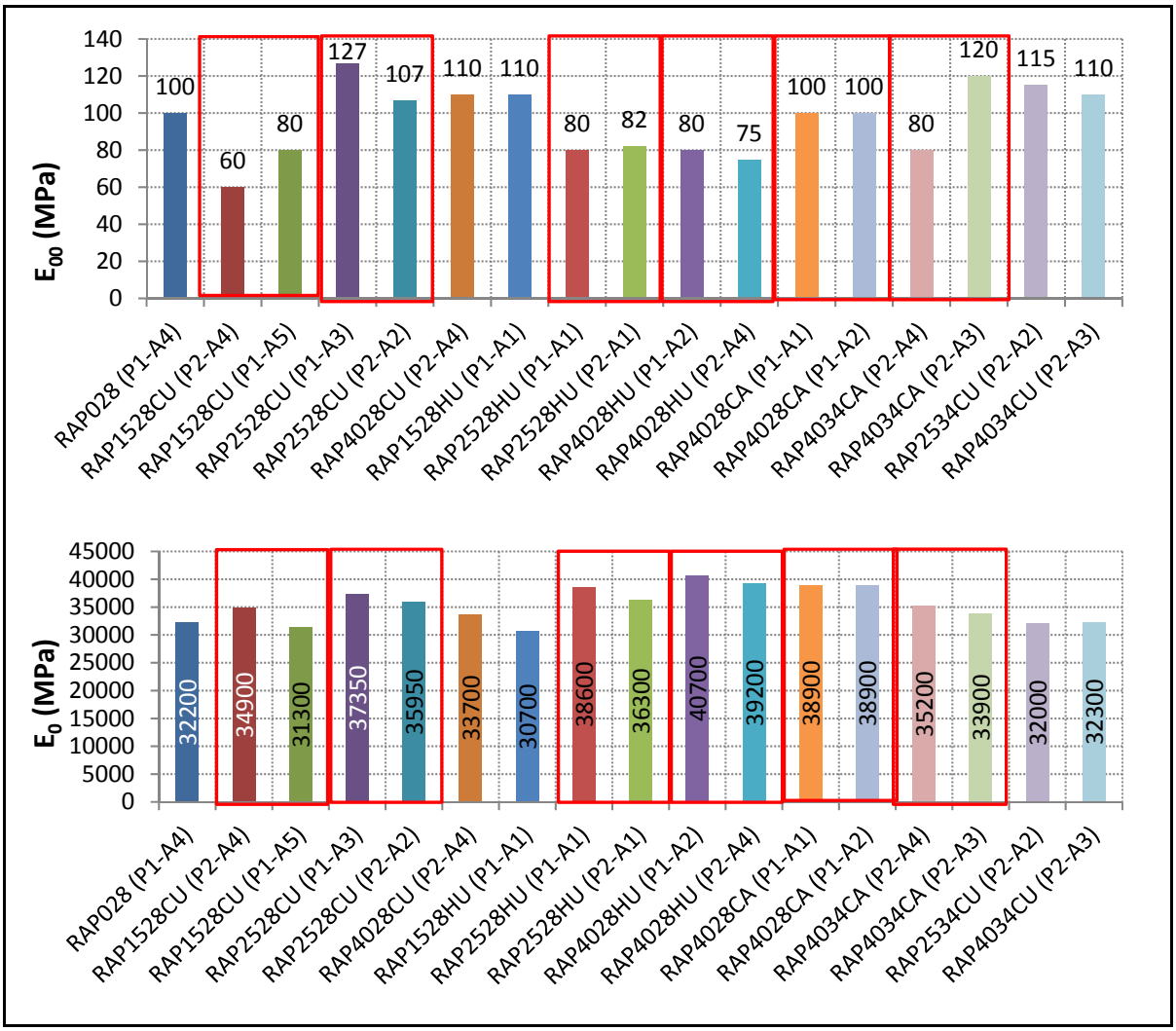

Figure 5.8 E_{00} and E_0 values for the tested specimens of different mixes

5.4 Statistical analysis

To evaluate the performance of the predicted 2S2P1D model, the correlation of the measured and predicted values was assessed using the coefficient of determination (R^2). The R^2 is used to observe the predicted data's dispersion from the equality line, with 1,0 as the perfect value. The R^2 calculation is done exactly as it will be presented in section 7.2 (equation 7.2). Table 5.3 shows the goodness of fit statistics for all the samples tested in this study. It was observed that the 2S2P1D model shows a good correlation (R^2 ranged from 0,9829 to 0,9994). These

results suggest that the 2S2P1D model can provide an “excellent” accuracy for the prediction of |E*|.

Table 5.3 Goodness of fit statistical analysis for the recycled mixture

Mix No.	Mix ID	Specimen	S_e/S_y	R^2
1	**RAP028**	P1-A4	8,08E-17	0,9994
2	**RAP1528CU**	P2-A4	5,55E-13	0,9964
		P1-A5	1,48E-09	0,9829
3	**RAP2528CU**	P1-A3	7,77E-16	0,9990
		P2-A2	1,12E-14	0,9984
4	**RAP4028CU**	P2-A4	2,77E-45	0,9992
5	**RAP1528HU**	P1-A1	8,15E-12	0,9939
6	**RAP2528HU**	P1-A1	3,48E-12	0,9949
		P2-A1	4,51E-14	0,9979
7	**RAP4028HU**	P1-A2	1,5E-15	0,9989
		P2-A4	1,43E-16	0,9993
8	**RAP4028CA**	P1-A1	2,32E-14	0,9981
		P1-A2	2,31E-12	0,9953
9	**RAP4034CA**	P2-A4	1,38E-13	0,9973
		P2-A3	1,75E-13	0,9972
10	**RAP2534CU**	P2-A2	1,02E-12	0,9960
11	**RAP4034CU**	P2-A3	1,16E-12	0,9959

5.5 Complex modulus results’ repeatability

The aim of this section is to demonstrate the difference in |E*| results between the two repetitions that have been tested for the same mix. The results of this section are important even if we focus to present our analysis by doing comparisons between mixes using only the one-to-one sample. With this, it’s possible to know if the existing variation due to the influence of a specific parameter is significant or if it occurs in the range of repeatability

between samples. As presented previously in Table 5.1, we have repetitions (two specimens) for only six mixes, of the 11, used in the complex modulus test. A summary of the tests data is presented in Figures 5.9 and 5.10 for the different mixes. Master curves were constructed using the method described in section 5.2.3. The reference temperature for all master curves is 10°C. While the figures placed at the right part of the page present the test data in Cole-Cole plane.

The statistical parameter (R^2) for the 2S2P1D models that represents the two repetitions of each mix in the master curves is given in these figures. The calculations can be done using the least square method as will be shown in details in section 7.2. The R^2 for the models of the defined six mixes ranged from 0,9957 to 0,9991, which indicates very low variation. Our results show that a difference in the modulus values between the two samples with the same air void content is low. This difference is also low for the two samples with different air void contents.

Even if the E* results in the Cole-Cole plane for mix RAP1528CU have shown that there is a difference between the two samples, their maximum storage moduli is still comparable. Their values are 34 900 and 33 440 MPa for samples P2-A4 and P1-A5, respectively. Indeed, we compare between these two values, we can consider that 11% variation is acceptable. However, in order to find a suitable tool to quantify the difference between the values of complex modulus, we calculate the variability coefficient evolution $|C^*_{VCE}|$. $|C^*_{VCE}|$ calculates the ratio of the |E*| between the two repetitions in the same way we do the $|C^*_{RCE}|$ presented in section 5.9. This section can provide a more reasonable and brief discussions, and accurate analysis about the changes in |E*| values between repetitions.

Moreover, one important issue in the repeatability study of dynamic modulus which has not been addressed is the coefficient of variation for dynamic modulus testing (CV). CV will show how much a testing parameter such as dynamic modulus should be different due to inherent variability in the dynamic modulus. Table 5.4 shows the average complex dynamic

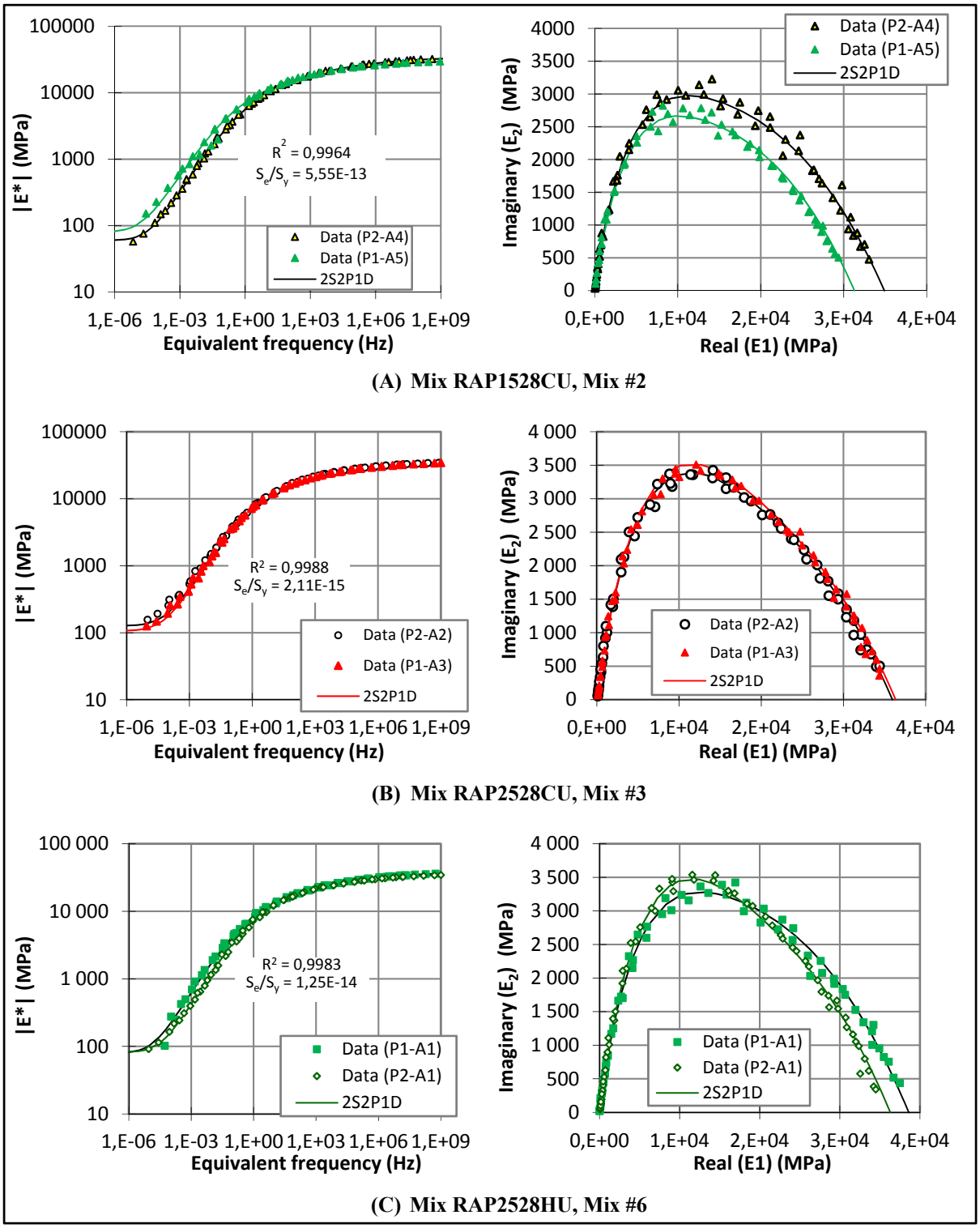

Figure 5.9 Master curves & Cole-Cole plane of different asphalt mixtures according to complex modulus repeatability. Simulation with the model 2S2P1D

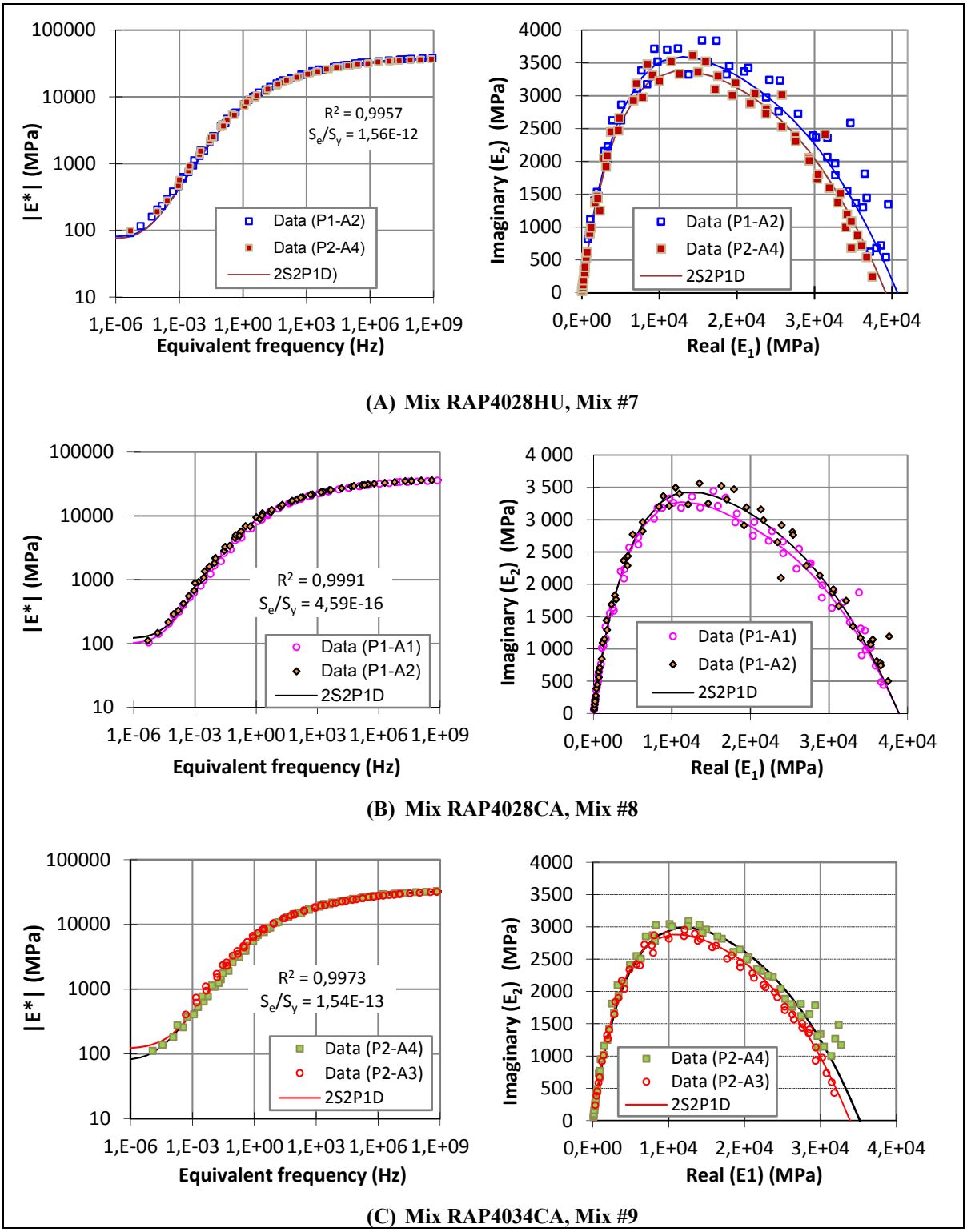

Figure 5.10 Following Master curves & Cole-Cole plane of different asphalt mixtures according to complex modulus repeatability. Simulation with the model 2S2P1D

moduli of the two samples and the CV of the replicate specimens for each mixture at three tested temperatures and at 20 Hz. The coefficient of variation of the data ranged from 2,4 to 29,8%.

Table 5.4 Average complex dynamic modulus of mixtures that have repeatability and CV

Mix No.	Mix ID	T (°C)	Average |E*| (MPa)	CV (%)
2	RAP1528CU	15	8 370	3,8
		25	2 816	29,9
		35	938	29,8
3	RAP2528CU	15	9 833	3,6
		25	4 769	2,4
		35	1 715	8,9
6	RAP2528HU	15	10 070	3,6
		25	5 058	8,1
		35	1 326	10,8
7	RAP4028HU	15	9 616	4,8
		25	4597	2,5
		35	N.A.*	N,A,
8	RAP4028CA	15	10 655	3,7
		25	5 492	4,4
		35	2 130	3,6
9	RAP4034CA	15	8 735	1,5
		25	4 196	6
		35	N.A.	N.A.

(*): The testing data is missing for one sample from the two

5.6 Analysis and Discussion

As mentioned previously, analysis on test data for the eleven different mixtures shows that the 2S2P1D model fits quite well the test data measurement. Again, a visual inspection of the

data contained in these plots indicates that the complex modulus increased as test temperature decreased and the complex modulus increased as loading frequency was increased. These results are in agreement with Sondag, Chadbourn and Drescher (2002) and Daniel, Kim and Lee (1998). There were four objectives to our sequence of complex modulus testing:

1. To evaluate the change in complex modulus with the addition of RAP on the mixtures;
2. To evaluate the asphalt binder grade effect on asphalt mixture complex modulus;
3. To evaluate the RAP conditioning effect on asphalt mixture complex modulus; and
4. To evaluate the effect of aged RAP on asphalt mixture complex modulus.

The figures in the following sections show the experimental data and the data calculated from the 2S2P1D model for each test specimen.

5.6.1 Effect of RAP content on complex modulus

This section focuses on showing the effect of the addition of RAP to the mixture on the complex modulus. The master curves for specimens with a PG 64-28 binder and with 0%, 15%, 25%, and 40% of RAP added cold are shown in Figure 5.11a. This Figure illustrates the effect of RAP content on complex modulus for four mixtures at 10°C. All mixtures show similar complex modulus at high temperature and/or low frequency. While at high testing frequency or low temperature, a difference is visible. However, with this presentation of the results, it is not possible to precisely analyze the results. From Figure 5.11a, it seems that the mixes can be ranked by stiffness starting with the control mix as the lowest, then followed by the 15% RAP mix, the 40% RAP and the 25% RAP mix as the stiffest. Complex modulus test results indicate that the stiffness of the mixtures increases with the addition of RAP, as would be expected, except for the 25% RAP mix, were it shows a E* a bit higher than those of the 40% RAP mixture. This is probably due to the variability of aggregate gradation. It is well known that variability of RAP stockpiles is possible.

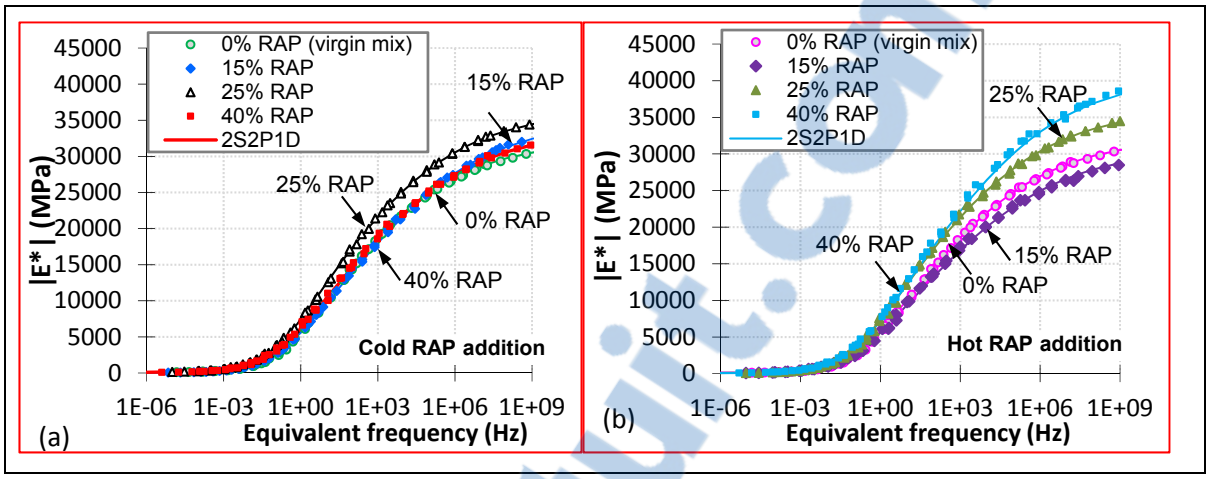

Figure 5.11 Master curves of the norm of the complex modulus at 10°C for mixes with binder grade PG 64-28, Cold RAP addition, and different percentages of RAP, 2S2P1D model of a single test (a) Cold RAP addition (b) Hot RAP addition

It is interesting to note that we can show the impact of the addition of RAP by introducing another comparison based on another group of recycled mixtures that were tested in this study. This group is also made with the addition of different percentages of RAP, but RAP was heated to 110°C for few minutes. Materials of that group were RAP028 (mix #1), RAP1528HU (mix #5), RAP2528HU (mix #6), and RAP4028HU (mix #7). Figure 5.11b summarizes test results by ranking mixtures based on the stiffness modulus (|E*|) master curves. In general at lower temperatures, the 40% mixture (mix #7) was the stiffest followed by the 25% mixture (mix #6) mixture. The softest mixture evaluated was the 15% mixture (mix #5). As we can see the ranking of this group between mixes did not show a larger difference than the one of the mixes made with cold added RAP. The only difference between them is that the 40% RAP mixture made with heated RAP to the hot virgin aggregates are stiffer than the mixtures made with cold added RAP to the superheated virgin aggregates. The variation could be explained by the slight heterogeneity among tested samples or because heating RAP in a microwave may produce stiffer RAP materials, which contributes to increase the stiffness of the mixture when very high-content RAP are used. More samples need to be tested to verify that hypothesis, so this aspect should be studied in a future project.

The complex modulus laboratory results for the four mixes made with cold added RAP are shown again but in a Cole-Cole plan in Figure 5.12. It is a much better way to distinguish between mixtures. The plotted data reflects the ability of the test results to effectively discriminate between the four mixtures known to produce different responses and consequently performance. The ranges of the storage modulus between the four mixes are close, which reflect that the different RAP content does not have a significant effect on the mixture stiffness. On the other hand, the ranking seen previously in Figure 5.11 is more obvious in this Figure (5.12a). If the E_0 of each mix is compared, the ranking stays the same with values ranking from 31 300 to 36 350 MPa with an average of 33 388. This means all calculated E_0 falls within 1913 MPa standard deviation from the average.

The data for the four mixtures prepared by adding heated RAP to 110°C are also plotted in a Cole-Cole diagram as shown in Figure 5.12b. The range of the storage modulus of the 40% mixture (mix #7) is greater than the one of the 25% mixture (mix #6) and 15% mixture (mix #5) as we observed before (see Figure 5.11).

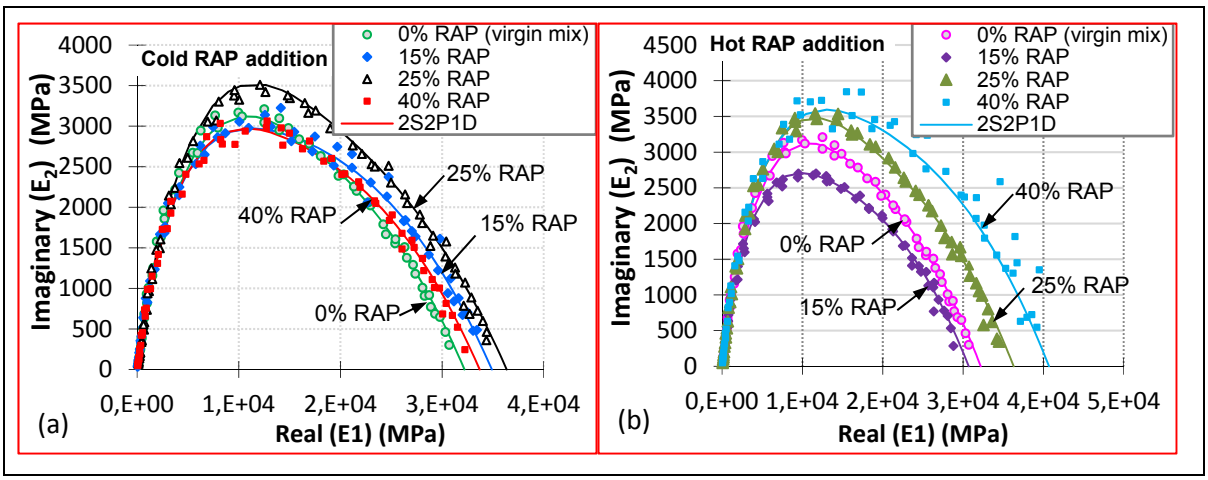

Figure 5.12 Cole-Cole diagram for the four RAP mixes prepared with different RAP content (0%, 15%, 25%, and 40%), 2S2P1D model of a single test (a) Cold RAP addition (b) Hot RAP addition

Figure 5.13 shows the E_0 stiffness ratio of the recycled mixes made by adding cold RAP to the mix and also by adding hot RAP to the mix relative to the virgin mix. For the mixtures made with cold RAP, the mix with 25% RAP was 1,16 times stiffer than the reference and with 15% RAP, the ratio goes from 0,97 to 1,08. With 40% RAP, it was 1,05 stiffer than the control mix. In fact, we consider that a change in stiffness of more or less 10% do not significantly alter the stiffness property of the mixture. In addition, the same trend was seen with the mixtures made with hot RAP. The 40% mixture was 1,25 times higher than the control mixture. The stiffness of the 25% mixtures was about 1,13 to 1,20 times higher, but the 15% mixture did not change the ratio a lot. Those observations confirm the above discussions. It should be noted that the values of E_0 shown previously in Table 5.2 were used for the calculations.

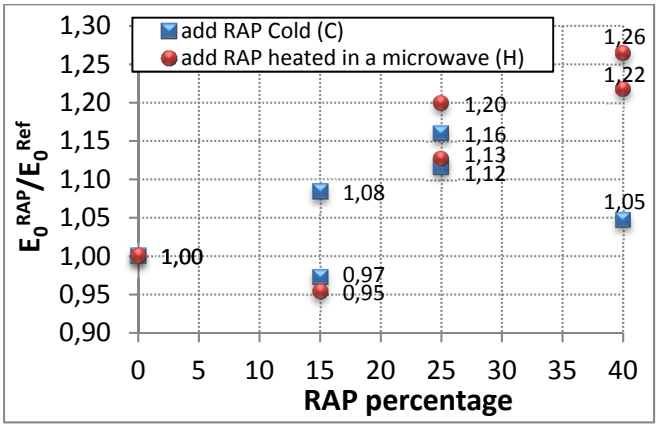

Figure 5.13 E_0 stiffness ratios of the recycled mixtures made with RAP added cold and RAP added hot relative to the virgin mix

5.6.2 Effect of other parameters on complex modulus

This section examined the influence of other parameters such as binder type, aging RAP, and RAP conditioning on the complex modulus of recycled mixtures. Figure 5.14 illustrates the typical behaviour of complex modulus for different recycled mixtures used in this research. In general, the data shown in Figure 5.14 clearly show how the complex modulus is affected by the binder grade and aging RAP. These effects are discussed in details later on.

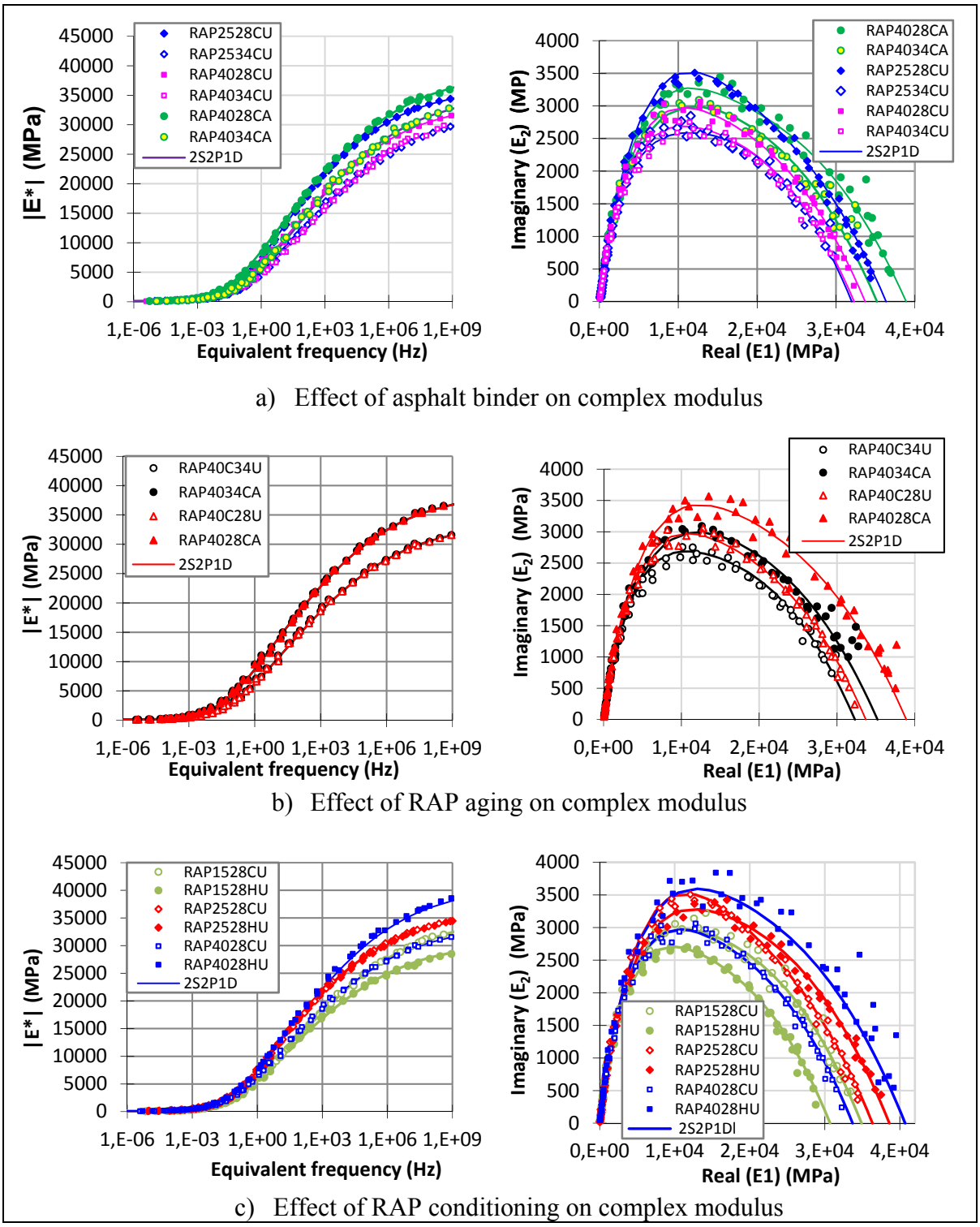

Figure 5.14 Master curves of the norm of the complex modulus (T_{ref} = 10°C) and Cole-Cole diagram different mixes with different conditioning

5.7 Shift factors

The shift factors obtained during the master curve construction of some selected materials are presented in Figures 5.15a and 5.15b. This figure shows how shift factors vary between mixtures with repetitions which have been carried out. On these figures, two evolution types of a(T) can be distinguished: the first one corresponds to materials made with various percentages of RAP where RAP was added at the room temperature 23°C (cold), and the second one corresponds to the materials composed of added RAP heated in a microwave. These figures show how shift factors vary in the case of the different selected materials. The shift factors are defined graphically after we used the classical WLF law to fit the C_1 and C_2 values. The values of coefficients C_1 and C_2 are shown previously in Table 5.2 corresponding to each sample.

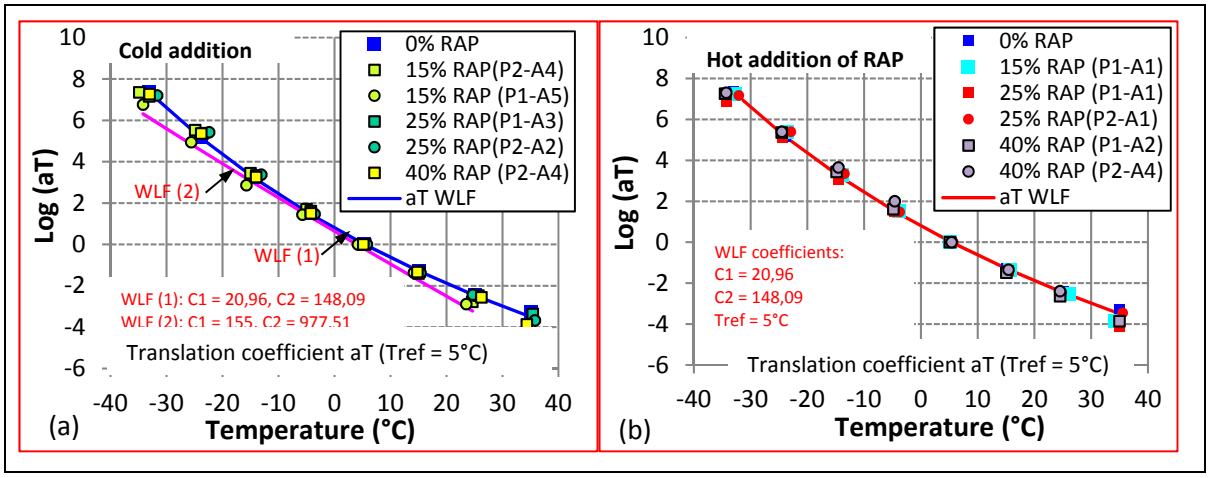

Figure 5.15 Shift factors of the tested materials made with different RAP dosage and RAP added cold or hot (a) Cold RAP addition (b) Hot RAP addition

The shift factors of the two samples of the same mix are similar (Figure 5.15). Based on the testing results and the results shown on Table-A II-1 in appendix II, for the mix RAP1528CU, a 4% change in shift factor would produce about 2% lower or higher modulus values (at 15°C and at 10 Hz), and a 17% change in shift factor would produce about 10% lower or higher modulus values (at -15°C and at 10 Hz). It appears that the equivalent frequencies (f_e) used for the sample (P2-A4) master curve corresponds very closely to the

same frequency-temperature for the sample (P2-A5). This mix seemed to have a bit of variability in its complex modulus values between its repetitions, as presented previously in section 5.5

Besides, on Figure 5.15, the shift factors for the materials shown in these figure are very close and with little variation at low temperatures. At -35°C, the log a(T) values range from 6,75 to 7,35, and at 25°C, they range from -2,43 to -2,88 (Figure 5.15a). Similar results were shown in Figure 5.15b, at -35°C, the log a(T) values ranged from 6,18 to 7,35, and at 25°C they range from -2,34 to -2,88.

Shift factors are fitted by the WLF law (equation (2.20)). The calculated coefficients are:
C_1 = 20,96 and C_2 = 148,09 for WLF (1), and C_1 = 155 and C_2 = 977,51 for WLF (2).

5.8 RAP coefficient of evolution C^*_{RCE}

In this research, in order to compare objectively the results of complex modulus of mixes with RAP, the RAP coefficient of evolution, C^*_{RCE} is introduced. The calculation of the RAP coefficient evolution (C^*_{RCE}) was proposed by Di Benedetto (Delaporte et al., 2007). The complex coefficient of evolution C^*_{RCE} is defined as the ratio between the complex modulus of a specific mix at the equivalent frequency f_e (defined by equation (5.1)), and the complex modulus of a reference mix at the same frequency f_e as written in equation (5.5).

$$C^*_{RCE}(f_e) = \frac{E^*_{mix}}{E^*_{ref-mix}} = |C^*_{RCE}|e^{i\phi_{RCE}} \tag{5.5}$$

C^*_{RCE} is a complex number, as shown in equation (5.5). Its norm is the ratio of the norms of the complex modulus of the recycled mixture to the one of the reference as calculated by equation (5.6). Its phase angle is the difference between the phase angle of the recycled mixture and the one of the reference as determined by equation (5.7).

$$|C^*_{RCE}| = \left|\frac{E^*_{mix}}{E^*_{ref-mix}}\right| \tag{5.6}$$

$$\phi_{RCE} = \phi_{E^*_{mix}} - \phi_{E^*_{ref-mix}} \tag{5.7}$$

It is important to note that the $|C^*_{RCE}|$ value is calculated in reference to the reference mix.

5.8.1 Variation coefficient evolution between replicates of complex modulus specimen's ($|C^*_{VCE}|$)

This section was used to investigate the differences in stiffness between the two samples of the same mix using the variation coefficient evolution ($|C^*_{VCE}|$) as a quantification tool to evaluate the repeatability of the stiffness of asphalt mixture. We would like to know if there will be change in the modulus value or not and what is the difference. There are 6 mixtures with two replicates per a mix (Total of 12 specimens). Now we have two groups of specimens; specimen replicates containing similar air void contents, and one specimen with different air void levels.

This section consists of two parts:

- The first part shows the difference of stiffness between 2 samples of the same mix using the $|C^*_{VCE}|$) calculated from the 2S2P1D model data; and
- The second part shows the difference between $|C^*_{VCE}|$ obtained from modelling and the one obtained from data.

In the first part we compare the results. To do that, we must have the same conditioning effect by keeping in mind that the testing temperatures of the two samples are not exactly the same but it is more or less the same. Thus, to do the calculations of ($|C^*_{VCE}|$), we fix one ($|E^*|$) sample as a reference and we calculate the ratio of the modulus of the second sample relative to the modulus of the first sample (the one that we choose to be as a reference), exactly as proposed previously in equation 5.5. It should be noted that we always select the

reference sample as the one that have the lowest air void to keep the consistency during our analysis.

Table 5.5 summarizes the maximum and the minimum $|C^*_{VCE}|$ values between the two repetitions. As shown in Table 5.5, the results of the two repetitions with the similar air void content (Mixes No. 2, 6, 7, 8, and 9) show that the maximum variation in $|C^*_{VCE}|$ value is around 5% at low temperature and/or high temperature. However, in some cases even with small variation in air voids contents ($\pm$0,5), (Mixes No 2, and 7) and the results show a large variation between the modulus, as it happens for the two repetitions of the mix RAP1528CU (samples P2-A4 and P1-A5) ($|C^*_{VCE}|$ = 43%). The sample P2-A4 with the air void content of 6,1% was 0,57 times less stiff than the sample P1-A5 with the air void content of 5,5% at low frequency (0,1 Hz) and/or high temperature. In fact we are not concerned about that ratio because when we checked deeply the two modulus values of the 2S2P1D model, we found that their values were 560 and 319 MPa for the sample P2-A4 and the sample (P1-A5), respectively. It means that the values of the modulus are low and the difference between the two values is also low and it is still in the range of the accuracy of the machine measurement. Other mixes may be showing only a few percentages difference between the two repetitions. With this, we can have more confidence to perform a comparison between mixes using one-to-one sample keeping in mind that the variations between the samples repetitions are respected. The synthesis of all the results will be shown later in Figure 5.16.

5.8.1.1 Comparison between $|C^*_{VCE}|$ obtained from experimental data or using 2S2P1D model

Since $|C^*_{VCE-2S2P1D}|$ results are coming from 2S2P1D model, those results are considered tricky. It is because there might be errors in the analysis by using modelling for some parts especially at low frequency and/or high temperature. The results could be sensitive to the calibration process which affects the resulting modelling parameters. Therefore, there might be an error in the variation calculations if the model fitting was not done properly.

Table 5.5 Summary of max and min $|C^*_{VCE}|$ value calculated from the ratio of modulus values obtained from 2S2P1D model for two repetitions of different mixes

Mix No.	Mix ID	Sample	Air void %	$\|C^*_{VCE}\|$							
				Max				Min			
				Value	Δ $\|C^*_{VCE}\|$ (%)	freq. (Hz)	Low or high freq.	Value	Δ $\|C^*_{VCE}\|$ (%)	Place (Hz)	Low or high Freq.
2	RAP1528CU	P2-A4	6,06	0,57	43	Less than 0,1	Low	1,10	10	Greater than 1E08	High
		P1-A5	5,46								
3	RAP2528CU	P1-A3	3,06	0,92	8	Less than 0,1	Low	0,99	1	Greater than 1E08	High
		P2-A2	4,52								
6	RAP2528HU	P1-A1	3,78	1,04	4	At 0,6	Low	0,99	1	At 1E05	High
		P2-A1	3,38								
7	RAP4028HU	P1-A2	3,30	0,95	5	At 30	Low	0,96	4	1E11	High
		P2-A4	3,78								
8	RAP4028C	P1-A1	4,63	0,96	4	At 1000	Low	0,99	1	1E11	High
		P1-A2	3,81								
9	RAP4034C	P2-A4	3,21	1,04	4	At 0,6	Low	0,97	3	1E11	High
		P2-A3	3,22								

Nevertheless, we propose to use always $|C^*_{VCE-2S2P1D}|$ obtained from modelling because it is an easy way to show the differences at the same conditions (temperature and frequency). Moreover, we know that the errors should be low because the accuracy of the 2S2P1D model for all our results is high, as we presented previously in section 6.4. Inconsequently, this section introduces another way for the analysis by using the experimental data at the same conditioning. It means that we would remove some data and calculate the true $|C^*_{VCE}|$ which comes directly from the test measurements.

It is important to note that to build the true $|C^*_{VCE}|$ curves, we selected the points from complex modulus test results that have the same or almost the same equivalent frequency f_e, and other values were not taken into account in the calculations. We then computed the

"true" values of $|C^*_{VCE}|$ according to the experimental data obtained. It is important to note that the obtained 2S2P1D model was not done exactly at the reference temperature 5,0°C for all the specimens (see Figure 5.16). The selected reference temperature of each mix differs more or less from 5,0°C (more or less than about 0,7°C).

The syntheses of the true $|C^*_{VCE}|$ calculated values are plotted against the equivalent frequency and given in Figure 5.16. We are keen to present the $|C^*_{VCE-2S2P1D}|$ calculated from the 2S2P1D model and the true $|C^*_{VCE}|$ calculated directly from experimental data side by side for each mix to make it easy to find out the difference and where this difference is occurring. It is interesting to show that the values of the true $|C^*_{VCE}|$ follow the same trend as the results of $|C^*_{VCE-2S2P1D}|$ from modelling. These results reveal that at high frequency (low temperature), the variations between two samples in all our cases are low. For example, for the mix RAP1528CU (Mix No.2) which showed only 0,5 variation of air void between its repetitions the maximum true $|C^*_{VCE}|$ of sample P2-A4 was found to be 10% stiffer than the reference sample P1-A5, exactly the same as the $|C^*_{VCE-2S2P1D}|$ value from modelling gave at high frequency and/or low temperature (at 4,2E+08 Hz). However, the results of the true $|C^*_{VCE}|$ of sample P2-A4 indicates that it is a 25% less stiffer than sample P1-A5, at low frequency and/or high temperature (at 0,01 Hz). Whereas its value from modelling indicates that the sample is 39% softer than sample P1-A5, at the same conditioning. This difference comes from the two replicates of this mixture which have different air voids content.

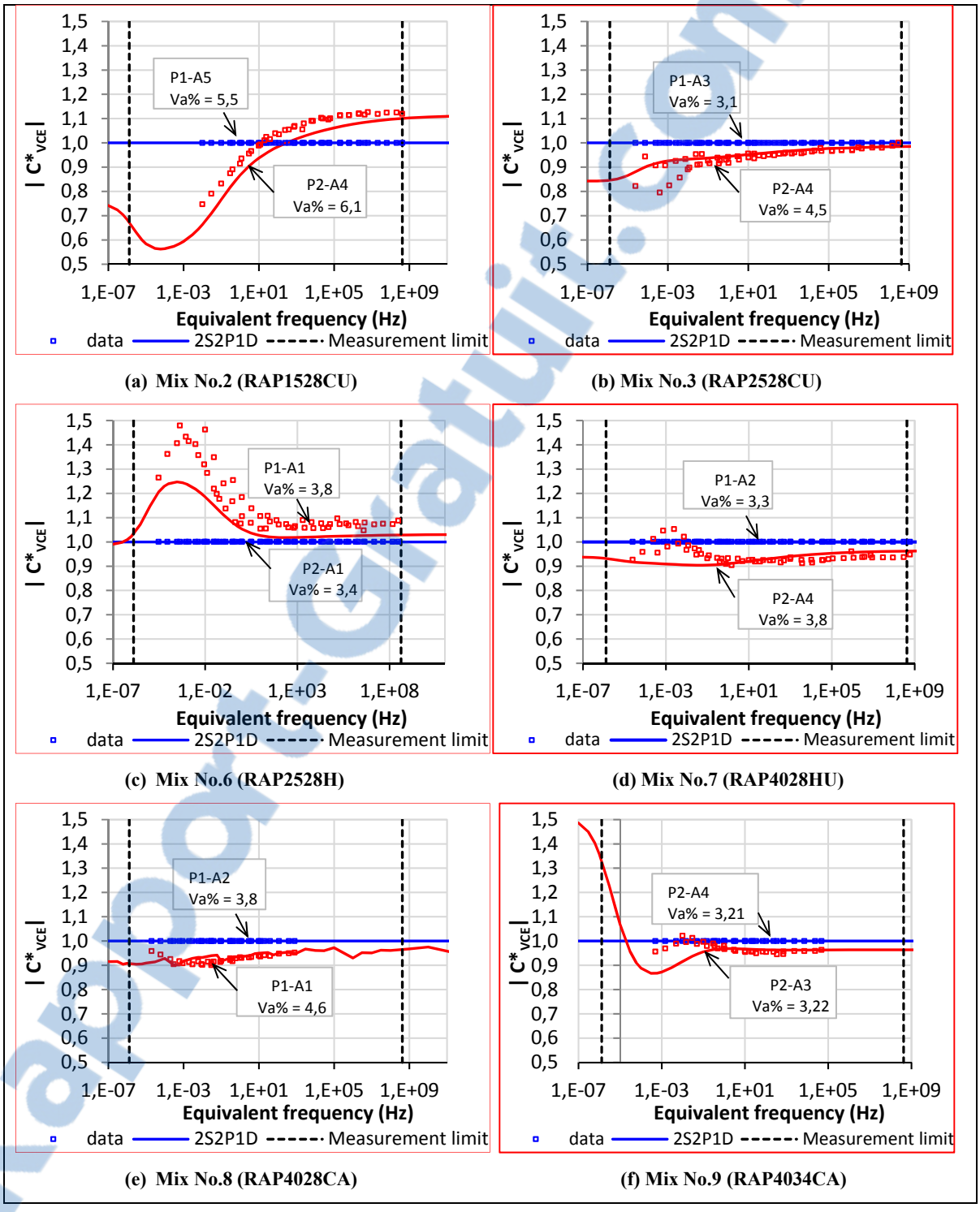

(a) Mix No.2 (RAP1528CU) (b) Mix No.3 (RAP2528CU)

(c) Mix No.6 (RAP2528H) (d) Mix No.7 (RAP4028HU)

(e) Mix No.8 (RAP4028CA) (f) Mix No.9 (RAP4034CA)

Figure 5.16 $|C^*_{VCE-data}|$ and $|C^*_{VCE-2S2P1D}|$ vs. equivalent frequency (T_{ref} = 5°C)

5.8.1.2 Summary of the results corresponding to the repeatability of complex modulus

We compared the $|C^*_{VCE}|$ obtained from data and $|C^*_{VCE-2S2P1D}|$ obtained from modelling for the specimen's replicates with and without the same air void. The summary of the analysis results is shown below:

- Results reported for replicates with the same air void of the mix RAP4034CA (mix No.9) showed that the true $|C^*_{VCE}|$ values were similar to the $|C^*_{VCE-2S2P1D}|$ from modelling. The maximum variation in the true value of $|C^*_{VCE}|$ is 4% at a range of frequency less than 0,1 Hz and the maximum variation between the two samples in the $|C^*_{VCE-2S2P1D}|$ obtained from modelling showed only 2% in the same range of frequency. However, the mixture RAP2528HU (Mix No.6) showed that the maximum true $|C^*_{VCE}|$ of sample P1-A1 was high, 43% stiffer than the reference sample P2-A1 at 1,0E-3 Hz. The maximum variation in their $|C^*_{VCE-2S2P1D}|$ obtained from modelling showed only 20% at the same range of frequency. As we mentioned previously, the variation appears to be large but in fact it isn't. It appears only at low frequency;

- Results of the RAP2528HU mix (Mix No.6) have shown that there was only 2% difference between the true $|C^*_{VCE}|$ and the $|C^*_{VCE}|$ obtained from modelling at 2,0E+5 Hz;

- In general, results show that there may be 2% differences between the true $|C^*_{VCE}|$ and the $|C^*_{VCE}|$ comes from modelling. These differences are very low and are not significant in the high range of frequency (>1E-02 Hz). However, it can have sometimes a higher difference near the limit of the lower frequency (at 1E-03 Hz). It can reach 20%;

- In some case, we can also get a difference of 10% or less between the two repetitions of the same mixture at high frequency. It means there is no difference between them. At low frequency, we can also sometimes get some difference up to 40%. In these cases, we would not consider it that we had a big difference. This could be attributed to the common

explanation of these differences that the variability of the results increases on a logarithmic scale as the |E*| value decreases;

- The results coming from the two replicates with different air voids content does not show a huge difference than the one comes from the two replicates with the same air voids contents for our case of study;

- More importantly, the complex modulus testing performed herein does not induce unexpected results between the replicates of the same mix; however the higher variability of the RAP is expected to be visible especially with increasing amounts of RAP according to Solaimanian and Tahmoressi (1996). In order to fabricate specimens containing RAP, the specific quantity of RAP was added using representative sampling methods. This process introduces a greater variability into the real sample because the RAP stockpile has various sizes which cannot be separated and added exactly according to the gradation (the individual aggregate particles are combined with the asphalt and impossible to separate into individual size fraction). This indicates that the variability in RAP mixture sometimes could be evident in complex modulus tests results. However, a well-managed RAP stockpile could show very low variability. To keep in mind that the two samples for comparisons could be from two different slabs conducting for the same mix;

- In general the variation between experimental results and the model was suitable to be used to predict data because of errors and variation between the experimental and the predicted values are minor at high frequency. However, variation observed in some cases at low frequency can be considered low and acceptable. This could be attributed to the $|C^*_{RCE-2S2P1D}|$ which is probably very sensitive to errors in the shifting procedure for the construction of the master curve. The 2S2P1D model was generally found to be useful because it helps to compare results at the same reduced frequency;

- Based on the discussion presented in this section, RAP coefficient evolution (C^*_{RCE}) values obtained from modelling have been used in the sections below. These sections focus on the influence of various parameters (RAP content, binder type, RAP aging, RAP conditioning) on complex modulus of the recycled asphalt mixture with the help of $|C^*_{RCE}|$ obtained from modelling. We will compare one sample with one sample for each mix. Also we can use the 2-samples for the same mix in the comparison just for the case that we have observed some level of variations in their moduli.

5.8.2 Effect of RAP content

In this section, mixes with PG 64-28 asphalt binder with various percentages of unaged RAP are considered (unaged RAP were added to the hot virgin aggregate). The results have been validated for four mixtures.

The influence of RAP content is analyzed using the RAP coefficient of evolution for RAP content effect ($C^*_{RCE-2S2P1D}$). The norm of the complex RAP coefficient of evolution for RAP content in reference to the mix without RAP is plotted on Figure 5.17a for the considered mixtures. Results show that coefficients $C^*_{RCE-2S2P1D}$ are very close to each other at high frequency and/or low temperature. At low frequency or high temperature, the mixtures with 25% RAP shows much higher complex modulus than the mixtures with 40% RAP. The 40% mixture exhibited slightly stiffer behaviour than the control mixture especially in the lower reduced frequency range. These results are in agreement with Shah *et al.* (2007). The 25% mixture exhibited slightly higher stiffer behaviour, especially in the lower reduced frequency range (at 6E-03 Hz). Nevertheless, this variation of 30% would be considered as low variance because that happens at very low frequency. As we noted in the previous section, we can have about 10% variation between the two repetitions for the same mix at high frequency and/or low temperature. At low frequency and/or high temperature the variation in the |E*| value can reach up to 30%. Even in this case, it would be considered low. Consequently, any variation less than 10% could not be directly associated to the direct influence of RAP content exclusively but that the variability of the test must also be taken

into account. Moreover, it is well known that the variability of the results increases on a logarithmic scale as the |E*| value decreases, which means that it is possible to observe the relatively high variability in specimens for low |E*| values from the existing research. It is important to note that not all the specimens would show the large variance of the |E*| values. When temperature increases, the RAP coefficient slowly increases for mixes with 25 and 40% RAP but slightly decrease for the 15% RAP. At high temperature, the C^*_{RCE} of the 25% RAP mixture (RAP1528CU) and the 40% RAP mixture (RAP2528CU) are the highest.

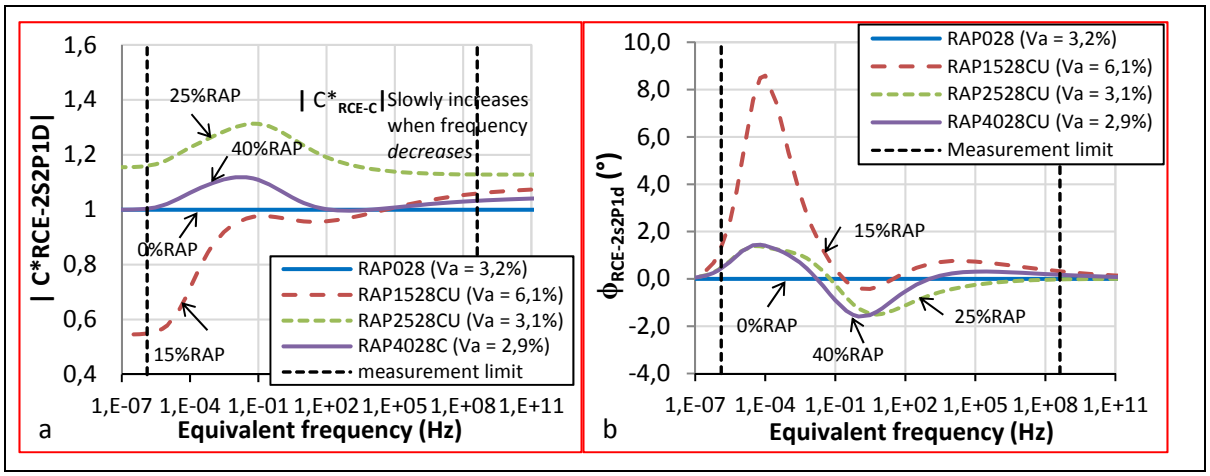

Figure 5.17 Coefficient of damage ($|C^*_{RCE}|$, ϕ_{RCE}) vs. equivalent frequency of mixtures made of PG64-28 bitumen and cold added RAP (unaged), at different RAP content: 0%, 15%, 25%, 40%, RAP028 mix (mix No.1) is the reference. T_{ref}=10°C
(a) $|C^*_{RCE-2S2P1D}|$ (b) $\phi_{RCE-2S2P1D}$

In fact, the detailed analysis of $|C^*_{RCE-2S2P1D}|$ evolution shows that:

- The results of the calculations of $|C^*_{RCE-2S2P1D}|$ shown in Figure 5.17a shows that there are small difference between the mixes and also that the percentage of RAP contained in the mixture was found to have small effects on the dynamic modulus at different frequencies and/or temperatures. At high frequency and/or low temperature, the modulus is very similar whatever the RAP content, for the four selected recycled mixtures;

- At low frequency and/or high temperature, materials made with 25% of RAP seem to exhibit higher stiffness in comparison with materials made of 40% RAP. Whereas the mix with 15% RAP shows the lowest dynamic modulus values at high temperatures and low frequencies;

- The RAP coefficient of evolution for RAP content effect increases when temperature increases for the two materials (25% RAP and 40% RAP). It should be noted that the increase is higher for the 25% RAP mixture;

- The moduli of the 15% RAP mixture are very close to the modulus of the virgin mixture on a large range of equivalent frequencies from about 1,0E02 Hz to 1,0E11 Hz (Figure 5.16a). For equivalent frequencies lower than 1,0E02 Hz and higher than 1,0E-03 Hz, the $|C^*_{RCE-2S2P1D}|$ is also very low;

- The values of $|C^*_{RCE-2S2P1D}|$ for RAP contents are not so different for the four considered mixtures. They are situated within a range of 1,0 to 1,3.

The data presented here support that adding different amounts of RAP, small, intermediate, and high amounts, which represent the percentages 15 to 25 and 40%, respectively, may not change greatly the mixtures stiffness. There are several explanations for these results. First, the asphalt content was kept constant for all the RAP asphalt mixtures. Secondly, the gradation of the 15, 25, and 40% processed RAP mixtures were very close to the control mixtures. This was done because, as shown in the literature review (Lachance, 2006), gradation does affect stiffness.

Generally the addition of RAP to a mixture adds a proportion of aged binder, however the effects of RAP on the rheological properties of the RAP mixtures might be so close to that reported for the virgin mixture. It is based on the RAP source.

For the RAP mixtures investigated in this section, the phase angles ϕ_{RCE} of the RAP content coefficient are close to 0, except for 15% RAP added mix. It shows an absolute value of ϕ_{RCE} less than 6° in the range of frequencies higher than 1,0E-04 Hz and lower than 1,0E02 Hz (see Figure 5.17b).

$|C^*_{RCE-2S2P1D}|$ calculated for mixtures made with various percentages of RAP (RAP is added hot to the mix) are presented in in Figure 5.18. Results show that for a large range of frequencies, the 40% RAP mixture were the stiffest followed by the 25% RAP mixture. The softest mixtures evaluated were the 15% RAP mixture. The 40% RAP mixture was approximately 21% stiffer than the control mixture while the sample (V_a=3,8%) of the RAP2528HU mix has shown about 75% higher than the virgin mix on a frequency of about 1,0E-02 Hz. It makes the repetitions of the mix RAP2528HU to look very different. The other sample (V_a=3,4%) of the same mix, on the other hand, shows only a 21% difference.

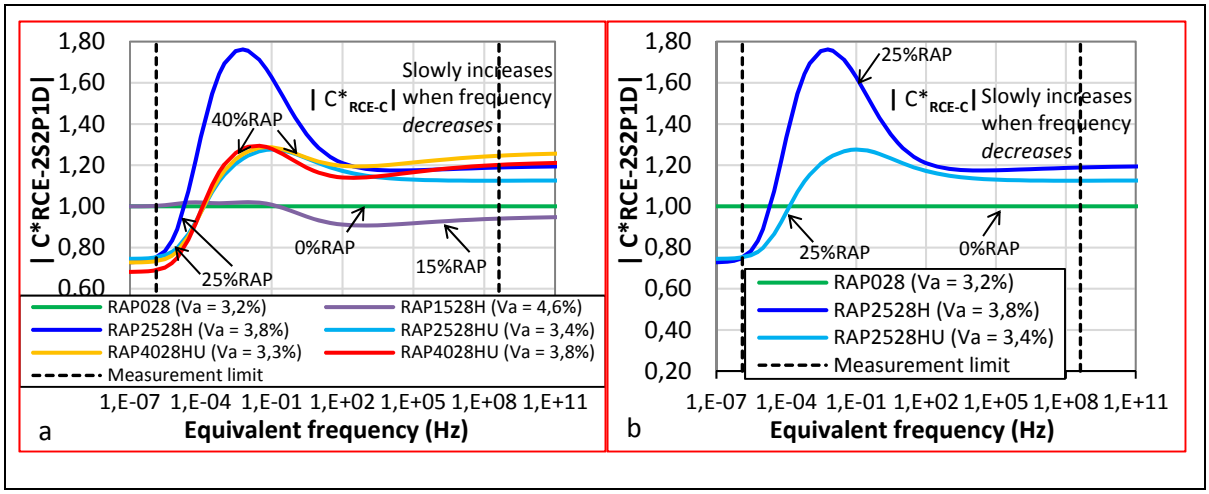

Figure 5.18 Coefficient of damage ($|C^*_{RCE-2S2P1D}|$) vs. equivalent frequency of mixtures made of PG64-28 bitumen and RAP is added hot, at different RAP content: 0%, 15%, 25%, 40%, RAP028 mix (mix No.1) is the reference. T_{ref}=10 °C
(a) mixes with 0-40% (b) mixes with 0% and 25%

In general, the effect of the stiffer asphalt binder contained in the RAP is responsible for the higher dynamic modulus values for the mixtures containing RAP than the control mixtures that made only with adding virgin asphalt binder (Li et al., 2008). However, this does not

explain the trends mentioned in this analysis at different temperatures. The behaviour of asphalt mixtures are mainly determined by the asphalt binder: a stiffer asphalt binder results in a mix with a higher modulus. Other researchers arrived at similar conclusions related to the scatter in the data for the mixes containing RAP and they showed that there was no big change in the modulus values (Li et al., 2008, Sondag, Chadbourn et Drescher, 2002). A number of reasons were introduced regarding this. One hypothesis that implied in the literature to explain the properties of asphalt mixtures at low temperatures is that the addition of aged and brittle binder coming from RAP mixtures results in a formation of micro cracks. Unfortunately, there are no simple experiments that can show evidence of the occurrence of this phenomenon. The experimental data show a much higher variability at high temperature (low frequency) compared to other test temperatures. Moreover, the addition of RAP further increased the variability of the test data.

5.8.3 Influence of binder grade

The effect of the binder grade on complex modulus is analyzed for the mixtures made with the PG 64-28 and the PG 58-34 bitumen. Then, in this section, six types of mixtures are selected for comparisons:

- The mix RAP2528CU (mix #3) composed of PG 64-28 bitumen and the mix RAP2534CU (mix #10) composed of PG 58-34 bitumen. Those mixes are made with 25% unaged RAP;
- The mix RAP4028CU (mix #4) composed of PG 64-28 bitumen and the mix RAP4034CU (mix #11) composed of PG 58-34 bitumen. Those mixes are made with the 40% unaged RAP;
- The mix RAP4028CA (mix #8) composed of PG 64-28 bitumen and the mix RAP4034CA (mix #9) composed of PG 58-34 bitumen. Those mixes are made with 40% aged RAP.

The researchers concluded (Li, Clyne et Marasteanu, 2004): ‘‘the complex modulus of the mixtures increases as the stiffness of the asphalt binder increases’’. This was observed for all our mixtures tested. The value of $|C^*_{RCE-2S2P1D}|$ is always higher than 1,0 because the norm

of the complex modulus for the mixtures made with PG 64-28 asphalt binder is always higher than the one of the mixtures made with a softer PG 58-34 asphalt binder, considering the other variables constant (testing temperature and frequency). It should be noted that $|C^*_{RCE-2S2P1D}|$ is defined as the ratio between the complex modulus of specimens containing the PG 64-28 virgin binder and the one of the PG 58-34 virgin binder.

The effect of the binder grade on $|C^*_{RCE-2S2P1D}|$ is illustrated in Figure 5.19. For the mixtures with 25% RAP (Figure 5.19a), the $|C^*_{RCE-2S2P1D}|$ coefficients are close at high frequency and/or low temperature. When temperature increases (lower frequency), the $|C^*_{RCE-2S2P1D}|$ slowly increases. At high temperature (low frequency), the modulus of the mix RAP2528CU is higher than the modulus of the mix RAP2534CU. The variations between those mixes are from 14% to 40% at 1,E11 Hz and 3,0E00 Hz.

For mixture containing 40% RAP (unaged), a similar tendency is observed (Figure 5.19b):

- At low temperature, $|C^*_{RCE-2S2P1D}|$ of the mix RAP4028CU seems to exhibit slightly higher stiffness in comparison with the mix RAP4034CU. It seems that it is influenced by the type of binder but not greatly. The variations between those mixes are from 5% to 33% at 1,0E11 Hz and 6,0E-02 Hz;

- The RAP coefficient evolution for the type of binder ($|C^*_{RCE-2S2P1D}|$) increases when temperature increases.

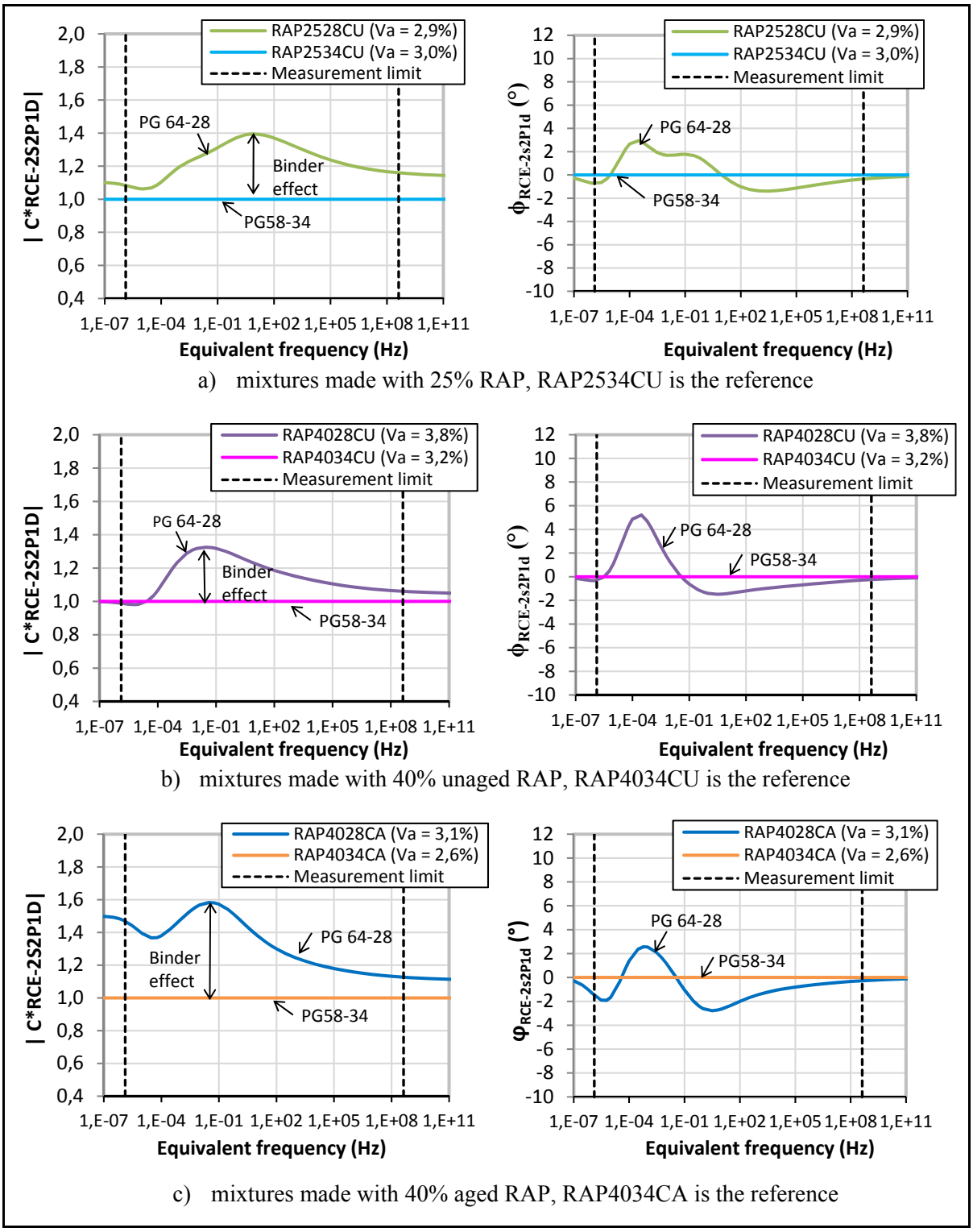

Figure 5.19 Norm and Phase angle of the complex RAP coefficient of evolution vs. equivalent frequency for mixtures composed of PG 64-28 bitumen or PG 58-34 bitumen and made with different RAP contents. T_{ref}=10°C

Finally, when the aged RAP is used for the 40% RAP mixture, results of Figure 5.19 show that the binder grade has more influence than the case of using the 40% RAP unaged on $|C^*_{RCE-2S2P1D}|$ at high frequency (low temperature). The effect of the type of binder increases when the temperature increases. Note that the maximum increase shown in Figure 5.19c is approximately 58% at 3,0E-02 and this increase is the highest in comparison with the mixtures made with 40% RAP unaged (a 33% difference). It is interesting to show that a larger difference is obtained when there is 25% RAP compared to 40% RAP. Generally when 40% RAP is added we can see a small difference between the results because there is less addition of virgin binder.

For the six mixtures investigated in this section, the phase angle $\phi_{RCE-2S2P1D}$ of the RAP coefficient evolution for type of binder is close to 0. The absolute value is always less than 4° in the range of frequencies lower than 1,0E-01 Hz (see the plots placed on the right side of the page in Figure 5.19). The phase angles ($\phi_{RCE-2S2P1D}$) are positive and it is probably sensitive to the binder grade for equivalent frequencies lower than 1,0E-01 Hz.

5.8.4 Effect of RAP aging

The loose RAP materials were aged for 3 months in a draft oven at 55°C before used in the mix design productions as explained in section 3.2.3. The properties of RAP mixtures made with the aged RAP are investigated and compared with RAP mixtures made with the unaged RAP.

Two RAP mixtures made with the oven aged RAP and with two different binder grades (PG 64-28 and PG 58-34) were used for this part of the study. The influence of the aging values is determined when comparing RAP complex modulus results of 40% RAP mixtures made of aged RAP to 40% RAP mixtures results made of unaged RAP.

Like stated earlier; the complex modulus of the mixture increases with increasing the stiffness of the incorporated RAP. Considering the other variables constant (testing

temperature and frequency), it was observed that complex modulus for the mixtures made with oven-aged RAP is always higher than that from the mixtures made with an unaged RAP. These results are also in agreement with a previous research (Carter, Stoup-Gardiner et Perraton, 2006). Aging coefficients of the mixtures are plotted in Figure 5.20 as a function of equivalent frequency. In this case, $C^*_{RCE-2S2P1D}$ is calculated by the ratio between the modulus of the mixture made with the aged RAP and the one of the mixture made with the unaged RAP. Often, our reference mixture is the mixture with unaged RAP.

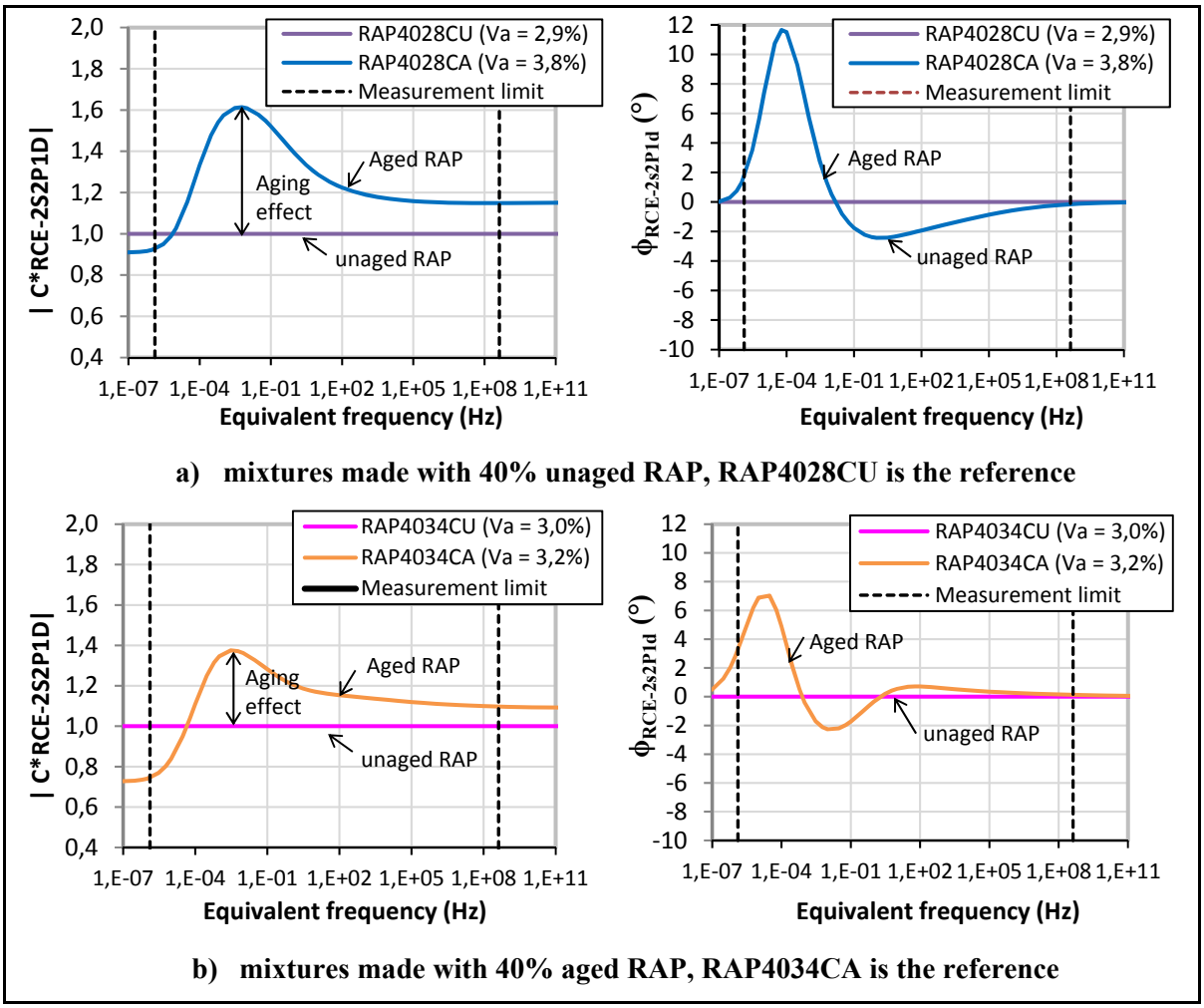

Figure 5.20 Complex aging coefficient (norm and phase angle) of 40% recycled asphalt mixtures made with PG 64-28 (RAP is added cold). T_{ref}=10°C

As shown in this figure, there is a clear influence due to aging for the 40% RAP mixtures. It is easy to see that the norm of the moduli of the RAP4028CA mix is higher than the RAP4028CU mix for all frequency ranges (or temperature ranges). It means that the aging process has an effect but not greatly on the complex modulus for the entire temperature and frequency range.

It can be seen that the maximum variation in the norm of the complex modulus of the mixture with aged RAP is 20% at high frequency ($f_e < 10^{+2}$ Hz) and reach to 60% higher than the mixture with unaged RAP at low frequency below about $f_e = 10^{-3}$ Hz. That looks like there was a huge difference between the modulus due to aging process but in fact it was not because as we have shown previously that the norm of the complex modulus is considered low at that range of frequency and it still in the range of the accuracy of the load capacity of the machine testing ($\pm$250MPa).

Phase angle is also plotted in this figure (phase angle $\phi_{RCE-2S2P1D}$) as a function of equivalent frequency.

Other conclusions were drawn from results of aged study of RAP mixtures:

- Aging has no effect at high frequency (or low temperature). $|C^*_{RCE-2S2P1D}|$ tends toward 1;
- Aging effect increases when frequency decreases (temperature increases). The norm of $|C^*_{RCE-2S2P1D}|$ is close to 1,6 and 1,4 at an equivalent frequency of 10^{-3} Hz for the recycled mixtures made with PG 64-28 and PG 58-34, respectively. In addition, Figure 6.19 points out the non-monotonic evolution of aging effect on the phase angle.

A brief summary of the aged study provided in this section is the addition of aged RAP makes the mixture stiffer. Carter, Stoup-Gardiner and Perraton (2006) stated that oven aging of loose mix has a great influence of the modulus because aging of the asphalt binder gets it harder. On the other hand, it is found in the literature that the complex modulus is not controlled only by the stiffness of the binder but also by many other factors including the

gradation and the angularity of the aggregate (Li, Clyne et Marasteanu, 2004). The finer gradation and round aggregate in the mixture may be a contributor to lower dynamic modulus. The mixture with more RAP materials and more fine aggregates were used and therefore, the increased stiffness brought about the addition of RAP may be offset by the use of finer and round aggregate.

For the mixture incorporating oven-aged RAP, the RAP material has likely aged further and RAP particles have hardened and even fewer of them are able to break down as it was reported in the literature (Lachance, 2006). This indicates that there are fine aggregates created in the mixes due to the aging process. That's why our results show that the mixture made with oven-aged 40% RAP has a slightly higher stiffness than the one made with the unaged 40% RAP. Influence of RAP conditioning

As part of the mixing procedure, some RAPs were preheated in the microwave until it reached the target temperature, 110°C, before being mixed with the heated virgin aggregate and the heated virgin binder. This is the procedure that the Minister of transports of Quebec uses to simulate plant operations. In the same manner, cold RAP is handled in the lab to simulate other type of plant operation. Hence, two different RAP conditions were used in this study. Unheated RAP and heated RAP in a microwave were used when adding RAP to prepare the recycled mix specimens for complex modulus testing. The influence of the RAP conditioning is analyzed using the RAP coefficient of evolution for RAP conditioning effect ($C^*_{RCE-2S2P1D}$). The norm of the complex conditioning effect coefficient $C^*_{RCE-2S2P1D}$ is plotted to compare complex modulus of mixtures made with the ambient temperature RAP (cold RAP) to mixtures made with heated RAP prior to mixing with the heated virgin aggregate (hot RAP). In this section, six types of recycled asphalt mixtures are selected:

- RAP1528CU mix made with 15% cold RAP (mix #2);
- RAP2528HU mix made with 15% hot RAP (mix #5);
- RAP2528CU mix made with 25% cold RAP (mix #3);
- RAP2528CU mix made with 25% hot RAP (mix #6);

- RAP4028CU mix made with 40% cold RAP (mix #4);
- RAP4028HU mix made with 40% hot RAP (mix #7).

The effect of RAP conditioning on the value of $|C^*_{RCE-2S2P1D}|$ is illustrated in Figure 5.21. Those Figures show that the $|C^*_{RCE-2S2P1D}|$ difference between mixtures made with cold RAP and hot RAP is low on a large range of frequencies whatever the RAP content. The moduli of the mixture made with heated RAP in microwave are higher than the moduli of mixtures made with unheated RAP in the range of frequencies higher than 10^{-3} Hz, when RAP content = 40%. In this case, there is a 20% difference between $|C^*_{RCE-2S2P1D}|$ for mixes with RAP added cold or hot (Figure 5.21c). However, at high temperature (low frequency), the 25% RAP mixture exhibit a slight lowering in modulus with respect to the heated RAP by microwave on a range of equivalent frequencies lower than 1,0E-4,0 Hz (Figure 5.21b).

Our results show clearly that it could balance from one side to the other side. At a first glance it suggests that there is no significant change in the modulus between the mixture made of cold-added RAP and the one of the mixture made of the hot-added RAP. Some difference also refers partly to sampling variability since it has been shown that specimens of the RAP mixtures itself could result in large variability especially at low frequency and. Part of variation could be attributed to the behaviour of an asphalt mixture as well.

The findings presented are generally consistent with the literature review. Results reported that as heating the RAP with microwaves avoids causing an excessive aging because microwave can provide optimum heating of the aggregate without affecting the asphalt binder with surrounds the aggregate particles. It means that the possibility of increased stiffness brought about increase of the binder stiffness in the case of aging RAP by heating in a microwave is very low. Further research and more analysis are needed to provide necessary information for the impact of RAP conditioning of HMA mixtures with very high amounts of RAP.

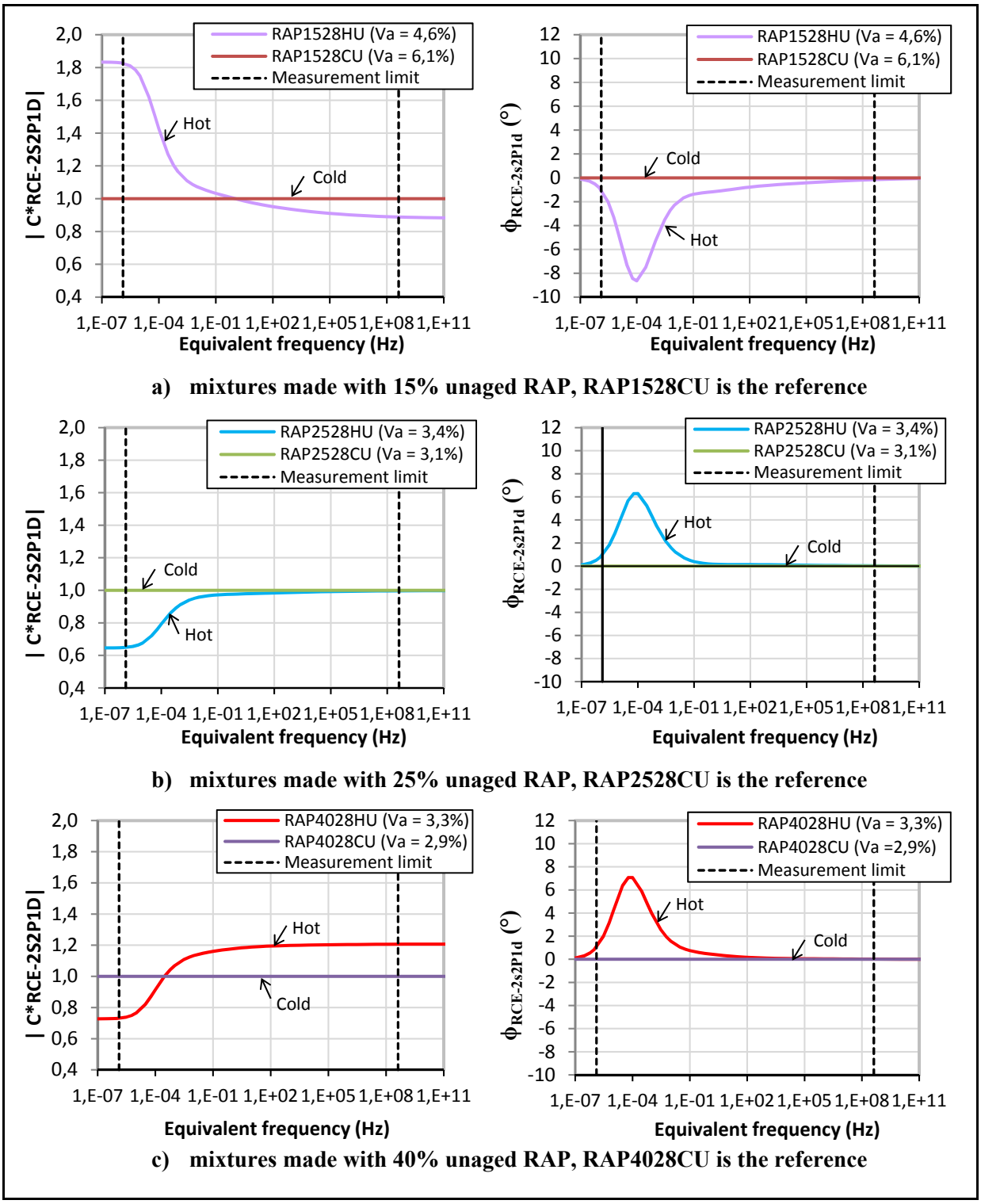

Figure 5.21 Evolution of $|C^*_{RCE-2S2P1D}|$ and $|\phi_{RCE-2S2P1D}|$ vs. equivalent frequency of mixtures made of PG 64-28 bitumen (RAP is added cold or hot), at RAP contents: 15%, 25%, and 40%. T_{ref}=10°C, RAP1528CU (mix No.2) is the reference

Finally, phase angle $\phi_{RCE-2S2P1D}$ of the RAP coefficient of evolution for RAP conditioning, plotted in Figure 5.21, are close to 0 (absolute difference less than about 4°) for the 6 mixtures, for frequencies higher than 10^{-3} Hz at 10°C.

The influence of the RAP conditioning values on the phase angle in this range of frequencies can be considered as low for the considered RAP processes and RAP content.

5.8.4.1 Sensitivity of RAP conditioning evolution values ($|C^*_{RCE-2S2P1D}|$) of mixes made with 25% RAP

This section focuses on two mixtures: RAP2528CU (Mix #3) and RAP2528HU (Mix #6). As mentioned previously one-to-one sample comparison between two samples is done. Herein, we would like to know if the tendency will change or not if only the other sample was used as a reference instead of the one that we selected. We focus the discussion in this section to investigate of the impact of RAP adding conditioning. To do that, it is important to calculate the RAP conditioning evolution values ($|C^*_{RCE-2S2P1D}|$). Thus, we plot two graphs in Figure 5.22. Figure 5.22a shows the $|C^*_{RCE-2S2P1D}|$ difference between mix #3 (RAP2528CU) by using sample (P1-A3) as a reference and mix #6 (RAP2528HU) with the use of its two repetitions: P1-A1, and P2-A1. Figure 5.22b shows the $|C^*_{RCE-2S2P1D}|$ difference between mix #3 (RAP2528CU) by using sample (P2-A2) as a reference and mix #6 (RAP2528HU) mix with showing the data of its repetitions.

It should be noticed that the moduli of the two repetitions of mix #3 (RAP2528CU) are identical since we the have the same tendency in both graphs. At low frequency and/or high temperature, sample P1-A1 of the mix #6 seems to exhibit higher stiffness (about 1,36 to 1,46 times) in comparisons with the two repetitions of the mix #3: P1-A3 and P2-A2, respectively. We will presume some assumptions that could explain those results in the section below (section 5.9).

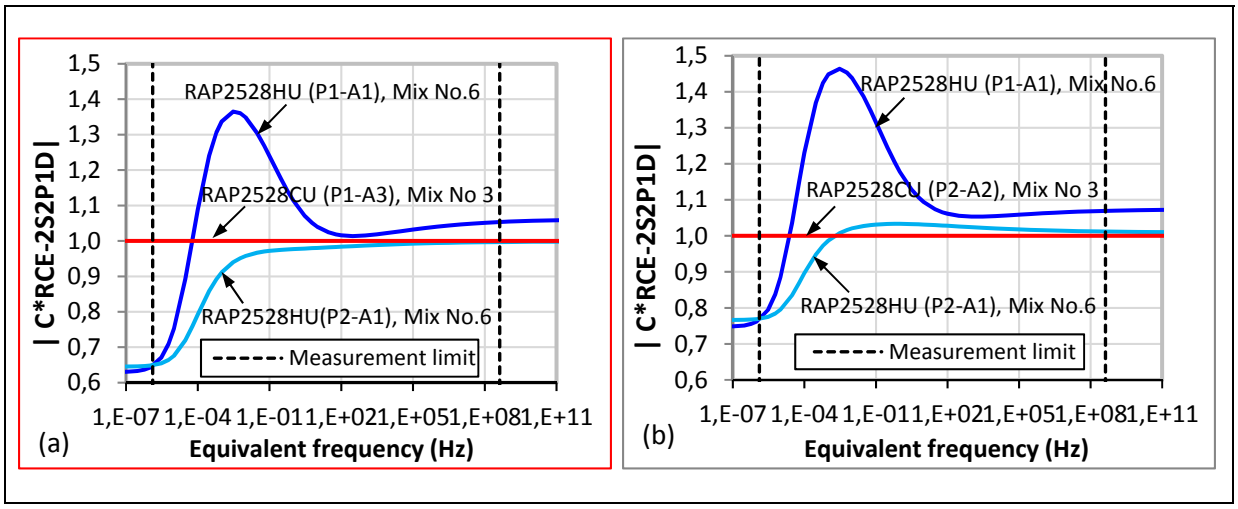

Figure 5.22 $|C^*_{RCE-2S2P1D}|$ vs. equivalent frequency of mixtures made of PG 64-28 bitumen and cold adding RAP or hot adding RAP, at different RAP content: 25%. T_{ref}=10°C
(a) Sample (P1-A3) of the RAP2528CU (mix No.3) is the reference
(b) Sample (P2-A1) of the RAP2528CU (mix No.3) is the reference.

5.9 Normalized curves

The normalized complex modulus (E^*_{norm}) as proposed by Di Benedetto is introduced in the following equation (Nguyen, Di Benedetto et Sauzéat, 2012):

$$E^*_{norm} = \frac{E^* - E_{00}}{E_0 - E_{00}} \tag{5.8}$$

Where:

E_{00} and E_0 are asymptotic values of the norm of complex modulus when the frequency tends towards 0 and infinity.

As presented previously in section 5.7, we focus on presenting our analysis for the same materials that dealt with studying the repeatability of complex modulus and the influence of RAP contents.

Regarding our study of the repeatability of E* when plotted in a Cole-Cole diagram (Figure 5.23 and Figure 5.24), the normalized moduli are superimposed on one another. The lines shown in those Figures represent the normalized complex modulus (E^*_{norm}) as a vector for the different materials. The group of lines with different colours shown in the middle of the curves represent the results at the same conditioning temperature and frequency (5°C, 3Hz) and the other group represented the results at high temperature -35°C and at 3Hz.

From Figures 5.23 and 5.24, we can see that the materials behaves almost the same as the two lines of the two repetitions are superimposed, except for the mix #6 (RAP25HU) as shown in Figure 5.23c. They look a little bit different at temperature 5°C, but we can say that they have 'conservative' behaviour. It's probably because the parameter δ used for the calibration of the 2S2P1D model of the sample P2-A1 was a bit higher than the sample P1-A1. The things that can explain the results are:

1) It is possible that something happened during materials preparation and mixing process and it was out of control;

2) It could probably be due to the variability of the RAP itself even if we show that we try to reduce it by adding RAP using representative methods for testing (see section 4.2) and the within specimen variability associated to the specimen inhomogeneity. Moreover, it is reviewed that the variability of recycled mixes is expected in the material properties (Lachance, 2006): the aggregate structure (grading) for each mixture was designed using the overall grading for the RAP stockpile and the RAP stockpile cannot be added exactly according to the grading as it was previously presented in section 5.8.1.2. In addition, it is mentioned that the specimen geometry and compaction do affect the dynamic modulus. Besides, the probability to have more variable could be found in our study because the maximum aggregate size is 20 mm, and it is supposed that the size of the sample to be 10 times the size of the maximum aggregate size to say it is homogenous material;

3) Generally, we have to keep in mind that it is a raw black material containing a recycled material and to control everything is not an easy task. This suggests to the author that the term associated with the variability between samples should be further studied with mixes with different percentages of RAP (0, 15, 25, and 40%) by doing at least 3 plates for each mix, and testing 3 samples from each plate to get more information regarding this aspect.

Based on data presented herein, we concluded that it would be acceptable to do our comparisons between mixtures using one-to-one sample. Moreover, it is well known that when the complex modulus test is done well, we can get more information from one sample in comparison with the results obtained with two or more samples and our results confirm that.

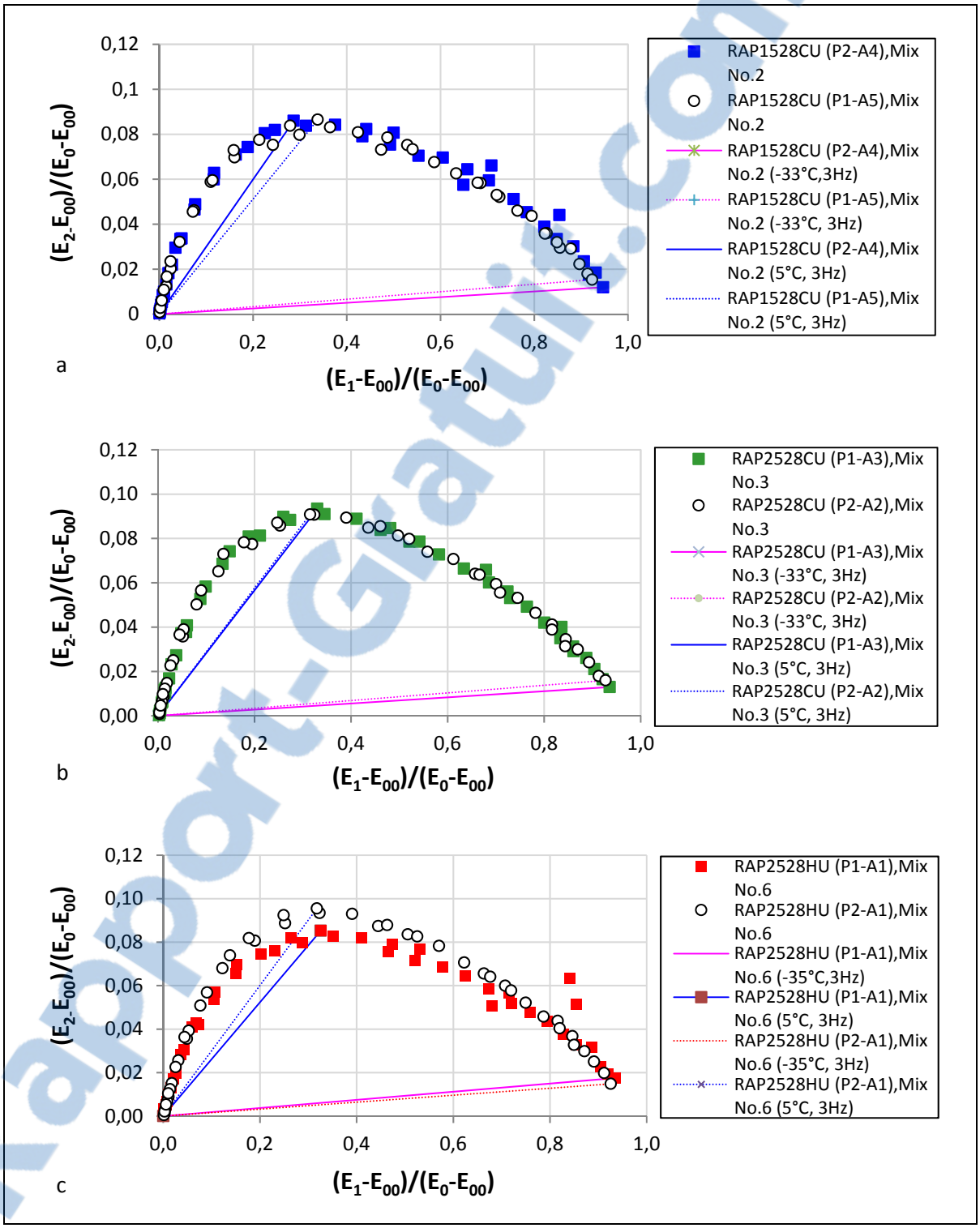

Figure 5.23 Normalized complex modulus curves in Cole-Cole diagram of the mixes with two repetitions

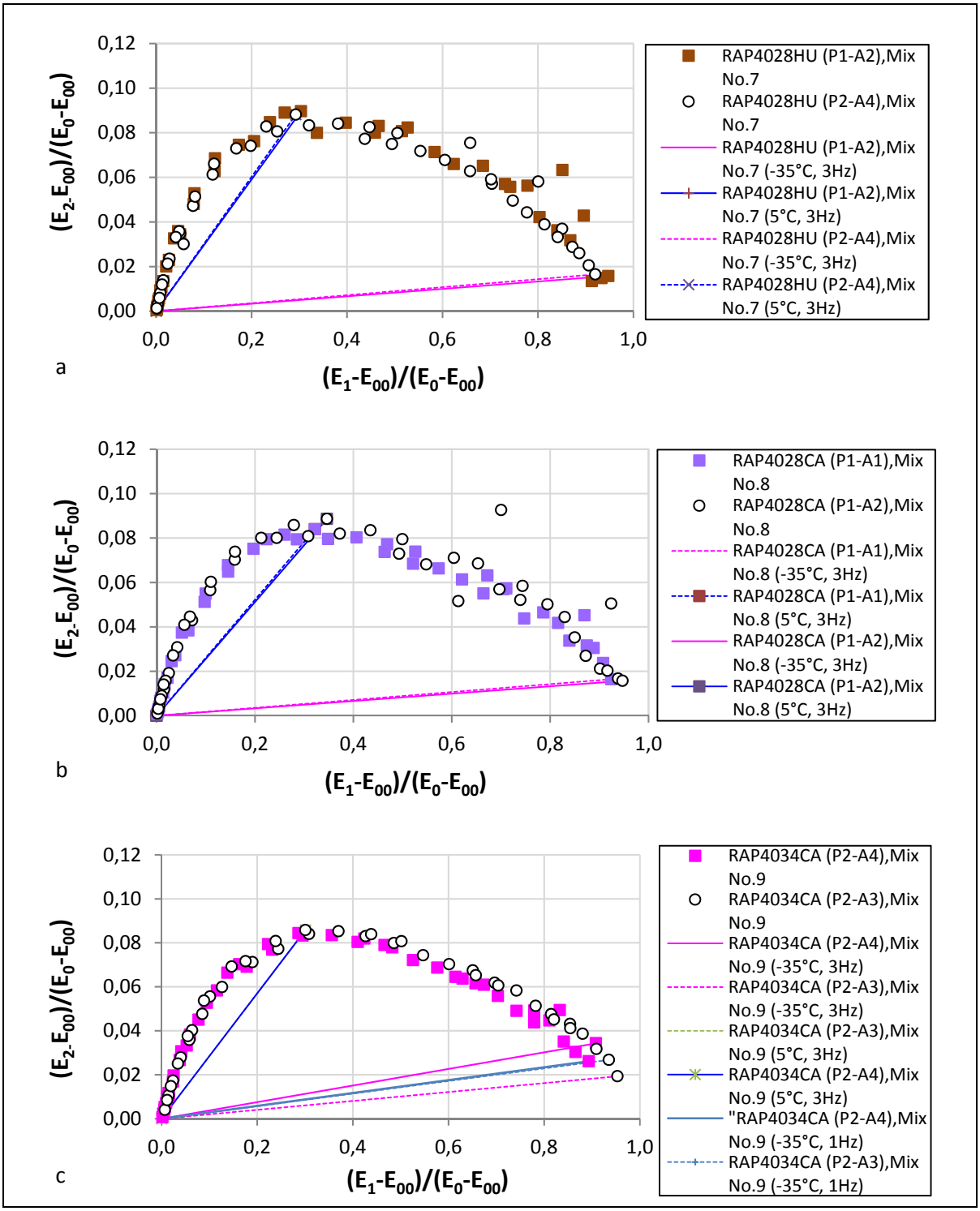

Figure 5.24 Following Normalized complex modulus curves in Cole-Cole diagram of the mixes with two repetitions

Similarly, the lines shown in Figure 5.25 show the normalized complex modulus (E^*_{norm}) as a vector for the different mixes containing different percentages of RAP (RAP added cold). The figure shows that we have almost no much effect using the temperature effect. If we judge the four mixes globally, the material with RAP can change the behaviour but it is more or less the same and it is not presume too much affect to have an effect on the behaviour.

We expect that the material will be sensible to the temperature effect especially by adding high amount of RAP (40%) but this is not the case. As we can see the points of light green and yellow are related to the 15% RAP and 40% RAP mixes and it seems that it is basically different than the virgin mix. That's curious to see that the normalized E* of the mix 40% RAP is the lowest at 5°C and 3 Hz (see the yellow line shown in the middle of the figure). That's why we said that the material with RAP can change the behaviour but it keeps it as 'conservative'. Also, as we can see the dark green line which represents the results of the 25% RAP mix is higher than those of 15% and 40% RAP and that in agreement with what we found in the literature that some people noted that at 25% RAP, there is something different (Li et al., 2008). This aspect was discussed previously in section 5.8.2.

The results for the other group of mixtures containing different percentages of RAP and made with RAP hot addition are shown in Figure 5.26. These figure's results were not so far from what we discussed above for the other group of mixtures made with cold RAP addition. Figure-A II-9 in Appendix II shows the results when plotted in a black diagram.

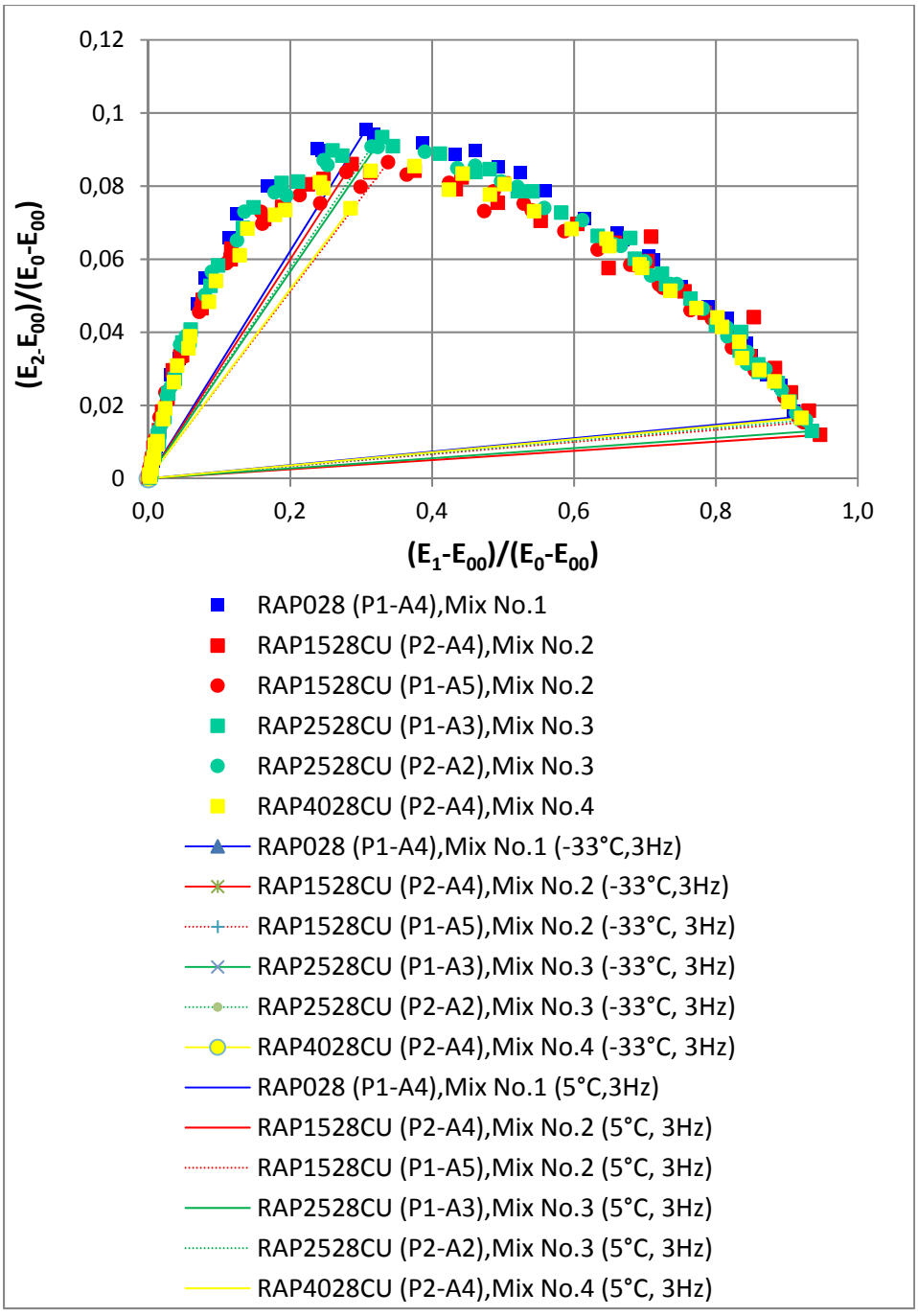

Figure 5.25 Normalized complex modulus curves in Cole-Cole diagram of the mixtures made with different percentages of RAP (the RAP at the room temperature was added to the mix)

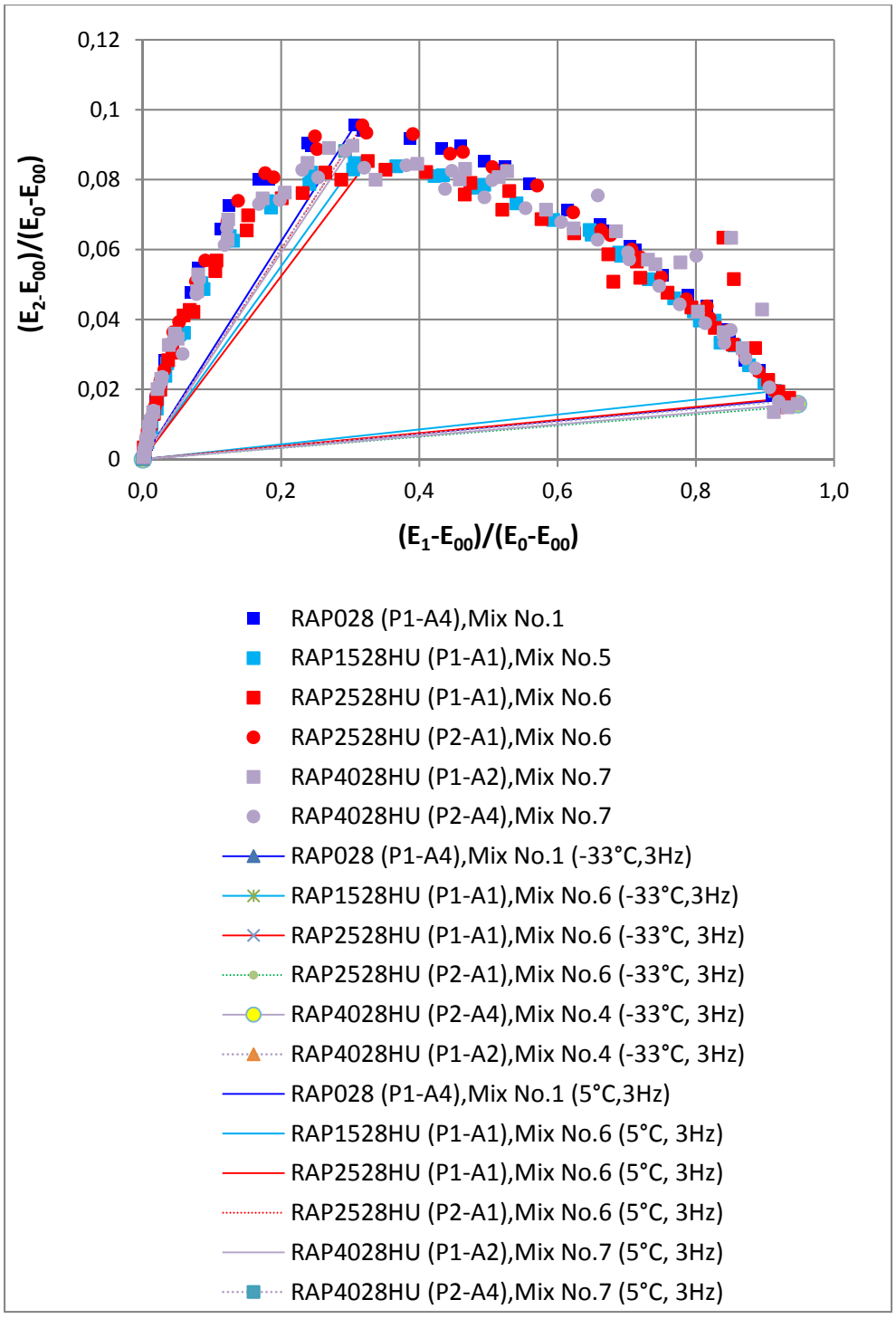

Figure 5.26 Normalized complex modulus curves in Cole-Cole diagram of the mixtures made with different percentages of RAP (the heated RAP to 110°C was added to the mix)

5.10 Chapter conclusion

The following conclusions are drawn as a result of the contents of this chapter:

- The 2S2P1D model generally simulate well the linear viscoelastic behaviour of HMA mixture with RAP in the measured temperatures and frequencies range;

- Repeatability of complex modulus test was found to be good on a large range of temperatures and equivalent frequencies. This not surprising since the variation in air voids in the specimen was deemed to be acceptable;

- Little change was observed in complex modulus when cold RAP was added to the mix whatever the RAP content (15, 25, or 40%) on a large range of frequencies and temperatures. Some very slight difference in complex modulus can only be notable at high frequency. The mixtures can be ranked in complex modulus amplitude as 15% RAP mix as the lowest, then followed by the virgin mix, the 40% RAP mix, and the 25% RAP mix as the stiffest;

- At lower temperatures, the ranking of mixtures mixed with hot added RAP (microwave condition at 110°C) was as follow: the lowest moduli were observed for the virgin mix and the 15% RAP mix, which have similar modulus. Then, the 25% RAP mixtures have higher modulus and the 40% RAP modulus is the stiffest. The ranking here is different than what was observed for cold RAP addition. It could be explained by the slight heterogeneity among tested samples due to the RAP heating process in a microwave. In fact, not enough materials were tested in this research program to verify if the RAP materials are affected by microwave heating. This aspect should be studied in another project;

- The complex modulus was higher for the mixture incorporating the stiffer PG 64-28 asphalt binders compared to PG 58-34 at all testing temperatures or frequencies whatever the RAP content (25% or 40%);

  A large stiffness difference for the mixture with 25% RAP and the mixtures with 40% RAP was noticed. This could be due to the amount of virgin binder. As the percentage of RAP materials is increasing, less virgin binder is used;

- The RAP conditioning before to add to the mix had low effect on the complex modulus values. Mixtures with cold added RAP did not show a big difference compared to the mixtures with hot added RAP;

- Adding up to 40% RAP to the virgin mixture did not show any significant difference in its stiffness compared to the virgin mixture, so it is concluded that high quality HMA with up to 40% RAP can be designed and can attain the desired performance, i.e. fatigue resistance.

CHAPTER 6

ANALYSIS OF FATIGUE TEST RESULTS

6.1 Introduction

This chapter summarizes the results of fatigue tests for the four tested mixes containing RAP. It has five main parts. The first part provides the description of the tested mixes which is presented in section 6.2. Then, the second part summarizes the experimental campaign as presented in section 6.3. The third part is devoted to the presentation of results and the analysis. The content of this part is broken up into a few sections (sections 6.4, 6.5, 6.6, 6.7, 6.8). Section 6.4 shows the analysis and the presentation of fatigue data. Section 6.5 suggests the correction of fatigue tests results. Section 6.6 shows the comparison of the fatigue test results. The evaluation of the fatigue test results is presented in section 6.7. The last section of this part (Section 6.8) addresses the finding of the investigation of the effect of RAP content on the fatigue characteristic of asphalt mixtures. Then, the part four discusses a method developed by Di Benedetto et al. (2013) that is used to predict fatigue life of recycled asphalt mixtures when considering only the 300 000 first cycles of any test. The component of the discussion of this part is presented in two sections (sections 6.9-6.10). The experimental procedure and the fatigue test were presented in chapter 4. The Part five shows a summary of the content of this chapter as it is presented in the last section of this chapter.

6.2 Tested mixes

Four selected recycled hot mix asphalt (RHMA) from the eleven recycled mixtures produced in our experimental program were investigated in this research. These mixes contained 0%, 15%, 25%, and 40% cold added RAPs with a PG64-28 binder. The RAP addition process was kept constant for all these mixes.

The four tested mixes are “0RAP28”, “RAP1528CU”, “RAP2528CU”, and “RAP4028CU” as presented in Table 6.1 and as it was referred in Section 3.2.5 of chapter 3. At least five specimens for each mix are suitable for fatigue testing.

Table 6.1 Characteristics of specimens for the four mixes

Sample No.	Mix Name	RAP %	Notation of the sample at the coring	Dimension (mm)		Weight (g)	Air voids (%)
				Diameter (mm)	Height (mm)		
1	**0RAP28**	0	P1-A2	73,90	121,6	1323,2	4,0
2	**0RAP28**	0	P1-A5	73,96	122,5	1332,6	4,1
3	**0RAP28**	0	P2-A4	73,97	118,0	1278,3	4,5
4	**0RAP28**	0	P1-A3	73,87	122,2	1325,8	3,9
5	**0RAP28**	0	P3-A3	73,97	123,7	1309,7	6,7
6	**0RAP28**	0	P3-A5	74,01	123,2	1304,2	6,8
7	**0RAP28**	0	P4-A5	74,04	124,4	1339,2	5,1
8	**0RAP28**	0	P3-A4	73,97	124,7	1323,1	6,6
9	**RAP1528CU**	15	P2-A1	73,90	125,0	1318,1	6,3
10	**RAP1528CU**	15	P2-A2	73,95	123,3	1294,6	6,7
11	**RAP1528CU**	15	P1-A3	73,97	121,6	1287,7	5,9
12	**RAP1528CU**	15	P2-A3	73,90	125,0	1306,9	6,3
13	**RAP1528CU**	15	P1-A2	73,95	122,6	1287,3	6,7
14	**RAP2528CU**	25	P4-A2	74,03	122,9	1296,6	6,1
15	**RAP2528CU**	25	P4-A4	74,02	123,9	1320,1	5,6
16	**RAP2528CU**	25	P4-A5	73,96	123,7	1311,3	5,8
17	**RAP2528CU**	25	P3-A1	73,91	124,4	1306,8	6,8
18	**RAP2528CU**	25	P1-A2	74,03	124,0	1311	6,2
19	**RAP4028CU**	40	P1-A2	73,92	122,1	1325,0	3,3
20	**RAP4028CU**	40	P2-A3	73,97	124,1	1333,9	3,3
21	**RAP4028CU**	40	P2-A2	73,93	123,9	1364,6	2,1
22	**RAP4028CU**	40	P1-A3	74,01	124,7	1353,0	3,6
23	**RAP4028CU**	40	P1-A4	73,97	121,6	1330,4	2,7
24	**RAP4028CU**	40	P1-A2	73,95	125,8	1378,5	2,5

The specimens have dimensions of 120mm$\pm$5mm in height and 74mm$\pm$1mm in diameter. The measurements of sample’s size and weight were performed and used to calculate the

percentage of air voids of specimens as we discussed in section 4.4.4. The height and the diameter are the average of the three measurements taken with the height gauge and the sliding gauge, respectively. The air voids of the specimens were calculated using the theoretical maximum specific gravity (G_{mm}) and bulk specific gravity (G_{mb}) and shown in Table 6.1 and Figure 6.1. Air voids of these samples range from 2,1% to 6,8% which indicated a compacted levels of 97,9 % to 92,6%. This difference in air voids was taken into account in the fatigue test results analysis, as it will be explained in section 6.5.

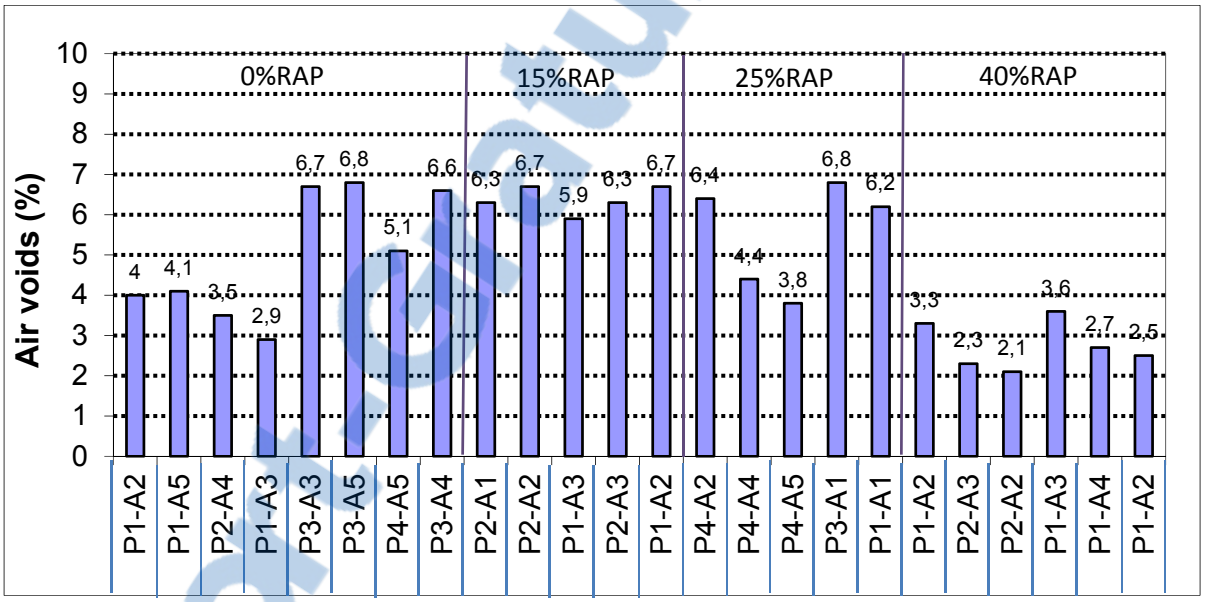

Figure 6.1 Air voids content for the specimens of the four mixtures

6.3 Experimental campaign

An experimental campaign of fatigue tests has been carried out on several asphalt mixes containing different percentages of RAP. The main goal of this study is to evaluate the effect of RAP addition on the fatigue resistance of those mixes. The experimental campaign was conducted using the experimental device presented in section 4.5.1. The tests were performed in strain-controlled mode of loading at a frequency of 10 Hz and at 10°C.

Table 6.2 shows the initial modulus and the applied strain for all the specimens tested. The coefficient of variation is equal to 13,5 percent of the initial modulus. This shows that test specimens are fairly constant. The initial modulus $|E_0^*|$ shown in Table 6.2, is determined as the value of the y-coordinate of intercept of the first 50 cycles for test in the LCMB (see section 2.7.5). Some specimens fatigue test results were rejected because they didn't verified the criteria of acceptance of the measure between each extensometer as presented in section 2.7.4.2. Moreover, some specimens were broken before they could be tested.

We proposed a simple nomenclature to name our tests which can provide information about the tested parameters (see Figure 6.2). Thus, the name is composed of four parts. The first part is the percentage of RAP used in the mix. The second is the number assigned to the specimen in a given plate. The third represents the mode of solicitation (D refers to Deformation), and the last number gives the level of solicitation in μm/m or in 10^{-6} m/m.

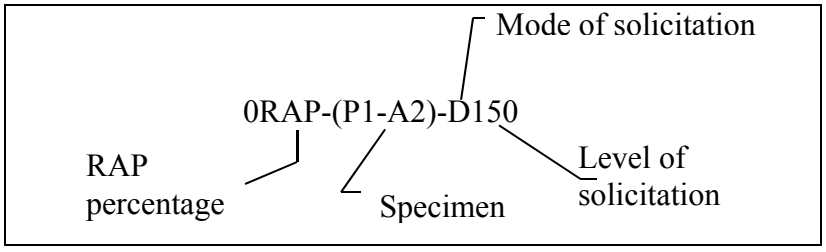

Figure 6.2 Notation of the name of the fatigue test

Table 6.2 Summary table of the performed fatigue tests

Test Name	Compacted level	Initial modulus, $\|E_0^*\|$(MPa)				
		Value	Average	Std Deviation	Average amplitude of deformation (µm/m)	
					Target	Real
0RAP-(P1-A2)-D150	96,0	10540	10756	676	150	148,9
0RAP-(P1-A5)-D140	95,9	11089			140	138,1
0RAP-(P2-A4)-D130	95,5	12057			130	126,5
0RAP-(P1-A3)-D140	96,1	11475			140	136,5
0RAP-(P3-A3)-D110	93,3	10393			110	106,8
0RAP-(P3-A5)-D105	93,2	10036			105	102,2
0RAP-(P4-A5)-D115	94,9	10436			115	112,0
0RAP-(P3-A4)-D115	93,2	10023			115	111,4
15RAP-(P2-A1)-D150	93,7	9607	10327	771	150	149,0
15RAP-(P2-A2)-D120	93,3	9193			120	118,7
15RAP-(P1-A3)-D115	94,1	10920			115	112,2
15RAP-(P2-A3)-D130	93,7	10861			130	129,4
15RAP-(P1-A2)-D140	93,3	11054			140	140,1
25RAP-(P4-A2)-D120	93,6	12090	10916	1074	120	119,0
25RAP-(P4-A4)-D140	94,4	10123			140	135,4
25RAP-(P4-A5)-D130	94,2	11962			130	128,5
25RAP-(P3-A1)-D150	93,2	11909			150	151,1
25RAP-(P1-A1)-D110	93,8	8760			110	108,8
40RAP-(P1-A2)-D130	96,7	11932	11930	492	130	130,5
40RAP-(P2-A3)-D140	96,2	12307			140	137,5
40RAP-(P2-A2)-D150	97,9	12541			150	147,0
40RAP-(P1-A3)-D160	96,4	11469			160	158,3
40RAP-(P1-A4)-D170	97,3	11125			170	168,0
40RAP-(P1-A2)-D180	97,5	12203			180	178,0

6.4 Results and analysis

In this section, we present a summary of fatigue tests carried out on the four tested recycled asphalt mixtures followed by the various comparisons of the results and analysis according to the various fatigue resistance criteria.

In order to show the steps to treat rigorously the results of a fatigue test and to simplify the presentation, we first present an example of the results of a fatigue test in the control strain mode before analyzing the results section of comparison fatigue test results (§ 6.6) and before going deeply into the analysis of the entire next chapter.

6.4.1 Interpretation of fatigue test results

Eleven curves are used for graphical presentation of a fatigue test. These curves are used initially to verify the validity of the test and to observe the changes in mechanical properties as a function of time (the number of cycle of solicitation) and also to have an idea about the initiation and the evolution of cracks inside the specimen. The following curves are used in this presentation:

- (N – T): evolution of temperature with the number of cycles;
- (N - QI): curves of the quality indices (QI) for signals of stress, strain gauges and the three extensometers. These curves are used to validate the test;
- (|E*| - N): evolution of the norm of the complex modulus with the number of cycles;
- (N – ε_{iA}) and (N – ε_A): evolution of the amplitude of deformation for the three extensometers (ε_{iA}) and the average deformation (ε_A) with the number of cycles;
- (N- average deviation of deformation): evolution of the average deviations of the amplitude of deformation of the three extensometers relative to the amplitude of axial average deformation with the number of cycles;
- (N – ε_{i0}) and (N – ε_0): evolution of the center of deformation for the three extensometers and the average deformation with the number of cycles;
- (σ_A - N): evolution of the amplitude of stress with the number of cycles;
- (σ_o - N): evolution of the center of stress (mean value) with the number of cycles;
- (ϕ_E - N): evolution of the phase angle of complex modulus (ϕ_E) with the number of cycles;
- (ϕ_E - |E*|): evolution of the norm of complex modulus with the phase angle (Black space).

The following sections will explain the different curves mentioned above one by one. Test results of sample 25RAP-(P1-A1)-D110 will be presented as an example for the eleven curves. As to the presentation of these curves, relevant comments are given regarding their interpretation. If necessary, some typical outcomes are also presented in the context of the analysis of the results of fatigue tests. Note that all the curves obtained for each test are given in Appendix III.

6.4.1.1 Evolution of temperature

Figure 6.3 shows the evolution of the temperature measured with the two temperature sensors of the type PT 100 placed at the surface of the specimen as a function of number of cycles for the sample P1-A1 of the test 25RAP-(P1-A1)-D110. While the chamber temperature was thermo-regulated to 10°C, it was noted a rapid heating of 0,5°C at the beginning of the test up to 10 000 cycles. Subsequently, the temperature stabilizes during the second phase to approximately 10,3°C. According to Baaj (2002), changes in temperature during fatigue testing are a consequence of direct energy dissipation. Thus, the evolution curve of the energy dissipated is often a decreasing curve leading to a cooling in the third phase until the end of the test.

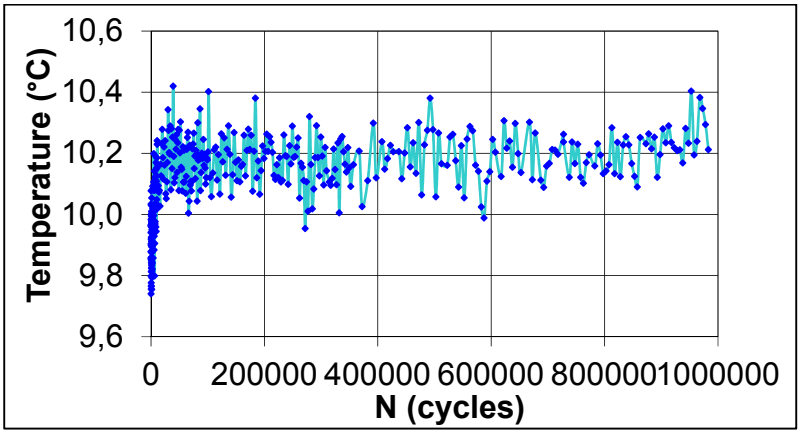

Figure 6.3 Evolution of the temperature at the surface of the specimen according to the number of cycles for the test 25RAP-(P1-A1)-D110 (ε_A = 108,8 µm/m; T = 10°C)

6.4.1.2 Evolution of the heating on the surface of the specimen

The evolution of the heating is established based on the initial temperature at the surface of the test specimen. Figure 6.4 illustrates the evolution of the heating on the surface of the specimen of the test 25RAP-(P1-A1)-D110. The warm-up progresses rapidly during the 9806 cycles and reaches a maximum of 0,4°C after 39 105 cycles. Also, after the first 40 000 cycles of solicitation, the warm-up stabilizes and marks the end of phase I. Although the ventilation within the thermal chamber is very high and can further reduce the heating of the specimen, the heating measured at the surface is low for a specimen solicited at amplitude of deformation of 108,8 µm/m. This heating should be almost the double (Nguyen et al., 2012). Furthermore, a temperature drop of about 0,2°C measured at the start of the test is inconsistent.

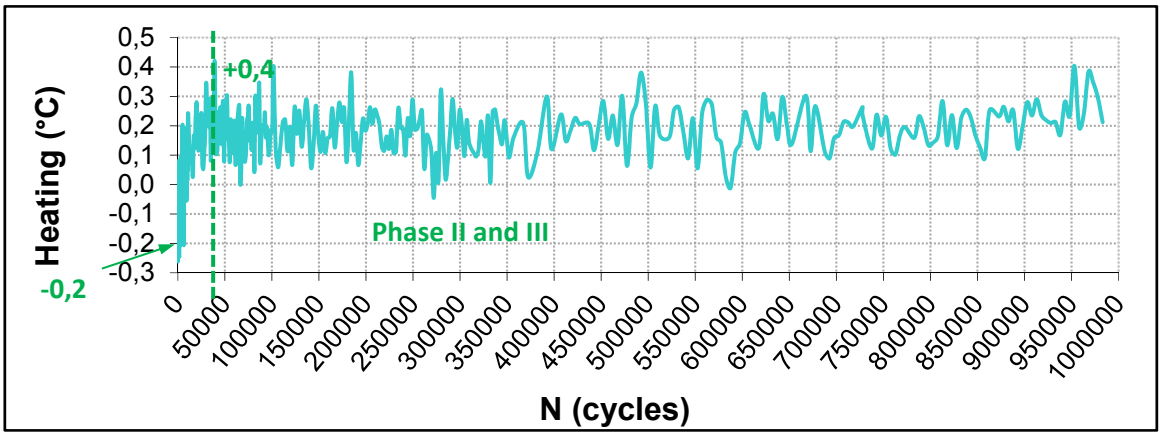

Figure 6.4 Evolution of the heating on the surface of the specimen of the test 25RAP-(P1-A1)-D110 (ε_A = 108,8 µm/m; T = 10°C)

It is possible to find that the surface heat of the specimen can vary up to ±0,4°C (Figure 6.4). This variation of surface heat of the sample is important. This can be explained by the fact that the temperature sensor placed at the surface was not covered with dough (simply supported on the surface) and so it was subjected to the temperature variation and the strong air flow within the thermal chamber of the press MTS. Indeed, the temperature sensor not only measures the temperature at the surface of the specimen, but also that of the air of the

thermal chamber. The use of a temperature probe covered with rubber would allow better measuring the surface heat of the specimen (Lamothe, 2014).

6.4.1.3 Curves of the quality index

To assess the quality of the signals for the stress, strain and the three extensometers and to validate the quality of a test, the calculation of quality indicators (QI) is introduced for each analyzed cycle. The quality index is used to quantify the average deviation of the measured values with those calculated for two consecutive cycles. In the case of a good quality of solicitation, this difference tends to zero. The QI is calculated with equation 6.1 as presented by Lamothe (2014).

$$QI(\%) = \sum_{i=1}^{n} \frac{G_{measured} - G_{calculated}}{n * A} * 100 \tag{6.1}$$

Where:

- $G_{measured}$: Magnitude of the measured signal;
- $Gc_{calculated}$: Magnitude of the calculated signal;
- n : Number of the analyzed point (200 points); and
- A : Amplitude of the signal.

Figure 6.5 shows the curves of the quality indices according to the number of cycles for the fatigue test on specimen 25RAP-(P1-A1)-D110. Note that as for the complex modulus tests, the limit was set at 15%. Beyond this limit, the test is canceled and subsequent cycles are no longer considered valid.

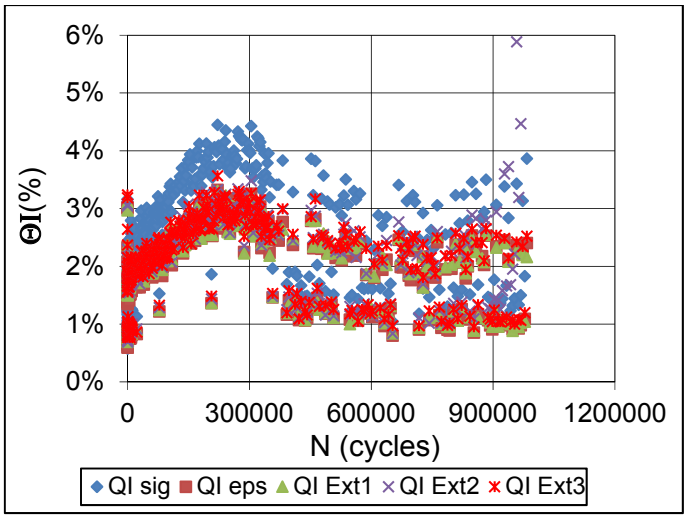

Figure 6.5 Evolution of quality indices according to the number cycles for the test 25RAP-(P1-A1)-D110 (ε_A = 108,8 µm/m; T = 10°C)
('QI sig' means QI of the signal, 'QI esp' means QI of Epsilon or deformation)

6.4.1.4 Evolution of the norm of complex modulus

From the amplitudes of deformation (ε_A) and stress (σ_A), the norm of the complex modulus is calculated (|E*|). Figure 6.6 illustrates the evolution of the complex modulus the specimen 25RAP-(P4-A1)-D110, tested at 10°C and 10 Hz, as a function of the number of cycles of solicitation. The decrease in |E*| is very rapid during the first 100 cycles of solicitation. This is due to the non-linear behaviour of the asphalt cement. Then, up to 40 000 cycles of solicitation, the decrease in |E*| becomes much more attenuated, it is due to the heating and the thixotropy of bitumen (phase I). It is followed by the second phase which corresponds to a more regular, almost linear, decrease in stiffness. We noted the presence of the third phase where there is again a rapid decrease of the stiffness. For some of our tests, we observed only the two first phases in the evolution of the stiffness.

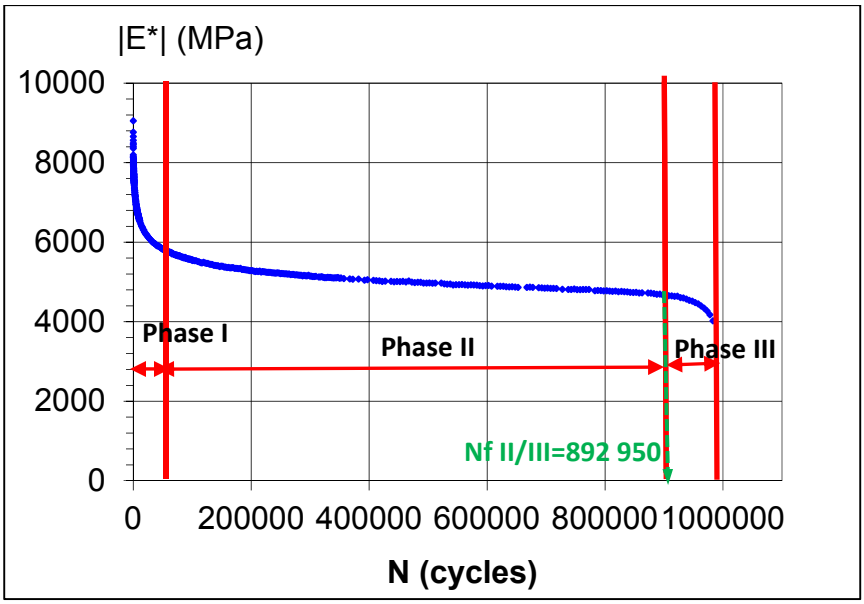

Figure 6.6 Evolution of the modulus according to the number of cycles for the test 25RAP-(P1-A1)-D110 (ε_A = 108,8 µm/m; T = 10°C)

6.4.1.5 Evolution of axial deformation

Figure 6.7 shows the change of the magnitude of the axial deformations for the test 0RAP-(P2-A4)-D130. During our fatigue tests, the average of the three axial deformations is used to control the deformation. That is why the amplitude of the mean strain is kept constant by the hydraulic press until the end of the test. However, the amplitudes of deformation measured by each of the three axial extensometers evolve separately during the test. The difference between the amplitudes of the three axial sensors and the average value increases with the progress of the test. Generally, differences between the measured strains by each extensometer are due to the non-homogeneity of the sample and (or) the eccentricity of the applied force.

Non-homogeneity within the samples is common in asphalt mixtures. In the manufacture of asphalt mixtures plates, good preparation, good mixing of the materials and a well-studied compaction plan can increase the homogeneity of the prepared asphalt mixture sample. It is

also very important to core the specimen away from the edge of the slabs, which minimize the heterogeneity due to the wall effect.

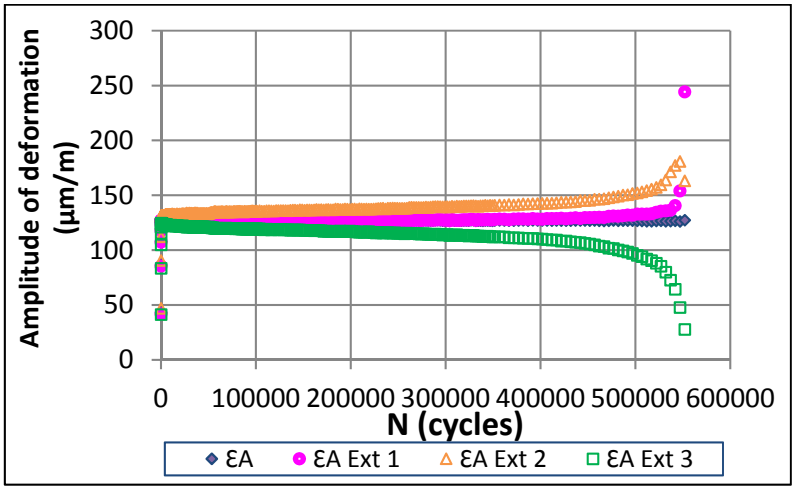

Figure 6.7 Evolution of the amplitude of the deformation as a function of the number of cycles for the test 0RAP-(P2-A4)-D130 (ε_A = 124,7 µm/m; T = 10°C)

To avoid the eccentricity of the applied force, it is important to core and saw the specimens carefully in order to obtain cylindrical specimens with parallel ends. Moreover, the connecting plates should be well machined and parallel, and the specimen perfectly centered during the gluing process.

In Figure 6.8, the differences of the amplitudes of deformation curves (corresponding to the three axial extensometers) relative to the amplitude of the average of the three extensometers are presented in function of number of cycles. These curves are important because they can judge the state of homogeneity or non-homogeneity of the field of deformation in the test specimen during the test. The values of these differences must remain low during the test. Baaj (2004) proposed a criterion to verify the validity of the fatigue test. The test is rejected if a difference of ±25% is observed, which is higher than the acceptable value for complex modulus because of the intrinsic variations associated with the fatigue phenomenon.

For the test 25RAP-(P1-A1)-D110, The deviations of the extensometers are relatively low at the beginning of the test. At 300 000 cycles, the average difference for extensometer 1 reached -16,53%, -10,78% for extensometer 2 and 5,67% for extensometer 3. These values are lower than 25%, making it possible to analyze this test.

With the advancement of the test, the differences are increasing. The state of deformation in the specimen is considered non-homogeneous beyond the cycle 800 000, where the deviation is 54% for extensometer 1 and -83% for extensometer 2, and 57% for extensometer 3.

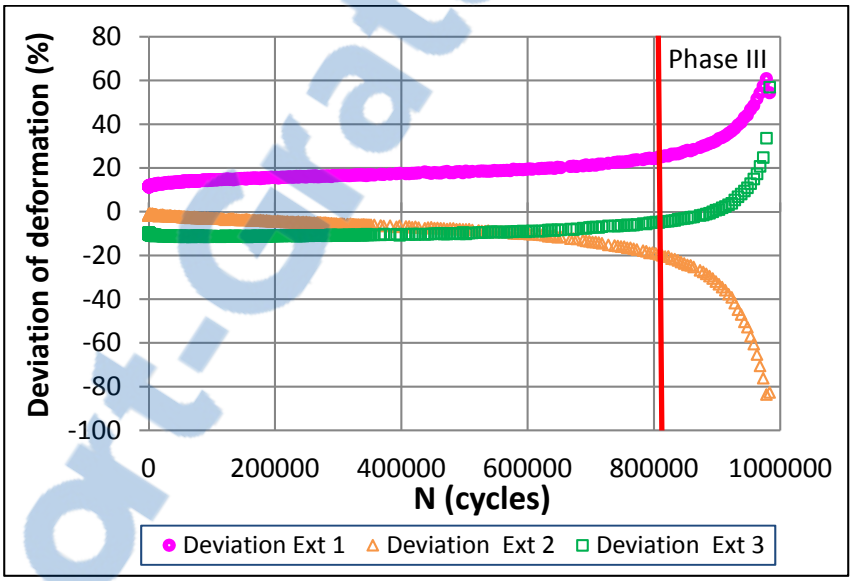

Figure 6.8 Differences relative to the mean of the deformation (average deviations of deformation) depending on the number of cycles for the test 25RAP-(P1-A1)-D110 (εA = 108,8 µm/m; T = 10°C)

6.4.1.6 Axial Strain's signal centered value

Our fatigue tests were conducted in a deformation control mode, in tension-compression, and the target of the average deformation of the specimen (εAax) is centered on a null value (ε_0). Figure 6.9 shows an example of the results for the fatigue test 25RAP-(P4-A5)-D130 in strain control mode. This zero value (ε_0) is illustrated in this figure.

Although, during the test, the average strain (ε_0) could stay around zero deformation, the deformation measured by each of the gauges (ε_0 Ext1, ε_0 Ext2 or ε_0 Ext3) evolves quite rapidly during the test. For example, in Figure 6.9, it is possible to observe that during the fatigue test, the specimen relaxes (up +113 µm/m) of the side of gauges 2 and 3 (ε_0 Ext2 and ε_0 Ext3) and contracts (up to -204 µm/m) on the side of gauge 1 (ε_0 Ext) before entering the rupture phase (Phase III). However, this might not really be the beginning of phase III since the limit was attained at only 501 000 cycles. In this case, it is possible that this evolution between the different extensometers is accountable on a differential deformation due to the setup problem, sample not centered, or because of a heterogeneity in the sample, different air voids on each side of the specimen.

However, for some cases this value (ε_0) could not be zero as illustrated in Figure 6.10 for the fatigue test 25RAP-(P1-A1)-D110. This value (ε_0) is based on the measured values of the three extensometers (ε_0 Ext1, ε_0 Ext2, ε_0 Ext3) because it is the average value of these numbers.

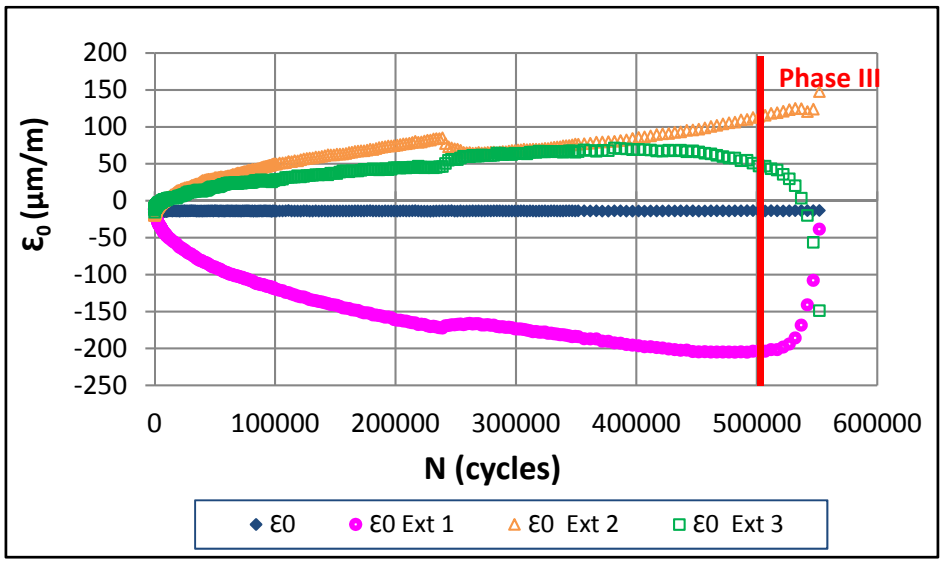

Figure 6.9 Changes in the center of the deformation as a function of the number cycles for the test 25RAP-(P4-A5)-D130 (ε_A = 128,5 µm/m; T = 10°C)

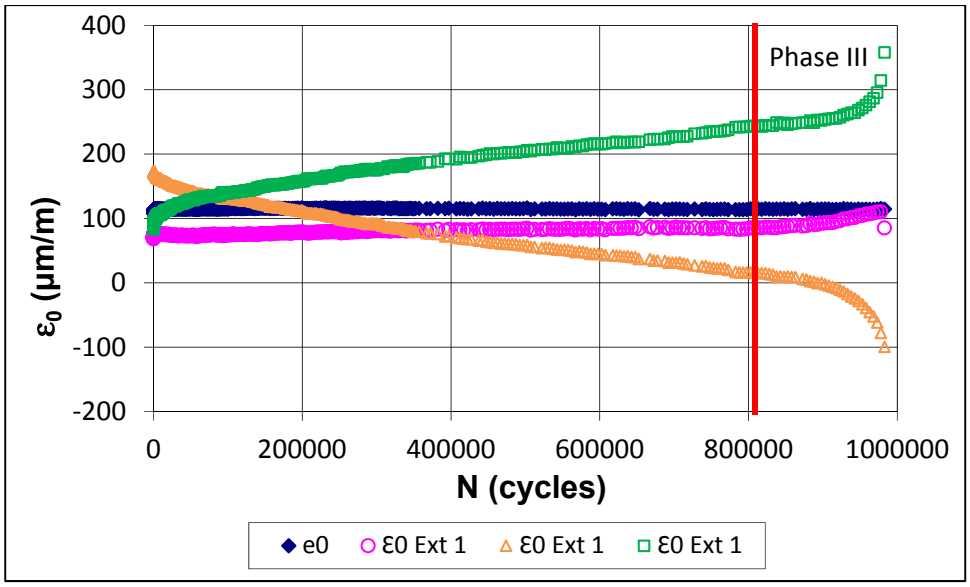

Figure 6.10 Changes in the center of the deformation as a function of the number cycles for the test 25RAP-(P1-A1)-D110 (ε_A = 108,8 µm/m; T = 10°C)

6.4.1.7 Stress amplitude

The fatigue damage of a sample is quantified by calculating the modulus of the specimen during test. To calculate this value, it is necessary to know the particular evolution of the applied stress to maintain the imposed strain at the target value. Figure 6.11 shows the change in the amplitude of the stress signal according to the number of cycles for a fatigue test carried out in the strain control mode for test 25RAP-(P4-A1)-D110. Since the amplitude of the deformation is kept constant, the stress amplitude is dropped at the beginning of the test due to biasing effects (heating, thixotropic and non-linearity) and fatigue damage. The rate of decrease is smaller after phase I up until the end of Phase II. The end of the test is marked by another significant drop. The curve of the stress amplitude has the same shape to that of the change of the modulus.

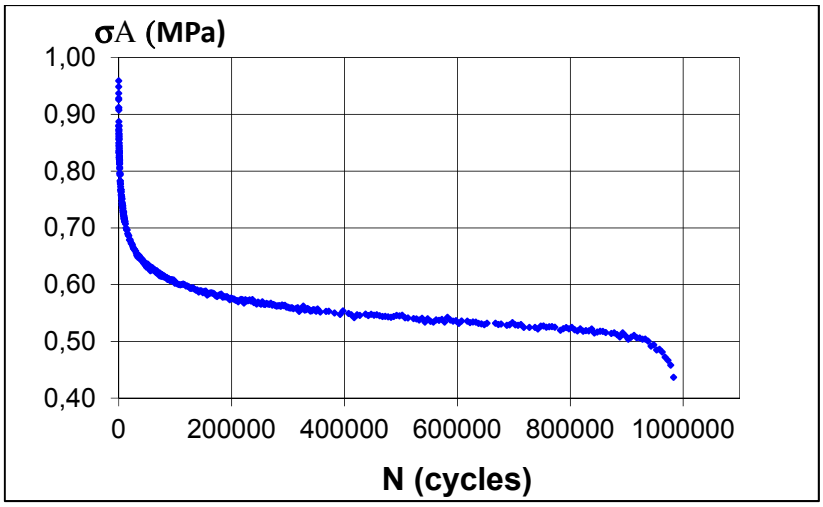

Figure 6.11 Evolution of the signal of the stress according to the number of cycles for the test 25RAP-(P1-A1)-D110 (ε_A = 110 µm/m; T = 10°C)

6.4.1.8 Center of stress's signal

Figure 6.12 shows the evolution of the center of the stress for fatigue test in strain control mode (σ_0). The center of the signal of the stress is changing very rapidly at the beginning of the test and after that at the 25 000th cycle it still increasing but it shows a steady or rapid slowdown of the high increased rate according to the results of Figure 6.12. The values of the center of the stress are very close to zero, indicating that there is stress relaxation during the test.

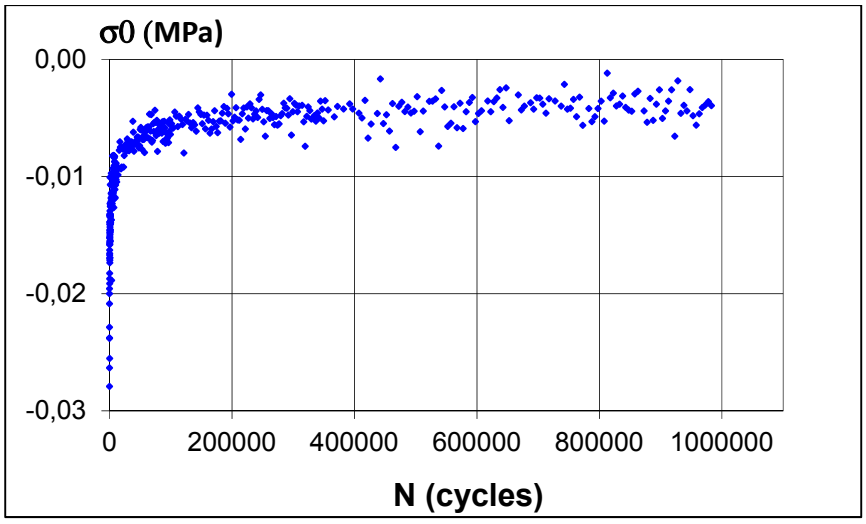

Figure 6.12 Evolution of the stress signal according to the number of cycles for the test 25RAP-(P1-A1)-D110 (ε_A = 110 µm/m; T = 10°C)

6.4.1.9 Phase angle evolution

For the evolution of the phase angle, we have two scenarios. First, the phase angle of the complex modulus increases rapidly at the beginning (phase I and II) of the test, then the rate of increase slows down (Figure 6.13a). The end of the test is marked by a decrease or a rapid decline of the phase angle reflecting the severity of the damage. Because of this, it can be concluded that the change in phase angle is a parameter closely related to fatigue and damage (Baaj, 2002).

In the second scenario, the phase angle increases rapidly from 17,48° to 26,87° during the first 6 357 cycles as it is shown in Figure 6.13b. Afterwards, this increase becomes much slower. The phase angle reaches at 33,24° at 551 984 cycles and continues to increase until the end of the test.

The above evolution of phase angle will affect the evolution of E* in Black space (|E*| versus ϕ_E) as we will see in the next section.

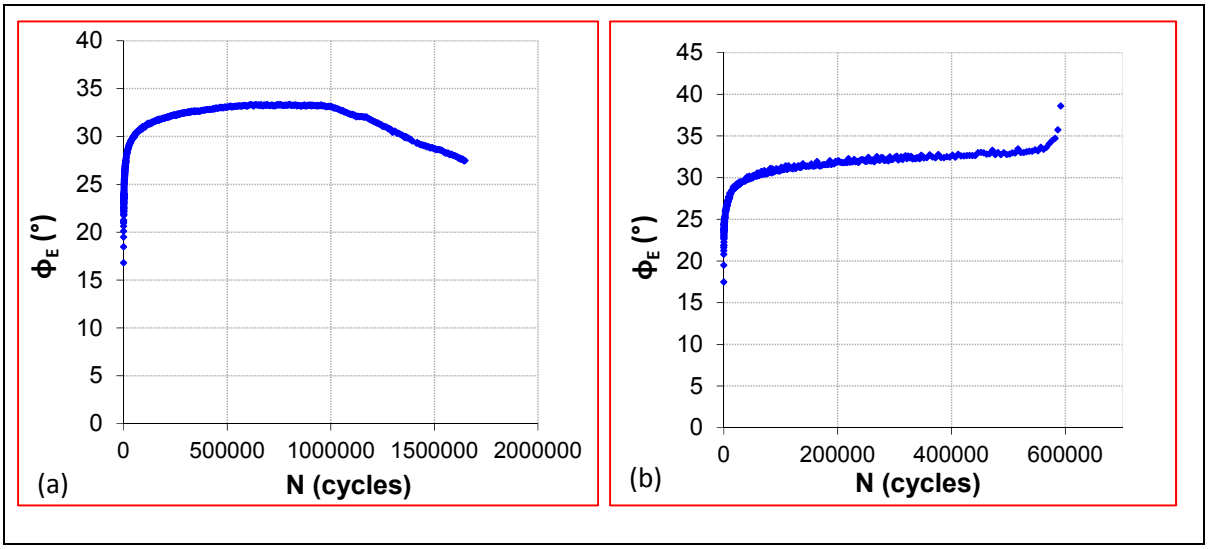

Figure 6.13 Evolution of the phase angle of the complex modulus according to the number of cycles for the test
(a) 40RAP-(P1-A3)-D170 (ε_A = 168,0 µm/m; T = 10°C)
(b) 25RAP-(P4-A5)-D130 (ε_A = 128,5 µm/m; T = 10°C)

6.4.1.10 Presentation in the black space

The complex modulus results of the fatigue tests were also plotted in the Black space. To get a better overview of changes in parameters (modulus and phase angle), we adopted the modification proposed by Soltani (1998) on the Black space. This change is to present the values of the modulus of rigidity in normal range and not in a logarithmic scale. Figure 6.14a and b present the modified Black space for the tests 40RAP-(P1-A3)-D170 and 25RAP-(P4-A5)-D130, respectively.

At the beginning of the test, the phase angle (ϕ_E) rapidly increases of a few degrees (Figure 6.14a). This is due to the nonlinearity of the asphalt mixture (details in § 6.4.1.4). Thereafter, this increase is more moderate, but still significant, up to 40 000 cycles where, at this time, the temperature (or heating) stabilizes. This more moderate change in the phase angle (ϕ_E) is due to heating and thixotropic bitumen (Phase I). The value of |E*| is 6 909 MPa at this solicitation cycle. Then, the slope of the phase angle vs the norm of the modulus is almost linear (phase II) until it reaches the failure (phase III). During the break phase, the phase

angle (ϕ_E) undergoes a decrease or increase rapidly, reflecting the importance of material damage (Baaj, 2002). In the context of the fatigue test on the test specimen 40RAP-(P1-A3)-D170, this rapid change in the phase angle (ϕ_E) occurs at 33,3°.

As indicated in Figure 6.14b, the end of Phase II which is the beginning of phase III is associated with the decrease in phase angle (see section 2.7.4.2). The test is marked by a decrease in the phase angle at the phase III.

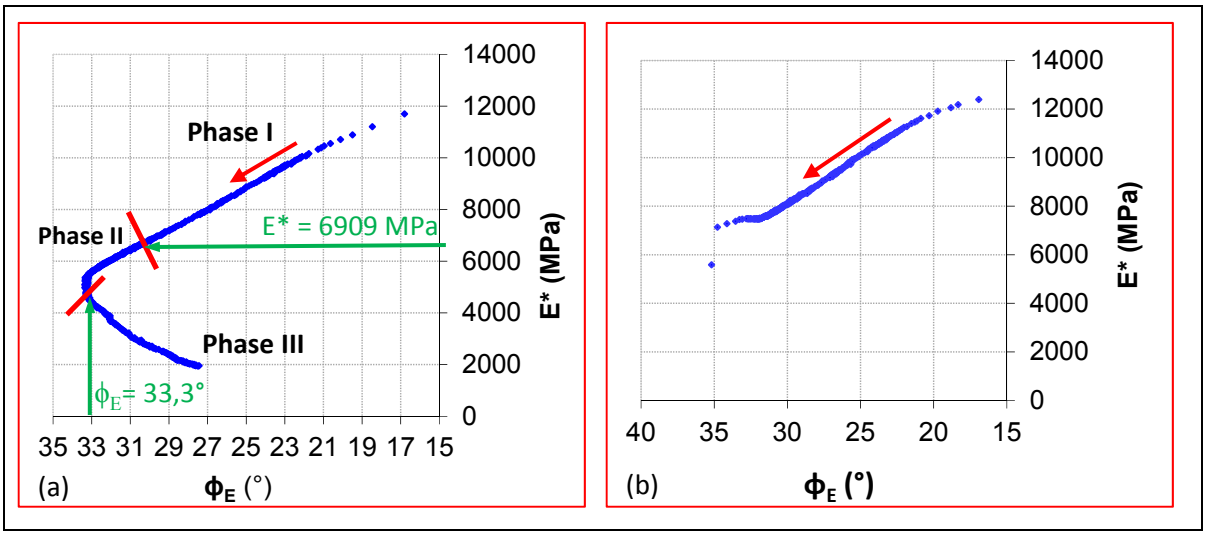

Figure 6.14 Presentation for the black space for the tests
(a) 40RAP-(P1-A3)-D170 (ε_A = 168 µm/m; T = 10°C)
(b) 25RAP-(P4-A5)-D130 (ε_A = 128,5 µm/m; T = 10°C)

6.4.1.11 Dissipated energy evolution

The failure criterion using the dissipated energy is not studied in this research, but the parameter itself will be used in the method DGCB to characterize the damage at the end of phase II. The dissipated energy has an important role in fatigue testing since it is converted into heat and raises the temperature of the specimen. Generally, in strain control mode, the dissipated energy is decreasing with the number of cycles (its increasing in stress control mode). But as the evolution of the dissipated energy depends on the stress, strain and the phase angle ($W_d = \pi \times \varepsilon_A \times \sigma_A \times \sin \phi_E$), one may encounter cases which disobey this rule

(especially for strain control mode). For tests with the strain control mode, the phase angle increases during the test. The average amplitude of the deformation is kept constant by the press. In tests controlled by one of the three extensometers, the amplitude of the average strain may increase or decrease slightly during the test. The stress amplitude does not cease to decrease during the test and before the rupture phase.

You can observe an increasing curve of dissipated energy in the case where the decrease in the amplitude of stress is very low compared to the increase in the phase angle or in the case where the average amplitude of the deformation increases during the test. Otherwise, the energy dissipation remains stable. The increase in the phase angle compensates the change in stress and strain.

The curve of the dissipated energy per unit volume with respect to the number of cycle is presented in Figure 6.15. These curves obey the following general rule: the dissipated energy is decreasing in function of the number of cycles in strain control mode.

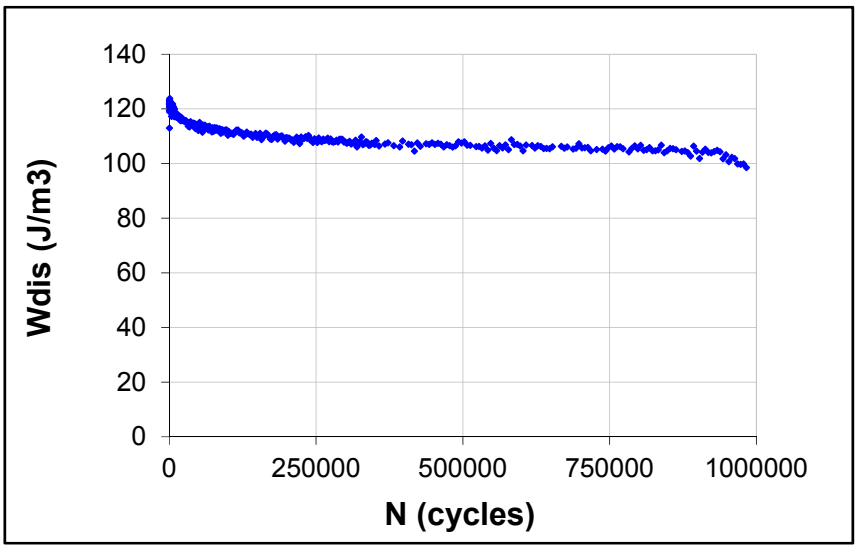

Figure 6.15 Evolution of the dissipated energy according to the number of cycles for the test 25RAP-(P1-A1)-D110 (ε_A = 110 µm/m; T = 10°C)

6.4.1.12 Fatigue test validation

There are some essential factors to verify for the successful implementation and analysis of a fatigue test. We always checked the following factors:

1) The chosen maximum difference in deformation amplitude relative to the average deformation amplitude (§ 6.4.1.5);
2) The quality of the signal (§ 6.4.1.3);
3) The temperature: it should be controlled precisely during the test (± 0,5°C);
4) The chosen imposed deformation: it needs to be chosen properly. Indeed, in some trials, the intensity of the imposed deformation largely reduces service life. In this regard, according Di Benedetto et al. (2004), it is important to subject to no less than 60 000 cycles to assess the performance in fatigue. That means if the specimen break before 60 000 cycles, it will lead to the elimination of a test. This last point highlights the importance of the imposed deformation amplitude.

The fatigue test is considered 'good' or acceptable if all these factors are respected. In this study, only the fatigue tests that did respect all the criteria were used in the analysis.

6.5 Correction of the test results based on air voids of the specimens

As presented previously in Table 6.1, specimen's air voids are different. To be able to represent fatigue resistance of a mix, we need to build the Wöhler curve from samples tested at similar air void content. Since, it is not our case, we need to correct all the fatigue tests results based on the content of voids of the specimens. In this study, the average content of void $\bar{V}$ for all the specimens used for the measure of the resistance of fatigue is 5,1%. This average void content allows calculating the corrected value of deformation ε_{cor} based on the corresponding processed value of imposed deformationε_m. This calculation is performed using the value of ε_m measured for a recycled mixture for which the air void content of a tested specimen is V_{sample}. The correction is performed according to the calculation specified

by Moutier (1991) in equation 6.2. This relationship has been established on the basis of Moutier's results obtained on trapezoidal specimens that had the same bitumen and even the same nature of aggregates at imposed displacement.

$$\varepsilon_{cor} = \varepsilon_m + 3{,}3(V_{sample} - \bar{V}) \quad (6.2)$$

The details regarding equation (6.2) are given in Appendix III. Figure-A III-1 shows the characteristic of fatigue before and after correcting the fatigue test results based on air voids for the four recycled mixtures. It is important to note that all the fatigue values in chapter 6 and 7 are corrected, based on $\bar{V}$ equal to 5,1%.

6.6 Comparison of fatigue test results

This section presents the analysis of the results of fatigue tests performed on the four selected recycled mixtures tested in this work and presented in Table 6.1. These tests are analyzed with two different criteria: classical failure criterion and end of phase II criterion as defined in sections 2.7.4.1 and 2.7.4.2, respectively. A comparative study of the measured fatigue life and the predicted fatigue life using the method DGCB is presented at the end of this chapter.

6.6.1 Comparison of initial values of the dynamic modulus

As explained in section 2.7.5, the initial values of the complex modulus are not measured directly. They are obtained by extrapolation, taking into account the initial modulus values over a range of 50 cycles. Figure 6.16 shows the initial dynamic modulus and phase angle for the four tested recycled mixtures. For each mix, these values are the average values of all specimens tested (see Table 6.2). The standard deviations are also shown. It should be noted that the amplitudes of the deformations on tested samples are relatively large in some cases and greater than what is generally called 'the field of small deformations (10^{-4}) (Di Benedetto and al., 2005). The results presented in Figure 6.16 show that the initial stiffness of the specimens, $|E_0^*|$, is relatively constant over the entire range of imposed deformations, which

means that, during the first cycles, the tested mixtures remains in the region of linear viscoelastic behaviour. The results presented in Figure 6.16 show that there is no increase in the initial stiffness with the addition of 15% and 25% RAP compared to the control mixture, but the addition of 40% RAP resulted in a slightly increase in mixture's stiffness, but not as much as we expected. The average values of the initial complex modulus are ranged between 10 327 and 11 929 MPa.

It was possible to notice that the phase angle does not seem to increase or decrease by the addition of RAP. Thus, there can be no conclusion made regarding this. The mean values of the phase angle of the complex modulus of different mixes range between 18,5° and 19,4°.

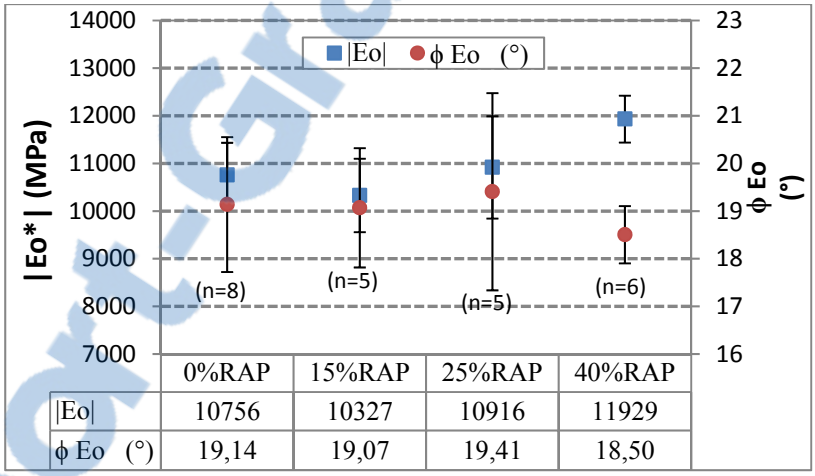

	0%RAP	15%RAP	25%RAP	40%RAP
|Eo|	10756	10327	10916	11929
ϕ Eo (°)	19,14	19,07	19,41	18,50

Figure 6.16 Initial complex modulus and phase angle for the four tested mixtures

6.6.2 Comparison of fatigue tests results performed on the same asphalt mixtures at different levels of deformation

In this section, we compare the results of various tests on the same type of mix to study the influence of the strain level amplitude on fatigue resistance. This influence is analyzed by plotting the normalized modulus (the ratio between the norm of the modulus after a given number of cycle and the norm of the initial modulus, ($|E^*/E_0|$), based on the progress of the test. For the virgin mixture (0RAP) curves, the normalized stiffness moduli are plotted against the number of cycles in logarithmic coordinates (Figure 6.17) using six different

target strain amplitudes (105, 110, 115, 130, 140, and 150 µm/m). The corresponding corrected real strains which used in the plot of the curves are (107,9, 112,1, 112,1, 116,4, 124,7, 134,8, 132,6, and 145,3 µm/m). All values of the true corrected strain will be presented later (Table 6.3). On Figure 6.17, we observe distinct curves corresponding to different levels of imposed deformation associated with the transition between phases II and III of the damage. As it can be seen, the rate of decrease of the normalized modulus increases with the increase of the strain amplitude.

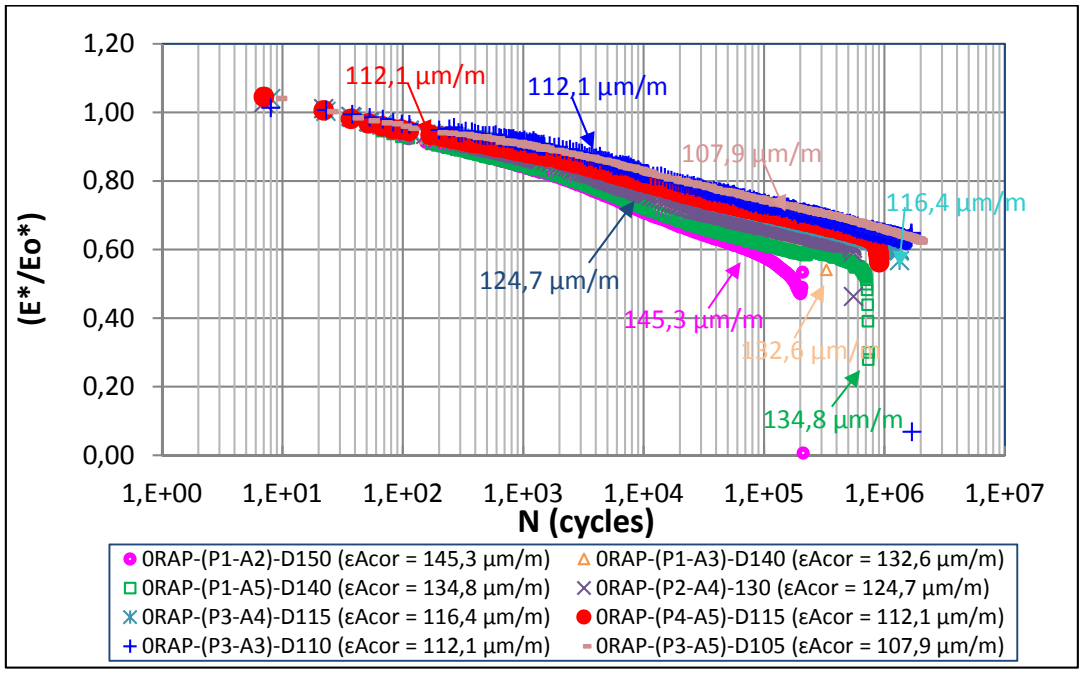

Figure 6.17 Comparison of ($|E^*/E_0|$), - log (N)) for six different strain level tests for the virgin mix (0RAP28)

6.6.3 Comparison of fatigue tests at the same imposed strain level for different recycled mixtures

Figures 6.18 to 6.20 show the results for the various fatigue tests carried out at the same strain amplitude, namely 130 µm/m, 140 µm/m and 150 µm/m, for the four recycled mixtures. The corrected strain values were used in the curves. We know that the strains values were not exactly the same but it is very close, and it may give some information about

the influence of the addition of RAP. For example, for the imposed strain values measured for the specimens of 130 µm/m, the real strain values range between 124,6 to 133,3 µm/m.

With these figures, we can compare the fatigue behaviour of different mixtures. In general, the 15% RAP, 25% RAP, and 40% RAP mixes show behaviour that are relatively close to the reference mix in terms of the drop of the normalized modulus for all the strains amplitudes (130, 140 and 150 µm/m), even if there exists a small difference in the real deformation for the four mixes.

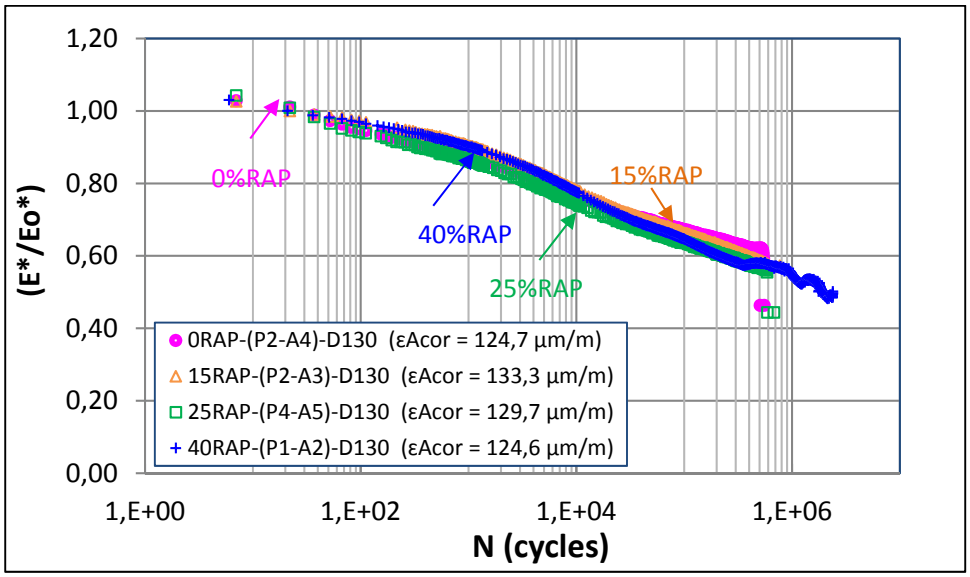

Figure 6.18 Comparison of a fatigue test at 130 µm/m strain level, real strain values range from 125 to 133 µm/m, for 4 recycled mixtures in the axes $|E^*/E_0|$) - log (N) (0% RAP, 15% RAP, 25% RAP, and 40% RAP)

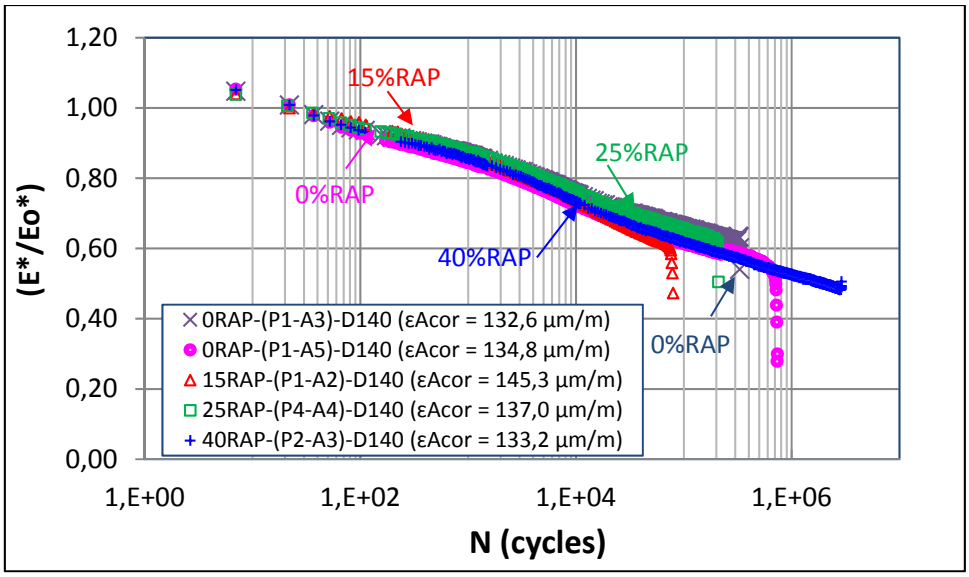

Figure 6.19 Comparison of a fatigue test at test at 140 µm/m strain level, values of real strain range from 133 to 145 µm/m, for 4 recycled mixtures in the axes $|E^*/E_0|$) - log (N) (0% RAP, 15% RAP, 25% RAP, and 40% RAP)

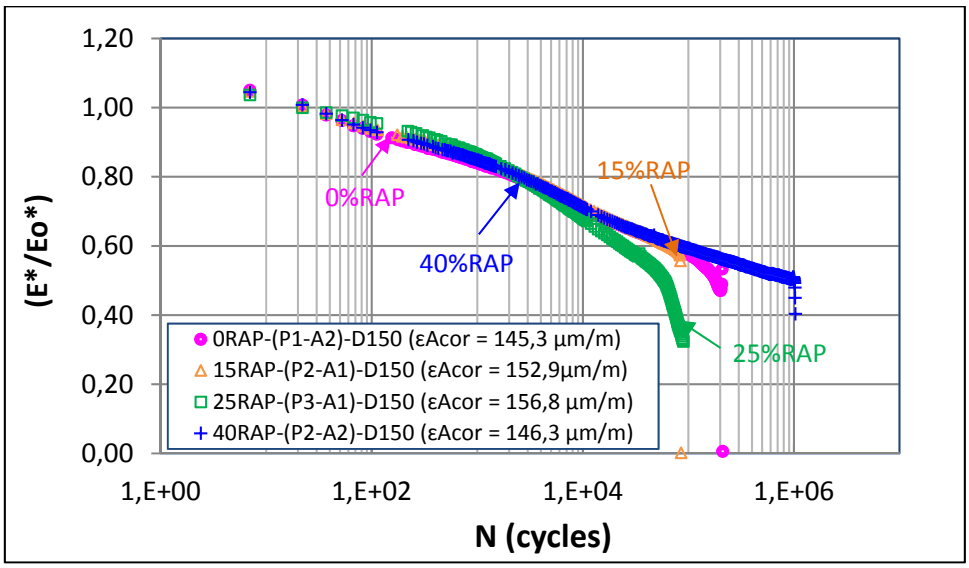

Figure 6.20 Comparison of a fatigue test at test at 150 µm/m strain level, real strain values lie in the range of 145 to 157 µm/m, for 4 recycled mixtures in the axes $|E^*/E_0|$) - log (N) (0% RAP, 15% RAP, 25% RAP, and 40% RAP)

6.7 Evaluation of the fatigue life

Two criteria were used to determine the service life of the tested asphalt mixtures: 1) The traditional criterion ($N_{f50\%}$ criterion), 2) The change criterion phase II/III ($N_{fII/III}$). These criteria were defined in section 2.7.4.1 and 2.7.4.2, respectively.

Table 6.3 summarizes the fatigue life derived from the results for fatigue tests performed on selected mixtures by different strains.

The values of the complex modulus calculated by the model 2S2P1D, with which we can calculate the value of the norm of the initial complex modulus for the conditions corresponding to the fatigue test (T=10°C and 10 Hz) (see section 5.2.3), are presented in Table 6.3. They are quite comparable to the dynamic modulus determined during fatigue testing.

Table 6.3 Presentation of the obtained fatigue test results

TN o.	Test Name	Void (%)	$\varepsilon_{avr\ real}$ (µm/m)	ε_{cor} (µm/m)	Initial dynamic modulus, |E*|(MPa)			Criterion (cycles)				Er(2) (%)	$\varepsilon_{6,cor}$ ($N_{f50\%}$)	$\varepsilon_{6,cor}$ ($N_{fII/II}$)
					Experimental		Modelling(1) 2S2P1D	$N_{f50\%}$	*Curves of extens* ($N_{f\Delta ext}$)	*Black space* ($N_{f\varphi}$)	$N_{fII/III}$ = $(N_{f\varphi}+N_{f\Delta ext})/2$			
					Value	Average								
1	0RAP-(P1-A2)-D150	4,0	148,9	145,3	10540	10756	10258	161 375	N/A	206 478	206 478	27,9	117,5	115.8
2	0RAP-(P1-A5)-D140	4,1	138,1	134,8	11089			692 216	406 884	692 216	549 550	-92,1		
3	0RAP-(P2-A4)-D130	4,5	126,5	124,7	12057			501 909	501 909	546 958	524 434	4,5		
4	0RAP-(P1-A3)-D140	3,9	136,5	132,6	11475			314 163	314 163	N/A	314 163	0,0		
5	0RAP-(P3-A3)-D110	6,7	106,8	112,1	10393			1 639 096	1 639 096	N/A	1 639 096	0,0		
6	0RAP-(P3-A5)-D105	6,8	102,2	107,9	10036			1 874 412	N/A	1 874 412	1 874 412	0,0		
7	0RAP-(P4-A5)-D115	5,1	112,0	112,1	10436			902 680	752 488	902 680	827 584	-8,3		
8	0RAP-(P3-A4)-D115	6,6	111,4	116,4	10023			1 328 140	1 172 944	1 333 145	1 253 045	-5,7		
9	15RAP-(P2-A1)-D150	6,3	149,0	152,9	9607	10327	9771	84 158	81 141	84 158	82 650	-90,2	117,0	113.3
10	15RAP-(P2-A2)-D120	6,7	118,7	124,1	9193			351 791	331 745	351 791	341 768	-2,8		
11	15RAP-(P1-A3)-D115	5,9	112,2	114,9	10920			1 027 737	932 622	1 027 737	980 180	-90,5		
12	15RAP-(P2-A3)-D130	6,3	129,4	133,3	10861			607 602	607 602	N/A	607 602	0,0		
13	15RAP-(P1-A2)-D140	6,7	140,1	145,3	11054			76 374	76 386	76 381	76 375	0,0		
14	25RAP-(P4-A2)-D120	6,1	119,0	122,4	12090	10916	10031	241 937	241 937	244 444	243 191	0,5	112,1	112.1
15	25RAP-(P4-A4)-D140	5,6	135,4	137	10123			203 910	203 910	206 416	205 163	0,6		
16	25RAP-(P4-A5)-D130	5,8	128,5	129,7	11962			577 019	577 019	587 030	582 025	0,9		
17	25RAP-(P3-A1)-D150	6,8	151,1	156,8	11909			53 227	N/A	64 309	64 309	20,8		
18	25RAP-(P1-A2)-D110	6,2	108,8	112,3	8760			943 017	812 841	973 058	892 950	-90,5		
19	40RAP-(P1-A2)-D130	3,3	130,5	124,6	11932	11930	10513	1 812 821	2 383 335	2 388 339	2 385 837	31,6	134,8	142,8
20	40RAP-(P2-A3)-D140	3,8	137,5	133,2	12307			1 028 208	2 865 932	2 800 844	2 835 891	175,8		
21	40RAP-(P2-A2)-D150	2,1	147,0	137,2	12541			542 579	943 107	1 023 215	985 665	81,7		
22	40RAP-(P1-A3)-D160	3,6	158,3	153,4	11469			214 108	254 196	417 001	335 599	56,7		
23	40RAP-(P1-A4)-D170	2,7	168,0	160,3	11125			296 783	792 452	802 465	797 459	168,7		
24	40RAP-(P1-A2)-D180	2,5	178,0	169,4	12203			54 043	401 998	427 016	414 507	667,0		

(1) Based on 2S2P1D determined for data mix presented in chapter 5

(2) $E_r = (N_{fII/III} - N_{f50\%} / N_{f50\%}) * 100$

To put into perspective the differences between the fatigue lives determined using the traditional criterion to the fatigue lives corresponding to the change of phases II and III, a relative error is calculated by the equation 6.3:

$$E_r(\%) = \left[\frac{N_{fII/III} - N_{f50\%}}{N_{f50\%}} \right] * 100 \qquad (6.3)$$

The results are shown in Table 6.3. Value of the relative error close to zero indicates a zero gap between the two criteria. Negative values show that the classical criterion overestimates the fatigue life, while positive values show that the fatigue life is underestimated.

It should be noted that many other criteria can be defined to determine the fatigue life in fatigue. The value of $N_{f50\%}$ does not appear directly linked to the appearance of macro crack. In addition, the evolution of the dynamic modulus is highly dependent on the bias phenomena (nonlinearity, heating and thixotropy). This thing plays an important role, especially in the first few cycles.

Also, it is important to note that the lowest imposed strain value for the 40% mixture was 130 µm/m. We decided not to go lower than this value since the resulted fatigue life was long. In order to achieve the rupture of the specimen quickly or to reach phase III, higher levels of deformation were applied.

In fact, this section will deal with fatigue life of asphalt concrete containing RAP. This section (section 6.7 – subsections 6.7.1 to 6.7.2) is separated in three main parts. In the first part, we deal with the Wöhler curve presentation, then with the characterization of fatigue life data. The second (section 6.8 – subsection 6.8.1) and the third parts (section 6.9 to section 6.10) present other main results which deal with different aspects of characterization of the fatigue life properties of the HMA mixtures containing RAP.

6.7.1 Relationship between the fatigue life and the amplitude of deformation: fatigue lines

The Wöhler curve is used to describe the fatigue behaviour of material in respect to the applied amplitude of the strain (ε_0), in logN-logε space. The Wöhler curve could be considered as a linear relationship and two key criteria are defined: 1) slope (k_2) and 2) the intercept (k_1). The fatigue life (N_f) is expressed as the basic fatigue model as follow:

$$N_f = k_1(\varepsilon_0)^{-k_2} \tag{6.4}$$

Where:

k_1 : Coefficient corresponding to the fatigue life of the material for a magnitude of imposed deformation of 1 m/m; and

k_2 : Coefficient related to the slope of the fatigue line of a material (without unit).

By plotting the relationship between fatigue life and the strain amplitude, the two coefficients k_1 and k_2, of the basic fatigue model, can be determined. For each series of the tests conducted as part of our experimental program, these two coefficients related to the Wöhler curve are specified. Figure 6.21 shows the typical relationship obtained in the system of log (N_f) vs log (ε_0) for fatigue tests performed at different magnitudes of strain.

The coefficients k_1 and k_2 are dependent on the material, and, in principle, on the temperature and the frequency of testing (Perraton et al., 2011). For the French method, the axis are interchanged, which means that the fatigue lines are shown in the system of log (ε_0) vs. log (N_f) in order to get the coefficient ε_6 and the coefficient b.

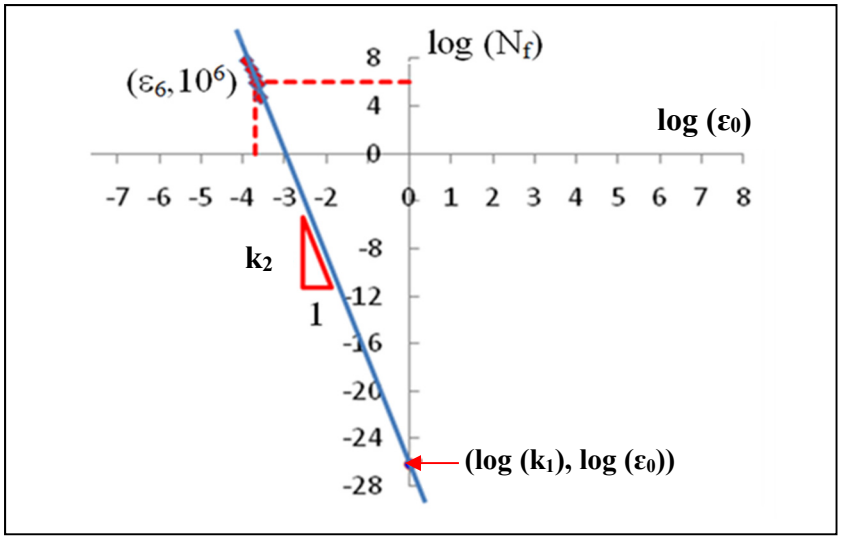

Figure 6.21 Wöhler curve in the domain log N_f vs log ε_0 (m/m)
Adapted from Perraton et al. (2011 p. 41)

The coefficient b refers to the slope of the fatigue line in the relevant axis system. The value of b in the system of log (ε_0) vs. log (N_f) is equivalent to $-1/k_2$ in the system log (N_f) vs. log (ε_0). Furthermore, ε_6 refers to the strain for which the fatigue life of the mixture is equal to 1 million cycles of solicitation for a mixture tested at a given temperature and frequency.

For each mix, the fatigue lines (Wöhler curve) were plotted in the log (N_f) vs. log (ε_0) system and we have determined the value of the coefficient of determination R^2. Figure 6.22a and Figure 6.22b show comparisons between the values of the fatigue life determined with the criterion $N_{f50\%}$ and the criterion $N_{fII/III}$ for the four tested mixes in function of the magnitude of the deformation of the test before doing the required correction to take into account difference in air void content between mixes. Similarly, Figure 6.23a and Figure 6.23b show comparisons between the values of the fatigue life measured with the criterion $N_{f50\%}$ and the criterion $N_{fII/III}$ in function of the magnitude of the deformation after doing the required correction for air voids.

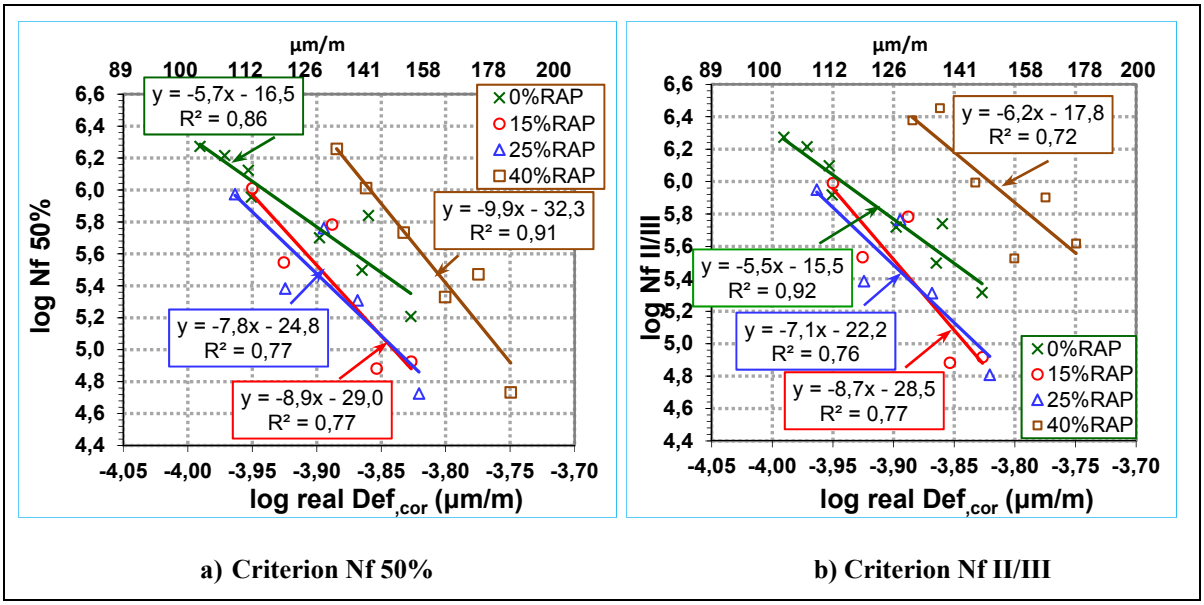

a) Criterion Nf 50% b) Criterion Nf II/III

Figure 6.22 Wöhler curves for the four mixes (0% RAP, 15% RAP, 25% RAP, 40% RAP) determined with the classical criteria (left) and with the criterion of the end of phase II (right) and the corresponding regression lines in the logarithmic axis log N_f-log ε

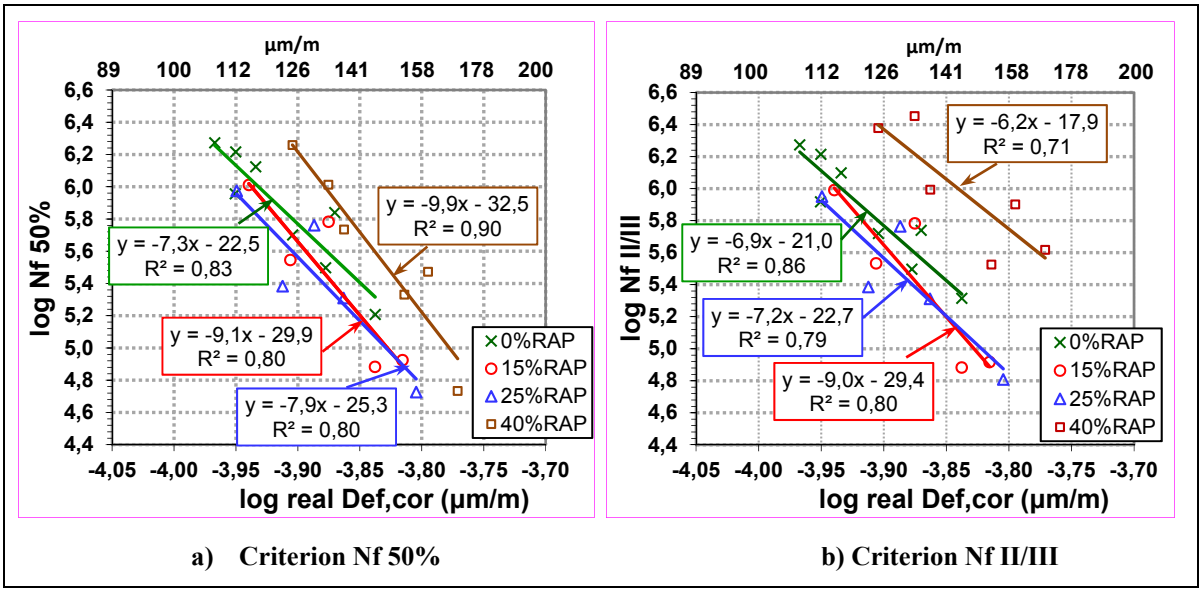

a) Criterion Nf 50% b) Criterion Nf II/III

Figure 6.23 Wöhler curves for the four mixes after corrected to air void of 5,1% determined with the classical criteria (left) and with the criterion of the end of phase II (right) and the corresponding regression lines in the logarithmic axis log N_f-log ε

From fatigue lines, it is possible to determine the constants (k_1 and k_2) of the fatigue lines. Tables 6.4 and 6.5 provide the synthesis of the results for the different series of the tests carried out before and after the correction process that take into account the variation of air voids between samples, respectively. For $N_{f50\%}$ criterion shown in Figure 6.23a, the R square value of the 40% RAP mix is high (90%) while those of 0% RAP, 15% RAP, and 25% RAP are lower (83%, 81%, and 81% respectively).The coefficients of the fatigue model will depend on the criteria used to determine the fatigue life of each specimen tested for fatigue.

It should be noted that the values of $\varepsilon_{6,cor}$ were determined from mathematical calculations using the best fit curve equations, by considering the corrected Wöhler curve for each mix. The suitable fatigue parameters for each mix $k_{1,cor}$ *and* $k_{2,cor}$ were used for this purpose, while fixing the fatigue life of the mix to 1 million cycles;

Table 6.4 Characteristics of the fatigue lines for different performed tests

Mix	No. of tests	Criterion of failure	k_1	k_2	ε_6 µm/m	b= -1/ k_2	R^2	Voids Mean (Std dev.)
0RAP	8	$N_{f50\%}$	3,0E-17	5,7	116	-0,175	0,86	5,2 (1,2)
		$N_{fII/III}$	3,2E-16	5,5	114	-0,183	0,92	
15RAP	5	$N_{f50\%}$	1,0E-29	8,9	111	-0,113	0,77	6,4 (0,3)
		$N_{fII/III}$	2,9E-29	8,7	111	-0,115	0,77	
25RAP	5	$N_{f50\%}$	1,7E-25	7,8	107	-0,129	0,77	6,1 (0,4)
		$N_{fII/III}$	6,2E-23	7,1	106	-0,141	0,76	
40RAP	6	$N_{f50\%}$	4,7E-33	9,9	138	-0,101	0,91	3,0 (0,6)
		$N_{fII/III}$	1,7E-18	6,2	151	-0,161	0,72	

Table 6.5 Characteristics of the fatigue lines for the corrected tests results for a specific air void of 5,1%

Mix	No, of tests	Criterion of failure	$k_{1,cor}$	$k_{2,cor}$	$\varepsilon_{6,cor}$ µm/m	$b_{cor} = -1/k_{2cor}$	R^2	Voids Mean
0RAP	8	$N_{f50\%}$	2,8E-23	7,3	117	-0,138	0,83	5,1
		$N_{fII/III}$	1,0E-21	6,9	116	-0,146	0,86	
15RAP	5	$N_{f50\%}$	1,3E-30	9,1	115	-0,110	0,81	
		$N_{fII/III}$	4,0E-30	9,0	115	-0,111	0,80	
25RAP	5	$N_{f50\%}$	4,8E-26	7,9	110	-0,0126	0,81	
		$N_{fII/III}$	2,1E-23	7,2	109	-0,138	0,79	
40RAP	6	$N_{f50\%}$	2,8E-33	9,9	132	-0,101	0,90	
		$N_{fII/III}$	1,2E-18	6,2	143	-0,161	0,71	

Tables 6.4 and 6.5 show that there is no big change in ε_6 and $\varepsilon_{6,cor}$ values. The fatigues lines (corrected data) have a greater slope than the lines of raw data except for 40% RAP. It means that there may be small variation of the values of X axis as the values of ε_6 and $\varepsilon_{6,cor}$ showed which will give us little effect on the fatigue resistance of the mixtures.

The influence of the correction of the air voids on the coefficients of the fatigue can be observed from the results in Table 6.4 and 6.5. The values of the coefficients ($logk_1$ and k_2) before doing the correction are close to the value after correction. However, there is a small gap between the results in the case of virgin mix (0% RAP) and that is because there is some variation of the air voids content of the tested samples ranges from 3,5 to 6,8. As we can see, the standard deviation is a bit high for that mix in comparison to the other 3 mixes.

6.7.1.1 Relationship between the fatigue line parameters and RAP content of a mix

In this section, we try to plot a linear relationship between the percentage of RAP and $logk_1$, and another relationship between the percentage of RAP and k_2. These relationships were

used to find out the general fatigue models which are obtained and explained later in chapter 7. The need for the improvement of the basic fatigue model is important because it can be used as a surrogate fatigue model to predict fatigue life of recycled mixtures without the necessity for producing the mixture itself for testing for fatigue (except for the virgin mixture). In the next chapter, the effect of added RAP content in the new model will be focused in applying a vertical shift factor obtained from these relationships to get these models. The only mixture that is required to define the fatigue parameters in these models is the virgin mixture.

The graphical representations of the relation between %RAP and $logk_1$, before and after the announced correction process using the two criteria ($N_{f50\%}$ and $N_{fII/III}$), are presented in Figure 6.24. The graphical representations of the relationship between %RAP and k_2 , before and after the correction done based on the average air void equal to 5,1%, according to the two criteria used in this study ($N_{f50\%}$ and $N_{fII/III}$) are presented in Figure 6.25.

Results show that with the classical criterion, $logk_1$ values for different mixtures at different percentages of RAP were fitted with good R-square value of 0,73 and 0,61 before and after correction (Figure 6.24a). However, the criterion of the end of phase II shows very poor of correlation between $logk_1$ and % RAP (R^2 = 0,0 to 0,15) (Figure 6.24b).

The influence of the percentage of RAP on k_2 can be observed on Figure 6.25. The results provided by the classical criterion show high R-square value of 75 and 62 in comparison with the criterion of the end of phase II (R^2 = 0 and 0,13). These results suggest that the classical criterion is capable of successfully providing a good correlation between the fatigue lines coefficients ($logk_1$ and k_2) and the percentages of RAP in comparison with the criterion of the end of phase II.

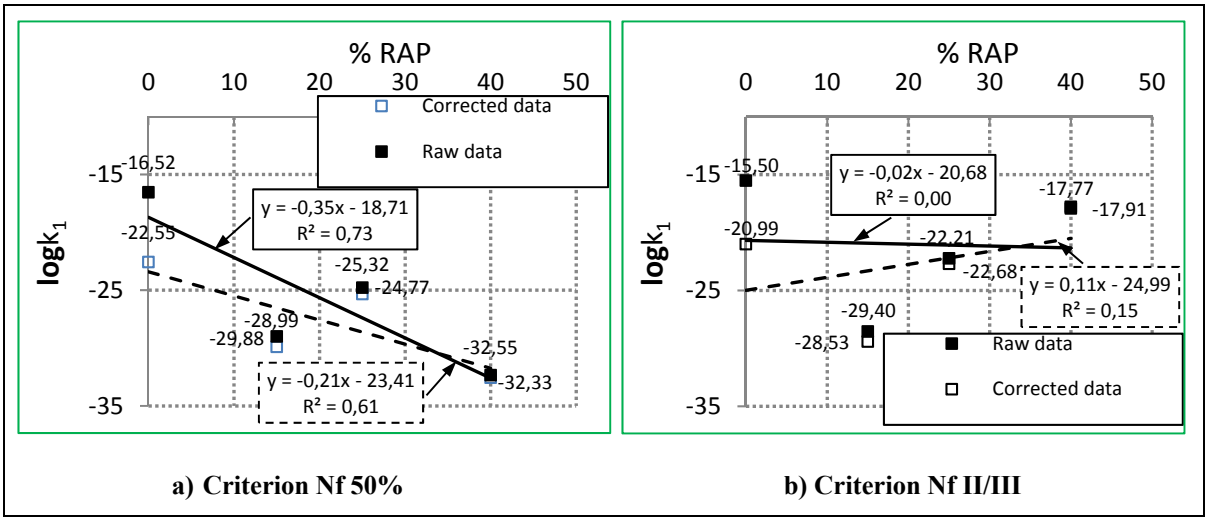

a) Criterion Nf 50% **b) Criterion Nf II/III**

Figure 6.24 Relation between %RAP and $logk_1$ before and after correction for a specific air void of 5,1% according to the classical criterion ($N_{f50\%}$) and the criterion of the end of phase II ($N_{fII/III}$)

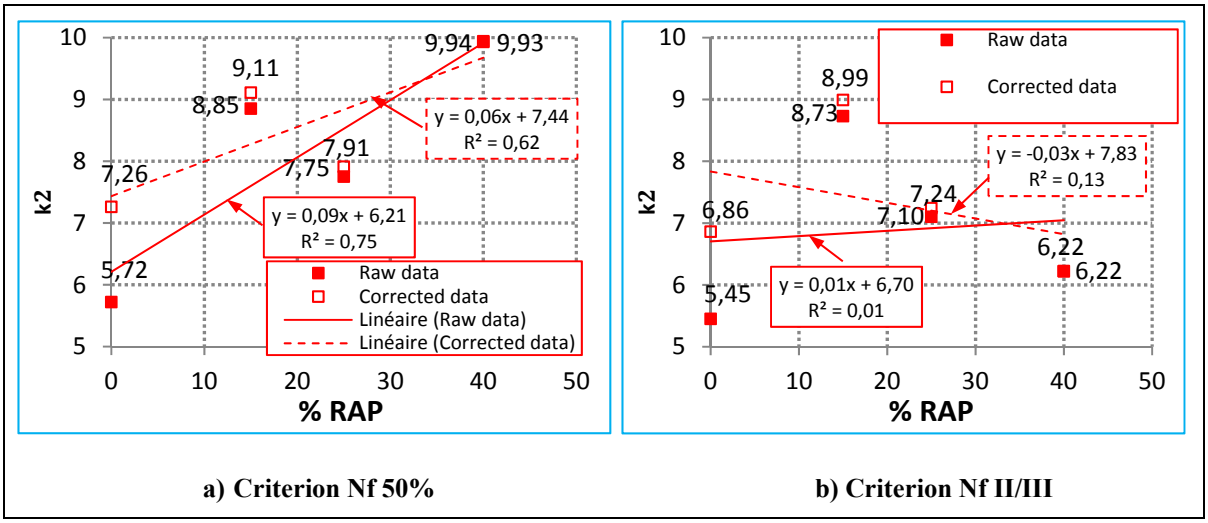

a) Criterion Nf 50% **b) Criterion Nf II/III**

Figure 6.25 Relation between %RAP and k_2 before and after correction for a specific air void of 5,1% according to the classical criterion ($N_{f50\%}$) and the criterion of the end of phase II ($N_{fII/III}$)

6.7.2 Measurement of the correlation between the N_f predicted by the basic model and the measured N_f

In this study, it can be beneficial to show the quality of the basic fatigue model presented in equation 6.4 for all combined mixes because, in the next chapter, we will present our attempts to improve the basic fatigue model. In this analysis, the fatigue effective parameters $k_{1,cor}$ and $k_{2,cor}$ (Table 6.5) for all the four recycled mixes are used to estimate the $N_{f50\%}$ and $N_{fII/III}$ values at each imposed corrected value of deformation and the results are presented in appendix III in Table-A III-2.

Figure 6.26 shows the plot of the measured fatigue values versus the predicted values for the basic fatigue model defined in equation (6.4). The coefficient of determination (R^2) is used to denote the strength of the linear association between $N_{f\text{-}pred.}$ and $N_{f\text{-}measured}$. The R^2 values were 0,88 and 0,80 for the $N_{f50\%}$ and $N_{fII/III}$ criterion, respectively. We can conclude that our experimental data are properly modelled by the basic fatigue model. The ratings of the fatigue model are good measures of accuracy for the two criteria. Nevertheless, to get fatigue line parameters in reference to the basic fatigue model is not useful due to the fact that a full series of laboratory tests is required. We will discuss in the next chapter on how we can modify the basic model to take into account the inclusion of RAP content in the hot mix asphalt to predict their fatigue lives.

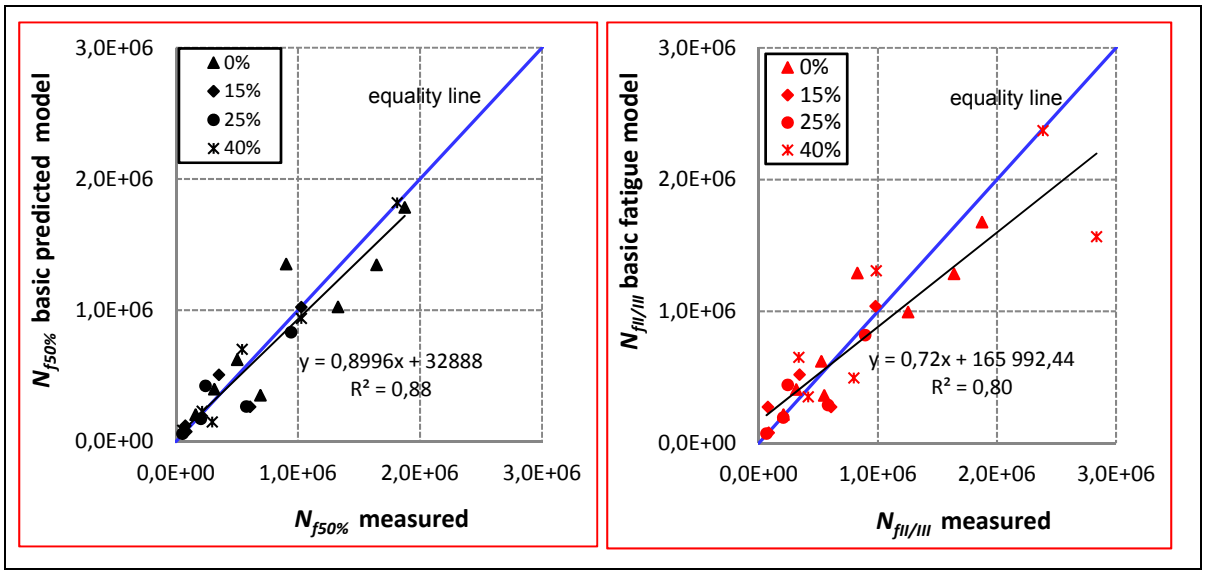

Figure 6.26 Basic predicted model versus measured N_f using the fatigue parameters k_1, and k_2 defined for each mix

6.8 Effect of the addition of RAP

One of the main goals of this research project is to verify the influence of the addition of RAP on the fatigue life of asphalt mixes. The next section will present a comparison between the four recycled mixtures.

6.8.1 Comparison between recycled asphalt mixtures

According to the classical criterion ($N_{f50\%}$: Figure 6.23a) the fatigue lines of the four mixes are different from each other. The fatigue line corresponding to the 40% RAP mix is the highest, which means that for any level of deformation, the fatigue life of the 40% RAP mix is the highest of the tested mixes. Moreover, the mixture 40% RAP has the highest ε_6 values. For the three other mixes, the ε_6 values are close to each other. However, these results show that the four recycled mixes (0% RAP, 15% RAP, 25% RAP and 40% RAP) have relatively similar fatigue behaviour. In the same manner, we also determined the fatigue life for the selected mixtures using the transition between phase II and phase III criterion ($N_{fII/III}$: Figure 6.23b). We get the same thing in this case.

In extrapolating the regression line in the axes (log (N_f) – log (ε)) for the corresponding values for each mix, it is possible to determine the strain to which the fatigue life of the mix is equal to 1 million cycles. The resulting value is conventionally referred to as $\varepsilon_{6,cor}$ which is used in the French pavement design method (Setra-LCPC, 1994). Figure 6.27 shows the values of $\varepsilon_{6,cor}$ which represent the failure at one million cycles according to the traditional criteria $N_{f50\%}$ and $N_{fII/III}$ as related to the transition between phase II and phase III. According to the criterion $N_{f50\%}$, the $\varepsilon_{6,cor\text{-}50\%}$ value ranged from 134,8 µm/m for the 40% RAP mix to 112,0 µm/m which was obtained with the 25% RAP mix. However, according to the criterion of the end of phase II, the values of $\varepsilon_{6,cor\text{-}II/III}$ ranges from 142,8 µm/m for the 40% RAP mix to 112,1 µm/m for the 25% RAP mix.

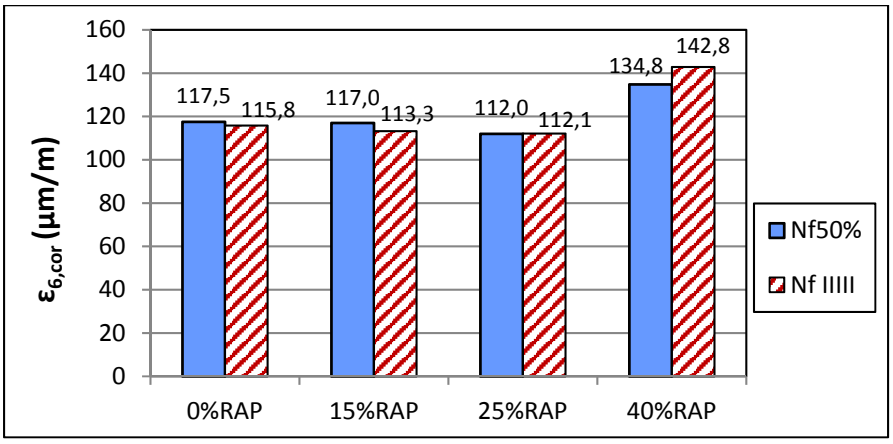

Figure 6.27 ε_6 values of the four tested mixes determined with the criteria of 50% decrease of the initial modulus and the criteria of transition between II and III

Here, we did a classification for the tested mixes according to the value in a descending order. The results show that the classification of the mix is slightly different according to the criteria used. Nevertheless, on the basis of these criteria the patterns show:

- The 25% RAP mix has a lower fatigue resistance;
- The 0% RAP and 15% RAP mixes have similar fatigue performance, slightly higher than the 25% RAP mix; and

- The 40% RAP presents fatigue performance higher than others.

To highlight the difference between the results of fatigue by considering the two criteria, fatigue lives are calculated using equation 6.4 at similar magnitude of deformation as shown in Table 6.6.

According to the two criteria used, at 110 microns strain level (Table 6.6), 40 percent RAP mixture had better fatigue performances than the control mixture (0% RAP) and 15 percent RAP mixture performed similar to the control mixture (0% RAP). However, the 25% RAP mixture has lower fatigue performance as compare to the control mixtures. At the 120 microns strain level (Table 6.6), 40 percent RAP added had better fatigue performance than the control mixture, whereas the 15%RAP and 25% RAP mixes have poor or did not affect the resistance of the mix to fatigue . Finally, at 130, 140, and 150 μm/m levels, the 40% RAP mixture also performed better than the control mixture. However, 15 and 25 percent performed worse than the control mixture. Our hypothesis that can support the results is that it looks in Figure 6.16 that the 40% RAP exhibited initial stiffness values at the testing temperature (10°C) which will stiffen the mixtures and it is well known that by increasing the stiffness, the estimated fatigue life will increase (Hajj, Sebaaly et Shrestha, 2007; McDaniel et Anderson, 2001).

Like for the classical criterion, we get the same trend of fatigue performance at various strain levels with the criterion of the end of phase II.

In summary, the results indicate that both the 15% RAP and 25% RAP mixes performed similar or worse than the control mixture, and the 40% RAP mix performs better than the rest. Furthermore, the 15% RAP mix performed slightly better than the 25% RAP mix at almost all strain levels. The 40% RAP mixture performed much better than the control mixtures at lower strain levels as compared to higher strain levels. These last findings are in agreement to what we concluded before when we analyzed the results based on the evaluation of the value of ε_6, as presented above.

Table 6.6 Comparison between the estimated laboratory fatigue life values of the two failure criteria using the corrected fatigue test results for a specific air void of 5,1%

The mix	Imposed deformation (µm/m)	$N_{f\text{-calculated}}$ (cycles)		Relative error Er (%)(1)
		By considering the coefficients k_1 and k_2 established from $N_{f50\%}$	By considering the coefficients k_1 and k_2 established from $N_{fII/III}$	
GB20 0% RAP	110	1 547 883	1 460 987	-5,95
	120	822 988	804 298	-2,32
	130	460 278	464 460	0,90
	140	268 757	279 358	3,79
	150	162 865	174 026	6,41
GB20 **15% RAP**	110	1 525 761	1 540 859	0,98
	120	690 610	704 764	2,01
	130	333 081	343 188	2,95
	140	169 569	176 276	3,80
	150	90 445	94 803	4,60
GB20 25% RAP	110	983 828	956 012	-2,91
	120	494 324	509 183	2,92
	130	262 448	285 231	7,99
	140	146 037	166 794	12,44
	150	84 616	101 215	16,40
GB20 40% RAP	110	6 292 248	5 157 540	-22,00
	120	2 649 644	3 001 911	11,73
	130	1 195 782	1 824 641	34,46
	140	572 449	1 150 771	50,26
	150	288 338	749 234	61,52

(1) Calculated in accordance to equation 6.3 (§ 6.7)

It should be noted that the calculated fatigue life for different mixtures at different strain levels were derived from the curve that are fitted to R-square value (Table 6.5) between 81 to

90 for the classical method and between 71 to 86 for the end of phase II method. These R-square values are good which indicates that our results fit the fatigue model well.

As shown in Table 6.6, the fatigue life determined by the criteria of transition between phase II and III can be close or shorter or longer than those determined by the traditional criteria with relative error quite important. Therefore, the situation requires special attention when using the traditional criteria to predict the fatigue life of the bituminous layers in the pavement, since the fatigue life of the pavement material can be overestimated or underestimated.

6.8.2 Summary of the results

This study shows that the addition of 15% RAP and 25% RAP may not change the fatigue performance of the mix greatly. However, the addition of 40% RAP to a mixture resulted in a better resistance to fatigue than the control mix in the case of our RAP source. As the RAP percentage increases some effects on the mixture properties are noted. Our explanation is that when the percentage of RAP in the mix is high enough, the RAP binder could create a change in the mixture properties and therefore we can conclude that the influence of RAP on the final HMA property also varies with the amount of RAP. It is postulated that the 40% RAP provided a good aggregate structure which lead to increase mixture stiffness and ultimately the estimated fatigue performance.

A previous study (Roohi, Tashman et Bahia, 2012) has demonstrated that the binder may have affected the internal structure of asphalt mixtures for the same gradation due to the rheological properties. Based on that, we can postulate in this study that the difference in structures can be explained with the mixture's combined binder.

In the literature, the majority of mix designs and compaction consider a specific of density or air void content (i.e. 3,5 - 4,5% for the superpave mix design, AASHTO M 323-07, 2007) as a target for compaction and quantify the workability based on that metric alone. The basic

assumption is that density can be used as an indicator for the mixture performance. However, a previous study has demonstrated that materials with the same density may perform significantly different under service loading (Olard, 2012). Based on the contact mechanism analysis, Roohi, Teymourpour and Bahia, (2013) demonstrated that the transmission of load in the asphalt mixture is mainly determined by the interaction of aggregates and binder at the proximity zones of adjacent aggregates. Based on this concept, specific microstructural indices such as total aggregate proximity length in the aggregate skeleton (i.e. in two dimension section images of mixtures), could be a good indicator of mixture load bearing aggregate structure and performance. The aggregate structure indices show sensitivity to compaction such as compaction temperature, method, and mix design properties (Roohi, Teymourpour et Bahia, 2013).

Therefore, there is still a need for a more comprehensive understanding of the mechanics governing the compaction process to better understand the virgin aggregate and RAP aggregate combination referred here as aggregate mobility. The mechanisms resisting aggregate mobility control the formation of the aggregate skeleton, the main load bearing structure in asphalt mixtures. A deeper understanding of this process can be invaluable for the control and optimisation of the construction process and enhancement of the pavement performance.

As we presented in section 2.7.9, it is reviewed that the fatigue of asphalt mixtures containing RAP could be worse or better or equivalent to the control mix depending on the source of RAP and the type of the virgin binder used. But, as for our source, we concluded that the fatigue test results show that the evaluated RAP mixtures had similar fatigue performance except for the laboratory prepared with the 40% RAP which exhibited a higher fatigue performance than the control mixture. Therefore, again in some cases, an increase in RAP content can lead to increase in fatigue performance.

6.9 Prediction of the fatigue life according to the DGCB method

The results of fatigue tests obtained from the experimental program are presented in the previous sections. In order to be able to get the fatigue lines with rigour, it is needed to perform several tests which take more times for which some have significant durations (1 to 2 weeks).

The DGCB method was used to analyze the data obtained for the 24 fatigue tests employed in this study. The DGCB method presented in chapter 2 (§ 2.7.7), permits to predict the value of the fatigue life of a specimen from a limited number of cycling loads (300 000 cycles). That means it allows to stop the test after 300 000 cycles. Di Benedetto et al. (2004) showed that the DGCB proposed prediction method is relevant for the tested materials and testing conditions.

The method DGCB for calculating damage rate shows the presence of several biased effects during fatigue testing. Among these effects we identify thermal effects (heating or cooling), and the thixotropic or a phenomenon of local restructuring in the material. The nonlinear evolution of the damage is a unique characteristic of the material that must be taken into account when studying fatigue behaviour of asphalt. The experimental damage parameter which has to be corrected from the biases effects is given by:

$$D = 1 - \frac{\left|E_N^*\right|}{\left|E_0^*\right|} \tag{6.5}$$

Where:

$|E_0^*|$ is the initial stiffness (at the beginning of the test) and $|E_N^*|$ is the current cyclic stiffness.

For homogenous tension-compression tests, the end of the phase II which also marks the beginning of the phase III, represents the appearance and the spread of macro crack in the specimen. The criteria that lead to rigorously identify this transition between phase II and III

which corresponds to the value of $N_{fII/III}$ are clearly established in chapter 2. The critical damage at the transition point (D_{III}) is given by the following equation:

$$D_{III} = \frac{(|E_0^*| - |E_{III}^*|)}{|E_0^*|} \tag{6.6}$$

Where, $|E_0^*|$ is the modulus at the beginning of the test and $|E_{III}^*|$ is the modulus at the transition point between phase II and III. However, the calculation of the damage from the equation (6.6) for fatigue testing shows typically that the value of D_{III} changes according to the amplitude of the imposed deformation for the same material. In fact, by increasing the amplitude of deformation, the difference between the initial stiffness and the stiffness at the transition between phase II and III is not only related to the fatigue damage, but also related to the biasing effects. Figure 6.28 shows typical results obtained by Di Benedetto et al. (2004). Hence, Di Benedetto (2004) proposes the calculation of a corrected damage (D_{IIIc}) to differentiate between the loss of stiffness due to artefact effects to the loss associated with material damage due to fatigue.

6.9.1 Calculation of the corrected damage at the end of phase II: D_{IIIc}

With the DGCB methods, different intervals, representing number of cycles, are needed to be considered. In this study, the four considered intervals are: a) interval i=-1 from 30 000 to 60 000 cycles, b) interval i=0 from 40 000 to 80 000 cycles, c) interval i=1 from 50 000 to 150 000 cycles, and d) interval i=2 from 150 000 to 300 000. As these intervals have to be situated within phase II, it is not always possible to consider all the intervals when evaluating individual tests. The corrected damage is calculated from equation (6.7) using the damage analysis of ENTPE as presented in Di Benedetto et al. (2004) (Cf. Section 2.7.7).

$$D_{IIIc} = D_{III} - \frac{C_i \times (|E_0^*| - |E_{III}^*|)}{|E_0^*|} \tag{6.7}$$

The correction term, $\frac{C_i \times (|E_0^*| - |E_{III}^*|)}{|E_0^*|}$ introduces the modulus E_{00i}, which is the initial stiffness for the considered interval (i) in the calculation of the damage. This correction term represents the biased effects: heating and thixotropy.

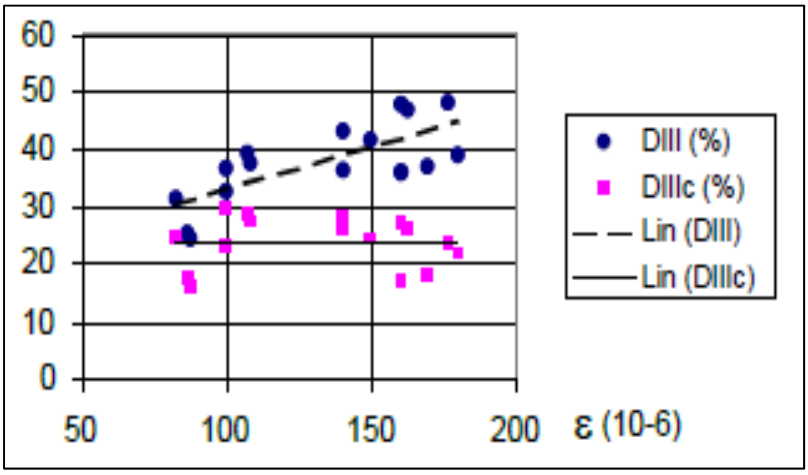

Figure 6.28 Damage values at the transition between phases II and phases III (beginning of macro-crack propagation) for Tension/compression strain control tests: D_{III} no correction; D_{IIIc} correction from artefact effects Di Benedetto et al. (2004)

In our analysis, the last interval of the four considered intervals is used to determine and plot the fixed damage curve as it will be shown after in the figures in § 6.9.2 which is close to the phase III to validate the concept of fixed damage as that proposed by Di Benedetto et al. (2004). The corrected and not corrected values of D_{III} for all our mixes are presented in Table 6.7.

Table 6.7 Damage values at the transition between phases II and phases III for the four recycled mixtures: D_{III} no correction; D_{IIIc} correction from artefact effects

%RAP	Air voids %	D_{III}%	D_{IIIc}%	D_{IIIc} mean (St. dev.)
0RAP-(P1-A2)-D150	4,0	52,9	25,5	
0RAP-(P1-A5)-D140	4,1	46,2	17,9	
0RAP-(P2-A4)-D130	4,5	40,0	17,6	
0RAP-(P1-A3)-D140	3,9	39,3	15,6	19,9
0RAP-(P3-A3)-D110	6,7	37,7	20,0	(2,8%)
0RAP-(P3-A5)-D105	6,8	40,2	21,5	
0RAP-(P4-A5)-D115	5,1	41,4	21,2	
0RAP-(P3-A4)-D115	6,6	40,3	20,0	
15RAP-(P2-A1)-D150	6,3	44,5	17,0	
15RAP-(P2-A2)-D120	6,7	43,8	15,9	18,7
15RAP-(P1-A3)-D115	5,8	42,3	23,4	(3,0%)
15RAP-(P2-A3)-D130	6,3	44,1	21,2	
15RAP-(P1-A2)-D140	6,7	36,9	16,1	
25RAP-(P4-A2)-D120	6,1	54,3	28,8	
25RAP-(P4-A4)-D140	5,6	44,4	28,7	23,6
25RAP-(P4-A5)-D130	5,8	40,8	16,1	(4,8%)
25RAP-(P3-A1)-D150	6,8	45,8	21,2	
25RAP-(P1-A2)-D110	6,2	48,3	23,1	
40RAP-(P1-A2)-D130	3,3	54,8	29,0	
40RAP-(P2-A3)-D140	3,3	51,4	27,9	
40RAP-(P2-A2)-D150	2,1	53,4	27,2	27,3
40RAP-(P1-A3)-D160	3,6	50,8	23,1	(2,0%)
40RAP-(P1-A4)-D170	2,7	56,8	28,3	
40RAP-(P1-A2)-D180	2,5	58,0	28,3	
		Mean value		
By considering the results of the mixes containing from 0 to 40% RAP		46,2	22,3	
By considering the results of the mixes containing from 0 to 25% RAP		43,5	20,6	
By considering the results of the mixes containing 40% RAP		54,2	27,3	

6.9.2 Level of damage leading to rupture (D_{III})

Figure 6.29 illustrates the relationship between the level of damage that leads to rupture (D_{III}) and the corrected strain imposed for all the specimens tested (group). The results show that D_{III} increases continuously with the imposed strain amplitude for all the mixes in group. This was also observed by Di Benedetto, et al. (2004), Touhara (2012) and Lamothe (2014). The increase in damage (D_{III}) with the amplitude of deformation is explained by the accentuation of the biasing effects (heating and thixotropy) during the endurance test. In order to properly define the relation between D_{III} and the strain level, results from a wide range of strains are needed. By taking into account the content of voids for each mix individually, the D_{III} correlated with the magnitude of deformation takes a different turn (Figure 6.30).

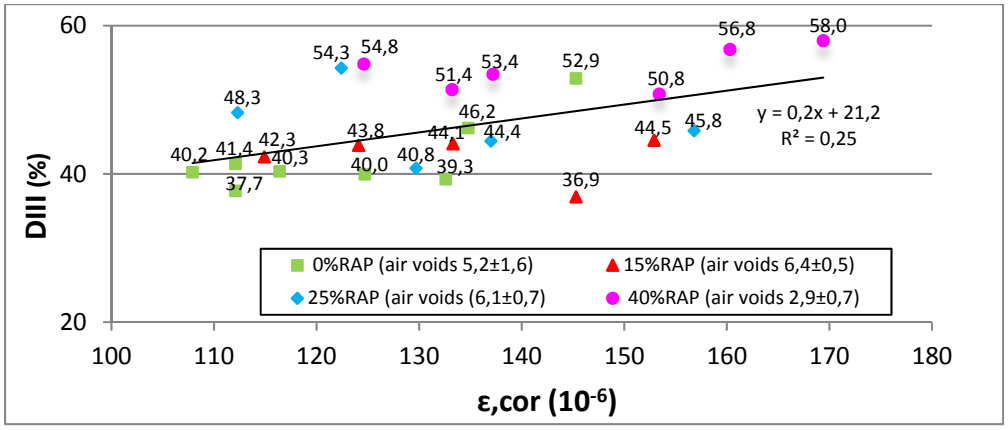

Figure 6.29 Level of damage leading to rupture (D_{III}) for all tested specimens (group), tested at +10°C and 10 Hz, depending on the corrected deformation amplitude

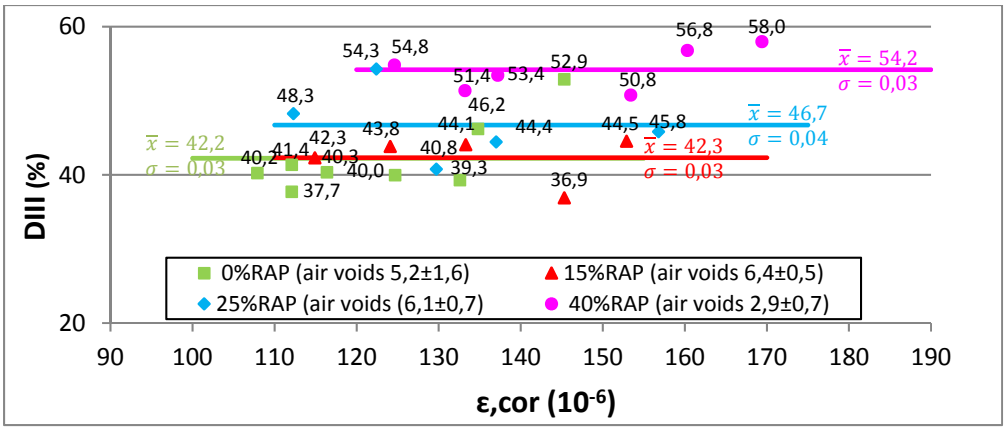

Figure 6.30 Level of damage leading to fracture the specimens group of each mix separately, tested at +10°C and 10 Hz, in function of the amplitude of corrected deformation and voids content

6.9.3 Evolution of the corrected damage leading to rupture (D_{IIIc})

By considering the artefact effects (heating and thixotropy), and by defining the corrected damage D_{IIIc}, it shows that the D_{IIIc} values appear to be independent of the applied strain amplitude (Figure 6.31). Hence, this finding suggests calculating D_{IIIc} as a failure criterion to evaluate the fatigue damage in the specimen.

As we can see in Figure 6.31 we didn't get a single value for D_{IIIc}, but we get the tendency and it is the same as proposed by Di Benedetto et al. (2004). The average value of D_{IIIc} is 22,3% with a standard deviation of 4,6%. The synthesis of the calculated damage values was shown previously in Table 6.7. However, we can note that this value really differs for 40% RAP mix. For the group of 40% RAP mix, we reached to D_{IIIc} equal to 27,3% and it is higher than the assumed value of D_{IIIc} (23%). But some authors found that the average values of D_{IIIc} ranging from 22,7 to 30,4% with a standard deviation of 1,4 to 6,2% depending on the type of asphalt mixture (Di Benedetto et al., 2004; Touhara, 2012). However, we also plotted the relationship between D_{IIIc} and ε_0 by considering data from each mix. Figure 6.32 also shows that the relationship between D_{IIIc} and ε_0 appears to be independent of the strain level when grouped according to the air voids content of the mix.

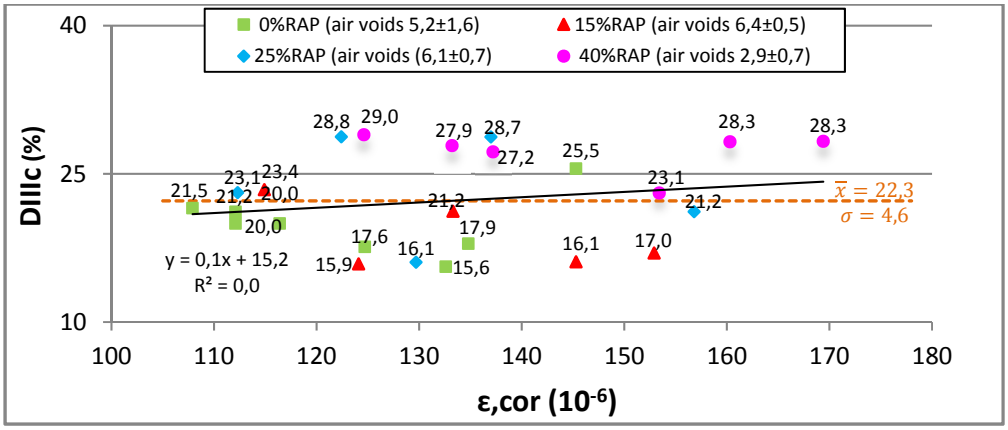

Figure 6.31 Evolution of damage leading to failure, corrected for artefact effects, depending on the corrected deformation amplitude for all the data at +10°C and 10Hz

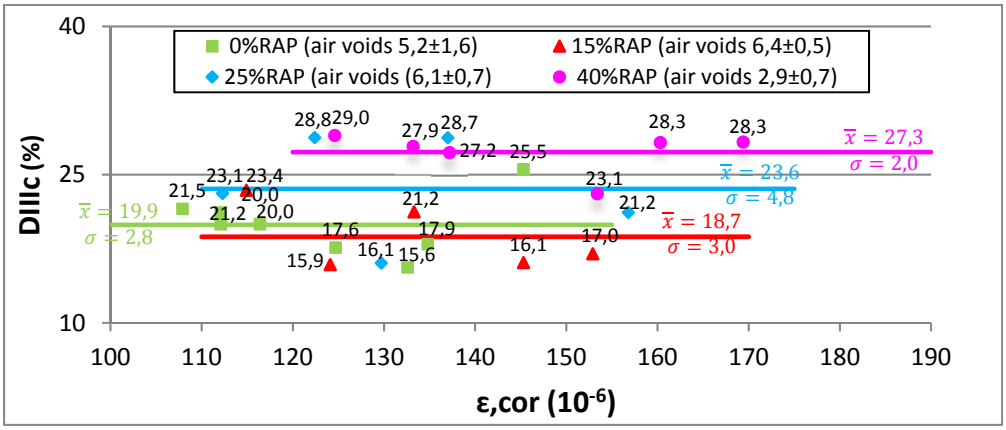

Figure 6.32 Evolution of damage leading to failure, corrected for artefact effects, depending on the magnitude of corrected deformation and voids content for each mix separately (group of the specimens of the same mix) at +10°C and 10Hz

6.9.4 Effect of air voids content on the critical damage (D_{IIIc})

Di Benedetto et al. (2004) suggested that the critical damage value (D_{IIIc}), mean 23%, is a threshold over which a macro-crack appears in the sample. Lamothe (2014) found that the D_{IIIc} value is a function of air void content in the mixture: as the air void content increases, the threshold decreases. The mix having a higher void content will have a reduced fatigue life. Voids are acting as defaults that promote crack propagation. Figure 6.33 shows the

relationship as established by Lamothe (2014). Figure 6.33a shows the present relationship for all the data points and the amplitude of deformation (ε_0) while Figure 6.33b shows trend lines for each mix identified in the analysis.

We found similar trends to those from Lamothe (2014) in the relationship between D_{IIIc} and air voids. It is generally shown that increasing air void will reduce fatigue and damage. The asphalt mixtures having a higher air void will withstand for shorter life. The short life indicates a lower critical internal damage, which corresponds to uniformly distributed micro-damage in the asphalt mixture and making the breaking point associated with the spread of macro-cracking in the asphalt mixture.

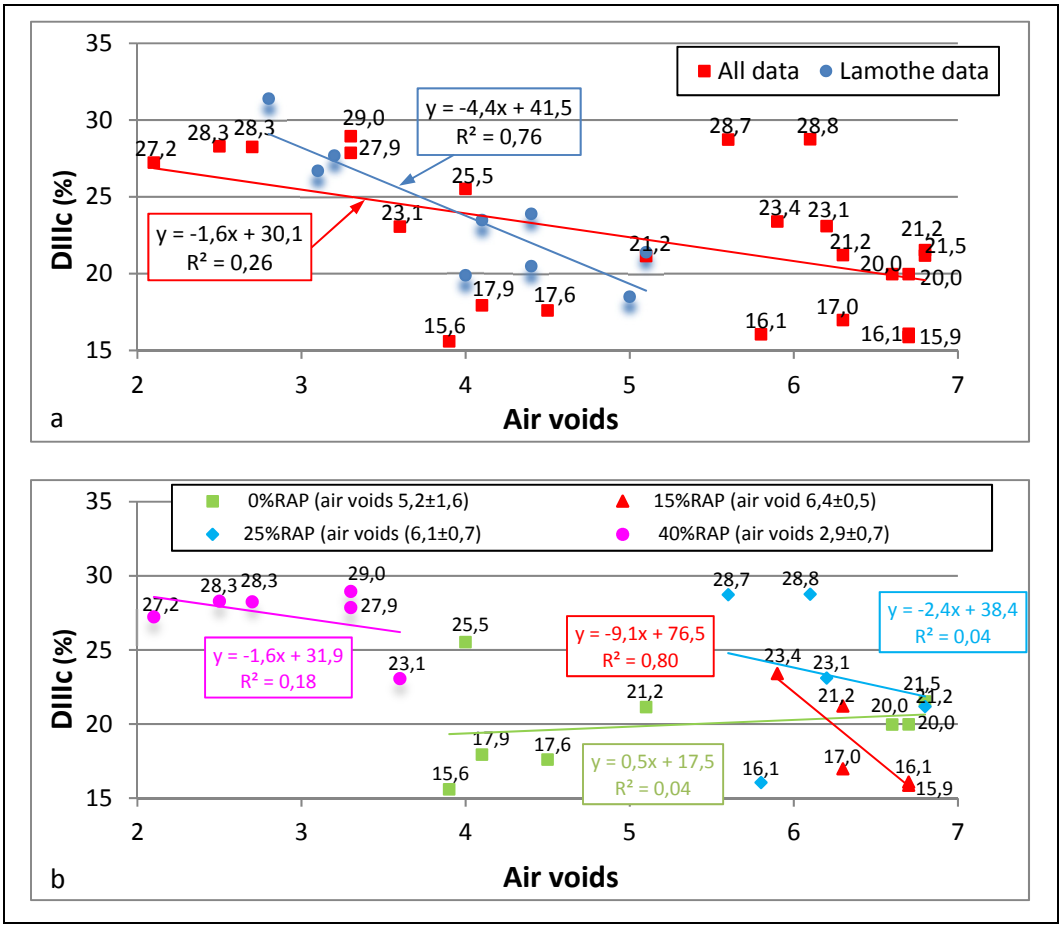

Figure 6.33 Evolution of damage leading to failure, corrected for artefact effects, depending on the air void content for all the data at +10°C and 10Hz

6.10 Predicting the number of cycles to failure when considering only the 300 000 first cycles ($N_{fII/III}^{DGCB}$)

When performing laboratory fatigue tests, there are several problems that can lead to the rejection of a test which imply a loss of time and sample. The most common problems are:

- Variation of temperature during the test due to an air conditioning system that is inappropriate;
- Bad alignment due to the less quality gluing process;
- Lack of homogeneity of test specimens;
- Errors in the measurement of the signals;
- Random stops of the hydraulic unit; etc.
- Based on that, the test should be repeated for the same imposed deformation. Since the time is important in the measuring of fatigue resistance of bituminous mixtures, the DGCB method presents a tool leading to increase effectiveness through the measurement of fatigue resistance of bituminous materials. Indeed, assuming a linear evolution of the loss of stiffness of the material at the defined intervals in Phase II, we can assume that there is a threshold value of the corrected damage that can extrapolates the expected fatigue life of the specimen with a limited number of cycles of loading. This approach is illustrated in Figure 6.34. By considering equation 6.8, we can evaluate the loss of stiffness during the interval "i" (Touhara, 2012):

$$N_{fII/III}^{DGCB} = \frac{|E_{00i}^*| - |E_{F00i}^*| + D_{IIIc}\,|E_0^*|}{-a_{T_{00i}}\,X\,|E_{00i}^*|} \tag{6.8}$$

The synthesis of the calculation of the $N_{fII/III}^{DGCB}$ for the four mixes at different imposed strain levels are shown in Appendix III in Tables-A from III-2 to III-5.

More information about the previous equation is provided in Touhara (2012).

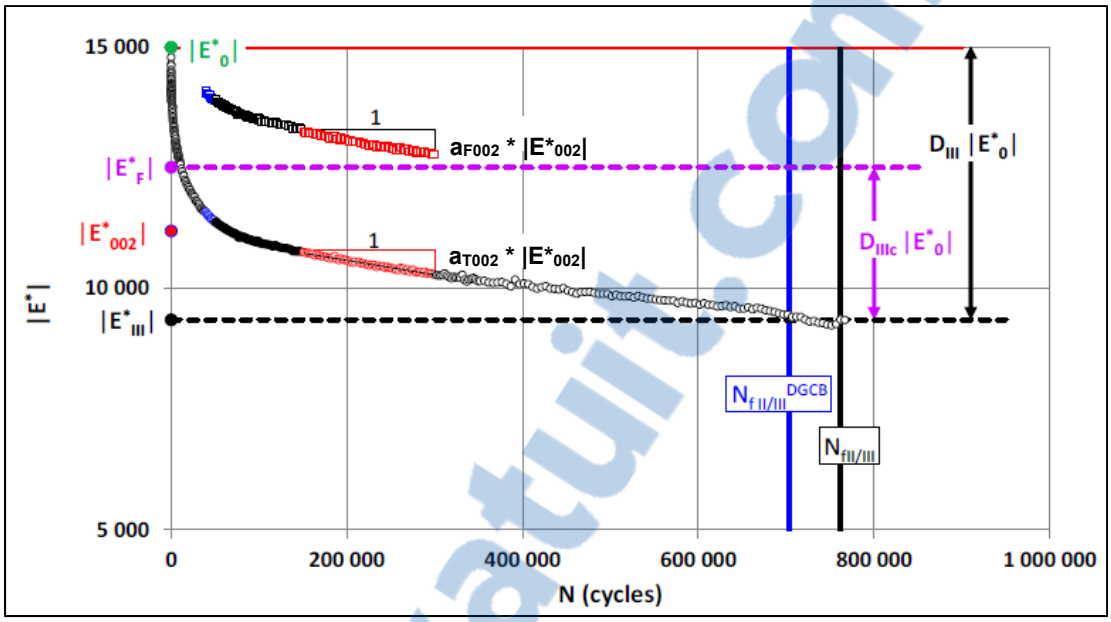

Figure 6.34 Prediction of the fatigue life according to the DGCB method
Taken from Touhara (2012)

As for the presented campaigns, 4 asphalt mixtures with and without RAP have been used, so we will first assume a unique value of D_{IIIc} (23%) for all the mixes as proposed by Di Benedetto et al. (2004), and after that, we will validate the results by calculating the standard deviation because it will show us how much variation or dispersion from the average is existing. Results are presented before in Figure 6.31. Since the value of the standard deviation is small (4,6%), it means that our results are comparable to what Di Benedetto et al. (2004) found and the error that could be found from our assumption with using a unique value of D_{IIIc} for all the recycled mixes is minor. However, we can see that the mean value of D_{IIIc} for the mixes of RAP percentages from 0% to 25% RAP is equal to 20,6%, and it is not so far from the first assumption (D_{IIIc} = 23%). It means that the damage process is influenced by the air void content in the mix and the high RAP may also have an effect on the D_{IIIc} value. To reduce the errors as possible we decide to use the specific D_{IIIc} value for each mix.

In order to validate this approach, all the results of fatigue are treated by considering the only first 300 000 cycles of loading. Referring to the DGCB method, the predicted values ($N_{fII/III}^{DGCB}$) are calculated from equation (6.8) with the values of corrected damage described above. The resulting values are compared with the corresponding actual values ($N_{fII/III}$). To do this, the measured stiffness has been corrected according to the method DGCB for all fatigue tests carried out in this program. The equation used in this analysis presented in Touhara (2012).

Figure 6.35a shows the relationship between the fatigue life determined experimentally using the failure criterion ($N_{fII/III}$) and the predicted fatigue life using the DGCB method ($N_{fII/III}^{DGCB}$).

Figure 6.35b presents the number of cycles at failure determined with the prediction method (N_{fpred}) as a function of the number of cycles at failure determined from tests with the N_f criterion.

As shown in Figure 6.35a, for the 0%RAP mix, the slope of regression line of $N_{fII/III}$ and $N_{fII/III}^{DGCB}$ is different (-6,9. and -4,7, respectively) and the value of R^2 of $N_{fII/III}$ and $N_{fII/III}^{DGCB}$ are 0,86 and 0,69, respectively.

For the 15% RAP mix, Figure 6.35b shows the value of R^2 and the slope of the regression line with $N_{fII/III}$ and $N_{fII/III}^{DGCB}$ where the slope values for the $N_{fII/III}$ and $N_{fII/III}^{DGCB}$ are -9,0 and -5,7 respectively which shows that the predicted and the experimental results are close to each other just a little bit. In the same manner, for the 25% RAP mix, in Figure 6.35c, the value of R^2 and the slope of the regression line with $N_{fII/III}$ and $N_{fII/III}^{DGCB}$ are -7,2 and -6,9, respectively which yields good predicted fatigue life using the DGCB method in comparison with the measured fatigue life ($N_{fII/III}$).

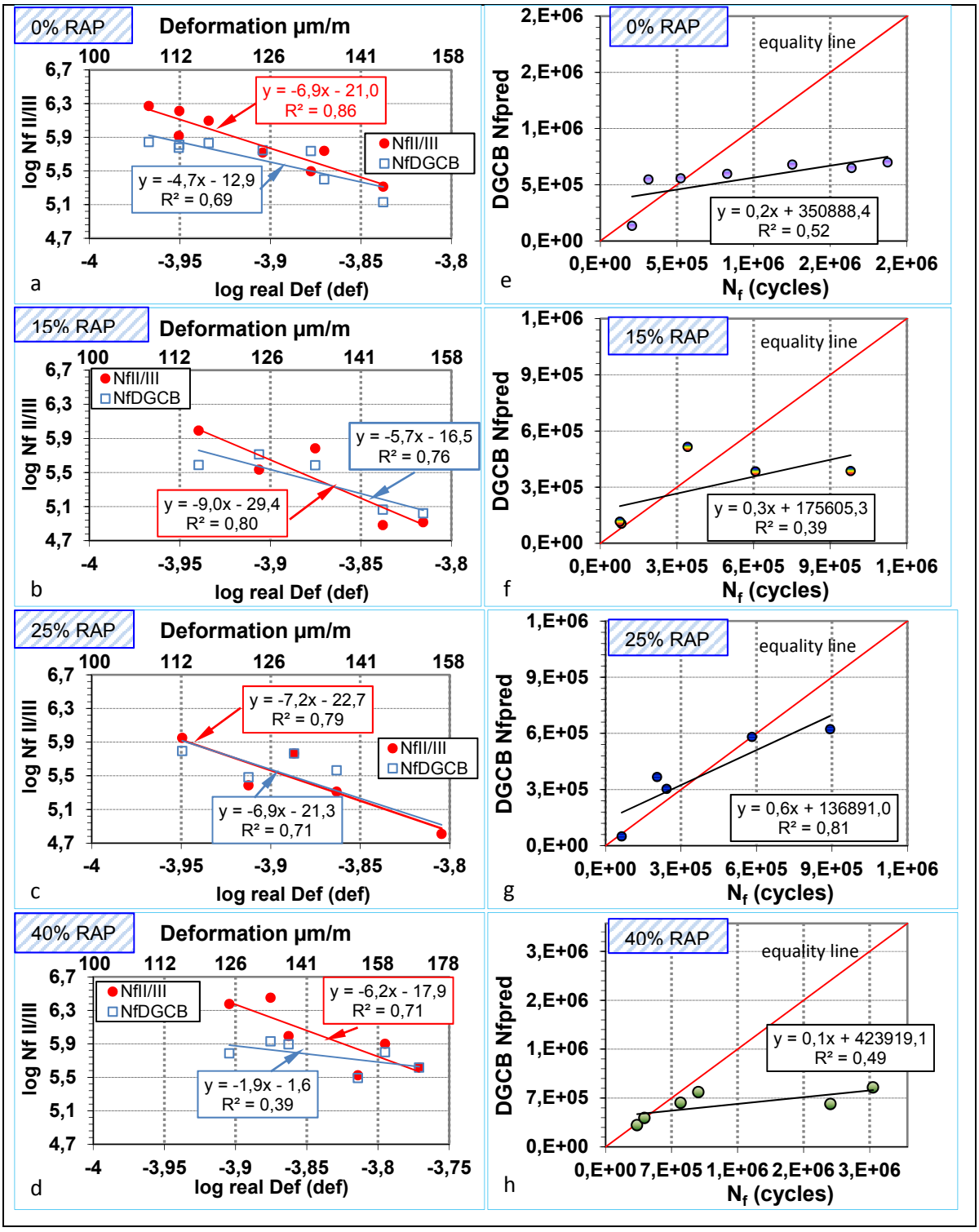

Figure 6.35 The N_f for the 4 recycled mixtures: (a to d) Wöhler curves determined using the failure criterion ($N_{fII/III}$) and the DGCB N_{fpred}, (e to h) Correlation between the DGCB N_{fpred} and the $N_{fII/III}$

6.11 Summary of the results

Several difficulties are present for the achievement of the fatigue tests, the most important is the time needed to characterize a bituminous mixture, and in this sense, the DGCB method was used to predict the fatigue life with 300 000 cycles only (8 hours). Comparison of the results gives fairly low regarding errors, which encourages applying this method on other RAP mixes using different sources of RAP to have a more general conclusion.

From the DGCB method, the measured damage can be corrected in order to obtain the actual damage of the material at the transition between phase II and III or at the rupture at phase III. We can obtained the corrected damage at the transition between phase II and III (D_{IIIc}), which is adjusted to takes into account skewing effects occurring mainly (but not only) during phase I. The corrected damage (D_{IIIc}) was obtained for each mixture tested. Our results show that D_{IIIc} varies from mix to mix. D_{IIIc} is equal to 19,9% for 0% RAP mixture and to 18,3% for 15% RAP mixture and to 23,6% for 25% RAP mixture and to 27,3 for 40% RAP mixture. The results show that D_{IIIc} appears independent of the strain amplitude for tension/compression test and could be used successfully with HMA mixtures containing up to 40% RAP. However this result needs to be checked and validated.

Damage in asphalt mixture refers to loss in strength. The results show that the damage could increase with the decreased air voids and reduce fatigue life because, in general, the material exhibited high levels of cracking before the appearance of micro-cracks will enhance its resistance to damage. We got the same trend to D_{IIIc} obtained by Lamothe in the relationships D_{IIIc} – air voids and in D_{IIIc} and ε. However, only two data points did not show exactly these results and it is probably due to one of the following reasons;

1) The utilization of RAP in a mix can cause an increase in the variability of the mix;
2) The non-homogeneity of the material itself;
3) There are some data points in the results that may have small variation of the modulus and can affect their D_{IIIc} value and therefore it will affect their predictive fatigue life;
4) The difficulty of performing the fatigue test.

CHAPTER 7

PROPOSED MODIFICATIONS TO THE BASIC FATIGUE MODEL TO TAKE INTO ACCOUNT THE EFFECT OF RAP CONTENT ON THE FATIGUE CRACKING RESISTANCE OF HMA MIXTURES

7.1 Introduction

Fatigue tests require time, and are expensive to perform. For this reason, a model that could be used to estimate fatigue resistance of asphalt mixtures containing RAP is needed. Such a model could eliminate or at least limit the need for more extensive fatigue testing in the pavement design process.

Fatigue consideration in the structural thickness design of HMA pavements has traditionally been based on the relationship between the tensile strain and the number of loads to a predetermined failure level as expressed by the basic fatigue model introduced in § 6.7. Because of the phenomenological nature of this relationship, some have proposed adjustments to this relation in order to obtain a better fit with observed behaviour differences. We can find that most of the fatigue models take the relationship presented in equation (6.4) and repeat it with different forms in various pavement design methods (Thompson et Carpenter, 2006). The most notable adjustment being the addition of a modulus term as expressed in Perraton et al. (2011):

$$N_f = k_{1,\theta_{test}}(\varepsilon_t)^{-k_2}\left[\frac{\left|E^*_{\theta_i}\right|}{\left|E^*_{\theta_{test}}\right|}\right]^{-k_3} \tag{7.1}$$

With $k_{1,\theta_{test}}$ corresponding to the fatigue life of the mix for the applied deformation equal to 1 µm/m at the fatigue test temperature (θ_{test})(10°C). $\left|E^*_{\theta_i}\right|$ and $\left|E^*_{\theta_{test}}\right|$ correspond respectively to the norm of the complex modulus at the considered temperature (θ_i) and at the test temperature. Generally, tests are done at (10°C). The coefficient k_3 represents the slope of

the relationship $k_{1,\theta_{test}}$ vs. $log\left|E^*_{\theta_i}\right|$ and is introduced to express temperature effect on fatigue behaviour.

As presented in section 6.5, air voids content vary between our tested samples and we referred to the correction of the fatigue tests using $\varepsilon_{t,cor}$. Once again we remind the reader that the corrected value is used in our analysis of the imposed deformation based on the value of average air void of 5,1% ($\varepsilon_t = \varepsilon_{t,cor}$).

The most recent work to develop a nationally calibrated fatigue model for the NCHRP 1-37A in the Pavement ME design software is based on the assumption of constants $k_{1,\theta_{test}}$, k_2, k_3 values for all HMA materials. Basically $k_{1,\theta_{test}}$ and k_2 are different for each mix. But we believe that with adding RAP at small concentrations, the parameters $k_{1,\theta_{test}}$ and k_2 in the basic fatigue model of the virgin mixture can be managed in accordance to the concentration of RAP to predict fatigue behaviour. This is because the binder and aggregate in the mixture are, for the most part, those of virgin mixes. In Canada, typical mix designs are made with less than 25% RAP. Actually, if we add small amounts of RAP, we presume that we can predict precisely the fatigue life of RAP mixtures by considering $k_{1,\theta_{test}}$ and/or k_2 values of the virgin mix based on the RAP content. However, we know that the RAP percentages used in Canada can be increased, so we need to see if we can have a model that works for low and high percentages of RAP. In this study, we start to manage our modelling in accordance to the RAP concentrations by limiting the RAP percentages from 0 to 40%, which are the percentages that were covered in our experimental program. We pointed out in section 6.7.1.1 that some relationships between fatigue parameters and RAP concentrations can be found when RAPs are used in HMA mixture.

To do this, we determine first $k_{1,\theta_{test}}$ and/or k_2 values for the virgin mixture and we explore ways to adapt the basic model to take into account the RAP content in the mix to predict their fatigue life. Then, we start our adaptation on mixes incorporating RAP up to 40%. In the next step, we check the model based on the RAP concentration up to 25%. As the bitumen part

significantly affect fatigue behaviour of HMA mixture, we assume that a small amount of RAP would not drastically change the fatigue behaviour of the mix. By modifying the basic model in accordance to the RAP content in the mix, we figure that it could be realistic to get an appropriate fatigue prediction of the mix.

Basically, we focus on improving the model in two different ways. The first method is by trying to make a modification based on phenomenological approach. That means we are trying to get relationships between the basic fatigue parameters (k_1 and k_2) against the concentration of RAPs. The second method is based on the statistical approach by using all the data that we have to fix universal values of the fatigue parameters (k_1 and k_2) and implement some parameters as shift factors for k_1 to take into account the effect of the RAP addition.

We validated the quality of the proposed predicted fatigue models in three different strategies. First, the predicted and the measured values at the material level are compared. The second way quantifies our proposed models in terms of predicting the fatigue life at the structure level by comparing the prediction of fatigue life based on the new models against the prediction of fatigue life of the basic model. Finally, for the third method, we present a comparison of fatigue models for predicting fatigue lives of HMA mixtures at material and structure levels at a specifically selected strain value. We check the impact of the addition of RAP by comparing the fatigue life of mixes made with 15, 25, and 40 percent RAP relative to the reference mix (0 percent RAP) at the two levels using the different models developed for this study.

7.2 Statistical approach: goodness-of-fit

The goodness-of-fit statistics for all predictions in arithmetic scale were performed using statistical parameters such as the coefficient of determination (R^2) and the standard error of predicted values (S_e) divided by the standard deviation of measured values (S_y). The R square value is a measure of correlation between the predicted and the measured values and

therefore, determines the accuracy of the fitting model (higher R^2 equal to higher accuracy). Also, the S_e/S_y indicates the relative improvement in accuracy and thus a smaller value indicate better accuracy. Having the S_e/S_y as a base, R^2 value can be calculated for comparative purposes using the following equation:

$$R = 1 - \left(\frac{S_e}{S_y}\right)^2 \tag{7.2}$$

To be consistent throughout the analysis, a subjective criterion was established to appropriately use goodness-of-fit parameters in modelling as shown in Table 7.1. All the comparisons and analyses were performed following this criterion.

Table 7.1 Subjective criterion for goodness-of-fit statistical parameters for modelling
Taken from Abojaradeh (2003)

Rating	**Goodness-of-fit Parameters**	
	R^2	S_e/S_y
Excellent	> 0,89	< 0,35
Good	Between 0,70 to 0,89	Between 0,36 to 0,55
Fair	Between 0,40 to 0,69	Between 0,56 to 0,75
Poor	Between 0,20 to 0,39	Between 0,76 to 0,90
Very poor	Lower than 0,19	Between 0,9 to 1,00

7.3 Modification of the basic fatigue model based on phenomenological approach

We noted in section 6.7.1 that the basic model of fatigue life is based on a linear relationship between log N_f and log ε_0, where k_1 (intercept) and k_2 (slope) are used to define the line in the plan. It is well known that road agency often manages fatigue model of HMA mixture by assuming a relatively constant slope. For example, the French Pavement Design Manual

(Setra-LCPC, 1994) refers to a constant slope, k_2, fixed at a value of 5,0 for the Wöhler curve for all HMA mixes. Also, the pavement ME design method assumed slopes k_2 of fatigue lines to be constant. So we can say that it is generally assumed, in the literature, that the slopes of fatigue lines are constant (NCHRP- National Cooperative Highway Research Program, 2004; Setra-LCPC, 1994).

To reach our goal to modify the model to estimate fatigue life of mixes containing RAP, it is assumed, in first approximation, that the effect of adding RAP will just translate the fatigue line without affecting the slope. In other words, the incorporation of RAP into the virgin mixture will simply affect the intercept of the fatigue line obtained from the virgin mix itself. It means that the slope of the fatigue lines established from the virgin mix is kept constant for mixes containing RAP.

By assuming a linear relationship between intercepts values $k_1^{\%RAP}$ obtained for mixes containing RAP as expressed in logarithmic scale and the RAP content. The basic fatigue model can be rewritten as shown in equation 7.3. The relative details of equation 7.3 are given in Annex IV.

$$N_f = k_{1,\theta_{test}}^0 \times (\varepsilon_t)^{-k_2^0} \times SF \tag{7.3}$$

Where:

SF is the y-axis shift factor which value depends on the RAP percentage and is equal to $SF = 10^{-k_4 \times \%RAP}$;

k_4 is the slope of the relationship between $logk_1^{\%RAP} and\ \%RAP$.

In fact, there exist two values of k_4: $k_4^{0/25}$ is used for up to 25% RAP, and $k_4^{0/40}$ is used for mixes with up to 40% RAP.

In equation (7.3), the term $(10^{-k_4 \times \%RAP})$ is a shift factor applied on the intercept of fatigue line associated to the virgin mix $(k^0_{1,\theta test})$.

k_4 values (slope of $log\ k_1$ vs %RAP) were defined for the two main failure criteria as shown in Figure 7.1 and reported in Table 7.2. We wish to remind that the modelling is first done from 0% to 40% RAP $(k_4^{0/40})$ and the results from 0% to 25% were verified $(k_4^{0/25})$.

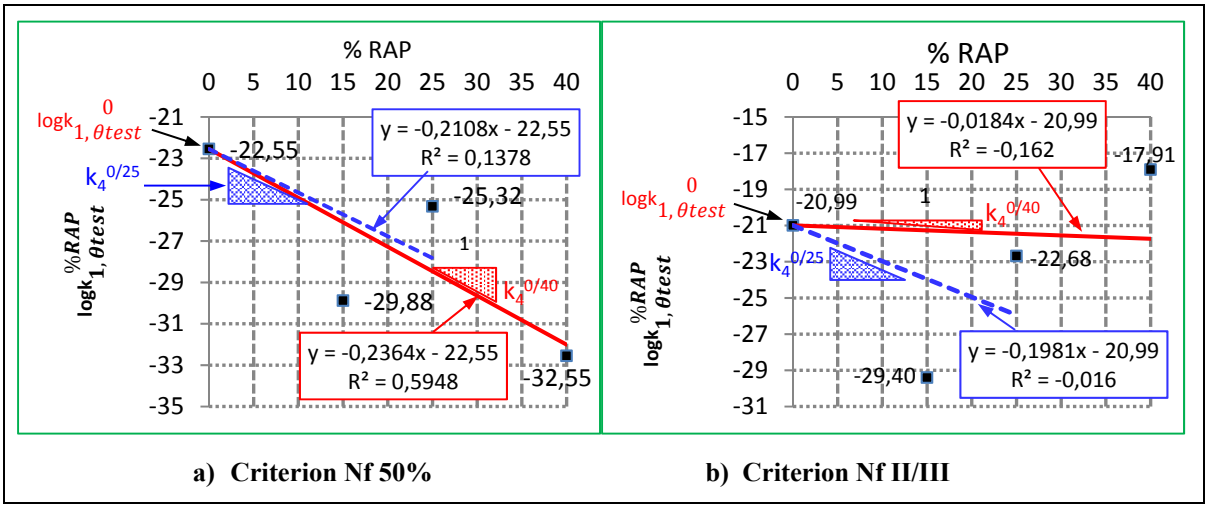

Figure 7.1 Relationship between $logk^{\%RAP}_{1,\theta test}$ and %RAP for the two studied criteria
dotted line: $k_4^{0/25}$ extrapolated from data for 0 to 25% RAP
dashed line: $k_4^{0/40}$ extrapolated form all data (0 to 40% RAP)

As shown in Figure 7.1, we have two lines on each graph. The red line (continuous) represents the relationship between k_1 and %RAP using the entire RAP percentages used in this study (from 0 to 40%), and the blue line (dashed) uses only the percentages from 0% to 25% RAP. For $N_{f50\%}$ criteria (Figure 7.1a), the R^2 are fair for the relationship mixes made with RAP percentages up to 40% and poor for the one described mixes made with RAP percentages up to 25%. For $N_{fII/III}$ criteria (Figure 7.1b), it is not a good relationship for neither considerations.

Table 7.2 Fatigue parameters of the general fatigue model established from $N_{f50\%}$ and $N_{fII/III}$ using the corrected fatigue test results for a specific air void of 5,1%

Mix	Failure criterion / Coefficient	$N_{f50\%}$	$N_{fII/III}$
Virgin mix	$k^0_{1,\theta_{test}}$ (Table 7.5)	2,8E-23	1,0E-21
	k^0_2 (Table 7.5)	7,3	6,9
RAP mixes	$k_4^{0/40}$(Figure 8.1)	0,2364	0,0184
	$k_4^{0/25}$ (Figure 8.1)	0,2108	0,1981
	$A^{0/40}$	0,00850	0,00095
	$A^{0/25}$	0,00713	0,00711

We assumed a linear relationship between $log\ k_1$ and %RAP because we are trying to correct k_1 by adding a shift factor (SF) in log based on the data. SF, in log, is considered a linear relationship. This is can be done exactly in the same way as it has been done for the introduction of the stiffness ratio (SF) to manage the temperature effect of fatigue life in the basic fatigue model. SF means that k_1 is moving in the y-direction with keeping the slope constant. Moreover, it is a relatively easy way to get a pretty accurate representation of a best fit line. We tried fitting curves with polynomial terms in linear regression but the above procedure did not work.

The next step is to find corresponding value of k_4 values from this relationship. This is easy to find since we already know what k_4 is. Basically we have two values of k_4 for each criterion. First, k_4 represents the slope of the curve $logk_1$ vs %RAP for the results from 0 to 40% RAP. Second, k_4 represents the slope of the curve $logk_1$ vs %RAP for the results from 0 to 25% RAP. Thus, k_4 has in total 4 values since we have two criteria. The parameters (k_1^0, k_2^0) were determined from the analysis of fatigue tests on the control mixtures, where k_4 values were obtained from the combined analysis of fatigue tests on all the recycled mixtures. Then, N_f values were obtained using equation 7.3 as we will describe in the section

below. It is important to note that in all the existing models for the calculation of fatigue life described in this chapter, we used the same strain level measured by the fatigue tests and as a reminder, we used the real and the corrected values for air voids.

7.3.1 Evaluation of the Accuracy of the newly developed model by the phenomenological approach

When referring to the fatigue parameters $k^0_{1,\theta test}$ and k^0_2 of the virgin mix, N_f-values calculated for different RAP contents in accordance to equation (7.3), in accordance to data in Table 7.2, are compared to the measured N_f-values as shown in Figure 7.2.

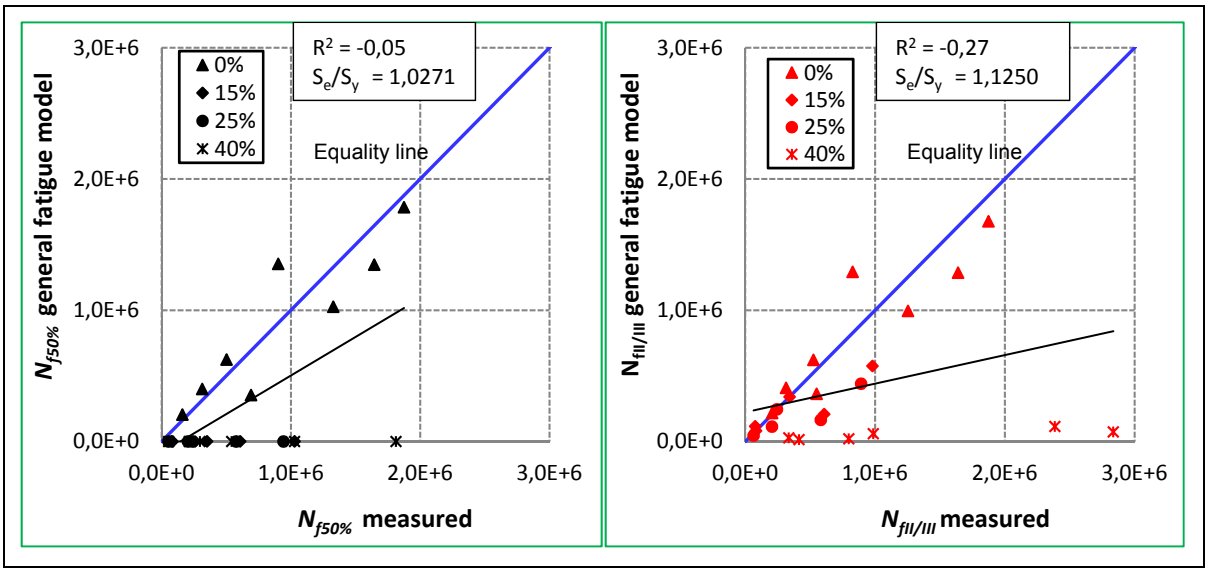

Figure 7.2 Predicted N_f in accordance with equation 7.3 versus observed N_f in accordance to the two criterion $N_{f50\%}$ and $N_{fII/III}$ using the parameters of Table 7.2 as defined in § 7.3

The predicted N_f-values obtained from § 7.3 are not acceptable based on the statistical regression because it shows very poor goodness of fit ($R^2 = 0$). We also see that most of the calculated N_f values are very far from the equality line. Most of those results didn't fell in the range of the fatigue testing measurements. It seems that the assumption of constant slopes for the fatigue lines is not appropriate.

Obviously, by plotting the relationship between $k_2^{\%RAP}$ versus %RAP using the two N_f criterion ($N_{f50\%}$ and $N_{fII/III}$) as shown in Figure 7.3, we can see that the slope can no longer be assumed constant when RAP is incorporated in a HMA mix. Based on this observation, $k_{1,\theta test}^0$ is not the only fatigue parameter that requires correction, but the slope k_2^0 does need correction to take into account the inclusion of RAP. We propose to correct the slope of the Wöhler curves ($\log N_f - \log \varepsilon_t$) of the virgin mix ($k_2^0$) in the fatigue model (equation 7.3) by considering a linear relationship between $k_2^{\%RAP}$ versus %RAP. We can write:

$$k_2^{RAP} = (1 + A \times \%RAP)k_2^0 \tag{7.4}$$

$$k_2^{RAP} = (A \times k_2^0) \times \%RAP + k_2^0 \tag{7.5}$$

$$y = ax + b \tag{7.6}$$

Based on that, we can show that:

$A = \frac{a}{k_2^0}$ with: a: The slope of the assumed linear relationship between $k_2^{\%RAP}$ and %RAP as shown in Figure 7.3. There exists $A^{0/25}$ value that corresponds to $a = a^{0/25}$ and $A^{0/40}$ value that corresponds to $a = a^{0/40}$.

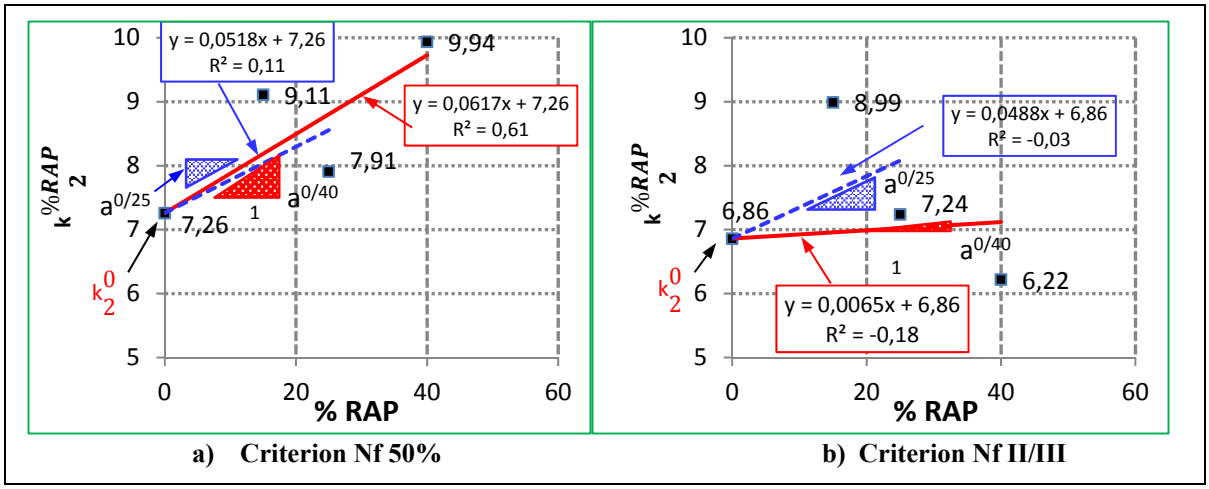

Figure 7.3 Relationship between $k_2^{\%RAP}$ and %RAP for the two studied criteria dotted line:
dotted line: $k_4^{0/25}$ extrapolated form data for 0 to 25% RAP
dashed line: $k_4^{0/40}$ extrapolated form all data (0 to 40% RAP)

Since the beginning, we focused on providing the results on the RAP percentages from 0 to 40% ($A^{0/40}$) and from 0 to 25% ($A^{0/25}$). The fatigue parameters $k^0_{1,\theta_{test}}$, k^0_2, k_4, and A values are reported in Table 7.2. For $N_{f50\%}$ criteria, Figure 7.3 shows that the R^2 of the linear relationship between $k_2^{\%RAP}$ and %RAP for all data (0 to 40% RAP) are fair and poor when we refer to 0 to 25% data. Even for $N_{fII/III}$ criterion this relationship shows a very poor correlation. Even if we do not have a good relationship in both cases, it was decided to use the models anyway because we need those models and also because in the end the most important things is to see what is going on in the prediction of fatigue life using the new models.

Therefore, we modified the equation 7.3 to take into account the influence of RAP content on the slope. The new model named general fatigue model is as follows:

$$N_f = k^0_{1,\theta_{test}} \times (\varepsilon_t)^{-(1+A\times\%RAP)k^0_2} \times SF \tag{7.7}$$

Where: $SF = 10^{-k_4\times\%RAP}$

For the results with up to 40% RAP, the parameters $A^{0/40}$and $k_4^{0/40}$ are used in equation 7.7. Similarly, the parameters $A^{0/25}$ and $k_4^{0/25}$ are used in equation 7.7 when dealing with the results with up to 25% RAP.

The predicted values of N_f based on equation 7.7 are compared to the measured values as shown in Figure 7.4. Fatigue parameters $k^0_{1,\theta_{test}}$, k^0_2, k_4 and A, presented in Table 7.2, were used in the substitution in equation 7.7 to calculate fatigue life of RAP mixes. Details are given in Appendix IV.

As shown from the results, this method enables us to estimate $N_f^{0/40}$ in the range of testing measurements comparable to the previous consideration at which the slope is kept constant. Basically, if we consider all the results, fatigue lives predicted with the general fatigue model

are still so far from the measured fatigue lives using the two criteria. The general fatigue model shows a fair goodness-of-fit statistics (R^2= 0,52) using the classical criteria, and provide a poor prediction of $N_f^{0/40}$ using the criteria of the end of phase II (R^2= 0,26). It means that our model doesn't work well for 0 to 40 percent of RAP. Therefore, in the next step, we focused on mixtures containing up to 25% RAP. The values of the parameters: $k_4^{0/25}$ and $A^{0/25}$ are then used in equation 7.7 to determine the predicted values and compared to the measured values as reported in Figure 7.5 (details for the results are given in Appendix IV).

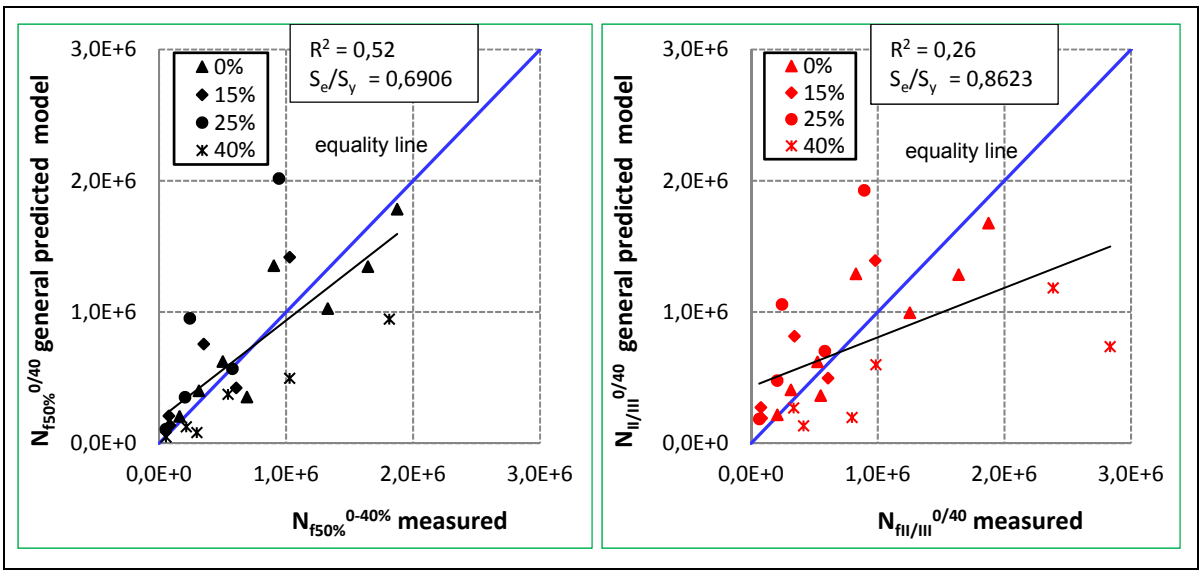

Figure 7.4 Predicted versus observed N_f using the two criterion $N_{f50\%}$ and $N_{fII/III}$ using the testing data up to 40% with the value of the parameter $A^{0/40}$ (Table 7.2) fixed from the $k_2^{\%RAP} - \%RAP$ relationship ($k_2^{0/40}$ versus %RAP)

As expected, the general fatigue model gives much better results by using k_1^0 and k_2^0 defined for the virgin mix to predict fatigue life of the mixes made with up to 25% RAP. Figure 7.5 can provide better accuracy (R^2 = 0,85). These results suggest that the general fatigue model can provide a good prediction of N_f for the two criteria using the two proposed values of $k_4^{0/25}$ and $A^{0/25}$.

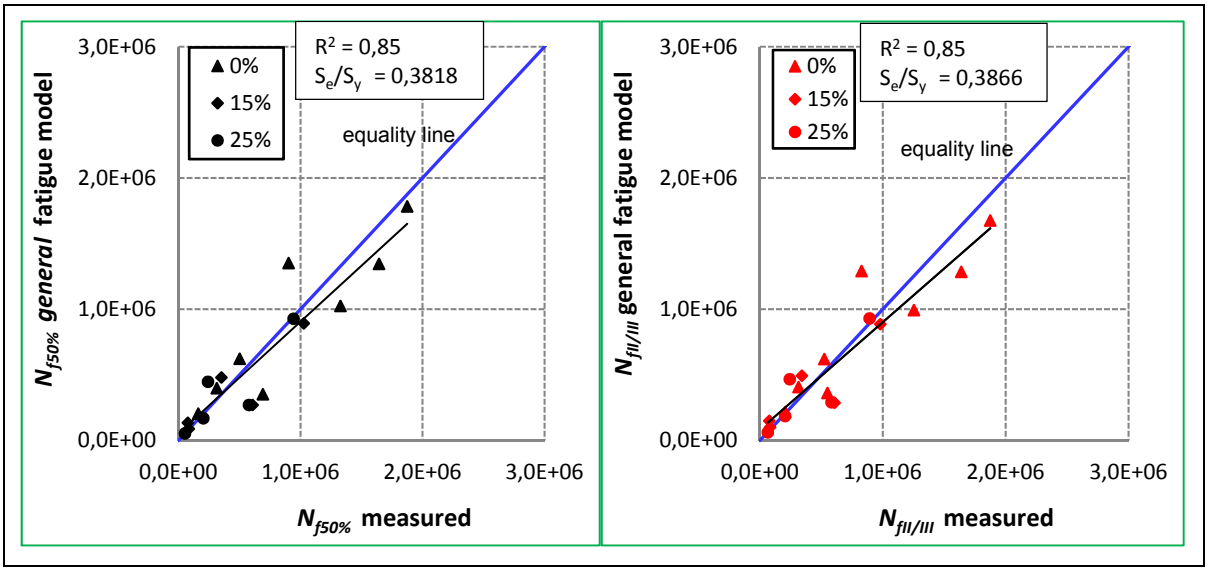

Figure 7.5 Predicted versus observed N_f using the two criterion $N_{f50\%}$ and $N_{fII/III}$ using the testing data up to 25% with the value of the parameter $A^{0/25}$ (Table 7.2) fixed from the $k_2^{\%RAP} - \%RAP$ relationship ($k_2^{0/25}$ versus RAP %)

7.3.2 Determination of the *A* parameter value acting in the slope by the optimization process

In this section, we used another innovative method to define the value of the A parameter proposed in the form 7.7. It is different from the first method discussed above in section 7.3.1 that determined the value of A from the equation $A = \frac{a}{k_2^0}$. It is based on the least square method. To do this, we first compare the predicted and the measured N_f values then the model will minimize the sum of the squared errors of prediction from measured data used. The fatigue parameters k_1^0 and k_2^0 were kept constant for the virgin mixture. Basically, we used the solver in MS Excel for the only unknown parameter 'A^i' with the least square method for each mix independently. In this case, the A value has now a specific value for each RAP mix tested (15, 25 and 40%). In other words, three different values of A are determined for the RAP mixes, as summarize in Table 7.3 (i = 15, 25, or 40%).

Table 7.3 Summary of A values based on an optimum process used to minimize the error between the predicted and measured fatigue life values ($k_4 = k_4^{0/40}$)

Parameter / Criteria	$N_{f50\%}^{0/40}$	$N_{fII/III}^{0/40}$
$k_4^{0/40}$	0,2364	0,0184
A^{15} (considered data for 15% RAP mix which means the 5 fatigue tests)	0,00815	0,00052
A^{25} (considered data for 25% RAP mix which means the 5 fatigue tests)	0,00804	0,00045
A^{40} (considered data for 40% RAP min which means the 6 fatigue tests)	0,00875	0,00130
***Average* $A^{0/40}$**	0,00831	0,00075

The 'A^i' values were determined for all the three mixes individually, and then the arithmetic mean value of A is used to calculate the predicted value of N_f. This can represent the effect of the value of 'A' on our results. We note that the A and k_4 values change with the failure criterion.

The $A^{0/40}$ value (Table 7.3) is used to calculate the predictive value of N_f using equation 7.7, the general fatigue model, for all tested mixtures. The results obtained are shown in Figure 7.6 and all the calculations results are summarized in Appendix IV.

The R^2 values for the combined mixes are 0,55 and 0,14 using the $N_{f50\%}$ and $N_{fII/III}$ criterion, respectively. Thus, the general fatigue model is 'fair' for the $N_{f50\%}$ criterion and 'poor' for the $N_{fII/III}$ criterion. It means that the general fatigue model is not working properly again. These results are very close to what we have observed previously in simulation by fixing the value of the constant 'A' from the relationship $k_2^{\%RAP}$ versus %RAP. We can also note that all N_f values predicted by the general fatigue model for 40% RAP mixtures are always underestimated in comparison to the real fatigue life data. Thus, we decided to evaluate the scatter of the results around the equality line if we try to apply the model for the results without considering the test sets data for 40% RAP mixture. To do it again, we used $k_4^{0/25}$ and redo the optimization process to find out the optimized values of the parameter 'A' for the 15 (A^{15}) and 25 (A^{25}) RAP mixes as shown in Table 7.4.

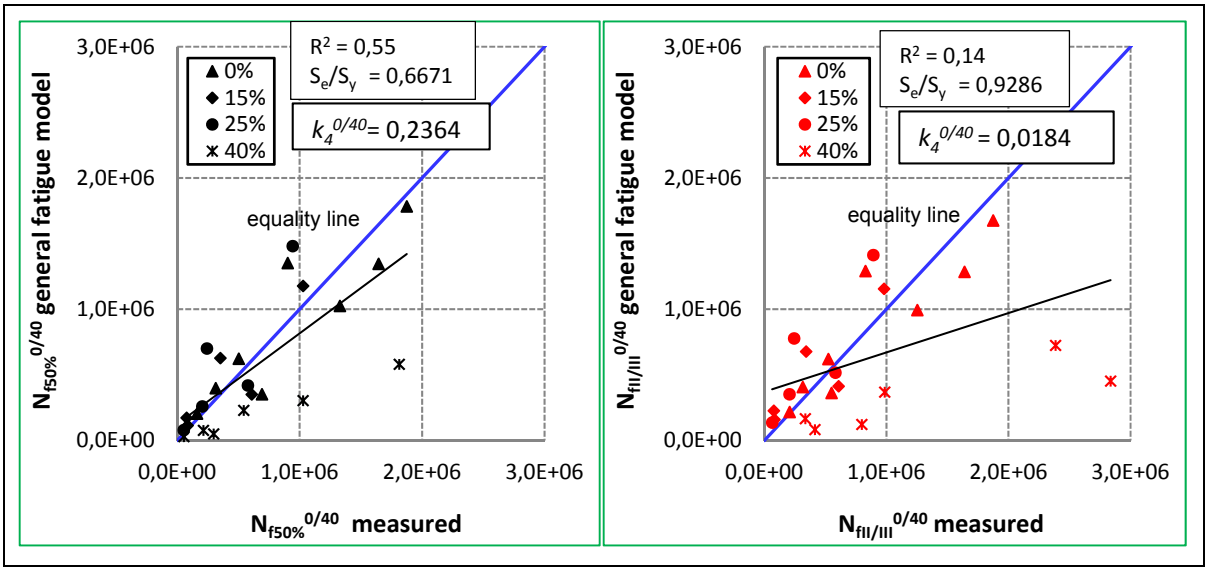

Figure 7.6 Predicted versus measured N_f using testing data by assuming variable slopes of the fatigue lines by considering *A* as the average of the three results obtained for each mix (15, 25, 40% of RAP) with both failure criteria

Table 7.4 Summary of *A* values based on an optimum process used to minimize the error between the predicted and measured fatigue life values ($k_4 = k_4^{0/25}$)

Parameter \ Criteria	$N_{f50\%}^{0/25}$	$N_{fII/III}^{0/25}$
$k_4^{0/25}$	0,2108	0,1985
A^{15} **(considered data for 15% RAP mix which means the 5 tests)**	0,00725	0,00719
A^{25} **(considered data for 25% RAP mix which means the 5 tests)**	0,00714	0,00709
Average $A^{0/25}$	0,00720	0,00714

The values of the parameters $k_4^{0/25}$ and $A^{0/25,average\ value}$ shown in Table 7.4 were used in the equation 7.7 while The N_f predicted values are compared with N_f (measurements) and reported graphically in Figure 7.7.

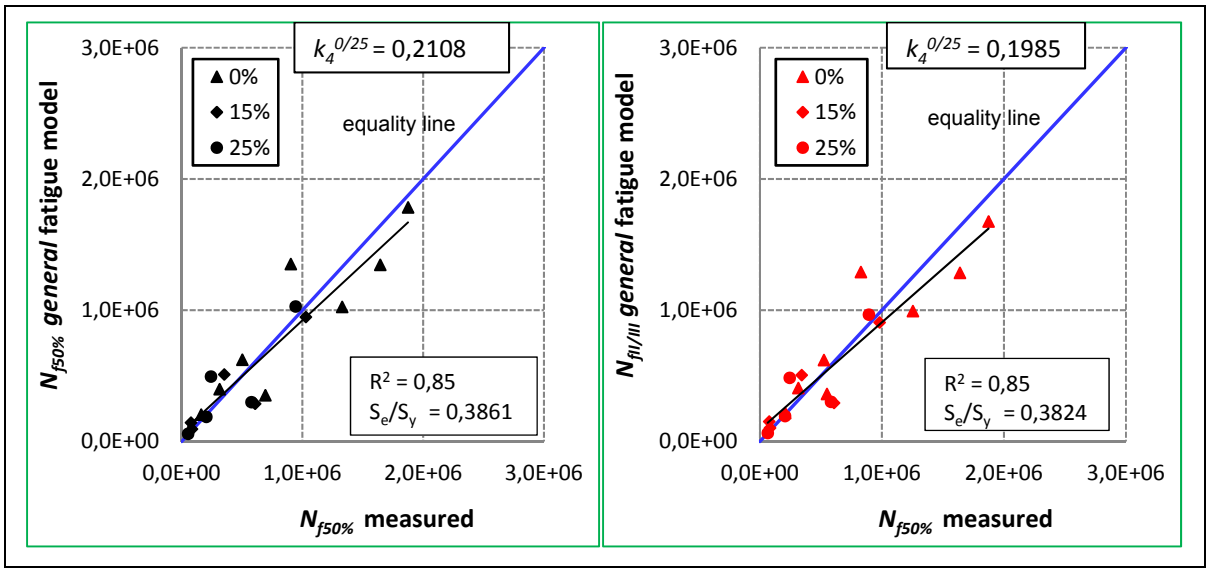

Figure 7.7 Predicted versus measured N_f using testing data by assuming the slope of the fatigue line is variant and by considering the A value determined from the optimization process as an average of A^{15} and A^{25}

In conclusion, when comparing simulations based on optimization for 0-25% RAP mixes to the one determined for mixes with up to 40% RAP, the R^2 values are strongly improved (R^2 = 0,85). But in this case, it is not valid anymore for the 40% RAP mixture. It seems that improving the fatigue model to take into account the percentage of RAP up to 40% becomes critical because there are lots of RAP (old) binder added to the virgin binder and the assumption to keep the fatigue parameters of the virgin mix ($k^0_{1,\theta_{test}}$, and k^0_2) constant could be incorrect in this case. We know that if we increase the percentages of RAP to a very high amount, like 50% or more, it will be questionable to keep those parameters as constant.

The results as shown in Figure 7.7 indicate that this method gives good results in predicting fatigue life for the mixes containing three RAP contents (0, 15, 25%). All results are quite close, but some predicted fatigue life numbers are a bit different from the corresponding observed one. This can be expected since past studies have shown significant dispersion in the results of fatigue life. This is due to the heterogeneity of the material and the fatigue phenomenon itself (Baaj, 2002).

7.3.3 Specific validation of the general fatigue model

In this section, we present how the general fatigue model has been found to be effective with its added new parameters (k_4 and A). Thus, we used the optimized values of A of each mix and k_4 values (Table 7.3) to make our calculations for $N_f^{0/40}$ like what we did before. The synthesis of the results is presented in Table-A IV-6 and in Figure 7.8. Of course, as shown from the results, the R^2 were improved. It is interesting that the predictions of N_f using the general fatigue model can provide a better accuracy (R^2= 0,90 and 0,80 using the $N_{f50\%}$ and $N_{fII/III}$ criterion, respectively) than when using a single value of A (the average value). These results suggest that the general fatigue model can provide an 'excellent' to 'good' prediction of N_f using the two criteria. It is interesting to note that we have, more or less, the same precision of what we presented in chapter 6 when we used specific values of k_1 and k_2 for each mix in the basic fatigue model. We reached almost the same level of accuracy (R^2).

Of course, the calculated predictions are close to the equality line by using the optimized A value specific for each mix. However, it is not useful since we can get the same thing by using the corresponding fatigue parameter k_1 and k_2 defined of each mix in the basic fatigue model. However, the general fatigue model is excellent for all mixes combined by using the optimized A value defined for each mix. In this case, laboratory fatigue testing continues to be essential to evaluate mixes containing any percentage of RAP. This means that there is still need to do fatigue tests in the mix design process. However, that's not our goal because in this case, the priority is to use the fatigue coefficient k_1 and k_2 defined for each mix in the basic traditional model.

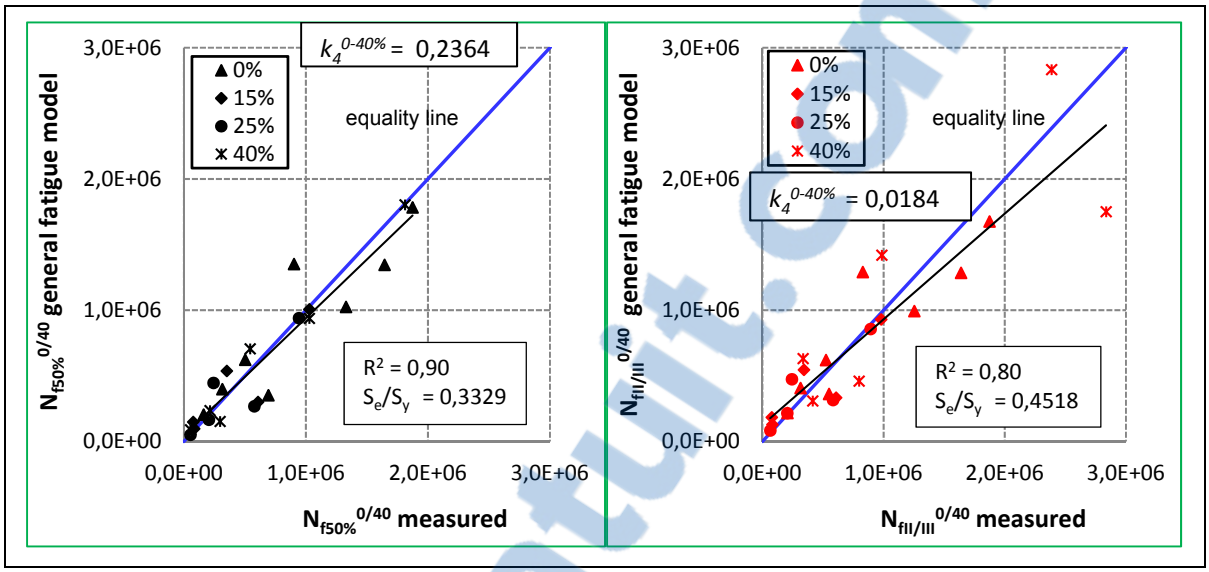

Figure 7.8 Predicted versus measured N_f using testing data by assuming the slope of the fatigue line as variant and using the optimum values of A for each mix (those values are shown in Table 7.3)

7.3.4 Conclusion

In the beginning of our modelling investigation, we suggested using the fatigue parameters of the virgin mix k_1^0 and k_2^0 to model the fatigue behaviour of recycled asphalt mixture made with small amounts of RAP. Based on the study findings, it was found that the general fatigue model is capable of capturing the influence of the addition of RAP up to 25% on N_f. It has been highlighted that the constant 'A' of the general model plays a determining role towards the fatigue life of the recycled mixtures. The general fatigue model had lower accuracy to predict N_f than the basic fatigue model when a single value of A was used. This is only occurring if we consider all mixes combined at up to 40% RAP.

We can conclude that the general fatigue model could be used considering the A value determined either from the relationship k_2 versus %RAP or from the optimization process using the mean value of optimized A for mixes combined up to 25%. In this case, the results show a bit higher accuracy (R=0,85) for the $N_{f50\%}$ and $N_{fII/III}$ criteria than for mixes combined up to 40%. But it is not validated for mixes made with RAP at up to 40%.

The proposed general fatigue model for RAP mixes made with RAP at up to 25% is:

$$N_f^{0/25} = k_{1,\theta_{test}}^0 \times (\varepsilon_t)^{-(1+A^{0/25}\times\%RAP)k_2^0} \times SF^{0/25} \quad (7.8)$$

Where $SF^{0/25} = 10^{-k_4^{0/25}}$

R^2 = 0,85 (for the $N_{f50\%}$ criteria and the $N_{fII/III}$ criteria)

The assumed values of A and k_4 are presented in Table 7.5

Table 7.5 Parameters used in the proposed general fatigue model for RAP mixtures listed in this research program

Mix	**Parameters**	**Ref.**	**Criteria**	
			$N_{f50\%}$	$N_{fII/III}$
RAP content: up to 25%	$k_4^{0/25}$	Table 7.2	0,2108	0,1981
	$A^{0/25}$	Table 7.2 (obtained from relationship k_2 vs RAP %)	0,00713	0,00711
		Table 7.4 (obtained optimization process)	0,00720	0,00714
RAP content: up to 40%	$k_4^{0/40}$	Table 7.2	0,2364	0,0184
	$A^{0/40}$	Table 7.2(obtained from relationship k_2 vs RAP %)	0,00850	0,00095
		Table 7.3(obtained optimization process)	0,00831	0,00075

If we want to model mixes with 40% RAP, we will refer to the $A^{0/40}$ and $k^{0/40}$ values as reported in Table 7.5.

7.4 Statistical fatigue model

As we have shown in section 7.3.1, we were not able to predict adequately the fatigue life by considering the effect of RAP addition by only shifting the Wöhler curve established for the virgin mix in the y-axis direction. To obtain a unique Wöhler curve that considers the effect

of RAP addition for fatigue by simply shifting the Wöhler curves in the y-axis, we need to consider a statistical value for the slope that is not related to the slope of the virgin mix. To do this, we refer to a statistical multi–regression analysis by considering 3 variables (log N_f, $log\ \varepsilon_t$, and %RAP) with the assumption that the variables $log\ \varepsilon_t$, and %RAP are independent. STATGRAPHICS software was used for this purpose to find the appropriate models for the two criteria used in this study. Similarly to what we did before in the first proposed approach, we will first analysis all the data from 0 to 40% RAP and after that we will repeat the analysis by considering the results only from 0 to 25% RAP. We obtain from the analysis an equation in the basic fatigue modelling form proposed in equation 6.4. By rearranging the form of the obtained equation for $N_{f50\%}$ criteria, as an example, we can obtain:

$$N_{f50\%}^{0/40} = 8{,}7E-27 \times (\varepsilon_t)^{-8{,}1} \times SF_{N_{f50\%}^{0/40}}^{stat} \tag{7.9}$$

Where: $SF_{N_{f50\%}^{0/40}}^{stat} = 10^{0{,}00696 \times \%RAP}$

As we can see, it is exactly in the same form as the basic model given in equation 7.3. We obtained the statistical fatigue parameters k_1^{stat} and k_2^{stat} from STATGRAPHICS and applied again RAP effect by shifting in Y-axis direction. These values are specific and do not relate to the fatigue parameters of the virgin mixtures ($k_{1,\theta_{test}}^0$, and k_2^0).

Table 7.6 contains a summary of the fatigue regression parameters $k_1^{stat-0/40}$ *and* $k_2^{stat-0/40}$ and the shift factor (SF^{stat}) that take into account the translation of the fatigue lines keeping the slope constant considering the effect of adding RAP, for all the recycled mixes combined in the statistical fatigue models $N_{f50\%}^{0/40}$ and $N_{fII/III}^{0/40}$.

Table 7.6 Statistical fatigue model regression coefficients for all the recycled mixes combined up to 40%

Parameters / Criteria	$k_1^{stat-0/40}$	$k_2^{stat-0/40}$	$SF^{stat-0/40}$
$N_{f50\%}^{0/40}$	$8{,}7\times 10^{-27}$	8,1	$10^{0{,}00696\times\%RAP}$
$N_{fII/III}^{0/40}$	$3{,}0\times 10^{-21}$	6,7	$10^{0{,}01343\times\%RAP}$

The tabulated results of the predicted values using these models are presented in Table-A IV-7. Values of the corrected deformation (ε_{cor}) were used in the calculation as stated previously. Figure 7.9 shows the plot of the predicted values for the statistical models versus the measured fatigue values.

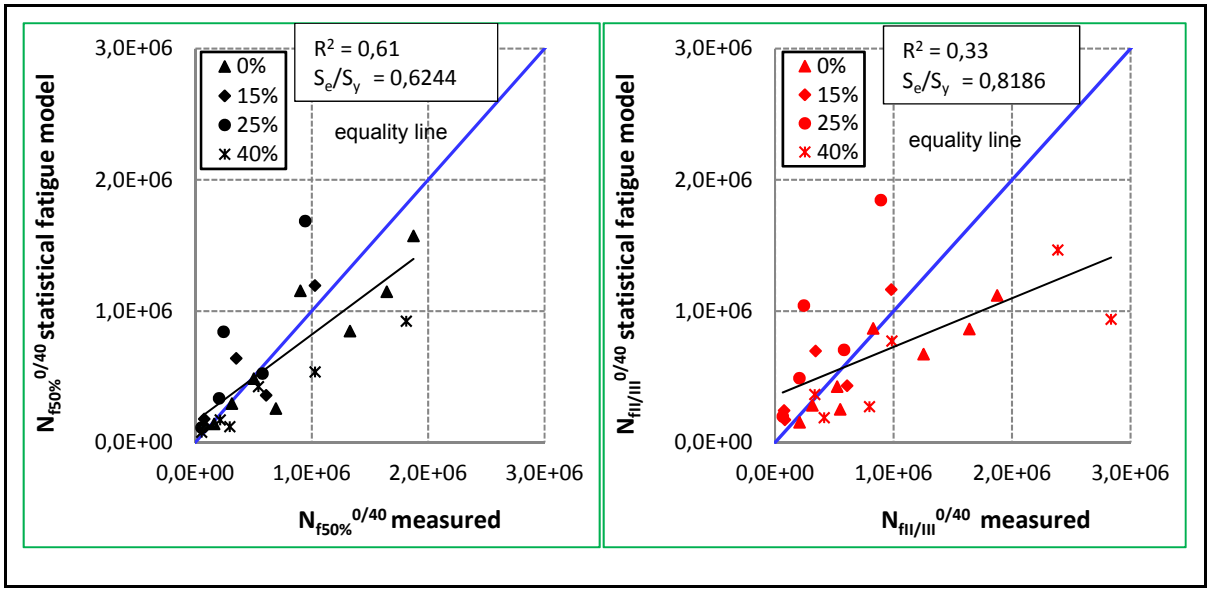

Figure 7.9 Statistical fatigue model versus measured N_f using the statistical fatigue parameters $k_1^{stat-0/40}$, and $k_2^{stat-0/40}$ and the $SF^{stat-0/40}$ defined for all the mixes combined up to 40%

A comparison between the R^2 values resulted from the analysis of the last improvement of the basic fatigue model and the analysis of statistical models show that the R^2 was improved from 0,52 to 0,61 for the general fatigue model $N_{f50\%}^{0/40}$ and statistical fatigue model,

$N_{f50\%}^{0/40}$ respectively, and from 0,26 to 0,33 for the general fatigue model $N_{fII/III}^{0/40}$ and statistical fatigue model $N_{fII/III}^{0/40}$, respectively. We mean with the last improvement correcting the slope of the Wöhler curve with using the values of the parameters k_1^0, k_2^0, $k_4^{0/40}$, and $A^{0/40}$ suggested in Table 7.2 and used in equation 7.7. So we have, so far, been able to obtain similar accuracy with what we found previously. Our results still show fair and poor accuracy for the $N_{f50\%}$ and $N_{fII/III}$ criterion, respectively if we use the best-fit line (predicted values) in our analysis. We rerun the software by considering the mixes made with RAP at up to 25% and STATGRAPHICS gives the results that shown in Table 7.7.

Table 7.7 Statistical fatigue model regression coefficients for all the recycled mixes combined up to 25% RAP

Parameters / Criteria	$\boldsymbol{k_1^{stat-0/25}}$	$\boldsymbol{k_2^{stat-0/25}}$	$\boldsymbol{SF^{stat-0/25}}$
$\mathbf{N_{f50\%}^{0/25}}$	$3{,}7\times 10^{-26}$	8,0	$10^{-0{,}00793\times\%RAP}$
$\mathbf{N_{fII/III}^{0/25}}$	$1{,}1\times 10^{-24}$	7,6	$10^{-0{,}00783\times\%RAP}$

The tabulated results of the predicted values of the statistical fatigue model, $N_{f50\%}^{0/25}$ and model $N_{fII/III}^{0/25}$ are presented in Table-A IV-8. Figure 7.10 shows the plot of the predicted values for the Statistical fatigue models developed for recycled mixtures made up to 25% RAP versus the measured fatigue values.

By doing this, the results show a higher level of accuracy than when using the results of combined mixtures made with RAP at up to 40% developed for $N_{f50\%}^{0/25}$ and $N_{fII/III}^{0/25}$ criteria. The most interesting thing is that the predictions made by the statistical method give the same level of accuracy than the general fatigue model's predictions assuming that the model used a single value of the A (the model parameter) for the slope of the fatigue line. However, even if the statistical predictions are getting better, it is not useful because we still need to perform all the tests. Again, these models cannot be validated for the 40% RAP mixture. This

confirms that it may be possible to improve the fatigue model made to incorporate small amounts of RAP. All the results are summarized in Table 7.8.

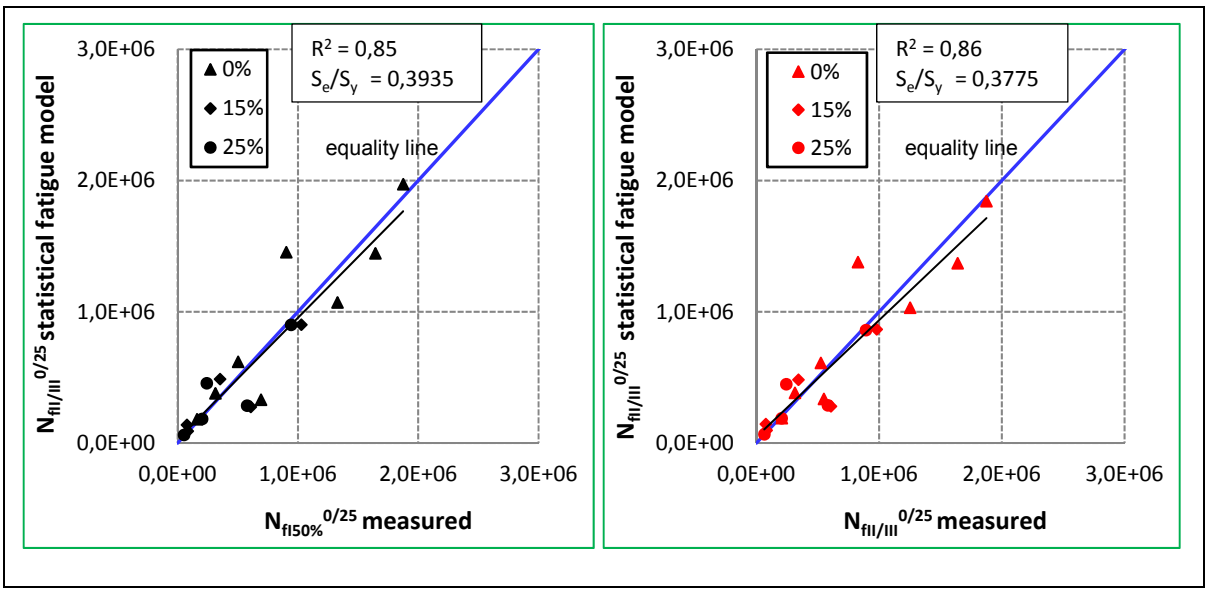

Figure 7.10 Statistical fatigue model versus measured N_f using the statistical fatigue parameters $k_1^{stat-0/25}$, and $k_2^{stat-0/25}$ and the $SF^{stat-0/25}$ defined for the mixes combined up to 25% RAP

7.5 Prediction of fatigue life at the pavement structure level

We presented in chapter 5 the fact that the addition of RAP to the virgin materials affects mix stiffness at the material level. Also, fatigue analysis of recycled mixture indicates the effects of the presence of RAP on resistance to fatigue damage at the material level. We found that the fatigue parameter ε_6 changes with the percentage of added RAP. The results indicated that 40 percent RAP mixture perform better than mixtures with 0, 15 and 25 percent RAP at all strain levels. However, the fatigue performances of mixes with 15 and 25 percent of RAP were similar or worse than that of the no-RAP-mixture at the same level of deformation.

Table 7.8 Summary of all the models newly developed in this study

Model	condition		Model data	R^2	Eq.
Basic model		**Form**	$\boldsymbol{N_f = k_{1,\theta_{test}}^{\%RAP} . (\varepsilon_t)^{-k_2^{\%RAP}}}$	**See Table 7.5**	**7.4**
General fatigue model	**Constant slope**	Form	$N_f^{0/40} = k_{1,\theta_{test}}^{0} \times (\varepsilon_t)^{-k_2^0} \times SF^{0/40}$		8.3
		$SF^{0/40}$	$10^{-k_4^{0/40} \times \%RAP}$		
		$N_{f50\%}^{0/40}$	$k_4^{0/40}$ = 0,2364	-0,05	
		$N_{fII/III}^{0/40}$	$k_4^{0/40}$= 0,0184	-0,27	
	Varying slope	Form	$N_f^{0/40} = k_{1,\theta_{test}}^{0} \times (\varepsilon_t)^{-(1+A^{0/40} \times \%RAP)k_2^0} \times SF^{0/40}$		8.7
		$SF^{0/40}$	$10^{-k_4^{0/40} \times \%RAP}$		
		$N_{f50\%}^{0/40}$	$k_4^{0/40}$ = 0,2364 and $A^{0/40}$ = 0,00850	0,52	
		$N_{fII/III}^{0/40}$	$k_4^{0/40}$ = 0,0184 and $A^{0/40}$ = 0,00095	0,27	
		Form	$N_f^{0/25} = k_{1,\theta_{test}}^{0} \times (\varepsilon_t)^{-(1+A^{0/25} \times \%RAP)k_2^0} \times SF^{0/25}$		8.7
		$SF^{0/25}$	$10^{-k_4^{0/25} \times \%RAP}$		
		$N_{f50\%}^{0/25}$	$k_4^{0/25}$ = 0,2108 for $A^{0/25}$ = 0,00713	0,85	
		$N_{fII/III}^{0/25}$	$k_4^{0/25}$ = 0,1981 for $A^{0/25}$ = 0,00711	0,86	
Statistical fatigue models	**Criteria**	Model data			
	$\boldsymbol{N_{f50\%}^{0/40}}$	Model 1	$N_{f50\%}^{0/40} = k_1^{stat-0/40} \times (\varepsilon_t)^{-k_2^{0/40}} \times SF^{stat-0/40}$	0,61	8.9
		$SF^{stat-0/40}$	$10^{0,00696 \times \%RAP}$		
		Fatigue parameters	$k_1^{stat-0/40}$ = 8,70$\times$ 10^{-27}, and $k_2^{stat-0/40}$ = 8,11		
	$\boldsymbol{N_{fII/III}^{0/40}}$	Model 2	$N_{fII/III}^{0/40} = k_1^{stat-0/40} \times (\varepsilon_t)^{-k_2^{stat-0/40}} \times SF^{stat-0/40}$	0,33	8.9
		$SF^{stat-0/40}$	$10^{0,01343 \times \%RAP}$		
		Fatigue parameters	$k_1^{stat-0/40}$ = 2,96$\times$ 10^{-21}, and $k_2^{stat-0/40}$ = 6,70		
	$\boldsymbol{N_{f50\%}^{0/25}}$	Model 3	$N_{f50\%}^{stat-0/25} = k_1^{0/25} \times (\varepsilon_t)^{-k_2^{stat-0/25}} \times SF^{ststst-0/25}$	0,85	8.9
		$SF^{stat-0/25}$	$10^{-0,00793 \times \%RAP}$		
		Fatigue parameters	$k_1^{stat-0/25}$ = 3,70$\times$ 10^{-26}, and $k_2^{stat-0/25}$ = 8,0		
	$\boldsymbol{N_{fII/III}^{0/25}}$	Model 4	$N_{fII/III}^{0/25} = k_1^{stat-0/25} \times (\varepsilon_t)^{-k_2^{stat-0/25}} \times SF^{stat-0/25}$	0,86	8.9
		$SF^{stat-0/25}$	$10^{-0,00783 \times \%RAP}$		
		Fatigue parameters	$k_1^{stat-0/25}$ = 1,1$\times$ 10^{-24}, and $k_2^{stat-0/25}$ = 7,61		

In a pavement structure, the mixture stiffness is linked to fatigue resistance. The Burmister's approach assumes that pavement materials behave as a linear, elastic and isotropic material (a function of its own stiffness). This means that the deformation will change with the stiffness of the mix, which in turn will change the fatigue damage of the pavement. So in order to properly evaluate the fatigue resistance of asphalt mixtures in a pavement, it is important to study both at the material scale and at the pavement structure scale. High HMA mixtures stiffness will lead to low deformation, but not necessarily to higher fatigue life since a very stiff material could also have a very low fatigue life.

This section focuses on studying the fatigue life of a pavement structure made of HMA mixtures containing recycled mixtures containing different percentages of RAP. Therefore, we make calculations to take into account stiffness of the material which gives us the deformation at the bottom of the surface asphalt layer in a reference structure composed of a bituminous layer over two granular layers (base course and sub-base). The calculations of the deformations of the asphalt pavement layer material were conducted considering the material stiffness obtained from each percentage of RAP and were done using LCPC Alizé software. This computer program, developed by LCPC (*Laboratoire Central des Ponts et Chaussées* = Central Laboratory of Bridges and Roads), is the reference program used in the "French pavement structures design method" (LCPC, 1994). This computer program, Alizé, is based on analytical solving of the stress and strain state of the pavement structure under load, by using the Burmister's multilayered elastic model (Burmister, 1943). We used Alizé to calculate stresses and strains in the flexible pavement structure chosen for this study. Then, we can estimate the fatigue life at different temperatures and frequencies. In all the structures, we assume the same characteristics for the subgrade, the granular base, and sub-base courses.

The aim of this section is to compare the fatigue life of the various bituminous mixes (GB-20) made with different percentages of RAP (0, 15, 25, and 40%) based on the structure level (see Figure 7.11).

The complex modulus of the GB-20 mix depends on the recycled material percentages and varies as a function of temperature and frequency. The value of the Poisson's ratio is set at 0,35 for all mixes. For the two granular layers, the stiffness values are E = 360 MPa and E = 180 MPa, respectively and Poisson's ratio = 0,45. And finally, the subgrade which has the modulus of 20 MPa, and a Poisson's ratio = 0,45. It was assumed that the link between the first layer and the second layer to be unbounded because it is composed of two different materials and between the second layer and the third layer to be bonded, and finally between the third layer and the subgrade existing soil to be bonded. No wearing course was used in this structure since it has a very limited impact on the calculated stresses and strains.

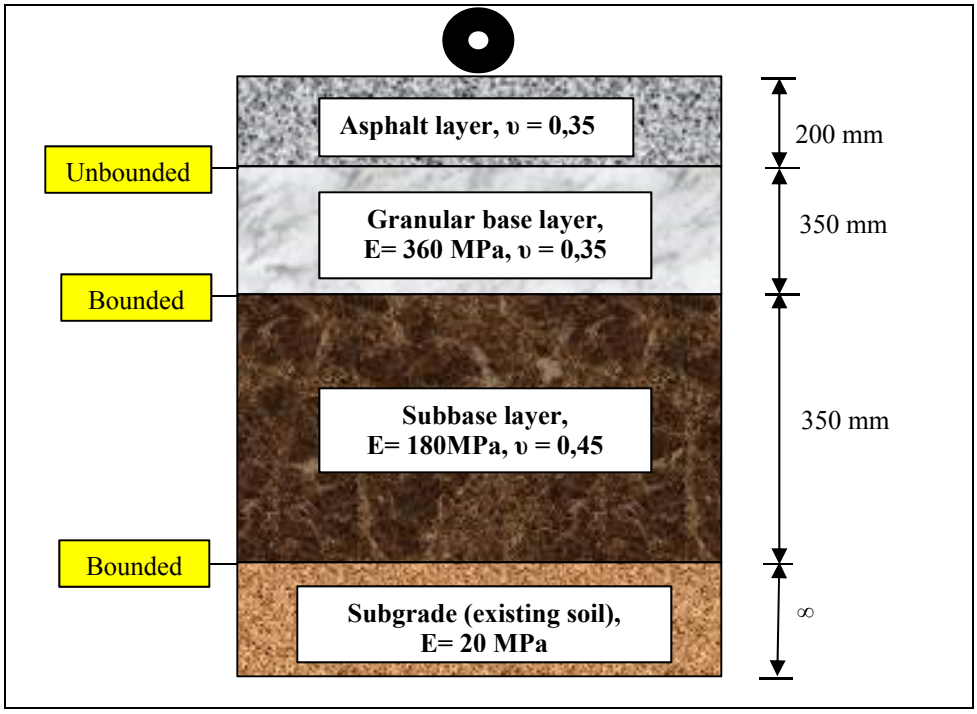

Figure 7.11 Studied pavement structure

All simulations were performed with the standard French ESAL corresponding to a single axle load of 130 kN dual tires with an inflation pressure of 6,62 bars.

We are focusing on the evolution of the strain at the bottom of the base asphalt layer (recycled materials) because the tensile horizontal strain at the bottom of HMA layer causes fatigue crack to initiate at the bottom of the layer and then propagates upwards (Yang, 2004). Based on that, the fatigue life of asphalt pavement was predicted at three selected temperatures (10, 25, and 40°C) and 2 selected frequencies (3, and 10 Hz). To do this, the 2S2P1D model established by simulating the experimental results is used because it allows predicting the bituminous mix complex modulus from the experimental data at a given temperature and frequency. These temperatures were selected because it is well known that the fatigue behaviour mostly occurs in summer times when asphalt pavement has a high surface temperature. Also, these three temperatures are close to expected surface temperature of the pavement in summer (Meunier, 2012). For this simulation, we used the complex modulus test results for the same HMA mixtures that were selected for the fatigue resistance test (Table 7.9). The samples used for this purpose were RAP028 (P1-A4), RAP1528CU (P2-A4), RAP2528CU (P1-A3), and RAP4028CU (P2-A4), as presented in chapter 5.

Table 7.9 Modulus of the mixtures predicted by
2S2P1D model and used in the input parameters of Alizé software

Modulus |E*| at different temperatures and frequencies (MPa)	**% RAP**			
	0	**15**	**25**	**40**
|E*| (40 °C, 10 Hz)	739	438	740	702
|E*| (40 °C, 3 Hz)	436	248	435	412
|E*| (25 °C, 10 Hz)	3 187	2 609	3 795	3 287
|E*| (25 °C, 3 Hz)	1 992	1 590	2 349	2 061
|E*| (10 °C, 10 Hz)	10 253	9 771	12 578	10 513
|E*| (10 °C, 3 Hz)	7 917	7 589	9 913	8 284

For each predicted complex moduli on each mix at a given frequency and temperature shown in Table 7.9, the software computes the strains as reported in accordance with the studied pavement structure (see Figure 7.11). The Alizé-LCPC software computations were done between the wheels at the bottom of the asphalt layer (point 1) as shown in Figure 7.12. The

strains at the bottom of the bituminous layer were computed as a function of temperature for all the structures made of mixtures containing different percentages of RAP as shown in Table 7.10 and Figure 7.13. The strains at the bottom of the HMA layer containing RAP were relatively low and varied between 84 and 323 μm/m at 10°C and 25°C, respectively and high at 40°C and varied between 524 to 1097 μm/m. Those results are for 10 Hz and 3 Hz.

As shown in Figure 7.13, at 10°C and 25°C at 10 Hz, the difference in strain values between the mixtures is negligible, but at 40°C, the mixture incorporating 25 and 40% RAP, as well as the reference mix (no RAP) exhibited similar strain values, but the 15% RAP mixture shows the highest strain. We get the same tendency at 3Hz. The results obtained from the different mixtures show that the strain values depend significantly on the modulus values. The trend is the same in all the conditions of frequency used.

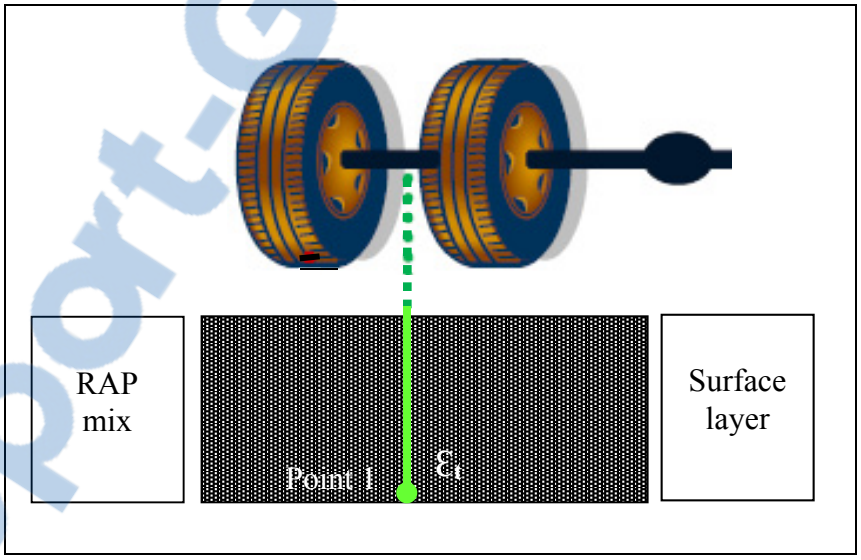

Figure 7.12 Location of the calculation of the strain considered in Alizé software

7.5.1 Determination of the fatigue lives values at the pavement level

In the previous sections, it has been highlighted that the general fatigue model and the statistical models play a critical role in determining the fatigue life of the asphalt mixtures containing RAP. The aim of this section is to quantify this aspect associated with fatigue

prediction of recycled mixture at the pavement level by testing the accuracy of the fatigue life data under a range of different models, namely the basic fatigue model, the general model and the statistical models. The strains calculated with Alizé were used to predict fatigue behaviour for pavement using the different models. The analyses were conducted at the 10, 25, and 40°C.

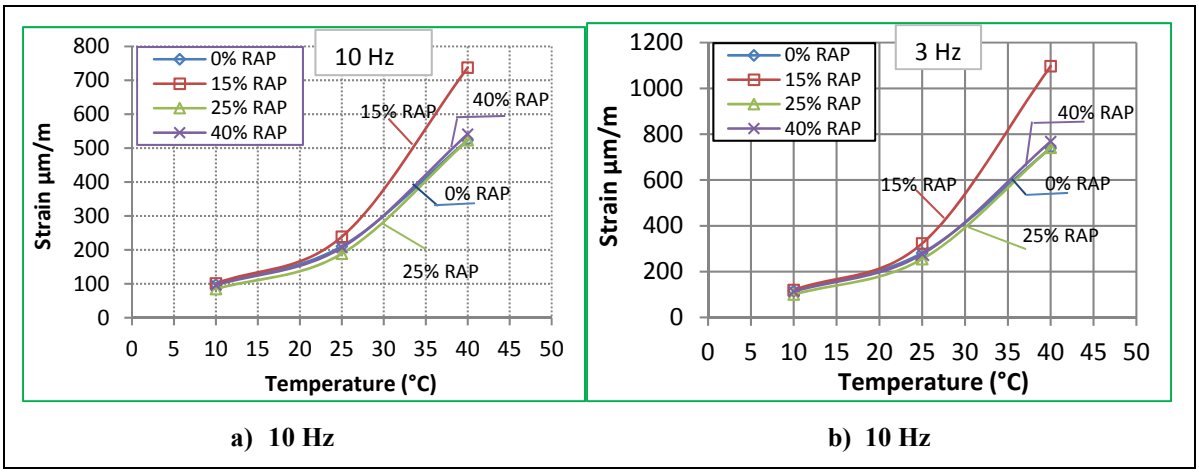

Figure 7.13 Relations between the computation strains at the bottom of the bituminous layer, between the dual tire of standard 18,000-lb single axle with (an ESAL), and the temperatures for the mixtures containing different percentages of RAP at 10 Hz and 3 Hz

Table 7.10 Resulted strain at the bottom of the bituminous layer of Alizé software

	Computed strain at different temperatures and frequencies (µm/m)			
% RAP	**0**	**15**	**25**	**40**
ε_t (40 °C, 10 Hz)	523,8	737,5	523,3	541,3
ε_t (40 °C, 3 Hz)	739,8	1097,4	740,9	768,6
ε_t (25 °C, 10 Hz)	210,8	238,8	188,8	206,7
ε_t (25 °C, 3 Hz)	281,9	323,2	254,8	276,1
ε_t (10 °C, 10 Hz)	97,7	101,2	84,8	96,0
ε_t (10 °C, 3 Hz)	116,6	120,0	100,0	113,1

As pointed out in section 7.1, there is a 'shift factor' in the prediction of laboratory fatigue life $\left[\frac{|E^*_{\theta_i}|}{|E^*_{\theta_{test}}|}\right]^{-k_3}$ to take into account the temperature effect on the fatigue behaviour based on the stiffness ratio. Obviously, this argument should be taken into account for all of the models shown in Table 7.8. It is important to note that when we refer to the basic model, it is as shown in equation 7.1. Since we don't have our own data to improve the statistical model at different temperatures, we apply the same shift factor to correct the fatigue life predicted from the statistical models to consider the temperature difference.

We need to focus discussions on two steps of the analysis: the first step in this analysis is to use the general and the statistical fatigue models designed to take into account mixes containing up to 40% RAP to predict fatigue life for all mixes in the four typical pavement structures. Even if these models show poor accuracy, there is still a need to predict fatigue lives for the 40% RAP mix at the pavement level at different temperature. In addition, we aim to conduct a comparative study for fatigue behaviour of recycled mixtures at the structure level focusing on all the RAP percentages tested in this study and after that to compare with the results at the material level. That can be done by using specific parameters values proposed for this model.

In the first step, we use the pertinent fatigue coefficients, k_1, and k_2 for all the four recycled mixes individually (presented in Table 6.5) to estimate the fatigue life based on equation 7.1. We fix the k_3, parameter in accordance with the value of the slope of the fatigue line divided by 2 as reported by the French design method (Perraton et al., 2011). For the basic model, we have four k_3 values because we have four k_2 values defined for each mix for each criterion.

In the same manner, we use the general model parameters values $k^0_{1,\theta_{test}}$, k^0_2, $k^{0/40}_4$, and $A^{0/40}$ (presented in Table 7.2) to estimate the fatigue lives of the model ($N_{f50\%}$ and $N_{fII/III}$) using equation 7.7. In that case, we determine the k_3 value by dividing the slope of the fatigue line of the virgin mix (k^0_2) by 2 (Perraton et al., 2011). Consequently, in the

general fatigue model, we have one value of k_3 for each criterion because we considered only the slope of the fatigue line of the virgin mix (k_2^0).

For Statistical modelling predictions of N_f, we use the parameters shown in Table 7.5 to calculate predictive values for each criterion. For this model, we have one value of k_3 for each criterion because we have one value of the slope for each criterion. The determined statistical slopes ($k_2^{0/40}$) shown in Table 7.5 were used in the calculation of the parameter k_3. Appropriate mixtures' moduli shown in Table 7.8 were considered in all the calculations for all the models.

Table 7.11 and Table 7.12 show the number of load repetitions to fatigue failure and the tensile strains at the bottom of the recycled hot mix asphalt layer for the four pavement structures computed by each model for the two criteria $N_{f50\%}$ and $N_{fII/III}$. A pavement structure with a higher number of cycles to failure indicates a HMA mix with a better resistance to fatigue cracking. The tensile strain at the bottom of the HMA layer were ranged from low to high (ranged between 84,8 to 1097,5 μm/m), therefore, a high and a low number of cycles to fatigue failure were found.

Table 7.11 Comparison between the fatigue life values predicted from the basic and the general fatigue models according to the criteria $N_{f50\%}$ based on the structure level ($k_3 = k_2{}^{a}/2$): modelling up to 40%

The mix	Temp. – freq.	Alizé resulted strain µm/m (Pavement structure: Figure 7.12)	$N_{f50\%\text{-calculated}}$ (cycles)		
			Basic model (equation 7.1) P. 281	General fatigue model (equation 7.7) P.290	Statistical model (equation 7.9 - model 1 table 7.8)
			By considering the coefficients $k_1^{\%RAP}$ and $k_2^{\%RAP}$ established from $N_{f50\%}$	By considering the coefficients k_1^0, k_2^0, $k_4^{0/40}$, and universal value of $A^{0/40}$ and $SF^{0/40}$ established from $N_{f50\%}$	By considering the statistical coefficients $k_1^{0/40}$ and $k_2^{\%RAP}$ and $SF^{0/40}$ established from $N_{f50\%}$
GB20 0% RAP	40°C – 10Hz	523,8	109 554	109 554	66 565
	40°C – 3Hz	739,8	143 691	143 691	89 127
	25°C– 10Hz	210,8	956 779	956 779	768 484
	25°C – 3Hz	281,9	638 673	638 673	485 135
	10°C– 10Hz	97,7	3 659 026	3 659 026	3 515 512
	10°C – 3Hz	116,6	2 590 493	2 590 493	2 378 270
GB20 15% RAP	40°C – 10Hz	737,5	62 736	27 407	94 109
	40°C – 3Hz	1097,5	22 384	8 344	37 179
	25°C– 10Hz	238,8	535 567	429 811	656 027
	25°C – 3Hz	323,2	324 413	217 836	416 152
	10°C– 10Hz	101,2	3 261 215	4 014 162	3 358 237
	10°C – 3Hz	120	2 183 556	2 490 409	2 338 338
GB20 25% RAP	40°C – 10Hz	523,3	317 081	77 531	597 898
	40°C – 3Hz	740,9	165 682	24 993	304 272
	25°C– 10Hz	188,8	1 567 982	1 620 107	3 171 434
	25°C – 3Hz	254,8	975 932	660 259	1 933 459
	10°C– 10Hz	84,8	7 704 143	24 004 657	16 598 435
	10°C – 3Hz	100	5 361 770	13 346 443	11 393 070
GB20 40% RAP	40°C – 10Hz	541,3	577 512	10 909	345 865
	40°C – 3Hz	768,6	250 224	2 493	173 051
	25°C– 10Hz	206,7	3 848 148	469 086	171 625
	25°C – 3Hz	276,1	2 203 246	152 781	1 051 642
	10°C– 10Hz	96	24 348 547	11 980 238	7 698 642
	10°C – 3Hz	113,1	15 601 239	5 775 267	5 329 279

a: In the case of the basic model, the slope of the fatigue line for each mix is varied and considered in the k_3 calculation (k_2 values that used were shown in Table 6.4. In the case of the general fatigue model the only slope value that was considered in the calculation was the slope of the mixture without RAP (k_2^0). and In the case of the statistical model, the determined statistical slope shown in Table 7.5 was taken into account in the calculation.

Table 7.12 Comparison between the estimated fatigue life values of the basic and the general fatigue models according to the criteria $N_{fII/III}$ based on the structure level ($k_3 = k_2/2$): (modelling up to 40%)

The mix	Temp. – freq.	Alizé resulted strain µm/m (Pavement structure: Figure 7.12)	$N_{fII/III-calculated}$ (cycles)		
			Basic model (equation. 7.1) P.281	General fatigue model (equation. 7.7) P.290	Statistical model (model 2–Table 7.8)
			By considering the coefficients $k_1^{\%RAP}$ and $k_2^{\%RAP}$ established from $N_{fII/III}$	By considering the coefficients $k_1^0, k_2^0, k_4^{0/40}$, and universal value of $A^{0/40}$ and the $SF^{0/40}$ established from $N_{fII/III}$	the statistical coefficients $k_1^{0/40}$ and $k_2^{\%RAP}$ and the $SF^{0/40}$ established from $N_{fII/III}$
GB20 0%RAP	40°C – 10Hz	523,8	120 099	120 099	85 304
	40°C – 3Hz	739,8	155 185	155 185	109 590
	25°C– 10Hz	210,8	930 821	930 821	629 968
	25°C – 3Hz	281,9	635 337	635 337	433 910
	10°C– 10Hz	97,7	3 306 156	3 306 156	2 171 403
	10°C – 3Hz	116,6	2 385 633	2 385 633	1 578 961
GB20 15%RAP	40°C – 10Hz	737,5	66 077	141 834	149 417
	40°C – 3Hz	1097,5	23 898	62 792	70 036
	25°C– 10Hz	238,8	548 377	795 813	722 832
	25°C – 3Hz	323,2	334 373	529 727	500 028
	10°C– 10Hz	101,2	3 260 696	3 372 536	2 727 911
	10°C – 3Hz	120	2 194 775	2 452 191	2 031 170
GB20 25%RAP	40°C – 10Hz	523,3	339 130	649 794	815 519
	40°C – 3Hz	740,9	187 219	349 754	470 708
	25°C– 10Hz	188,8	1 464 668	3 067 237	3 156 141
	25°C – 3Hz	254,8	948986	1 936 438	2 112 573
	10°C– 10Hz	84,8	6 288 692	13 894 411	12 149 910
	10°C – 3Hz	100	4 513 129	9 878 346	8 938 800
GB20 40%RAP	40°C – 10Hz	541,3	1 157 130	366 022	676 577
	40°C – 3Hz	768,6	685 628	187 602	385 099
	25°C– 10Hz	206,7	3791492	1 740 505	2 428 143
	25°C – 3Hz	276,1	2 674 604	1 098 606	1 667 640
	10°C– 10Hz	96	12 027 574	7 589 774	8 416 592
	10°C – 3Hz	113	9 103 554	5 349 402	6 235 569

The second step was to redo the above simulation but with using the general and the statistical fatigue models that take into account mixes containing up to 25% RAP to see the results. We apply again the parameters specific for each mix when considering a model of data up to 25% RAP. We finally obtain the synthesis results as shown in appendix IV.

Figure 7.14 and Figure 7.15 show the number of load repetitions to fatigue failure relative to the virgin mixture for the four structures under the various strains level resulted from a given analysis: step 1 and step 2, respectively. We placed the results of the two steps in these figures side by side. The results shown in the left side (part a) are for a data modelling that can account for up to 40% RAP. In fact, we can't consider the statistical model in the comparison between the models because the value of N_f of the virgin mix (the mix of no RAP) is not the same as in the other models. In another word, N_f^{stat} of the virgin coming from the statistical calculation differs from those coming from other models. When comparing the basic model with the other new models, it is important to keep the denominator consistent by the same amount.

It is important to note that the fatigue may occur more rapidly at high temperature, so as the temperature increases the fatigue cracking increases or the materials show less fatigue resistance. If we want to explain this, we need to show that the engineering parameters considered in grading the asphalt binder are related to the following mechanisms: rutting, fatigue cracking, and thermal cracking. At high temperatures, the asphalt binder behaves like a viscous fluid and has a low rigidity. Many researchers came up to the conclusions that mixtures with hard bitumen have longer fatigue life (Racanel et Burlacu, 2013). Based on that, we can say that the fatigue cracking is more pronounced at high temperatures.

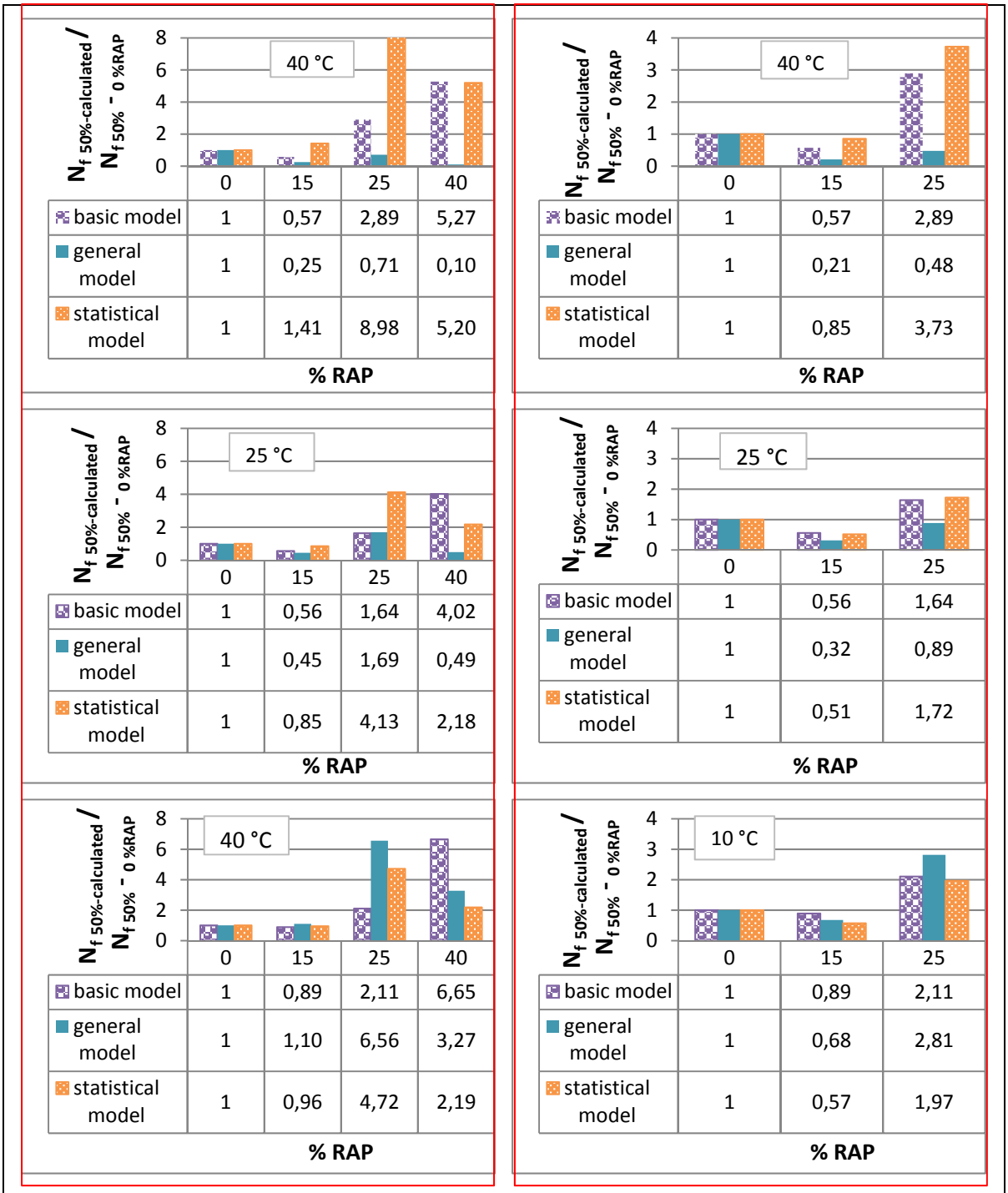

a) Modelling up to 40% RAP b) Modelling up to 25% RAP

Figure 7.14 $N_{calculated}^{0-40\%}$ relative to $N_{0\%RAP}^{0/40}$ determined based on the structure level at different temperatures and at 10 Hz according to the $N_{f50\%}^{0/40}$ using three different models

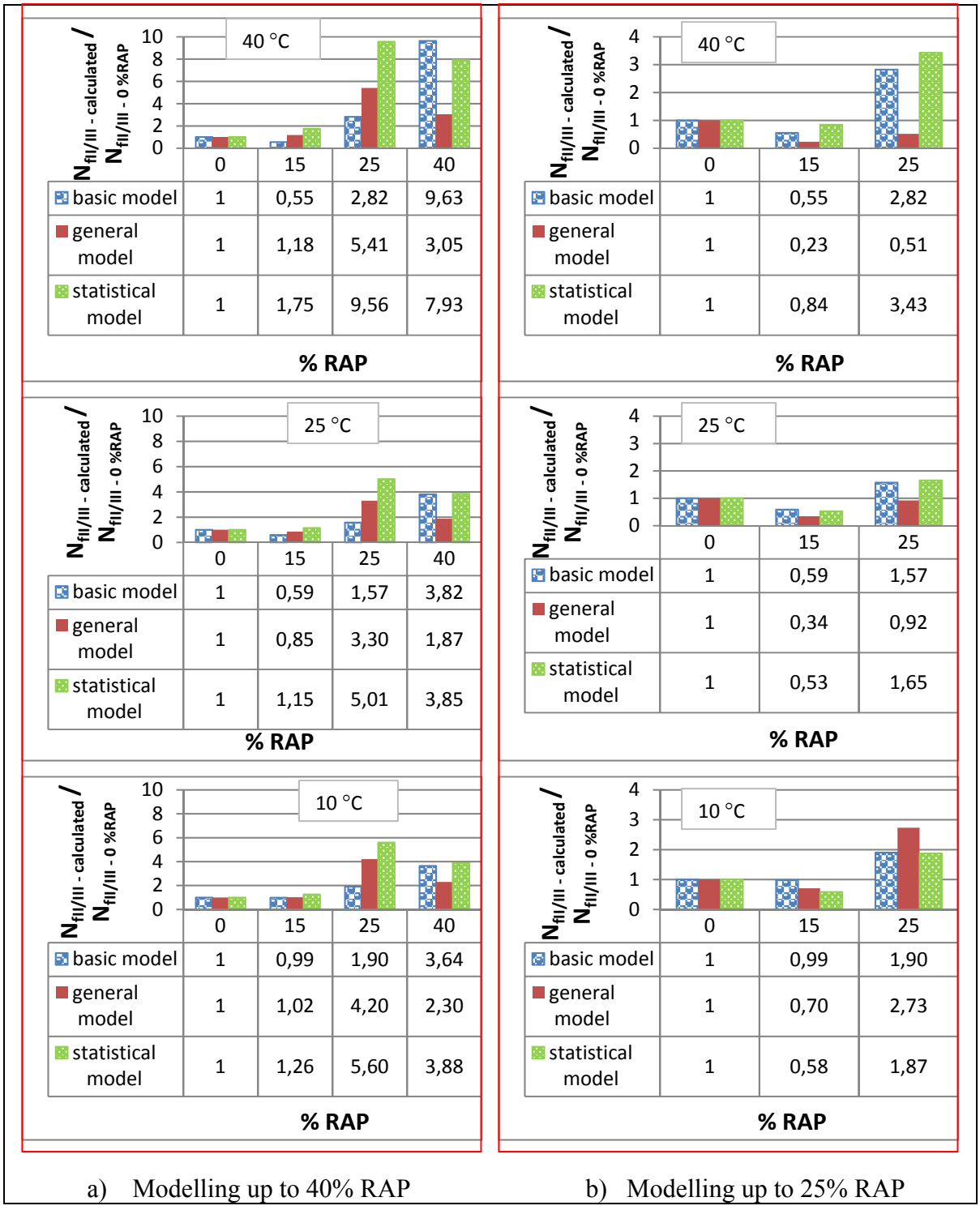

Figure 7.15 $N_{calculated}^{0/40}$ relative to $N_{0\%RAP}^{0/40}$ determined based on the structure level at three different temperatures and at 10 Hz according to the $N_{fII/III}^{0/40}$ using three different models.

When we examine the results of the N_f prediction using our models, we find that it is difficult to see a general trend in Figure 7.14. Probably because it was shown that there is a difference of the accuracy of prediction between the models. Our results clearly show that there is a difference in fatigue life which may be affected by the duration of the exposure to elevated temperature.

At 25°C, the basic model shows that the 40% RAP structures exhibited slightly higher $N_{f50\%}^{0/40}$ than the mixture without RAP. At 10°C, the basic model shows that the structure with 40% RAP mix exhibits the highest $N_{f50\%}^{0/40}$ ratio, thus a better fatigue resistance. The structures with 15% RAP and 25% RAP mixes have fatigue resistance similar to the structure with the conventional mix.

Basically, at 40°C and 25°C, the general and the statistical fatigue models do not seem to follow the same tendency. The stiffness ratio term that shifts the results according to the temperature has a bigger effect on the developed model than on the basic model because the stiffness ratio is raised to the power k_3. We have previously discussed how to assume a fixed value of the k_3 parameter and unfortunately this assumption has as large an effect on the prediction of fatigue life. This could explain the discrepancies found. Other models are probably required to describe the fatigue behaviour of asphalt mixtures at different testing temperature.

In Figure 7.15a, at 25°C, the basic model shows that the structure with 40% RAP mix exhibited the highest $N_{fII/III}^{0/40}$ ratio, followed by the structure with 25% RAP mix. The $N_{fII/III}$ criterion shows very close results to $N_{f50\%}^{0/40}$ for the 40% RAP mix at this temperature. The structure with 15% RAP mix exhibits a lower $N_{fII/III}^{0/40}$ ratio but not significantly. At 10°C, the basic model shows that the structure of 40% RAP mix exhibit the highest $N_{fII/III}^{0/40}$ ratio, thus a better fatigue resistance; followed by the structure with 25% RAP mix and the structure with 15% RAP mix. This observation is consistent with the results of previous

$N_{fII/III}^{0/40}$ ratio comparisons. In fact we can't compare between any kind of RAP percentage on the graphs at different temperatures because the N_f reference is changing with the temperature.

The results, shown in Figure 7.14b, clearly show that the use of data modelling for mixes up to 25% reduces the difference between fatigue life predictions using different models. We can get the same trend for the basic fatigue model using our models. It is more or less the same magnitude. It means that the prediction has improved greatly. It is evident that making modelling up to 40% RAP is not a good way because the new models show completely different fatigue life ratio and it might be difficult to obtain consistent results with the basic model. However, it is interesting to see that the inclusion of RAP materials in the HMA can improve its fatigue resistance but the way we used to make the modelling could be tricky.

Figure 7.16a shows the plot of $N_{f50\%}^{0/40}$ basic fatigue model versus the predicted values from the general fatigue model and the statistical fatigue model for data model up to 40% of RAP, and Figure 7.16b shows these graphs but for data model up to 25% of RAP. Figure 7.17a and Figure 7.17b show the same relationship but for $N_{fII/III}$ criterion. All data used in this analysis are coming from the fatigue life prediction of the structure considering different temperatures and frequencies. Data presented in Tables 7.11 and 7.12 are used for the Graphs 7.16a and 7.17a, respectively.

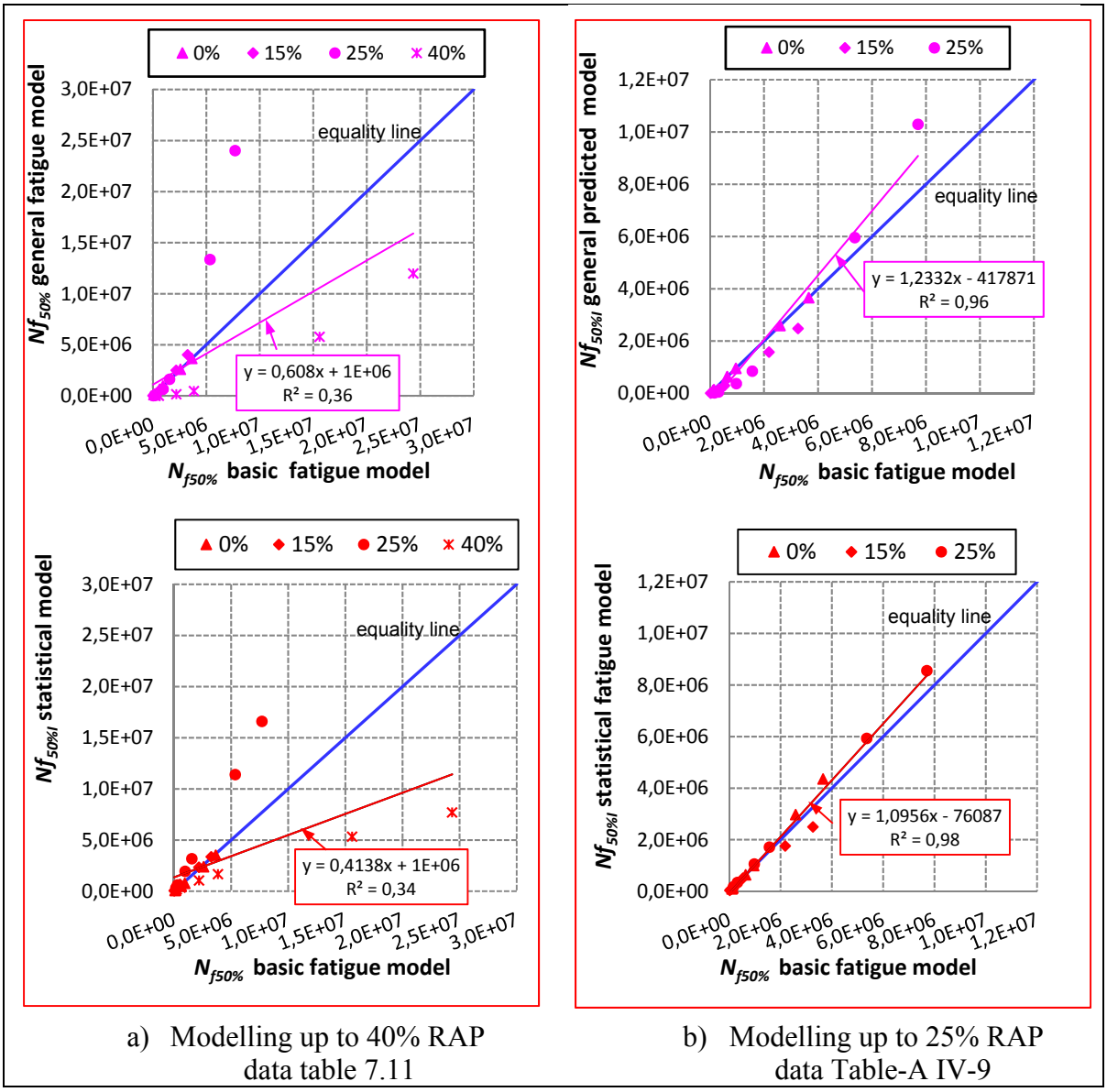

a) Modelling up to 40% RAP data table 7.11

b) Modelling up to 25% RAP data Table-A IV-9

Figure 7.16 Basic predicted model values versus the new predicted models values using the suitable coefficients fatigue factors established from $N_{f50\%}$ criterion based on the structure level point of view (top: the general model, and down: the statistical model)

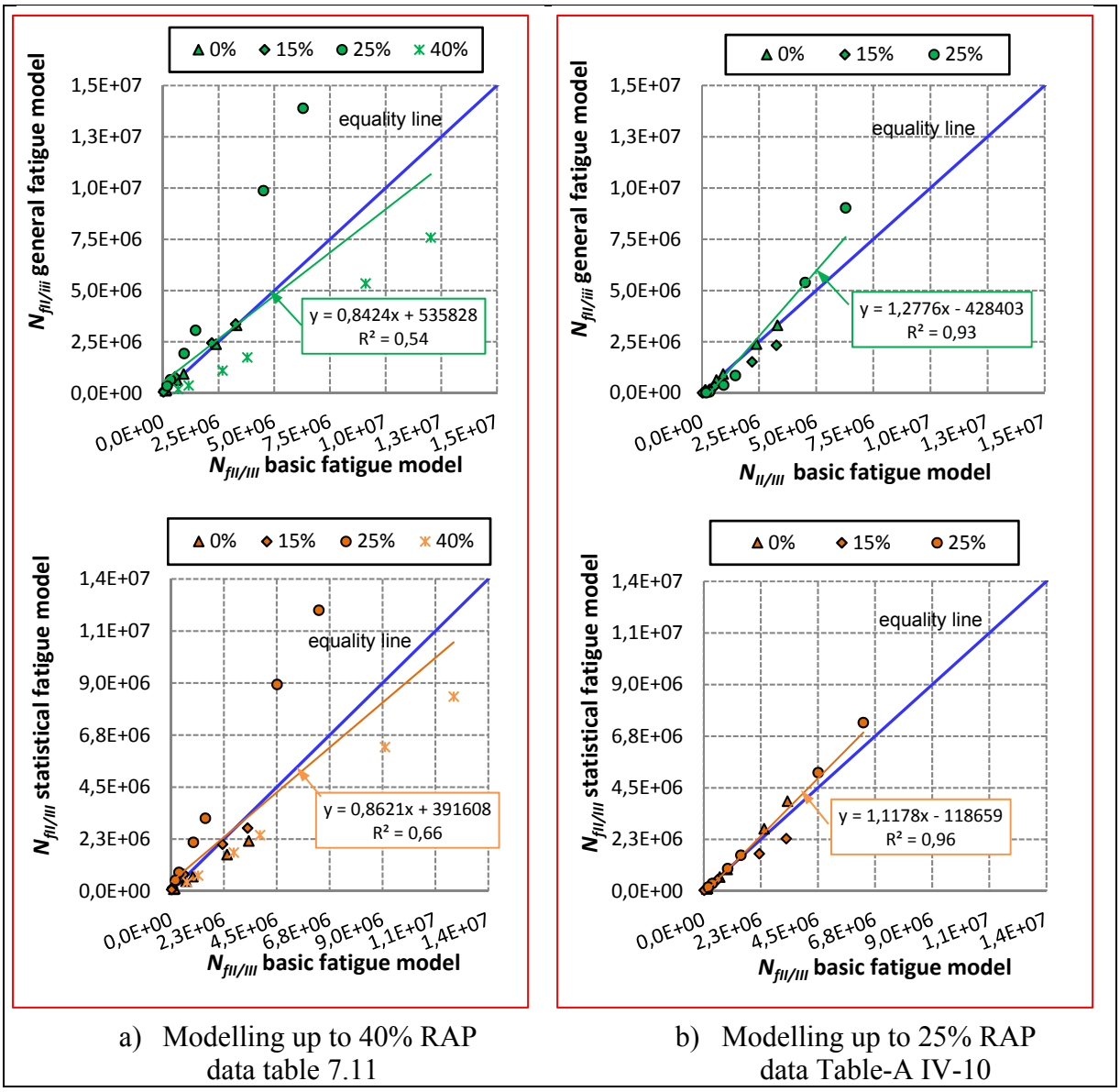

a) Modelling up to 40% RAP data table 7.11

b) Modelling up to 25% RAP data Table-A IV-10

Figure 7.17 Basic predicted model values versus the new predicted models values using the suitable coefficients fatigue factors established from $N_{fII/III}$ criterion based on the structure level point of view (top: the general model, and down: the statistical model)

The relationship between the $N_{f50\%}^{0/40}$ basic fatigue model values versus the $N_{f50\%}^{0/40}$ general fatigue model values show poor goodness-of fit statistics (R^2 = 0,36), and the R^2 value obtained from the relationship between the $N_{f50\%}^{0/40}$ basic fatigue model values versus the $N_{f50\%}^{0/40}$ statistical fatigue model was also poor (R^2 = 0,34). It is noticed that the predicted

values for the 40% RAP mixture using the new models developed in this study are more scattered below the line of equality for most of our results especially in the case of the 40%RAP mixtures. However, the fatigue lives predicted using the new models are in some cases overestimated compared with the N_f prediction using the basic fatigue model. We are not concern about that because this overestimation can be corrected with a correction factor in the pavement design.

There is a large difference between the fatigue life predictions determined using different prediction models using the $N_{f50\%}$ criterion. This happened at some points of the 40% RAP mix, especially at 10°C, 10 Hz. The difference is probably due to that the fatigue life calculation applied at low level of strain (96 μm/m) compared to the strain level used in fatigue testing. We never use level of strain lower than 130 μm/m in our fatigue testing. It is not noticed at other temperature (25°C, 40°C) because the values of N_f are calculated at high-strain level. This was observed clearly for mixes made with the 25% and 40% RAP. For 25% RAP mixture, the lowest applied strain level in the fatigue testing was 115 μm/m and the lowest calculated value of strain was 84,7 μm/m. It means that the calculated strain may be outside of the strain range where the model has been developed.

On the other hand, if we look at the results for mixes containing up to 25% of RAP, it appears that the prediction has been getting better. There is a high correlation between the measured and the predicted fatigue life, very high value of R^2, as shown on the right-hand side of the Figures 7.16 and 7.17. Also, it does not show any problem to predict fatigue life for strain levels outside the range for which the modelling process was used. In general, these models work well and are applicable for different strain levels.

The most interesting results of our studies about this part are that at the structure level the fatigue life is not only affected by the percentage of RAP, but also affected by the modulus of the mixes. Even that, we found that the new models for fatigue work and the predicted number of repetitions is not so far from making predictions using the basic fatigue model. We keep in mind that, in some cases, there could be some existing exception and as we have

discussed before. And we know that there are some assumptions behind the calculation of the N_f predictions especially that the k_3 factor is defined by slope/2. This big assumption can have a big effect on the predictions.

7.5.2 Comparisons between the predicted pavement fatigue lives (structure level) and the predicted fatigue lives of recycled asphalt mixtures (material level)

In order to compare the fatigue behaviour of all test materials, we can also use ε_6 or use a specific strain. First, we have the material level. It means that we compare the N_f prediction based on our lab testing results. In this case, the strain at the bottom of the asphalt concrete layer which made of the virgin mix is selected to be used in the calculations (ε = 97,7 μm/m).

This level of strain is close to the calculated strain levels determined at the bottom of other HMA layers made of 15% RAP mixture or 40% RAP mixture except for the layer made of the mixture of 25% of RAP. The calculated strains at the bottom of HMA layer of different asphalt pavements made of different recycled asphalt mixtures are used for the N_f predictions at the structure level.

We will continue considering the two steps presented previously. Again, the first step will be to consider the modelling of data for mixes containing up to 40% RAP. In the second step, we will consider the one for up to 25% RAP mixes. The results with respect to modelling for up to 40% RAP are always plotted on the left side of the figure and the other one is shown on the right side of the figure.

For the first step, the syntheses of the calculated values for the comparisons of the various mixtures are summarized in Table 7.13 and Table 7.14 for the two criteria. Figure 7.18 (a_1 to a_3) shows the number of load repetitions relative to the 0% RAP mix.

Table 7.13 Comparison between the estimated fatigue life values determined based on the structure level at 10°C – 10Hz and based on the material level determined at an equivalent deformation ε_t = 97,7 µm/m determined according to the $N_{f50\%}$ using the basic model (modelling up to 40%)

The mix	$N_{f50\%-calculated}$ *(cycles)*					
	Material level: (constant strain: ε_t)			**Structure level: (constant bituminous thickness)**		
	Basic model	**General predicted model**	**Statistical model**	**Basic model**	**General predicted model**	**Statistical model**
	By considering the coefficients $k_1^{\%RAP}$ and $k_2^{\%RAP}$ established from $N_{f50\%}$ (at strain = 97,7 µm/m	By considering the coefficients k_1^0, k_2^0, $k_4^{0/40}$, and universal value of $A^{0/40}$ established from $N_{f50\%}$ (at strain = 97,7 µm/m)	By considering the universal statistical fatigue coefficients $k_1^{0/40}$ and $k_2^{0/40}$ established from $N_{f50\%}$ (at strain = 97,7 µm/m	By considering the coefficients $k_1^{\%RAP}$ and $k_2^{\%RAP}$ established from $N_{f50\%}$ and used Alizé deformation resulted at 10°C – 10Hz (Table 7.10)	By considering the coefficients k_1^0, k_2^0, $k_4^{0/40}$, and universal value of $A^{0/40}$ established from $N_{f50\%}$ and used Alizé deformation resulted At 10°C – 10Hz (Table 7.10)	By considering the universal statistical fatigue coefficients $k_1^{0/40}$ and $k_2^{0/40}$ and the $SF^{0/40}$ established from $N_{f50\%}$ and used Alizé deformation resulted at 10°C – 10Hz (Table 7.10)
0 % RAP	3 659 026 (at strain = 97,7 µm/m)	3 659 026 (at strain = 97,7 µm/m)	3 515 512 (at strain = 97,7 µm/m	3 659 026 (at strain = 97,7 µm/m)	3 659 026 (at strain = 97,7 µm/m)	3 515 512 (at strain = 97,7 µm/m)
15% RAP	4 494 014 (at strain = 97,7 µm/m)	5 354 489 (at strain = 97,7 µm/m)	4 470 986 (at strain = 97,7 µm/m)	3 261 215 (at strain = 101,2 µm/m)	4 014 162 (at strain = 101,2 µm/m)	3 358 237 (at strain = 101,2 µm/m)
25% RAP	2 513 446 (at strain = 97,7 µm/m	6 901 653 (at strain = 97,7 µm/m)	5 248 233 (at strain = 97,7 µm/m)	7 704 143 (at strain = 84,8 µm/m)	24 004 657 (at strain = 84,8 µm/m)	16 598 435 (at strain = 84,8 µm/m)
40% RAP	20 450 180 (at strain = 97,7 µm/m)	10 099 635 (at strain = 97,7 µm/m)	6 674 640 (at strain = 97,7 µm/m)	24 348 547 (at strain = 96 µm/m)	11 980 238 (at strain = 96 µm/m)	7 698 642 (at strain = 96 µm/m)

Table 7.14 Comparison between the estimated fatigue life values determined based on the structure level at 10°C – 10Hz and based on the material level determined at an equivalent deformation ε_t = 97,7 µm/m determined according to the $N_{fII/III}$ using the basic model (modelling up to 40%)

The mix	$N_{fII/III-calculated}$ *(cycles)*					
	Material level: (constant strain: ε_t)			**Structure level: (constant bituminous thickness)**		
	Basic model	**General predicted model**	**Statistical model**	**Basic model**	**General predicted model**	**Statistical model**
	By considering the coefficients $k_1^{\%RAP}$ and $k_2^{\%RAP}$ established from $N_{fII/III}$ (at strain = 97,7 µm/m)	By considering the coefficients k_1^0, k_2^0, $k_4^{0/40}$, and universal value of $A^{0/40}$ established from $N_{fII/III}$ (at strain = 97,7 µm/m)	By considering the universal statistical fatigue coefficients $k_1^{0/40}$, $k_2^{0/40}$ and the $SF^{0/40}$ established from $N_{fII/III}$ (at strain = 97,7 µm/m)	By considering the coefficients $k_1^{\%RAP}$ and $k_2^{\%RAP}$ established from $N_{fII/III}$ and used Alizé deformation resulted at 10°C – 10Hz (Table 7.10)	By considering the coefficients k_1^0, k_2^0, $k_4^{0/40}$, and universal value of $A^{0/40}$ established from $N_{fII/III}$ and used Alizé deformation resulted At 10°C – 10Hz (Table 7.10)	By considering the universal statistical fatigue coefficients $k_1^{0/40}$, $k_2^{0/40}$ and the $SF^{0/40}$ established from $N_{fII/III}$ and used Alizé deformation resulted at 10°C – 10Hz (Table 7.10)
0% RAP	3306156 (at strain = 97,7 µm/m	3306156 (at strain = 97,7 µm/m)	2171403 (at strain = 97,7 µm/m)	3306156 (at strain = 97,7 µm/m)	3306156 (at strain = 97,7 µm/m)	2171403 (at strain = 97,7 µm/m)
15% RAP	4474360 (at strain = 97,7 µm/m)	4308326 (at strain = 97,7 µm/m)	3453321 (at strain = 97,7 µm/m)	3260696 (at strain = 101,2 µm/m)	3372536 (at strain = 101,2 µm/m)	2727911 (at strain = 101,2 µm/m)
25% RAP	2255847 (at strain = 97,7 µm/m)	5140027 (at strain = 97,7 µm/m)	4705090 (at strain = 97,7 µm/m)	6288692 (at strain = 84,8 µm/m	13894411 (at strain = 84,8 µm/m)	12149910 (at strain = 84,8 µm/m)
40% RAP	10783529 (at strain = 97,7 µm/m)	6698086 (at strain = 97,7 µm/m)	7482806 (at strain = 97,7 µm/m)	12027574 (at strain = 96 µm/m)	7589774 (at strain = 96 µm/m	8416592 (at strain = 96 µm/m)

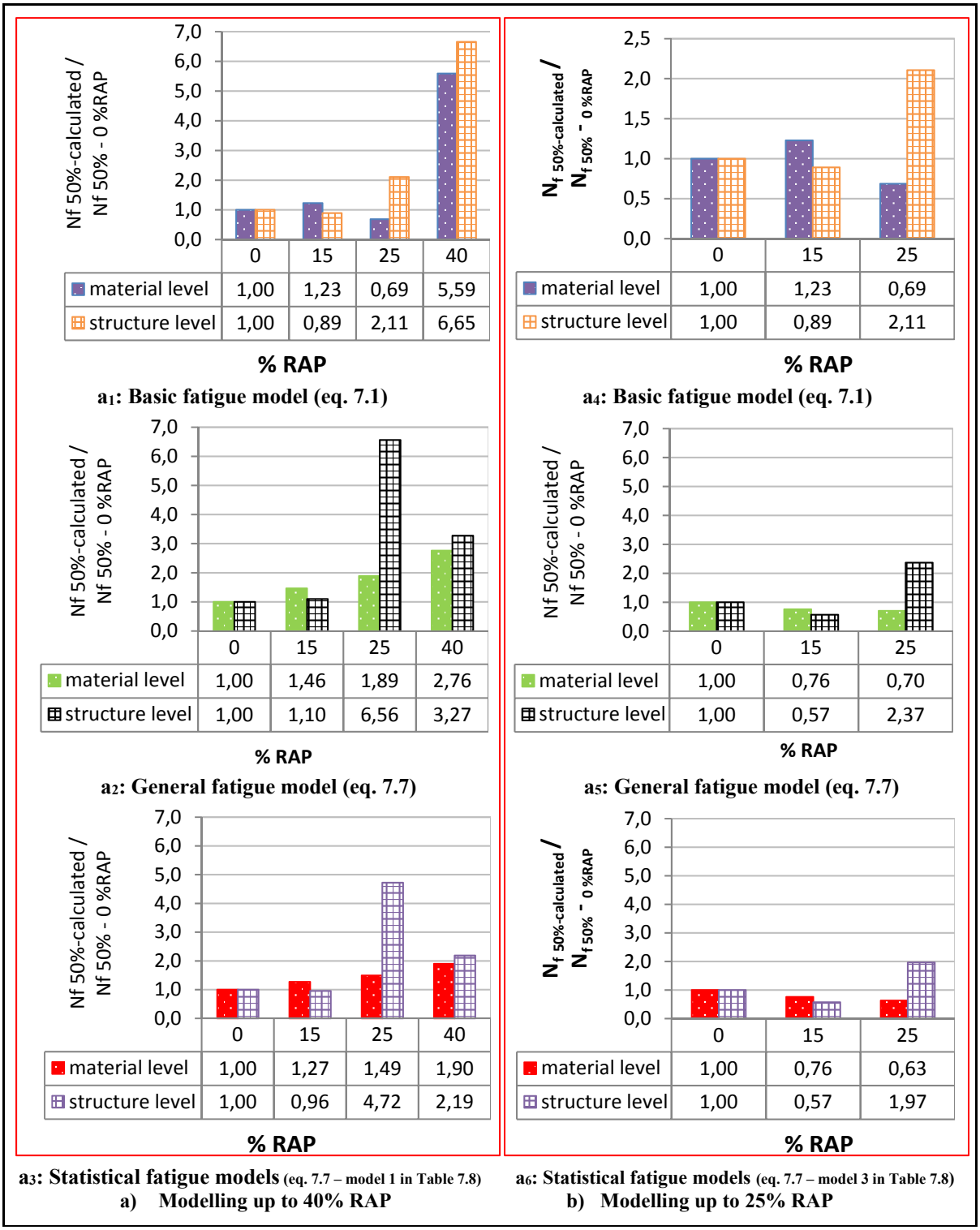

Figure 7.18 $N_{f\text{-}calculated}$ relative to $N_{f\text{-}0\%RAP}$ determined based on the material level and the structure level at 10°C and 10 Hz according to the $N_{f50\%}$ using the basic model and the general model

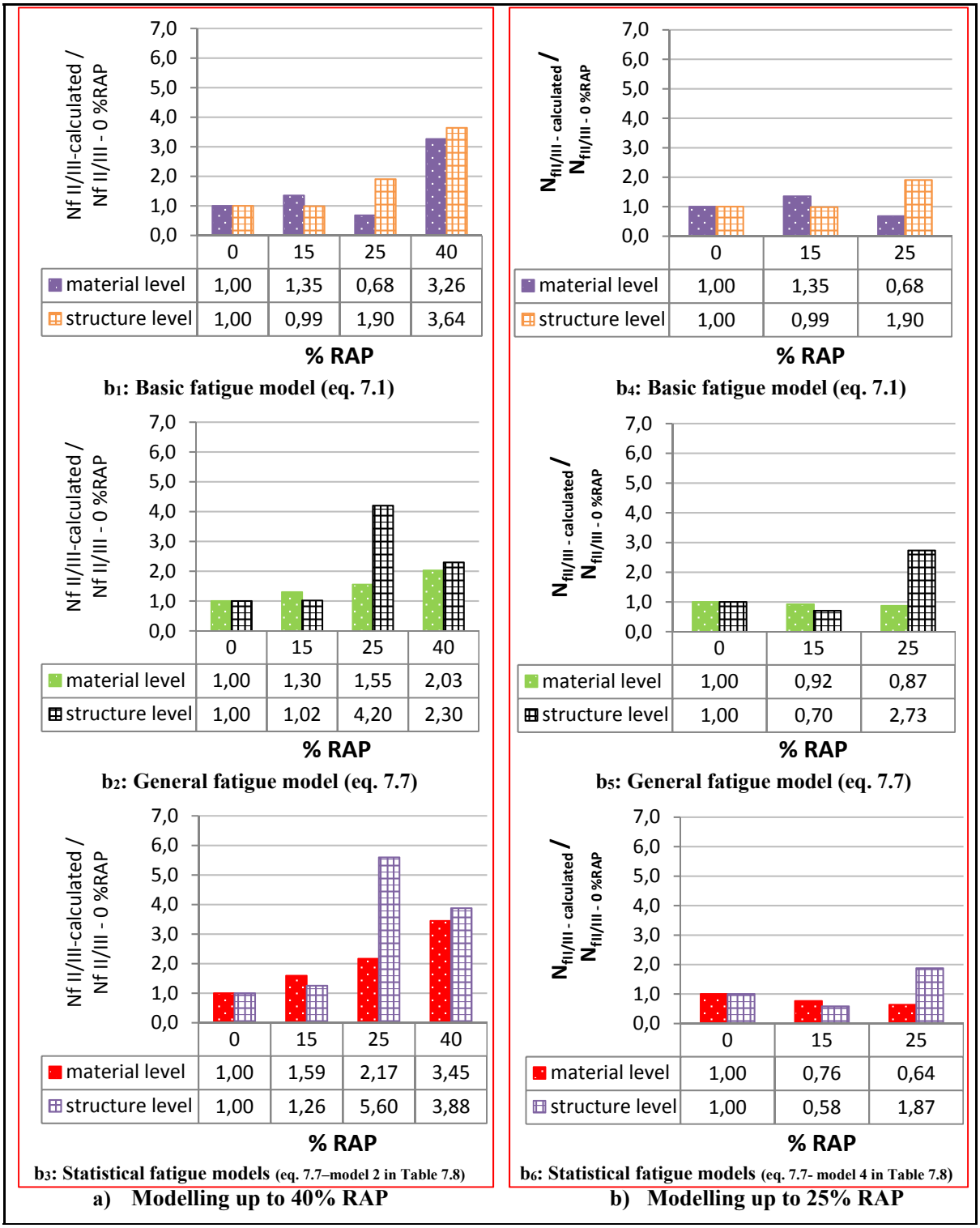

Figure 7.19 $N_{f\text{-}calculated}$ relative to $N_{f\text{-}0\%RAP}$ determined based on the material level and the structure level at 10°C and 10 Hz according to the $N_{fII/III}$ using the basic model and the general model

As shown in Figure 7.18a, it was found that the ratios of $N_{f50\%-calculated}/N_{f50\%-0\%\,RAP}$ for the mixes based on the material level and the structure level show little differences between models except when $N_{f-calculated}$ of 25% RAP mixture is used. Comparison of $N_{fII/III}$ ratios among the models shows similar results (Figure 7.19a). With both criterions, the general trends which are obtained in the basic model are: the 15% RAP mix and the 25% RAP mix exhibit number of load repetitions which are relatively close to the virgin mix, followed by the 40% RAP mix which show better fatigue resistance than the 0% RAP mixture. These trends were based on the two criteria.

When using modelling up to 40% RAP, we can see that fatigue analysis for the 25% RAP mix gives different performance especially if we use the new fatigue models at the two levels: material and structure (general fatigue model and statistical model). This is done because N_f is here calculated based on the material level on the selected strain level (ε = 97,7 μm/m) and on 84,8 μm/m at structure level. We should exclude it from our comparison because the two values are not close. Moreover, it is well known that level of the strain will significantly affect the fatigue life. We note that we keep the thickness of the asphalt mix layer constant and we know strain is dictated by the thickness and stiffness of the asphalt mix layer. However, at 10°C, we did the comparison without considering the E-modulus of the mix layer which could express the difference in the strain values of 25% and 0% RAP mix layers. Based on that, we are not able to dilute the difference regarding the strain values of the two mix layers.

First, according to the basic model (Figure 7.18a_1 and 7.19b_1), at the material level, the numbers of load repetitions to fatigue failure of the 15% RAP mix were about 1,23 and 1,35 times higher than the number of load repetitions to fatigue failure of the control mixture for $N_{f50\%}$ criterion and $N_{fII/III}$ criterion, respectively. On the other hand, at the structure level, the numbers of load repetitions to fatigue failure of the 15% RAP mix represent 0,89 and 0,99 times the number of load repetitions to fatigue failure of the control mixture for $N_{f50\%}$ criterion and $N_{fII/III}$ criterion, respectively. This means that from a purely material

point of view, mixes with 15% RAP perform better than virgin mix in fatigue, but in the pavement, mixes with 15% RAP perform worse than the reference mix.

For $N_{f50\%}$ criterion and $N_{fII/III}$ criterion, the ratios of the numbers of load repetitions to fatigue failure to the number of load repetitions to fatigue failure of the mixture with 40% RAP are relatively the same for the analysis done at material and structure levels. For both analyses the incorporation of RAP into HMA mixtures improves significantly the fatigue performance of the bituminous structure.

For the 25% RAP mixture, the same trend is observed with the basic model as noted for the two levels. There is a difference between the two levels with two new models. Overall, the incorporation of RAP in HMA resulted in little or high improvement to fatigue resistance of materials and structures. It's all because of the stiffness of each mix.

The same comparisons conducted between the mixes using the statistical fatigue models results reveal almost results that are close to what we obtained using the general model presented above. We almost have the same trend for $N_{fII/III}$ as shown with the results of $N_{f50\%}$ fatigue prediction.

Figure 7.18b (a_4 to a_6) shows the results of the second step (the number of load repetitions relative to the 0% RAP mix) and the syntheses of their calculated values for the comparisons of the various mixtures are summarized in Appendix IV in Table-A IV-11 and Table-A IV-12 for the two criteria.

Figure 7.18b shows that the ratios calculated from the new models have become more closely to the one from the basic model at the two levels. So by doing these two steps in our analysis we can show again that the model designed to account for up to 25% would highly improve the predictions. It means we can now make these predictions even better - to show us more information about the fatigue behaviour on the two levels. Figure 7.19b has shown the same trend as the $N_{f50\%}$ criterion for a model doing for up to 25% RAP.

In summary, when we compare the four mixtures, we found that the 40% RAP mix performed the best against fatigue failure at the material and the structure levels and followed by the 15% RAP mix and the 25% RAP mix. However, it is interesting to note that all four mixtures are expected to perform well in fatigue since all four mixes exhibited a high number of cycles to fatigue failure in reference to the virgin mixture. Mixes with 40% RAP perform better than the virgin mix in fatigue in both a purely material and structure point of view. Again, this could be explained by their better stiffness.

Finally, it is interesting to see that the addition of high RAP contents can lead to improved fatigue resistance of the pavement structure. When RAP was added at 15% and 25% to the mixture, the fatigue resistance of RAP mixtures were very close to those of the virgin mixture, just like in the material level.

Making fatigue models that do account for up to 25% RAP gives good predictions results for fatigue analysis at the material and at the structure levels.

7.6 Chapter conclusion

Based on the data analysis presented in this chapter, the following conclusions can be made:

- In opposition to the information found in the literature review where the fatigue slopes are kept constant and a simple shift factor for k_1 can be used for the fatigue line represented in the system of axes log (N_f) vs log(ε_0), we found that it is not possible to simply assume constant fatigue line slope; we have to consider changes in the slope of the fatigue line for the recycled mixtures;

- The new modified fatigue model (the general fatigue model) that do account for mixes contain up to 25% RAP is able to predict the fatigue life of these mixes with a high degree of precision. A simple way for modifying the existing fatigue model was

introduced using the phenomenological approach with good results. The recommended general fatigue model is:

$$N_f^{0/25} = k_{1,\theta_{test}}^0 \times (\varepsilon_t)^{-(1+A^{0/25}\times\%RAP)k_2^0} \times SF^{0/25}$$

$$\text{Where } SF^{0/25} = 10^{-k_4^{0/25}}$$

- The best modelling is obtained when considering mixtures incorporating recycled asphalt pavement (RAP) for up to 25 percent of RAP.

- The ranking in mixtures at the structure level was more or less the same to the one at the material level;

- Our new modified model predicts the fatigue life of our HMA mixtures containing RAP from a single source. This model cannot be used to predict the fatigue life for every asphalt mixture containing RAP without a proper verification and calibration.

SUMMARY AND CONCLUSION

This Ph.D. dissertation focuses on the use of complex modulus and fatigue testing to investigate reclaimed asphalt pavement (RAP) effect on hot-mix and to compare these properties with those of the virgin mixture. Cyclic tension/compression (T/C) test on cylindrical specimen developed at the DGCB laboratory of ENTPE was used. The data obtained from fatigue laboratory testing program were extended by the use of phenomenological and statistical approaches to predict fatigue life of recycled mixtures for materials. This study presents the attempts done to modify the basic fatigue model as defined by Wöhler curve by applying shift factors. For this, the determination of the fatigue calibration parameters for three selected recycled mixtures that were studied in this study. The modified fatigue models were used to provide predictions of the fatigue life for also one typical pavement section through the recycled mix used in it.

For the evaluation of the mixes stiffness, a total of 11 HMA mixtures were mixed, compacted, tested and analysed in this study. Those mixtures including one RAP source, four different RAP content percentages (0%, 15%, 25%, and 40%), two different asphalt binders (PG 64-28 and PG 58-34), two RAP additions (cold or hot), and/or two RAP processes (Unaged or Aged) were also part of our experimental program. Complex Young's modulus repeatability study was conducted to demonstrate the effect of the variability of the HMA samples (data of one mix) on the complex modulus results. The effects of the addition of RAP, asphalt binder grade, aging, and the prior conditioning of the RAP have been analyzed. Some curves and parameters were used for the investigation, here summarized as master curves for the norm of E*, shift factors a_T, and normalized Cole-Cole (or Black) curve. RAP coefficient evolution ($\left|C^*_{RCE}\right|$) was also used to quantify the effect of RAP on HMA. A rheological model (2S2P1D) developed at the ENTPE/DGCB laboratory was used to simulate the experimental results for all materials.

The laboratory test program in this study included complex modulus (|E*|) testing under controlled strain on a large range of temperatures (from -35°C to 35°C) and frequencies (0,01

Hz to 20 Hz). The following conclusions were drawn from the measurements of stiffness mixtures:

- The 2S2P1D model can correctly model the behaviour of (LVE) of recycled asphalt mixtures over a wide range of temperatures and frequencies. It was found to fit favorably to experimental results;

- Overall, cold added RAP (room temperature) at up to 40% to the hot-mix had little effect on asphalt mixture complex modulus on a large range of frequency whatever the RAP content. The complex modulus master curves constructed at 10°C using experimental results show the ranking of the asphalt mixtures containing RAP as follow: The virgin mixture (0% RAP) , 15% RAP specimen, 25% RAP specimen and 40% RAP specimens have similar complex modulus behaviour. No significant change in stiffness at high temperature and/or low frequency. But, at high testing frequency or low temperature, a difference is notable. It seems that the mixes can be ranked by stiffness starting with 15% RAP mix as the lowest, then followed by the virgin mix, the 40% RAP mix, and the 25% RAP mix as the stiffest;

- At lower temperatures, the ranking of mixtures mixed with adding hot RAP (microwave condition using up to 110°C) was as follow: the mixture containing 40% RAP were the stiffest followed by the mixture containing 25% RAP. The complex modulus of the mixture containing 15% RAP was similar to the virgin mixture. The ranking here was a bit different as compared to the RAP Cold addition process. Based on the laboratory test results conducted on the RAP adding conditions, the following were also drawn:

    - When the hot RAP was added to the mixture, there were no significant difference noted when compared to the control mixture for 15, 25, and 40% RAP;
    - The effect of RAP conditioning is rather small; The modulus difference between mixtures made with RAP added cold and RAP added hot is low over a wide range of frequencies when the RAP concentrations are 15% or 25% or even 40%;

- However, we did not find significant difference between these two added conditions of RAP into HMA mixes with Cold and Hot RAP addition, we cannot recommend one method of conditioning over another since each method has its advantage and disadvantages. But we could say that we would go to select or choose heating RAP in a microwave if we can get some larger microwaves in our laboratory that are big enough to accommodate large amounts of RAP materials.

- The asphalt binder grade was found to have some effects on the stiffness of the resulting asphalt mixture but it was not greatly; the mixtures containing PG 64-28 had slightly greater complex modulus values than those made with PG 58-34 at high temperature and low frequency;

- From the results conducted to evaluate the effect of added RAP that artificially aged in the laboratory, it could be said that adding the RAP samples in cold condition after it was long term oven aged for 3 months at 55°C into the HMA effectively increases the modulus of the mixtures. For example, the addition of 40% aged RAP to the HMA containing PG 64-28 caused 40% increase in the stiffness ($|C^*_{RCE}|$) compared with the addition of 40% unaged RAP to the same mixture;

- Repetitions of the complex Young's modulus was investigated on some selected RAP mixes. Based on the values of $|C^*_{VCE}|$, we concluded that the repetitions between two samples are quite good. They are suited within a range of 10%. In some cases, the modulus ratio ($|C^*_{VCE}|$) difference could reach to 40% only at low frequency and/or at high temperature. It is likely that a combination of variables is influencing the material behaviour of these specimens in that range of measurement. The repeatability of the complex modulus was quite good. Data from stiffness at high temperatures indicated coefficient of variation from 1,5 – 29,9%. Based on that it is concluded that:

- There were no major differences between samples of the same mix with the exception of the results achieving at lower frequency (high temperature). This is probably related to the heterogeneity among tested samples or due to precision measurement equipment itself. However, we consider those differences as not significant (not large) because the modulus values ($|E^*|$) are very low;

- It is interesting to see in the repeatability complex modulus study that the values of the true $|C^*_{VCE}|$ calculated from the experimental data follow the same trend of the $|C^*_{VCE}|$ calculated from 2S2P1D data. For most of cases, the two values are identical. In some cases, the difference between them could be few percentages. This happens because we achieve best fit for our data using the modelling and the probability of getting errors in the results due to modelling calibration process is also low.

The fatigue behaviour of four recycled mixtures out of the total 11 mixtures was studied. These specific mixtures containing different percentages of RAP and mixed with adding RAP in cold condition and the PG 64-28 virgin binder. This study exploits the advantage of a homogeneous fatigue test, namely the tension/compression test on a cylindrical specimen and performed under strain controlled.

In order to determine the fatigue life of the tested samples, two criteria were studied; criterion $N_{f50\%}$ and criterion of end of phase II/III ($N_{fII/III}$) as defined in sections 2.7.4.1-2.7.4.2. Results indicated that the inclusion of less than 25% of RAP in HMA had only very limited influence in the fatigue performance of the mix. The inclusion of 40% of RAP in the HMA mixtures in this study intended to improve its resistance to fatigue.

The method developed at the laboratory DGCB of ENTPE was used to analyse the data obtained from the fatigue test results employed in this study. The purpose of this method is to take into account bias effects (heating and thixotropy) occurring mainly (but not only) during phase I to determine the 'true' ratio of fatigue evolution of the modulus with numbers of applied cycles within given intervals. From this method the criteria; damage associated with

the transition between phase II to III and linked to the start of the spread of a macro-crack leading to failure could be corrected from the bias effect to obtain the intrinsic critical damage to the material. A constant intrinsic damage at failure (D_{IIIc}) was obtained for each tested material. D_{IIIc} values were found to be within the range of values found in the literature. Based on this intrinsic damage at failure, an innovative method of prediction could be used for mixtures containing 0%, 15%, 25%, and 40% RAP to determine the number of cycles at failure considering only the first 300 000 cycles.

It was shown that D_{IIIc} value decreases with the increase in air void content in asphalt mixture. Indeed, voids in the material can be considered as specific damage to the materials which results in a lower intrinsic damage (corrected) leading to asphalt mixture failure.

This study was the first to modify the basic fatigue model to take into account the incorporation of RAP in the HMA mix. Two different approaches are used for this purpose. First, it is done using the phenomenological approach and then after that using a statistical approach which provided the best fit to the experimental data of fatigue test results. The primary advantage of our first approach is that we only need to conduct fatigue tests in the laboratory for the control mix. Note that the attempts were made to find availability for fatigue model modification to take into account up to a high RAP content of up to 40 percent and/or to use up to 25 percent RAP by total weight in hot mix asphalt.

In opposition to the information found in the reviews of the literature where the fatigue slopes are kept constant and a simple shift factor for k_1 can be used for the fatigue line represented in the system of axes log (N_f) vs log(ε_0), we found that it is not possible to do it. Our results show that by only shifting the fatigue lines in the y-axis direction (log (N_f)) and keeping the slope the same, there is a huge difference between a measurement and the prediction of fatigue life. It means that keeping the slope constant is not a good way to make good predictions using the models. Therefore, it is better to consider slopes as a function of the RAP content in the modelling of fatigue cracking of recycled asphalt mixtures. The basic model was updated by introducing a dimensionless parameter (A) that acting on the slope

combined to the shift factor as a function of k_4 and acting on k_1 and we found that it has a major effect on the fatigue life predictions. The general fatigue model shows lower prediction accuracy than the basic fatigue model when using the fatigue parameters of the virgin mix (k_1 and k_2) and also by using the new parameters "A" and "k_4" that added to a basic fatigue model especially when it is used for N_f predictions for asphalt mixtures containing very high amount of RAP (at up to 40%).

The best modelling is obtained when considering mixtures incorporating recycled asphalt pavement (RAP) for up to 25 percent of RAP with using the specific values of A and k_4 in the formula as constant.

The main conclusions to be drawn as related to the study of the modification of the basic fatigue model are that:

- The basic fatigue model available in the literature produced a good fit for the RAP mixes individually but we still need to perform fatigue tests for each mix. By applying shift factors to this model a significant modification was achieved in order to predict the fatigue life of RAP mixes containing up to 25%.

- The new modified fatigue model (the general fatigue model) can be used as a surrogate model to predict the fatigue life of RAP mixes up to 25% with a high degree of precision. A simple way for modifying the existing fatigue model was introduced using the phenomenological approach with good results. The recommended general fatigue model is:

$$N_f^{0/25} = k_{1,\theta_{test}}^0 \times (\varepsilon_t)^{-\left(1+A^{0/25}\times\%RAP\right)k_2^0} \times SF^{0/25}$$

$$\text{Where } SF^{0/25} = 10^{-k_4^{0/25}}$$

$R^2 = 0{,}85$; $S_e/S_y \simeq 0{,}38$ (for the $N_{f50\%}$ criteria and the $N_{fII/III}$ criteria)

- When the RAP mix was used for surface layer of a reference pavement, there were no great differences noted between RAP mixes and virgin mixture in terms of fatigue resistance. The results revealed that the 40% RAP mix becomes more resistant to fatigue cracking compared to the virgin mixture while the addition of 15% and 25% RAP resulted in a slight increase or decrease in fatigue life. It is almost what happened at the material level. Generally, it can be said that the ranking in mixtures was more or less the same to the one at the material level by considering double action of stiffness and fatigue variation by adding RAP in the fatigue analysis of the structure level.

- The newly models designed to account up to 25% of RAP would be able to predict fatigue life for an asphalt pavement subjected to dual axle tire loadings by considering the change in the stiffness of the mixture with changing RAP content.

- Our new modified model defines the fatigue failure of our HMA mixtures containing RAP using a given RAP source. However, more tests are needed to verify the applicability of this model to mixes made with other sources of RAP.

Finally, more tests with a different RAP source is recommend in order to validate the models and the factors established here. Therefore, we can say that the fatigue performance of recycled asphalt mixtures is difficult to predict not only because many of the input parameters needed for the analysis are difficult to obtain but also because the fatigue phenomenon itself is not well understood.

APPENDIX I

CHARACTERIZATION OF RAP PROPERTIES AND FORMULATION OF RECYCLED MIXTURES

Table-A I-1 Detailed results for the tests (with taking into account correction factor)

RAP ignition asphalt content		
Place: Lab ETS	Date sampled Mai 26. 2010	Date tested Mai 27. 2010
No of samples: 3	Time sampled: 45 min	

Ignition data

		Sample 1	Sample 2	Sample 3
A. WT. of ignition basket @ room temperature	g	3090,6	3098,9	3099,3
B. WT. of dry RAP material+ ignition basket@ room temperature	g	4228,7	4182,3	4057,1
C. Dry WT. of RAP material	g	1138,8	1083,8	957,5
D. Dry WT. of RAP material without the fine aggregates before ignition-$\mathbf{m_i}$	g	1133,1	1078,4	952,7
E. WT. of dry RAP material+ basket from ignition	g	4178,4	4134,3	4014
F. WT. of dry RAP sample from ignition $\mathbf{m_f}$	g	1087,9	1035,5	914,7
G. WT. of asphalt ($m_i - m_f$)	g	45,21	42,9	38,0
H. RAP asphalt content non corrected ($\frac{m_i - m_f}{m_i}$ x 100)	%	3,99	3,98	3,99
I. RAP asphalt content corrected [($\frac{m_i - m_f}{m_i}$ x 100 + Correction factor)] Correction factor = -0,09 (LC 26-150) [see Table I.3]	%	3,9	3,89	3,9
Time stated	h-min	12:55	2:48	4:30
Time completed	h-min	1:40	3:37	5:15
Ignition time	h-min	0:45	0:45	0:45

The difference between the tests' replicates

Sample Number	RAP asphalt content %
Difference between 1 & 2	0,01
Difference between 1 & 3	0,00
Difference between 2 & 3	0,01
Averages	3,9
Std. Deviation	0,0050
Maximum acceptable Difference between 3 tests (LC 26-006)	0,13
Maximum acceptable Std. Deviation (LC 26-006)	0,04%

Table-A I-2 Detailed results for determining the correction factor of lost fine aggregates of EB–10s

RAP fine aggregate content		
Place: Lab ETS	Date sampled July 22. 2010	Date tested july 22. 2010
No of samples: 3	Time sampled: 45 min	

Ignition data

			Sample 1	Sample 2
A	WT. of ignition basket @ room temperature	g	3089,8	3090,0
B	WT. of dry sample + ignition basket@ room temperature	g	4189,5	4190,4
C	Dry WT. of sample [B - A]	g	1099,7	1100,4
D	WT. of dry sample + basket from ignition	g	4184,4	4184,5
E	WT. of dry sample from ignition	g	1094,6	1094,47
F	WT. of fine aggregates lost [B - D]	g	5,1	5,93
G	WT. of fine aggregates lost [F / C x100]	%	0,464	0,539
	Time stated	h-min	11 AM	11:45 AM
	Time completed	h-min	12 AM	12 :45 AM
	Ignition time	h-min	1:00 PM	1 :45 PM

The difference between the tests' replicates

Sample Number	RAP fine aggregate content %
Difference between 1 & 2	0,075
Averages	0,502
Std. Deviation	0,0375
Maximum acceptable Difference between 3 tests (LC 26-006)	0,13
Maximum acceptable Std. Deviation (LC 26-006)	0,04%

Table-A I-3 Detailed results for determining the correction factor of the percentage of binder of EB–10s

RAP ignition asphalt content		
Place: Lab ETS	Date sampled July 22. 2010	Date tested July 22. 2010
No of samples: 3	Time sampled: 45 min	

Ignition data

		Sample 1	Sample 2
A. WT. of ignition basket @ room temperature	g	3102,4	2089,3
B. WT. of dry sample + ignition basket@ room temperature	g	4159,2	4174,9
C. Dry WT. of sample	g	1056,8	1085,6
D. Dry WT. of sample without the fine aggregates before ignition $\mathbf{m_i}$	g	1052,2	1080,9
E. WT. of the dry sample + basket from ignition	g	4111,1	4126,4
F. WT. of dry sample from ignition $\mathbf{m_f}$	g	1008,7	1037,1
G. WT. of asphalt ($m_i - m_f$)	g	43,5	43,8
H. Sample asphalt content non corrected $\mathbf{B_o}$ ($B_o = \frac{m_i - m_f}{m_i}$ x 100)	%	4,13	4,05
H. Average asphalt content non corrected $\mathbf{B_o moy}$	%	4,09	
H. Correction factor (b - $B_o$moy) b: Sample asphalt content = 4 %	g	-0,09	
I. Sample asphalt content corrected **B** [(B = $\frac{m_i - m_f}{m_i}$ x 100 + Correction factor)	%	4,04	3,96
Time stated	h-min	3:00 PM	3:45 PM
Time completed	h-min	4:00 PM	5:45 PM
Ignition time	h-min	6:00 PM	6:45 PM

The difference between the tests' replicates

Sample Number	RAP asphalt content %
1 & 2	0,08
Averages	4%
Std. Deviation	0,04
Maximum acceptable Difference between 3 tests (LC 26-006)	0,13
Maximum acceptable Std. Deviation (LC 26-006)	0,04%

Table-A I-4 Detailed results for the extraction using solvent tests of the RAP

Volume of balloon and specific gravity of trichloroethylene

		Sample 1	Sample 2	
A.	Mass balloon + stopper + water	1362,4	1368,8	g
B.	Mass of balloon + stopper	292,8	300,1	g
C.	Volume of balloon not corrected (A-B)	1069,6	1068,7	cm^3
D.	Volume of balloon corrected (C x αeau)	1072,77	1071,08	cm^3
E.	Mass of balloon + stopper + trichlo	1855,5	1863,1	g
F.	Mass of balloon + stopper	292,8	300,1	g
G.	Mass of trichloroethylene (E-F)	1562,7	1563	g
H.	Specific gravity of trichloroethylene (G/D)	1,457	1,459	g/cm^3
I.	Temperature of trichloroethylene	25,2	23,7	C°
J.	Temperature of water	25	22	C°

BEFORE EXTRACTION

	Sample 1	Sample 2	
Mass of bowl of extraction	973,5	973,5	g
Mass of filter ring	14,1	14	g
Masse du bowl + filtre ring + RAP mixture	2147,3	2093,6	g
Mass of RAP mixtures sample	1159,7	1106,1	g
AFTER EXTRACTION			
Mass of bowl + filter ring + aggregates	2087,4	2047,7	g
Mass of aggregate	1099,8	1060,2	g
Mass of aggregate + filler	1113,0	1064,4	g
Correction factor (LC 26-150) [see tables-A I-3]	-0,25		
% of asphalt binder (non corrected)	**4,03**	**3,78**	**%**
% of asphalt binder (corrected)	**3,78**	**3,53**	**%**
Average of % of asphalt binder (corrected)	**3,66**	**%**	

Table-A I-5 Calculation of the percentage of asphalt binder - Volumetric method for the RAP

Calculation of the percentage of asphalt binder - Volumetric method for the RAP				
		Sample 1	**Sample 2**	
A.	Masse of balloon + asphalt binder + filler + trichlo	1841,9	1847	g
B.	Mass of balloon (N°)	292,8	300,1	g
C.	Mass of asphalt binder + filler + trichlo (A - B)	1549,1	1546,9	g
D.	Mass of asphalt binder + filler (from extraction test)	59,9	45,9	g
E.	Mass of trichloroethylene(C - D)	1489,2	1501	cm^3
F.	Volume of balloon (N°)	1072,77	1071,08	cm^3
G.	Volume of trichloroethylene (E/MVt)	1022,10	1028,60	cm^3
H.	Volume of asphalt binder + filler (F - G)	50,67	42,49	
I.	Mass of asphalt binder K [(MVf x H) - D]	46,69	41,78	g
J.	Masse du filler (D - I)	13,21	4,12	g
K.	MVb MVf - MVb	0,6071429	0,607143	
L.	* MVb (Specific gravity of asphalt binder at 25°C	1,020	1,020	g/cm^3
M.	* MVf (Specific gravity of filler)	2,700	2,700	g/cm^3
N.	* MVt (Specific gravity of trichloroethylene)	1,457	1,459	g/cm^3
O.	Temperature of trichloroethylene	25,7	23,7	C°

Table-A I-6 Detailed results for the extraction using solvent tests for EB-10 using correction factor

Volume of balloon and specific gravity of trichloroethylene				
		Sample 1	**Sample 2**	
A.	Mass balloon + stopper + water	1363,4	1367,5	g
B.	Mass of balloon + stopper	293,5	300,1	g
C.	Volume of balloon not corrected (A-B)	1069,9	1067,4	cm^3
D.	Volume of balloon corrected (C x αeau)	1073,07	1070,56	cm^3
E.	Mass of balloon + stopper + trichlo	1857,6	1861,1	g
F.	Mass of balloon + stopper	293,5	300,1	g
G.	Mass of trichloroethylene (E-F)	1564,1	1561,5	g
H.	Specific gravity of trichloroethylene (G/D)	1,457	1,458	g/cm^3
I.	Temperature of trichloroethylene	23,8	23,8	C°
J.	Temperature of water	25	25	C°

BEFORE EXTRACTION			
	Sample 1	**Sample 2**	
Mass of bowl of extraction	973,1	815,4	g
Mass of filter ring	14,1	14	g
Masse du bowl + filtre ring + RAP mixture	2075,5	1907,7	g
Mass of RAP mixtures sample	1088,3	1078,3	g
AFTER EXTRACTION			
Mass of bowl + filter ring + aggregates	2020,9	1843,1	g
Mass of aggregate	1033,7	1013,7	g
Mass of aggregate + filler	1041,721	1032,773	g
Correction factor (LC 26-150) [see tables-A I-3]	-0,25		
% of asphalt binder	**4,28**	**4,22**	
Average of % of asphalt binder (non corrected)	**4,25**	**%**	
Average of % of asphalt binder (corrected)	**4,00**	**%**	

Table-A I-7 Calculation of the percentage of asphalt binder - Volumetric method for EB-10

Calculation of the percentage of asphalt binder - Volumetric method for EB-10				
		Sample 1	**Sample 2**	
A.	Masse of balloon + asphalt binder + filler + trichlo	1840,7	1850,2	g
B.	Mass of balloon (N°)	293,5	300,1	g
C.	Mass of asphalt binder + filler + trichlo (A - B)	1547,2	1550,1	g
D.	Mass of asphalt binder + filler (from extraction test)	54,6	64,6	g
E.	Mass of trichloroethylene(C - D)	1492,6	1485,5	cm³
F.	Volume of balloon (N°)	1073,07	1070,56	cm³
G.	Volume of trichloroethylene (E/MVt)	1024,43	1018,86	cm³
H.	Volume of asphalt binder + filler (F - G)	48,64	51,70	cm³
I.	Mass of asphalt binder K [(MVf x H) - D]	46,58	45,53	g
J.	Masse du filler (D - I)	8,02	19,07	g
K.	MVb			
L.	MVf - MVb	0,607143	0,607143	
M.	* MVb (Specific gravity of asphalt binder at 25°C	1,020	1,020	g/cm³
N.	* MVf (Specific gravity of filler)	2,700	2,700	g/cm³
O.	* MVt (Specific gravity of trichloroethylene)	1,457	1,458	g/cm³
P.	Temperature of trichloroethylene	23,8	23,7	C°

Table-A I-8 Calculation of the percentage of asphalt binder - Volumetric method for EB-10

Calculation of the percentage of asphalt binder - Volumetric method for EB-10				
		Sample 1	**Sample 2**	
A.	Masse of bowl (hot)	973,1	815,4	g
B.	Mass of bowl + aggregates	2017,9	1850,56	g
C.	Mass of aggregates (B-A)	1044,8	1035,16	g
D.	Mass of bowl + aggregates + binder (before mixing)	2061,4	1893,7	g
E.	Mass of asphalt binder (D-B)	43,5	43,13	g
F.	Mass of aggregates + asphalt binder (D-A)	1088,30	1078,3	g
G.	Mass of bowl + mixture (immediately after mixing)	2061,40	1893,7	g
H.	Mass of bowl + filter ring + mixture	2075,50	1907,7	g
I.	Mass of bowl + aggregates + filter (after extraction)	2020,90	1843,1	g
J.	Mass loss by washing (H-I)	54,60	64,60	g
K.	Mass of lost filler (volumetric method)	8,02	19,07	g
L.	Mass of found asphalt binder (J-K)	46,58	45,53	g
M.	Mass of asphalt binder retained (E-L)	-3,08	-2,40	g
N.	Correction factor (Fc) (M/F *100)	-0,28	-0,22	g
O.	Average correction factor	-0,25		

Table-A I-9 Viscosity of recovery bitumen binder of unaged RAP

Test Temperature (ºC)	Speed (RPM)	Torque (%)	Viscosity (mPa.s)	Average Viscosity (mPa.s)
135	12	64,3	2679	
135	12	61,8	2579	2586,0
135	12	60,0	2500	
140	12	45,8	1908	
140	12	43,4	1808	1838,7
140	12	43,2	1800	
145	12	35,0	1475	
145	12	32,3	1345	1382,0
145	12	31,8	1325	
150	12	24,0	1000	
150	12	23,5	979	986,0
150	12	23,5	979	
155	12	18,0	750	
155	12	18,0	750	750,0
155	12	18,0	750	
160	12	14,1	588	
160	12	14,1	588	588,0
160	12	14,1	588	
165	12	11,3	471	
165	12	11,3	471	471,0
165	12	11,3	471	

Table-A I-10 Viscosity of recovery bitumen binder of heated microwave RAP (HM)

Test Temperature (ºC)	Speed (RPM)	Torque (%)	Viscosity (mPa.s)	Average Viscosity (mPa.s)
135	20	83,6	2090	
135	20	82,4	2060	2070,0
135	20	82,4	2060	
140	20	61,2	1530	
140	20	61,3	1533	1534,3
140	20	61,6	1540	
145	20	46,4	1160	
145	20	46,4	1160	1160,0
145	20	46,4	1160	
150	20	35,4	895	
150	20	35,4	895	895,0
150	20	35,4	895	
155	20	27,8	695	
155	20	27,6	690	693,3
155	20	27,8	695	
160	20	22,2	555	
160	20	22,2	555	555,0
160	20	22,2	555	
165	20	18	450	
165	20	18	450	450,0
165	20	18	450	

Table-A I-11 Viscosity of recovery bitumen binder of aged RAP

Test Temperature (ºC)	Speed (RPM)	Torque (%)	Viscosity (mPa.s)	Average Viscosity (mPa.s)
135	12	71,2	2967	
135	12	71,2	2967	2965,3
135	12	71,2	2962	
140	12	53,3	2225	
140	12	52,8	2200	2201,3
140	12	52,3	2179	
145	12	39,5	1646	
145	12	39,5	1646	1643
145	12	39,3	1637	
150	12	30,5	1271	
150	12	30,2	1258	1262,3
150	12	30,2	1258	
155	12	23,7	987,5	
155	12	23,7	987,5	986,1
155	12	23,6	983,3	
160	12	18,9	787,5	
160	12	18,9	787,5	787,5
160	12	18,9	787,5	
165	12	15,5	650,0	
165	12	15,5	650,0	650,0
165	12	15,5	650,0	

Table-A I-12 Formulation of different trials of virgin aggregate

Aggregate	Class		10-20 mm	5-10 mm	0-5 mm	1.25-0 mm	80 um
	Type		Stone	Stone	Stone	Sand	F
	From		Raycar	Raycar	Raycar	Bomix	Filler
Aggregate a properties	S.G. of aggregate	Bulk	2,867	2,842	2,821	2,702	
		Apparent	2,953	2,959	2,976	2,715	2,700
	% absrop. of water		1,02	1,4	1,61	0,45	1,00
	gradation (% of passing)	Sieve in mm 28,0	100	100	100	100	100
		Sieve in mm 20,0	96	100	100	100	100
		Sieve in mm 14,0	49	100	100	100	100
		Sieve in mm 10,0	12	92	100	100	100
		Sieve in mm 5,0	2,0	9,0	96	100	100
		Sieve in mm 2,5	1,0	3,0	61	100	100
		Sieve in mm 1,25	0,0	2,0	39	98	100
		Sieve size in um 630	0,0	2,0	26	87	100
		Sieve size in um 315	0,0	2,0	18	46	100
		Sieve size in um 160	0,4	1,0	13	11	100
		Sieve size in um 80	0,8	0,7	9,1	1,2	98

2*: averager of samples of the mix
1*: average of one sample of the mix

Mixes	Mix No.	ID mix	Description	The percentage used					Gradation for combination: Sieve size in mm 28,0	20,0	14,0	10,0	5,0	2,5	1,25	Sieve size in µm 630	315	160	80	Volumetric properties: Date	Voids at S.G.C. (%) No of gyration 10	120	200	Max theoretical S.G. G_{mm}
	1	Trial 1	0% of RAP PG64-28	43%	19%	35%	2%	1%	100	98,3	78,1	60,6	39,2	25,4	17	12,2	8,6	6,0	4,7	12-08-2010	17,5	7,9	6,6	2,626*2
	2	Trial 2	0% of RAP PG64-28	43%	14%	40%	2%	1%	100	98,3	78,1	61,0	43,5	28,3	18,8	13,4	9,4	6,6	5,1	13-08-2010	16,2	7,1	5,7	2,645*2
	3	Trial 3	0% of RAP PG64-28	43%	11%	40%	4%	2%	100	98,3	78,1	61,3	46,3	31,2	21,7	16,1	11,3	7,7	6,1	15-08-2010	14,2	5,8	4,5	2,641*2
	4	Trial 3 Replicate 2	0% of RAP PG64-28	43%	11%	40%	4%	2%	100	98,3	78,1	61,3	46,3	31,2	21,7	16,1	11,3	7,7	6,1	18-08-2010	14	5,2	4,3	2,641*2
	5	Trial 3 Replicate 3	0% of RAP PG58-28	43%	11%	40%	4%	2%	100	98,3	78,1	61,3	46,3	31,2	21,7	16,1	11,3	7,7	6,1	18-08-2010	14,6	5,7	4,3	2,631*1

Table-A I-13 Characteristics of virgin mix [RAP028]

	Type of mix "GB-20"	

Aggregates			Gradation (percentage of passing)											used	Density		% absotp.
Aggregate class	C: Coarse S: Sand F: Filler		Sieve size in mm							Sieve size in um					Bulk	Apparent	
	Type	From (Production code)	28,0	20,0	14,0	10,0	5,0	2,5	1,25	630	315	160	80				
10-20 mm	S	RAYCAR	100	96	49	12	2,0	1,0	0,0	0,0	0,0	0,0	0,8	43%	2,867	2,953	1,02
5-10 mm	S	RAYCAR	100	100	100	92	9,0	3,0	2,0	2,0	2,0	1,0	0,7	11%	2,842	2,959	1,40
0-5 mm	S	RAYCAR	100	100	100	100	96	61	39	26	18	13	9,1	40%	2,821	2,979	1,61
1,25-0 mm	Sand	BOMIX	100	100	100	100	100	100	97,9	86,6	45,8	10,9	1,2	4,%	2,702	2,715	0,45
0-0,315 mm	F	FILLER	100	100	100	100	100	100	100	100	100	100	98	2%	2,700	2,700	1,00
Gradation of combination			**100**	**98,3**	**78,1**	**61,3**	**46,3**	**31,2**	**21,7**	**16,1**	**11,3**	**7,7**	**6,1**	100%	2,835	2,948	1,27

Formula		Sieve size in mm							Sieve size in um				Binder %	Voids %	V.M.A. %	V.F.A. %	Stability N	Creep mm	Density		Binder absorb. %
		28,0	20,0	14,0	10,0	5,0	2,5	1,25	630	315	160	80							Theoretical	Max.	
		100	98,3	78,1	61,3	46,3	31,2	21,7	16,1	11,3	7,7	6,1									
Specification	Max.	100	100	90	75	50	-	-	-	-	-	8,0	4,5	4,5	13,9	70,4			2,666	2,641	0,25
	Min.	100	95	67	52	35	-	-	-	-	-	4,0									

Additional characteristics				Recycling asphalt mixtures			Resistance of rutting		Spec.
Class of asphalt binder performance (PG)	64-28	Total particle size		Percentage of binder		0	1 000 cycles		
Class of bitumen used in formulation	64-28	Predicted compatibility	94.5%	Voids at S.G.C. (%)		Spec.	3 000 cycles		
Density of the used asphalt binder. Gb (g/cm3)	1,020	Report bitumen / total particle size		10 gyrations	14,1	≥ 11%	10 000 cycles		
Combined aggregate specific gravity	2,835	Factor correction of binder		60 gyrations	-		30 000 cycles		
Percentage of effective asphalt binder	4,26	Total surface area (m2/kg)		120 gyrations	5,5	(4%-7%)	Ressuage		
Volume of effective binder at 0 % void (%)	10,2			200 gyrations	4,5	≥ 2%	Content of water (%)		Spec.
Note :				Ressuage			Stability restraint		≥ 70%

Table-A I-14 Formulation of virgin and different mixes of 25% RAP

Aggregate properties				10-20 mm	5-10 mm	0-5 mm	1,25-0 mm	80 um	2,5-5 mm	0-5 mm	RAP
	Class			10-20 mm	5-10 mm	0-5 mm	1,25-0 mm	80 um	2,5-5 mm	0-5 mm	RAP
	Type			Stone	Stone	Stone	Sand	F	Stone	Stone	Stone
	From			Raycar	Raycar	Raycar	Bomix	Filler	Raycar	St. Phylippe	St.P.
	S. G of agreegate		Bulk	2,867	2,842	2,821	2,702	2,700	2,827	2,718	2,365
			Apparent	2,953	2,959	2,979	2,715	2,700		2,766	2,496
	% absrop. of water			1,02	1,4	1,61	0,45	1,00	1,4	0,64	2,21
	gradation (% of passing)	Sieve in mm	28,0	100	100	100	100	100	100	100	100
			20,0	96	100	100	100	100	100	100	100
			14,0	49	100	100	100	100	100	100	100
			10,0	12	92	100	100	100	100	100	98
			5,0	2,0	9,0	96	100	100	91	94	71
			2,5	1,0	3,0	61	15,0	100	15	58	52
			1,25	0,0	2,0	39	98	100	5	29	41
		Sieve size in um	630	0,0	2,0	26	87	100	3	14	32
			315	0,0	2,0	18	46	100	2	10	23
			160	0,4	1,0	13	11	100	2	8	16
			80	0,8	0,7	9,1	1,2	98	1,2	7	10

Mixes	Mix No.	ID mix	Description	The percentage used								gradation for combination										Voids at S.G.C. (%)		
												Sieve size in mm							Seive size in µm				No of gyration		
												28,0	20,0	14,0	10,0	5,0	2,5	1,25	630	315	160	80	10	120	200
	1	RAP0 (Trial 3)	0% of RAP (Virgin mix) - PG64-28	43%	11%	40%	4%	2%	0%	0%	0%	100	98,3	78,1	61,3	46,3	31,2	21,7	16,1	11,3	7,7	6,1	14,1	5,5	4,2
	3	RAP25 (Trial 1)	25% of RAP (hot addition) – PG64-28	37%	18%	0%	0%	3%	2%	15%	25%	100	98,5	81,1	65,5	39	25,9	18,1	13,5	10,7	8,4	6,9	16,4	6	4,6
	4	RAP25 (Trial 2)	25% of RAP (hot addition)– PG64-28	37%	18%	0%	0%	2%	5%	13%	25%	100	98,5	81,1	65,5	38,9	24,2	16,6	12,3	9,5	7,3	5,9	17,3	7,8	5,9
	5	RAP25 (Trial 3)	25% of RAP (hot addition)– PG64-28	36%	18%	0%	0%	3%	5%	13%	25%	100	98,6	81,6	66,4	39,9	25,2	17,6	13,3	10,5	8,3	6,8	15,8	5,6	4,1
	6	RAP25 (Trial 3) Replicate 2	25% of RAP (hot addition)– PG64-28	36%	18%	0%	0%	3%	5%	13%	25%	100	98,6	81,6	66,4	39,9	25,2	17,6	13,3	10,5	8,3	6,8	17,4	6,8	5,2
	7	RAP25 (Trial 3) Replicate 3	25% of RAP (hot addition)– PG64-28	36%	18%	0%	0%	3%	5%	13%	25%	100	98,6	81,6	66,4	39,9	25,2	17,6	13,3	10,5	8,3	6,8	16,9	6,7	5,1
	8	RAP25 (Trial 3) Replicate 4	25% of RAP (hot addition) – PG64-28	36%	18%	0%	0%	3%	5%	13%	25%	100	98,6	81,6	66,4	39,9	25,2	17,6	13,3	10,5	8,3	6,8	16,1	5,3	3,5
	9	RAP25 (Trial 3) Replicate 5	25% of RAP (Cold addition)– PG64-28	36%	18%	0%	0%	3%	5%	13%	25%	100	98,6	81,6	66,4	39,9	25,2	17,6	13,3	10,5	8,3	6,8	16,7	5,6	4,1
	10	RAP25 (Trial 3) Replicate 6	25% of RAP (Cold addition)– PG58-34	36%	18%	0%	0%	3%	5%	13%	25%	100	98,6	81,6	66,4	39,9	25,2	17,6	13,3	10,5	8,3	6,8	14,9	5,3	3,8

Table-A I-15 The properties of different mixes of 25% RAP

Mix No.	Date	The mixture	Gradation (percent of passing)											Percentage of binder			Type of Binder	Voids at S.G.C. (%)			Theoretical	Notes
			Sieve size in mm							Sieve size in µm				total	RAP	Virgin		No of gyration			S.G.	
			28	20	14	10	5,0	2,50	1,25	630	315	160	80	binder				10	120	200	G_{mm}	
1	18-08-2010	RAP0 (Trial3)	100	98,3	78,1	61,3	46,3	31,2	21,7	16,1	11,3	7,7	6,1	4,5	0,0	4,5	PG64-28	14,1	5,5	4,2	2,641	0% of RAP
3	18-06-2010	RAP25-Trial 1	100	98,5	81,1	65,5	39	25,9	18,1	13,5	10,7	8,4	6,9	4,5	1,0	3,5	PG64-28	16,4	6	4,6	2,630	25% of RAP (hot addition)
		Difference	0	0	3	4	-7	-5	-4	-3	-1	1	1	0	1,0	-1						
		Coff, of variation	0	0	4	7	-16	-17	-17	-16	-5	9	13	0		-22						
4	16-06-2010	RAP25-Trial 2	100	98,5	81,1	65,5	38,9	24,2	16,6	12,3	9,5	7,3	5,9	4,5	1,0	3,5	PG64-28	17,3	7,8	5,9	2,628	25% of RAP (hot addition)
		Difference	0	0	3	4	-7	-7	-5	-4	-2	-0,4	-0,2	0	1,0	-1						
		Coff, of variation	0	0	4	7	-16	-22	-24	-24	-16	-5	-3	0		-22						
5	16-06-2010	RAP25-Trial 3	100	98,6	81,6	66,4	39,9	25,2	17,6	13,3	10,5	8,3	6,8	4,5	1,0	3,5	PG64-28	15,8	5,6	4,1	2,616	25% of RAP (hot addition)
		Difference	0	0	4	5	-6	-6	-4	-3	-1	1	1	0	1,0	-1						
		Coff, of variation	0	0	4	8	-14	-19	-19	-17	-7	8	11	0		-22						
6	18-06-2010	RAP25 (Trial 3)Replicate 2	100	98,6	81,6	66,4	39,9	25,2	17,6	13,3	10,5	8,3	6,8	4,5	1,0	3,5	PG64-28	17,4	6,8	5,2	2,617	25% of RAP (hot addition)
		Difference	0	0	4	5	-6	-6	-4	-3	-1	1	1	0	1,0	-1						
		Coff, of variation	0	0	4	8	-14	-19	-19	-17	-7	8	11	0		-22						
7	18-06-2010	RAP25(Trial 3)Replicate 3	100	98,6	81,6	66,4	39,9	25,2	17,6	13,3	10,5	8,3	6,8	4,5	1,0	3,5	PG64-28	16,9	6,7	5,1	2,617	25% of RAP (hot addition)
		Difference	0	0	4	5	-6	-6	-4	-3	-1	1	1	0	1,0	-1						
		Coff, of variation	0	0	4	8	-14	-19	-19	-17	-7	8	11	0		-22						
8	22-06-2010	RA25 (Trial 3) Replicate 4	100	98,6	81,6	66,4	39,9	25,2	17,6	13,3	10,5	8,3	6,8	4,5	1,0	3,5	PG64-28	16,1	5,3	3,5	2,617	25% of RAP (hot addition)
		Difference	0	0	4	5	-6	-6	-4	-3	-1	1	1	0	1,0	-1						
		Coff, of variation	0	0	4	8	-14	-19	-19	-17	-7	8	11	0		-22						
9	22-06-2010	RAP25 (Trial 3) Replicate 4	100	98,6	81,6	66,4	39,9	25,2	17,6	13,3	10,5	8,3	6,8	4,5	1,0	3,5	PG64-28	16,7	5,6	4,1	2,622*1	25% of RAP (Cold addition)
		Difference	0	0	4	5	-6	-6	-4	-3	-1	1	1	0	1,0	-1						
		Coff, of variation	0	0	4	8	-14	-19	-19	-17	-7	8	11	0		-22						
10	30-06-2010	RAP25 (Trial 3) Replicate 5	100	98,6	81,6	66,4	39,9	25,2	17,6	13,3	10,5	8,3	6,8	4,5	1,0	3,5	PG58-34	14,9	5,3	3,8	2,624*1	25% of RAP (Cold addition)
		Difference	0	0	4	5	-6	-6	-4	-3	-1	1	1	0	1,0	-1						
		Coff, of variation	0	0	4	8	-14	-19	-19	-17	-7	8	11	0		-22						

Table-A I-16 The properties of different mixes of 25% RAP

Mix No,	Date	The mixture	Gradation (percent of passing)											Percentage of binder			Type of Binder	Voids at S,G,C, (%)			Theoretical S.G.	Notes
			Sieve size in mm							Sieve size in µm				total binder	RAP	Virgin		No of gyration				
			28	20	14	10	5,0	2,50	1,25	630	315	160	80					10	120	200	Gmm	
1	1-09-2009	RAP0 (Trial 3)	100	98,3	78,1	61,3	46,3	31,2	21,7	16,1	11,3	7,7	6,1	4,5	0,0	4,5	PG64-28	14,1	5,5	4,2	2,641*1	0% of RAP
3	16-06-2010	RAP25 (Trial 1)	100	98,5	81,1	65,5	39	25,9	18,1	13,5	10,7	8,4	6,9	4,5	1,0	3,5	PG64-28	16,4	6	4,6	2,630*1	25% RAP (Hot addition)
4	16-06-2010	RAP25 (Trial 2)	100	98,5	81,1	65,5	38,9	24,2	16,6	12,3	9,5	7,3	5,9	4,5	1,0	3,5	PG64-28	17,3	7,8	5,9	2,628*1	25% RAP (Hot addition)
5	16-06-2010	RAP25 (Trial 3) Replicate 1	100	98,6	81,6	66,4	39,9	25,2	17,6	13,3	10,5	8,3	6,8	4,5	1,0	3,5	PG64-28	15,8	5,6	4,1	2,616*1	25% RAP (Hot addition)
6	18-06-2010	RAP25 (Trial 3) Replicate 2	100	98,6	81,6	66,4	39,9	25,2	17,6	13,3	10,5	8,3	6,8	4,5	1,0	3,5	PG64-28	17,4	6,8	5,2	2,617*2	25% RAP (Hot addition)
7	18-06-2010	RAP25 (Trial 3) Replicate 3	100	98,6	81,6	66,4	39,9	25,2	17,6	13,3	10,5	8,3	6,8	4,5	1,0	3,5	PG64-28	16,9	6,7	5,1	2,617*2	25% RAP (Hot addition) Unaged condition
8	22-06-2010	RAP25 (Trial 3) Replicate 4	100	98,6	81,6	66,4	39,9	25,2	17,6	13,3	10,5	8,3	6,8	4,5	1,0	3,5	PG64-28	16,1	5,3	3,5	2,617*2	25% RAP (Hot addition)
9	22-06-2010	RAP25 (Trial 3) Replicate 5	100	98,6	81,6	66,4	39,9	25,2	17,6	13,3	10,5	8,3	6,8	4,5	1,0	3,5	PG64-28	16,7	5,6	4,1	2,622*2	25% RAP (Cold addition)
10	30-06-2010	RAP25 (Trial 3) Replicate 6	100	98,6	81,6	66,4	39,9	25,2	17,6	13,3	10,5	8,3	6,8	4,5	1,0	3,5	PG58-34	14,9	5,3	3,8	2,624*1	25% RAP (Cold addition)

Table-A I-17 Characteristics of 25% RAP mix # 3 [RAP2528CUN]

	Type of mix "GB-20"	

Aggregates			**Gradation (percentage of passing)**											**used**	**Density**		**% absotp .**
Aggregate class	**C: Coarse S: Sand F: Filler**		**Sieve size in mm**							**Sieve size in um**					**Bulk**	**Apparent**	
	Type	**From (Production code)**	**28,0**	**20,0**	**14,0**	**10,0**	**5,0**	**2,5**	**1,25**	**630**	**315**	**160**	**80**				
10-20 mm	s	RAYCAR	100	96	49	12	2,0	1,0	0,0	0,0	0,0	0,0	0,8	36,0%	2,867	2,953	1,02
5-10 mm	s	RAYCAR	100	100	100	92	9,0	3,0	2,0	2,0	2,0	1,0	0,7	18,0%	2,842	2,959	1,40
0-5 mm	s	Construction DJL, St-Philippe	100	100	100	100	94	58	29	14	10	8,0	7,0	13,0%	2,718	2,766	0,64
2,5-5 mm	s	RAYCAR	100	100	100	100	91	15	5	3	2	2	1,2	5,0%	2,827	2,926	1,40
0-0,315 mm	F	FILLER	100	100	100	100	100	100	100	100	100	100	98	3,0%	2,700	2,700	1,00
0-10 mm		RAP	100	100	100	98	71	52	41	32	23	16	10	25,0%	2,365	2,496	2,21
Gradation of combination			100	98,6	81,6	66,4	39,9	25,2	17,6	13,3	10,5	8,3	6,8	100%	2,706	2,819	1,48

Formula		**Sieve size in mm**							**Sieve size in um**				**Binder %**	**Voids %**	**V.M.A. %**	**V.F.A. %**	**Stability N**	**Creep mm**	**Density**		Binder absorb. %
		28,0	**20,0**	**14,0**	**10,0**	**5,0**	**2,5**	**1,25**	**630**	**315**	**160**	**80**							**Theoretical**	**Max.**	
		100	98,6	81,6	66,4	39,9	25,2	17,6	13,3	10,5	8,3	6,8									
Specification	**Max.**	100	100	90	75	50	-	-	-	-	-	8,0	4,5	4,1	13,9	70,5			2,539	2,622	1,84
	Min.	100	95	67	52	35	-	-	-	-	-	4,0									

Additional characteristics				**Recycling asphalt mixtures**			**Resistance of rutting**		**Spec.**
Class of asphalt binder performance (PG)	64-28	**Total particle size**		**Percentage of binder**		0	1 000 cycles		
Class of bitumen used in formulation	64-28	**Predicted compatibility**		**Voids at S.G.C. (%)**		**Spec.**	3 000 cycles		
Density of the used asphalt binder. Gb (g/cm3)	1,020	**Report bitumen / total particle size**		10 gyrations	16,7	≥ 11%	10 000 cycles		
Combined aggregate specific gravity	2,706	**Factor correction of binder**		60 gyrations	-		30 000 cycles		
Percentage of effective asphalt binder	2,74	**Total surface area (m2/kg)**		120 gyrations	5,6	(4%-7%)	Ressuage		
Volume of effective binder at 0 % void (%)	10,2			200 gyrations	4,1	≥ 2%	**Content of water (%)**		**Spec.**
Note :				Ressuage 200			Stability restraint		≥ 70%

Table-A I-18 Characteristics of 25% RAP mix # 6 [RAP2528HUN]

	Type of mix “GB-20”	

Aggregates			Gradation (percentage of passing)											used	Density		% absotp.
Aggregate class	C: Coarse S: Sand F: Filler		Sieve size in mm							Sieve size in um					Bulk	Apparent	
	Type	From (Production code)	28.0	20.0	14.0	10.0	5.0	2.5	1.25	630	315	160	80				
10-20 mm	S	RAYCAR	100	96	49	12	2,0	1,0	0,0	0,0	0,0	0,0	0,8	36,0%	2,867	2,953	1,02
5-10 mm	S	RAYCAR	100	100	100	92	9,0	3,0	2,0	2,0	2,0	1,0	0,7	18,0%	2,842	2,959	1,40
0-5 mm	S	Construction DJL, St-Philippe	100	100	100	100	94	58	29	14	10	8,0	7,0	13,0%	2,718	2,766	0,64
2,5-5 mm	S	RAYCAR	100	100	100	100	91	15	5	3	2	2	1,2	5,0%	2,827	2,926	1,40
0-0,315 mm	F	FILLER	100	100	100	100	100	100	100	100	100	100	98	3,0%	2,700	2,700	1,00
0-10 mm		RAP	100	100	100	98	71	52	41	32	23	16	10	25,0%	2,365	2,496	2,21
Gradation of combination			100	98,6	81,6	66,4	39,9	25,2	17,6	13,3	10,5	8,3	6,8	100%	2,706	2,819	1,48

Formula		Sieve size in mm							Sieve size in um				Binder %	Voids %	V.M.A. %	V.F.A. %	Stability N	Creep mm	Density		Binder absorb. %
		28,0	20,0	14,0	10,0	5,0	2,5	1,25	630	315	160	80							Theoretical	Max.	
		100	98,6	81,6	66,4	39,9	25,2	17,6	13,3	10,5	8,3	6,8									
Specification	Max.	100	100	90	75	50	-	-	-	-	-	8,0	4,5	4,1	14,5	66,9			2,539	2,617	1,77
	Min.	100	95	67	52	35	-	-	-	-	-	4,0									

Additional characteristics				Recycling asphalt mixtures			Resistance of rutting		Spec.
Class of asphalt binder performance (PG)	64-28	Total particle size		Percentage of binder		0	1 000 cycles	Apparent	
Class of bitumen used in formulation	64-28	Predicted compatibility		Voids at S.G.C. (%)		Spec.	3 000 cycles		
Density of the used asphalt binder. Gb (g/cm³)	1,020	Report bitumen / total particle size		10 gyrations	16,7	≥ 11%	10 000 cycles		
Combined aggregate specific gravity	2,706	Factor correction of binder		60 gyrations	-		30 000 cycles		
Percentage of effective asphalt binder	2,81	Total surface area (m2/kg)		120 gyrations	6,4	(4%-7%)	Ressuage		
Volume of effective binder at 0 % void (%)	10,2			200 gyrations	4,8	≥ 2%	Content of water (%)		Spec.
Note :				Ressuage			Stability restraint		≥ 70%

Table-A I-19 Characteristics of 25% RAP mix # 10 [RAP2534CUN]

	Type of mix "GB-20"	

Aggregates			Gradation (percentage of passing)											used	Density		% absot p.
Aggregate class	C: Coarse S: Sand F: Filler		Sieve size in mm							Sieve size in um					Bulk	Apparent	
	Type	From (Production code)	28.0	20.0	14.0	10.0	5.0	2.5	1.25	630	315	160	80				
10-20 mm	S	RAYCAR	100	96	49	12	2,0	1,0	0,0	0,0	0,0	0,0	0,8	36,0%	2,867	2,953	1,02
5-10 mm	S	RAYCAR	100	100	100	92	9,0	3,0	2,0	2,0	2,0	1,0	0,7	18,0%	2,842	2,959	1,40
0-5 mm	S	Construction DJL, St-Philippe	100	100	100	100	94	58	29	14	10	8,0	7,0	13,0%	2,718	2,766	0,64
2,5-5 mm	S	RAYCAR	100	100	100	100	91	15	5	3	2	2	1,2	5,0%	2,827	2,926	1,40
0-0,315 mm	F	FILLER	100	100	100	100	100	100	100	100	100	100	98	3,0%	2,700	2,700	1,00
0-10 mm		RAP	100	100	100	98	71	52	41	32	23	16	10	25,0%	2,365	2,496	2,21
Gradation of combination			100	98,6	81,6	66,4	39,9	25,2	17,6	13,3	10,5	8,3	6,8	100%	2,706	2,819	1,48

Formula		Sieve size in mm							Sieve size in um				Binder %	Voids %	V.M.A. %	V.F.A. %	Stability N	Creep mm	Density		Binder absorb. %
		28,0	20,0	14,0	10,0	5,0	2,5	1,25	630	315	160	80							Theoretical	Max.	
		100	98,6	81,6	66,4	39,9	25,2	17,6	13,3	10,5	8,3	6,8									
Specification	Max.	100	100	90	75	50	-	-	-	-	-	8,0	4,5	3,8	13,7	71,8			2,539	2,624	1,87
	Min.	100	95	67	52	35	-	-	-	-	-	4,0									

Additional characteristics				Recycling asphalt mixtures			Resistance of rutting		Spec.
Class of asphalt binder performance (PG)	58-34	Total particle size		Percentage of binder		0	1 000 cycles		
Class of bitumen used in formulation	58-34	Predicted compatibility		Voids at S.G.C. (%)		Spec.	3 000 cycles		
Density of the used asphalt binder. Gb (g/cm3)	1,020	Report bitumen / total particle size		10 gyrations	14.9	≥ 11%	10 000 cycles		
Combined aggregate specific gravity	2,706	Factor correction of binder		60 gyrations	-		30 000 cycles		
Percentage of effective asphalt binder	2,714	Total surface area (m2/kg)		120 gyrations	5,3	(4%-7%)	Ressuage		
Volume of effective binder at 0 % void (%)	10,2			200 gyrations	3,8	≥ 2%	Content of water (%)		Spec.
Note :				Ressuage			Stability restraint		≥ 70%

Table-A I-20 Formulation of virgin and different mixes of 15% RAP

Aggregate	Class		10-20 mm	5-10 mm	0-5 mm	1,25-0 mm	80 um	2,5-5 mm	0-5 mm	RAP
	Type		Stone	Stone	Stone	Sand	F	Stone	Stone	Stone
	From		Raycar	Raycar	Raycar	Bomix	Filler	Raycar	St, Phylippe	St,P,
Aggregate a properties	S. G of agreegate	Bulk	2,867	2,842	2,821	2,702	2,700	2,827	2,718	2,365
		Apparent	2,953	2,959	2,979	2,715	2,700		2,766	2,496
	% absrop. of water		1,02	1,4	1,61	0,45	1,00	1,4	0,64	2,21
	gradation (% of passing) Sieve in mm	28,0	100	100	100	100	100	100	100	100
		20,0	96	100	100	100	100	100	100	100
		14,0	49	100	100	100	100	100	100	100
		10,0	12	92	100	100	100	100	100	98
		5,0	2,0	9,0	96	100	100	91	94	71
		2,5	1,0	3,0	61	15,0	100	15	58	52
		1,25	0,0	2,0	39	98	100	5	29	41
	Sieve size in um	630	0,0	2,0	26	87	100	3	14	32
		315	0,0	2,0	18	46	100	2	10	23
		160	0,4	1,0	13	11	100	2	8	16
		80	0,8	0,7	9,1	1,2	98	1,2	7	10

Mixes	Mix No.	ID mix	Description	The percentage used								gradation for combination												Voids at S.G.C. (%)		
												Sieve size in mm							Seive size in µm				No of gyration		
												28,0	20,0	14,0	10,0	5,0	2,5	1,25	630	315	160	80	10	120	200
	1	RAP0 (Trial 3)	0% of RAP (Virgin mix) - PG64-28	43%	11%	40%	4%	2%	0%	0%	0%	100	98,3	78,1	61,3	46,3	31,2	21,7	16,1	11,3	7,7	6,1	14,1	5,5	4,2
	2	RAP15 (Trial 1)	15% of RAP (Cold addition-unaged RAP) – PG64-28	42%	11%	28%	0%	2%	2%	0%	15%	100	98,3	78,6	61,9	43,2	27,9	19,4	14,4	10,8	8,2	6,4	16,6	7,1	5,7
	3	RAP15 (Trial 1)	15% of RAP (Hot addition-unaged RAP) – PG64-28	42%	11%	28%	0%	2%	2%	0%	15%	100	98,3	78,6	61,9	43,2	27,9	19,4	14,4	10,8	8,2	6,4	15,8	6,0	4,6
	4	RAP15 (Trial 1) Replicate 2	15% of RAP (Hot addition-unaged RAP) – PG64-28	42%	11%	28%	0%	2%	2%	0%	15%	100	98,3	78,6	61,9	43,2	27,9	19,4	14,4	10,8	8,2	6,4	17,3	7,7	6,4
	5	RAP15 (Trial 2)	15% of RAP (Cold addition-unaged RAP) – PG64-28	40%	11%	30%	0%	2%	2%	0%	15%	100	98,4	79,6	63,2	39,6	27	20,7	16,4	12,4	9,2	6,8	14,3	4,5	3,0
	6	RAP15 (Trial 2) Replicate 2	15% of RAP (Cold addition-aged RAP) – PG58-34	40%	11%	30%	0%	2%	2%	0%	15%	100	98,4	79,6	63,2	39,6	27	20,7	16,4	12,4	9,2	6,8	13,3	3,5	2,2
	7	RAP15 (Trial 2) Replicate 3	15% of RAP (Hot addition-unaged RAP) – PG58-34	40%	11%	30%	0%	2%	2%	0%	15%	100	98,4	79,6	63,2	39,6	27	20,7	16,4	12,4	9,2	6,8	13,8	4,1	2,6
	8	RAP15 (Trial 2) Replicate 4	15% of RAP (Hot addition-unaged RAP) – PG58-34	40%	11%	30%	0%	2%	2%	0%	15%	100	98,4	79,6	63,2	39,6	27	20,7	16,4	12,4	9,2	6,8	15,7	6,0	4,5

Table-A I-21 The Formulation of virgin and different mixes of 15% RAP

Mix No.	Date	The mixture	Gradation (pecent of passing)											Percentage of binder			Type of Binder	Voids at S.G.C. (%)			Theoritical	Notes
			Seive size in mm							Seive size in µm				total	RAP	Virgin		No of gyration			S.G.	
			28	20	14	10	5,0	2,50	1,25	630	315	160	80	binder				10	120	200	Gmm	
1	18-08-2010	RAP0 (Trial3)	100	98,3	78,1	61,3	46,3	31,2	21,7	16,1	11,3	7,7	6,1	4,5	0,0	4,5	PG64-28	14,1	5,5	4,2	2.641	0% of RAP
2	6-04-2011	RAP15 (Trial 1)	100	98,3	78,6	61,9	43,2	27,9	19,4	14,4	10,8	8,2	6,4	4,5	0,6	2,9	PG64-28	16,6	7,1	5,7	2.642*1	15% of RAP (Cold addition) Unaged RAP
		Difference	0	0	1	1	-3	-3	-2	-2	-1	0	0	0	0,6	-1,6						
		Coff. of variation	0	0	1	1	-7	-11	-11	-11	-4	6	5	0		-36						
3	6-04-2011	RAP15 (Trial 1) Replicate 2	100	98,3	78,6	61,9	43,2	27,9	19,4	14,4	10,8	8,2	6,4	4,5	0,6	2,9	PG64-28	15,8	6	4,6	2,653*2	15% of RAP (hot addition) Unaged RAP
		Difference	0	0	1	1	-3	-3	-2	-2	-1	0,5	0,3	0	0,6	-1,6						
		Coff. of variation	0	0	1	1	-7	-11	-11	-11	-4	6	5	0		-36						
4	6-04-2011	RAP15 (Trial 1) Replicate 3	100	98,3	78,6	61,9	43,2	27,9	19,4	14,4	10,8	8,2	6,4	4,5	0,6	2,9	PG64-28	17,3	7,7	6,4	2,653*2	15% of RAP (hot addition) Unaged RAP
		Difference	0	0	1	1	-3	-3	-2	-2	-1	0	0	0	0,6	-1,6						
		Coff. of variation	0	0	1	1	-7	-11	-11	-11	-4	6	5	0		-36						
5	6-04-2011	RAP15 (Trial 2)	100	98,4	79,6	45,1	29,1	20,2	14,9	11,1	8,5	6,6	6,8	4,5	0,6	2,9	PG64-28	14,3	4,5	3	2,601*2	15% of RAP (Cold addition) Unaged RAP
		Difference	0	0	2	-16	-17	-11	-7	-5	-3	-1	1	0	0,6	-1,6						
		Coff. of variation	0	0	2	-26	-37	-35	-31	-31	-25	-14	11	0		-36						
6	6-04-2011	RAP15 (Trial 2) Replicate 2	100	98,4	79,6	63,2	39,6	27	20,7	16,4	12,4	9,2	6,8	4,5	0,6	2,9	PG64-28	13,3	3,5	2,2	2,601*2	15% of RAP (Cold addition) Unaged RAP
		Difference	0	0	2	2	-7	-4	-1	0	1	2	1	0	0,6	-1,6						
		Coff. of variation	0	0	2	3	-14	-13	-5	2	10	19	11	0		-36						
7	6-04-2011	RAP15 (Trial 2) Replicate 3	100	98,4	79,6	63,2	39,6	27	20,7	16,4	12,4	9,2	6,8	4,5	0,6	2,9	PG64-28	13,8	4,1	2,6	2,612*2	15% of RAP (hot addition) Unaged RAP
		Difference	0	0	2	2	-7	-4	-1	0	1	2	1	0	0,6	-1,6						
		Coff. of variation	0	0	2	3	-14	-13	-5	2	10	19	11	0		-36						
8	6-04-2011	RAP15 (Trial 2) Replicate 4	100	98,4	79,6	63,2	39,6	27	20,7	16,4	12,4	9,2	6,8	4,5	0,6	2,9	PG64-28	15,7	6	4,5	2,612*2	15% of RAP (hot addition) Unaged RAP
		Difference	0	0	2	2	-7	-4	-1	0	1	2	1	0	0,6	-1,6						
		Coff. of variation	0	0	2	3	-14	-13	-5	2	10	19	11	0		-36						

Table-A I.22 Formulation of virgin and different mixes of 15% RAP

Mix No.	Date	The mixture	Gradation (pecent of passing)											Percentage of binder			Type of Binder	Voids at S.G.C. (%)			Theoritical	Notes
			Seive size in mm							Seive size in µm				total	RAP	Virgin		No of gyration			S.G.	
			28	20	14	10	5,0	2,50	1,25	630	315	160	80	binder				10	120	200	Gmm	
1	18-08-2010	RAP0 (Trial3)	100	98,3	78,1	61,3	46,3	31,2	21,7	16,1	11,3	7,7	6,1	4,5	0,0	4,5	PG64-28	14,1	5,5	4,2	2,641	0% of RAP
2	6-04-2011	RAP15 (Trial 1)	100	98,3	78,6	61,9	43,2	27,9	19,4	14,4	10,8	8,2	6,4	4,5	0,6	2,9	PG64-28	16,6	7,1	5,7	2,642*1	15% of RAP (Cold addition) Unaged RAP
		Difference	0	0	1	1	-3	-3	-2	-2	-1	0	0	0	0,6	-1,6						
		Coff. of variation	0	0	1	1	-7	-11	-11	-11	-4	6	5	0		-36						
3	6-04-2011	RAP15 (Trial 1) Replicate 2	100	98,3	78,6	61,9	43,2	27,9	19,4	14,4	10,8	8,2	6,4	4,5	0,6	2,9	PG64-28	15,8	6	4,6	2,653*2	15% of RAP (hot addition) Unaged RAP
		Difference	0	0	1	1	-3	-3	-2	-2	-1	0,5	0,3	0	0,6	-1,6						
		Coff. of variation	0	0	1	1	-7	-11	-11	-11	-4	6	5	0		-36						
4	6-04-2011	RAP15 (Trial 1) Replicate 3	100	98,3	78,6	61,9	43,2	27,9	19,4	14,4	10,8	8,2	6,4	4,5	0,6	2,9	PG64-28	17,3	7,7	6,4	2,653*2	15% of RAP (hot addition) Unaged RAP
		Difference	0	0	1	1	-3	-3	-2	-2	-1	0	0	0	0,6	-1,6						
		Coff. of variation	0	0	1	1	-7	-11	-11	-11	-4	6	5	0		-36						
5	6-04-2011	RAP15 (Trial 2)	100	98,4	79,6	45,1	29,1	20,2	14,9	11,1	8,5	6,6	6,8	4,5	0,6	2,9	PG64-28	14,3	4,5	3	2,601*2	15% of RAP (Cold addition) Unaged RAP
		Difference	0	0	2	-16	-17	-11	-7	-5	-3	-1	1	0	0,6	-1,6						
		Coff. of variation	0	0	2	-26	-37	-35	-31	-31	-25	-14	11	0		-36						
6	6-04-2011	RAP15 (Trial 2) Replicate 2	100	98,4	79,6	63,2	39,6	27	20,7	16,4	12,4	9,2	6,8	4,5	0,6	2,9	PG64-28	13,3	3,5	2,2	2,601*2	15% of RAP (Cold addition) Unaged RAP
		Difference	0	0	2	2	-7	-4	-1	0	1	2	1	0	0,6	-1,6						
		Coff. of variation	0	0	2	3	-14	-13	-5	2	10	19	11	0		-36						
7	6-04-2011	RAP15 (Trial 2) Replicate 3	100	98,4	79,6	63,2	39,6	27	20,7	16,4	12,4	9,2	6,8	4,5	0,6	2,9	PG64-28	13,8	4,1	2,6	2,612*2	15% of RAP (hot addition) Unaged RAP
		Difference	0	0	2	2	-7	-4	-1	0	1	2	1	0	0,6	-1,6						
		Coff. of variation	0	0	2	3	-14	-13	-5	2	10	19	11	0		-36						
8	6-04-2011	RAP15 (Trial 2) Replicate 4	100	98,4	79,6	63,2	39,6	27	20,7	16,4	12,4	9,2	6,8	4,5	0,6	2,9	PG64-28	15,7	6	4,5	2,612*2	15% of RAP (hot addition) Unaged RAP
		Difference	0	0	2	2	-7	-4	-1	0	1	2	1	0	0,6	-1,6						
		Coff. of variation	0	0	2	3	-14	-13	-5	2	10	19	11	0		-36						

Table-A I-23 Characteristics of 15% RAP mix # 2 [RAP1528CUN]

	Type of mix "GB-20"	

Aggregates			Gradation (percentage of passing)											used	Density		% absot p.
Aggregate class	C: Coarse S: Sand F: Filler		Sieve size in mm							Sieve size in um					Bulk	Apparent	
	Type	From (Production code)	28.0	20.0	14.0	10.0	5.0	2.5	1.25	630	315	160	80				
10-20 mm	S	RAYCAR	100	96	49	12	2,0	1,0	0,0	0,0	0,0	0,0	0,8	42,0%	2,867	2,953	1,02
5-10 mm	S	RAYCAR	100	100	100	92	9,0	3,0	2,0	2,0	2,0	1,0	0,7	11,0%	2,842	2,959	1,40
0-5 mm	S	RAYCAR	100	100	100	100	96	61	39	26	18	13	9,1	28,0%	2,821	2,979	1,61
2,5-5 mm	S	RAYCAR	100	100	100	100	91	15	5	3	2	2	1,2	2,0%	2,827	2,926	1,40
0-0,315 mm	F	FILLER	100	100	100	100	100	100	100	100	100	100	98	2,0%	2,700	2,700	1,00
0-10 mm		RAP	100	100	100	98	71	52	41	32	23	16	10	15,0%	2,365	2,496	2,21
Gradation of combination			100	98,3	78,6	61,9	43,2	27,9	19,4	14,4	10,8	8,2	6,4	100%	2,760	2,876	1,41

Formula		Sieve size in mm							Sieve size in um				Binder %	Voids %	V.M.A. %	V.F.A. %	Stability N	Creep mm	Density		Binder absorb. %
		28,0	20,0	14,0	10,0	5,0	2,5	1,25	630	315	160	80							Theoretical	Max.	
		100	98,3	78,6	61,9	43,2	27,9	19,4	14,4	10,8	8,2	6,4									
Specification	Max.	100	100	90	75	50	-	-	-	-	-	8,0	4,5	2,6	12,6	78,6			2,599	2,602	0,63
	Min.	100	95	67	52	35	-	-	-	-	-	4,0									

Additional characteristics				Recycling asphalt mixtures			Resistance of rutting		Spec.
Class of asphalt binder performance (PG)	64-28	Total particle size		Percentage of binder		0	1 000 cycles	Apparent	
Class of bitumen used in formulation	64-28	Predicted compatibility		Voids at S.G.C. (%)		Spec.	3 000 cycles		
Density of the used asphalt binder. Gb (g/cm^3)	1,020	Report bitumen / total particle size		10 gyrations	13,8	≥ 11%	10 000 cycles		
Combined aggregate specific gravity	2,706	Factor correction of binder		60 gyrations	-		30 000 cycles		
Percentage of effective asphalt binder	3,9	Total surface area (m2/kg)		120 gyrations	4,0	(4%-7%)	Ressuage		
Volume of effective binder at 0 % void (%)	10,2			200 gyrations	2,6	≥ 2%	Content of water (%)		Spec.
Note :				Ressuage			Stability restraint		≥ 70%

Table-A I-24 Characteristics of 15% RAP mix # 5 [RAP1528HUN]

	Type of mix "GB-20"	

Aggregates			Gradation (percentage of passing)											used	Density		% absotp.
Aggregate class	C: Coarse S: Sand F: Filler		Sieve size in mm							Sieve size in um					Bulk	Apparent	
	Type	From (Production code)	28,0	20,0	14,0	10,0	5,0	2,5	1,25	630	315	160	80				
10-20 mm	s	RAYCAR	100	96	49	12	2,0	1,0	0,0	0,0	0,0	0,0	0,8	36,0%	2,867	2,953	1,02
5-10 mm	s	RAYCAR	100	100	100	92	9,0	3,0	2,0	2,0	2,0	1,0	0,7	18,0%	2,842	2,959	1,40
0-5 mm	s	RAYCAR	100	100	100	100	96	61	39	26	18	13	9,1	13,0%	2,821	2,979	1,61
2,5-5 mm	s	RAYCAR	100	100	100	100	91	15	5	3	2	2	1,2	5,0%	2,827	2,926	1,40
0-0,315 mm	F	FILLER	100	100	100	100	100	100	100	100	100	100	98	3,0%	2,700	2,700	1,00
0-10 mm		RAP	100	100	100	98	71	52	41	32	23	16	10	25,0%	2,365	2,496	2,21
Gradation of combination			100	98,6	81,6	66,4	39,9	25,2	17,6	13,3	10,5	8,3	6,8	100%	2,706	2,819	1,48

Formula		Sieve size in mm							Sieve size in um				Binder %	Voids %	V.M.A. %	V.F.A. %	Stability N	Creep mm	Density		Binder absorb. %
		28,0	20,0	14,0	10,0	5,0	2,5	1,25	630	315	160	80							Theoretical	Max.	
		100	98,6	81,6	66,4	39,9	25,2	17,6	13,3	10,5	8,3	6,8									
Specification	Max.	100	100	90	75	50	-	-	-	-	-	8,0	4,5	3,6	13,1	75,3			2,599	2,622	1,84
	Min.	100	95	67	52	35	-	-	-	-	-	4,0									

Additional characteristics				Recycling asphalt mixtures			Resistance of rutting		Spec.
Class of asphalt binder performance (PG)	64-28	Total particle size		Percentage of binder		0	1 000 cycles		
Class of bitumen used in formulation	64-28	Predicted compatibility		Voids at S.G.C. (%)		Spec.	3 000 cycles		
Density of the used asphalt binder. Gb (g/cm^3)	1,020	Report bitumen / total particle size		10 gyrations	14,8	≥ 11%	10 000 cycles		
Combined aggregate specific gravity	2,706	Factor correction of binder		60 gyrations	-		30 000 cycles		
Percentage of effective asphalt binder	3,74	Total surface area (m^2/kg)		120 gyrations	5,1	(4%-7%)	Ressuage		
Volume of effective binder at 0 % void (%)	10,2			200 gyrations	3,6	≥ 2%	Content of water (%)		Spec.
Note :				Ressuage 200			Stability restraint		≥ 70%

Table-A I-25 The Formulation of virgin and different mixes of 40% RAP

Aggregate	Class		10-20 mm	5-10 mm	0-5 mm	1,25-0 mm	80 um	2,5-5 mm	0-5 mm	RAP
	Type		Stone	Stone	Stone	Sand	F	Stone	Stone	Stone
	From		Raycar	Raycar	Raycar	Bomix	Filler	Raycar	St, Phylippe	St,P,
Aggregate a properties	S. G of agreegate	Bulk	2,867	2,842	2,821	2,702	2,700	2,827	2,718	2,365
		Apparent	2,953	2,959	2,979	2,715	2,700		2,766	2,496
	% absrop. of water		1,02	1,4	1,61	0,45	1,00	1,4	0,64	2,21
	gradation (% of passing) Sieve in mm	28,0	100	100	100	100	100	100	100	100
		20,0	96	100	100	100	100	100	100	100
		14,0	49	100	100	100	100	100	100	100
		10,0	12	92	100	100	100	100	100	98
		5,0	2,0	9,0	96	100	100	91	94	71
		2,5	1,0	3,0	61	15,0	100	15	58	52
		1,25	0,0	2,0	39	98	100	5	29	41
	Sieve size in um	630	0,0	2,0	26	87	100	3	14	32
		315	0,0	2,0	18	46	100	2	10	23
		160	0,4	1,0	13	11	100	2	8	16
		80	0,8	0,7	9,1	1,2	98	1,2	7	10

Mixes	Mix No.	ID mix	Description	The percentage used								gradation for combination										Voids at S.G.C. (%)		
												Sieve size in mm							Seive size in µm				No of gyration		
												28,0	20,0	14,0	10,0	5,0	2,5	1,25	630	315	160	80	10	120	200
	1	RAP0 (Trial 3)	0% RAP (Virgin mix) - PG64-28	43%	11%	40%	4%	2%	0%	0%	0%	100	98,3	78,1	61,3	46,3	31,2	21,7	16,1	11,3	7,7	6,1	14,1	5,5	4,2
	2	RAP40 (Trial 1)	40% RAP (Cold addition-unaged RAP) – PG64-28	40%	10%	5%	0%	2%	3%	0%	40%	100	98,4	79,6	63,2	39,6	27	20,7	16,4	12,4	9,2	6,8	15,1	5,1	3,7
	3	RAP40 (Trial 1) Replicate 2	40% RAP (Cold addition-unaged RAP) – PG64-28	40%	10%	5%	0%	2%	3%	0%	40%	100	98,4	79,6	63,2	39,6	27	20,7	16,4	12,4	9,2	6,8	16	6,7	5,3
	4	RAP40 (Trial 1) Replicate 3	40% of RAP (Cold addition-aged RAP) – PG64-28	40%	10%	5%	0%	2%	3%	0%	40%	100	98,4	79,6	63,2	39,6	27	20,7	16,4	12,4	9,2	6,8	12,4	3,4	2,0
	5	RAP40 (Trial 1) Replicate 4	40% RAP (Cold addition-aged RAP) – PG58-34	40%	10%	5%	0%	2%	3%	0%	40%	100	98,4	79,6	63,2	39,6	27	20,7	16,4	12,4	9,2	6,8	13,1	3,5	2
	6	RAP40 (Trial 1) Replicate 5	40% RAP (Cold addition-aged RAP) – PG58-34	40%	10%	5%	0%	2%	3%	0%	40%	100	98,4	79,6	63,2	39,6	27	20,7	16,4	12,4	9,2	6,8	13,1	3,9	2,5
	7	RAP40 (Trial 1) Replicate 6	40% RAP (Cold addition-unaged RAP) – PG58-34	40%	10%	5%	0%	2%	3%	0%	40%	100	98,4	79,6	63,2	39,6	27	20,7	16,4	12,4	9,2	6,8	14	4,4	3,0
	8	RAP40 (Trial 1) Replicate 7	40% RAP (Cold addition-unaged RAP) – PG58-34	40%	10%	5%	0%	2%	3%	0%	40%	100	98,4	79,6	63,2	39,6	27	20,7	16,4	12,4	9,2	6,8	15,1	5,5	4,1

Table-A I-26 The properties of different mixes of 40% RAP mixture

Mix No.	Date	The mixture	Gradation (percent of passing)											Percentage of binder			Type of Binder	Voids at S.G.C. (%)			Theoretical	Notes
			Sieve size in mm							Sieve size in µm				total	RAP	Virgin		No of gyration			S.G.	
			28	20	14	10	5.0	2.50	1.25	630	315	160	80	binder				10	120	200	G_{mm}	
1	2010	RAP0 (Trial 3)	100	98,3	78,1	61,3	46,3	31,2	21,7	16,1	11,3	7,7	6,1	4,5	0,0	4,5	PG64-28	14,1	5,5	4,2	2,641	0% of RAP
2	12-10-2010	RAP40 (Trial 1)	100	98,4	79,6	63,2	39,6	27	20,7	16,4	12,4	9,2	6,8	4,5	1,6	2,9	PG64-28	15,1	5,1	3,7	2,618*1	40% of RAP (Cold addition) Unaged RAP
		Difference	0	0	2	2	-7	-4	-1	0	1	2	1	0	1,6	-1,6						
		Coff. of variation	0	0	2	3	-14	-13	-5	2	10	19	11	0		-36						
3	22-10-2010	RAP40 (Trial 1) Replicate 2	100	98,4	79,6	63,2	39,6	27	20,7	16,4	12,4	9,2	6,8	4,5	1,6	2,9	PG64-28	16	6,7	5,3	2,627*2	40% of RAP (hot addition) Unaged RAP
		Difference	0	0	2	2	-7	-4	-1	0	1	1,5	0,7	0	1,6	-1,6						
		Coff. of variation	0	0	2	3	-14	-13	-5	2	10	19	10	0		-36						
4	2-11-2010	RAP40 (Trial 1) Replicate 3	100	98,4	79,6	63,2	39,6	27	20,7	16,4	12,4	9,2	6,8	4,5	1,6	2,9	PG64-28	12,4	3,4	2,0	2,601*2	40% of RAP (Cold addition) Aged RAP
		Difference	0	0	2	2	-7	-4	-1	0	1	2	1	0	1,6	-1,6						
		Coff. of variation	0	0	2	3	-14	-13	-5	2	10	19	11	0		-36						
5	2-11-2010	RAP40 (Trial 1) Replicate 4	100	98,4	79,6	63,2	39,6	27	20,7	16,4	12,4	9,2	6,8	4,5	1,6	2,9	PG58-34	13,14	3,5	2	2,599*2	40% of RAP (Cold addition) Aged RAP
		Difference	0	0	2	2	-7	-4	-1	0	1	2	1	0	1,6	-1,6						
		Coff. of variation	0	0	2	3	-14	-13	-5	2	10	19	11	0		-36						
6	2-11-2010	RAP40 (Trial 1) Replicate 5	100	98,4	79,6	63,2	39,6	27	20,7	16,4	12,4	9,2	6,8	4,5	1,6	2,9	PG58-34	13,14	3,9	2,5	2,599*2	40% of RAP (Cold addition) Aged RAP
		Difference	0	0	2	2	-7	-4	-1	0	1	2	1	0	1,6	-1,6						
		Coff. of variation	0	0	2	3	-14	-13	-5	2	10	19	11	0		-36						
7	2-11-2010	RAP40 (Trial 1) Replicate 6	100	98,4	79,6	63,2	39,6	27	20,7	16,4	12,4	9,2	6,8	4,5	1,6	2,9	PG58-34	14	4,4	3,0	2,621*2	40% of RAP (Cold addition) Unaged RAP
		Difference	0	0	2	2	-7	-4	-1	0	1	2	1	0	1,6	-1,6						
		Coff. of variation	0	0	2	3	-14	-13	-5	2	10	19	11	0		-36						
8	2-11-2010	RAP40 (Trial 1) Replicate 7	100	98,4	79,6	63,2	39,6	27	20,7	16,4	12,4	9,2	6,8	4,5	1,6	2,9	PG58-34	15,1	5,5	4,1	2,621*2	40% of RAP (Cold addition) Unaged RAP
		Difference	0	0	2	2	-7	-4	-1	0	1	2	1	0	1,6	-1,6						
		Coff. of variation	0	0	2	3	-14	-13	-5	2	10	19	11	0		-36						

Table-A I-27 The properties of different mixes of 40% RAP mixture: (*2: average of two samples of the mix)

Mix No.	Date	The mixture	Gradation (percent of passing)											Percentage of binder			Type of Binder	Voids at S.G.C. (%)			Theoretical	Notes
			Sieve size in mm							Sieve size in µm				total	RAP	Virgin		No of gyration			S.G.	
			28	20	14	10	5,0	2,50	1,25	630	315	160	80	binder				10	120	200	G_{mm}	
1	18-08-2010	RAP0 (Trial 3)	100	98,3	78,1	61,3	46,3	31,2	21,7	16,1	11,3	7,7	6,1	4,5	0,0	4,5	PG64-28	14,1	5,5	4,2	2,641	0% of RAP
2	12-10-2010	RAP40 (Trial 1)	100	98,4	79,6	63,2	39,6	27	20,7	16,4	12,4	9,2	6,8	4,5	1,6	2,9	PG64-28	15,1	5,1	3,7	2,618*1	40% of RAP (Cold addition) Unaged RAP
3	22-10-2010	RAP40 (Trial 1) Replicate 2	100	98,4	79,6	63,2	39,6	27	20,7	16,4	12,4	9,2	6,8	4,5	1,6	2,9	PG64-28	16	6,7	5,3	2,627*2	40% of RAP (hot addition) Unaged RAP
4	2-11-2010	RAP40 (Trial 1) Replicate 3	100	98,4	79,6	63,2	39,6	27	20,7	16,4	12,4	9,2	6,8	4,5	1,6	2,9	PG64-28	12,4	3,4	2,0	2,601*2	40% of RAP (Cold addition) Aged RAP
5	2-11-2010	RAP40 (Trial 1) Replicate 4	100	98,4	79,6	63,2	39,6	27	20,7	16,4	12,4	9,2	6,8	4,5	1,6	2,9	PG58-34	13,14	3,5	2	2,599*2	40% of RAP (Cold addition) Aged RAP
6	2-11-2010	RAP40 (Trial 1) Replicate 5	100	98,4	79,6	63,2	39,6	27	20,7	16,4	12,4	9,2	6,8	4,5	1,6	2,9	PG58-34	13,14	3,9	2,5	2,599*2	40% of RAP (Cold addition) Aged RAP
7	2-11-2010	RAP40 (Trial 1) Replicate 6	100	98,4	79,6	63,2	39,6	27	20,7	16,4	12,4	9,2	6,8	4,5	1,6	2,9	PG58-34	14	4,4	3,0	2,621*2	40% of RAP (Cold addition) Unaged RAP
8	2-11-2010	RAP40 (Trial 1) Replicate 7	100	98,4	79,6	63,2	39,6	27	20,7	16,4	12,4	9,2	6,8	4,5	1,6	2,9	PG58-34	15,1	5,5	4,1	2,621*2	40% of RAP (Cold addition) Unaged RAP

Table-A I-28 Characteristics of 40% RAP mix # 4 [RAP4028CUN]

	Type of mix “GB-20”	

Aggregates			Gradation (percentage of passing)											used	Density		% absotp.
Aggregate class	C: Coarse S: Sand F: Filler		Sieve size in mm							Sieve size in um					Bulk	Apparent	
	Type	From (Production code)	28,0	20,0	14,0	10,0	5,0	2,5	1,25	630	315	160	80				
10-20 mm	S	RAYCAR	100	96	49	12	2,0	1,0	0,0	0,0	0,0	0,0	0,8	40,0%	2,867	2,953	1,02
5-10 mm	S	RAYCAR	100	100	100	92	9,0	3,0	2,0	2,0	2,0	1,0	0,7	10,0%	2,842	2,959	1,40
0-5 mm	S	RAYCAR	100	100	100	100	96	61	39	26	18	13	9,1	5,0%	2,821	2,979	1,61
2.5-5 mm	S	RAYCAR	100	100	100	100	91	15	5	3	2	2	1,2	3,0%	2,827	2,926	1,40
0-0.315 mm	F	FILLER	100	100	100	100	100	100	100	100	100	100	98	2,0%	2,700	2,700	1,00
0-10 mm	S	RAP	100	100	100	98	71	52	41	32	23	16	10	40,0%	2,365	2,496	2,21
Gradation of combination			100	98,6	81,6	66,4	39,9	25,2	17,6	13,3	10,5	8,3	6,8	100%	2,634	2,748	1,24

Formula		Sieve size in mm							Sieve size in um				Binder %	Voids %	V.M.A. %	V.F.A. %	Stability N	Creep mm	Density		Binder absorb. %
		28,0	20,0	14,0	10,0	5,0	2,5	1,25	630	315	160	80							Theoretical	Max.	
		100	98,4	79,6	63,2	39,6	27	20,7	16,4	12,4	9,2	6,8									
Specification	Max.	100	100	90	75	50	-	-	-	-	-	8,0	4,5	3,7	13,5	72,7			2,488	2,618	2,63
	Min.	100	95	67	52	35	-	-	-	-	-	4,0									

Additional characteristics				Recycling asphalt mixtures			Resistance of rutting		Spec.
Class of asphalt binder performance (PG)	64-28	Total particle size		Percentage of binder		0	1 000 cycles	Apparent	
Class of bitumen used in formulation	64-28	Predicted compatibility		Voids at S.G.C. (%)		Spec.	3 000 cycles		
Density of the used asphalt binder. Gb (g/cm³)	1,020	Report bitumen / total particle size		10 gyrations	15,1	≥ 11%	10 000 cycles		
Combined aggregate specific gravity	2,634	Factor correction of binder		60 gyrations	-		30 000 cycles		
Percentage of effective asphalt binder	1,99	Total surface area (m²/kg)		120 gyrations	5,1	(4%-7%)	Ressuage		
Volume of effective binder at 0 % void (%)	10,2			200 gyrations	3,7	≥ 2%	Content of water (%)		Spec.
Note :				Ressuage			Stability restraint		≥ 70%

Table-A I-29 Characteristics of 40% RAP mix # 7 [RAP4028HUN]

Type of mix "GB-20"

Aggregates			Gradation (percentage of passing)											used	Density		% absotp.
Aggregate class	C: Coarse S: Sand F: Filler		Sieve size in mm							Sieve size in um					Bulk	Apparent	
	Type	From (Production code)	28,0	20,0	14,0	10,0	5,0	2,5	1,25	630	315	160	80				
10-20 mm	S	RAYCAR	100	96	49	12	2,0	1,0	0,0	0,0	0,0	0,0	0,8	40,0%	2,867	2,953	1,02
5-10 mm	S	RAYCAR	100	100	100	92	9,0	3,0	2,0	2,0	2,0	1,0	0,7	10,0%	2,842	2,959	1,40
0-5 mm	S	RAYCAR	100	100	100	100	96	61	39	26	18	13	9,1	5,0%	2,821	2,979	1,61
2,5-5 mm	S	RAYCAR	100	100	100	100	91	15	5	3	2	2	1,2	3,0%	2,827	2,926	1,40
0-0,315 mm	F	FILLER	100	100	100	100	100	100	100	100	100	100	98	2,0%	2,700	2,700	1,00
0-10 mm	S	RAP	100	100	100	98	71	52	41	32	23	16	10	40,0%	2,365	2,496	2,21
Gradation of combination			100	98,6	81,6	66,4	39,9	25,2	17,6	13,3	10,5	8,3	6,8	100%	2,634	2,748	1,24

Formula		Sieve size in mm							Sieve size in um				Binder %	Voids %	V.M.A. %	V.F.A. %	Stability N	Creep mm	Density		Binder absorb. %
		28,0	20,0	14,0	10,0	5,0	2,5	1,25	630	315	160	80							Theoretical	Max.	
		100	98,4	79,6	63,2	39,6	27	20,7	16,4	12,4	9,2	6,8									
Specification	Max.	100	100	90	75	50	-	-	-	-	-	8,0	4,5	5,3	14,9	64,9			2,488	2,627	2,78
	Min.	100	95	67	52	35	-	-	-	-	-	4,0									

Additional characteristics				Recycling asphalt mixtures			Resistance of rutting		Spec.
Class of asphalt binder performance (PG)	64-28	Total particle size		Percentage of binder		0	1 000 cycles	Apparent	
Class of bitumen used in formulation	64-28	Predicted compatibility		Voids at S.G.C. (%)		Spec.	3 000 cycles		
Density of the used asphalt binder. Gb (g/cm³)	1,020	Report bitumen / total particle size		10 gyrations	16	≥ 11%	10 000 cycles		
Combined aggregate specific gravity	2,634	Factor correction of binder		60 gyrations	-		30 000 cycles		
Percentage of effective asphalt binder	1,85	Total surface area (m2/kg)		120 gyrations	6,7	(4%-7%)	Ressuage		
Volume of effective binder at 0 % void (%)	10,2			200 gyrations	5,3	≥ 2%	Content of water (%)		Spec.
Note :				Ressuage			Stability restraint		≥ 70%

Table-A I-30 Characteristics of 40% RAP mix # 8 [RAP4028CA]

	Type of mix “GB-20”	

Aggregates			Gradation (percentage of passing)											used	Density		% absot p.
Aggregate class	C: Coarse S: Sand F: Filler		Sieve size in mm							Sieve size in um					Bulk	Apparent	
	Type	From (Production code)	28,0	20,0	14,0	10,0	5,0	2,5	1,25	630	315	160	80				
10-20 mm	S	RAYCAR	100	96	49	12	2,0	1,0	0,0	0,0	0,0	0,0	0,8	40,0%	2,867	2,953	1,02
5-10 mm	S	RAYCAR	100	100	100	92	9,0	3,0	2,0	2,0	2,0	1,0	0,7	10,0%	2,842	2,959	1,40
0-5 mm	S	RAYCAR	100	100	100	100	96	61	39	26	18	13	9,1	5,0%	2,821	2,979	1,61
2,5-5 mm	S	RAYCAR	100	100	100	100	91	15	5	3	2	2	1,2	3,0%	2,827	2,926	1,40
0-0,315 mm	F	FILLER	100	100	100	100	100	100	100	100	100	100	98	2,0%	2,700	2,700	1,00
0-10 mm	S	RAP	100	100	100	98	71	52	41	32	23	16	10	40,0%	2,365	2,496	2,21
Gradation of combination			100	98,6	81,6	66,4	39,9	25,2	17,6	13,3	10,5	8,3	6,8	100%	2,634	2,748	1,24

Formula		Sieve size in mm							Sieve size in um				Binder %	Voids %	V.M.A. %	V.F.A. %	Stability N	Creep mm	Density		Binder absorb. %
		28,0	20,0	14,0	10,0	5,0	2,5	1,25	630	315	160	80							Theoretical	Max.	
		100	98,4	79,6	63,2	39,6	27	20,7	16,4	12,4	9,2	6,8									
Specification	Max.	100	100	90	75	50	-	-	-	-	-	8,0	4,5	2,0	12,0	83			2,488	2,600	2,34
	Min.	100	95	67	52	35	-	-	-	-	-	4,0									

Additional characteristics				Recycling asphalt mixtures			Resistance of rutting		Spec.
Class of asphalt binder performance (PG)	64-28	Total particle size		Percentage of binder		0	1 000 cycles	Apparent	
Class of bitumen used in formulation	64-28	Predicted compatibility		Voids at S.G.C. (%)		Spec.	3 000 cycles		
Density of the used asphalt binder. Gb (g/cm³)	1,020	Report bitumen / total particle size		10 gyrations	12,4	≥ 11%	10 000 cycles		
Combined aggregate specific gravity	2,634	Factor correction of binder		60 gyrations	-		30 000 cycles		
Percentage of effective asphalt binder	2,27	Total surface area (m²/kg)		120 gyrations	3,4	(4%-7%)	Ressuage		
Volume of effective binder at 0 % void (%)	10,2			200 gyrations	2,0	≥ 2%	Content of water (%)		Spec.
Note :				Ressuage			Stability restraint		≥ 70%

Table-A I-31 Characteristics of 40% RAP mix # 9 [RAP4034CA]

	Type of mix "GB-20"	

Aggregates			Gradation (percentage of passing)											used	Density		% absot p.
Aggregate class	C: Coarse S: Sand F: Filler		Sieve size in mm							Sieve size in um					Bulk	Apparent	
	Type	From (Production code)	28,0	20,0	14,0	10,0	5,0	2,5	1,25	630	315	160	80				
10-20 mm	S	RAYCAR	100	96	49	12	2,0	1,0	0,0	0,0	0,0	0,0	0,8	40,0%	2,867	2,953	1,02
5-10 mm	S	RAYCAR	100	100	100	92	9,0	3,0	2,0	2,0	2,0	1,0	0,7	10,0%	2,842	2,959	1,40
0-5 mm	S	RAYCAR	100	100	100	100	96	61	39	26	18	13	9,1	5,0%	2,821	2,979	1,61
2,5-5 mm	S	RAYCAR	100	100	100	100	91	15	5	3	2	2	1,2	3,0%	2,827	2,926	1,40
0-0,315 mm	F	FILLER	100	100	100	100	100	100	100	100	100	100	98	2,0%	2,700	2,700	1,00
0-10 mm	S	RAP	100	100	100	98	71	52	41	32	23	16	10	40,0%	2,365	2,496	2,21
Gradation of combination			100	98,6	81,6	66,4	39,9	25,2	17,6	13,3	10,5	8,3	6,8	100%	2,634	2,748	1,24

Formula		Sieve size in mm							Sieve size in um				Binder %	Voids %	V.M.A. %	V.F.A. %	Stability N	Creep mm	Density		Binder absorb. %
		28,0	20,0	14,0	10,0	5,0	2,5	1,25	630	315	160	80							Theoretical	Max.	
		100	98,4	79,6	63,2	39,6	27	20,7	16,4	12,4	9,2	6,8									
Specification	Max.	100	100	90	75	50	-	-	-	-	-	8,0	4,5	2,2	12,2	81,7			2,488	2,597	2,31
	Min.	100	95	67	52	35	-	-	-	-	-	4,0									

Additional characteristics				Recycling asphalt mixtures			Resistance of rutting		Spec.
Class of asphalt binder performance (PG)	64-28	Total particle size		Percentage of binder		0	1 000 cycles	Apparent	
Class of bitumen used in formulation	64-28	Predicted compatibility		Voids at S.G.C. (%)		Spec.	3 000 cycles		
Density of the used asphalt binder. Gb (g/cm³)	1,020	Report bitumen / total particle size		10 gyrations	13,11	≥ 11%	10 000 cycles		
Combined aggregate specific gravity	2,706	Factor correction of binder		60 gyrations	-		30 000 cycles		
Percentage of effective asphalt binder	2,29	Total surface area (m²/kg)		120 gyrations	3,6	(4%-7%)	Ressuage		
Volume of effective binder at 0 % void (%)	10,2			200 gyrations	2,2	≥ 2%	Content of water (%)		Spec.
Note :				Ressuage			Stability restraint		≥ 70%

Table-A I-32 Characteristics of 40% RAP mix # 11 [RAP4028CA]

	Type of mix “GB-20”	

Aggregates			Gradation (percentage of passing)											used	Density		% absotp.
Aggregate class	C: Coarse S: Sand F: Filler		Sieve size in mm							Sieve size in um					Bulk	Apparent	
	Type	From (Production code)	28,0	20,0	14,0	10,0	5,0	2,5	1,25	630	315	160	80				
10-20 mm	S	RAYCAR	100	96	49	12	2,0	1,0	0,0	0,0	0,0	0,0	0,8	40,0%	2,867	2,953	1,02
5-10 mm	S	RAYCAR	100	100	100	92	9,0	3,0	2,0	2,0	2,0	1,0	0,7	10,0%	2,842	2,959	1,40
0-5 mm	S	RAYCAR	100	100	100	100	96	61	39	26	18	13	9,1	5,0%	2,821	2,979	1,61
2,5-5 mm	S	RAYCAR	100	100	100	100	91	15	5	3	2	2	1,2	3,0%	2,827	2,926	1,40
0-0,315 mm	F	FILLER	100	100	100	100	100	100	100	100	100	100	98	2,0%	2,700	2,700	1,00
0-10 mm	S	RAP	100	100	100	98	71	52	41	32	23	16	10	40,0%	2,365	2,496	2,21
Gradation of combination			100	98,6	81,6	66,4	39,9	25,2	17,6	13,3	10,5	8,3	6,8	100%	2,634	2,748	1,24

Formula		Sieve size in mm							Sieve size in um				Binder %	Voids %	V.M.A. %	V.F.A. %	Stability N	Creep mm	Density		Binder absorb. %
		28,0	20,0	14,0	10,0	5,0	2,5	1,25	630	315	160	80							Theoretical	Max.	
		100	98,4	79,6	63,2	39,6	27	20,7	16,4	12,4	9,2	6,8									
Specification	Max.	100	100	90	75	50	-	-	-	-	-	8,0	4,5	3,6	13,2	74,4			2,488	2,621	2,68
	Min.	100	95	67	52	35	-	-	-	-	-	4,0									

Additional characteristics				Recycling asphalt mixtures			Resistance of rutting		Spec.
Class of asphalt binder performance (PG)	64-28	Total particle size		Percentage of binder		0	1 000 cycles	Apparent	
Class of bitumen used in formulation	64-28	Predicted compatibility		Voids at S.G.C. (%)		Spec.	3 000 cycles		
Density of the used asphalt binder. Gb (g/cm³)	1,020	Report bitumen / total particle size		10 gyrations	14,5	≥ 11%	10 000 cycles		
Combined aggregate specific gravity	2,706	Factor correction of binder		60 gyrations	-		30 000 cycles		
Percentage of effective asphalt binder	1,94	Total surface area (m²/kg)		120 gyrations	4,95	(4%-7%)	Ressuage		
Volume of effective binder at 0 % void (%)	10,2			200 gyrations	3,6	≥ 2%	Content of water (%)		Spec.
Note :				Ressuage			Stability restraint		≥ 70%

Table-A I-33 An example spread sheet prepared for calculating the required RAP content of 25 percent RAP mix

Aggregate blending (Type GB-20, 25%RAP, Trial 3)

RAP source: No.1

(18/05/2010) **RAP25, Trial 3**

Binder to be used: PG 64-28

RAP binder content = 4,0%

Aggregate batching sheet:		Mix design	Mix design
Aggregates		2000 wt, g	5300
	Batch %	Aggregate wt, g	Aggregate wt, g
10-20mm	36	720	1908
5-10mm	18	360	954
0-5mm	13	260	689
2,5mm	5	100	265
Filler	3	60	159
RAP aggregate	25	500	1325
Total	100	2000	5300
Required RAP including binder	26	520	1378
Required total binder	4,5	94,2	249,7
Required net Binder	3,5	94,2 – 20 = 74,2	249,7 – 53 = 196,7

For the ease of the calculation of the actual amount of each material to add in each mix a spread sheet was developed as shown in Table A-I.32. This spread sheet shows the calculation of a total materials required to add into a batch of each mix design. For example, to prepare a mixture with 2000 grams of aggregates with 25 percent RAP aggregate (which would be 500 grams of RAP aggregates), a total of 520 grams of RAP material is required. The difference in weight 520–500 = 20 grams of RAP binder is contributing binder into the mix, which would be deducted from the total binder required for the mixture. To prepare a mixture with 2000 grams of aggregate at 4,5 percent optimum binder content, the total binder required will be 94,2 grams. Since the RAP contributes 20 grams of binder, a net required virgin binder will be 94,2-20 = 74,2 grams. This calculation process was adopted for all the

mix designs as well as sample preparations of 25%RAP mixtures. Once the net virgin binder is known, the preheated virgin binder was added into the blended mixture of preheated virgin aggregates and the pre-heated RAP materials.

Determination of voids content

In this study, voids content (V_i) was determined using the volumetric method. According to the LC 26 320 method (MTQ, 2015), the void content (V_i) is:

$$V_i(\%) = \left(1 - \frac{G_{mb}}{G_{mm}}\right) \times 100 \quad \text{(A I-1)}$$

Where:

G_{mb} Bulk density of compacted asphalt mixtures;

G_{mm} Maximum density of the mix.

Volumetric method, determination of density

This method is recommended for the mixtures of $V_i \geq 10\%$ (Test LC 26-040 method). The volume should be calculated from the dimensions of the sample, each dimension is equal to the average of three measurements performed at 120° from each other for the height, and at 60° to the diameter. These measures must be expressed with an accuracy of three significant numbers.

Density is:

$$MV = \frac{M_{dry}}{V} \quad \text{(A I-2)}$$

Where:

MV Mass to volume ratio (Density) (g/cm^3);

M_{dry} Dry mass (g); and

V Volume (cm^3).

Then, the density (MV) is converted into bulk density (G_{mb}) by dividing it by the density of water at 25°C (0,99704 g/cm^3).

APPENDIX II

COMPLEX MODULUS MEASUREMENT RESULTS OBTAINED BY THE AUTHORS ON RECYCLED MATERIALS

METHOD LC 26-700 (MTQ, 2015)
COMPLEX MODULUS OF ASPHALT MIXTURE

Specimen: P1-A4
Air void: 3,2%

Bulk density: 2,555
Maximum density: 2,641

Mixture ID: RAP028
Mixture No.: 1
Mixture type: GB-20
%RAP: 0
Bitumen type: PG 64-28
Bitumen content: 4,5%
Air void: 5,5%
Aggregate source:
Bitumen source:
Mixture source:

2S2P1D MODEL OF COMPLEX MODULUS, E* (MPa)

$$E^*(i\omega\tau) = E_{00} + \frac{E_0 - E_{00}}{1 + \delta(i\omega\tau)^{-k} + (i\omega\tau)^{-h} + (i\omega\beta\tau)^{-1}}$$

$$\log a_T = \frac{-C_1(T - T_0)}{C_2 + (T - T_0)}$$

E_0 (MPa)	32 200
E_{00} (MPa)	110
δ	1,82
k	0,182
h	0,530
β	500
τ_0 (sec)	0,135
C_1	20,96
C_2	148,09

Temp,(°C)	Freq,(Hz)	|E*|(MPa)	ϕ (°)	E1(MPa)	E2(MPa)
-33,0	0,03	27188	2,7	27157	1289
-33,0	0,1	28097	2,1	28079	1008
-33,0	0,3	28750	1,8	28735	916
-33,0	1	29313	1,3	29305	686
-33,0	3	29810	1,2	29803	646
-33,0	10	30328	0,9	30325	461
-23,8	0,03	22836	5,2	22743,	2058
-23,8	0,1	24289	4,2	24223	1789
-23,8	0,3	25476	3,6	25425	1605
-23,8	1	26576	3,0	26540	1376
-23,8	3	27390	2,5	27365	1178
-23,8	10	28297	1,8	28282	907
-14,1	0,03	16199	10,1	15949	2837
-14,1	0,1	18251	8,3	18061	2630
-14,1	0,3	19965	6,9	19821	2386
-14,1	1	21705	5,8	21593	2200
-14,1	3	23049	5,0	22961	2020
-14,1	10	24530	3,9	24474	1666
-4,3	0,03	8482	20,6	7941	2979
-4,3	0,1	10786	16,8	10325	3120
-4,3	0,3	12870	13,7	12504	3045
-4,3	1	15174	11,3	14880	2976
-4,3	3	17146	9,3	16919	2783
-4,3	10	19270	7,7	19096	2584
5,4	0,03	2857	34,8	2346	1631
5,4	0,1	4354	30,6	3748	2216
5,4	0,3	6097	26,0	5480	2672
5,4	1	8325	21,1	7765	3001
5,4	3	10445	17,7	9953	3168
5,4	10	12909	14,4	12503	3208
15,1	0,03	779	40,5	592	506
15,1	0,1	1263	40,3	963	816
15,1	0,3	2014	38,4	1578	1250
15,1	1	3268	34,6	2689	1857
15,1	3	4779	30,5	4118	2424
15,1	10	6919	25,2	6261	2944
25,1	0,03	290	34,1	240	162
25,1	0,1	403	38,0	318	248
25,1	0,3	588	40,6	446	383
25,1	1	950	41,9	707	634
25,1	3	1511	41,8	1126	1007
25,1	10	2494	39,3	1931	1578
35,0	0,03	145	27,6	129	67
35,0	0,1	189	30,9	162	97
35,0	0,3	255	34,9	209	146
35,0	1	379	38,9	294	238
35,0	3	581	42,3	429	391
35,0	10	976	44,3	699	682

Mixture RAP028-Mix No.1 (Specimen P1-A4)

Mixture ID: RAP028 Bitumen type: PG 64-28 Specimen: P1-A4
Mixture No.: 1 Bitumen content: 4,5% Air void: 3,24%
Mixture type: GB-20

Cole Cole Plan for Virgin mix RAP064 (P1-A4)-Mix No.1

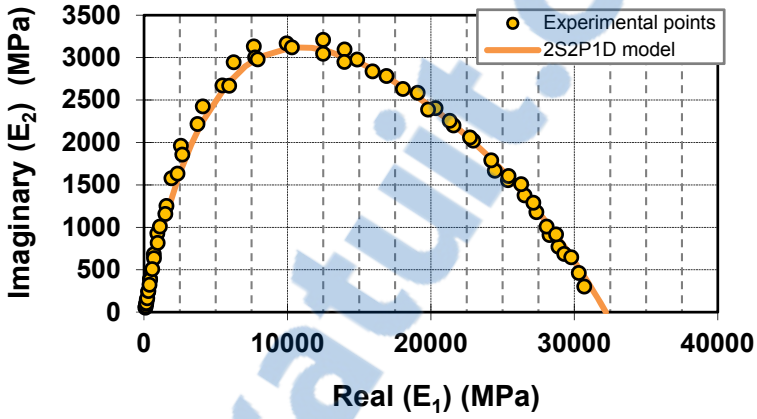

Black space for Virgin mix RAP064 (P1-A4)-Mix No.1

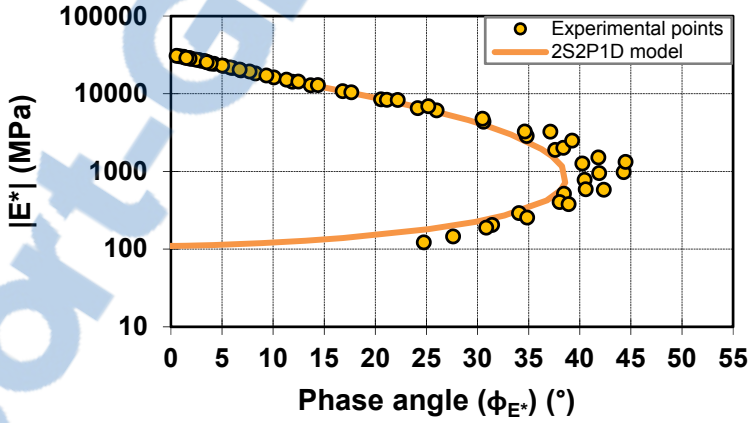

Master curver of the norm of complex modulus for Virgin mix RAP064 (P1-A4)-Mix No.1

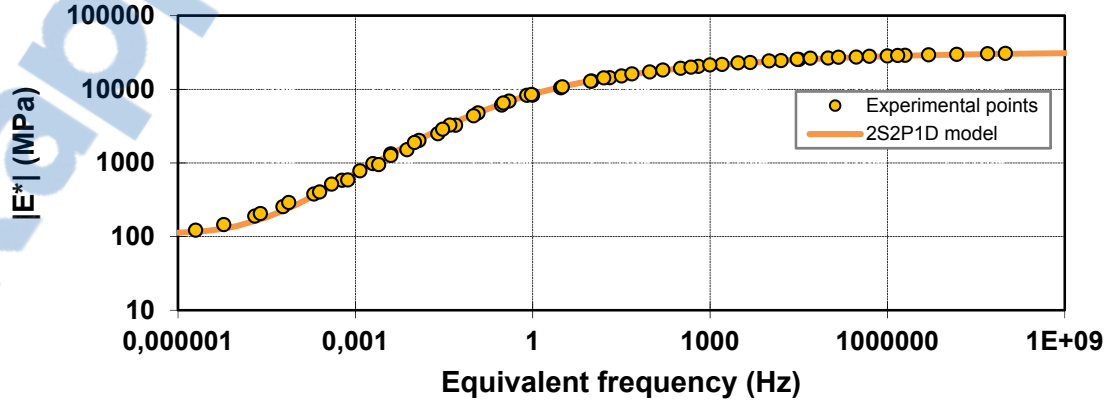

METHOD LC 26-700
COMPLEX MODULUS OF ASPHALT MIXTURE

Specimen: P2-A4
Air void: 6,1%

Bulk density: 2,443
Maximum density: 2,601

Mixture ID: RAP1528CU
Mixture No.: 2
Mixture type: GB-20
%RAP: 15
Bitumen type: PG 64-28
Bitumen content: 4,5%
Air void: 6,36%
Aggregate source:
Bitumen source:
Mixture source:

2S2P1D MODEL OF COMPLEX MODULUS, E* (MPa)

$$E^*(i\omega\tau) = E_{00} + \frac{E_0 - E_{00}}{1 + \delta(i\omega\tau)^{-k} + (i\omega\tau)^{-h} + (i\omega\beta\tau)^{-1}}$$

$$\log a_T = \frac{-C_1(T-T_0)}{C_2+(T-T_0)}$$

E_0 (MPa)	34 900
E_{00} (MPa)	60
δ	2,3
k	0,177
h	0,544
β	500
τ_0 (sec)	0,18
C_1	27,38
C_2	178,00

Temp(°C)	Freq.(Hz)	|E*|(MPa)	ϕ(°)	E1(MPa)	E2(MPa)
-34,8	0,03	29848	3,1	29792	1611
-34,8	0,1	30865	2,1	30842	1121
-34,8	0,3	31638	1,6	31626	879
-34,8	1	32026	1,2	32019	671
-34,8	3	32515	1,2	32506	704
-34,8	10	33062	0,8	33058	476
-24,9	0,03	24871	5,5	24740	2373
-24,9	0,1	26466	4,0	26399	1842
-24,9	0,3	27438	3,4	27389	1639
-24,9	1	28723	2,8	28688	1415
-24,9	3	29639	2,4	29613	1223
-24,9	10	30580	1,8	30565	939
-15,0	0,03	17438	8,9	17228	2687
-15,0	0,1	19501	7,4	19338	2514
-15,0	0,3	21283	6,7	21137	2486
-15,0	1	23091	5,7	22975	2305
-15,0	3	24667	5,0	24575	2132
-15,0	10	26294	4,0	26229	1829
-5,0	0,03	9142	18,6	8666	2913
-5,0	0,1	11368	15,2	10971	2977
-5,0	0,3	13478	12,8	13141	2993
-5,0	1	15726	10,7	15451	2929
-5,0	3	17723	9,3	17489	2871
-5,0	10	19887	7,9	19696	2745
5,0	0,03	3168	32,1	2684	1681
5,0	0,1	4643	27,6	4116	2148
5,0	0,3	6289	23,7	5756,6	2531
5,0	1	8413	19,9	7911	2863
5,0	3	10508	16,9	10054	3055
5,0	10	12957	14,0	12579	3138
15,0	0,03	789	41,2	594	520
15,0	0,1	1304	39,3	1008	826
15,0	0,3	2047	36,8	1640	1225
15,0	1	3256	32,7	2739	1762
15,0	3	4714	28,5	4143	2248
15,0	10	6792	24,0	6207	2759
24,6	0,03	219	41,3	164	144
24,6	0,1	358	43,9	258	248
24,6	0,3	587	44,1	42	409
24,6	1	1024	42,8	751	696
24,6	3	1674	40,6	1271	1089
24,6	10	2791	36,7	2239	1667
34,9	0,03	76	37,0	60	45
34,9	0,1	110	40,9	83	72
34,9	0,3	168	43,7	121	116
34,9	1	285	46,2	198	206
34,9	3	480	47,4	325	354
34,9	10	867	47,4	587	638

Mixture RAP1528CU-Mix No.2 (Specimen P2-A4)

Mixture ID: RAP1528CU Bitumen type: PG 64-28 Specimen: P2-A4
Mixture No.: 2 Bitumen content: 4,5% Air void: 6,1%
Mixture type: GB-20

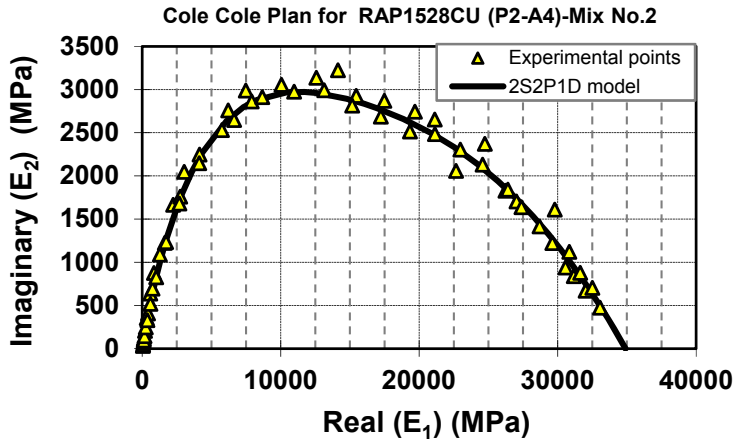

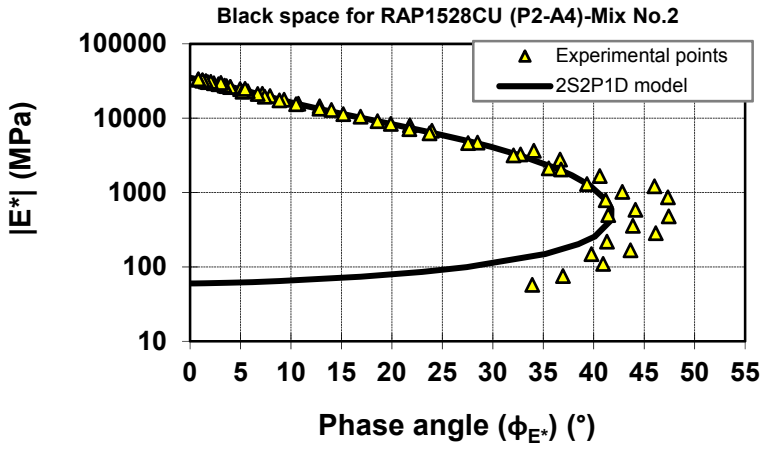

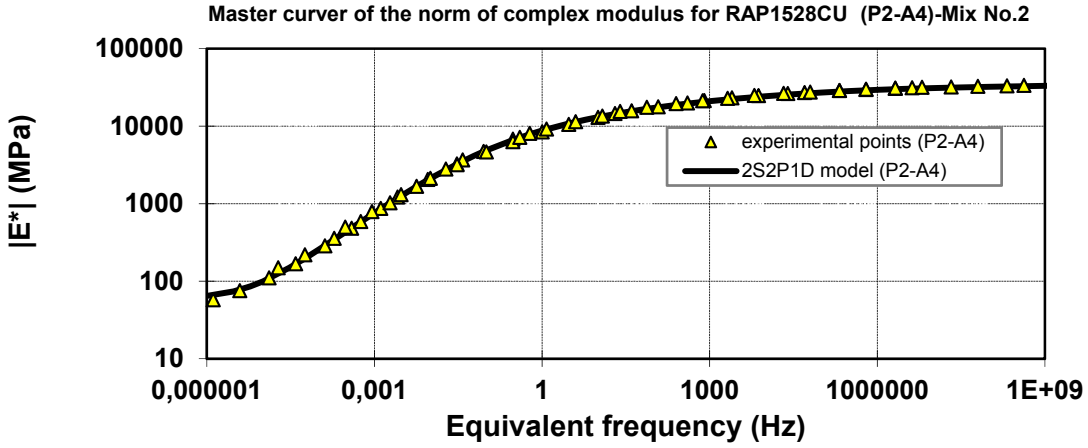

METHOD LC 26-700
COMPLEX MODULUS OF ASPHALT MIXTURE

Specimen: P1-A5
Air void: 5,5%

Bulk density: 2,459
Maximum density: 2,601

Mixture ID: RAP1528CU
Mixture No.: 2
Mixture type: GB-20
%RAP: 15
Bitumen type: PG 64-28
Bitumen content: 4,5%
Air void: 6,36%
Aggregate source:
Bitumen source:
Mixture source:

2S2P1D MODEL OF COMPLEX MODULUS, E* (MPa)

$$E^*(i\omega\tau) = E_{00} + \frac{E_0 - E_{00}}{1 + \delta(i\omega\tau)^{-k} + (i\omega\tau)^{-h} + (i\omega\beta\tau)^{-1}}$$

$$\log a_T = \frac{-C_1(T-T_0)}{C_2+(T-T_0)}$$

E_0 (MPa)	31 300
E_{00} (MPa)	80
δ	2,3
k	0,177
h	0,544
β	500
τ_0 (sec)	0,69
C_1	155,0
C_2	977,5

Temp.(°C)	Freq.(Hz)	|E*|(MPa)	ϕ (°)	E1(MPa)	E2(MPa)
-34,2	0,03	26791	2,1	26772	1003
-34,2	0,1	27514	2,1	27496	990
-34,2	0,3	28082	1,6	28072	775
-34,2	1	28619	1,3	28612	640
-34,2	3	28920	1,1	28915	559
-34,2	10	29381	1,0	29377	504
-25,6	0,03	22797	4,3	22733	1709
-25,6	0,1	23997	3,6	23948	1517
-25,6	0,3	24927	3,3	24885	1443
-25,6	1	25794	2,7	25766	1198
-25,6	3	26597	2,3	26575	1079
-25,6	10	27328	1,9	27313	896
-15,7	0,03	16779	8,3	16601	2428
-15,7	0,1	18526	6,8	18395	2192
-15,7	0,3	19963	5,9	19858	2035
-15,7	1	21376	5,1	21291	1905
-15,7	3	22627	4,4	22560	1735
-15,7	10	23898	3,7	23848	1542
-5,7	0,03	9769	15,2	9425	2571
-5,7	0,1	11768	13,1	11460	2675
-5,7	0,3	13573	11,1	13320	2605
-5,7	1	15488	9,4	15280	2532
-5,7	3	17123	8,0	16958	2369
-5,7	10	18850	6,8	18717	2237
4,2	0,03	4006	28,6	3517	1918
4,2	0,1	5576	23,9	5099	2257
4,2	0,3	7190	20,3	6741	2499
4,2	1	9203	17,0	8798	2696
4,2	3	10993	14,7	10636	2780
4,2	10	13115	12,3	12816	2783
14,2	0,03	1104	40,1	845	711
14,2	0,1	1800	37,0	1437	1083
14,2	0,3	2766	32,9	2322	1503
14,2	1	4114	28,1	3628	1939
14,2	3	5565	25,0	5041	2357
14,2	10	7465	21,4	6948	2729
24,6	0,03	227	47,6	153	167
24,6	0,1	370	46,9	253	270
24,6	0,3	567	47,5	383	418
24,6	1	838	45,8	584	601
24,6	3	1167	44,2	837	813
24,6	10	1603	42,5	1181	1083

Mixture RAP1528CU-Mix No.2 (Specimen P1-A4)

Mixture ID: RAP1528CU Bitumen type: PG 64-28 Specimen: P1-A5
Mixture No.: 2 Bitumen content: 4,5% Air void: 5,5%
Mixture type: GB-20

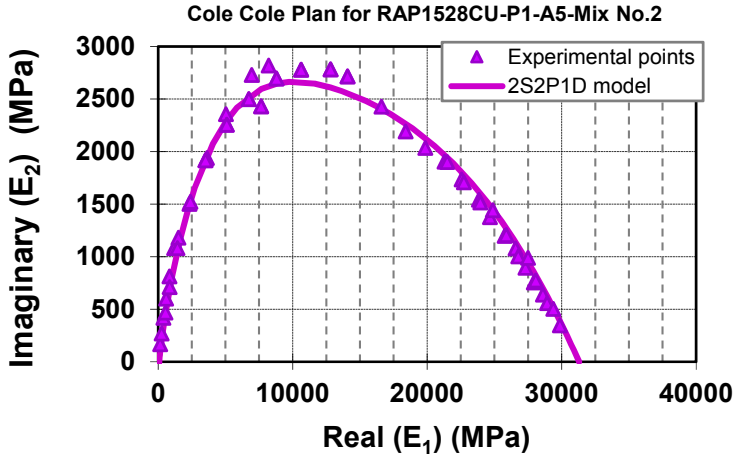

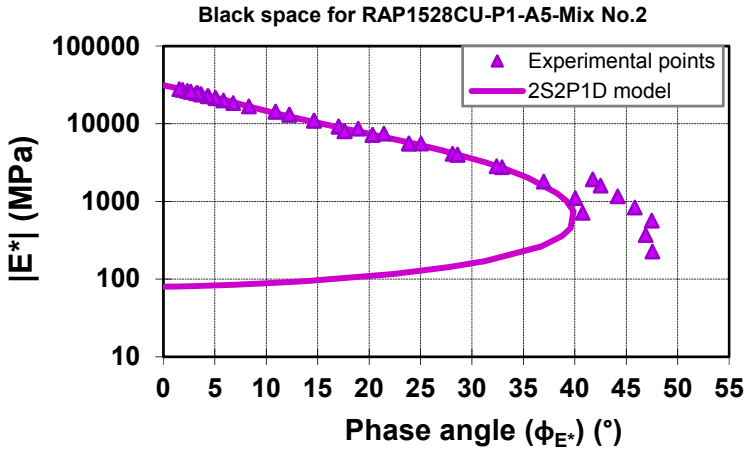

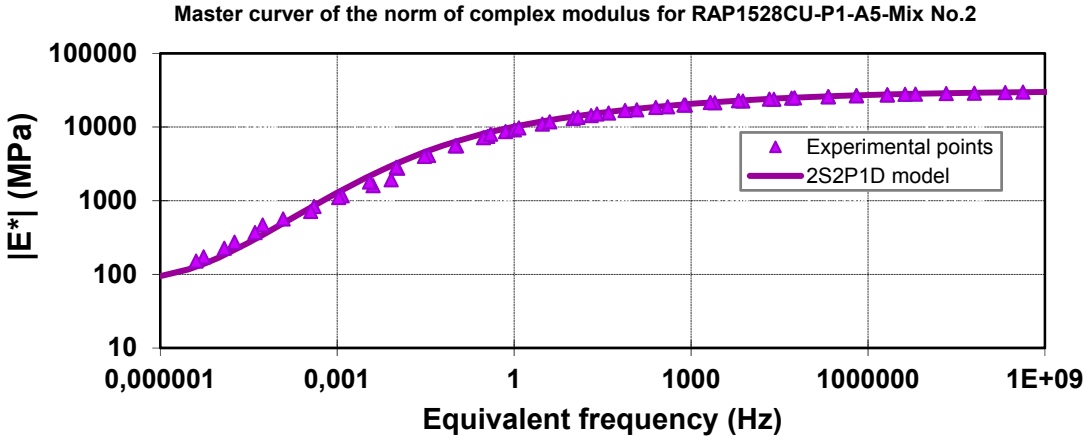

METHOD LC 26-700
COMPLEX MODULUS OF ASPHALT MIXTURE

Specimen: P1-A3
Air void: 3,1%

Bulk density: 2,542
Maximum density: 2,622

Mixture ID: RAP2528CU
Mixture No.: 3
Mixture type: GB-20
%RAP: 25
Bitumen type: PG 64-28
Bitumen content: 4,5%
Air void: 5,66%
Aggregate source:
Bitumen source:
Mixture source:

2S2P1D MODEL OF COMPLEX MODULUS, E* (MPa)

$$E^*(i\omega\tau) = E_{00} + \frac{E_0 - E_{00}}{1 + \delta(i\omega\tau)^{-k} + (i\omega\tau)^{-h} + (i\omega\beta\tau)^{-1}}$$

$$\log a_T = \frac{-C_1(T-T_0)}{C_2+(T-T_0)}$$

E_0 (MPa)	36 350
E_{00} (MPa)	127
δ	1,81
k	0,177
h	0,544
β	500
τ_0 (sec)	0,21
C_1	26,13
C_2	179,53

Temp. (°C)	Freq.(Hz)	|E*|(MPa)	ϕ (°)	E1 (MPa)	E2 (MPa)
-31,1	0,03	31303	2,3	31277	1256
-31,1	0,1	32288	1,9	32270	1071
-31,1	0,3	32891	1,5	32880	888
-31,1	1	33506	1,2	33498	723
-31,1	3	34025	1,0	34020	597
-31,1	10	34402	0,8	34399	462
-23,4	0,03	26446	4,7	26358	2156
-23,4	0,1	27883	3,9	27817	1909
-23,4	0,3	29165	3,2	29118	1648
-23,4	1	30361	2,6	30329	1392
-23,4	3	31330	2,2	31308	1181
-23,4	10	32135	1,4	32125	784
-13,9	0,03	19232	8,9	19001	2972
-13,9	0,1	21396	7,4	21216	2762
-13,9	0,3	23219	6,3	23081	2530
-13,9	1	25082	5,3	24976	2304
-13,9	3	26642	4,4	26563	2051
-13,9	10	28106	3,7	28048	1803
-4,2	0,03	10575	18,3	10039	3326
-4,2	0,1	13082	15,2	12626	3420
-4,2	0,3	15396	12,5	15029	3345
-4,2	1	17848	10,3	17560	3191
-4,2	3	19970	8,6	19747	2971
-4,2	10	22269	6,9	22109	2657
5,5	0,03	3885	31,6	3309	2035
5,5	0,1	5613	27,7	4970	2609
5,5	0,3	7580	23,8	6937	3055
5,5	1	10119	19,5	9539	3377
5,5	3	12576	16,2	12077	3509
5,5	10	15203	12,8	14823	3379
15,2	0,03	1208	37,5	959	735
15,2	0,1	1863	36,7	1493	1114
15,2	0,3	2802	34,9	2299	1602
15,2	1	4326	31,1	3702	2237
15,2	3	6185	27,1	5508	2813
15,2	10	8669	22,4	8016	3301
25,7	0,03	368	34,4	304	208
25,7	0,1	584	37,9	461	359
25,7	0,3	907	39,9	695	582
25,7	1	1503	40,0	1152	966
25,7	3	2386	38,1	1877	1474
25,7	10	3796	34,4	3133	2144
35,4	0,03	192	28,9	168	93
35,4	0,1	256	32,2	216	136
35,4	0,3	350	35,8	284	204
35,4	1	535	39,4	413	339
35,4	3	833	41,5	623	552
35,4	10	1389	42,5	1025	939

Mixture RAP2528CU-Mix No.3 (Specimen P1-A3)

Mixture ID: RAP2528CU
Mixture No.: 3
Mixture type: GB-20

Bitumen type: PG 64-28
Bitumen content: 4,5%

Specimen: P1-A3
Air void: 3,1%

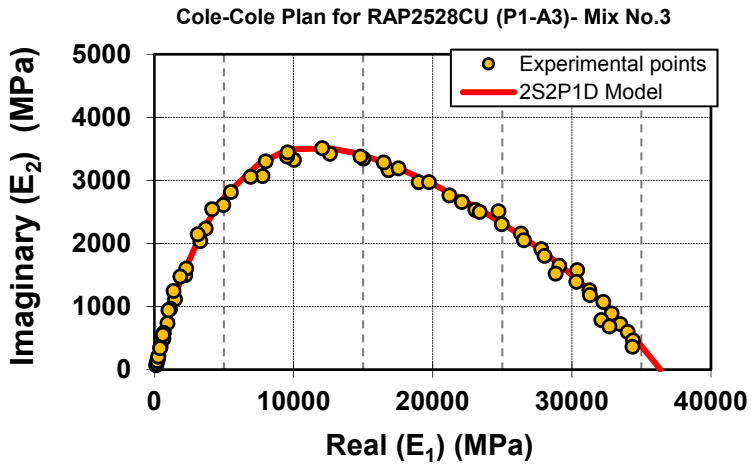

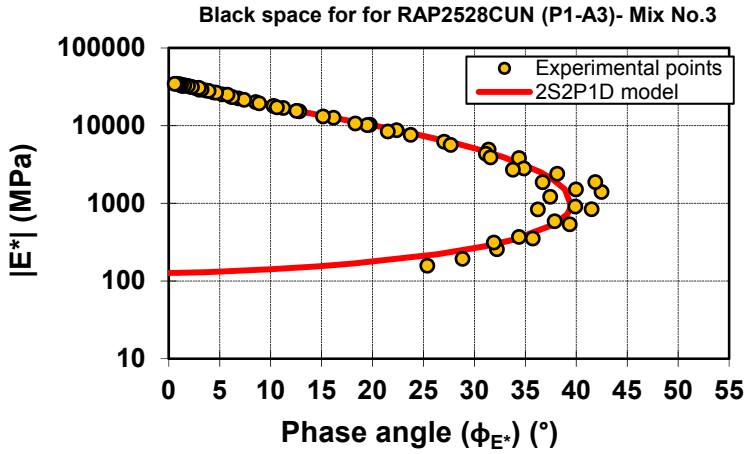

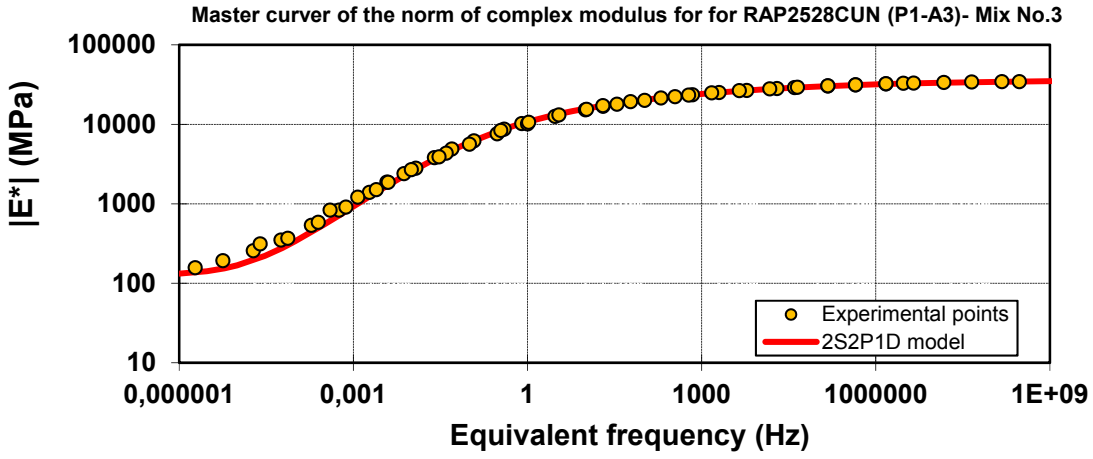

METHOD LC 26-700
COMPLEX MODULUS OF ASPHALT MIXTURE

Specimen: P2-A2
Air void: 4,5%

Bulk density: 2,542
Maximum density: 2,622

Mixture ID: RAP2528CU
Mixture No.: 3
Mixture type: GB-20
%RAP: 25
Bitumen type: PG 64-28
Bitumen content: 4,5%
Air void: 5,66%
Aggregate source:
Bitumen source:
Mixture source:

2S2P1D MODEL OF COMPLEX MODULUS, E* (MPa)

$$E^*(i\omega\tau) = E_{00} + \frac{E_0 - E_{00}}{1 + \delta(i\omega\tau)^{-k} + (i\omega\tau)^{-h} + (i\omega\beta\tau)^{-1}}$$

$$\log a_T = \frac{-C_1(T-T_0)}{C_2+(T-T_0)}$$

E_0 (MPa)	35 950
E_{00} (MPa)	107
δ	1,9
k	0,177
h	0,544
β	500
τ_0 (sec)	0,19
C_1	28,42
C_2	185,48

Temp.(°C)	Freq.(Hz)	|E*|(MPa)	ϕ(°)	E1 (MPa)	E2(MPa)
-31,7	0,03	30409	2,5	30380	1345
-31,7	0,1	31306	2,2	31284	1179
-31,7	0,3	32133	1,7	32118	972
-31,7	1	32846	1,3	32838	749
-31,7	3	33343	1,2	33336	680
-31,7	10	33989	0,8	33985	494
-22,4	0,03	25314	5,1	25215	2236
-22,4	0,1	26885	4,3	26809	2012
-22,4	0,3	28195	3,6	28140	1770
-22,4	1	29401	2,9	29363	1501
-22,4	3	30373	2,3	30348	1232
-22,4	10	31261	1,8	31246	965
-13,1	0,03	18182	9,6	17929	3021
-13,1	0,1	20309	7,8	20120	2758
-13,1	0,3	22199	6,8	22041	2640
-13,1	1	24104	5,7	23986	2387
-13,1	3	25594	4,7	25508	2097
-13,1	10	27215	3,8	27155	1812
-3,6	0,03	9704	19,1	9167	3181
-3,6	0,1	12180	16,0	11707	3358
-3,6	0,3	14469	13,2	14085	3310
-3,6	1	16923	10,8	16623	3172
-3,6	3	18996	9,0	18763	2966
-3,6	10	21259	7,5	21078	2765
5,8	0,03	3535	32,6	2977	1906
5,8	0,1	5201	28,0	4591	2442
5,8	0,3	7117	24,2	6493	2913
5,8	1	9532	19,8	8969	3229
5,8	3	11884	16,4	11398	3362
5,8	10	14534	13,6	14125	3426
15,4	0,03	996	39,6	768	635
15,4	0,1	1596	38,9	1242	1003
15,4	0,3	2516	36,7	2017	1504
15,4	1	3942	32,8	3316	2133
15,4	3	5665	28,7	4968	2723
15,4	10	8038	23,6	7365	3218
24,7	0,03	347	36,2	280	205
24,7	0,1	530	39,6	408	338
24,7	0,3	822	41,4	617	544
24,7	1	1391	41,1	1044	920
24,7	3	2228	39,5	1718	1418
24,7	10	3619	35,4	2952	2094
35,8	0,03	148	28,3	131	70
35,8	0,1	194	32,6	164	105
35,8	0,3	267	36,9	213	160
35,8	1	412	41,1	310	271
35,8	3	654	44,0	470	454
35,8	35,8	1137	44,9	805	803

Mixture RAP2528CU-Mix No.3 (Specimen P2-A2)

Mixture ID: RAP2528CU Bitumen type: PG 64-28 Specimen: P2-A2
Mixture No.: 3 Bitumen content: 4,5% Air void: 4,5%
Mixture type: GB-20

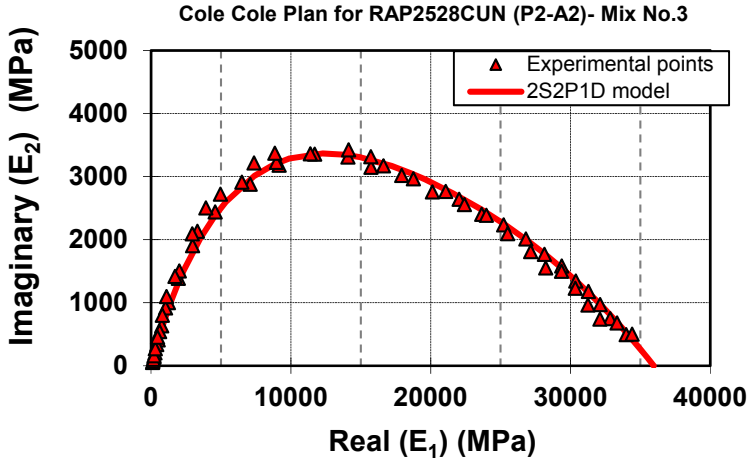

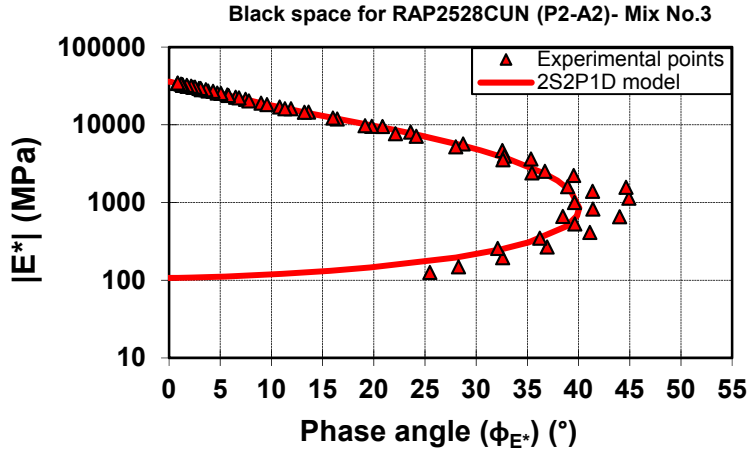

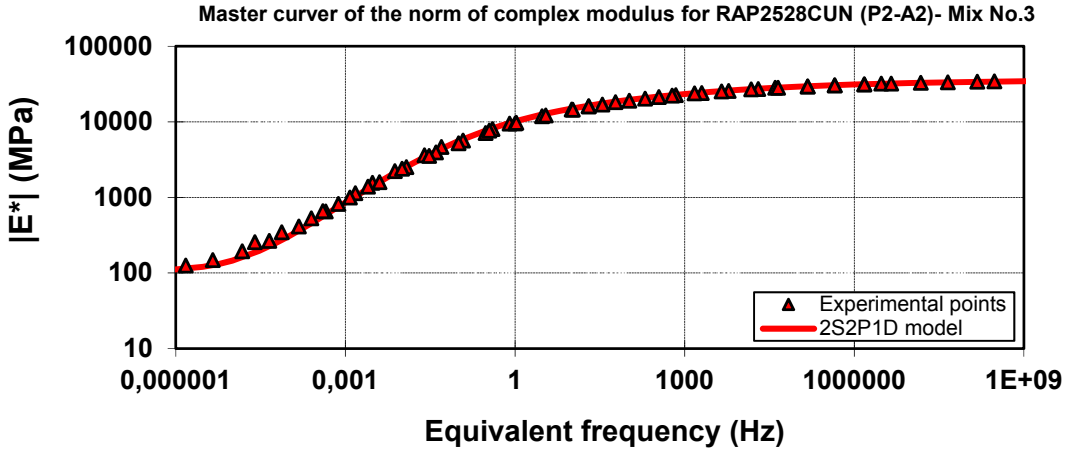

METHOD LC 26-700
COMPLEX MODULUS OF ASPHALT MIXTURE

Specimen: P2-A4
Air void: 2,9%

Bulk density: 2,540
Maximum density: 2,618

Mixture ID: RAP4028CU
Mixture No.: 4
Mixture type: GB-20
%RAP: 40
Bitumen type: PG 64-28
Bitumen content: 4,5%
Air void: 3,8%
Aggregate source:
Bitumen source:
Mixture source:

2S2P1D MODEL OF COMPLEX MODULUS, E* (MPa)

$$E^*(i\omega\tau) = E_{00} + \frac{E_0 - E_{00}}{1 + \delta(i\omega\tau)^{-k} + (i\omega\tau)^{-h} + (i\omega\beta\tau)^{-1}}$$

$$\log a_T = \frac{-C_1(T-T_0)}{C_2+(T-T_0)}$$

E_0 (MPa)	33 700
E_{00} (MPa)	110
δ	2,15
k	0,177
h	0,544
β	500
τ_0 (sec)	0,22
C_1	22,26
C_2	150,16

Temp,(°C)	Freq.(Hz)	|E*|(MPa)	ϕ (°)	E1 (MPa)	E2 (MPa)
-33,0	0,03	28131	2,8	28064	1365
-33,0	0,1	29071	2,2	29050	1106
-33,0	0,3	29775	1,9	29758	1001
-33,0	1	30435	1,5	30424	812
-33,0	3	31044	1,2	31036	664
-33,0	10	31555	0,9	31550	517
-23,8	0,03	23472	5,1	23379	2077
-23,8	0,1	24904	4,2	24836	1835
-23,8	0,3	26126	3,7	26073	1675
-23,8	1	27325	3,1	27284	1501
-23,8	3	28250	2,5	28224	1216
-23,8	10	29294	2,0	29276	1006
-14,0	0,03	16519	9,5	16294	2718
-14,0	0,1	18560	7,9	18381	2566
-14,0	0,3	20307	6,8	20164	2402
-14,0	1	22062	5,8	21948	2245
-14,0	3	23585	5,0	23496	2044
-14,0	10	25189	4,3	25117	1903
-4,2	0,03	8854	18,3	8407	2776
-4,2	0,1	11045	15,4	10648	2935
-4,2	0,3	13068	13,2	12723	2979
-4,2	1	15277	11,0	14997	2910
-4,2	3	17214	9,4	16983	2813
-4,2	10	19335	7,7	19159	2599
5,2	0,03	3452	30,1	2986	1732
5,2	0,1	4942	25,9	444	2159
5,2	0,3	6618	22,5	6114	2531
5,2	1	8712	19,0	8239	2831
5,2	3	10037	15,0	9640	2773
5,2	10	13166	13,4	12805	3060
14,8	0,03	1047	38,7	816	654
14,8	0,1	1660	36,8	1330	993
14,8	0,3	2529	34,0	2096	1418
14,8	1	3840	30,1	3324	1924
14,8	3	5373	26,6	4805	2404
14,8	10	7435	22,7	6860	2866
26,3	0,03	333	35,4	272	193
26,3	0,1	477	38,1	376	294
26,3	0,3	708	39,6	545	452
26,3	1	1185	39,4	916	753
26,3	3	1876	37,7	1484	1147
26,3	10	3029	34,7	2490	1724
34,3	0,03	104	36,1	84	61
34,3	0,1	148	38,9	116	93
34,3	0,3	220	41,2	165	145
34,3	1	362	43,7	262	250
34,3	3	596	44,7	424	419
34,3	10	1048	44,3	750	733

Mixture RAP4028CU-Mix No.4 (Specimen P2-A4)

Mixture ID: RAP4028CU
Mixture No.: 4
Mixture type: GB-20

Bitumen type: PG 64-28
Bitumen content: 4,5%

Specimen: P2-A4
Air void: 2,9%

Cole Cole Plan for RAP4028CUN (P2-A4)-Mix No.4

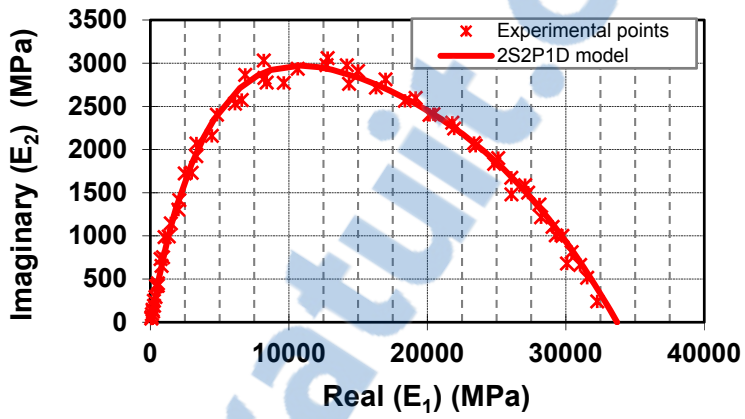

Black space for RAP4028CUN (P2-A4)-Mix No.4

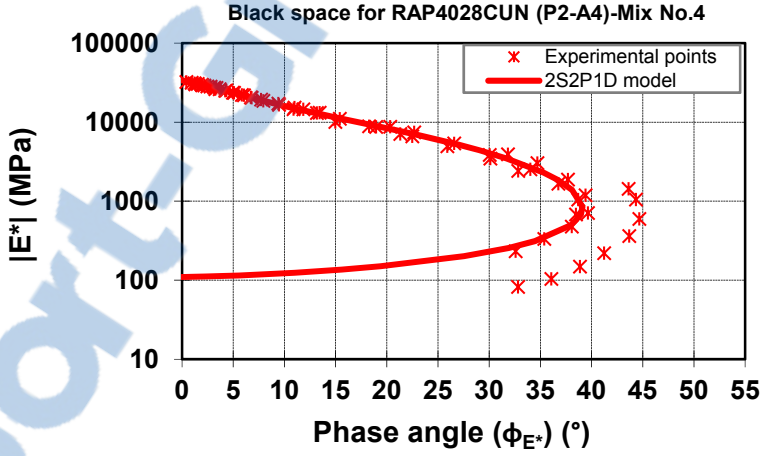

Master curver of the norm of complex for RAP4028CUN (P2-A4)-Mix No.4

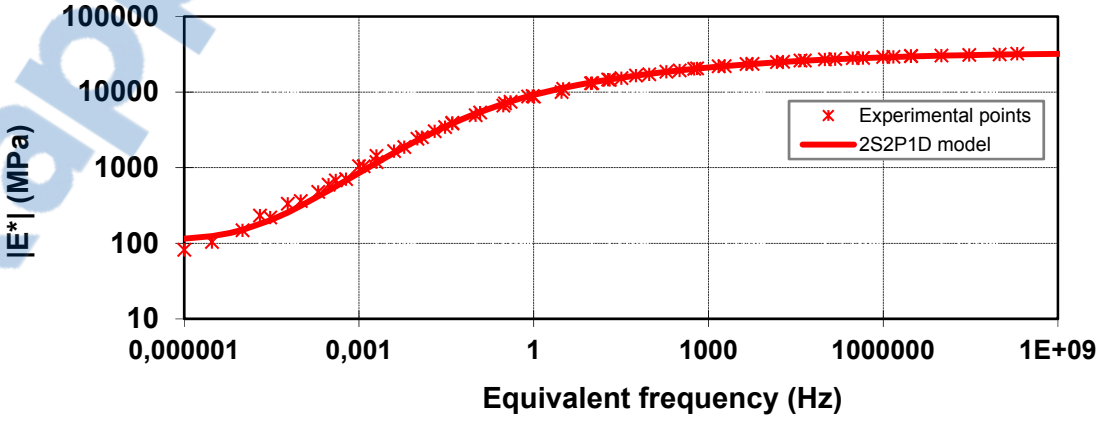

METHOD LC 26-700
COMPLEX MODULUS OF ASPHALT MIXTURE

Specimen: P1-A1
Air void: 4,6%

Bulk density: 2,491
Maximum density: 2,612

Mixture ID: RAP1528HU
Mixture No.: 5
Mixture type: GB-20
%RAP: 15
Bitumen type: PG 64-28
Bitumen content: 4,5%
Air void: 7,1
Aggregate source:
Bitumen source:
Mixture source:

2S2P1D MODEL OF COMPLEX MODULUS, E* (MPa)

$$E^*(i\omega\tau) = E_{00} + \frac{E_0 - E_{00}}{1 + \delta(i\omega\tau)^{-k} + (i\omega\tau)^{-h} + (i\omega\beta\tau)^{-1}}$$

$$\log a_T = \frac{-C_1(T-T_0)}{C_2+(T-T_0)}$$

E_0 (MPa)	30 700
E_{00} (MPa)	110
δ	2,15
k	0,177
h	0,544
β	500
τ_0 (sec)	0,22
C_1	22,42
C_2	150,14

Temp,(°C)	Freq.(Hz)	|E*|(MPa)	ϕ (°)	E1(MPa)	E2(MPa)
-32,7	0,03	25457	3,0	25422	1321
-32,7	0,1	26318	2,4	26295	1104
-32,7	0,3	26964	2,0	26948	931
-32,7	1	27634	1,6	27623	778
-32,7	3	28099	1,4	28090	706
-32,7	10	28486	1,1	28480	533
-23,6	0,03	21279	5,2	21193	1917
-23,6	0,1	22574	4,3	22510	1684
-23,6	0,3	23684	3,7	23635	1517
-23,6	1	24799	3,1	24764	1323
-23,6	3	25708	2,5	25683	1129
-23,6	10	26438	2,6	26397	1170
-13,9	0,03	15007	9,5	14800	2485
-13,9	0,1	16821	8,0	16656	2349
-13,9	0,3	18415	6,9	18282	2202
-13,9	1	20086	5,9	19979	2074
-13,9	3	21373	5,1	21289	1889
-13,9	10	22845	4,3	22782	1694
-3,7	0,03	7903	18,6	7492	2518
-3,7	0,1	9790	15,7	9426	2645
-3,7	0,3	11643	13,3	11332	2672
-3,7	1	13647	11,0	13398	2594
-3,7	3	15432	934	15226	2511
-3,7	10	17339	7,9	17173	2391
5,2	0,03	3229	29,7	2806	1598
5,2	0,1	4579	26,2	4109	2020
5,2	0,3	6105	22,8	5627	2367
5,2	1	8014	19,1	7575	2616
5,2	3	9874	15,9	9497	2700
5,2	10	11998	13,0	11690	2700
15,7	0,03	919	36,9	735	552
15,7	0,1	1394	36,9	1115	838
15,7	0,3	2102	34,8	1725	1201
15,7	1	3171	31,3	2708	1649
15,7	3	4471	27,5	3967	2062
15,7	10	6131	23,2	5634	2418
26,0	0,03	262	36,4	211	155
26,0	0,1	411	38,6	321	256
26,0	0,3	612	40,0	469	394
26,0	1	984	39,9	754	632
26,0	3	1529	38,4	1199	949
26,0	10	2412	35,5	1964	1400
34,2	0,03	116	33,0	97	63
34,2	0,1	160	37,4	127	97
34,2	0,3	234	39,8	180	150
34,2	1	382	42,3	283	257
34,2	3	622	43,3	453	427
34,2	10	1070	42,3	791	720

Mixture RAP1528HU-Mix No.5 (Specimen P1-A1)

Mixture ID: RAP1528HU Bitumen type: PG 64-28 Specimen: P1-A1
Mixture No.: 5 Bitumen content: 4,5% Air void: 4,6%
Mixture type: GB-20

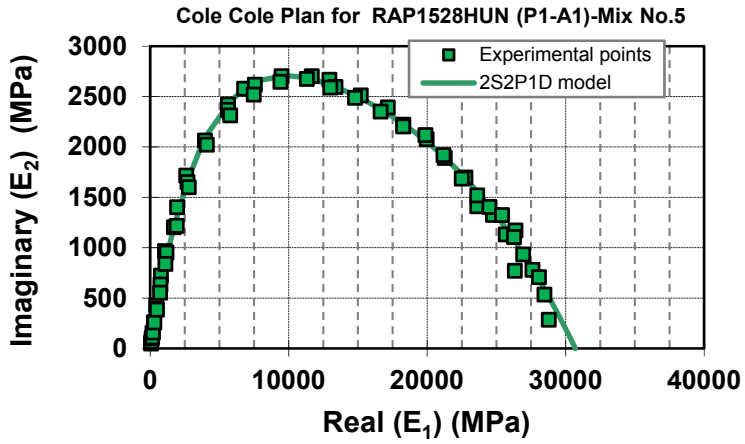

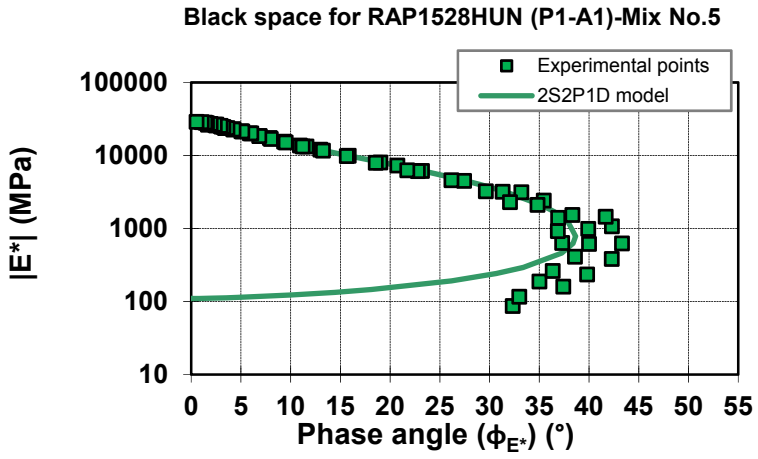

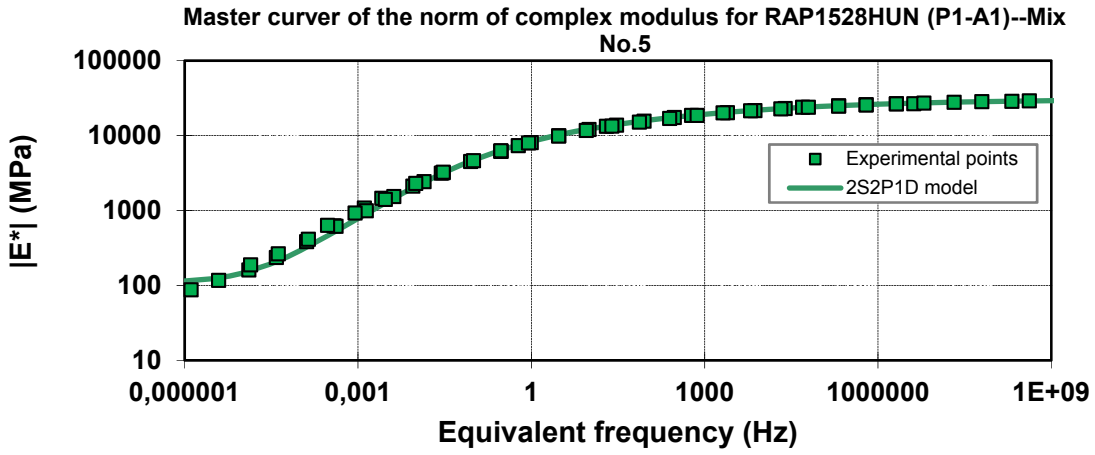

METHOD LC 26-700
COMPLEX MODULUS OF ASPHALT MIXTURE

Specimen: P1-A1
Air void: 3,8%

Bulk density: 2,518
Maximum density: 2,617

Mixture ID: RAP2528HU
Mixture No.: 6
Mixture type: GB-20
%RAP: 25
Bitumen type: PG 64-28
Bitumen content: 4,5%
Air void: 5%
Aggregate source:
Bitumen source:
Mixture source:

2S2P1D MODEL OF COMPLEX MODULUS, E* (MPa)

$$E^*(i\omega\tau) = E_{00} + \frac{E_0 - E_{00}}{1 + \delta(i\omega\tau)^{-k} + (i\omega\tau)^{-h} + (i\omega\beta\tau)^{-1}}$$

$$\log a_T = \frac{-C_1(T-T_0)}{C_2+(T-T_0)}$$

E_0 (MPa)	38 600
E_{00} (MPa)	80
δ	2,30
k	0,177
h	0,540
β	500
τ_0 (sec)	0,40
C_1	29,37
C_2	208,82

Temp, (°C)	Freq,(Hz)	|E*|(MPa)	ϕ (°)	E1 (MPa)	E2 (MPa)
-34,2	0,03	33086	3,6	33009	2061
-34,2	0,1	34234	2,2	34204	1303
-34,2	0,3	34947	1,6	34933	853
-34,2	1	35511	1,3	35501	824
-34,2	3	36118	1,2	36110	754
-34,2	10	36718	0,8	36714	517
-24,4	0,03	27888	4,3	27810	2077
-24,4	0,1	29392	3,7	29329	1913
-24,4	0,3	30709	3,3	30658	1750
-24,4	1	32003	2,7	31967	1526
-24,4	3	32992	2,3	32965	1342
-24,4	10	34058	2,0	34036	1208
-14,5	0,03	20322	8,0	20123	2828
-14,5	0,1	22477	7,0	22311	2725
-14,5	0,3	24257	6,1	24120	2567
-14,5	1	26131	5,1	26026	2336
-14,5	3	27713	4,7	27026	2257
-14,5	10	29337	3,9	29270	1989
-4,6	0,03	11587	15,8	11148	3158
-4,6	0,1	13994	13,5	13607	3267
-4,6	0,3	16203	11,5	15875	3242
-4,6	1	18608	9,7	18344	3123
-4,6	3	20734	8,4	20511	3034
-4,6	10	23025	7,2	22845	2871
5,4	0,03	4655	27,5	4129	2150
5,4	0,1	6428	23,8	5879	2599
5,4	0,3	8373	20,7	7835	2953
5,4	1	10757	17,5	10258	3239
5,4	3	16063	14,9	12623	3364
5,4	10	15673	12,5	15302	3390
15,4	0,03	1355	38,5	1061	843
15,4	0,1	2144	35,8	1739	1253
15,4	0,3	3202	32,6	2699	1724
15,4	1	4769	28,4	4195	2267
15,4	3	6569	24,9	5958	2766
15,4	10	8846	21,1	8251	3190
24,5	0,03	423	42,5	312	286
24,5	0,1	696	42,7	511	472
24,5	0,3	1136	40,7	861	740
24,5	1	1898	38,0	1495	1169
24,5	3	2884	35,2	2356	1663
24,5	10	4372	32,3	3692	2325
35,0	0,03	26	42,8	16	20
35,0	0,1	31	42,7	19	24
35,0	0,3	102	36,4	74	51
35,0	1	250	56,4	127	210
35,0	3	499	43,5	364	328
35,2	10	194	40,4	148	126

Mixture RAP2528HU-Mix No.6 (Specimen P1-A1)

Mixture ID: RAP2528HU
Mixture No.: 6
Mixture type: GB-20

Bitumen type: PG 64-28
Bitumen content: 4,5%

Specimen: P1-A1
Air void: 3,8%

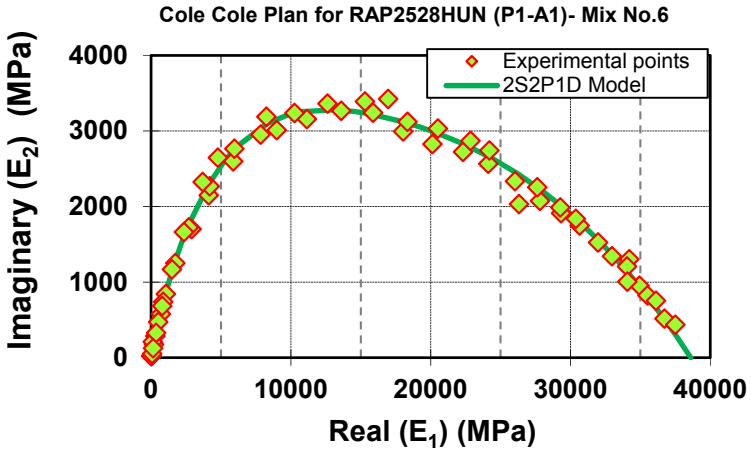

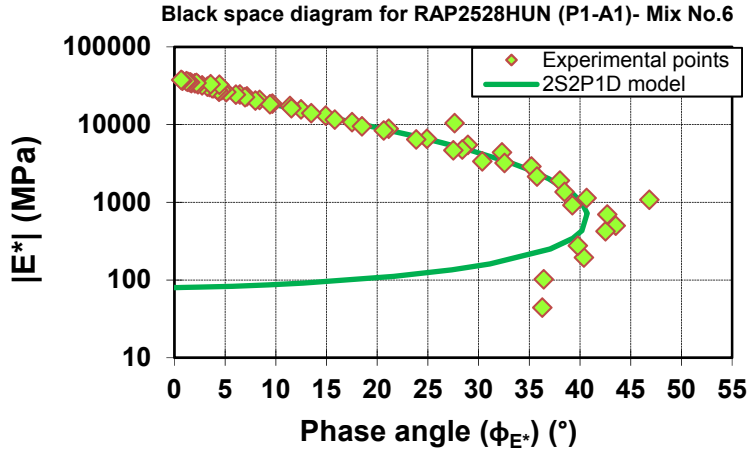

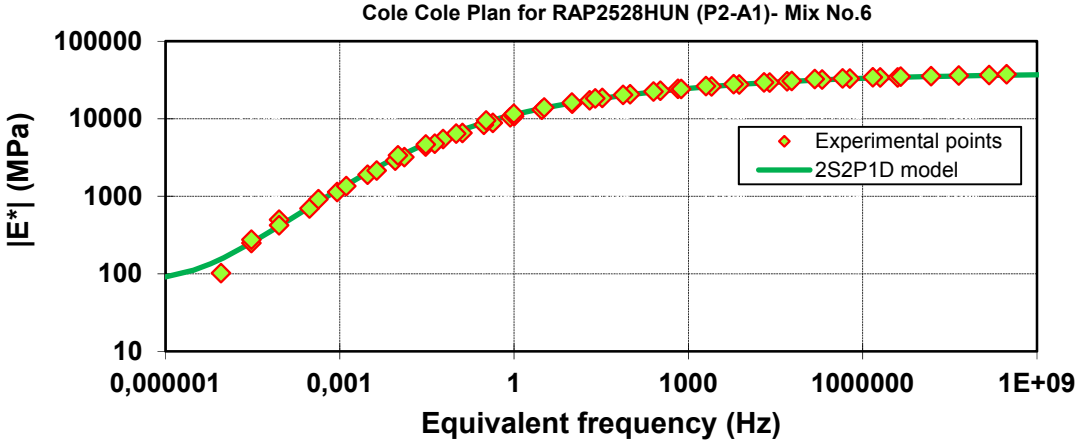

METHOD LC 26-700
COMPLEX MODULUS OF ASPHALT MIXTURE

Specimen: P2-A1
Air void: 3,4%

Bulk density: 2,518
Maximum density: 2,617

Mixture ID: RAP2528HU
Mixture No.: 6
Mixture type: GB-20
%RAP: 25
Bitumen type: PG 64-28
Bitumen content: 4,5%
Air void: 5%
Aggregate source:
Bitumen source:
Mixture source:

2S2P1D MODEL OF COMPLEX MODULUS, E* (MPa)

$$E^*(i\omega\tau) = E_{00} + \frac{E_0 - E_{00}}{1 + \delta(i\omega\tau)^{-k} + (i\omega\tau)^{-h} + (i\omega\beta\tau)^{-1}}$$

$$\log a_T = \frac{-C_1(T-T_0)}{C_2+(T-T_0)}$$

E_0 (MPa)	36 300
E_{00} (MPa)	82
δ	1,85
k	0,177
h	0,544
β	500
τ_0 (sec)	0,20
C_1	26,24
C_2	175,81

Temp,(°C)	Freq,(Hz)	|E*|(MPa)	ϕ (°)	E1 (MPa)	E2 (MPa)
-32,1	0,03	30763	2,6	30730	1413
-32,1	0,1	31661	2,1	31640	1163
-32,1	0,3	32374	1,8	32359	989
-32,1	1	33125	1,4	33116	799
-32,1	3	33615	1,1	33610	619
-32,1	10	34230	0,6	34228	385
-22,9	0,03	25801	5,0	25702	2254
-22,9	0,1	27310	4,1	27238	1970
-22,9	0,3	28626	3,5	28573	1740
-22,9	1	29823	3,0	29783	1545
-22,9	3	30883	2,4	30857	1269
-22,9	10	32005	1,9	31987	1053
-13,5	0,03	18665	9,6	18404	3109
-13,5	0,1	20947	8,0	20743	2916
-13,5	0,3	22786	6,7	22632	2640
-13,5	1	24701	5,6	24584	2402
-13,5	3	26236	4,8	26145	2173
-13,5	10	27768	3,7	27710	1797
-3,7	0,03	9784	19,7	9213	3295
-3,7	0,1	12296	16,4	11798	3464
-3,7	0,3	14646	13,6	14234	3451
-3,7	1	17171	11,0	16858	3264
-3,7	3	19357	9,1	19111	3074
-3,7	10	21735	7,4	21555	2785
5,7	0,03	3453	33,8	2868	1922
5,7	0,1	5181	29,4	4513	2544
5,7	0,3	7176	25,1	6498	3045
5,7	1	9730	20,6	9106	3427
5,7	3	12117	17,0	11588	3540
5,7	10	14868	13,7	14442	3533
15,2	0,03	958	41,1	722	629
15,2	0,1	1580	39,7	1215	1009
15,2	0,3	2494	37,1	1990	1504
15,2	1	3982	32,5	3357	2141
15,2	3	5778	28,5	5076	2759
15,2	10	8185	24,0	7476	3333
24,8	0,03	311	39,1	241	196
24,8	0,1	495	41,3	372	327
24,8	0,3	792	41,9	589	530
24,8	1	1353	41,6	1012	898
24,8	3	2187	39,7	1682	1398
24,8	10	3586	36,0	2899	2110
35,5	0,03	115	34,1	95	64
35,5	0,1	164	37,4	131	100
35,5	0,3	244	40,5	185	158
35,5	1	398	43,5	289	274
35,5	3	649	45,1	458	460
35,2	35,5	1151	45,4	809	820

Mixture RAP2528HU-Mix No.6 (Specimen P2-A1)

Mixture ID: RAP2528HU Bitumen type: PG 64-28 Specimen: P2-A1
Mixture No.: 6 Bitumen content: 4,5% Air void: 3,4%
Mixture type: GB-20

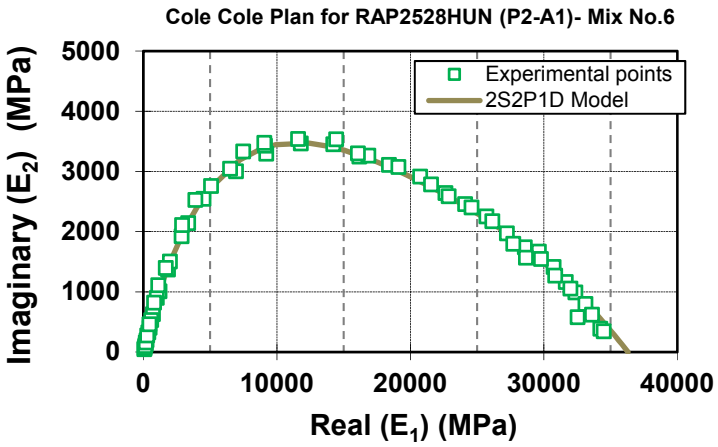

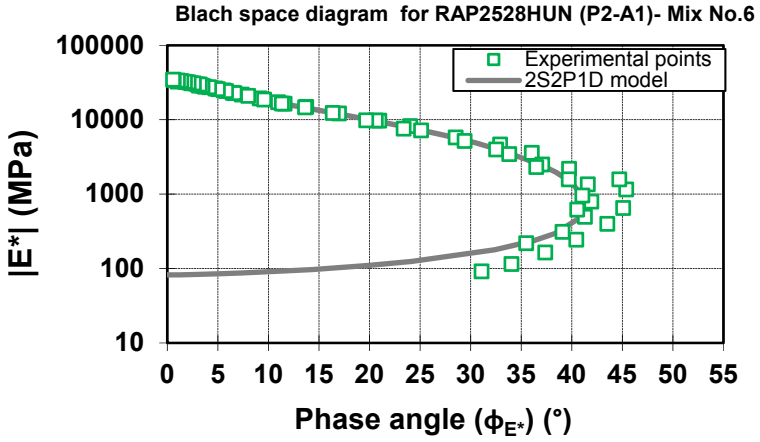

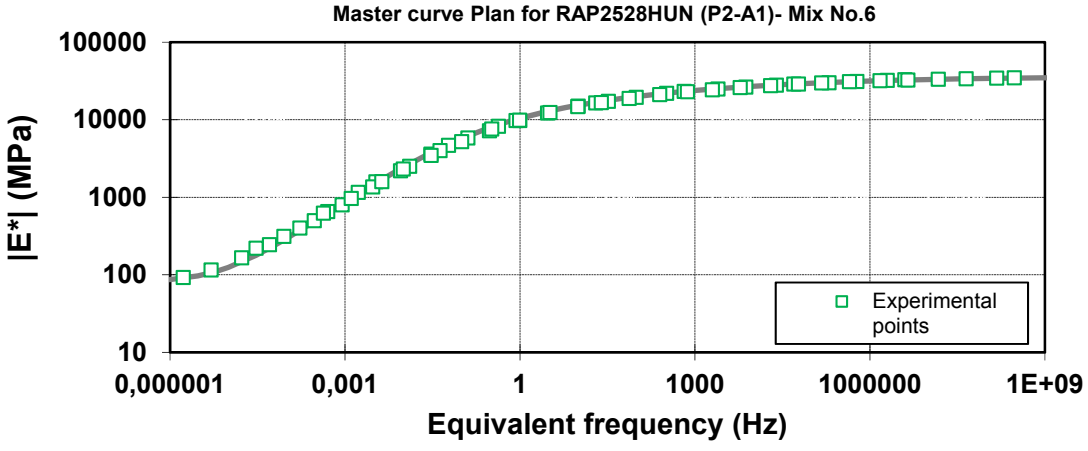

METHOD LC 26-700
COMPLEX MODULUS OF ASPHALT MIXTURE

Specimen: P1-A2
Air void: 3,3%

Bulk density: 2,507
Maximum density: 2,627

Mixture ID: RAP4028HU
Mixture No.: 7
Mixture type: GB-20
%RAP: 15
Bitumen type: PG 64-28
Bitumen content: 4,5%
Air void: 4,69%
Aggregate source:
Bitumen source:
Mixture source:

2S2P1D MODEL OF COMPLEX MODULUS, E* (MPa)

$$E^*(i\omega\tau) = E_{00} + \frac{E_0 - E_{00}}{1 + \delta(i\omega\tau)^{-k} + (i\omega\tau)^{-h} + (i\omega\beta\tau)^{-1}}$$

$$\log a_T = \frac{-C_1(T-T_0)}{C_2+(T-T_0)}$$

E_0 (MPa)	40 700
E_{00} (MPa)	80
δ	2,15
k	0,177
h	0,544
β	500
τ_0 (sec)	0,22
C_1	25,81
C_2	169,67

Temp.(°C)	Freq.(Hz)	|E*|(MPa)	ϕ (°)	E1(MPa)	E2(MPa)
-34,5	0,03	34760	4,4	34640	2584
-34,5	0,1	36529	2,9	36480	1815
-34,5	0,3	37175	1,0	37169	626
-34,5	1	37994	1,0	37987	683
-34,5	3	38580	1,1	38572	721
-34,5	10	39224	0,8	39219	544
-24,5	0,03	30303	4,4	30205	2368
-24,5	0,1	31771	4,3	31683	2359
-24,5	0,3	32759	3,1	32709	1793
-24,5	1	34262	2,6	34227	1553
-24,5	3	35356	2,2	35329	1369
-24,5	10	36277	2,1	36252	1301
-14,8	0,03	21269	9,1	20960	3372
-14,8	0,1	23972	7,1	23783	2977
-14,8	0,3	25558	6,2	25406	2763
-14,8	1	28027	5,6	27894	2728
-14,8	3	29871	4,6	29774	2396
-14,8	10	31728	3,7	31659	2068
-4,8	0,03	11627	18,5	11011	3702
-4,8	0,1	14167	13,6	13769	3324
-4,8	0,3	16595	12,2	16218	3510
-4,8	1	19341	10,3	19030	3453
-4,8	3	21765	9,1	21494	3425
-4,8	10	24414	7,6	24197	3243
5,1	0,03	3864	31,7	3287	2032
5,1	0,1	5711	27,4	5070	2628
5,1	0,3	7782	23,5	7133	3108
5,1	1	10387	19,8	9772	3521
5,1	3	1953	16,7	12407	3721
5,1	10	15977	13,9	15507	3842
15,1	0,03	936	42	695	626
15,1	0,1	1551	40,8	1175	1014
15,1	0,3	2496	38,0	1966	1538
15,1	1	4020	33,6	3348	2226
15,1	3	5851	29,3	5101	2864
15,1	10	8402	23,8	7688	3386
24,5	0,03	293	39,9	225	188
24,5	0,1	461	42,6	339	312
24,5	0,3	746	44,0	537	518
24,5	1	1303	43,3	948	894
24,5	3	2139	41,1	1613	1405
24,5	10	3609	36,7	2894	2155
35,0	0,03	116	33,7	97	65
35,0	0,1	161	38,1	126	99
35,0	0,3	233	41,4	175	154
35,0	1	384	44,4	274	269
35,0	3	633	46,2	439	457
35,0	10	1126	46,5	775	817

Mixture RAP4028HU-Mix No.7 (Specimen P1-A2)

Mixture ID: RAP4028HU Bitumen type: PG 64-28 Specimen: P1-A2
Mixture No.: 7 Bitumen content: 4,5% Air void: 3,3%
Mixture type: GB-20

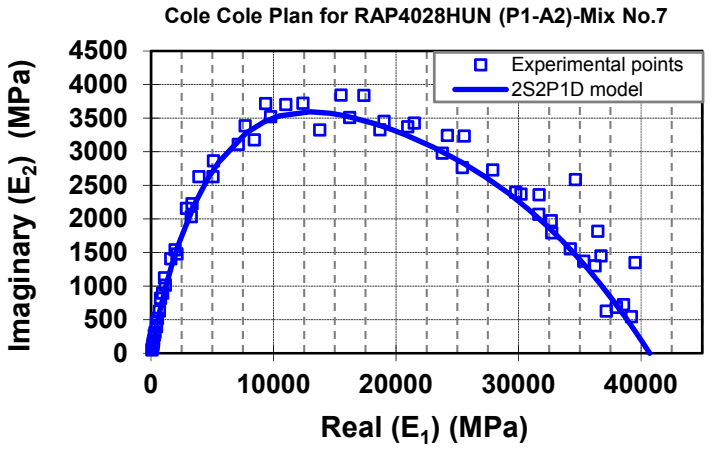

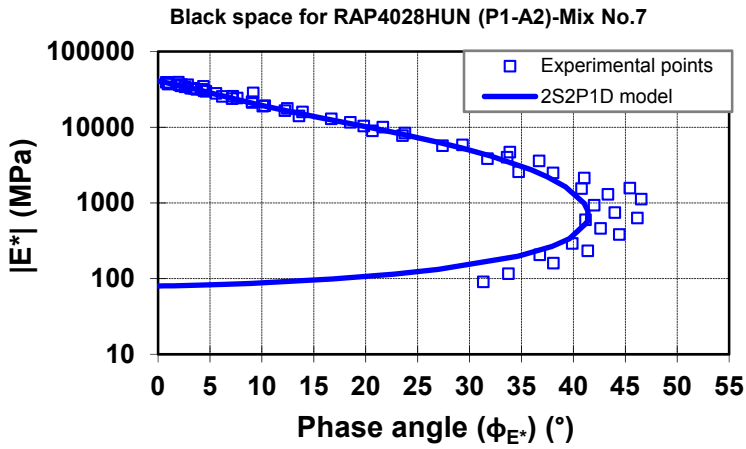

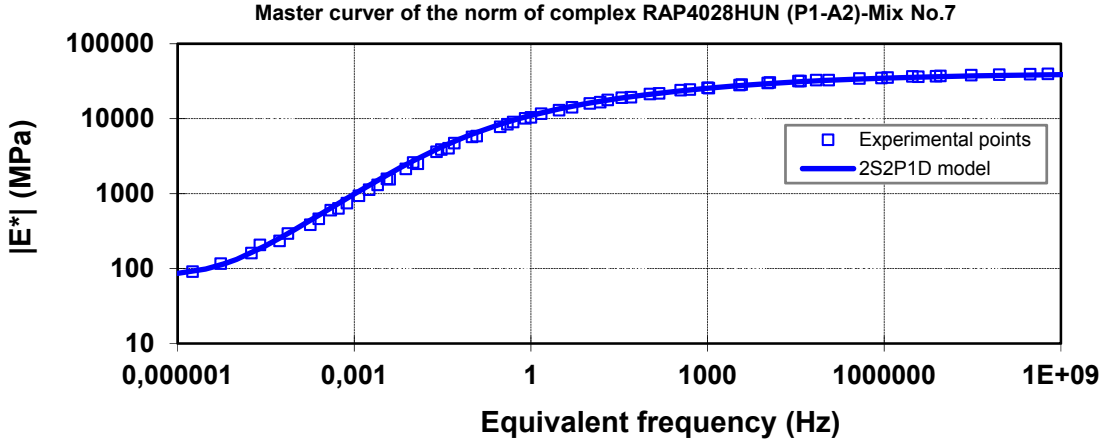

METHOD LC 26-700
COMPLEX MODULUS OF ASPHALT MIXTURE

Specimen: P2-A4
Air void: 3,8%

Bulk density: 2,528
Maximum density: 2,627

Mixture ID: RAP4028HU
Mixture No.: 7
Mixture type: GB-20
%RAP: 15
Bitumen type: PG 64-28
Bitumen content: 4,5%
Air void: 4,7%
Aggregate source:
Bitumen source:
Mixture source:

2S2P1D MODEL OF COMPLEX MODULUS, E* (MPa)

$$E^*(i\omega\tau) = E_{00} + \frac{E_0 - E_{00}}{1 + \delta(i\omega\tau)^{-k} + (i\omega\tau)^{-h} + (i\omega\beta\tau)^{-1}}$$

$$\log a_T = \frac{-C_1(T-T_0)}{C_2+(T-T_0)}$$

E_0 (MPa)	39 200
E_{00} (MPa)	75
δ	2,3
k	0,180
h	0,544
β	500
τ_0 (sec)	0,20
C_1	21,88
C_2	157,42

Temp,(°C)	Freq.(Hz)	|E*|(MPa)	ϕ (°)	E1(MPa)	E2(MPa)
-34,3	0,03	33390	2,6	33353	1518
-34,3	0,1	34223	2,0	34200	1196
-34,3	0,3	34776	1,8	34758	1091
-34,3	1	35555	1,4	35544	878
-34,3	3	36081	1,1	36074	720
-34,3	10	36747	0,8	36743	545
-24,5	0,03	27705	4,8	27600	2310
-24,5	0,1	29380	3,9	29310	2014
-24,5	0,3	30525	3,4	30471	1807
-24,5	1	31951	2,9	31911	1597
-24,5	3	33024	2,4	32995	1375
-24,5	10	34033	1,7	34018	1001
-14,5	0,03	19646	8,8	19413	3005
-14,5	0,1	21933	7,6	21743	2883
-14,5	0,3	23912	6,6	23756	2728
-14,5	1	25937	5,6	25813	2530
-14,5	3	27647	5,0	27544	2387
-14,5	10	29346	4,0	29273	2056
-4,6	0,03	10510	17,9	10002	3228
-4,6	0,1	13042	14,8	12608	3335
-4,6	0,3	15367	12,6	14994	3364
-4,6	1	17881	10,6	17573	3302
-4,6	3	20110	9,2	19854	3198
-4,6	10	22537	7,7	22332	3036
5,4	0,03	3660	31,7	3115	1923
5,4	0,1	5322	27,7	4713	2472
5,4	0,3	7267	23,8	6650	2930
5,4	1	9690	20,0	9106	3314
5,4	3	12054	17,0	11527	3524
5,4	10	14772	14,2	14323	3614
15,4	0,03	917	42,3	679	617
15,4	0,1	1540	40,2	1175	995
15,4	0,3	2458	36,8	1968	1474
15,4	1	3882	32,5	3274	2085
15,4	3	5522	28,8	4838	2662
15,4	10	7725	24,4	7037	3186
24,5	0,03	281	42,9	206	190
24,5	0,1	466	41,1	350	305
24,5	0,3	781	43,9	563	541
24,5	1	1372	41,5	1028	908
24,5	3	2184	39,0	1697	1375
24,5	10	3511	35,7	2851	2049
34,9	0,03	32	45,8	35	36
34,9	0,1	50	44,6	71	68
34,9	0,3	98	44,2	128	125
34,9	1	*	*	*	*
34,9	3	*	*	*	*
34,9	10	*	*	*	*

*bad results were rejected

Mixture RAP4028HU-Mix No.7 (Specimen P2-A4)

Mixture ID: RAP4028HU
Mixture No.: 7
Mixture type: GB-20

Bitumen type: PG 64-28
Bitumen content: 4,5%

Specimen: P2-A4
Air void: 3,8%

Cole Cole Plan for RAP4028HUN-P2-A4-Mix No.7

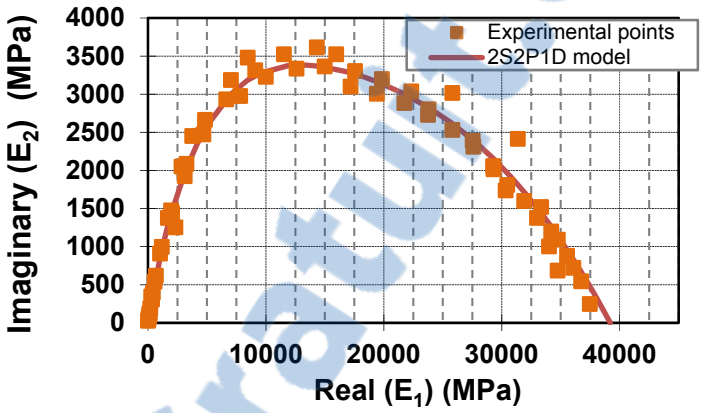

Black space for RAP4028HUN-P2-A4-Mix No.7

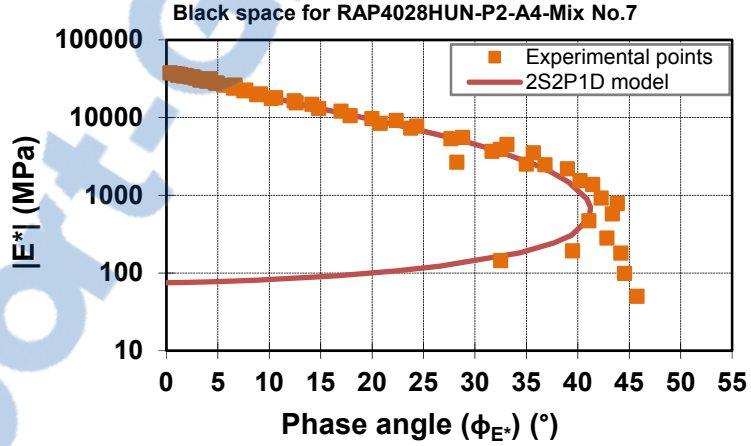

Master curver of the norm of complex RAP4028HUN-P2-A4-Mix No.7

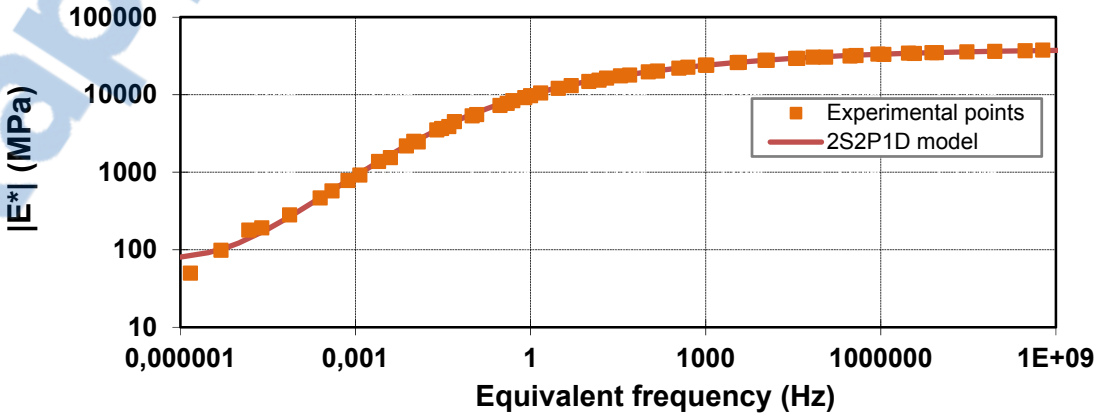

METHOD LC 26-700
COMPLEX MODULUS OF ASPHALT MIXTURE

Specimen: P1-A1
Air void: 4,6%

Bulk density: 2,481
Maximum density: 2,601

Mixture ID: RAP4028CA
Mixture No.: 8
Mixture type: GB-20
%RAP: 40
Bitumen type: PG 64-28
Bitumen content: 4,5%
Air void: 3,1
Aggregate source:
Bitumen source:
Mixture source:

2S2P1D MODEL OF COMPLEX MODULUS, E* (MPa)

$$E^*(i\omega\tau) = E_{00} + \frac{E_0 - E_{00}}{1 + \delta(i\omega\tau)^{-k} + (i\omega\tau)^{-h} + (i\omega\beta\tau)^{-1}}$$

$$\log a_T = \frac{-C_1(T-T_0)}{C_2+(T-T_0)}$$

E_{infini} (MPa)	38 900
E_{zero} (MPa)	100
δ	2,20
k	0,168
h	0,544
β	500
τ_0 (sec)	0,40
C_1	33,86
C_2	230,21

Temp,(°C)	Freq.(Hz)	|E*|(MPa)	ϕ(°)	E1(MPa)	E2 (MPa)
-34,2	0,03	33899	3,1	33828	1873
-34,2	0,1	34058	2,2	34028	1316
-34,2	0,3	34601	2,1	34574	1283
-34,2	1	35338	1,7	35322	1019
-34,2	3	35966	1,2	35958	738
-34,2	10	36657	0,8	36653	486
-24,3	0,03	27559	4,8	27460	2311
-24,3	0,1	29150	3,5	29092	1793
-24,3	0,3	30657	3,6	30597	1906
-24,3	1	31814	3,1	31766	1720
-24,3	3	32693	2,5	32661	1410
-24,3	10	34185	1,5	34171	990
-14,4	0,03	20519	7,7	20331	2752
-14,4	0,1	22508	6,8	22343	2673
-14,4	0,3	24318	5,9	24190	2480
-14,4	1	26314	5,6	26188	2549
-14,4	3	27777	4,8	27679	2325
-14,4	10	29251	3,8	29182	1983
-4,3	0,03	11620	15,9	11175	3183
-4,3	0,1	13997	13,2	13629	3188
-4,3	0,3	16193	11,4	15870	3215
-4,3	1	18552	9,6	18291	3096
-4,3	3	20723	8,2	20510	2965
-4,3	10	22941	7,1	22765	2822
5,6	0,03	4421	28,2	3896	2089
5,6	0,1	6312	24,5	5744	2616
5,6	0,3	8311	21,3	7744	3016
5,6	1	10708	17,7	10199	3263
5,6	3	13026	14,9	12585	3358
5,6	10	15686	12,7	15302	3444
15,5	0,03	1234	38,2	970	762
15,5	0,1	1957	36,2	1579	1156
15,5	0,3	2981	33,3	2492	1637
15,5	1	4560	29,3	3975	2234
15,5	3	6351	25,5	5734	2730
15,5	10	8777	21,3	8179	3183
24,9	0,03	400	40,1	306	258
24,9	0,1	624	41,3	469	412
24,9	0,3	987	41,1	744	649
24,9	1	1664	39,2	1289	1051
24,9	3	2611	36,4	2101	1550
24,9	10	4133	32,2	3497	2201
34,9	0,03	141	36,2	114	83
34,9	0,1	207	39,4	160	132
34,9	0,3	314	41,6	235	209
34,9	1	525	43,1	384	359
34,9	3	861	43,5	625	593
34,9	10	1499	42,7	1102	1016

Mixture RAP4028CA-Mix No.8 (Specimen P1-A1)

Mixture ID: RAP4028CA
Mixture No.: 8
Mixture type: GB-20

Bitumen type: PG 64-28
Bitumen content: 4,5%

Specimen: P1-A1
Air void: 4,6%

Cole Cole Plan for RAP4028CA-P1-A1-Mix No.8

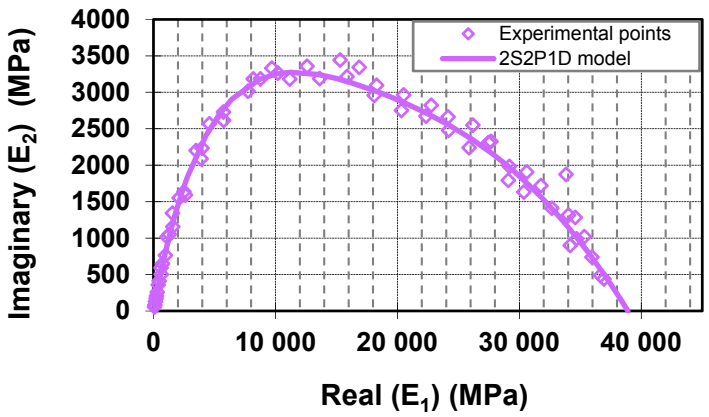

Black space for for RAP4028CA-P1-A1-Mix No.8

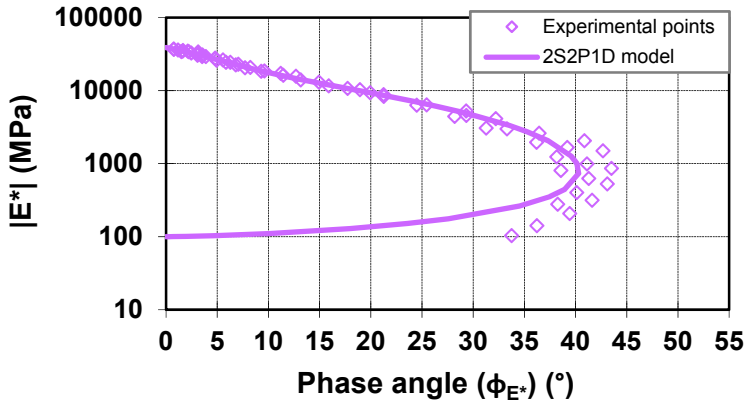

Master curver of the norm of complex for RAP4028CA-P1-A1-Mix No.8

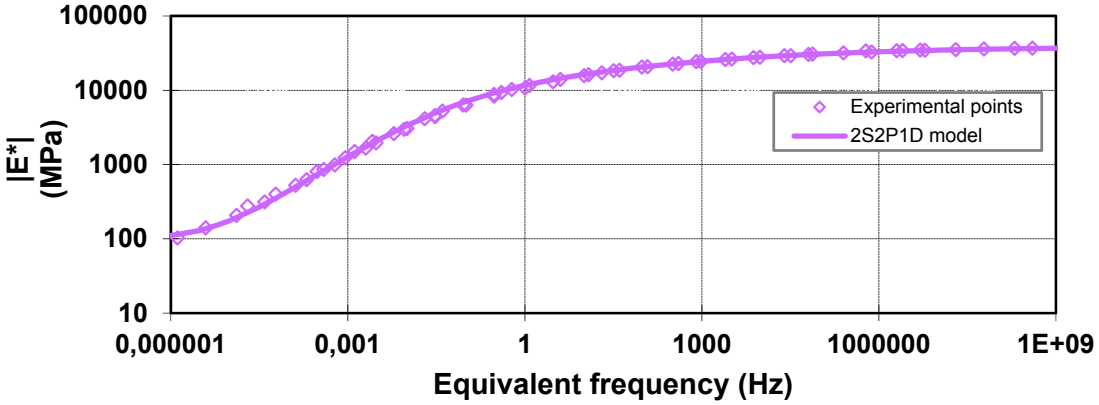

METHOD LC 26-700
COMPLEX MODULUS OF ASPHALT MIXTURE

Specimen: P1-A2
Air void: 3,8%

Bulk density: 2,502
Maximum density: 2,601

Mixture ID: RAP4028CA
Mixture No.: 8
Mixture type: GB-20
%RAP: 40
Bitumen type: PG 64-28
Bitumen content: 4,5%
Air void: 3,1
Aggregate source:
Bitumen source:
Mixture source:

2S2P1D MODEL OF COMPLEX MODULUS, E* (MPa)

$$E^*(i\omega\tau) = E_{00} + \frac{E_0 - E_{00}}{1 + \delta(i\omega\tau)^{-k} + (i\omega\tau)^{-h} + (i\omega\beta\tau)^{-1}}$$

$$\log a_T = \frac{-C_1(T-T_0)}{C_2+(T-T_0)}$$

E_0 (MPa)	38 900
E_{00} (MPa)	100
δ	2,15
k	0,177
h	0,544
β	500
τ_0 (sec)	0,40
C_1	34,38
C_2	230,13

Temp,(°C)	Freq,(Hz)	|E*|(MPa)	ϕ (°)	E1(MPa)	E2 (MPa)
-34,2	0,03	36017	3,3	35958	2060
-34,2	0,1	35318	1,7	35300	1067
-34,2	0,3	36084	1,3	36075	809
-34,2	1	36529	1,2	36519	788
-34,2	3	36593	1,2	36585	743
-34,2	10	37514	0,8	37508	501
-24,3	0,03	29636	5,2	29453	2773
-24,3	0,1	30620	3,5	30542	1922
-24,3	0,3	32232	3,1	32184	1745
-24,3	1	33074	2,3	33046	1348
-24,3	3	34022	2,0	34001	1171
-24,3	10	35331	1,8	35311	1108
-14,4	0,03	21618	8,4	21340	3160
-14,4	0,1	23608	6,4	23455	2653
-14,4	0,3	25596	6,2	25446	2767
-14,4	1	27217	4,8	27121	2286
-14,4	3	28902	4,2	28823	2138
-14,4	10	30469	3,5	30411	1869
-4,3	0,03	12492	15,0	12065	3236
-4,3	0,1	14989	12,5	14632	3254
-4,3	0,3	17300	11,1	16979	3316
-4,3	1	19769	9,3	19509	3193
-4,3	3	21866	7,9	21659	2994
-4,3	10	24155	6,9	23977	2916
5,6	0,03	4907	27,9	4339	2291
5,6	0,1	6878	24,3	6270	2825
5,6	0,3	8949	21,0	8355	3205
5,6	1	11478	17,3	10960	3406
5,6	3	13970	14,8	13507	365
5,6	10	16693	12,2	16317	3524
15,5	0,03	1358	38,5	1064	845
15,5	0,1	2164	36,7	1735	1294
15,5	0,3	3293	33,8	2738	1830
15,5	1	5017	29,1	4384	2437
15,5	3	6950	25,2	6287	2962
15,5	10	9519	20,7	8903	3367
24,9	0,03	424	40,3	323	274
24,9	0,1	675	41,4	506	446
24,9	0,3	1076	41,2	810	709
24,9	1	1821	39,2	1411	1152
24,9	3	2852	36,3	2299	1687
24,9	10	4517	31,6	3846	2368
34,9	0,03	147	36,1	119	86
34,9	0,1	217	39,4	168	138
34,9	0,3	328	42,2	243	220
34,9	1	556	43,9	400	386
34,9	3	922	44,3	660	643
34,9	10	1611	42,8	1182	1095

Mixture RAP4028CA-Mix No.8 (Specimen P1-A1)

Mixture ID: RAP4028CA
Mixture No.: 8
Mixture type: GB-20

Bitumen type: PG 64-28
Bitumen content: 4,5%

Specimen: P1-A2
Air void: 3,8%

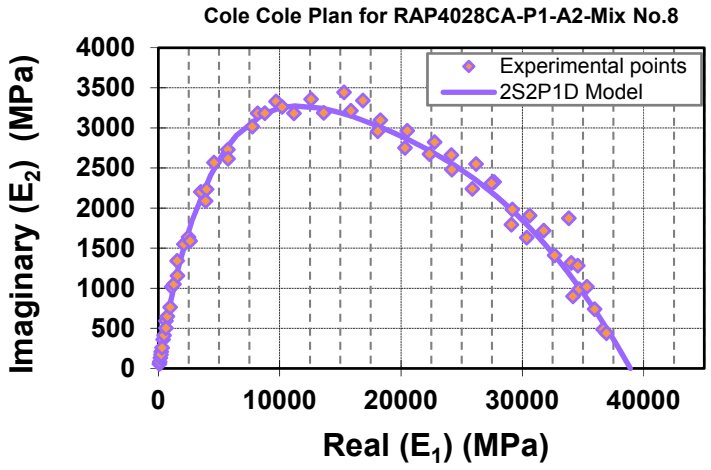

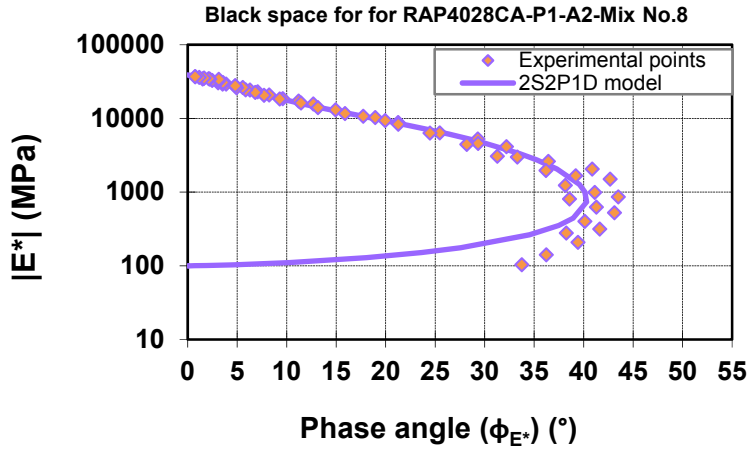

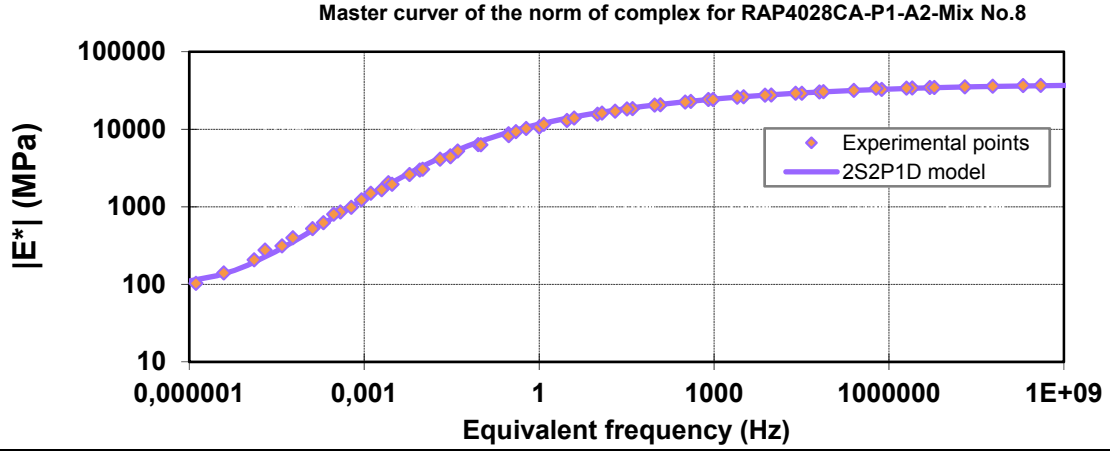

METHOD LC 26-700
COMPLEX MODULUS OF ASPHALT MIXTURE

Specimen: P2-A4
Air void: 3,2%

Bulk density: 2,514
Maximum density: 2,597

Mixture ID: RAP4034CA
Mixture No.: 9
Mixture type: GB-20
%RAP: 40
Bitumen type: PG 58-34
Bitumen content: 4,5%
Air void: 3,1
Aggregate source:
Bitumen source:
Mixture source:

2S2P1D MODEL OF COMPLEX MODULUS, E* (MPa)

$$E^*(i\omega\tau) = E_{00} + \frac{E_0 - E_{00}}{1 + \delta(i\omega\tau)^{-k} + (i\omega\tau)^{-h} + (i\omega\beta\tau)^{-1}}$$

$$\log a_T = \frac{-C_1(T-T_0)}{C_2+(T-T_0)}$$

E_0 (MPa)	35 200
E_{00} (MPa)	80
δ	2,20
k	0,175
h	0,510
β	2000
τ_0 (sec)	0,20
C_1	37,42
C_2	230,16

Temp,(°C)	Freq(Hz)	|E*|(MPa)	ϕ(°)	E1 (MPa)	E2 (MPa)
-32,7	0,03	28609	3,3	28561	1647
-32,7	0,1	29646	2,5	29617	1310
-32,7	0,3	30491	2,2	30469	1144
-32,7	1	31458	1,8	31442	998
-32,7	3	31992	2,3	31959	1266
-32,7	10	32782	2,0	32733	1169
-24,1	0,03	23244	5,5	23135	2241
-24,1	0,1	24862	4,7	24778	2039
-24,1	0,3	26204	3,9	26142	1802
-24,1	1	27494	3,4	27446	1617
-24,1	3	29379	3,5	29314	1782
-24,1	10	29675	2,2	29652	1131
-14,9	0,03	16701	9,8	16455	2852
-14,9	0,1	18723	8,0	18539	2611
-14,9	0,3	20478	7,0	20326	2491
-14,9	1	22301	6,0	22180	2316
-14,9	3	23844	5,3	23739	2221
-14,9	10	25437	4,2	25366	1884
-4,9	0,03	8663	18,7	8204	2777
-4,9	0,1	10861	16,1	10437	3004
-4,9	0,3	12936	13,5	12581	3009
-4,9	1	15259	11,2	14970	2955
-4,9	3	17256	9,4	17025	2814
-4,9	10	19550	7,8	19370	2645
4,9	0,03	3256	30,7	2800	1660
4,9	0,1	4664	27,1	4151	2127
4,9	0,3	6313	23,8	5776	2546
4,9	1	8413	19,9	7909	2867
4,9	3	10586	16,7	10139	3043
4,9	10	13002	13,7	12629	3090
14,0	0,03	1137	36,2	918	671
14,0	0,1	1744	35,6	1417	1016
14,0	0,3	2592	33,2	2168	1419
14,0	1	3916	29,5	3407	1930
14,0	3	5476	26,1	4917	2410
14,0	10	7557	22,2	6999	2849
24,7	0,03	369	37,5	293	225
24,7	0,1	527	38,6	411	329
24,7	0,3	772	39,3	597	489
24,7	1	1234	38,5	965	768
24,7	3	1913	37,2	1524	1156
24,7	10	3129	35,2	2546	1810
34,9	0,03	138	31,5	118	72
34,9	0,1	181	34,8	148	103
34,9	0,3	257	38,4	201	160
34,9	1	407	40,8	308	266
34,9	3	642	42,0	477	429
34,9	10	1081	42,1	802	725

Mixture RAP4034CA-Mix No.9 (Specimen P2-A4)

Mixture ID: RAP4034CA
Mixture No.: 9
Mixture type: GB-20

Bitumen type: PG 58-34
Bitumen content: 4,5%

Specimen: P2-A4
Air void: 3,2%

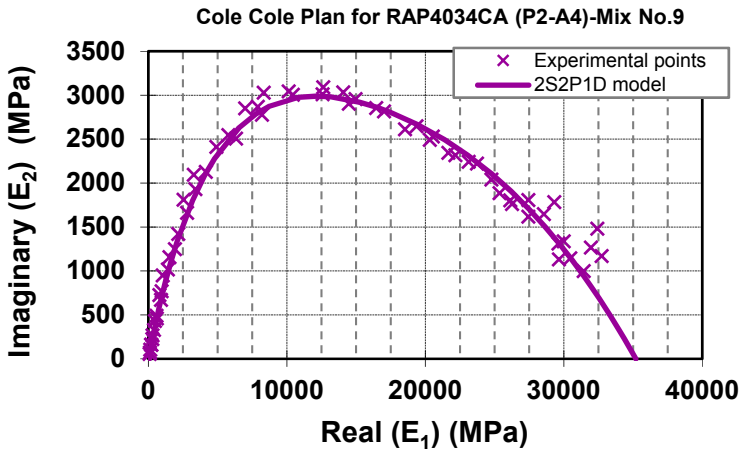

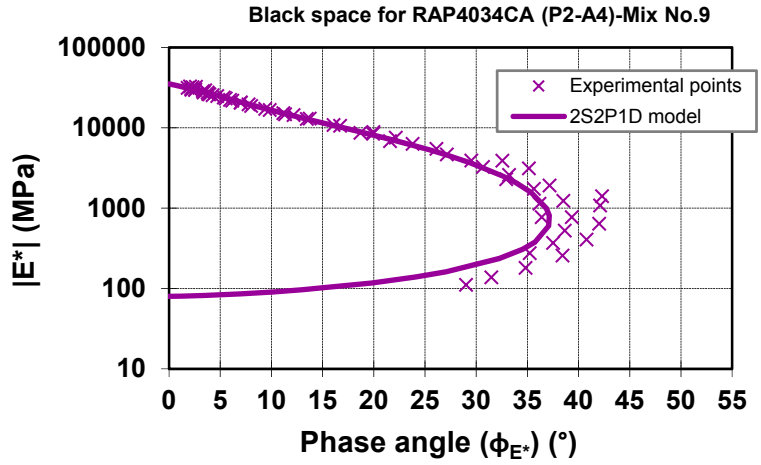

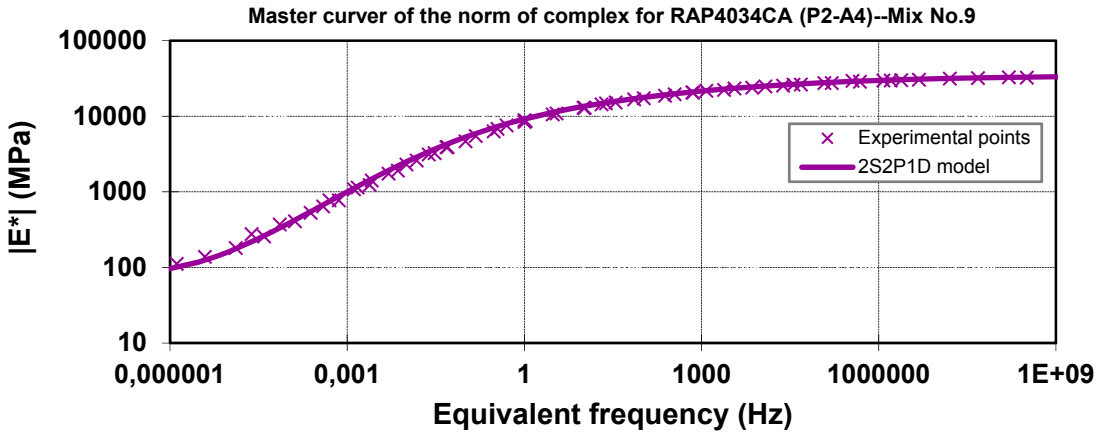

METHOD LC 26-700
COMPLEX MODULUS OF ASPHALT MIXTURE

Specimen: P2-A3
Air void: 3,2%

Bulk density: 2,513
Maximum density: 2,597

Mixture ID: RAP4034CA
Mixture No.: 9
Mixture type: GB-20
%RAP: 40
Bitumen type: PG 58-34
Bitumen content: 4,5%
Air void: 3,01
Aggregate source:
Bitumen source:
Mixture source:

2S2P1D MODEL OF COMPLEX MODULUS, E* (MPa)

$$E^*(i\omega\tau) = E_{00} + \frac{E_0 - E_{00}}{1 + \delta(i\omega\tau)^{-k} + (i\omega\tau)^{-h} + (i\omega\beta\tau)^{-1}}$$

$$\log a_T = \frac{-C_1(T-T_0)}{C_2+(T-T_0)}$$

E_0 (MPa)	32 300
E_{00} (MPa)	110
δ	2,40
k	0,177
h	0,544
β	2000
τ_0 (sec)	0,14
C_1	22,60
C_2	151,44

Temp,(°C)	Freq.(Hz)	|E*|(MPa)	ϕ (°)	E1(MPa)	E2 (MPa)
-33,0	0,03	27643	3,1	27602	1497
-33,0	0,1	28477	2,7	28445	1353
-33,0	0,3	29399	2,2	29377	1132
-33,0	1	30231	1,8	30215	972
-33,0	3	30789	1,4	30789	732
-33,0	10	31490	1,1	31483	593
-23,6	0,03	22624	5,3	22527	2100
-23,6	0,1	24078	4,7	23996	1986
-23,6	0,3	25349	4,0	25287	1762
-23,6	1	26560	3,4	26514	1563
-23,6	3	27655	3,0	27617	1435
-23,6	10	28610	2,8	28574	1410
-14,1	0,03	15974	9,7	15748	2681
-14,1	0,1	17892	8,0	17716	2503
-14,1	0,3	19602	7,0	19458	2372
-14,1	1	21373	5,9	21259	2210
-14,1	3	22859	5,2	22766	2061
-14,1	10	24402	4,5	24326	1907
-4,0	0,03	8373	18,1	7960	2595
-4,0	0,1	10418	15,7	10031	2815
-4,0	0,3	12354	13,4	12019	2855
-4,0	1	14492	11,2	14217	2811
-4,0	3	16474	9,5	16250	2707
-4,0	10	18483	8,0	18305	2558
5,5	0,03	3296	29,9	2857	1644
5,5	0,1	4648	26,0	4177	2037
5,5	0,3	6247	22,7	5761	2416
5,5	1	8246	19,2	7787	2711
5,5	3	10205	16,3	9792	2871
5,5	10	12461	13,7	12106	2952
14,8	0,03	1102	37,3	877	668
14,8	0,1	1725	35,7	1401	1007
14,8	0,3	2580	33,0	2164	1404
14,8	1	3869	29,4	3371	1898
14,8	3	5364	25,8	4828	2337
14,8	10	7327	21,8	6802	2724
24,4	0,03	405	36,4	326	240
24,4	0,1	617	38,4	484	383
24,4	0,3	946	38,3	742	586
24,4	1	1516	37,2	1209	916
24,4	3	2293	35,1	1876	1319
24,4	10	3492	31,8	2969	1838

Mixture RAP4034CA-Mix No.9 (Specimen P2-A3)

Mixture ID: RAP4034CA
Mixture No.: 9
Mixture type: GB-20

Bitumen type: PG 58-34
Bitumen content: 4,5%

Specimen: P2-A3
Air void: 3,2%

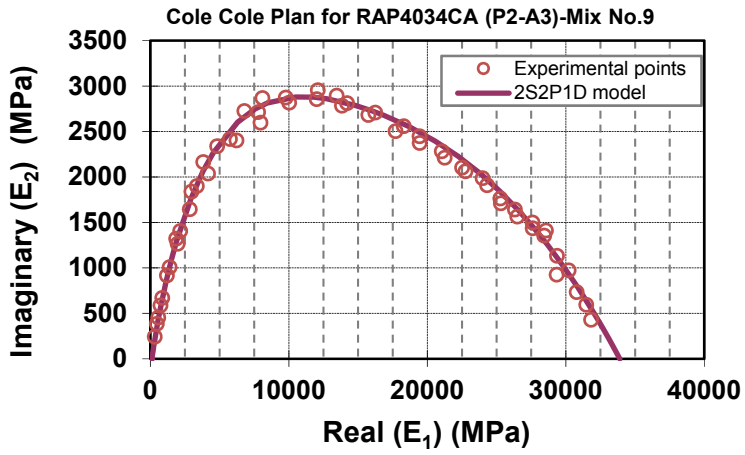

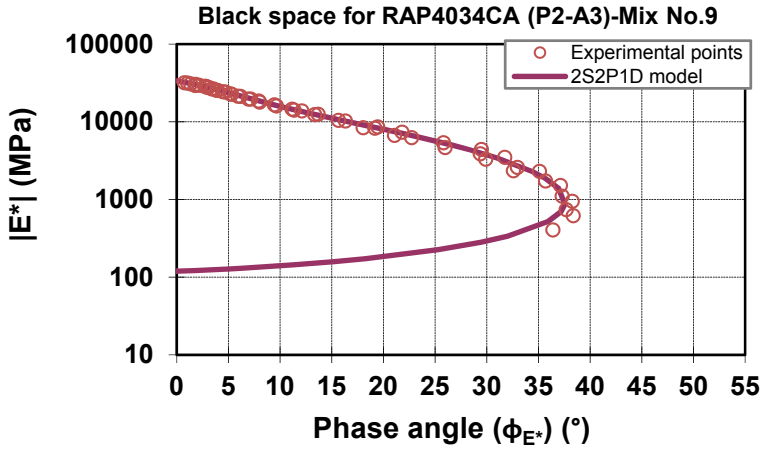

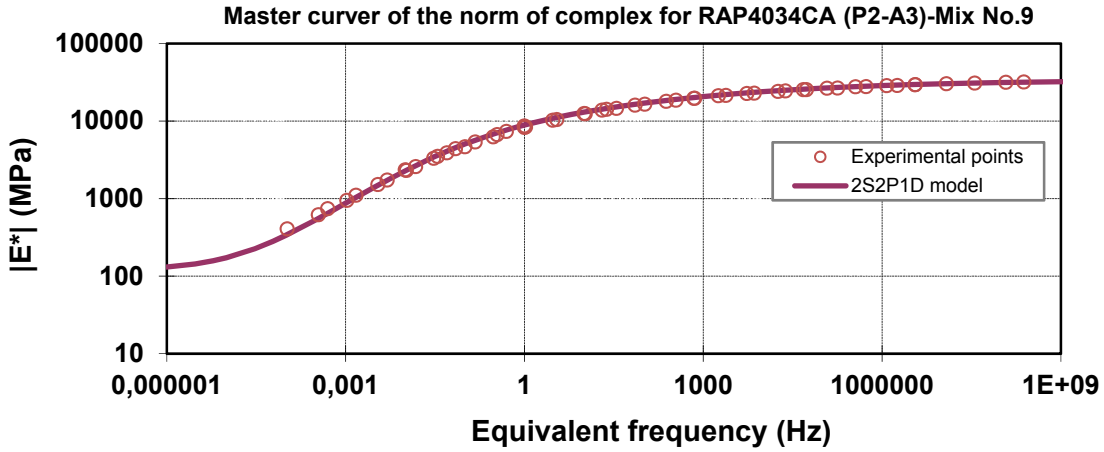

METHOD LC 26-700
COMPLEX MODULUS OF ASPHALT MIXTURE

Specimen: P2-A2
Air void: 2,6%

Bulk density: 2,555
Maximum density: 2,624

Mixture ID: RAP2534CU
Mixture No.: 10
Mixture type: GB-20
%RAP: 25
Bitumen type: PG 58-34
Bitumen content: 4,5%
Air void: 5,6%
Aggregate source:
Bitumen source:
Mixture source:

2S2P1D MODEL OF COMPLEX MODULUS, E* (MPa)

$$E^*(i\omega\tau) = E_{00} + \frac{E_0 - E_{00}}{1 + \delta(i\omega\tau)^{-k} + (i\omega\tau)^{-h} + (i\omega\beta\tau)^{-1}}$$

$$\log a_T = \frac{-C_1(T-T_0)}{C_2+(T-T_0)}$$

E_0 (MPa)	32 000
E_{00} (MPa)	115
δ	2,70
k	0,182
h	0,560
β	2000
τ_0 (sec)	0,198
C_1	20,64
C_2	150,43

Temp,(°C)	Freq.(Hz)	|E*|(MPa)	ϕ (°)	E1(MPa)	E2(MPa)
-32,9	0,03	24949	3,5	24902	1516
-32,9	0,1	26144	3,1	26106	1401
-32,9	0,3	27091	2,6	27062	1244
-32,9	1	27955	2,2	27934	1070
-32,9	3	28665	1,7	28652	851
-32,9	10	29270	2,4	29241	1204
-221,9	0,03	18576	7,0	18439	2253
-221,9	0,1	20242	6,0	20130	2115
-221,9	0,3	21684	5,2	21596	1948
-221,9	1	23156	4,4	23088	1774
-221,9	3	24502	3,8	24449	1607
-221,9	10	25530	4,0	25468	1757
-13,8	0,03	13036	11,4	12781	2567
-13,8	0,1	14903	9,5	14699	2452
-13,8	0,3	16618	8,3	16444	2398
-13,8	1	18470	7,1	18330	2270
-13,8	3	20036	6,2	19918	2164
-13,8	10	21702	5,7	21593	2157
-3,8	0,03	6792	20,3	6368	2361
-3,8	0,1	8509	17,4	8118	2549
-3,8	0,3	10213	15,1	9861	2662
-3,8	1	12159	12,7	11862	2671
-3,8	3	13952	10,8	16705	2617
-3,8	10	16055	9,1	15852	2544
5,6	0,03	2640	31,1	2256	1371
5,6	0,1	3828	28,2	3373	1809
5,6	0,3	5191	24,7	4715	2171
5,6	1	6991	21,1	6522	2516
5,6	3	8607	18,1	8183	2667
5,6	10	10738	14,9	10375	2767
15,4	0,03	817	36,0	661	480
15,4	0,1	1249	34,9	1024	715
15,4	0,3	1868	33,5	1559	1030
15,4	1	2912	30,9	2499	1494
15,4	3	4150	27,6	3678	1921
15,4	10	5870	23,9	5367	2377
27,1	0,03	303	32,4	256	163
27,1	0,1	370	35,1	303	213
27,1	0,3	517	36,9	414	311
27,1	1	821	37,5	652	500
27,1	3	1262	37,0	1008	7589
27,1	10	2023	35,2	1653	1167
35,2	0,03	170	26,9	152	77
35,2	0,1	223	29,9	193	111
35,2	0,3	298	32,8	250	161
35,2	1	438	35,6	356	255
35,2	3	647	37,7	512	395
35,2	10	1028	38,3	807	638

Mixture RAP2534CU-Mix No.10 (Specimen P2-A2)

Mixture ID: RAP2534CU
Mixture No.: 10
Mixture type: GB-20

Bitumen type: PG 58-34
Bitumen content: 4,5%

Specimen: P2-A2
Air void: 2,6%

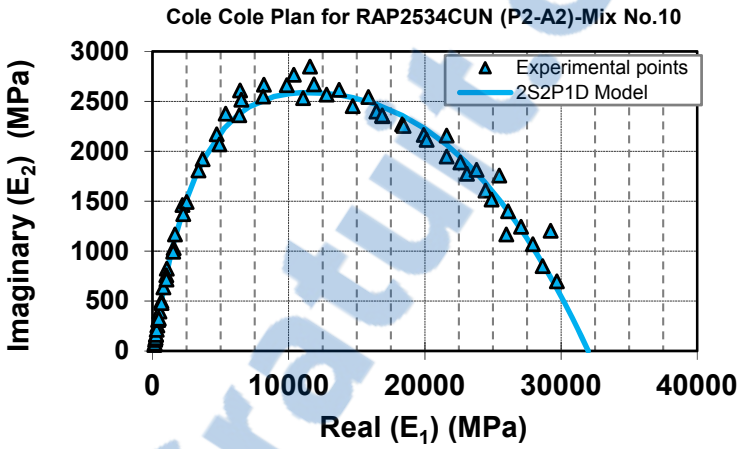

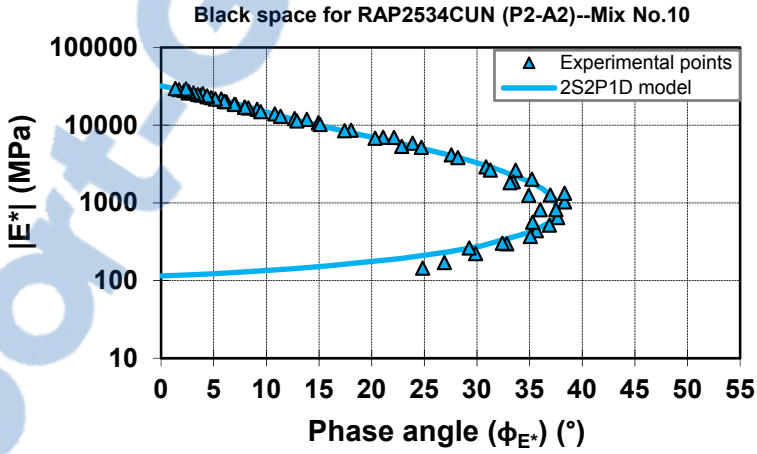

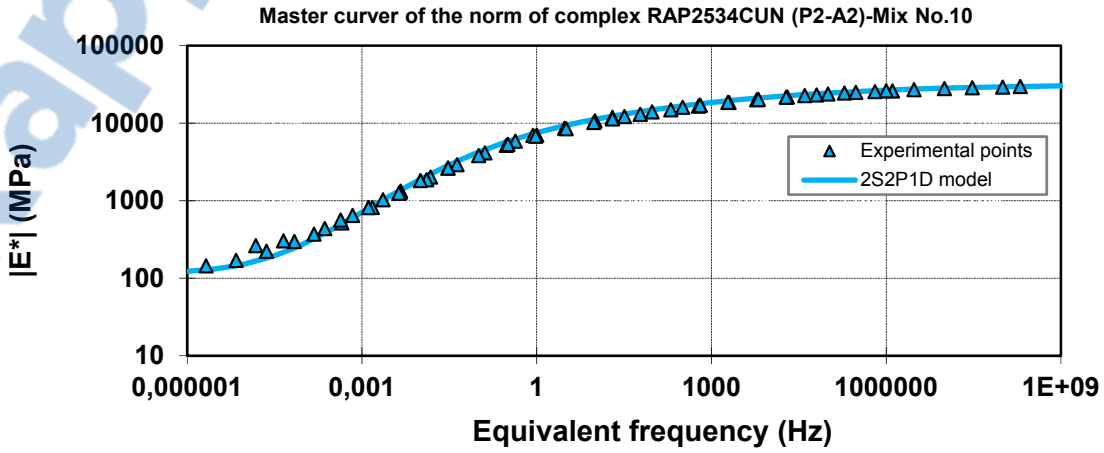

METHOD LC 26-700
COMPLEX MODULUS OF ASPHALT MIXTURE

Specimen: P2-A3
Air void: 3,0%

Bulk density: 2.542
Maximum density: 2,621

Mixture ID: RAP4034CU
Mixture No.: 11
Mixture type: GB-20
%RAP: 40
Bitumen type: PG 58-34
Bitumen content: 4,5%
Air void: 4,5%
Aggregate source:
Bitumen source:
Mixture source:

2S2P1D MODEL OF COMPLEX MODULUS, E* (MPa)

$$E^*(i\omega\tau) = E_{00} + \frac{E_0 - E_{00}}{1 + \delta(i\omega\tau)^{-k} + (i\omega\tau)^{-h} + (i\omega\beta\tau)^{-1}}$$

$$\log a_T = \frac{-C_1(T-T_0)}{C_2+(T-T_0)}$$

E_0 (MPa)	32 300
E_{00} (MPa)	110
δ	2,40
k	0,177
h	0,544
β	2000
τ_0 (sec)	0,14
C_1	22,60
C_2	151,44

Temp,(°C)	Freq,(Hz)	|E*|(MPa)	ϕ (°)	E1(MPa)	E2(MPa)
-33,2	0,03	25207	3,6	25158	1569
-33,2	0,1	26351	3,1	26311	1448
-33,2	0,3	27205	2,5	27178	1205
-33,2	1	28089	2,1	28070	1027
-33,2	3	28363	1,9	28341	957
-33,2	10	29337	1,4	29321	740
-24,0	0,03	20172	6,1	20058	2142
-24,0	0,1	21808	5,2	21717	1986
-24,0	0,3	23080	4,6	23005	1856
-24,0	1	24354	3,9	24298	1654
-24,0	3	25618	2,8	25585	1251
-24,0	10	26687	3,1	26615	1409
-14,4	0,03	13514,6	13515	10,8	13275
-14,4	0,1	15433	9,1	15238	2438
-14,4	0,3	17135	8,1	16965	2405
-14,4	1	18975	6,9	18839	2266
-14,4	3	20484	6,0	20372	2138
-14,4	10	22047	5,1	21949	1972
-4,2	0,03	6686	19,5	6303	2228
-4,2	0,1	8420	16,9	8057	2447
-4,2	0,3	10201	14,7	9866	2592
-4,2	1	12244	12,5	11954	2649
-4,2	3	14183	10,9	13929	2672
-4,2	10	16202	9,2	15994	2586
5,0	0,03	2573	30,4	2218	1303
5,0	0,1	3663	27,2	3259	1673
5,0	0,3	4962	23,9	4536	2011
5,0	1	6654	20,6	6229	2340
5,0	3	8425	17,8	8022	2573
5,0	10	10506	15,2	10138	2755
14,7	0,03	773	37,3	615	468
14,7	0,1	1218	36,5	979	724
14,7	0,3	1850	34,1	1513	1038
14,7	1	2821	30,9	2421	1447
14,7	3	3970	27,8	3513	1849
14,7	10	5510	24,0	50,33	2242
25,3	0,03	257	33,8	214	143
25,3	0,1	409	36,6	328	244
25,3	0,3	634	37,9	500	390
25,3	1	1029	37,7	814	630
25,3	3	1584	36,3	1276	938
25,3	10	2488	33,7	2069	1382
34,2	0,03	123	29,3	107	60
34,2	0,1	168	33,0	141	92
34,2	0,3	233	36,6	187	139
34,2	1	362	39,5	279	230
34,2	3	564	41,1	425	371
34,2	10	941	41,3	707	621

Mixture RAP4034CU-Mix No.11 (Specimen P2-A3)

Mixture ID: RAP4034CU
Mixture No.: 11
Mixture type: GB-20

Bitumen type: PG 58-34
Bitumen content: 4.5%

Specimen: P2-A3
Air void: 3.0%

Cole Cole Plan for RAP4034CUN-Mix No.11

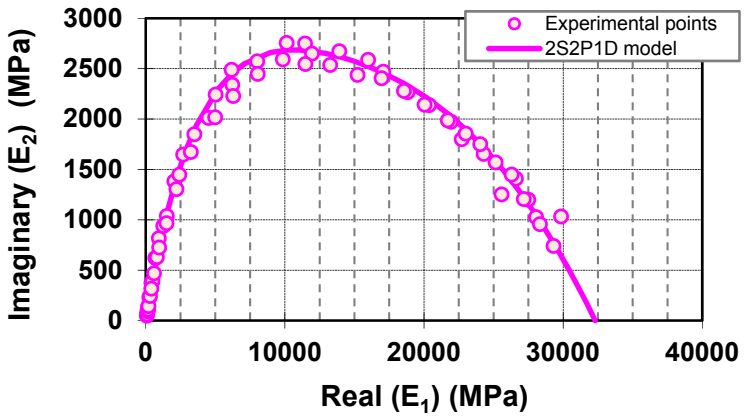

Black space for RAP4034CUN-Mix No.11

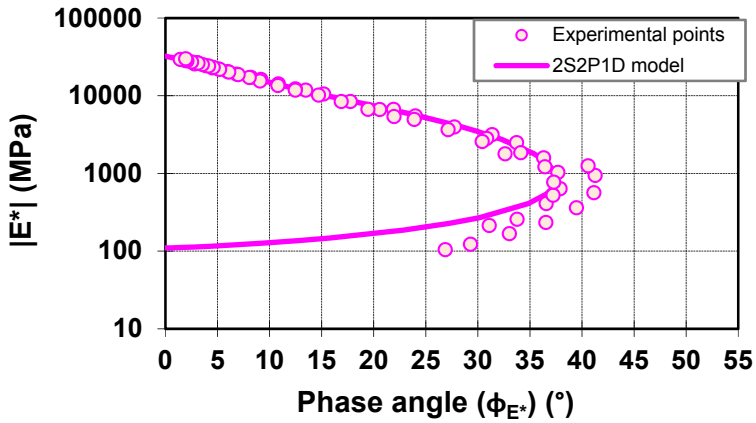

Master curver of the norm of complex RAP4034CUN-Mix No.11

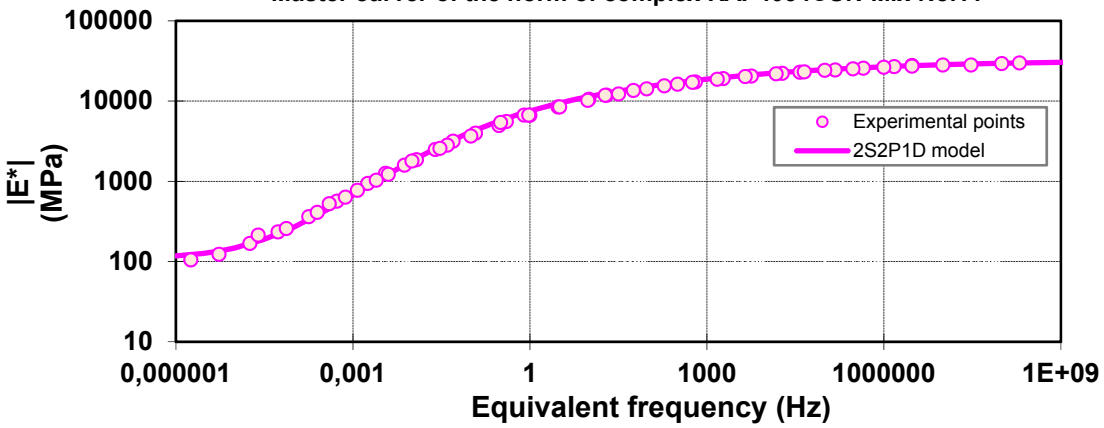

Table-A II-1 Shift factors log a(T) obtained from τ fitted values of experimental data for all the different tested samples

RAP028 (P1-A4), Mix No.1

Temperature (°C)	-33,0	-23,8	-14,1	-4,3	5,4	15,1	25,1	35,0
aT	2,22E+07	1,48E+05	1,85E+03	3,41E+01	1,00E+00	5,19E-02	3,70E-03	5,19E-04
log (aT)	7,35	5,17	3,27	1,53	0,00	-1,29	-2,43	-3,29

RAP1528CU (P2-A4), Mix No.2

Temperature (°C)	-34,8	-24,9	-15,0	-5,0	5,0	15,0	24,6	34,9
aT	2,22E+07	3,33E+05	2,78E+03	5,00E+01	1,00E+00	3,89E-02	1,67E-03	1,11E-04
log (aT)	7,35	5,52	3,44	1,70	0,00	-1,41	-2,78	-3,95

RAP1528CU (P1-A5), Mix No.2

Temperature (°C)	-34,2	-25,6	-15,7	-5,7	4,2	14,2	23,5	
aT	5,80E+06	8,70E+04	7,25E+02	2,75E+01	1,00E+00	4,35E-02	1,30E-03	
log (aT)	6,76	4,94	2,86	1,44	0,00	-1,36	-2,88	

RAP2528CU (P1-A3), Mix No.3

Temperature (°C)	-33,1	-23,4	-13,9	-4,2	5,5	15,2	25,7	35,4
aT	1,43E+07	2,38E+05	2,14E+03	4,05E+01	1,00E+00	4,76E-02	3,33E-03	4,29E-04
log (aT)	7,15	5,38	3,33	1,61	0,00	-1,32	-2,48	-3,37

RAP2528CU (P2-A2), Mix No.3

Temperature (°C)	-31,7	-22,4	-13,1	-3,6	5,8	15,4	24,7	35,8
aT	1,58E+07	2,63E+05	2,37E+03	2,95E+01	1,00E+00	4,21E-02	3,68E-03	2,11E-04
log (aT)	7,20	5,42	3,37	1,47	0,00	-1,38	-2,43	-3,68

Table-A II-1 Following shift factors log a(T) obtained from τ fitted values of experimental data for all the different tested samples

RAP028 (P1-A4), Mix No.1

Temperature (°C)	-33,0	-23,8	-14,1	-4,3	5,4	15,1	25,1	35,0
aT	2,22E+07	1,48E+05	1,85E+03	3,41E+01	1,00E+00	5,19E-02	3,70E-03	5,19E-04
log (aT)	7,35	5,17	3,27	1,53	0,00	-1,29	-2,43	-3,29

RAP1528CU (P2-A4), Mix No.2

Temperature (°C)		-24,9	-15,0	-5,0	5,0	15,0	24,6	34,9
aT	2,22E+07	3,33E+05	2,78E+03	5,00E+01	1,00E+00	3,89E-02	1,67E-03	1,11E-04
log (aT)	7,35	5,52	3,44	1,70	0,00	-1,41	-2,78	-3,95

RAP1528CU (P1-A5),Mix No.2

Temperature (°C)	-34.2	-25.6	-15.7	-5.7	4.2	14.2	23.5	
aT	5.80E+06	8.70E+04	7.25E+02	2.75E+01	1.00E+00	4.35E-02	1.30E-03	
log (aT)	6,76	4,94	2,86	1,44	0,00	-1,36	-2,88	

RAP2528CU (P1-A3), Mix No.3

Temperature (°C)	-33,1	-23,4	-13,9	-4,2	5,5	15,2	25,7	35,4
aT	1,43E+07	2,38E+05	2,14E+03	4,05E+01	1,00E+00	4,76E-02	3,33E-03	4,29E-04
log (aT)	7,15	5,38	3,33	1,61	0,00	-1,32	-2,48	-3,37

RAP2528CU (P2-A2), Mix No.3

Temperature (°C)	-31,7	-22,4	-13,1	-3,6	5,8	15,4	24,7	35,8
aT	1,58E+07	2,63E+05	2,37E+03	2,95E+01	1,00E+00	4,21E-02	3,68E-03	2,11E-04
log (aT)	7,20	5,42	3,37	1,47	0,00	-1,38	-2,43	-3,68

Table-A II-1 Following shift factors log a(T) obtained from τ fitted values of experimental data for all the different tested samples

RAP4028CU (P2-A4), Mix No.4

Temperature (°C)	-33,0	-23,8	-14,0	-4,2	5,2	14,8	26,3	34,4
aT	1,82E+07	2,27E+05	1,82E+03	3,18E+01	1,00E+00	4,55E-02	2,73E-03	1,36E-04
log (aT)	7,26	5,36	3,26	1,50	0,00	-1,34	-2,56	-3,87

RAP1528HU (P1-A1), Mix No.5

Temperature (°C)	-32,7	-23,6	-13,9	-3,7	5,2	15,7	26,0	34,2
aT	1,82E+07	2,27E+05	1,82E+03	3,18E+01	1,00E+00	4,55E-02	2,73E-03	1,36E-04
log (aT)	7,26	5,36	3,26	1,50	0,00	-1,34	-2,56	-3,87

RAP2528HU (P1-A1),Mix No.6

Temperature (°C)	-34,2	-24,4	-14,5	-4,6	5,4	15,4	24,5	35,0
aT	7,50E+06	1,25E+05	1,13E+03	3,00E+01	1,00E+00	4,00E-02	2,25E-03	7,50E-05
log (aT)	6,88	5,10	3,05	1,48	0,00	-1,40	-2,65	-4,12

RAP2528HU (P2-A1), Mix No.6

Temperature (°C)	-32,1	-22,9	-13,5	-3,7	5,7	15,2	24,8	35,5
aT	1,50E+07	2,50E+05	2,25E+03	3,00E+01	1,00E+00	4,50E-02	3,50E-03	3,50E-04
log (aT)	7,18	5,40	3,35	1,48	0,00	-1,35	-2,46	-3,46

RAP4028HU (P1-A2), Mix No.7

Temperature (°C)	-34,5	-24,5	-14,8	-4,8	5,1	15,1	24,5	35,0
aT	1,82E+07	2,27E+05	2,73E+03	4,09E+01	1,00E+00	3,18E-02	2,27E-03	1,36E-04
log (aT)	7,26	5,36	3,44	1,61	0,00	-1,50	-2,64	-3,87

Table-A II-1 Following shift factors log a(T) obtained from τ fitted values of experimental data for all the different tested samples

RAP4028HU (P2-A4), Mix No.7

Temperature (°C)	-34,3	-24,5	-14,5	-4,6	5,4	15,4	24,5	
aT	2,00E+07	2,50E+05	4,50E+03	1,00E+02	1,00E+00	4,50E-02	4,00E-03	
log (aT)	7,30	5,40	3,65	2,00	0,00	-1,35	-2,40	

RAP4028CA (P1-A1), Mix No.8

Temperature (°C)	-34,1	-24,3	-14,4	-4,3	5,6	15,5	24,9	34,9
aT	1,00E+07	1,25E+05	2,00E+03	5,00E+01	1,00E+00	3,75E-02	2,50E-03	1,50E-04
log (aT)	7,00	5,10	3,30	1,70	0,00	-1,43	-2,60	-3,82

RAP4028CA (P1-A2), Mix No.8

Temperature (°C)	-33,8	-24,0	-14,1	-4,2	5,7	15,6	24,9	34,9
aT	1,00E+07	1,25E+05	2,00E+03	5,00E+01	1,00E+00	3,75E-02	2,25E-03	1,50E-04
log (aT)	7,00	5,10	3,30	1,70	0,00	-1,43	-2,65	-3,82

RAP4034CA (P2-A4), Mix No.9

Temperature (°C)	-32,7	-24,1	-14,9	-4,9	4,9	14,0	24,7	34,9
aT	2,00E+07	2,50E+05	4,00E+03	5,00E+01	1,00E+00	4,00E-02	3,50E-03	1,50E-04
log (aT)	7,30	5,40	3,60	1,70	0,00	-1,40	-2,46	-3,82

RAP4034CA (P2-A3), Mix No.9

Temperature (°C)	-33,0	-23,6	-14,1	-4,0	5,5	14,8	24,4	
aT	1,82E+07	2,27E+05	3,64E+03	4,55E+01	1,00E+00	4,55E-02	4,55E-03	
log (aT)	7,26	5,36	3,56	1,66	0,00	-1,34	-2,34	

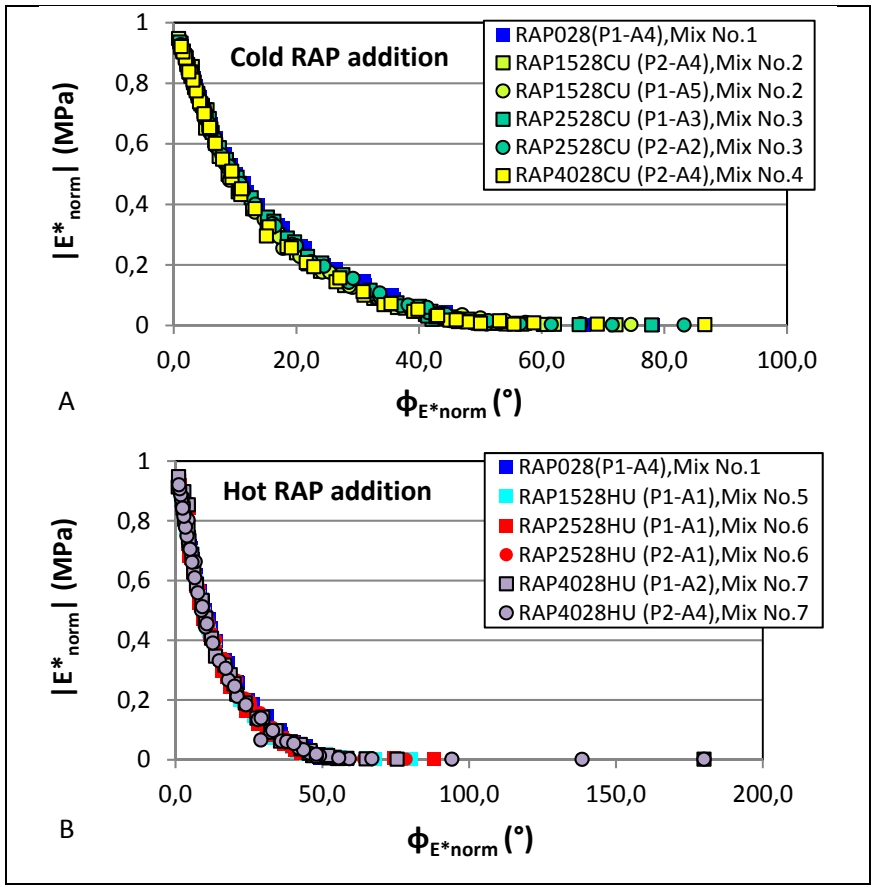

Figure-A II-9 Normalized Black diagrams for materials made of different percentage of RAP

APPENDIX III

PRESENTATION OF FATIGUE TEST RESULTS

TEST NAME: 0RAP-(P1-A2)-D150

GENERAL INFORMATION FOR FATIGUE TEST

Presse of sollicitation:

Presse of sollicitation:	Presse Bionix	**ACTUAL DATA**	
Date / hour:	19/08/2011 - 13h14	Frequency (Hz):	
Operator:	Asmaa/FB	Tº test (ºC) :	10,25
		ε real (µdef):	148,9
TARGET DATA			
Type of mix:	GB20	**Observations:**	
Especimen Nº:	P1-A2	Test name: 0RAP-(P1-A2)-D150	
Diameter (mm):	73,9		
Hight (mm):	121,5		
Vi(%):	4		
Frequency(Hz):	10		
Tº target (ºC):	10		
ε target (µdef):	150		

FATIGUE RESULTS

$\|E_O\|$ (MPa):	**11072**	$N_{f50\%}$ (cycles)	161375
$\|E_{O/2}\|$ (MPa):	**5536**	$N_{fII/III}$ (cycles)	206478

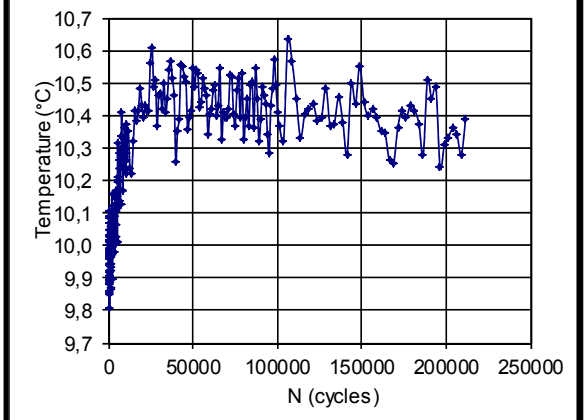

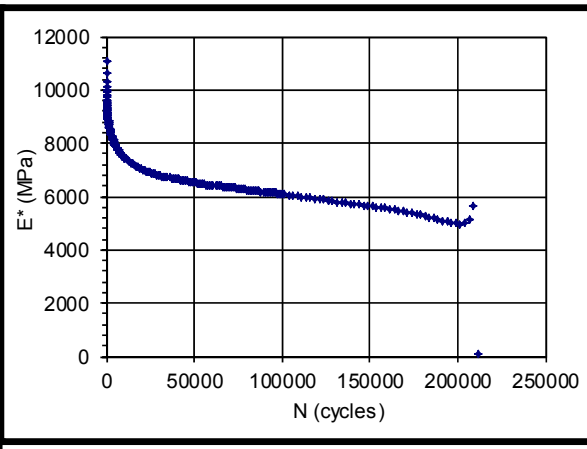

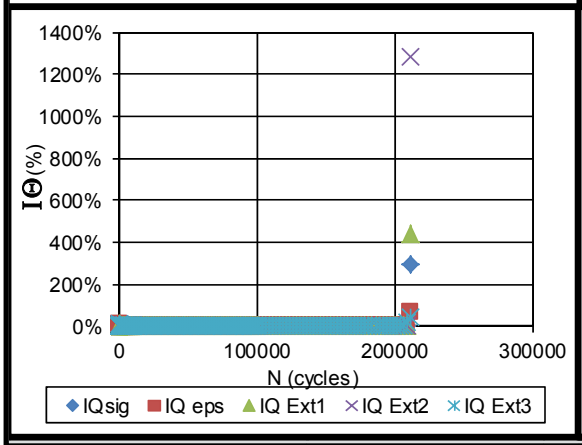

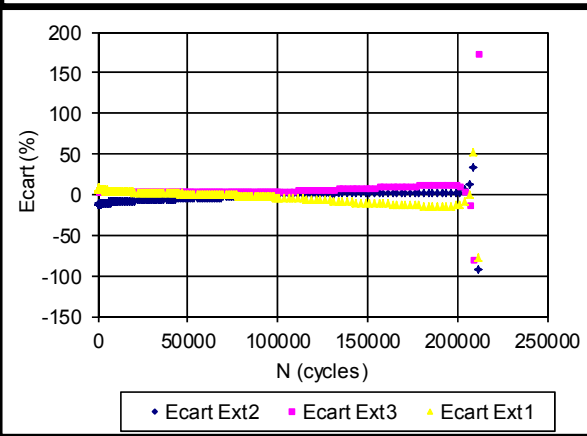

TEST NAME: 40RAP-(P1-A2)-D180

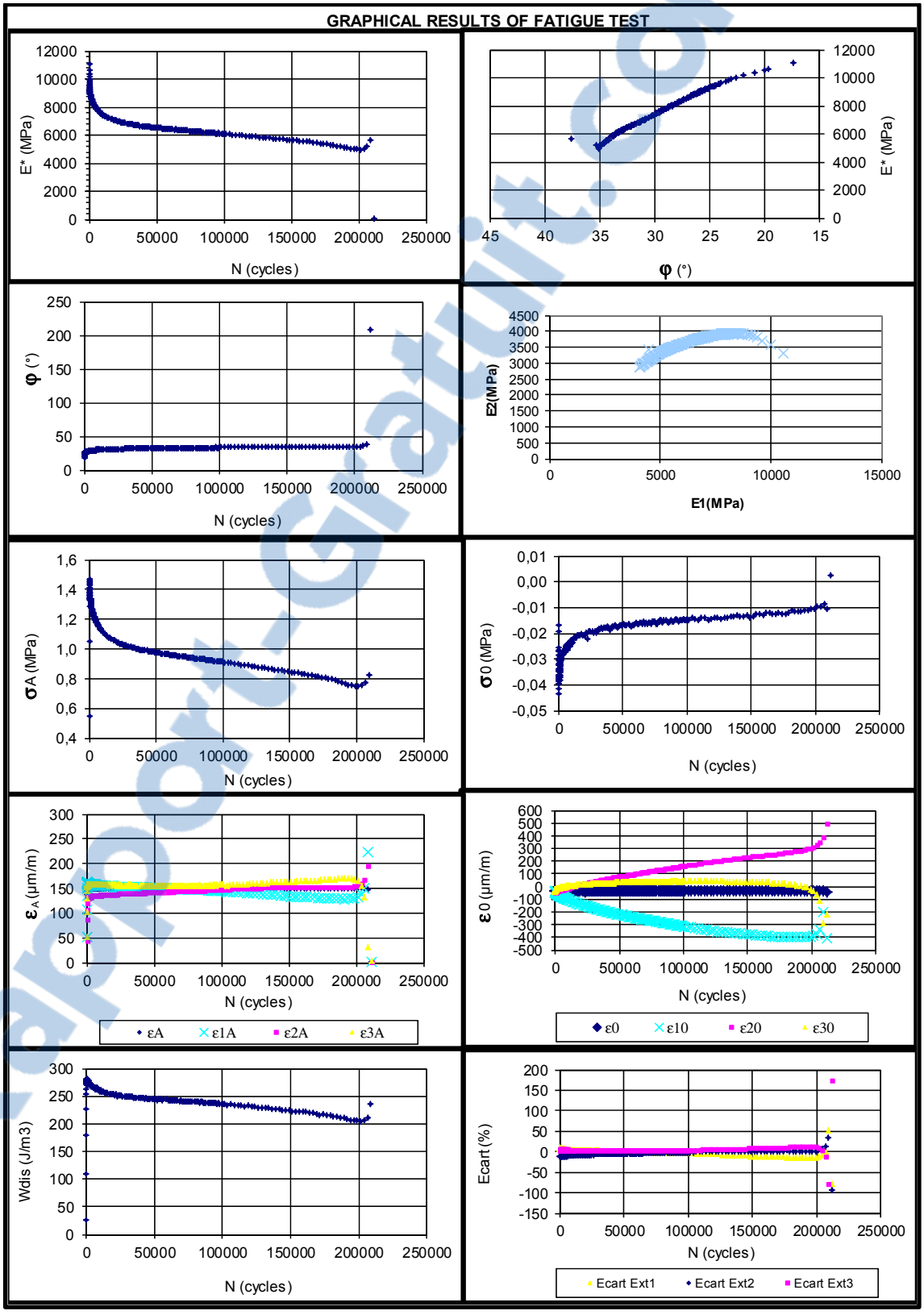

TEST NAME: 0RAP-(P1-A5)-D140

GENERAL INFORMATION FOR FATIGUE TEST

Presse of sollicitation:

Presse of sollicitation:	Presse Bionix	**ACTUAL DATA**	
Date / hour:	21/08/2011 - 13h14	Frequency (Hz):	
Operator:	Asmaa/FB	Tº test (ºC) :	10,23
		ε real (µdef):	138,1
TARGET DATA			
Type of mix:	GB20	**Observations:**	
Especimen Nº:	P1-A5	Test name: 0RAP-(P1-A5)-D140	
Diameter (mm):	73,96		
Hight (mm):	122,5		
Vi(%):	4,1		
Frequency(Hz):	10		
Tº target (ºC):	10		
ε target (µdef):	140		

FATIGUE RESULTS

$\|E_O\|$ (MPa):	**11682**	$N_{f50\%\ (cycles)}$	692216
$\|E_{O/2}\|$ (MPa):	**5841**	$N_{fII/III\ (cycles)}$	549550

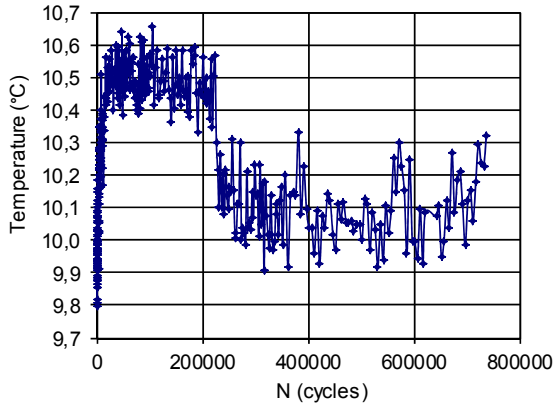

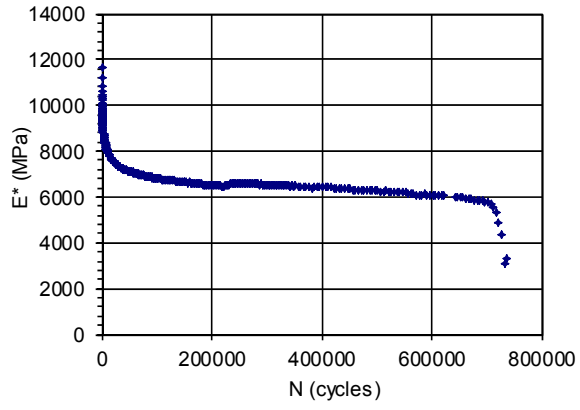

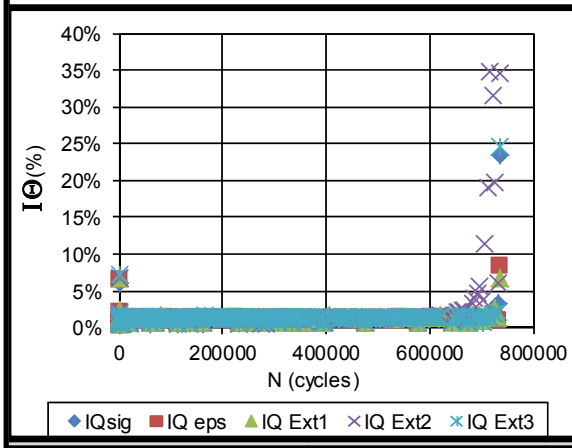

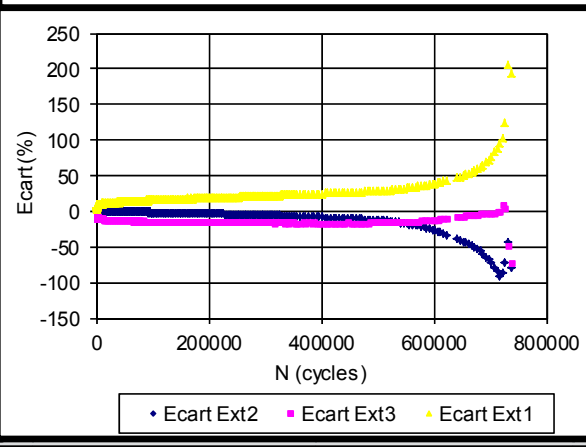

TEST NAME: 0RAP-(P1-A5)-D140

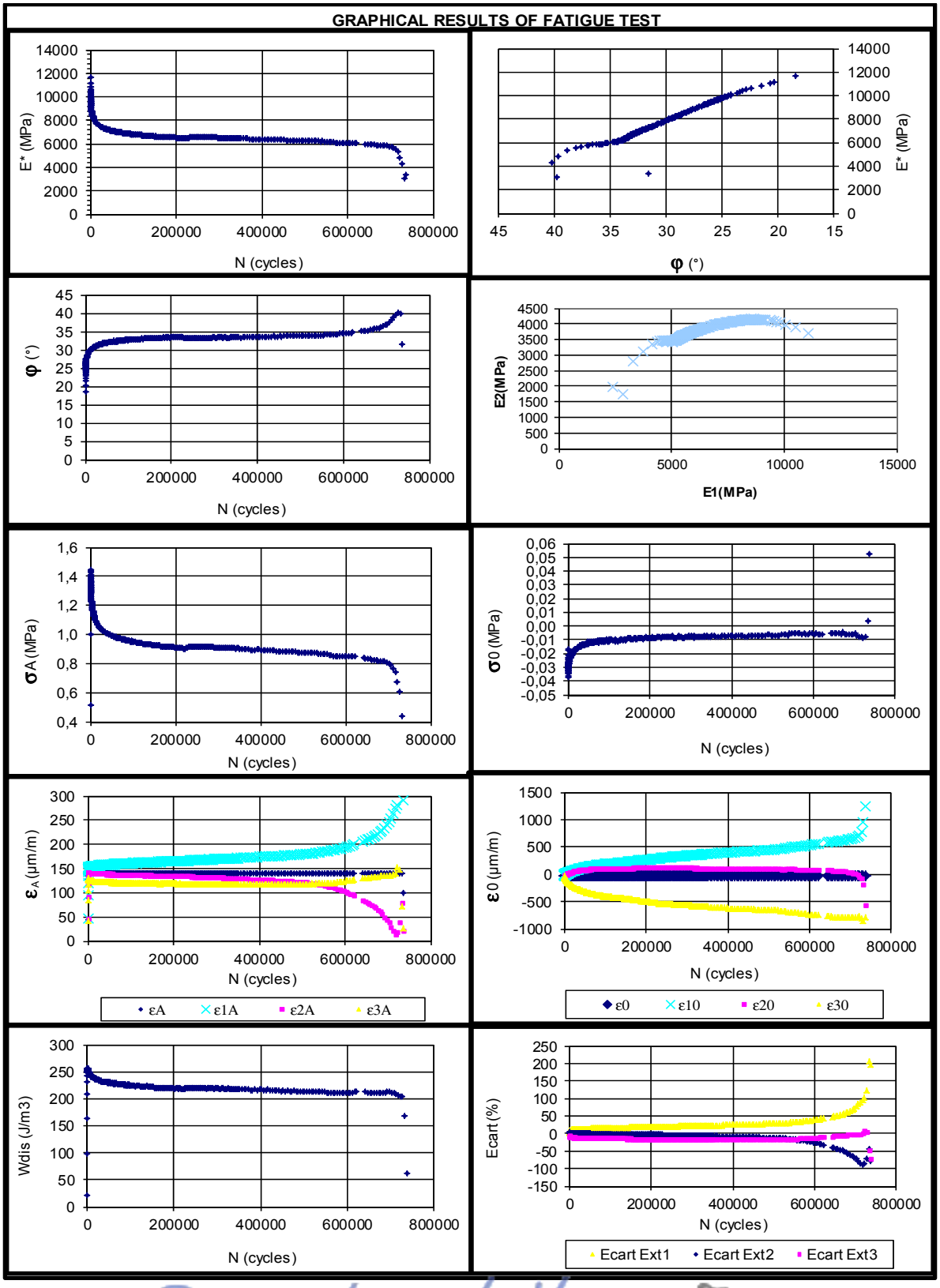

TEST NAME: 0RAP-(P2-A4)-D130

GENERAL INFORMATION FOR FATIGUE TEST

Presse of sollicitation:

Presse of sollicitation:	Presse Bionix	**ACTUAL DATA**	
Date / hour:	02/10/2011 - 13h14	Frequency (Hz):	
Operator:	Asmaa/FB	Tº test (ºC) :	10,3
		ε real (µdef):	126,5
TARGET DATA			
Type of mix:	GB20	**Observations:**	
Especimen Nº:	P2-A4	Test name: 0RAP-(P2-A4)-D130	
Diameter (mm):	73,97		
Hight (mm):	118		
Vi(%):	4,5		
Frequency(Hz):	10		
Tº target (ºC):	10		
ε target (µdef):	130		

FATIGUE RESULTS

$\|E_O\|$ (MPa):	12396	$N_{f50\%}$ (cycles)	501909
$\|E_{O/2}\|$ (MPa):	6198	$N_{fII/III}$ (cycles)	524434

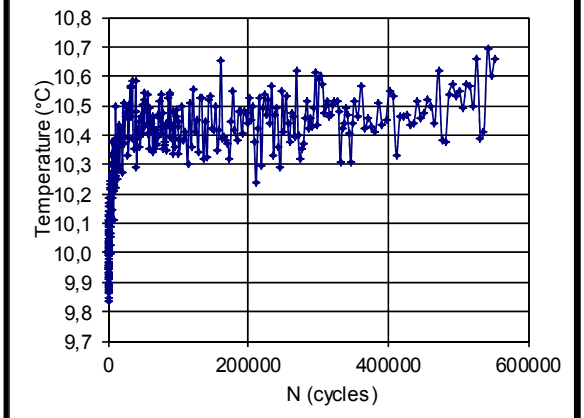

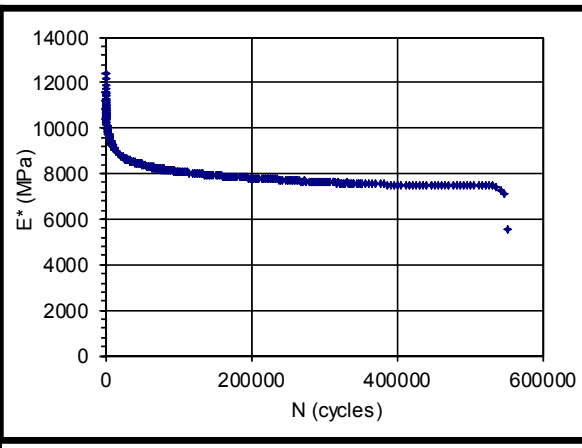

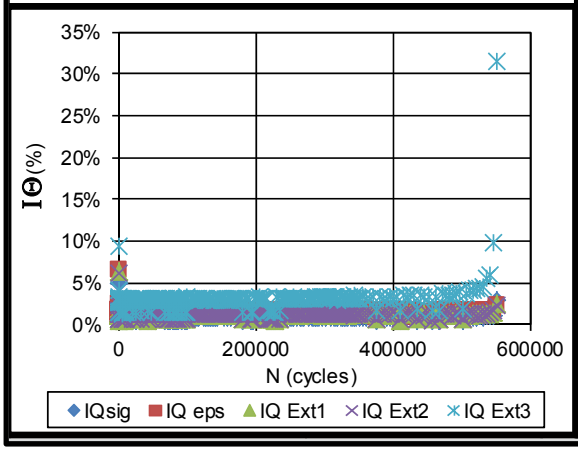

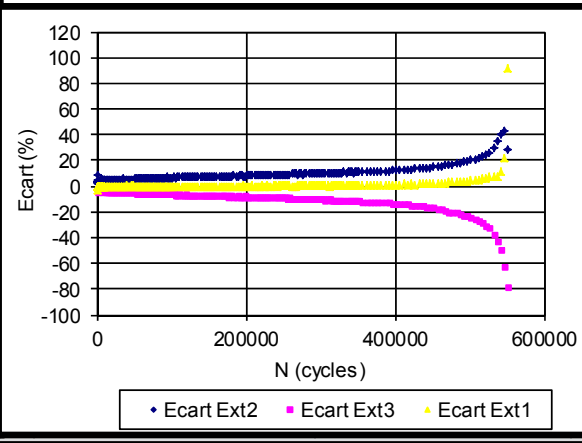

TEST NAME: 0RAP-(P1-A5)-D140

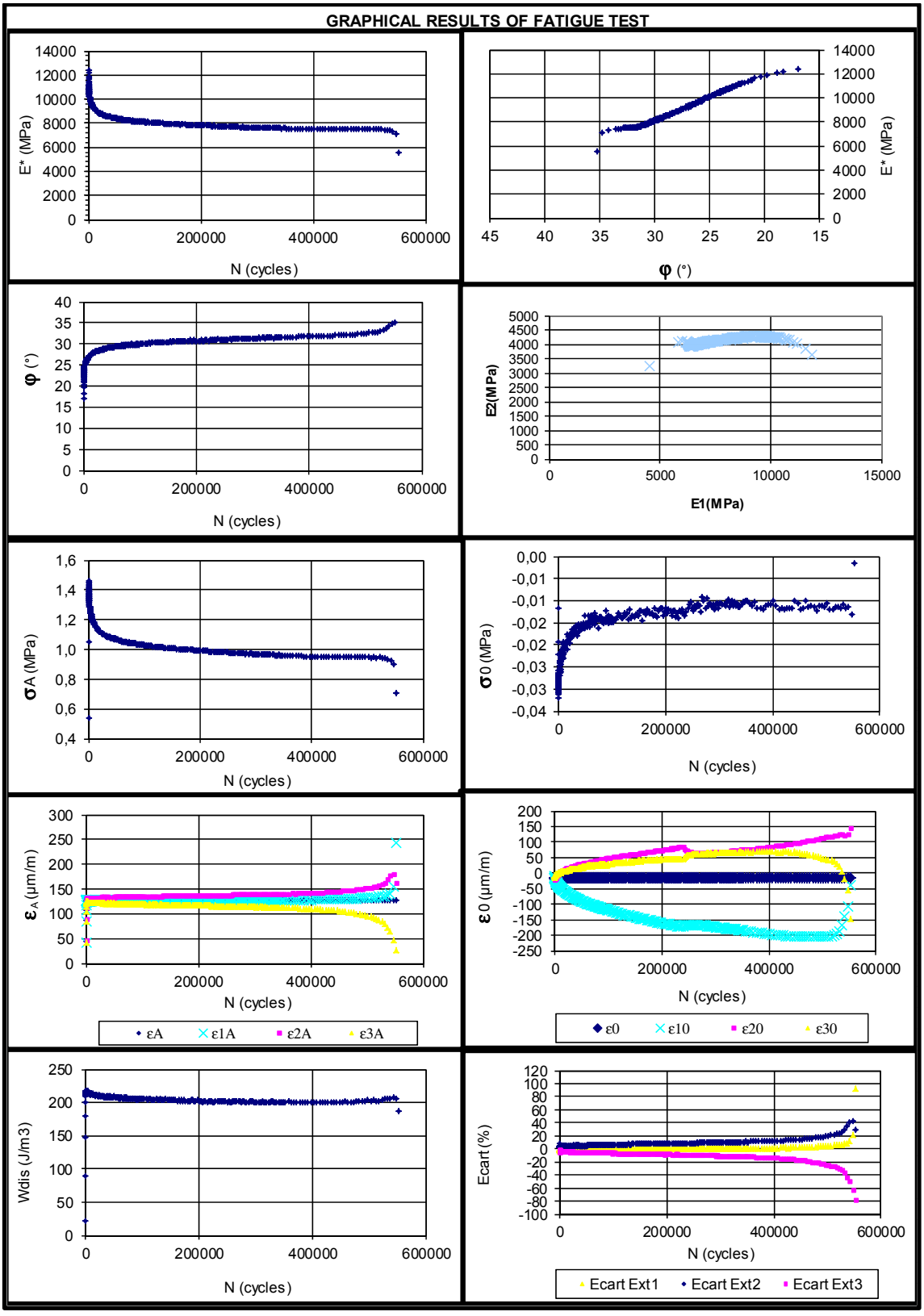

TEST NAME: 0RAP-(P1-A3)-D140

GENERAL INFORMATION FOR FATIGUE TEST

Presse of sollicitation:

Presse of sollicitation:	Presse Bionix	**ACTUAL DATA**	
Date / hour:	1/11/2011 - 16h14	Frequency (Hz):	
Operator:	Asmaa/FB	Tº test (ºC) :	10
		ε real (µdef):	136,5
TARGET DATA			
Type of mix:	GB20	**Observations:**	
Especimen Nº:	P1-A3	Test name: 0RAP-(P1-A3)-D140	
Diameter (mm):	73,87	Failure before to reach Nf50%	
Hight (mm):	122,2		
Vi(%):	3,9		
Frequency(Hz):	10		
Tº target (ºC):	10		
ε target (µdef):	140		

FATIGUE RESULTS

$\|E_O\|$ (MPa):	12023	$N_{f50\%\ (cycles)}$	314163
$\|E_{O/2}\|$ (MPa):	6011	$N_{fII/III\ (cycles)}$	314163

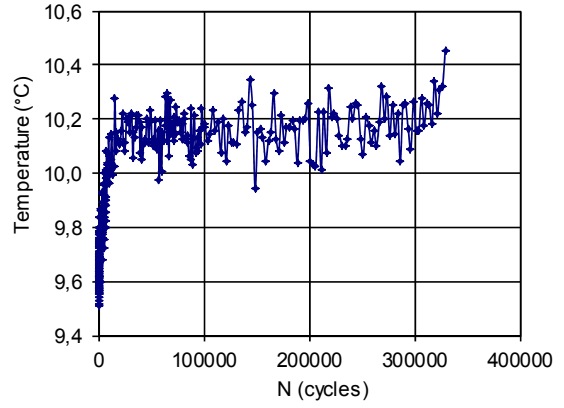

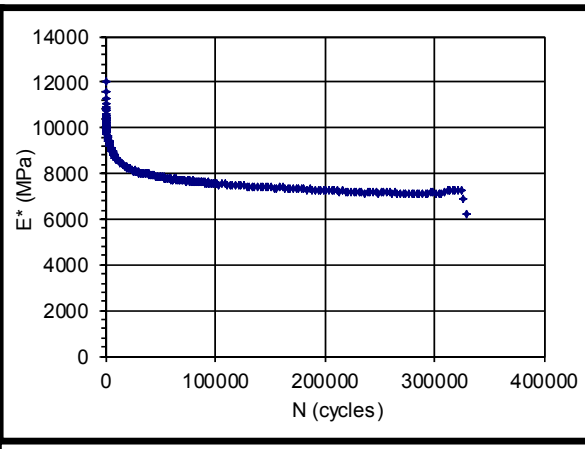

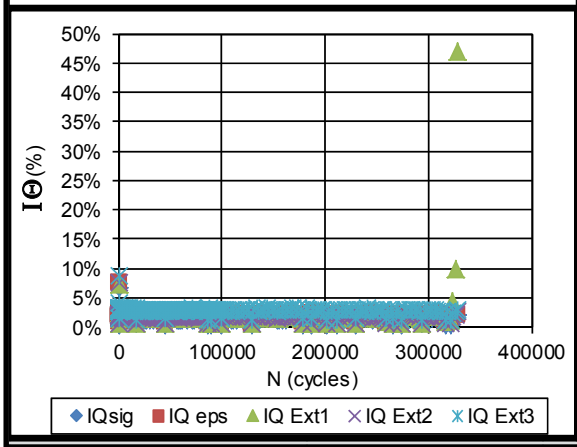

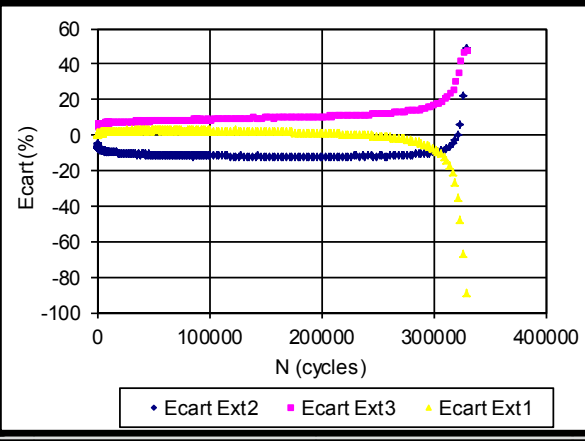

TEST NAME: 0RAP-(P1-A3)-D140

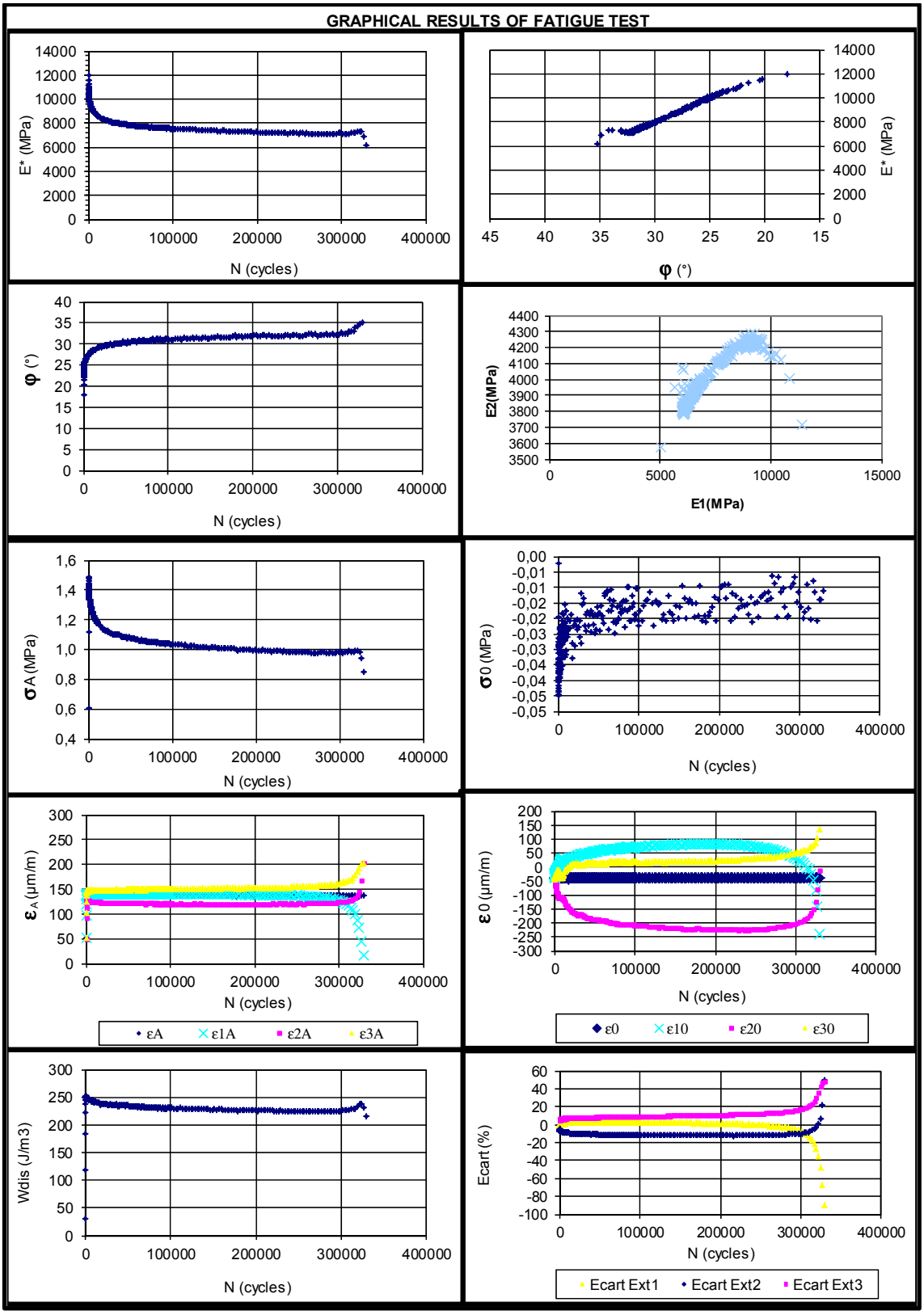

TEST NAME: 0RAP-(P3-A3)-D110

GENERAL INFORMATION FOR FATIGUE TEST

Presse of sollicitation:

Presse of sollicitation:	Presse Bionix	**ACTUAL DATA**	
Date / hour:	5/12/2011 - 11h0	Frequency (Hz):	
Operator:	Asmaa/FB	Tº test (ºC) :	10,1
		ε real (µdef):	106,8
TARGET DATA			
Type of mix:	GB20	**Observations:**	
Especimen Nº:	P3-A3	Test name: 0RAP-(P3-A3)-D110	
Diameter (mm):	73,97	Failure before to reach to Nf50%	
Hight (mm):	123,7		
Vi(%):	6,7		
Frequency(Hz):	10		
Tº target (ºC):	10		
ε target (µdef):	110		

Failure before Nf 50%

FATIGUE RESULTS

$\|E_O\|$ (MPa):	10532	$N_{f50\%\ (cycles)}$	1639096
$\|E_{O/2}\|$ (MPa):	5266	$N_{fII/III\ (cycles)}$	1639096

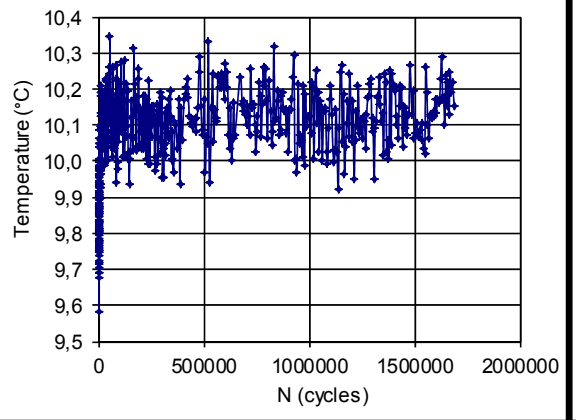

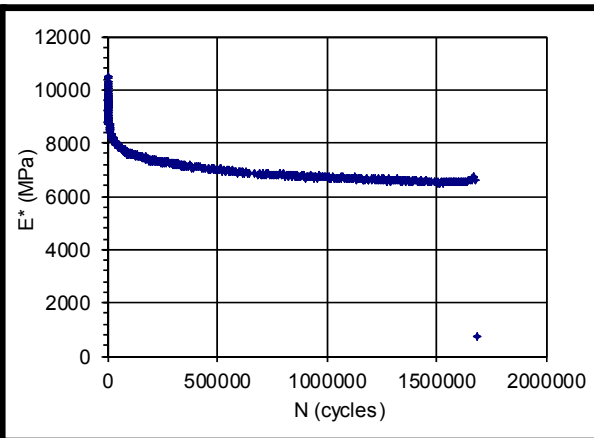

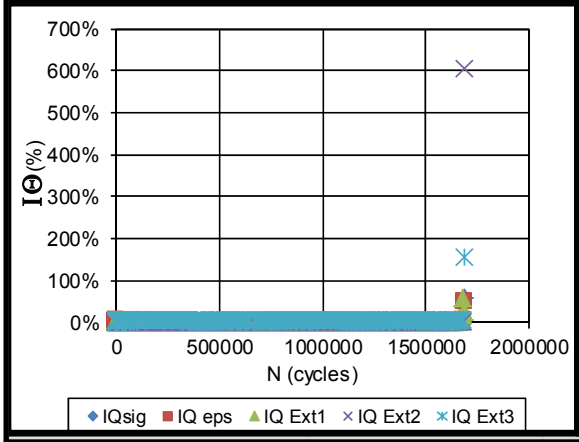

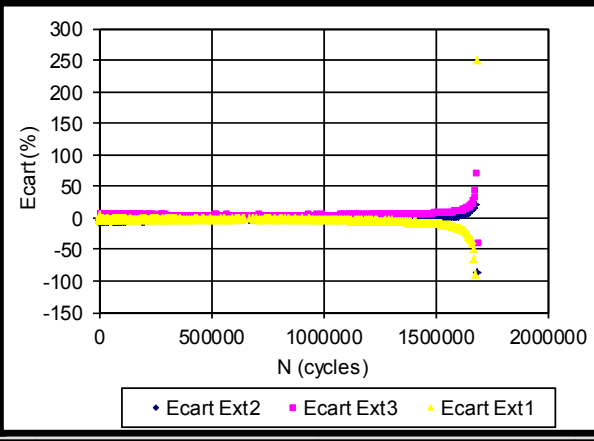

TEST NAME: 0RAP-(P3-A3)-D110

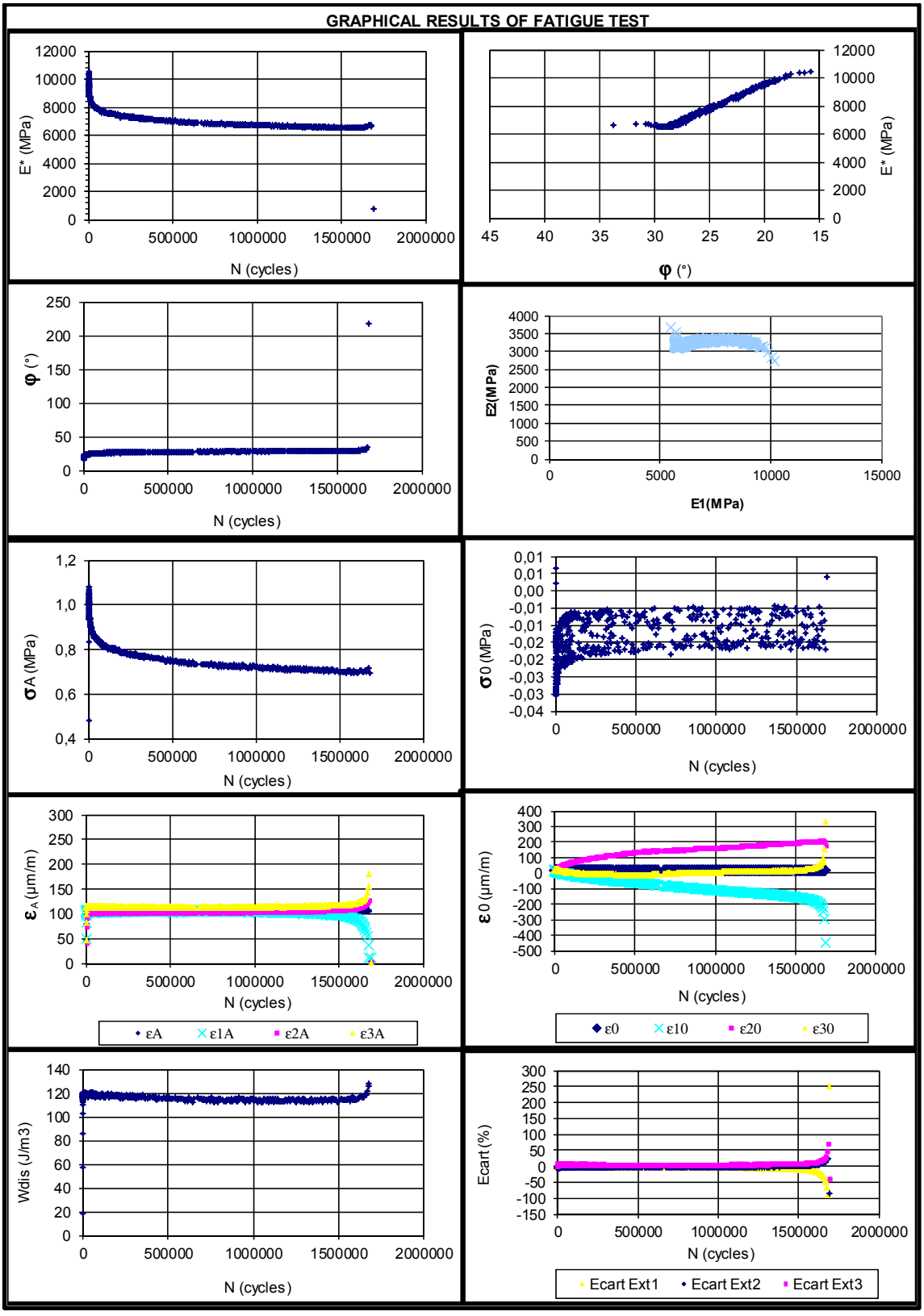

TEST NAME: 0RAP-(P3-A5)-D105

GENERAL INFORMATION FOR FATIGUE TEST

Presse of sollicitation:

Presse of sollicitation:	Presse Bionix	**ACTUAL DATA**	
Date / hour:	08/12/2011 - 15h10	Frequency (Hz):	
Operator:	Asmaa/FB	Tº test (ºC) :	10,06
		ε real (µdef):	102,2
TARGET DATA			
Type of mix:	GB20	**Observations:**	
Especimen Nº:	P3-A5	Test name: 0RAP-(P3-A5)-D105	
Diameter (mm):	74,01	Failure before to reach to Nf50%	
Hight (mm):	123,2		
Vi(%):	6,8		
Frequency(Hz):	10		
Tº target (ºC):	10		
ε target (µdef):	105		

Failture before 50%

FATIGUE RESULTS

$\|E_0\|$ (MPa):	10435	$N_{f\,50\%\,(cycles)}$	1874412
$\|E_{O/2}\|$ (MPa):	5218	$N_{fII/III\,(cycles)}$	1874412

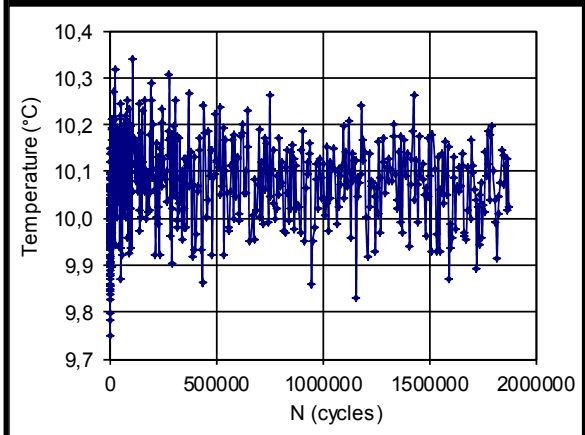

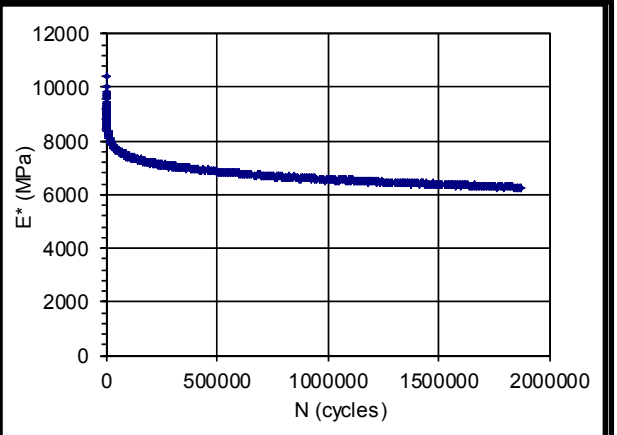

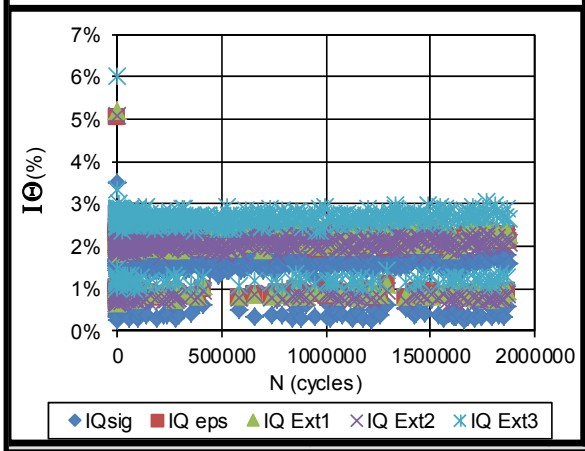

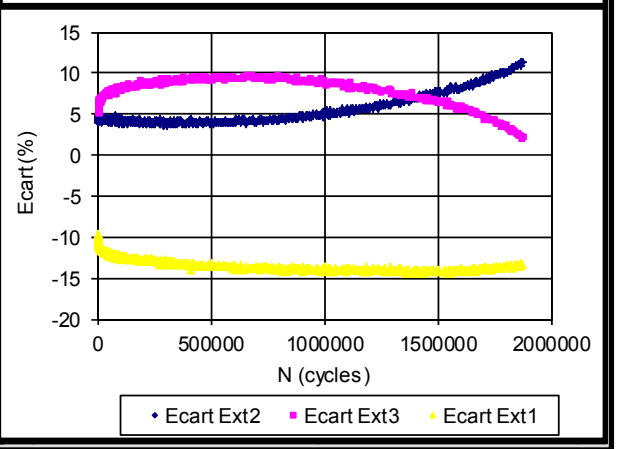

TEST NAME: 0RAP-(P3-A5)-D105

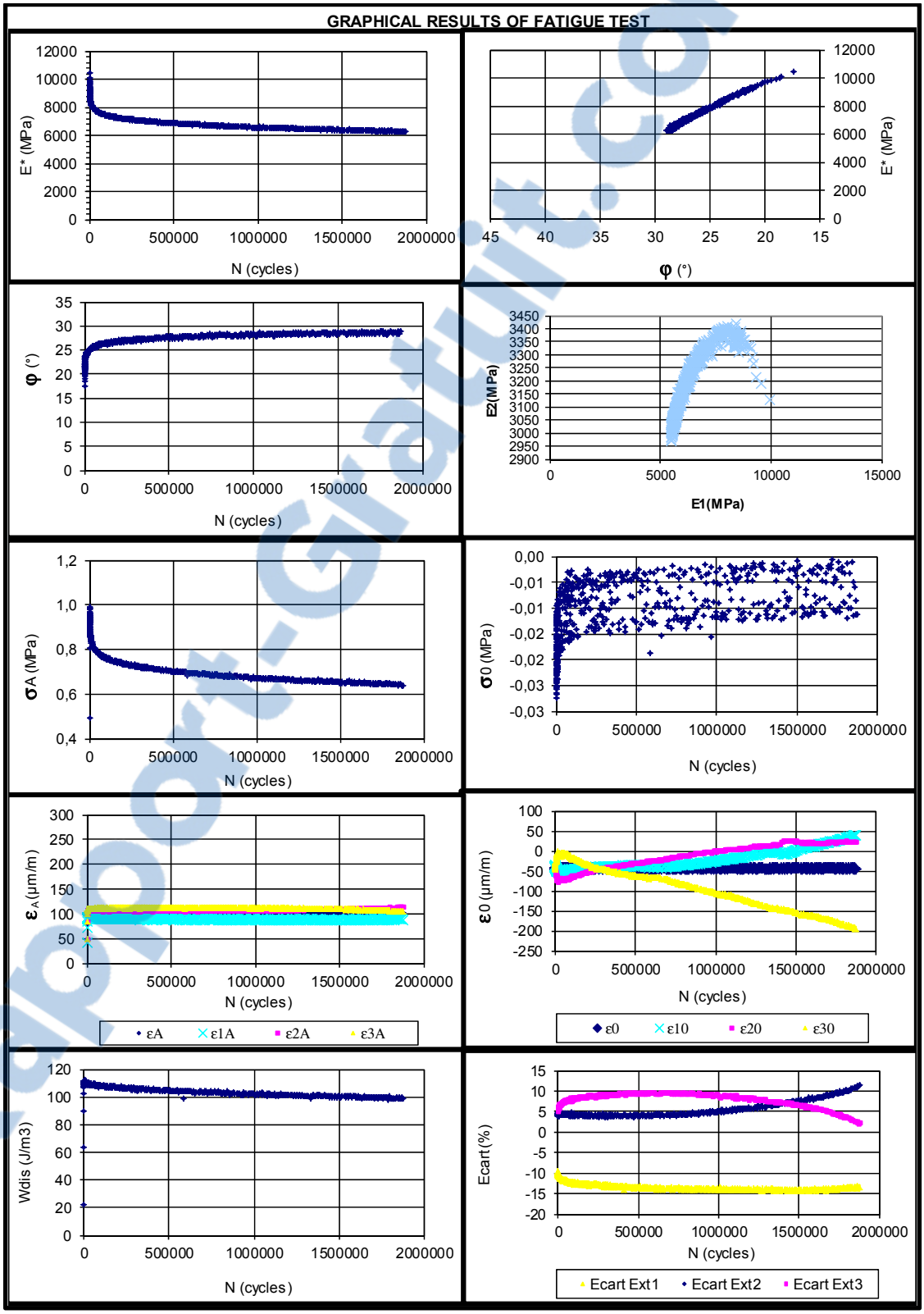

TEST NAME: 0RAP-(P4-A5)-D115

GENERAL INFORMATION FOR FATIGUE TEST

Presse of sollicitation:

Presse of sollicitation:	Presse Bionix	**ACTUAL DATA**	
Date / hour:	12/12/2011 - 11h45	Frequency (Hz):	
Operator:	Asmaa/FB	Tº test (ºC) :	10,16
		ε real (µdef):	112
TARGET DATA			
Type of mix:	GB20	**Observations:**	
Especimen Nº:	P4-A5	Test name: 0RAP-(P4-A5)-D115	
Diameter (mm):	74,04		
Hight (mm):	124,4		
Vi(%):	5,1		
Frequency(Hz):	10		
Tº target (ºC):	10		
ε target (µdef):	115		

Failture before 50%

FATIGUE RESULTS

$\|E_O\|$ (MPa):	10436	$N_{f\,50\%\,(cycles)}$	902680
$\|E_{O/2}\|$ (MPa):	5218	$N_{f\,II/III\,(cycles)}$	827584

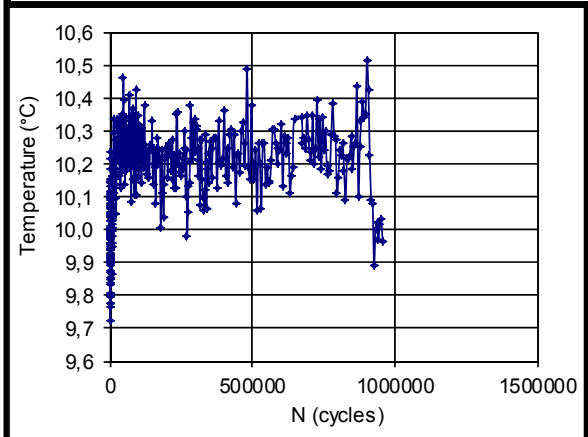

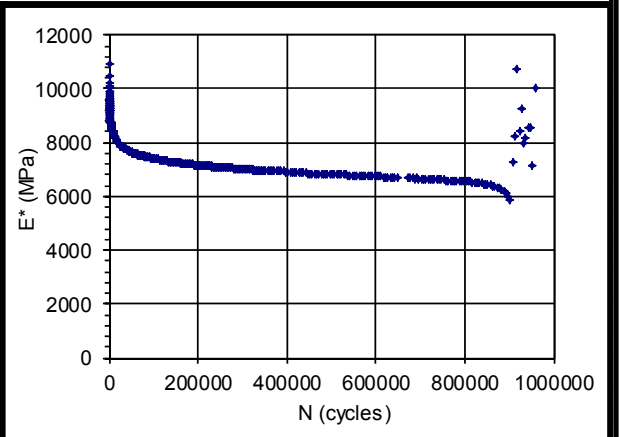

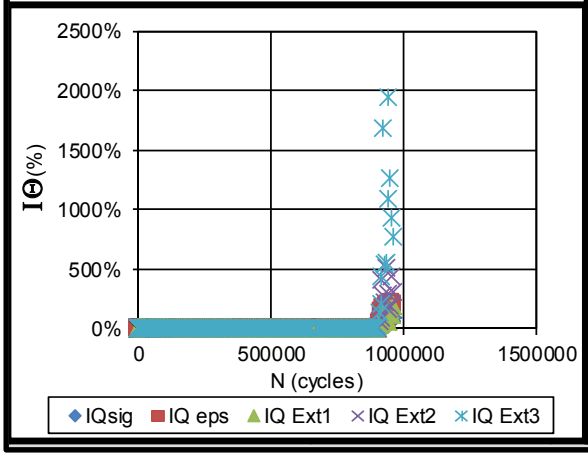

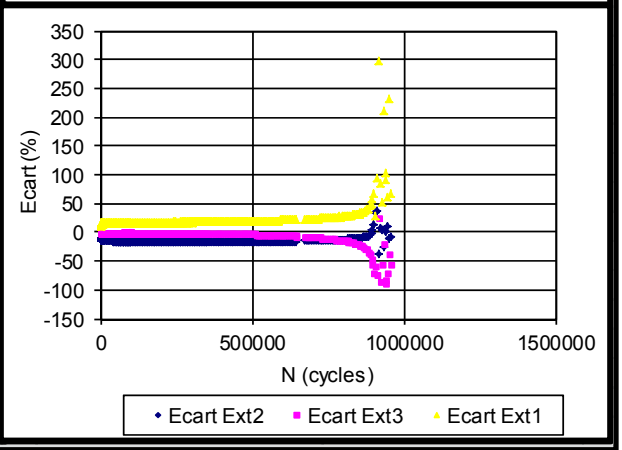

TEST NAME: 0RAP-(P4-A5)-D115

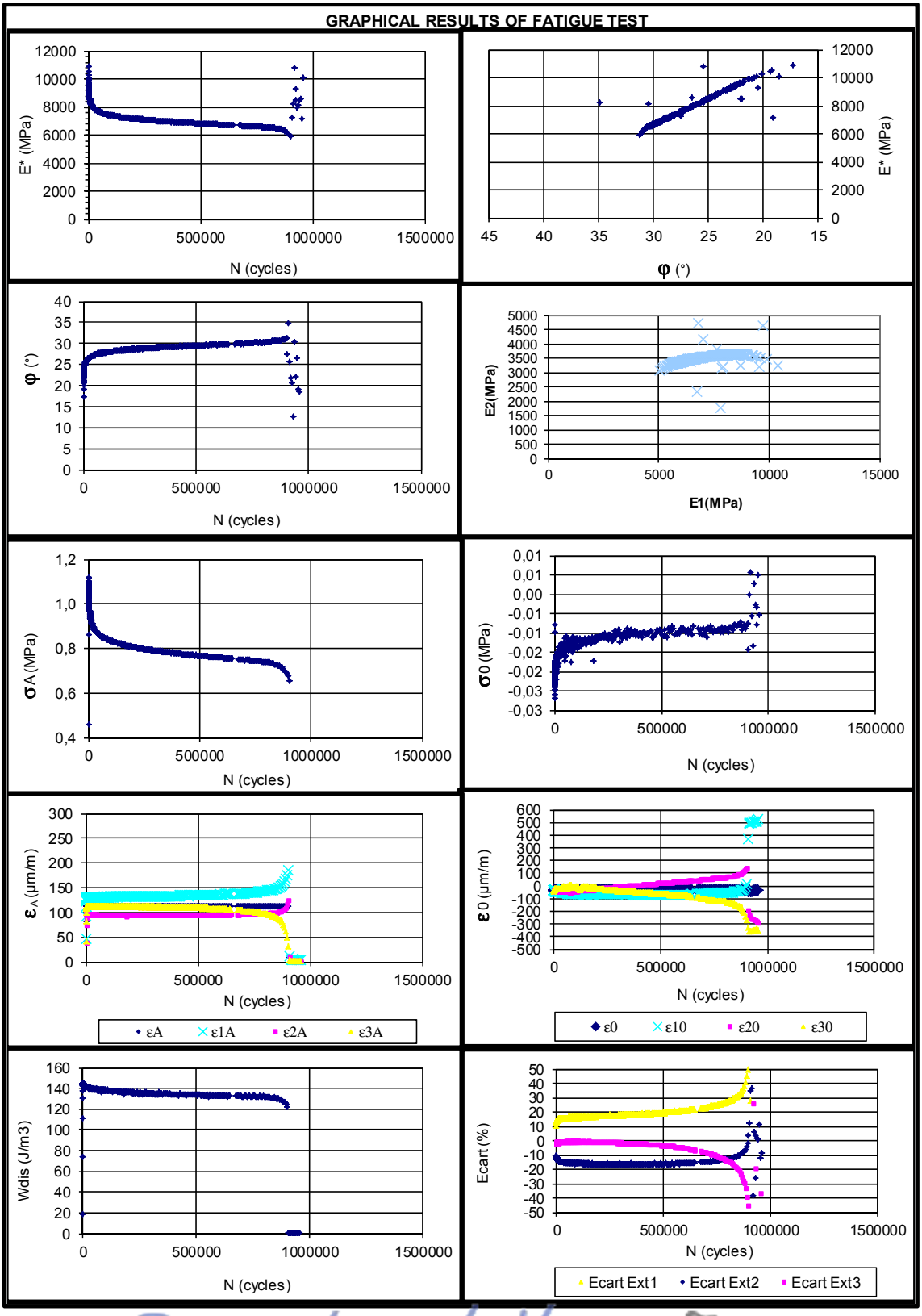

TEST NAME: 0RAP-(P3-A4)-D115

GENERAL INFORMATION FOR FATIGUE TEST

Presse of sollicitation:

Presse of sollicitation:	Bionix Presse
Date / hour:	19/12/2011 - 16h30
Operator:	Asmaa/FB

TARGET DATA

Type of mix:	GB20
Especimen Nº:	P3-A4
Diameter (mm):	73,97
Hight (mm):	124,7
Vi(%):	6,6
Frequency(Hz):	10
Tº target (ºC):	10
ε target (µdef):	115

ACTUAL DATA

Frequency (Hz):	
Tº test (ºC) :	10,12
ε real (µdef):	111,4

Observations:

Test name: 0RAP-(P3-A4)-D115

Failture before 50%

FATIGUE RESULTS

$\|E_0\|$ (MPa):	10430	$N_{f50\%\ (cycles)}$	1328140
$\|E_{0/2}\|$ (MPa):	5215	$N_{fII/III\ (cycles)}$	1253045

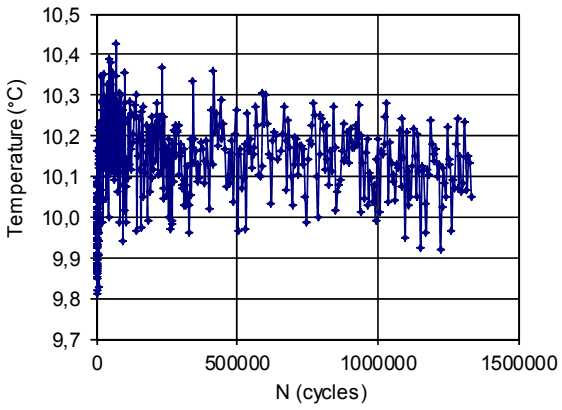

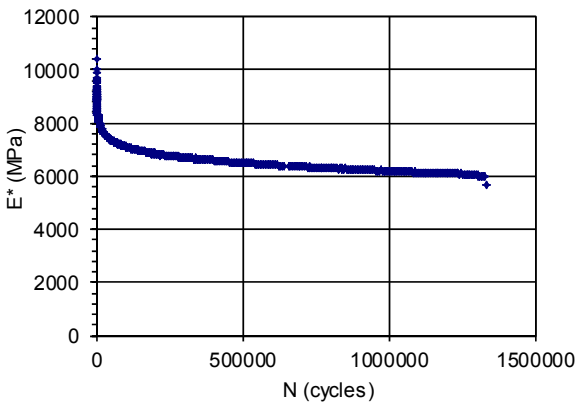

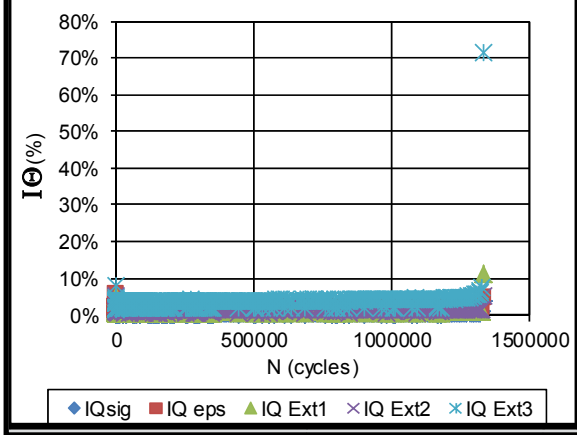

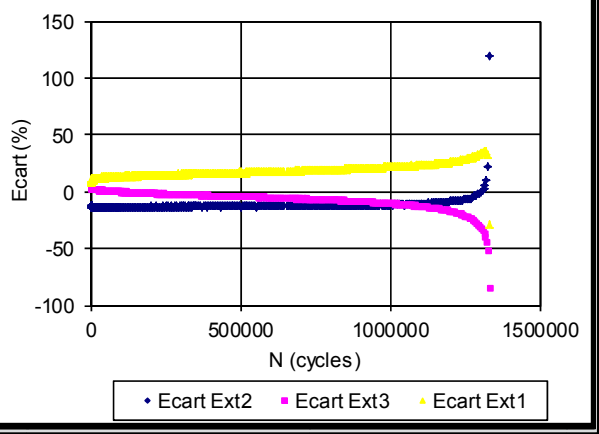

TEST NAME: 0RAP-(P3-A4)-D115

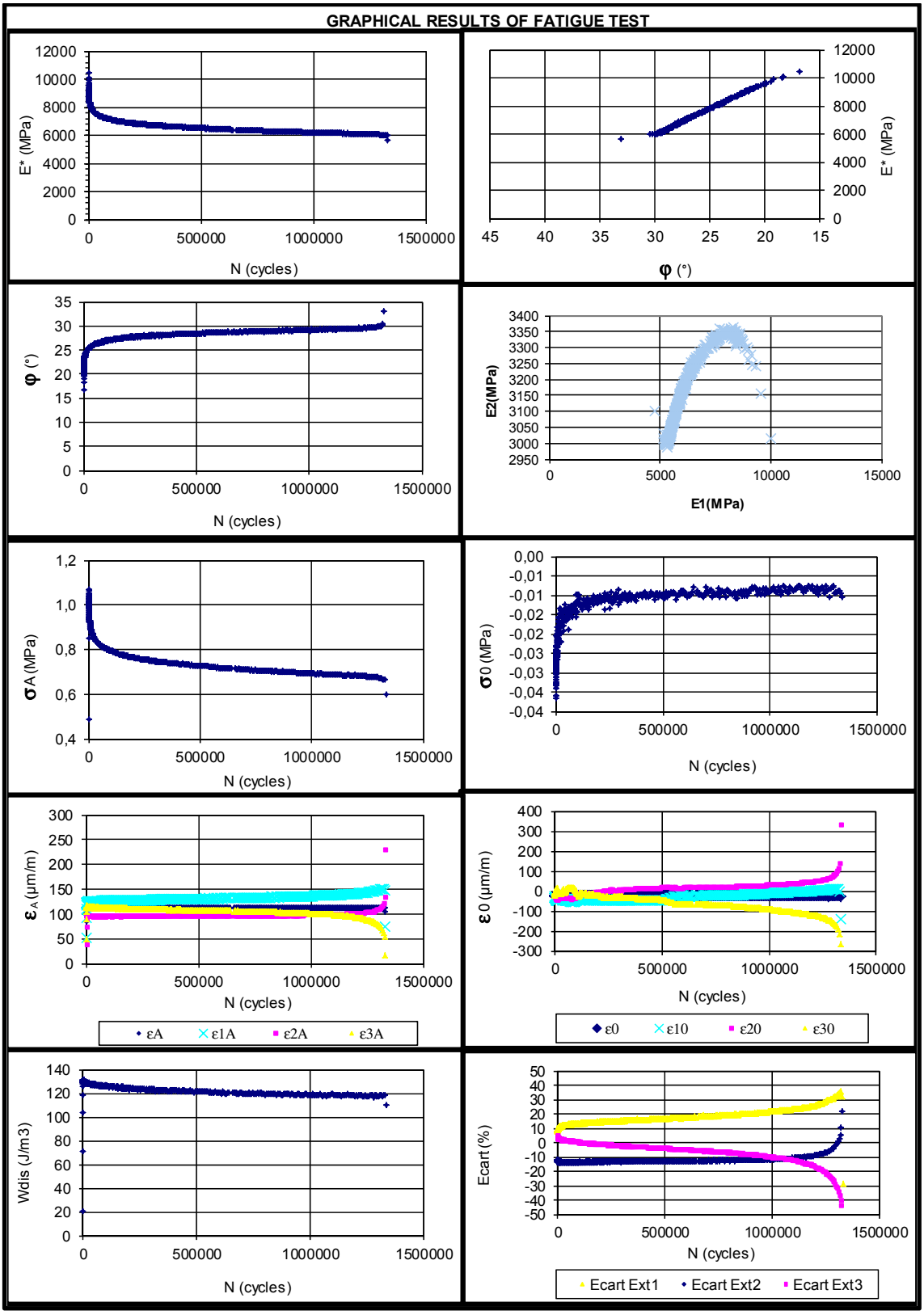

TEST NAME: 15RAP-(P2-A1)-D150

GENERAL INFORMATION FOR FATIGUE TEST

Presse of sollicitation:

Presse of sollicitation:	Presse Bionix
Date / hour:	16/08/2011 - 11h30
Operator:	Asmaa/FB

TARGET DATA

Type of mix:	GB20
Especimen Nº:	P2-A1
Diameter (mm):	73,9
Hight (mm):	125,0
Vi(%):	6,3
Frequency(Hz):	10
Tº target (ºC):	10
ε target (μdef):	150

ACTUAL DATA

Frequency (Hz):	
Tº test (ºC) :	9,86
ε real (μdef):	149

Observations:

Test name: 15RAP-(P2-A1)-D150

Failure before to reach to Nf50%

FATIGUE RESULTS

$\|E_O\|$ (MPa):	10058	$N_{f50\%\ (cycles)}$	84158
$\|E_{O/2}\|$ (MPa):	5029	$N_{fII/III\ (cycles)}$	82650

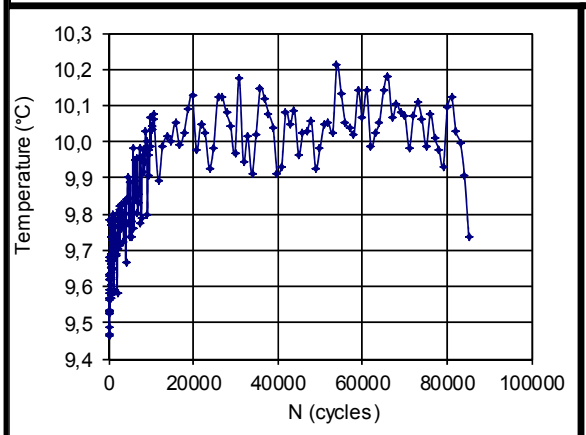

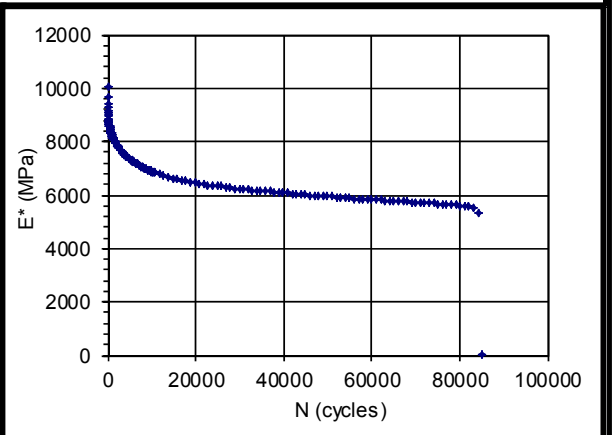

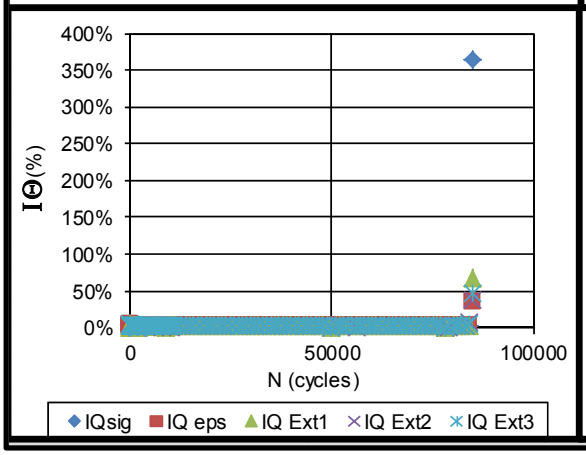

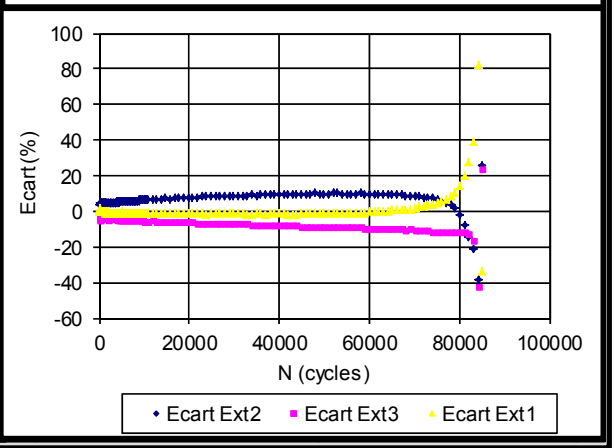

TEST NAME: 15RAP-(P2-A1)-D150

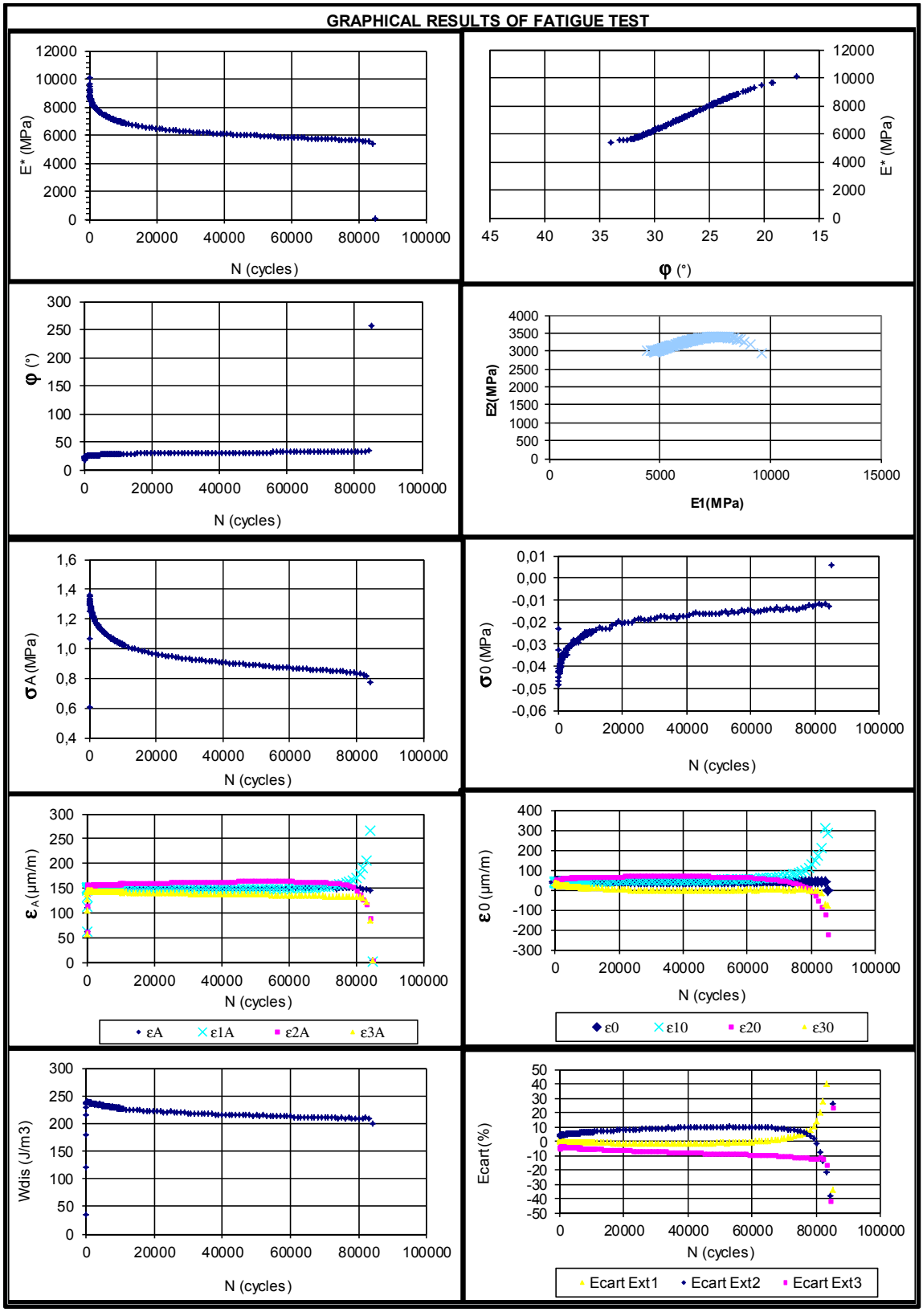

TEST NAME: 15RAP-(P2-A2)-D120

GENERAL INFORMATION FOR FATIGUE TEST

Presse of sollicitation:

Presse of sollicitation:	Presse Bionix	**ACTUAL DATA**	
Date / hour:	18/08/2011 - 14h9	Frequency (Hz):	
Operator:	Asmaa/FB	Tº test (ºC) :	10,2
		ε real (µdef):	118,7
TARGET DATA			
Type of mix:	GB20	**Observations:**	
Especimen Nº:	P2-A2	Test name: 15RAP-(P2-A2)-D120	
Diameter (mm):	73,95	Failure before to reach to Nf50%	
Hight (mm):	123,3		
Vi(%):	6,7		
Frequency(Hz):	10		
Tº target (ºC):	10		
ε target (µdef):	120		

FATIGUE RESULTS

$\|E_O\|$ (MPa):	9550	$N_{f50\%\ (cycles)}$	351791
$\|E_{O/2}\|$ (MPa):	4775	$N_{fII/III\ (cycles)}$	341768

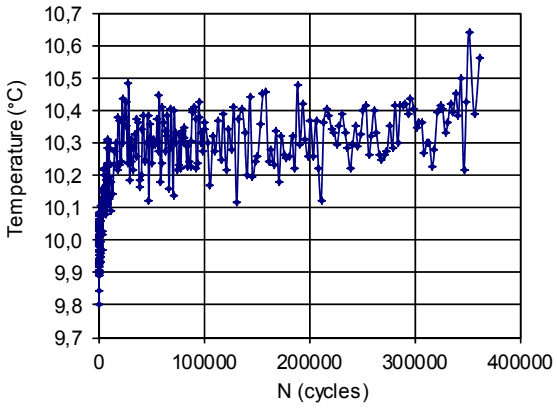

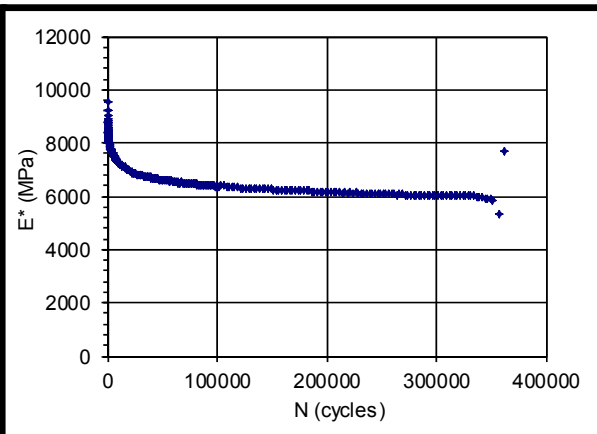

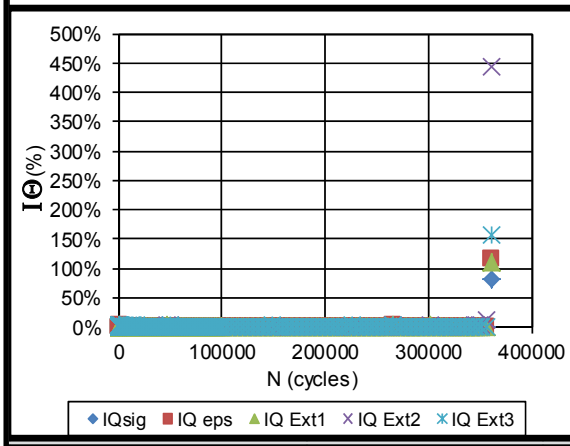

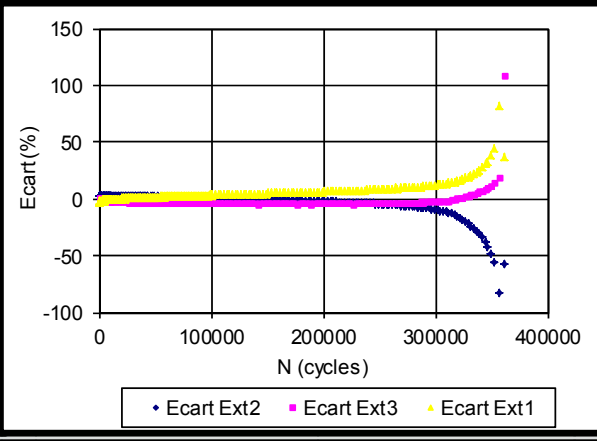

TEST NAME: 15RAP-(P2-A2)-D120

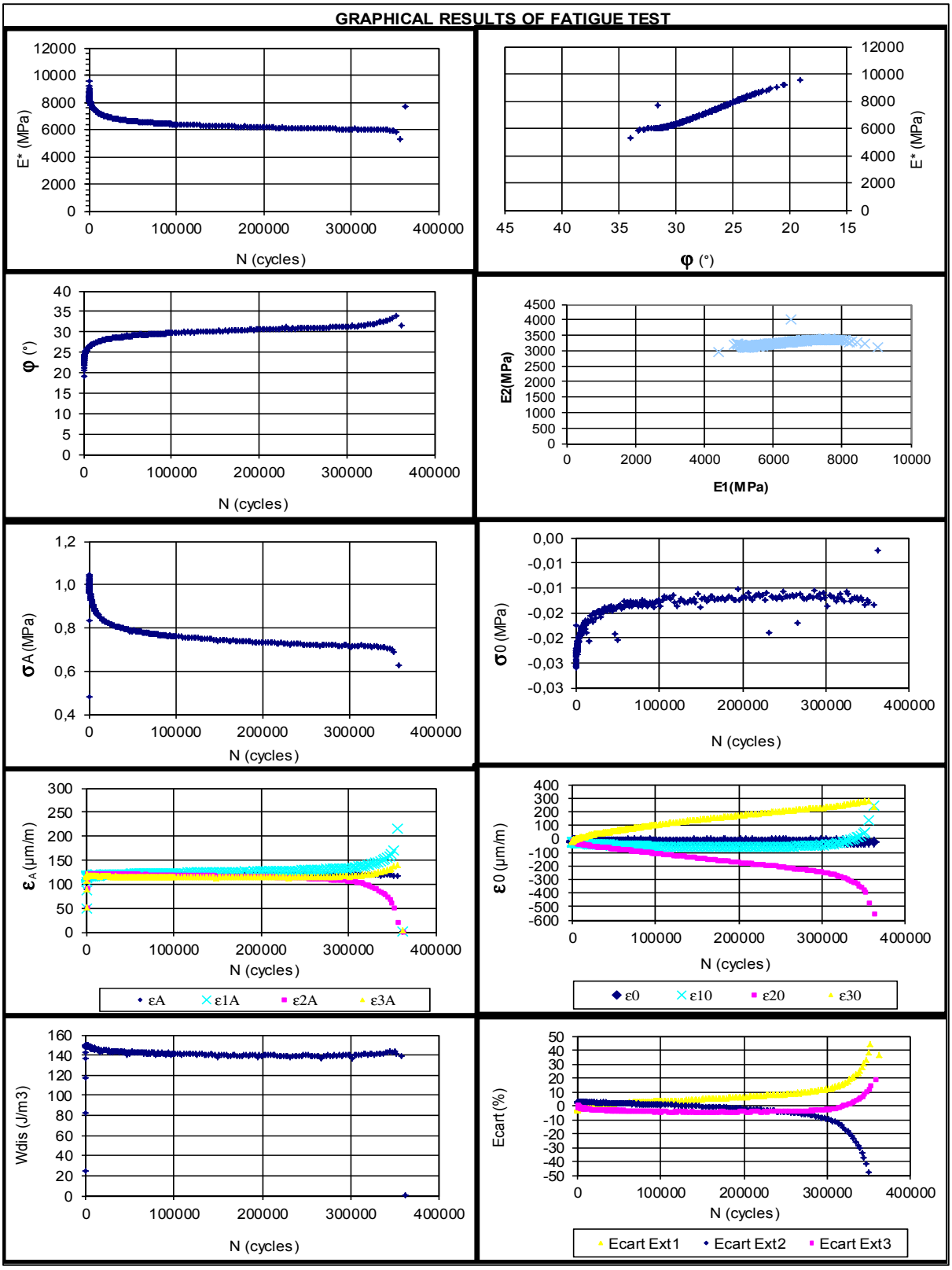

TEST NAME: 15RAP-(P1-A3)-D115

GENERAL INFORMATION FOR FATIGUE TEST

Presse of sollicitation:

Presse of sollicitation:	Presse Bionix
Date / hour:	17/12/2011 - 15h30
Operator:	Asmaa/FB
TARGET DATA	
Type of mix:	GB20
Especimen Nº:	P1-A3
Diameter (mm):	73,97
Hight (mm):	121,6
Vi(%):	5,9
Frequency(Hz):	10
Tº target (ºC):	10
ε target (µdef):	115

ACTUAL DATA

Frequency (Hz):	
Tº test (ºC) :	10,02
ε real (µdef):	112,2

Observations:
Test name: 15RAP-(P1-A3)-D115
Failure before to reach to Nf50%

FATIGUE RESULTS

$\|E_O\|$ (MPa):	11222	$N_{f50\%\ (cycles)}$	1027737
$\|E_{O/2}\|$ (MPa):	5611	$N_{fII/III\ (cycles)}$	980180

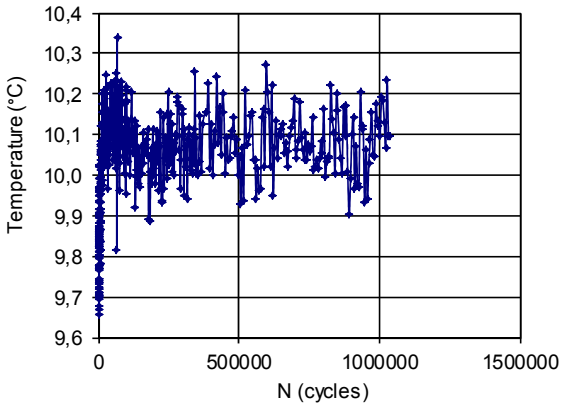

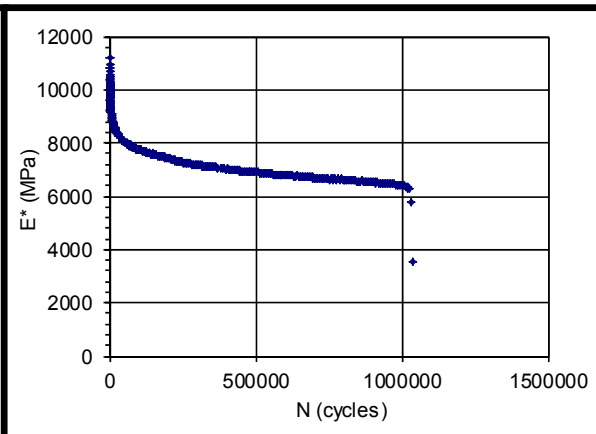

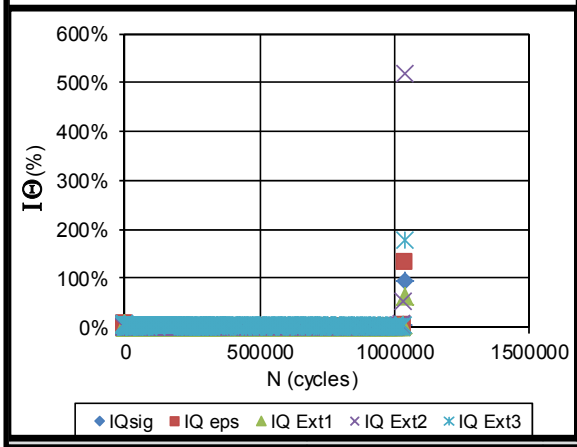

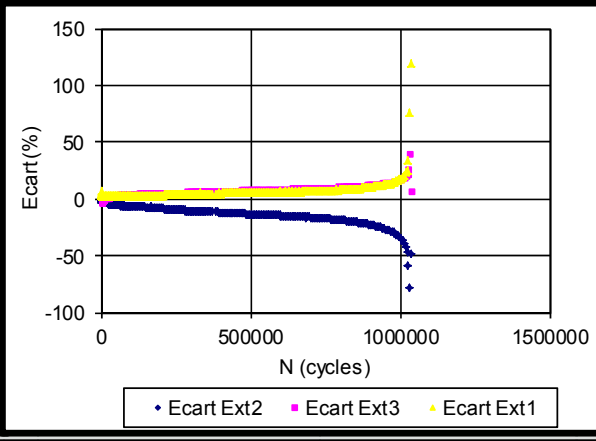

TEST NAME: 15RAP-(P1-A3)-D115

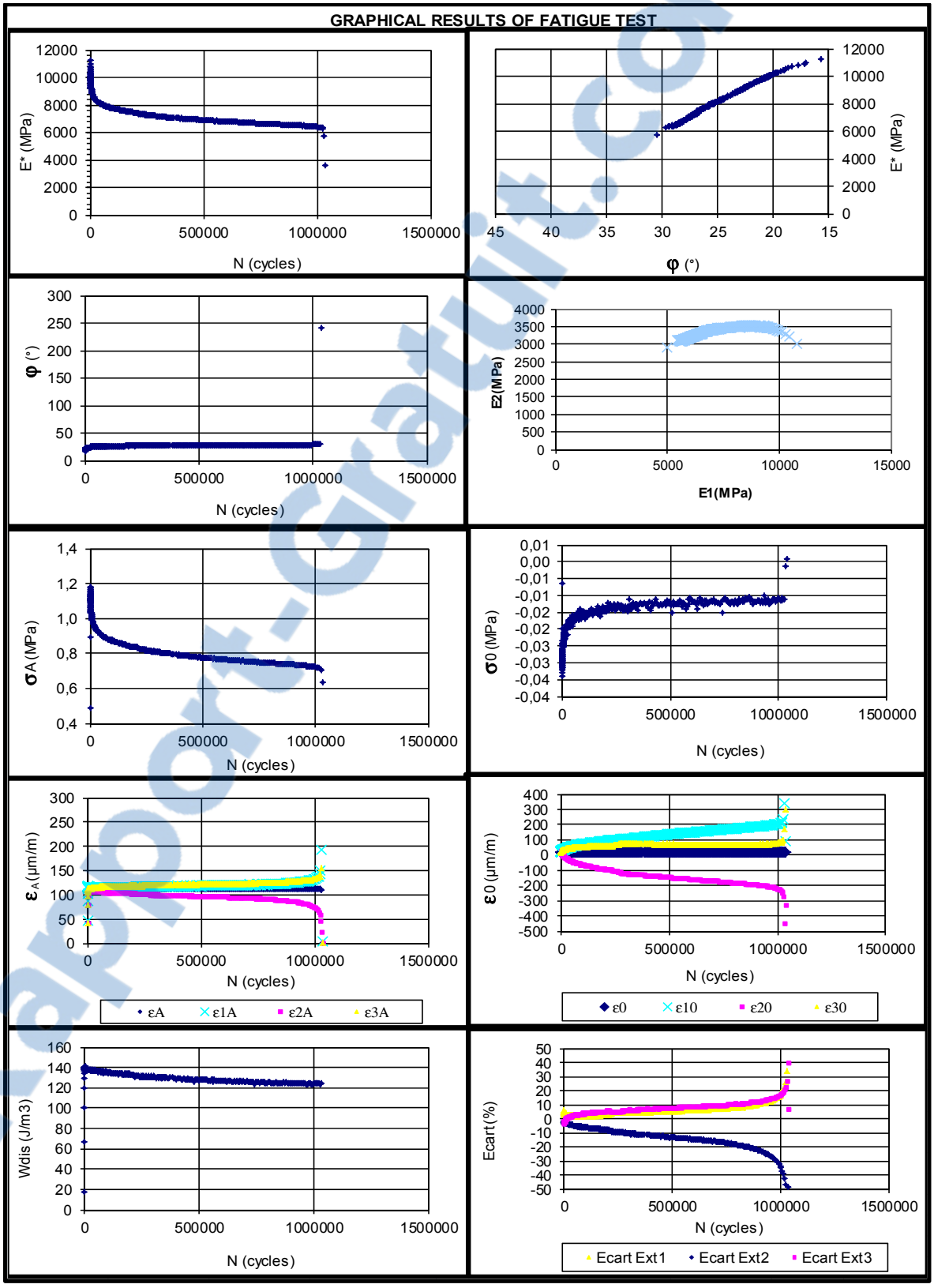

TEST NAME: 15RAP-(P2-A3)-D130

GENERAL INFORMATION FOR FATIGUE TEST

Presse of sollicitation:

Presse of sollicitation:	Presse Bionix
Date / hour:	19/06/2012 - 13h14
Operator:	Asmaa/FB
TARGET DATA	
Type of mix:	GB20
Especimen Nº:	P2-A3
Diameter (mm):	73,9
Hight (mm):	125,0
Vi(%):	6,3
Frequency(Hz):	10
Tº target (ºC):	10
ε target (µdef):	130

ACTUAL DATA

Frequency (Hz):	
Tº test (ºC) :	9,8
ε real (µdef):	129,4

Observations:

Test name: 15RAP-(P2-A3)-D130
Failure before to reach to Nf50%
Failure due to sudden break of the sample

FATIGUE RESULTS

$\|E_O\|$ (MPa):	11148	Nf50% (cycles)	607602
$\|E_{O/2}\|$ (MPa):	5574	Nfll/lll (cycles)	607602

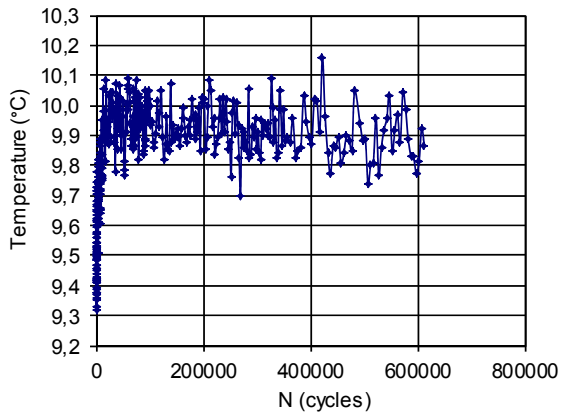

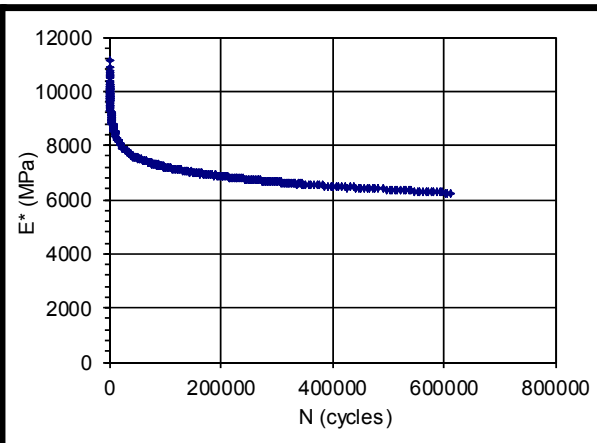

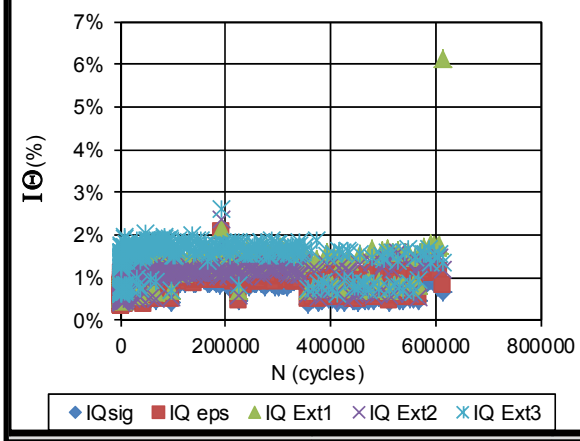

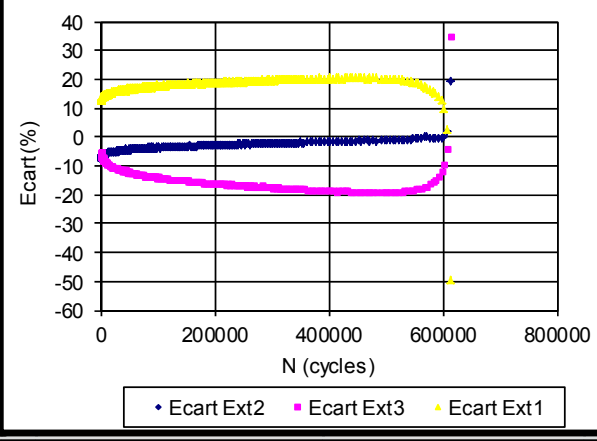

TEST NAME: 15RAP-(P2-A3)-D130

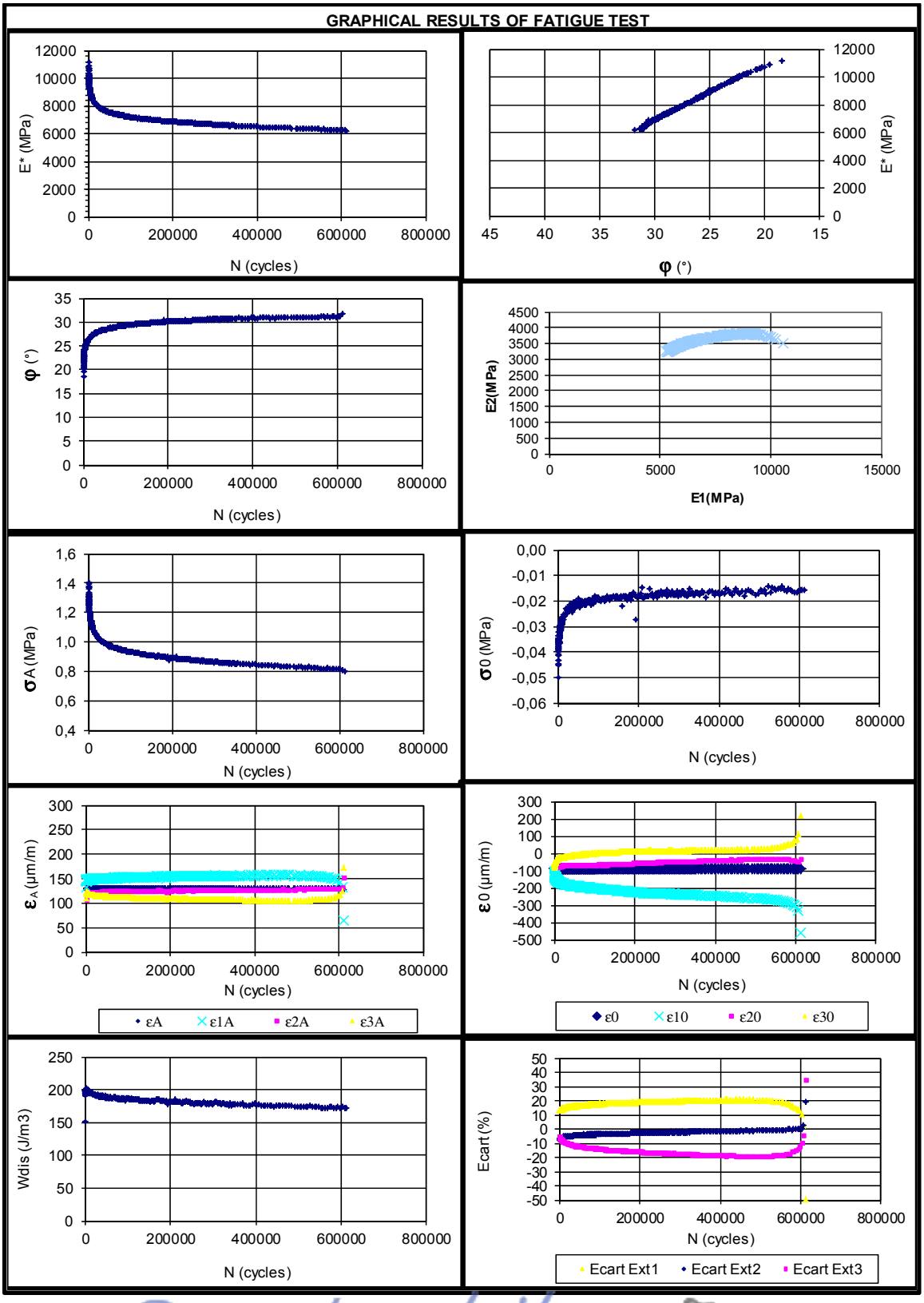

TEST NAME: 15RAP-(P1-A2)-D140

GENERAL INFORMATION FOR FATIGUE TEST

Presse of sollicitation:

Presse of sollicitation:	Presse MTS
Date / hour:	21/6/2012 - 13h00
Operator:	Asmaa/FB

TARGET DATA

Type of mix:	GB20
Especimen Nº:	P1-A2
Diameter (mm):	73,95
Hight (mm):	122,6
Vi(%):	6,7
Frequency(Hz):	10
Tº target (ºC):	10
ε target (μdef):	140

ACTUAL DATA

Frequency (Hz):	
Tº test (ºC) :	10,2
ε real (μdef):	140,1

Observations:

Test name: 15RAP-(P1-A2)-D140
Failure before to reach to Nf50%
Failure due to sudden break of the sample

FATIGUE RESULTS

$\|E_O\|$ (MPa):	11490	$N_{f50\%\ (cycles)}$	76374
$\|E_{O/2}\|$ (MPa):	5745	$N_{fII/III\ (cycles)}$	76375

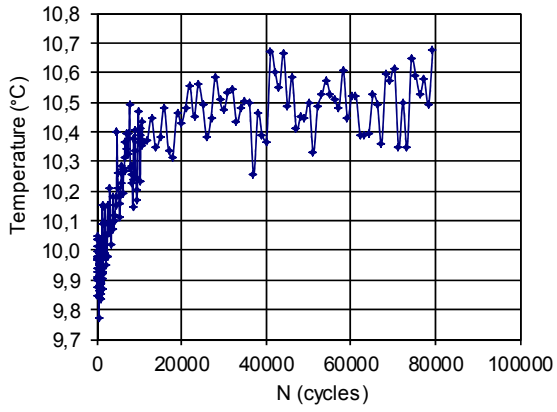

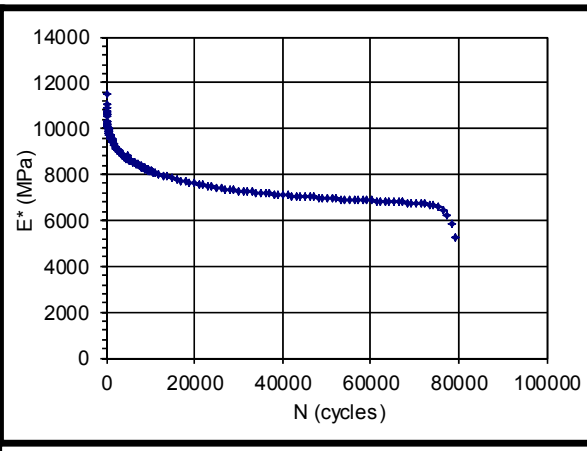

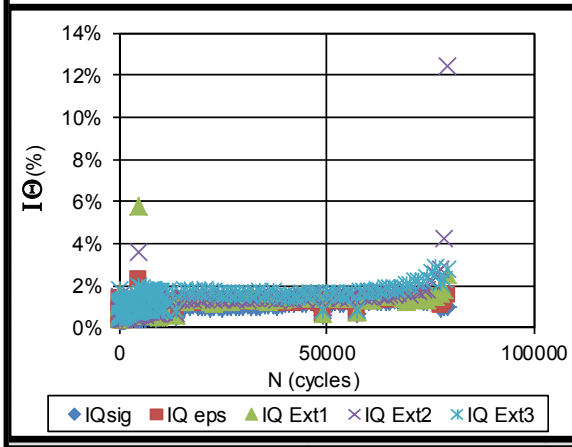

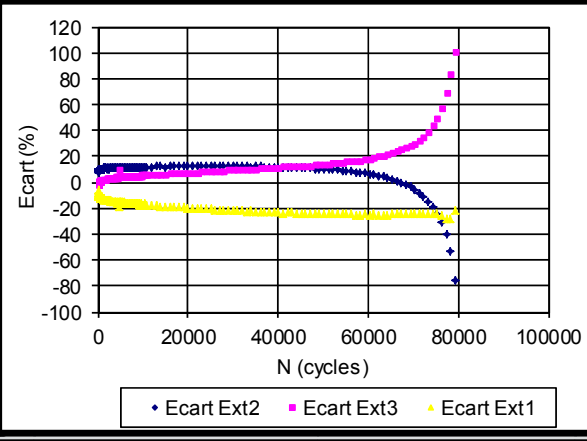

TEST NAME: 15RAP-(P1-A2)-D140

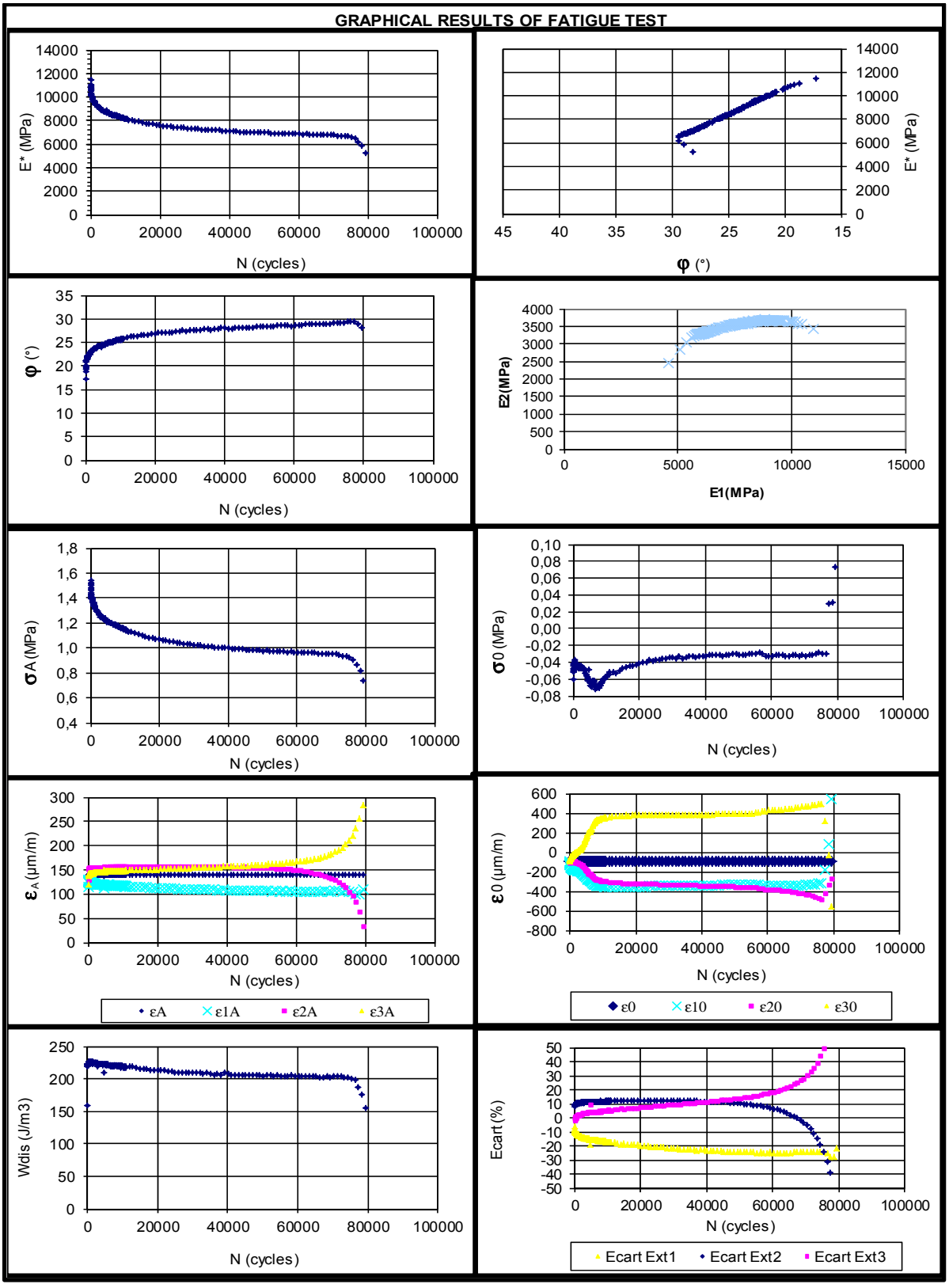

TEST NAME: 25RAP-(P4-A2)-D120

GENERAL INFORMATION FOR FATIGUE TEST

Presse of sollicitation:

Presse of sollicitation:	Presse MTS
Date / hour:	13/6/2012 - 14h15
Operator:	Asmaa/FB
TARGET DATA	
Type of mix:	GB20
Especimen Nº:	P4-A2
Diameter (mm):	74,03
Hight (mm):	122,9
Vi(%):	6,1
Frequency(Hz):	10
Tº target (ºC):	10
ε target (µdef):	120

ACTUAL DATA	
Frequency (Hz):	
Tº test (ºC) :	9,7
ε real (µdef):	119,0

Observations:
Test name: 25RAP-(P4-A2)-D120
Failure before to reach to Nf50%
Failure due to sudden break of the sample

FATIGUE RESULTS

$\|E_O\|$ (MPa):	12379	$N_{f50\%\ (cycles)}$	241937
$\|E_{O/2}\|$ (MPa):	6189	$N_{fII/III\ (cycles)}$	243191

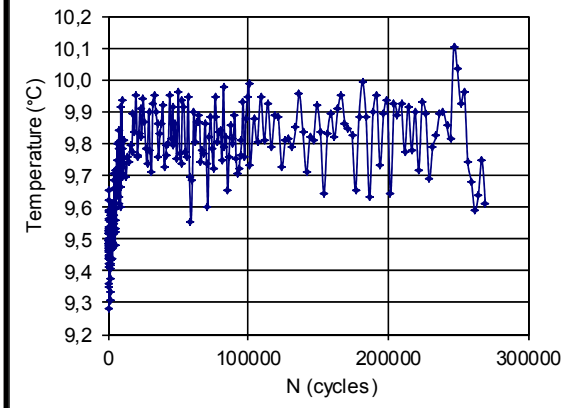

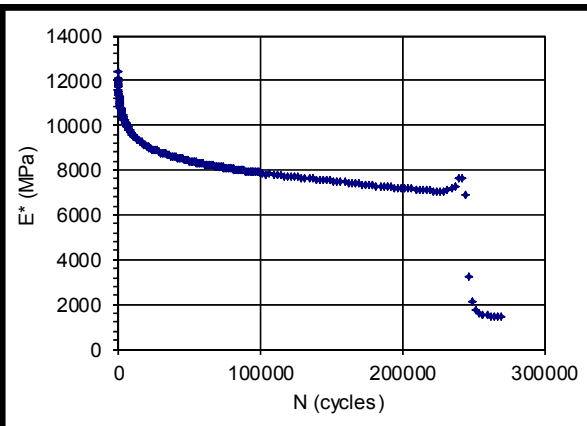

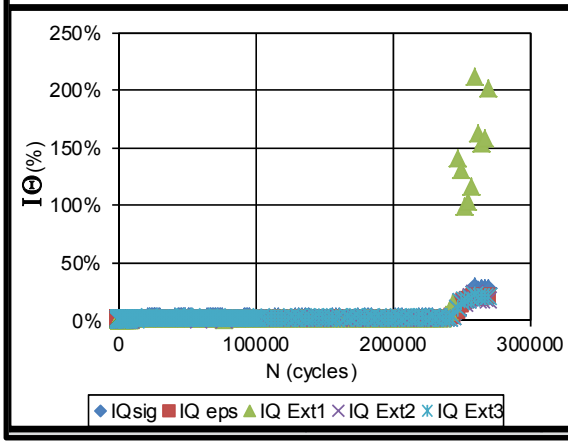

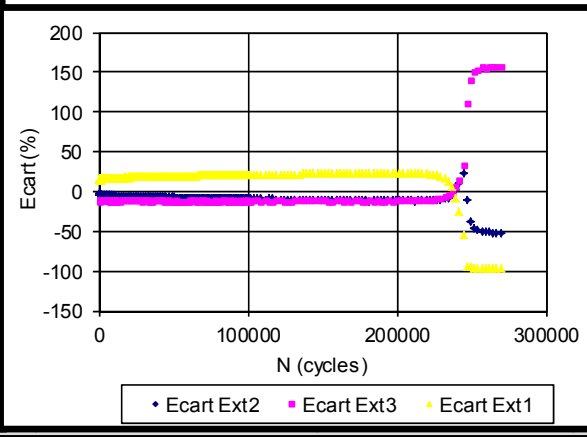

TEST NAME: 25RAP-(P4-A2)-D120

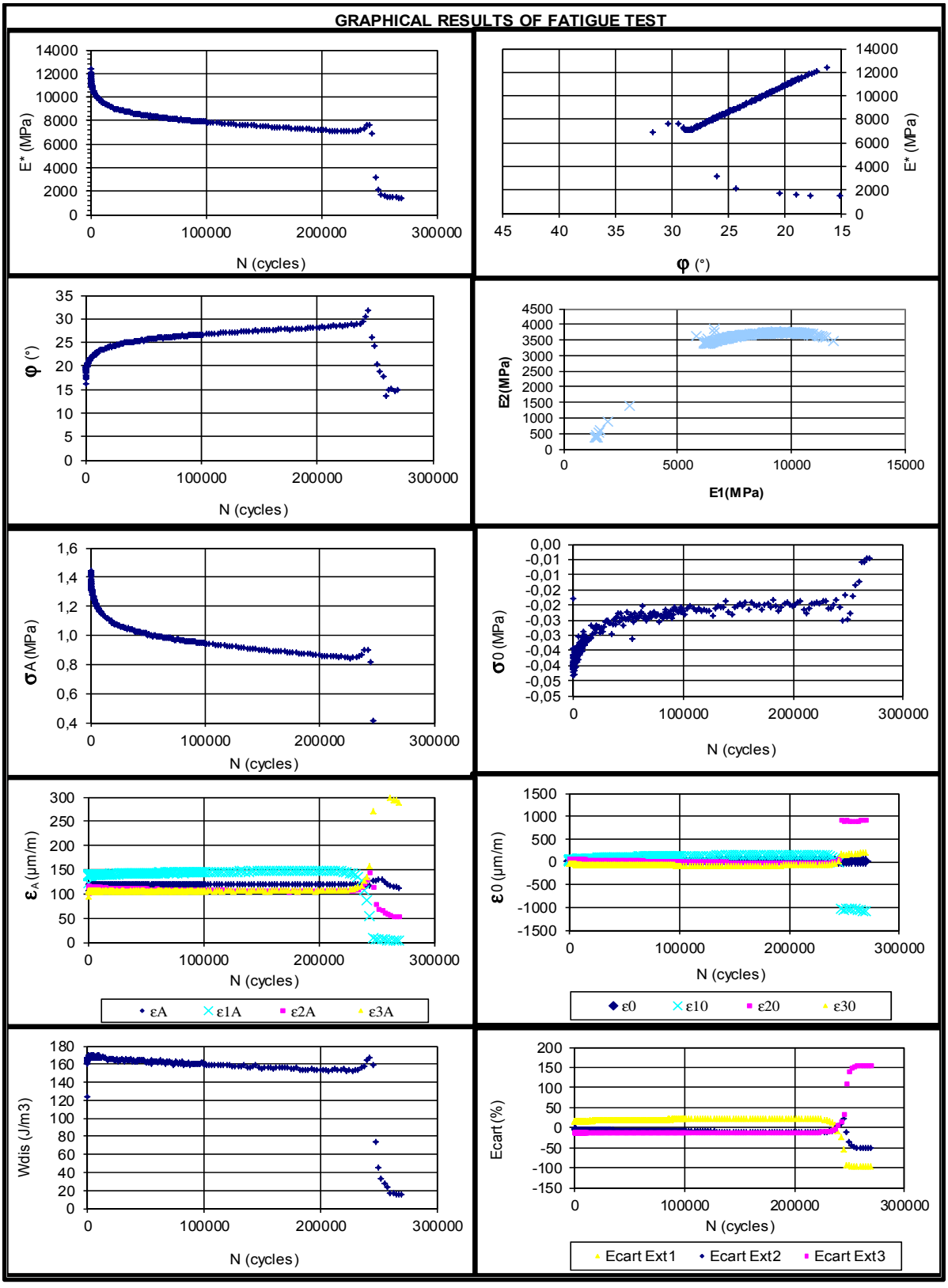

TEST NAME: 25RAP-(P4-A4)-D140

GENERAL INFORMATION FOR FATIGUE TEST

Presse of sollicitation:

Presse of sollicitation:	Presse MTS
Date / hour:	07/10/2011 - 14h30
Operator:	Asmaa/FB

TARGET DATA

Type of mix:	GB20
Especimen Nº:	P4-A4
Diameter (mm):	74,02
Hight (mm):	123,9
Vi(%):	5,6
Frequency(Hz):	10
Tº target (ºC):	10
ε target (μdef):	140

ACTUAL DATA

Frequency (Hz):	
Tº test (ºC) :	10,24
ε real (μdef):	135,4

Observations:

Test name: 25RAP-(P4-A4)-D140
Failure before to reach to Nf50%
Failure due to sudden break of the sample

FATIGUE RESULTS

$\|E_O\|$ (MPa):	10507	$N_{f50\%\ (cycles)}$	203910
$\|E_{O/2}\|$ (MPa):	5253	$N_{fII/III\ (cycles)}$	206416

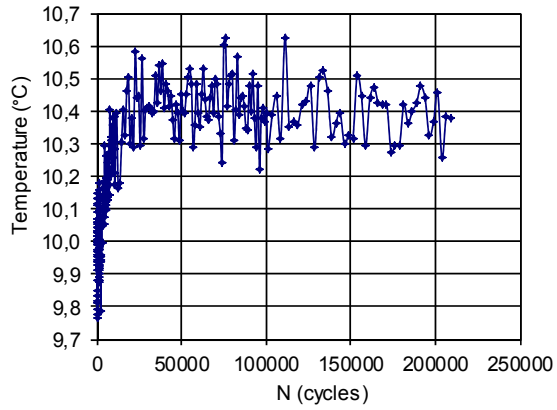

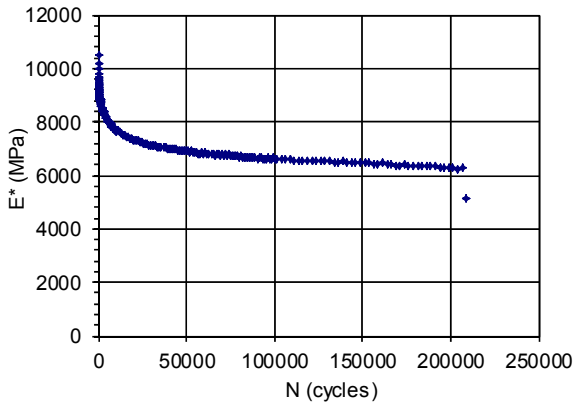

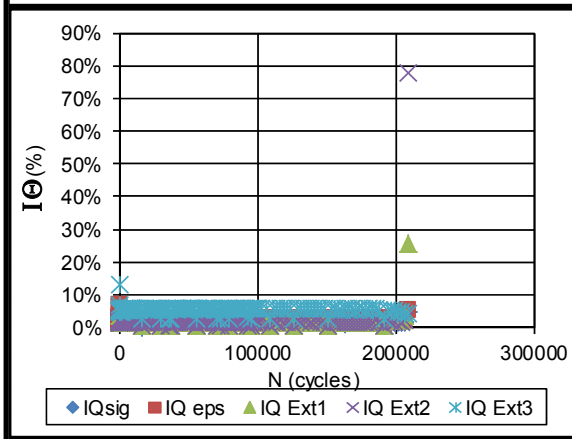

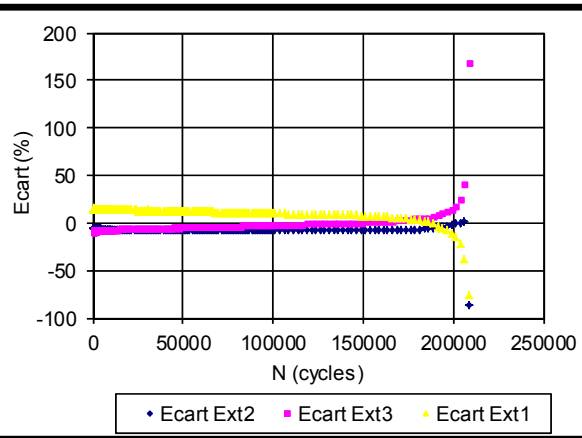

TEST NAME: 25RAP-(P4-A4)-D140

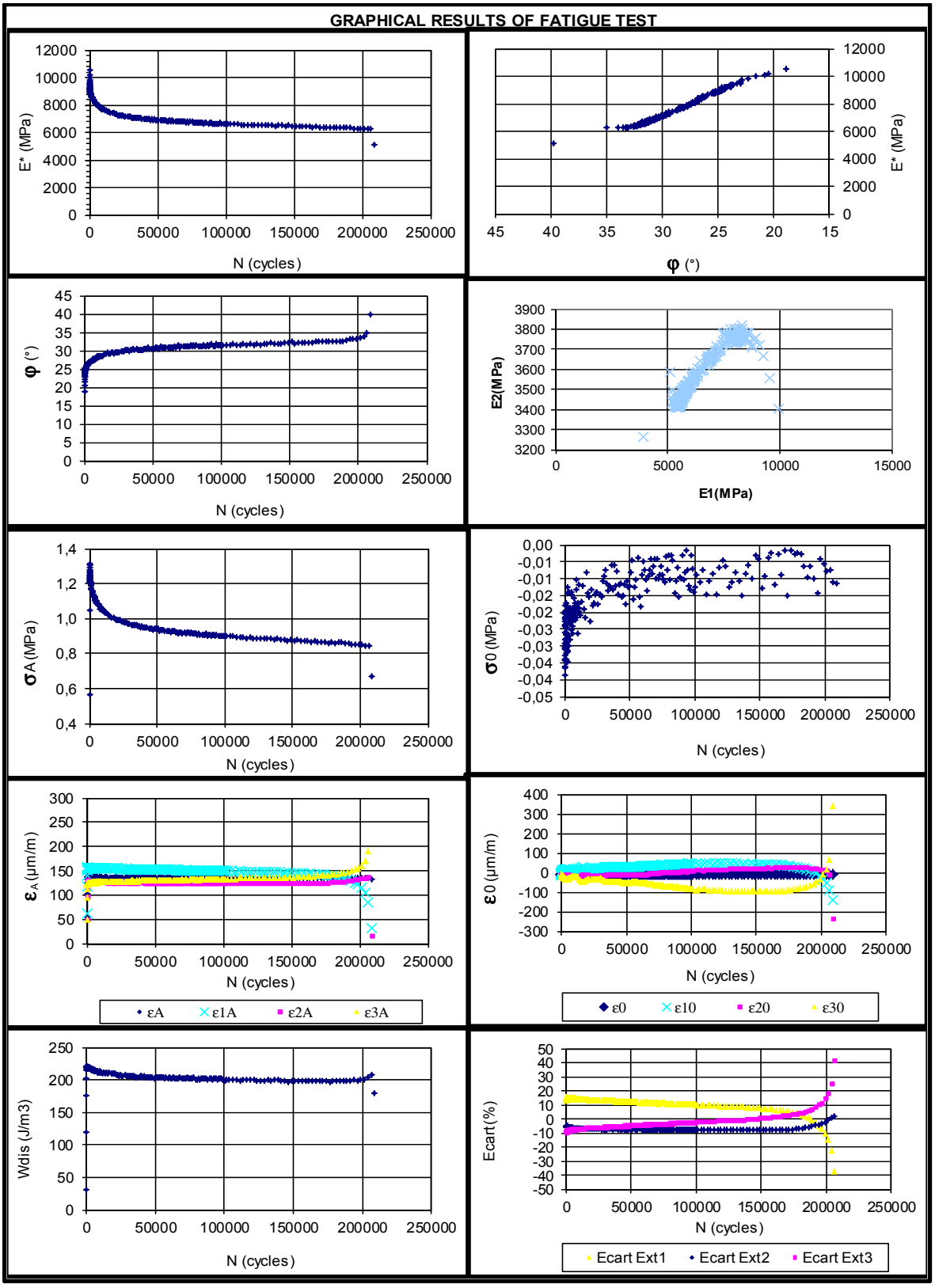

TEST NAME: 25RAP-(P4-A5)-D130

Presse of sollicitation:

Presse of sollicitation:	Presse MTS	Frequency (Hz):	
Date / hour:	10/10/2011 - 10h15	Tº test (ºC) :	
Operator:	Asmaa/FB	ε real (µdef):	10,4 128,5
TARGET DATA		**Observations:**	
Type of mix:	GB20	Test name: 25RAP-(P4-A5)-D130	
Especimen Nº:	P4-A5	Failure before to reach to Nf50%	
Diameter (mm):	73,96	Failure due to sudden break of the sample	
Hight (mm):	123,7		
Vi(%):	5,8		
Frequency(Hz):	10		
Tº target (ºC):	10		
ε target (µdef):	130		

FATIGUE RESULTS

$\|E_O\|$ (MPa):	12472	$N_{f50\%\ (cycles)}$	577019
$\|E_{O/2}\|$ (MPa):	6236	$N_{fII/III\ (cycles)}$	582025

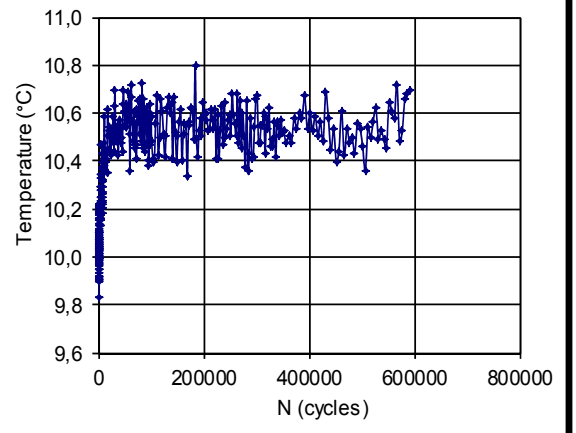

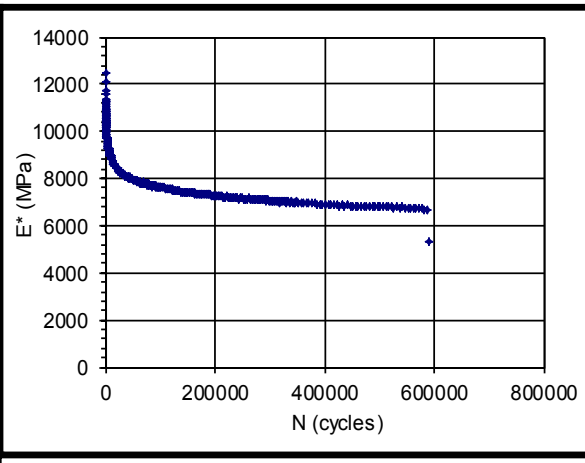

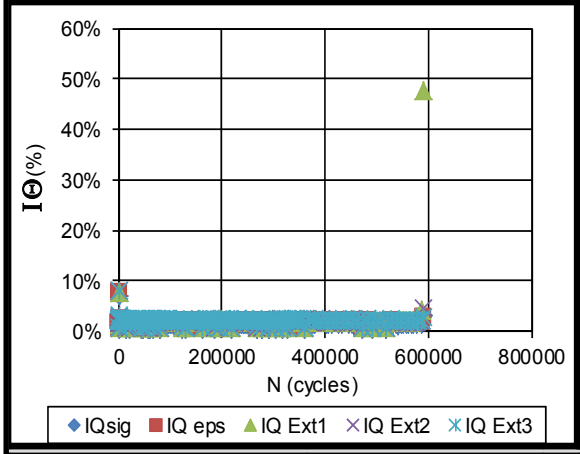

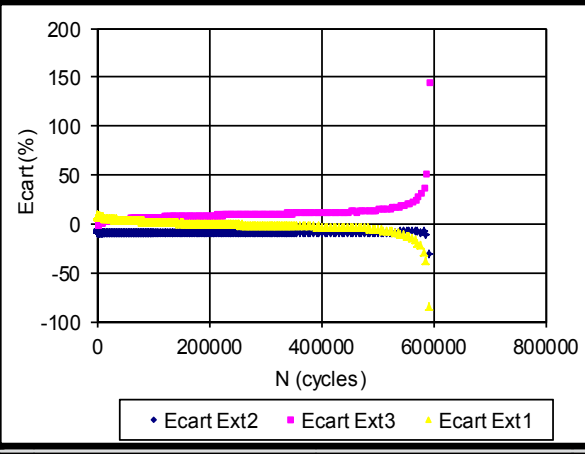

TEST NAME: 25RAP-(P4-A5)-D130

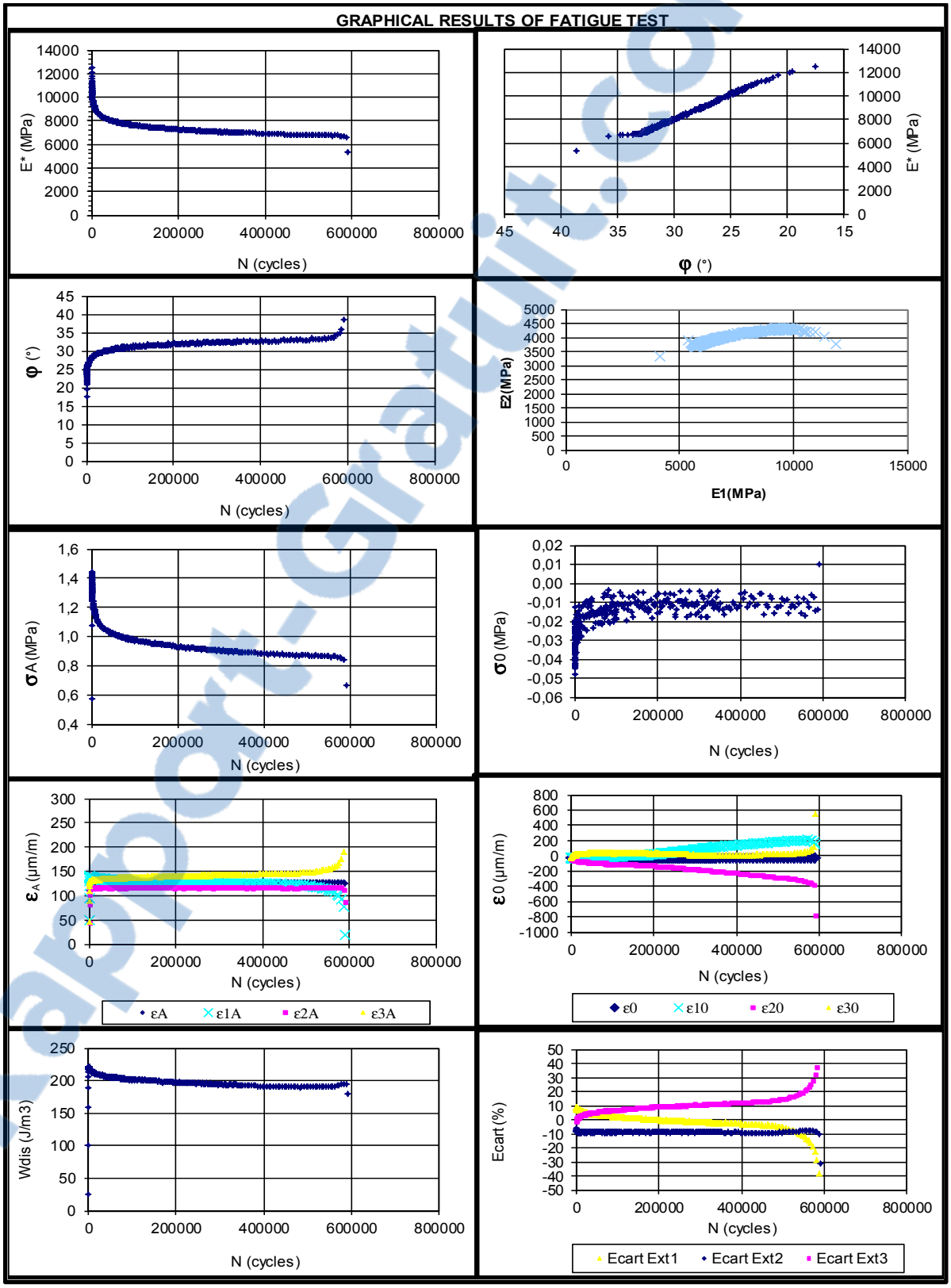

TEST NAME: 25RAP-(P3-A1)-D150

GENERAL INFORMATION FOR FATIGUE TEST

Presse of sollicitation:

Presse of sollicitation:	Presse MTS	**ACTUAL DATA**	
Date / hour:	31/5/2012 - 15h00	Frequency (Hz):	
Operator:	Asmaa/FB	Tº test (ºC) :	10,2
		ε real (µdef):	151,1
TARGET DATA			
Type of mix:	GB20	**Observations:**	
Especimen Nº:	P3-A1	Test name: 25RAP-(P3-A1)-D150	
Diameter (mm):	73,91		
Hight (mm):	124,4		
Vi(%):	6,8		
Frequency(Hz):	10		
Tº target (ºC):	10		
ε target (µdef):	150		

FATIGUE RESULTS

$\|E_O\|$ (MPa):	12351	$N_{f50\%\ (cycles)}$	53227
$\|E_{O/2}\|$ (MPa):	6175	$N_{fII/III\ (cycles)}$	64309

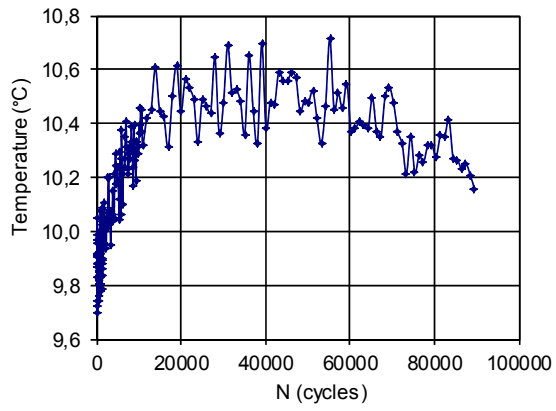

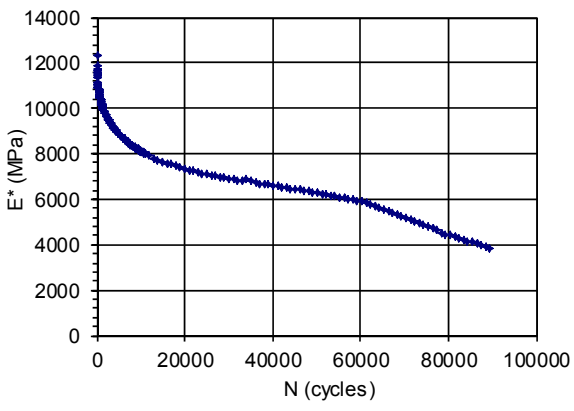

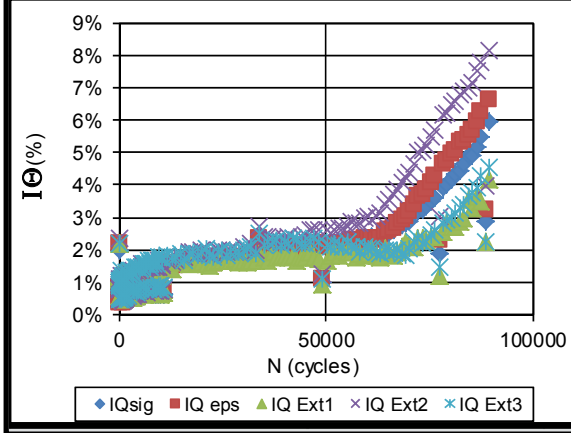

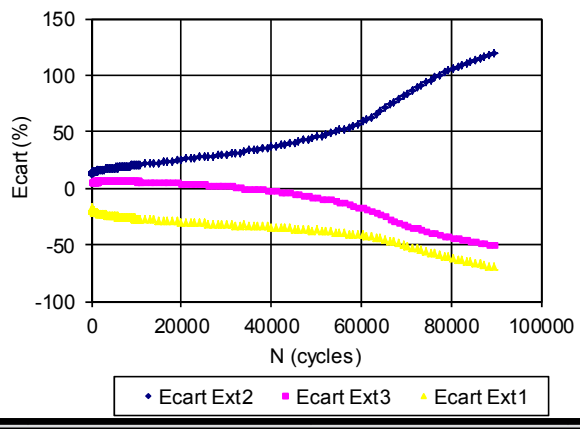

TEST NAME: 25RAP-(P3-A1)-D150

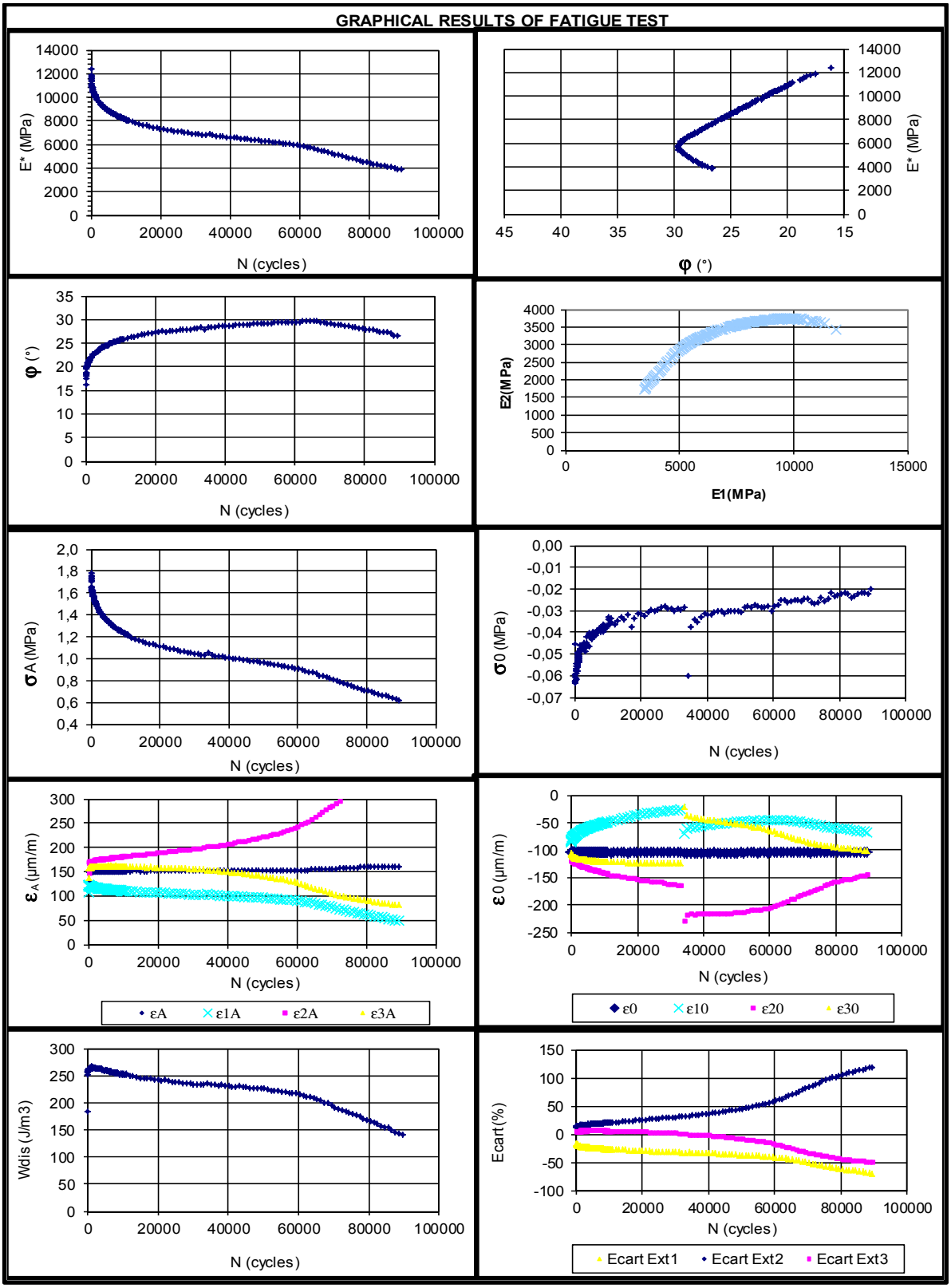

TEST NAME: 25RAP-(P1-A2)-D110

GENERAL INFORMATION FOR FATIGUE TEST

Presse of sollicitation:

Presse of sollicitation:	Presse MTS	**ACTUAL DATA**	
Date / hour:	8/6/2012 - 13h14	Frequency (Hz):	
Operator:	Asmaa/FB	Tº testi (ºC) :	10,12
		ε real (µdef):	108,8
TARGET DATA			
Type of mix:	GB20	**Observations:**	
Especimen Nº:	P1-A2	Test name: 25RAP-(P1-A2)-D110	
Diameter (mm):	74,03		
Hight (mm):	124,0		
Vi(%):	6,2		
Frequency(Hz):	10		
Tº target (ºC):	10		
ε target (µdef):	110		

FATIGUE RESULTS

$\|E_O\|$ (MPa):	9053	$N_{f50\%}$ (cycles)	943017
$\|E_{O/2}\|$ (MPa):	4527	$N_{fII/III}$ (cycles)	892950

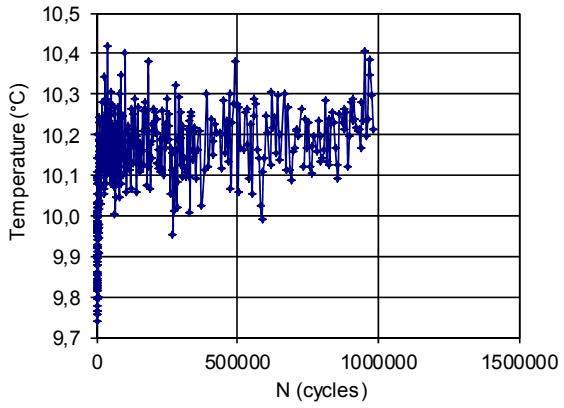

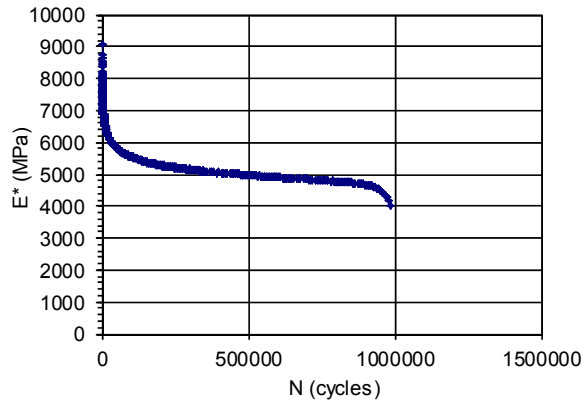

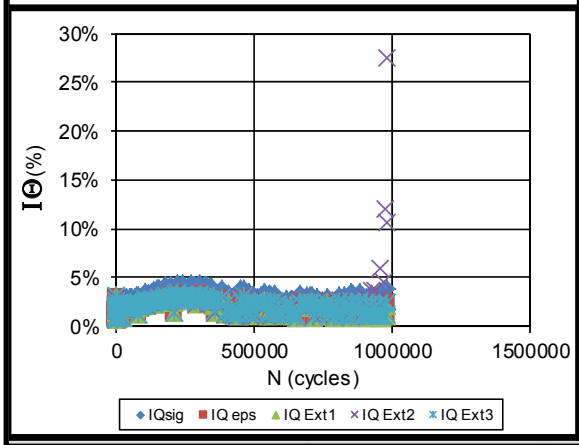

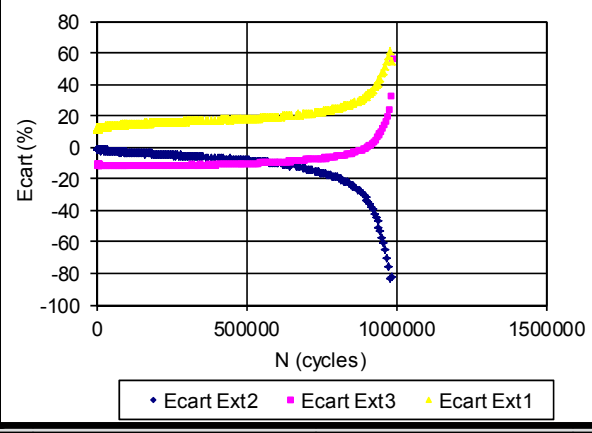

TEST NAME: 25RAP-(P1-A2)-D110

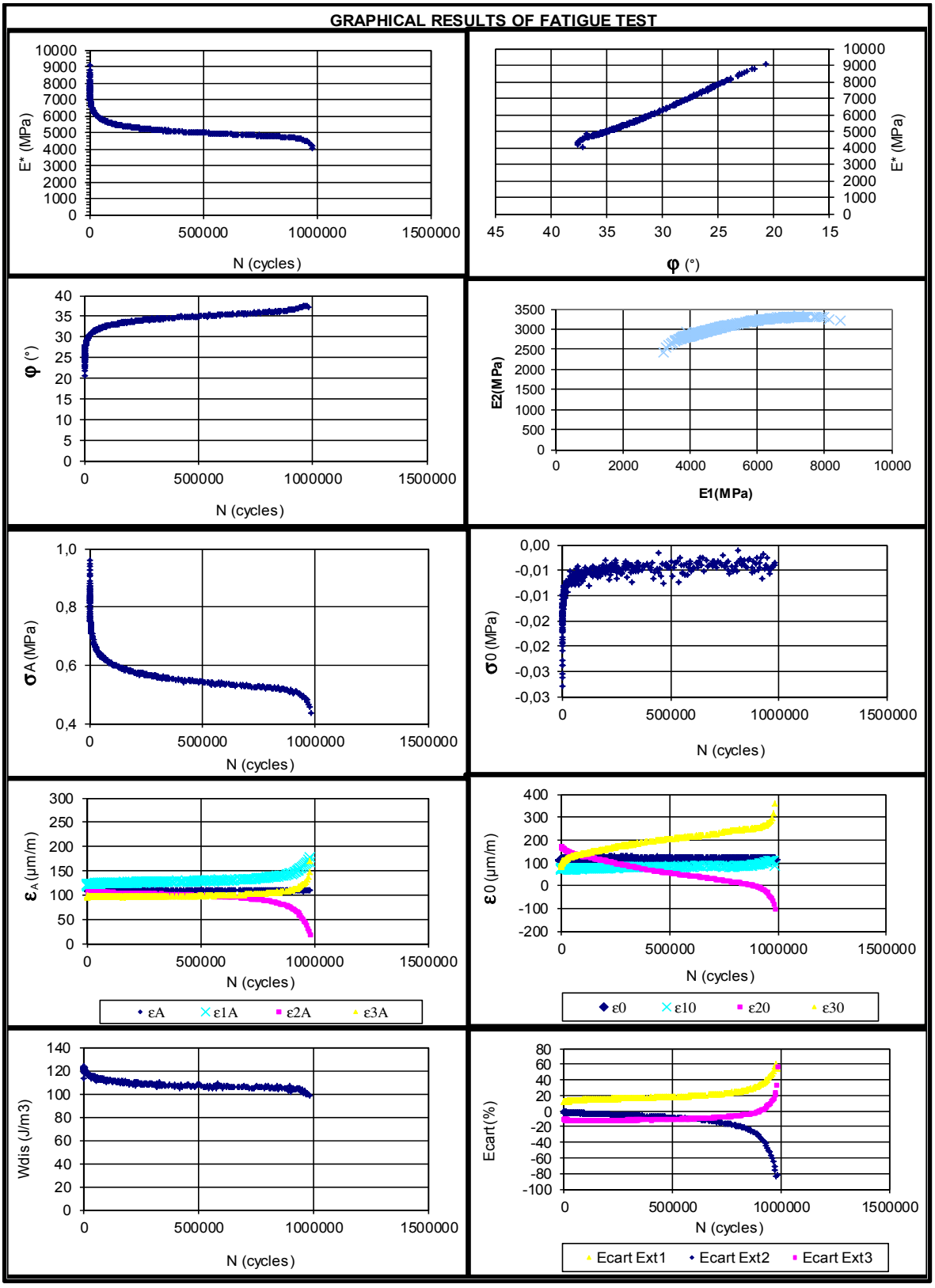

TEST NAME: 40RAP-(P1-A2)-D130

GENERAL INFORMATION FOR FATIGUE TEST

Presse of sollicitation:

Presse of sollicitation:	Presse Bionix
Date / hour:	2/06/2011 - 13h14
Operator:	AB
TARGET DATA	
Type of mix:	GB20
Especimen Nº:	P1-A5
Diameter (mm):	73,92
Hight (mm):	122,1
Vi(%):	3,3
Frequency(Hz):	10
Tº target (ºC):	10
ε target (µdef):	130

ACTUAL DATA

Frequency (Hz):	
Tº test (ºC) :	10,56
ε real (µdef):	130,5

Observations:

Test name: 40RAP-(P1-A2)-D130

Broken at the end of the test (the test was run for three days)

FATIGUE RESULTATS

$\|E_O\|$ (MPa):	12294	$N_{f50\%\ (cycles)}$	1812821
$\|E_{O/2}\|$ (MPa):	6147	$N_{fII/III\ (cycles)}$	2385837

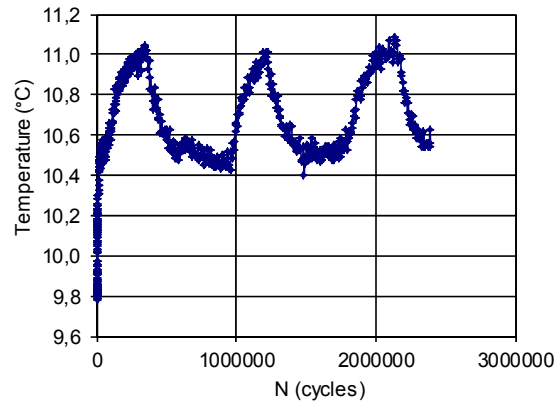

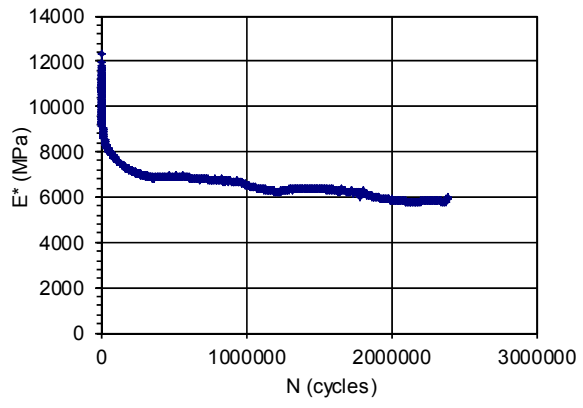

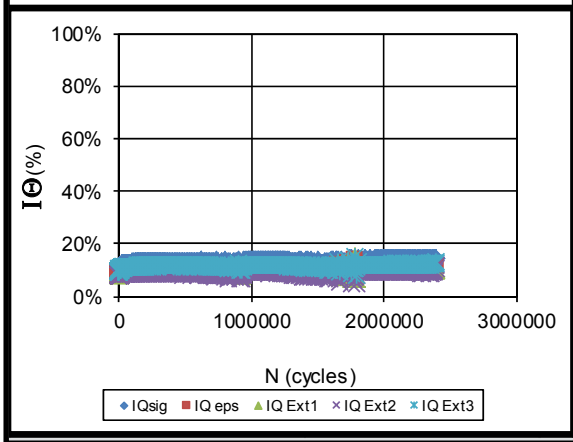

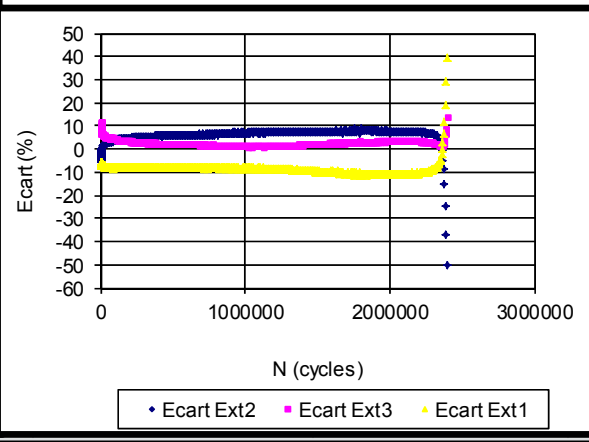

TEST NAME: 40RAP-(P1-A2)-D130

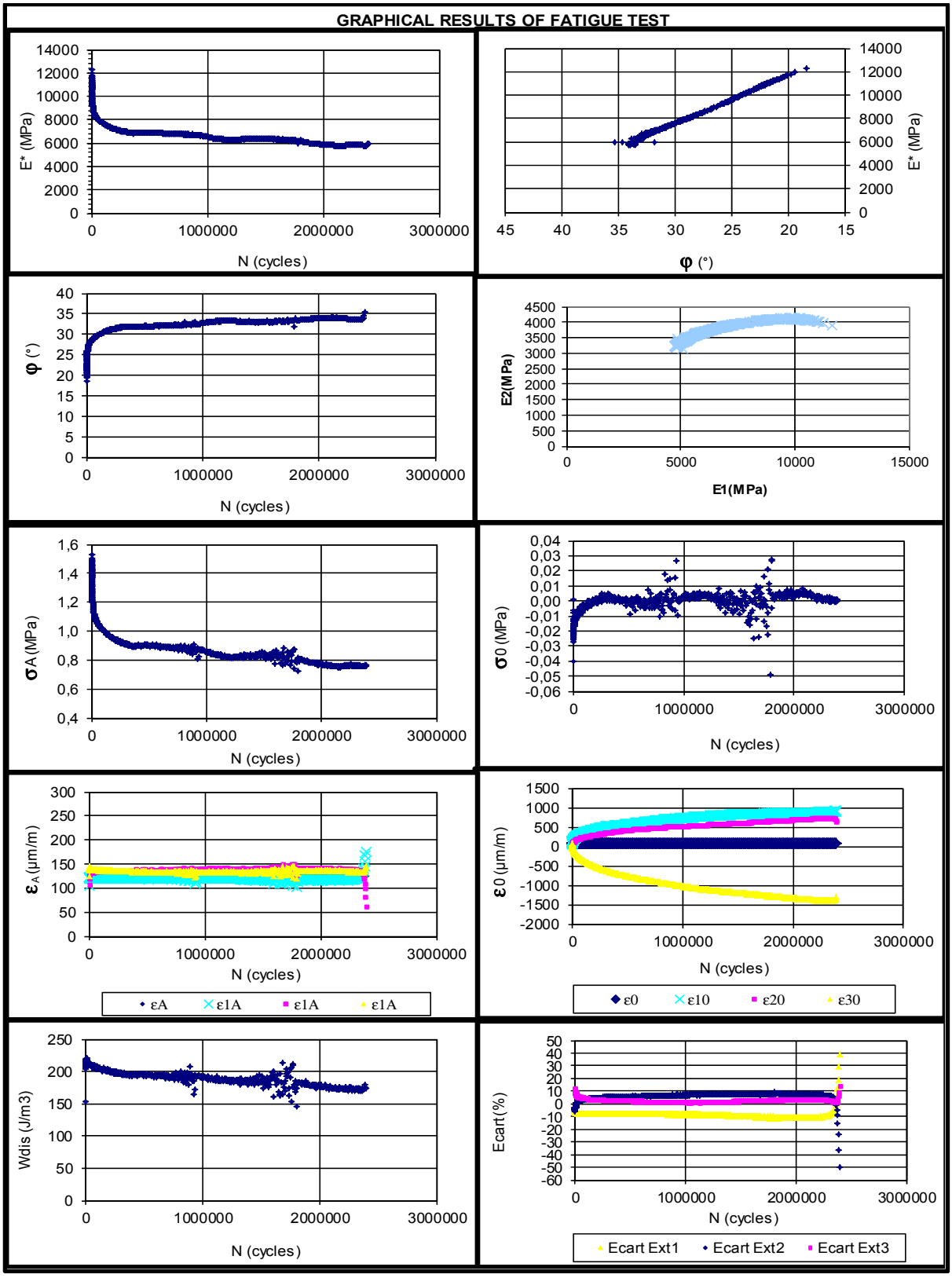

TEST NAME: 40RAP-(P2-A3)-D140

GENERAL INFORMATION FOR FATIGUE TEST

Presse of sollicitation:

Presse of sollicitation:	Presse Bionix	ACTUAL DATA	
Date / hour:	1/12/2011 - 13h14	Frequency (Hz):	
Operator:	AB	Tº test (ºC) :	10,3
		ε real (µdef):	142,2
TARGET DATA			
Type of mix:	GB20	Observations:	
Especimen Nº:	P2-A3	Test name: 40RAP-(P2-A3)-D140	
Diameter (mm):	73,97	Sample was broken at the end of the test	
Hight (mm):	124,1		
Vi(%):	3,8		
Frequency(Hz):	10		
Tº target (ºC):	10		
ε target (µdef):	140		

FATIGUE RESULTATS

$\|E_O\|$ (MPa):	12941	$N_{f50\%\ (cycles)}$	1028208
$\|E_{O/2}\|$ (MPa):	6471	$N_{fII/III\ (cycles)}$	2835891

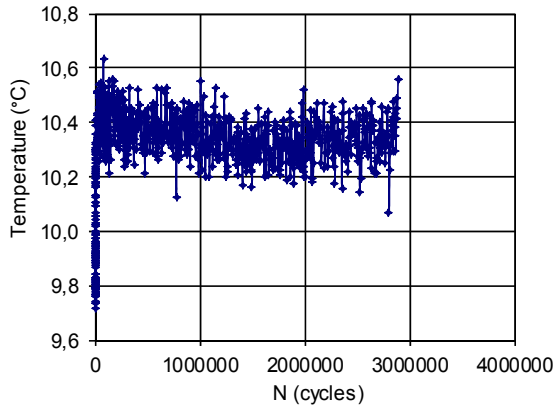

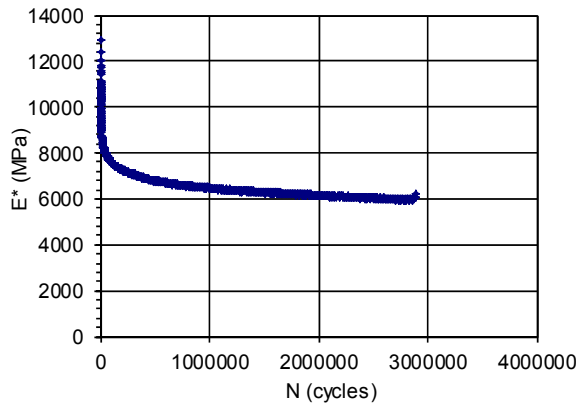

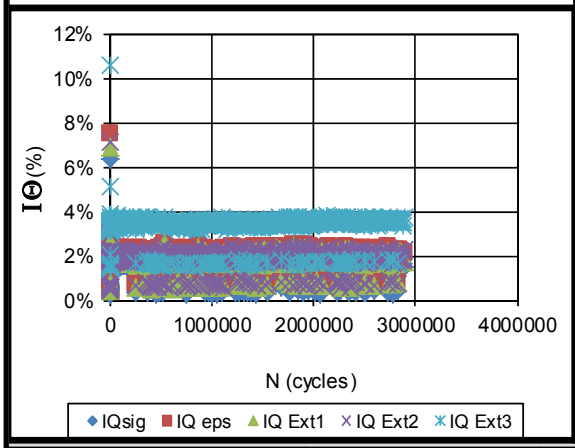

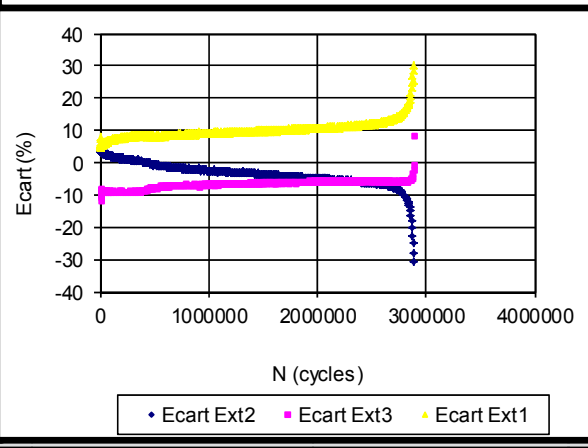

TEST NAME: 40RAP-(P2-A3)-D140

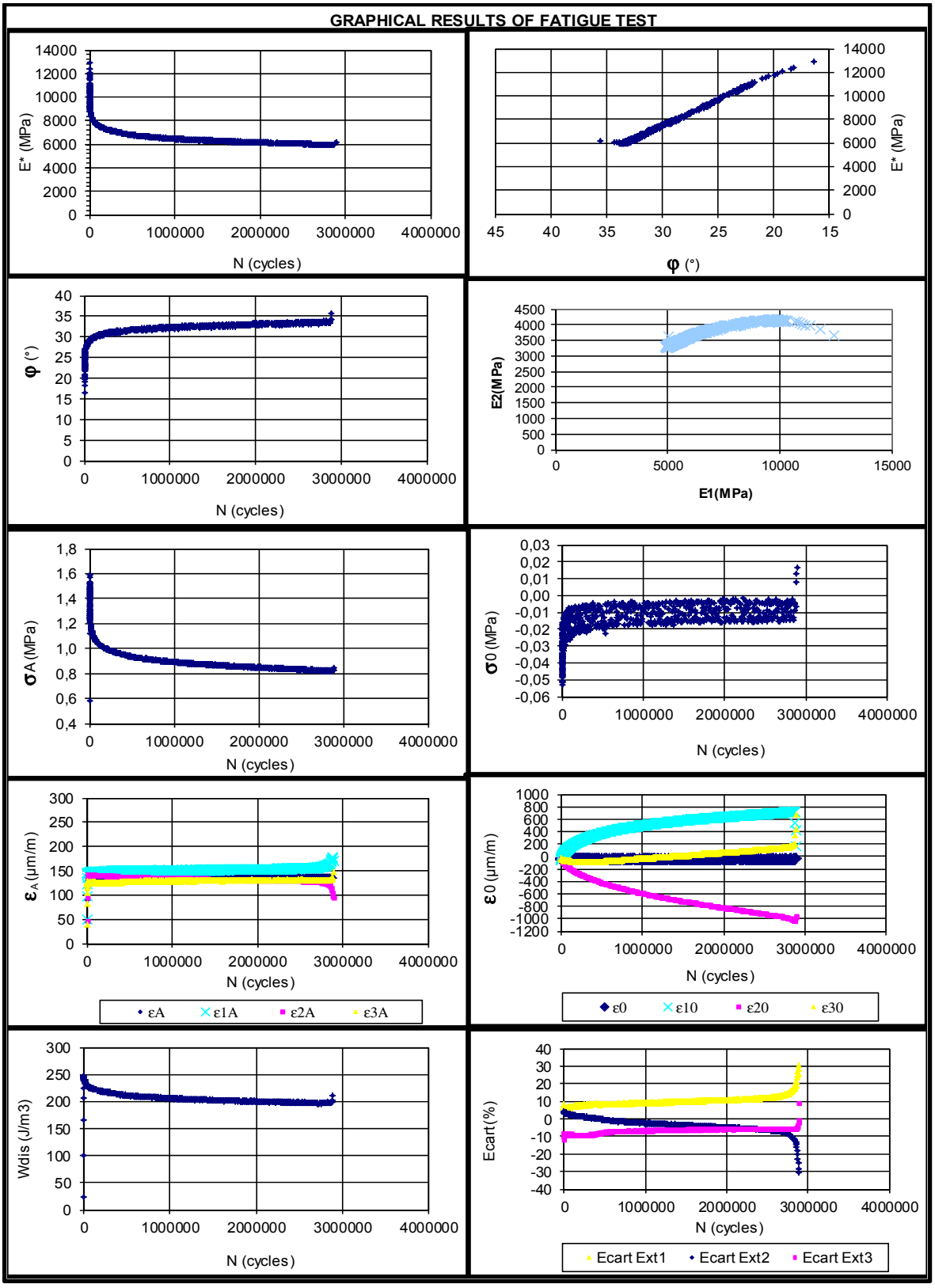

TEST NAME: 40RAP-(P2-A2)-D150

GENERAL INFORMATION FOR FATIGUE TEST

Presse of sollicitation:

Presse of sollicitation:	Presse MTS	ACTUAL DATA	
Date / hour:	1/12/2011 - 13h14	Frequency (Hz):	
Operator:	AB	Tº test(ºC) :	10,46
		ε real (µdef):	147,0
TARGET DATA			
Type of mix:	GB20	Observations:	
Especimen Nº:	P2-A2	Test name: 40RAP-(P2-A2)-D150	
Diameter (mm):	73,93		
Hight (mm):	123,9		
Vi(%):	2,1		
Frequency(Hz):	10		
Tº target (ºC):	10		
ε target (µdef):	150		

FATIGUE RESULTATS

$\|E_O\|$ (MPa):	13100	$N_{f50\%\ (cycles)}$	542579
$\|E_{O/2}\|$ (MPa):	6550	$N_{fII/III\ (cycles)}$	985665

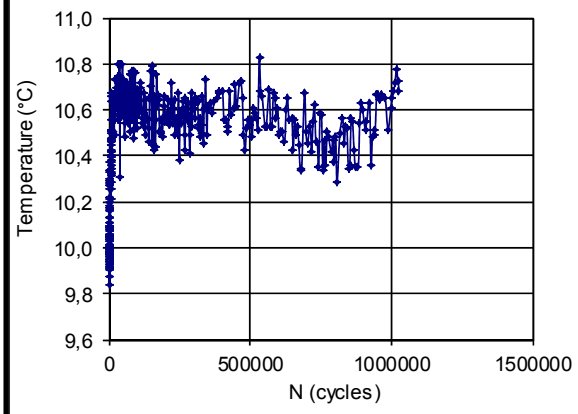

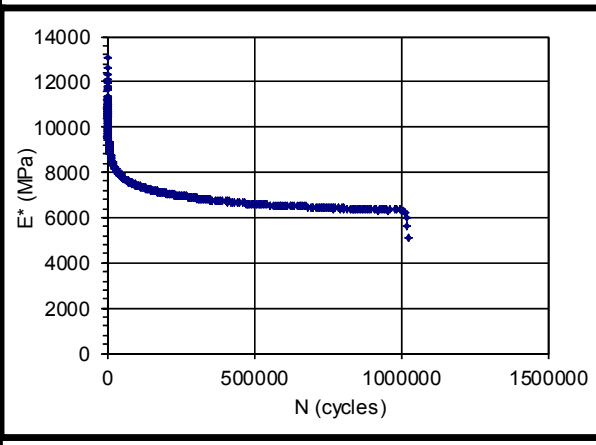

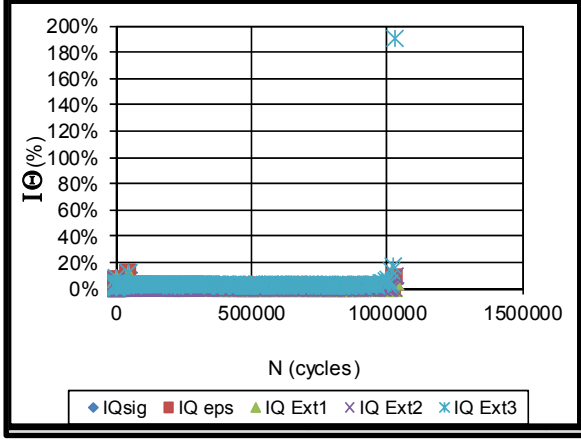

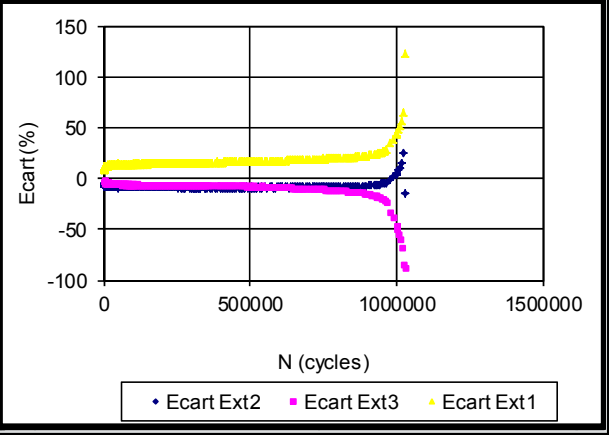

TEST NAME: 40RAP-(P2-A2)-D150

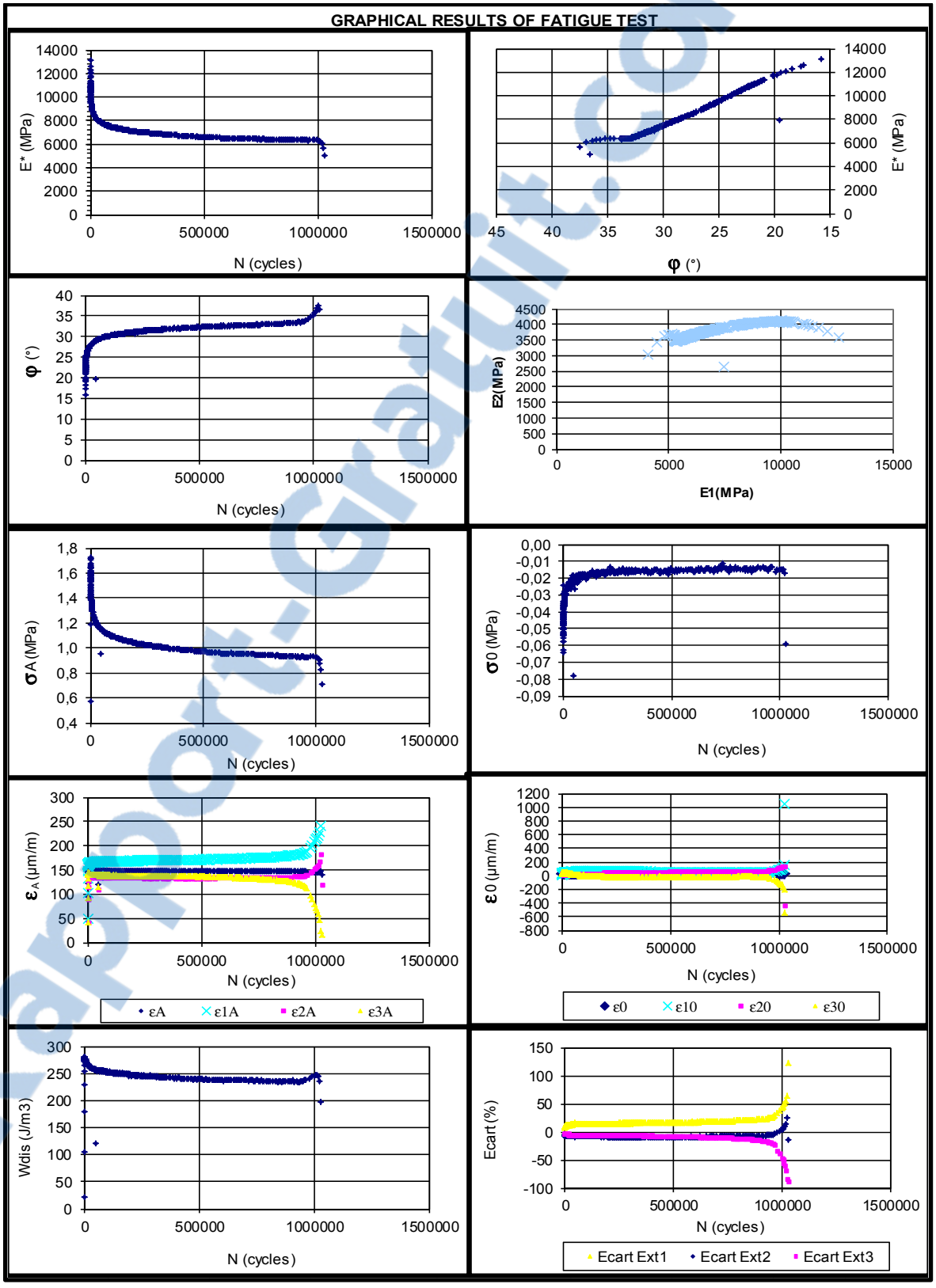

TEST NAME: 40RAP-(P1-A3)-D160

GENERAL INFORMATION FOR FATIGUE TEST

Presse of sollicitation:

Presse of sollicitation:	Presse Bionix	ACTUAL DATA	
Date / hour:	15/12/2011 - 13h14	Frequency (Hz):	
Operator:	AB	Tº test (ºC) :	10,46
		ε real (µdef):	158,3
TARGET DATA			
Type of mix:	GB20	Observations:	
Especimen Nº:	P1-A3	Test name: 40RAP-(P1-A3)-D160	
Diameter (mm):	74,01		
Hight (mm):	124,7		
Vi(%):	3,6		
Frequency(Hz):	10		
Tº target (ºC):	10		
ε target (µdef):	160		

FATIGUE RESULTATS

$\|E_O\|$ (MPa):	12030	$N_{f50\%}$ (cycles)	214108
$\|E_{O/2}\|$ (MPa):	6015	$N_{fII/III}$ (cycles)	335599

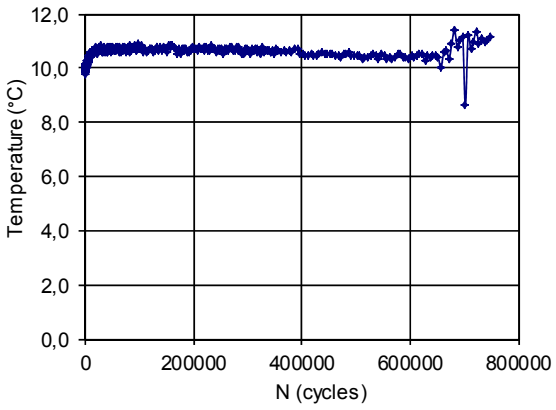

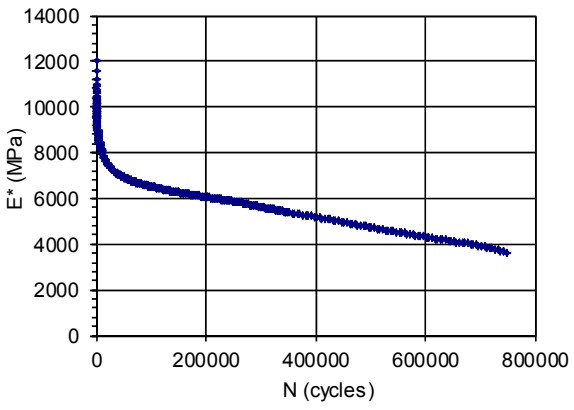

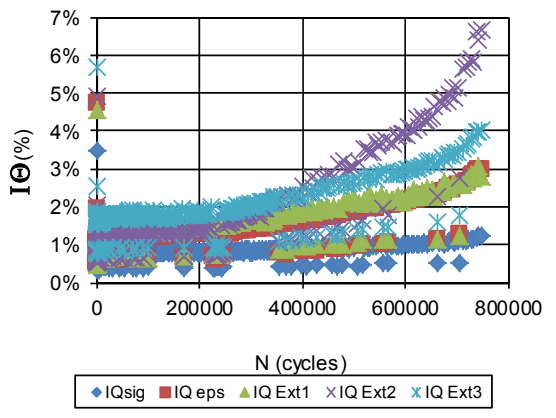

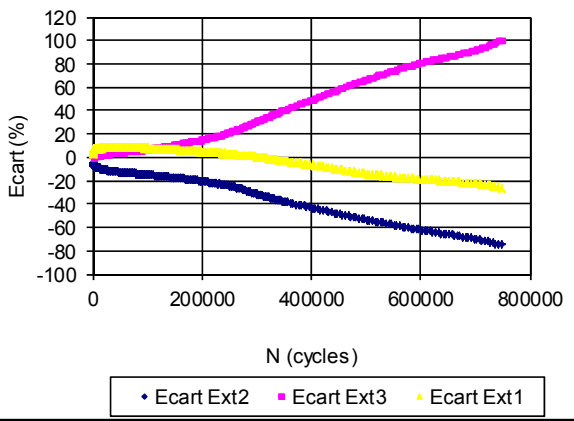

TEST NAME: 40RAP-(P1-A3)-D160

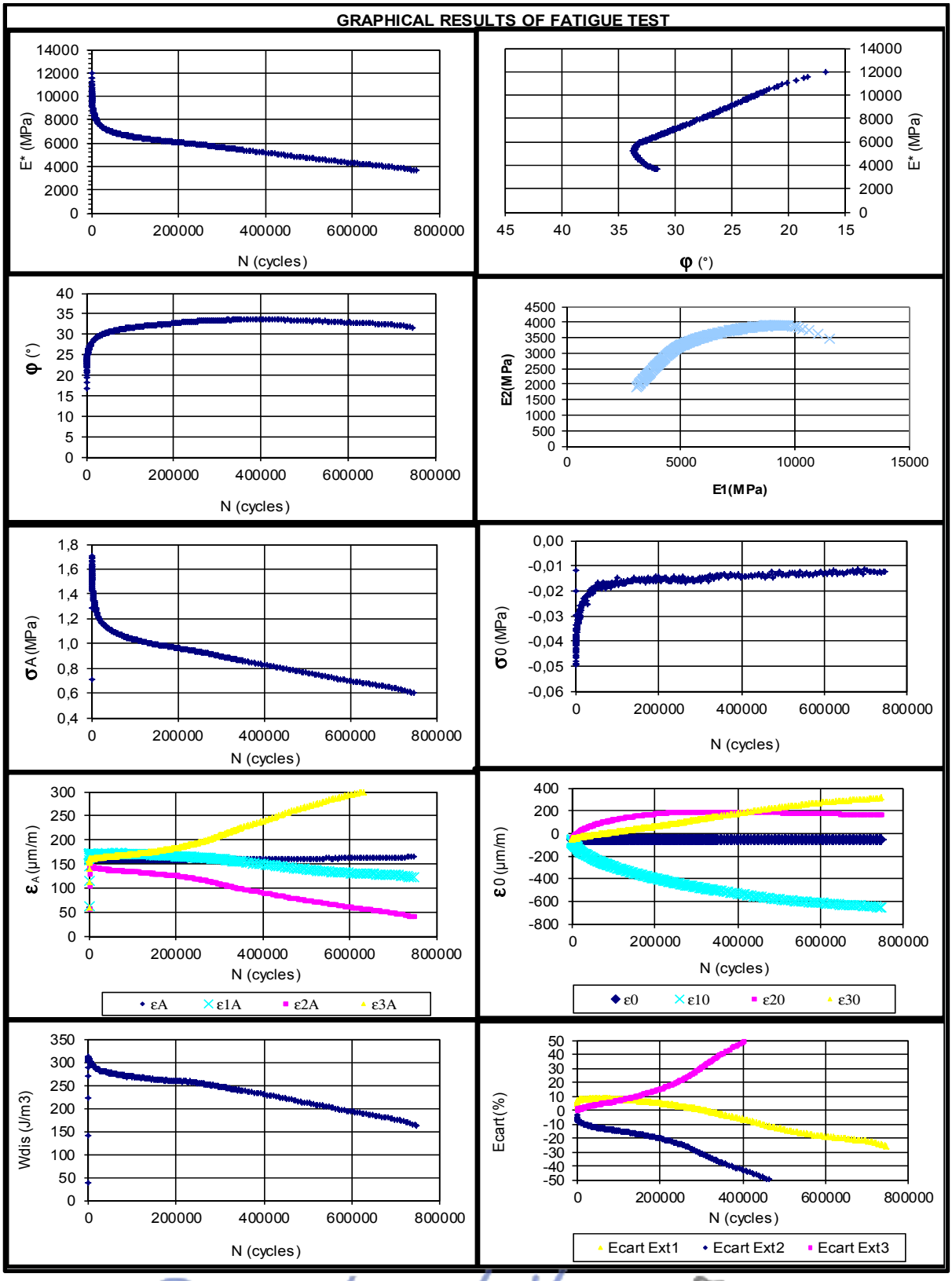

TEST NAME: 40RAP-(P1-A4)-D170

GENERAL INFORMATION FOR FATIGUE TEST

Presse of sollicitation:

Presse of sollicitation:	Presse Bionix	ACTUAL DATA	
Date / hour:	15/12/2011 - 13h14	Frequency (Hz):	
Operator:	AB	Tº test (ºC) :	10,4
		ε real (µdef):	168,0
TARGET DATA			
Type of mix:	GB20	Observations:	
Especimen Nº:	P1-A4	Test name: 40RAP-(P1-A4)-D170	
Diameter (mm):	73,97		
Hight (mm):	121,6		
Vi(%):	2,7		
Frequency(Hz):	10		
Tº target (ºC):	10		
ε target (µdef):	170		

FATIGUE RESULTATS

$\|E_O\|$ (MPa):	11698	$N_{f50\%\ (cycles)}$	296783
$\|E_{O/2}\|$ (MPa):	5849	$N_{fII/III\ (cycles)}$	797459

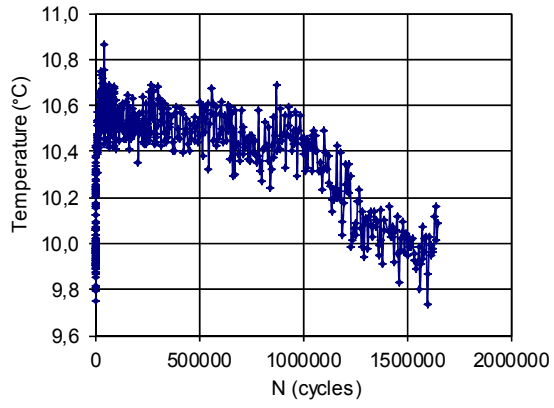

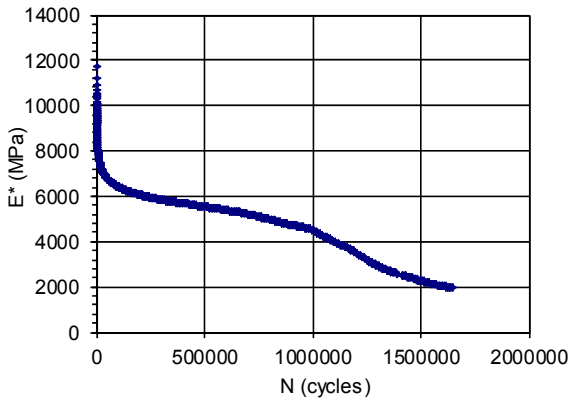

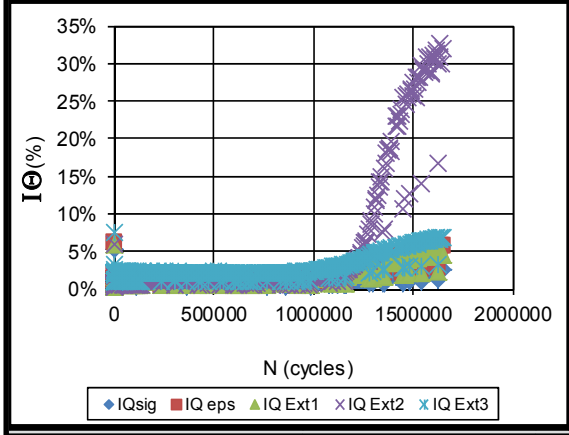

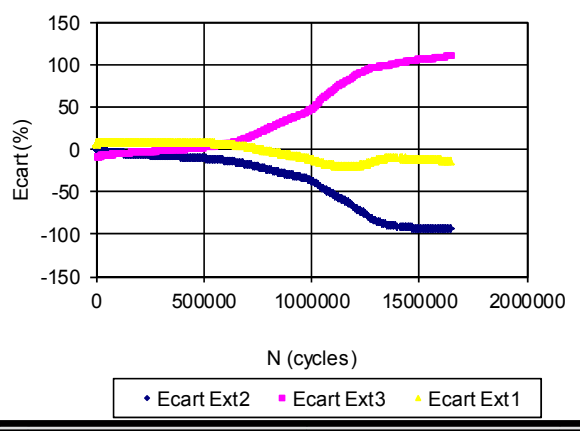

TEST NAME: 40RAP-(P1-A4)-D170

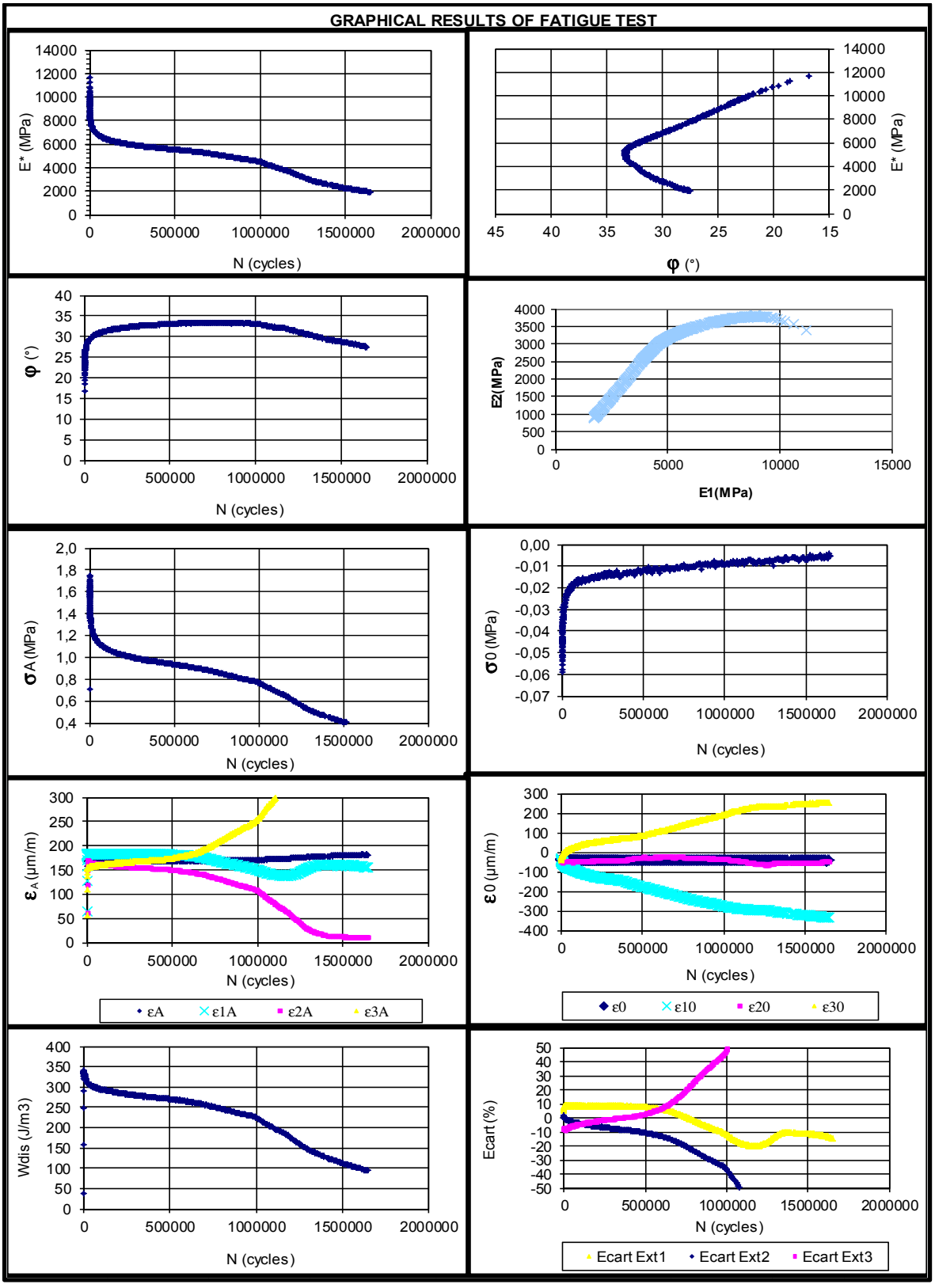

TEST NAME: 40RAP-(P1-A2)-D180

GENERAL INFORMATION FOR FATIGUE TEST

Presse of sollicitation:

Presse of sollicitation:	Presse Bionix	ACTUAL DATA	
Date / hour:	22/12/2011 - 13h14	Frequency (Hz):	
Operator:	AB	Tº test (ºC) :	10,54
		ε real (µdef):	178
TARGET DATA			
Type of mix:	GB20	Observations:	
Especimen Nº:	P1-A2	Test name: 40RAP-(P1-A2)-D180	
Diameter (mm):	73,95		
Hight (mm):	125,8		
Vi(%):	2,5		
Frequency(Hz):	10		
Tº target (ºC):	10		
ε target (µdef):	180		

FATIGUE RESULTATS

$\|E_O\|$ (MPa):	12914	$N_{f50\%\ (cycles)}$	55043
$\|E_{O/2}\|$ (MPa):	6457	$N_{fII/III\ (cycles)}$	414507

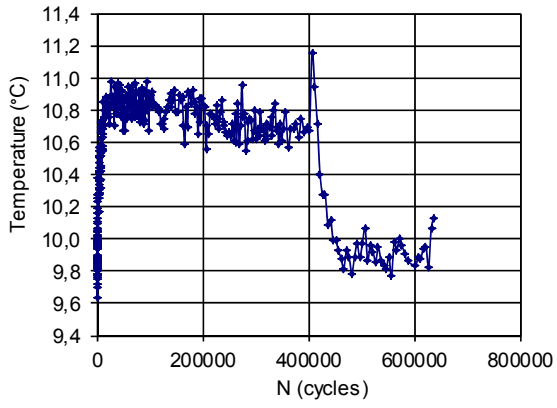

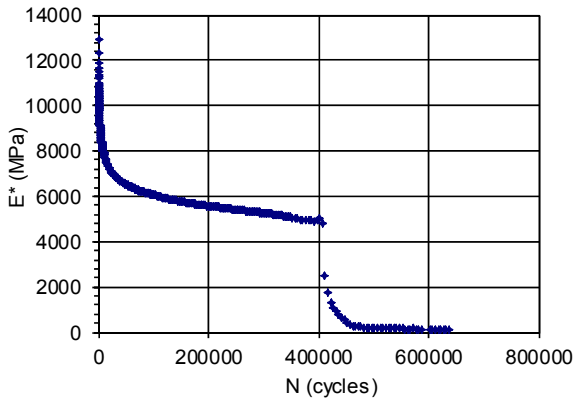

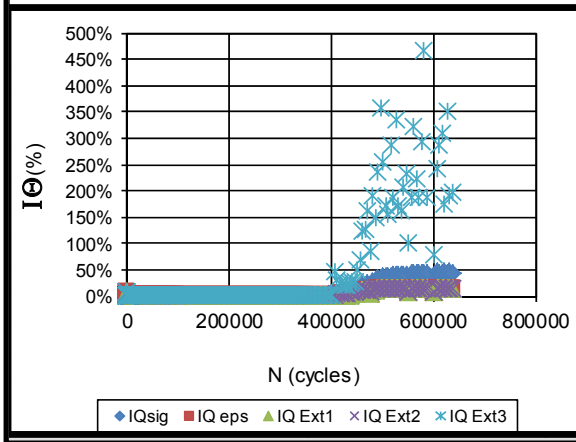

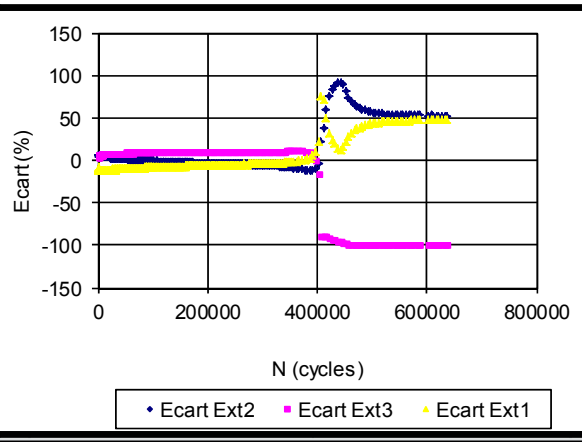

TEST NAME: 40RAP-(P1-A2)-D180

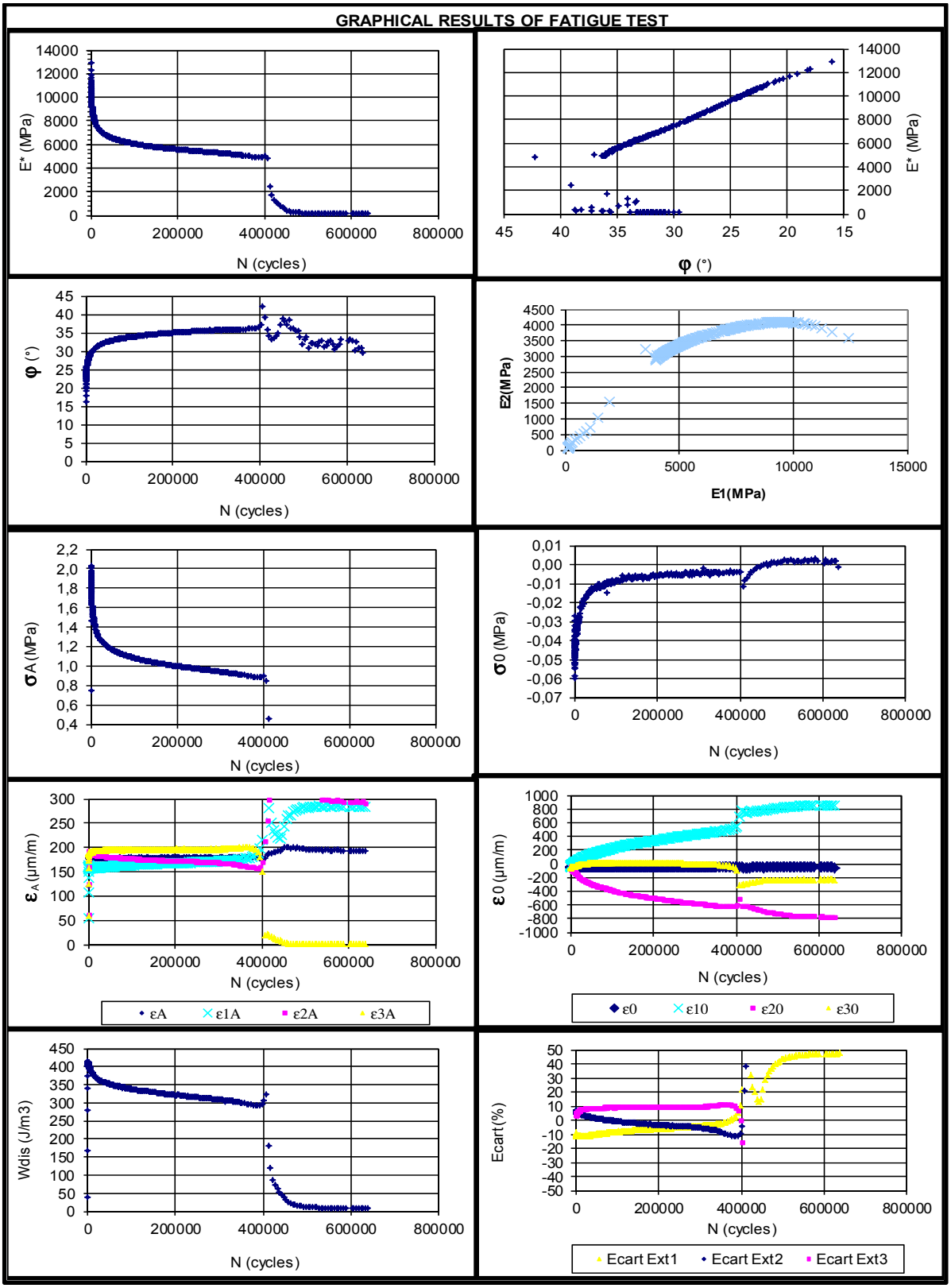

Correction of the fatigue test results based on the voids of the specimens

To do the Correction of the fatigue test results based on the voids of the specimens, the relationship that has been set by Moutier (1991) was used for this purpose. It is in the form:

$$\varepsilon_6 = (-125 + 72 * TL - 4{,}85 * TL^2 + 3{,}3 * \Delta C) * 10^{-6} \qquad \text{(A III-1)}$$

Where:

ε_6 Estimation of the deformation eligible for 10^6 cycles;

TL Binder content

ΔC Difference between the compaction obtained on the specimen and the compaction obtained by the test of gyratory shear compactor (C_{GSC})

Since the assumption derived for ε_6 can be applied for other deformations we can write:

$$\varepsilon_m = (-125 + 72 * TL - 4{,}85 * TL^2 + 3{,}3 * (C_{sample} - C_{GSC})) * 10^{-6} \qquad \text{(A III-2)}$$

In the same way we can write:

$$\varepsilon_{cor} = (-125 + 72 * TL - 4{,}85 * TL^2 + 3{,}3 * (C_{cor} - C_{GSC})) * 10^{-6} \qquad \text{(A III-3)}$$

Because we calculate the correction value for the same mix the TL parameter is the same and C_{GSC} is the same for the same sample.

Then we have:

$$\varepsilon_{cor} = \varepsilon_m + 3{,}3(C_{cor} - C_{sample}) \qquad \text{(A III-4)}$$

We have:

Compaction (%) = 100 – percentage of voids or C = 100 – V

Then: $\varepsilon_{cor} = \varepsilon_m + 3{,}3(V_{sample} - V_{cor})$

In our case V_{cor} is the averge void for all the specimens used

By replace $V_{cor} = \overline{V}$

We find finally:

$$\varepsilon_{cor} = \varepsilon_m + 3{,}3(V_{sample} - \overline{V}) \qquad \text{(A III-5)}$$

We did the correction on the deformation and keeping the number of cycle N_f as it is. By applying this principle we can get the new Wöhler curve.

We will show in the following section the fatigue results by taken into account the correction done based on air void for the selected tested mixtures to show what`s going on or what`s happen for the coefficients of fatigue.

Figures III.1 shows the old and the new Wöhler curve drawn before and after the correction done for all the selected mixtures using the classical criterion and the criteria of the transition between phase II and III.

This figure shows that the slope was less affected by the correction done in the case of the three recycled mixtures 15% RAP 25% RAP and 40% RAP because we have some point hide the difference. However, in the case of the control mix the slope is more affective that`s probably because we have scattering between these points.

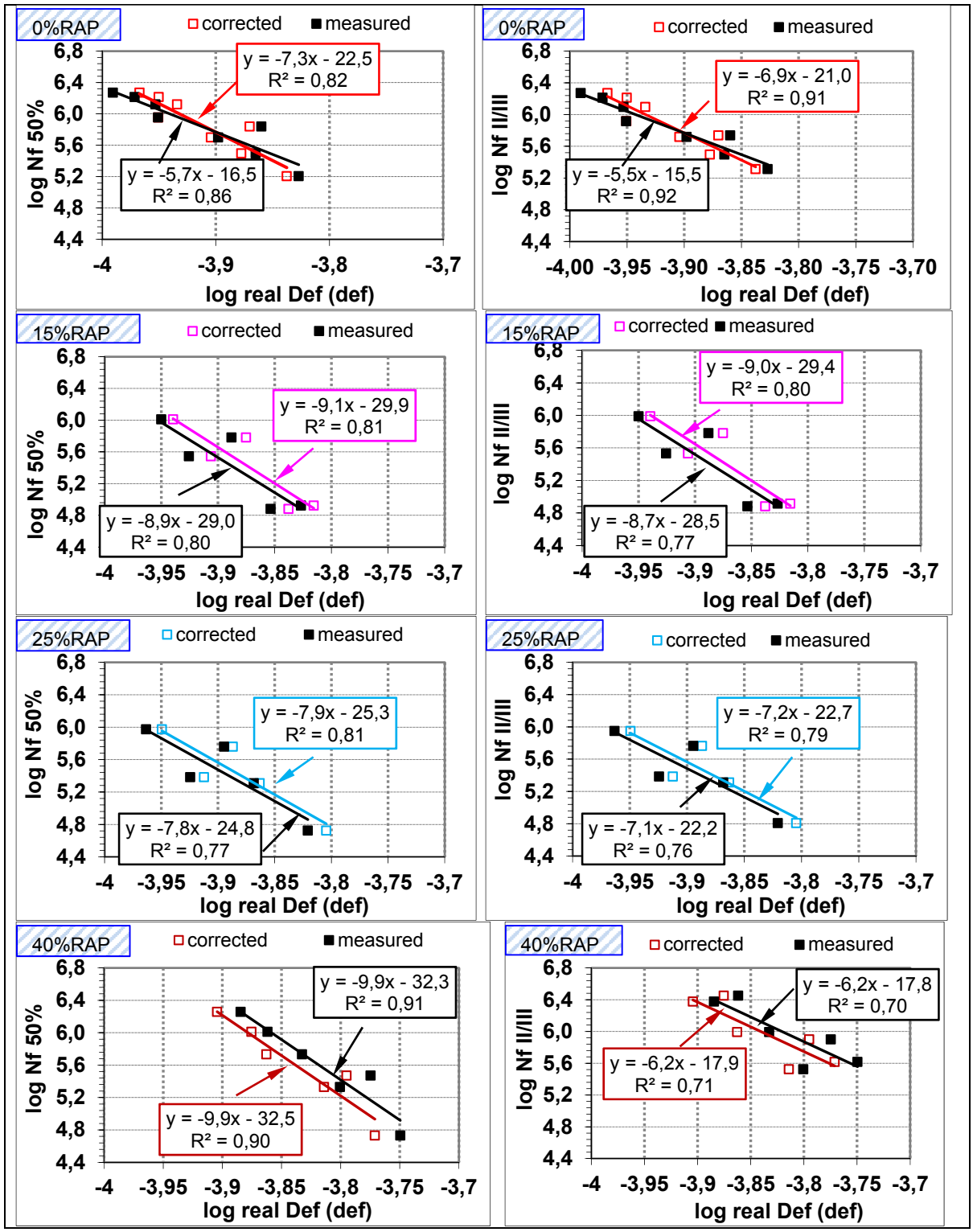

Figure-A III-1Characteristic of fatigue for the selected tested mixtures before and after correction based on air void of 5,1% using the two criterions

Table-A III-1 Comparison between the measured and the basic predicted model values for the two criteria

The mix	Imposed corrected strain (µdef)	$N_{f-50\%}$ (cycles)		Relative error Er (%)	$N_{f-II/III}$ (cycles)		Relative error Er (%)
		measured	basic predicted model		measured	basic predicted model	
GB20 0%RAP	145,3	161 375	204 757	-26,9	206 478	216 862	-5,0
	134,8	692 216	352 963	49,0	549 550	362 781	34,0
	124,7	501 909	623 407	-24,2	524 434	620 978	-18,4
	132,6	314 163	399 334	-27,1	314 163	407 660	-29,8
	112,1	1 644 105	1 345 845	18,1	1 639 096	1 284 947	21,6
	107,9	1 874 412	1 784 053	4,8	1 874 412	1 677 078	10,5
	112,1	902 680	1 352 836	-49,9	827 584	1 291 253	-56,0
	116,4	1 328 140	1 026 024	22,7	1 253 045	994 352	20,6
GB20 15%RAP	152,9	84 158	75 953	9,7	82 650	79 797	3,5
	124,1	351 791	508 120	-44,4	341 768	520 634	-52,3
	114,9	1 027 737	1 023 850	0,4	980 180	1 039 429	-6,0
	133,3	607 602	265 460	56,3	607 602	274 333	54,8
	145,3	76 374	121 133	-58,6	76 375	274 333	-259,2
GB20 25%RAP	122,4	241 937	423 998	-75,3	243 191	442 457	-81,9
	137,0	203 910	172 982	15,2	205 163	194 755	5,1
	129,7	577 019	266 769	53,8	582 025	289 526	50,3
	156,8	53 227	59 506	-11,8	64 309	73 333	-14,0
	112,3	943 017	832 409	11,7	892 950	820 406	8,1
GB20 40%RAP	124,6	1812 821	1 819 151	-0,3	2 385 837	2 372 468	0,6
	133,2	1 028 208	937 563	8,8	2 835 891	1 566 987	44,7
	137,2	542 579	702 256	-29,4	985 665	1 307 766	-32,7
	153,4	214 108	230 246	-7,5	335 599	650 841	-93,9
	160,3	296 783	148 742	49,9	797 459	495 145	37,9
	169,4	54 043	86 045	-59,2	414 507	351 549	15,2

Table-A III-2 The synthesis of the calculation of N_f for the conventional mixture (mixture without RAP)

Specimen	ε (µm/m)	$\varepsilon_{cor,real}$ (µm/m)	T °C	$E_{0\ test}$	$E_{III\ test}$	$N_{II/III\ test}$	$D_{II/III\ test}$	$E_{0\ DGCB}$	E_F	$E_{III\ cor}$	$D_{IIIc\ (0)}$
0RAP-(P1-A2)-D150	150	145,3	10	10952	5161	178 678	0,53	10952	7956.40	8005.00	0,24
0RAP-(P1-A5)-D140	140	134,8	10	11547	6214	549 550	0,46	11547	8397.05	8374.00	
0RAP-(P2-A4)-D130	130	124,7	10	12428	7463	524 434	0,40	12428	9564.20	9584.00	
0RAP-(P1-A3)-D140	140	132,6	10	11899	7226	314 163	0,39	11899	9004.10	9060.00	
0RAP-(P3-A3)-D110	110	112,1	10	10532	6560	1 639 096	0,38	10570	8704.90	8712.00	
0RAP-(P3-A5)-D105	105	107,9	10	10491	6271	1 874 412	0,40	10491	8498.90	8499.00	
0RAP-(P3-A4)-D115	115	112,1	10	10371	6082	1 253 045	0,41	10371	8239.60	8270.00	
0RAP-(P4-A5)-D115	115	116,4	10	10907	6508	827 584	0,40	10830	8566.20	8601.00	
											0,24

$D_{IIIc\ (0)}$	Interval -1 (30 000 to 60 000)			$D_{IIIc\ (0)}$	Interval 0 (40 000 to 80 000)			$D_{IIIc\ (1)}$	Interval 1 (50 000 to 150 000)			$D_{IIIc\ (2)}$	Interval 2 (150 000 to 300 000)		
	E_{00-1}	a_{T-1}	N_{fDGCB}		E_{000}	a_{T0}	N_{fDGCB}		E_{001}	a_{T1}	N_{fDGCB}		E_{002}	a_{T2}	N_{fDGCB}
0,24	7138	-1,70E-06	140 122	0,24	7015	-1,37E-06	163 783	0,26	6958	-1,26E-06	173578				
				0,18	7512	-1,03E-06	229 900	0,19	7317	-6,62E-07	325372	0,18	6606	-3,14E-08	2 442 426
				0,17	8807	-9,20E-07	259 481	0,17	8573	-5,38E-07	405090	0,18	8222	-2,46E-07	558 500
				0,15	8228	-9,14E-07	260 619	0,15	8029	-5,71E-07	384407	0,16	7631	-2,38E-07	547 174
				0,21	8306	-9,59E-07	255 134	0,20	8048	-5,13E-07	430146	0,20	7730	-2,25E-07	649 415
				0,21	7980	-7,52E-07	315 520	0,21	7842	-5,01E-07	447162	0,22	7520	-2,11E-07	699 190
				0,21	7673	-7,82E-07	302 965	0,21	7546	-5,47E-07	409499	0,21	7197	-2,37E-07	597 529
				0,19	7957	-7,58E-07	311 879	0,19	7809	-4,92E-07	451493	0,20	7489	-2,12E-07	679 997
0,24				0,19				0,20				0,19			

Table-A III-3 The synthesis of the calculation of the predicted N_{fDGCB} for the 15%RAP mixture

specimen	ε (µm/m)	$\varepsilon_{cor,real}$ (µm/m)	T °C	$E_{0\ test}$	$E_{III\ test}$	$N_{II/III\ test}$	$D_{II/III\ test}$	$E_{0\ DGCB}$	E_F	$E_{III\ cor}$
15RAP-(P2-A1)-D150	150	152,9	10	9939	5513	82 650	0,45	9939	7185,70	7193,50
15RAP-(P1-A2)-D140	140	145,3	10	11498	6459	76 375	0,44	11498	8270,80	9616,00
15RAP-(P1-A3)-D115	115	114,9	10	11164	6443	980 180	0,42	11164	9005,80	9005,00
15RAP-(P2-A3)-D130	130	133,3	10	11154	6240	607 602	0,44	11154	8554,50	8554,00
15RAP-(P2-A2)-D120	120	124,1	10	9461	5971	341 768	0,37	9461	7442,20	7442,00

$D_{IIIc\ (0)}$	Interval -1 (30 000 to 60 000)			$D_{IIIc\ (0)}$	Interval 0 (40 000 to 80 000)			$D_{IIIc\ (1)}$	Interval 1 (50 000 to 150 000)			$D_{IIIc\ (2)}$	Interval 2 (150 000 to 300 000)		
	E_{00-1}	a_{T-1}	N_{fDGCB}		E_{000}	a_{T0}	N_{fDGCB}		E_{001}	a_{T1}	N_{fDGCB}		E_{002}	a_{T2}	N_{fDGCB}
0,17	6635	-2,06E-06	126712	0,17	6517	-1,74E-06	104 943								
0,16	7625	-1,70E-06	115 818												
				0,23	8453	-9,11E-07	261 633	0,23	8263	-5,95E-07	371170	0,23	7969	-3,41E-07	386 424
				0,21	7882	-9,00E-07	266 953	0,21	7677	-5,84E-07	376427	0,21	7294	-2,95E-07	383 872
				0,15	6909	-8,39E-07	283 552	0,15	6759	-5,33E-07	414196	0,16	6479	-2,42E-07	514 809
0,16				0,19				0,20				0,20			

Table-A III-4 The synthesis of the calculation of the predicted N_{fDGCB} for the 25%RAP mixture

Specimen	Def (µm/m)	$\varepsilon_{cor,real}$ (µm/m)	T °C	$E_{0\ test}$	$E_{III\ test}$	$N_{II/III\ test}$	$D_{II/III\ test}$	$E_{0\ DGCB}$	E_F	$E_{III\ cor}$
25RAP-(P3-A1)-D150	150	156,8	10	12363	5651	64 309	0,54	12363	9193	
25RAP-(P4-A2)-D120	120	122,4	10	12391	6885	243 191	0,44	12391	9695	9695,10
25RAP-(P4-A4)-D140	140	137,0	10	10564	6256	205 163	0,41	10564	7952	7951,00
25RAP-(P4-A5)-D130	130	129,7	10	12373	6702	582 025	0,46	12373	9295	9295,30
25RAP-(P1-A1)-D110	110	112,3	10	9071	4693	892 950	0,48	9071	6769	6768,70

$D_{IIIc\ (0)}$	Interval -1 (30 000 to 60 000)			$D_{IIIc\ (0)}$	Interval 0 (40 000 to 80 000)			$D_{IIIc\ (1)}$	Interval 1 (50 000 to 150 000)			$D_{IIIc\ (2)}$	Interval 2 (150 000 to 300 000)		
	E_{00-1}	a_{T-1}	N_{fDGCB}		E_{000}	a_{T0}	N_{fDGCB}		E_{001}	a_{T1}	N_{fDGCB}		E_{002}	a_{T2}	N_{fDGCB}
0,29	8559	-5,34E-06	49 973												
0,24	9278	-1,86E-06	141 142	0,23	9056	-1,41E-06	173 399	0,29	9797	-1,02E-06	303 383				
0,41	10564	-1,36E-06	352 092	0,16	7254	-9,53E-07	250 639	0,16	7081	-6,25E-07	366 830				
				0,20	8425	-1,08E-06	217 553	0,20	8179	-6,68E-07	316475	0,21	7752	-3,06E-07	580 736
				0,23	6187	-1,13E-06	214 332	0,23	6012	-7,38E-07	299827	0,23	5612	-2,82E-07	621 876
0,31				0,20				0,22				0,22			

Table-A III-5 The synthesis of the calculation of the predicted N_{fDGCB} for the 40%RAP mixture

Specimen	Def (µm/m)	$\varepsilon_{cor,real}$ (µm/m)	T °C	$E_{0\ test}$	$E_{III\ test}$	$N_{II/III\ test}$	$D_{II/III\ test}$	$E_{0\ DGCB}$	E_F	$E_{III\ cor}$
40RAP-(P1-A3)-D160	160	153,4	10	11863,6	5359	335 599	0,55	11863,60	8354,10	8354,00
40RAP-(P1-A1)-D130	130	124,6	10	12125,53	5897	2 385 837	0,51	12125,15	9288,90	9288,00
40RAP-(P2-A3)-D140	140	133,2	10	12780,17	5950	2 835 891	0,53	12780,17	9350,00	9350,00
40RAP-(P2-A2)-D150	150	137,2	10	12997,97	6399	985 665	0,51	12997,97	9295,00	9295,00
40RAP-(P1-A4)-D170	170	160,3	10	11555,27	4993	797 459	0,57	11555,27	8170,60	8170,00
40RAP-(P1-A2)-D180	180	169,4	10	11365,57	4776,51	414 507	0,58	11365,57	7966,20	7966,20

Specimen	D_{IIIc} (0)	Interval 0 (40 000 to 80 000)			D_{IIIc} (1)	Interval 1 (50 000 to 150 000)			$D_{IIIc\ (2)}$	Interval 2 (150 000 to 300 000)		
		E_{000}	a_{T0}	N_{fDGCB}		E_{001}	a_{T1}	N_{fDGCB}		E_{002}	a_{T2}	N_{fDGCB}
40RAP-(P1-A3)-D160	0,26	7642	-1,84E-06	143 708	0,27	7460	-1,39E-06	176 627	0,29	7213	-9,34E-07	235 585
40RAP-(P1-A1)-D130	0,28	8563	-1,07E-06	225 339	0,28	8416	-8,34E-07	273 136	0,28	7808	-3,82E-07	438 943
40RAP-(P2-A3)-D140	0,26	8436	-1,08E-06	221 577	0,27	8203	-6,95E-07	314 575	0,27	7705	-2,81E-07	597 946
40RAP-(P2-A2)-D150	0,22	8312	-1,18E-06	204 264	0,22	8032	-7,16E-07	300 071	0,23	7544	-3,04E-07	540 626
40RAP-(P1-A4)-D170	0,27	7263	-1,28E-06	188 938	0,27	7035	-8,37E-07	258 540	0,28	6559	-3,72E-07	428 717
40RAP-(P1-A2)-D180	0,28	7122	-1,66E-06	150 147	0,28	6837	-1,10E-06	196 791	0,28	6255	-5,36E-07	269 257
	0,26				0,27				0,27			

Table-A III-6 A comparison between $N_{fII/III\text{-measured}}$ and $N_{fII/III}^{DGCB}$

Test Name	$\varepsilon_{cor,real}$ (μm/m)	$N_{fII/III\text{-measured}}$ (cycles)	$N_{fII/III}^{DGCB}$ (cycles)	Er (%)
0RAP-(P1-A2)-D150	145,3	178 678	134 818	25
0RAP-(P1-A5)-D140	134,8	549 550	251 437	54
0RAP-(P2-A4)-D130	124,7	524 434	558 500	-6
0RAP-(P1-A3)-D140	132,6	314 163	547 174	-74
0RAP-(P3-A3)-D110	112,1	1 639 096	649 415	60
0RAP-(P3-A5)-D105	107,9	1 874 412	699 190	63
0RAP-(P4-A5)-D115	112,1	827 584	597 529	52
0RAP-(P3-A4)-D115	116,4	1 253 045	679 997	18
15RAP-(P2-A1)-D150	152,9	82 650	104 943	-27
15RAP-(P2-A2)-D120	124,1	341 768	514 809	-51
15RAP-(P1-A3)-D115	114,9	980 180	386 424	61
15RAP-(P2-A3)-D130	133,3	607 602	383 872	37
15RAP-(P1-A2)-D140	145,3	76 375	115 818	-52
25RAP-(P4-A2)-D120	122,4	243 191	303 383	-25
25RAP-(P4-A4)-D140	137	205 163	366 830	-79
25RAP-(P4-A5)-D130	129,7	582 025	580 736	0
25RAP-(P3-A1)-D150	156,8	64 309	49 973	22
25RAP-(P1-A2)-D110	112,3	892 950	621 876	30
40RAP-(P1-A2)-D130	124,6	2 385 837	613 925	74
40RAP-(P2-A3)-D140	133,2	2 835 891	851 751	70
40RAP-(P2-A2)-D150	137,2	985 665	784 664	20
40RAP-(P1-A3)-D160	153,4	335 599	311 276	7
40RAP-(P1-A4)-D170	160,3	797 459	632 333	21
40RAP-(P1-A2)-D180	169,4	414 507	415 005	0

It should be noted that in Table-A III-6 for the test 0RAP-(P1-A5)-D140, we used the results of the second interval (interval 1) because we found that the third interval (interval 2) is not

good. We found that the temperature is more stable at the second interval comparable with the third one. Thus, we decide to make our prediction based on that. As we can see in the synthesis of the fatigue test of this mixture that shown in Appendix III that our thermo chamber was a bit high even if it is found that it is in the acceptable range of temperature to make a prediction. Even if we get less accuracy by doing this, we don't have the artefact effects that coming from the interval 2. We found that, in this test, the value of the modulus can show either an increasing or a decreasing during the phase II rather than to follow a linear decrease as expected. This happens specified at interval 2 only. This variance has more effect on the slope value of the test resulting in a huge difference between the two values of $N_{fII/III}$ measured and $N_{fII/III}$ predicted by the DGCB method.

In Table-A III-6, it can be seen that there are a wide difference between the $N_{fII/III}$ and $N_{fII/III}^{DGCB}$ values in the two tests 40RAP-(P1-A2)-D130 and 40RAP-(P2-A3)-D140. The reason in this case is that the predicted method may not able to give good prediction when the duration life of the sample continue for very long time (very high number of cycles) with a very low rate of decrease in the modulus. We know that when the propagation cracking is very low, we need to increase the applied deformation. Otherwise, the results show that the two values are close. Based on that, we can say that this method is more applicable with high level of accuracy for fatigue tests for materials with short fatigue life. Thus, according to our results we propose that up to actual one million cycles of failure that could happen for the material, we can use the DGCB method to predict the failure occurs. This last result still needs to be checked on a wider range of recycled mixes of different source of RAP is of a primary importance.

On the other hand, all the announced points for each mix were used to obtain the overall DGCB prediction accuracy statistics, as shown in Figure 6.35 (e to h). The range of R^2 values for the four recycled mixtures are between 0,39 and 0,81. Clearly, this method does not take into account the specimen's air void effects and also the measured $N_{fII/III}$. Because of this, it can be said that estimating of accuracy of the relationship between $N_{fII/III}$ and $N_{fII/III}^{DGCB}$ can be affected and part of an 'error' may be in the relationship. That can be one point; the second

point is that the accuracy of one test can dramatically affect the level of the presentation of accuracy between $N_{fII/III}$ and $N_{fII/III}^{DGCB}$. For example, by examining our results we found that there are big differences between the values of $N_{fII/III}$ and $N_{fII/III}^{DGCB}$ for the two tests 40RAP-(P1-A1)-D130 and 40RAP-(P2-A3)-D130 and that might affect the results and the precision of the relation $N_{fII/III}$ and $N_{fII/III}^{DGCB}$ curve itself.

In fact, we are more concern about the $N_{fII/III}$ Wöhler curves' accuracy because it is the traditional way that is used to present the accuracy of fatigue test result.

Therefore, we can generally say that the value of the predicted and the experimental results are comparable with acceptable errors in most of the fatigue tests done, which allows to generalize this calculation on other tests to validate this prediction and to characterize the fatigue behaviour of asphalt to 300 000 cycles of solicitation (which means run the test for only 8 hours of solicitation at a frequency of 10 Hz and stopped it before failure). But caution should be taken because of the reasons provided previously.

APPENDIX IV

DATA OF THE BASIC FATIGUE MODEL IMPROVEMENT

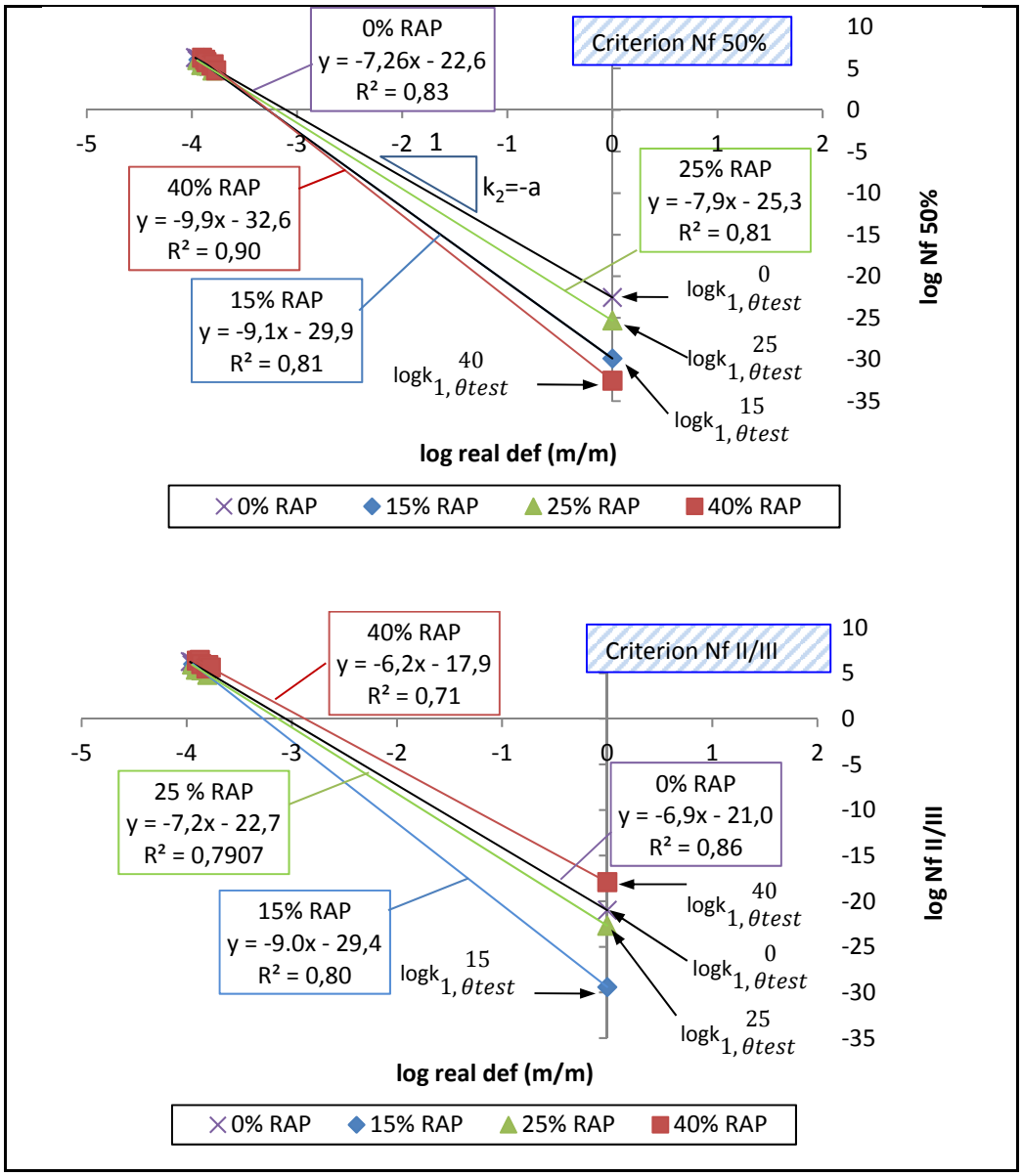

Figure-A IV-1 Corrected life duration based on air void of 5,1% for the four mixes (0% RAP, 15% RAP, 25% RAP, 40% RAP) determined with the classical criterion and the criterion of the end of phase II and the corresponding regression lines in the logarithmic axis log N-log ε

Basic steps to improve the basic fatigue model

The relationship of number cycle to failure N_f and the real applied deformation in logarithmic can be exhibited graphically as the Wöhler curve using the two criterion $N_{f50\%}$ and $N_{fII/III}$ as shown in Figure-A IV-1. This curve is generally negatively sloped. Wöhler curve is often graphed as a straight line of the form:

$$y = ax + b \quad \text{(A IV-1}$$

Where *a*, b are parameters. The constant '*a*' is the slope of the Wöhler curve and show how the applied deformation affects the number of cycle to failure. The constant 'b' is the intercept where $\log \varepsilon_t$ is zero where the Wöhler curve intercepts the y axis for the amplitude of deformation equal to 1 (m/m).

Consequently the graphical presentation is technically of the equation 6.4:

$$logN_f = a \times log\varepsilon_t + b \quad \text{(A IV-10)}$$

The basic fatigue form is in the form presented in equation 6.4. This equation was recast into linear form by taking natural logarithm of each side as follow:

$$y = ax + b \quad \text{(A IV-11)}$$

Where: $y = \log N_f$, $x = log\varepsilon_t$, $a = -k_2$, and $b = logk_{1,\theta_{test}}^{\%RAP}$

So equation 6.4 could be written as:

$$logN_f = -k_2 \times log\varepsilon_t + logk_{1,\theta_{test}}^{\%RAP} \quad \text{(A IV-12)}$$

We can find the values of $k_{1,\theta_{test}}^{\%RAP}$ for the four recycled asphalt mixtures that have been tested and the value of k_2 for each mix as shown in Table 6.5.

$k_{1,\theta_{test}}^{0}$, k_2^0, $k_4^{0/40}$

By assuming a linear relationship between $logk_{1,\theta_{test}}^{\%RAP}$ and % RAP with a slope k_4, thus we plot the required data and we add a trend line using the intercept of value equal to $logk_{1,\theta_{test}}^{0}$ to indicate the linear relationship between the $\%RAP$ and $logk_{1,\theta_{test}}^{\%RAP}$ (Figure-A IV-2). It is important to note that we use the intercept referred to the virgin mix because it is our reference mixture (common point). The mathematical relationship can be written in $y = ax + b$ form.

Where:

$y = logk_{1,\theta_{test}}^{\%RAP}$, $x = \%RAP$, $a = slope = -k_4$, and b = Y intercept

Where: %RAP = 0 = $\log k_{1,\theta_{test}}^{0}$

Consequently the graphical presentation is technically that of the equation:

$$logk_{1,\theta_{test}}^{\%RAP} = logk_{1,\theta_{test}}^{0} - k_4 \times \%RAP \qquad \text{(A IV-13)}$$

By substituting equation A IV-5 in equation A IV-4 we have:

$$logN_f = logk_{1,\theta_{test}}^{0} - k_4 \times \%RAP - k_2 \times log\varepsilon_t \qquad \text{(A IV-6)}$$

Then:

$$logN_f = logk_{1,\theta_{test}}^{0} - k_4 \times \%RAP - log\varepsilon_t^{-k_2} \qquad \text{(A IV-14)}$$

Then:

$$logN_f = -k_4 \times \%RAP + \log(k_{1,\theta_{test}}^{0} \times \varepsilon_t^{-k_2}) \quad \text{(A IV-15)}$$

Notice that $10^{\log_{10}(N_f)} = N_f$, therefore the logs can be inverted to find:

$$N_f = k_{1,\theta_{test}}^{0} \times \varepsilon_t^{-k_2} \times 10^{-k_4 \times \%RAP} \quad \text{(A IV-16)}$$

Table-A IV-1 Comparison between the measured and the general fatigue model predicted values for the two criteria

The mix	Imposed strain (µm/m)	$N_{f\text{-}50\%}$(cycles)		Relative error Er (%)	$N_{f\text{-}II/III}$(cycles)		Relative error Er (%)
		measured	General fatigue model		measured	General fatigue model	
GB20 0%RAP	145,3	161 375	204 757	26,9	206 478	216 862	5,0
	134,8	692 216	352 963	-49,0	549 550	362 781	-34,0
	124,7	501 909	623 407	24,2	524 434	620 978	18,4
	132,6	314 163	399 334	27,1	314 163	407 660	29,8
	112,1	1644 105	1 345 845	-18,1	1 639 096	1 284 947	-21,6
	107,9	1 874 412	1 784 053	-4,8	1 874 412	1 677 078	-10,5
	112,1	902 680	1 352 836	49,9	827 584	1 291 253	56,0
	116,4	1 328 140	1 026 024	-22,7	1 253 045	994 352	-20,6
GB20 15%RAP	152,9	84 158	40	-100,0	82 650	81 079	-1,9
	124,1	351 791	183	-99,9	341 768	339 207	-0,7
	114,9	1 027 737	320	-100,0	980 180	574 891	-41,3
	133,3	607 602	109	-100,0	607 602	208 035	-65,8
	145,3	76 374	58	-99,9	76 375	115 228	50,9
GB20 25%RAP	122,4	241 937	0,88	-100,0	243 191	244 915	0,7
	137,0	203 910	0,39	-100,0	205 163	112 548	-45,1
	129,7	577 019	0,57	-100,0	582 025	163 870	-71,8
	156,8	53 227	0,14	-100,0	64 309	44 608	-30,6
	112,3	943 017	1,63	-100,0	892 950	439 641	-50,8
GB20 40%RAP	124,6	1 812 821	0	-100,0	2 385 837	114 315	-95,2
	133,2	1 028 208	0	-100,0	2 835 891	72 349	-97,4
	137,2	542 579	0	-100,0	985 665	59 268	-94,0
	153,4	214 108	0	-100,0	335 599	27 452	-91,8
	160,3	296 783	0	-100,0	797 459	20 306	-97,5
	169,4	54 043	0	-100,0	414 507	13 918	-96,6

Table-A IV-2 Comparison between the measured and the general fatigue model predicted values for the two criteria using the testing data up to 40% with the value of the parameter A fixed from the relationship between $k_2^{0/40}$, versus %RAP

The mix	Imposed strain (µm/m)	$N_{f\text{-}50\%}$(cycles)		Relative error Er (%)	$N_{f\text{-}II/III}$(cycles)		Relative error Er (%)
		measured	General fatigue model		measured	General fatigue model	
GB20 0%RAP	145,3	161 375	204 757	26,9	206478	216862	5,0
	134,8	692 216	352 963	-49,0	549 550	362781	-34,0
	124,7	501 909	623 407	24,2	524 434	620978	18,4
	132,6	314 163	399 334	27,1	314 163	407660	29,8
	112,1	1 644 105	1 345 845	-18,1	1 639 096	1 284 947	-21,6
	107,9	1 874 412	1 784 053	-4,8	1 874 412	1 677 078	-10,5
	112,1	902 680	1 352 836	49,9	827 584	1 291 253	56,0
	116,4	1 328 140	1 026 024	-22,7	1 253 045	994 352	-20,6
GB20 15%RAP	152,9	84 158	136 920	62,7	82 650	190 954	131,0
	124,1	351 791	755 300	114,7	341 768	815 301	138,6
	114,9	1 027 737	1 417 463	37,9	980 180	1 392 181	42,0
	133,3	607 602	421 470	-30,6	607 602	496 562	-18,3
	145,3	76 374	208 262	172,7	76 375	272 739	257,1
GB20 25%RAP	122,4	241 937	952 442	293,7	243 191	1 058 716	335,3
	137,0	203 910	351 192	72,2	205 163	477 643	132,8
	129,7	577 019	568 730	-1,4	582 025	701 665	20,6
	156,8	53 227	107 105	101,2	64 309	185 208	188,0
	112,3	943 017	2 017 757	114,0	892 950	1 926 997	115,8
GB20 40%RAP	124,6	1 812 821	945 996	-47,8	2 385 837	1 183 708	-50,4
	133,2	1 028 208	494 494	-51,9	2 835 891	736 284	-74,0
	137,2	542 579	372 677	-31,3	985 665	598 613	-39,3
	153,4	214 108	125 129	-41,6	335 599	269 303	-19,8
	160,3	296 783	81 592	-72,5	797 459	196 932	-75,3
	169,4	54 043	47 754	-11,6	414 507	133 060	-67,9

Table-A IV-3 Comparison between the measured and the general fatigue model predicted values for the two criteria using the testing data up to 25% with the value of the parameter A fixed from the relationship between $k_2^{0/25}$, versus %RAP

The mix	Imposed strain (µm/m)	$N_{f\text{-}50\%}$(cycles)		Relative error Er (%)	$N_{f\text{-}II/III}$(cycles)		Relative error Er (%)
		measured	General fatigue model		measured	General fatigue model	
GB20 0%RAP	145,3	161 375	204 757	26,9	206 478	216 862	5,0
	134,8	692 216	352 963	-49,0	549 550	362 781	-34,0
	124,7	501 909	623 407	24,2	524 434	620 978	18,4
	132,6	314 163	399 334	27,1	314 163	407 660	29,8
	112,1	1 644 105	1345 845	-18,1	1 639 096	1 284 947	-21,6
	107,9	1 874 412	1 784 053	-4,8	1 874 412	1 677 078	-10,5
	112,1	902 680	1 352 836	49,9	827 584	1 291 253	56,0
	116,4	1 328 140	102 6024	-22,7	1 253 045	994 352	-20,6
GB20 15%RAP	152,9	84 158	89 919	6,8	82 650	101 488	22,8
	124,1	351 791	480 895	36,7	341 768	494 647	44,7
	114,9	1 027 737	892 242	-13,2	980 180	886 881	-9,5
	133,3	607 602	271 202	-55,4	607 602	287 947	-52,6
	145,3	76 374	135 735	77,7	76 375	149 746	96,1
GB20 25%RAP	122,4	241 937	447 220	84,8	243 191	467 342	92,2
	137,0	203 910	169 594	-16,8	205 163	187 027	-8,8
	129,7	577 019	270 948	-53,0	582 025	291 127	-50,0
	156,8	53 227	53 478	0,5	64 309	62 879	-2,2
	112,3	943 017	927 651	-1,6	892 950	930 904	4,3

Table-A IV-4 Comparison between the measured and the general fatigue model predicted values for the two criteria using testing data by assuming the slope of the fatigue line is variant and by considering *A* as the average of the three results obtained for each mix (15, 25, 40% of RAP) which fixed from the optimization process

The mix	Imposed strain (µm/m)	$N_{f\text{-}50\%}$(cycles)		Relative error Er (%)	$N_{f\text{-}II/III}$(cycles)		Relative error Er (%)
		measured	General fatigue model		measured	General fatigue model	
GB20 0%RAP	145,3	161 375	204 757	26,9	206 478	216 862	5,0
	134,8	692 216	352 963	-49,0	549 550	362 781	-34,0
	124,7	501 909	623 407	24,2	524 434	620 978	18,4
	132,6	314 163	399 334	27,1	314 163	407 660	29,8
	112,1	1 644 105	1 345 845	-18,1	1 639 096	1 284 947	-21,6
	107,9	1 874 412	1 784 053	-4,8	1 874 412	1 677 078	-10,5
	112,1	902 680	1 352 836	49,9	827 584	1 291 253	56,0
	116,4	1 328 140	1026024	-22,7	1 253 045	994 352	-20,6
GB20 15%RAP	152,9	84 158	114462	36,0	82 650	159 507	93,0
	124,1	351 791	628735	78,7	341 768	678 133	98,4
	114,9	1 027 737	1 178 091	14,6	980 180	1 156 135	18,0
	133,3	607 602	351 355	-42,2	607 602	413 622	-31,9
	145,3	76 374	173 921	127,7	76 375	227 585	198,0
GB20 25%RAP	122,4	241 937	701 253	189,8	243 191	778 447	220,1
	137,0	203 910	259 569	27,3	205 163	352 561	71,8
	129,7	577 019	419 573	-27,3	582 025	516 949	-11,2
	156,8	53 227	79 526	49,4	64 309	137 338	113,6
	112,3	943 017	1 481 311	57,1	892 950	1 412 754	58,2
GB20 40%RAP	124,6	1 812 821	580 207	-68,0	2 385 837	724 439	-69,6
	133,2	1 028 208	304 389	-70,4	2 835 891	452 256	-84,1
	137,2	542 579	229 767	-57,7	985 665	368 277	-62,6
	153,4	214 108	77 618	-63,7	335 599	166 698	-50,3
	160,3	296 783	50 733	-82,9	797 459	122 194	-84,7
	169,4	54 043	29 782	-44,9	414 507	82 811	-80,0

Table-A IV-5 Comparison between the measured and the general fatigue model predicted values for the two criteria using testing data by assuming the slope of the fatigue line is variant and by considering *A* as the average of the two results obtained for each mix (15, 25% of RAP) which fixed from the optimization process using the optimum values of *A* for each mix

The mix	Imposed strain (µm/m)	$N_{f\text{-}50\%}$ (cycles)		Relative error Er (%)	$N_{f\text{-}II/III}$ (cycles)		Relative error Er (%)
		measured	General fatigue model		measured	General fatigue model	
GB20 0%RAP	145,3	161 375	204 757	26,9	206 478	216 862	5,0
	134,8	692 216	352 963	-49,0	549 550	362 781	-34,0
	124,7	501 909	623 407	24,2	524 434	620 978	18,4
	132,6	314 163	399 334	27,1	314 163	407 660	29,8
	112,1	1 644 105	1 345 845	-18,1	1 639 096	1 284 947	-21,6
	107,9	1 874 412	1 784 053	-4,8	1 874 412	1 677 078	-10,5
	112,1	902 680	1 352 836	49,9	827 584	1 291 253	56,0
	116,4	1 328 140	1 026 024	-22,7	1 253 045	994 352	-20,6
GB20 15%RAP	152,9	84 158	95 477	13,4	82 650	103 772	25,6
	124,1	351 791	511 346	45,4	341 768	506 045	48,1
	114,9	1 027 737	949 238	-7,6	980 180	907 492	-7,4
	133,3	607 602	288 235	-52,6	607 602	294 528	-51,5
	145,3	76 374	144 175	88,8	76 375	153 135	100,5
GB20 25%RAP	122,4	241 937	495 487	104,8	243 191	485 456	99,6
	137,0	203 910	187 655	-8,0	205 163	194 183	-5,4
	129,7	577 019	299 990	-48,0	582 025	302 336	-48,1
	156,8	53 227	59 083	11,0	64 309	65 247	1,5
	112,3	943 017	1 028 767	9,1	892 950	967 332	8,3

Table-A IV-6 Comparison between the measured and the general fatigue model predicted values for the two criteria using testing data by assuming the slope of the fatigue line as variant and using the optimum values of *A* for each mix

The mix	Imposed strain (µm/m)	$N_{f\text{-}50\%}$(cycles)		Relative error Er (%)	$N_{f\text{-}II/III}$(cycles)		Relative error Er (%)
		measured	General fatigue model		measured	General fatigue model	
GB20 0%RAP	145,3	161 375	204 757	26,9	206 478	216 862	5,0
	134,8	692 216	352 963	-49,0	549 550	362 781	-34,0
	124,7	501 909	623 407	24,2	524 434	620 978	18,4
	132,6	314 163	399 334	27,1	314 163	407 660	29,8
	112,1	1 644 105	1345 845	-18,1	1 639 096	1 284 947	-21,6
	107,9	1 874 412	1784053	-4,8	1 874 412	1 677 078	-10,5
	112,1	902 680	1 352 836	49,9	827 584	1 291 253	56,0
	116,4	1 328 140	1 026 024	-22,7	1 253 045	216 862	-82,7
GB20 15%RAP	152,9	84 158	98 342	16,9	82 650	129 236	56,4
	124,1	351 791	538 243	53,0	341 768	546 699	60,0
	114,9	1 027 737	1 007 192	-2,0	980 180	930 340	-5,1
	133,3	607 602	301 156	-50,4	607 602	334 025	-45,0
	145,3	76 374	149 294	95,5	76 375	184 168	141,1
GB20 25%RAP	122,4	241 937	446 788	84,7	243 191	474 787	95,2
	137,0	203 910	166 320	-18,4	205 163	216 374	5,5
	129,7	577 019	268 106	-53,5	582 025	316 310	-45,7
	156,8	53 227	51 302	-3,6	64 309	84 913	32,0
	112,3	943 017	939 766	-0,3	892 950	857 636	-4,0
GB20 40%RAP	124,6	1 812 821	1 803 299	-0,5	2 385 837	2 833 113	18,7
	133,2	1 028 208	938 126	-8,8	2 835 891	1 750 867	-38,3
	137,2	542 579	705 548	30,0	985 665	1 419 477	44,0
	153,4	214 108	234 994	9,8	335 599	631 674	88,2
	160,3	296 783	1 52 747	-48,5	797 459	459 955	-42,3
	169,4	54 043	89 047	64,8	414 507	309 119	-25,4

Table-A IV-7 Comparison between the Statistical fatigue model versus measured N_f using the statistical fatigue parameters $k_1^{0/40}$, and $k_2^{0/40}$ and the $SF^{0/40}$ defined for all the mixes combined up to 40%

The mix	Imposed strain (µm/m)	$N_{f\text{-}50\%}$(cycles)		Relative error Er (%)	$N_{f\text{-}II/III}$(cycles)		Relative error Er (%)
		measured	General fatigue model		measured	General fatigue model	
GB20 0%RAP	145,3	161 375	139 193	-13,7	206 478	151 809	-26,5
	134,8	692 216	256 145	-63,0	549 550	250 916	-54,3
	124,7	501 909	484 363	-3,5	524 434	424 125	-19,1
	132,6	314 163	294 120	-6,4	314 163	281 187	-10,5
	112,1	1 644 105	1 146 827	-30,2	1 639 096	862 801	-47,4
	107,9	1 874 412	1 572 530	-16,1	1 874 412	1 119 105	-40,3
	112,1	902 680	1 153 501	27,8	827 584	866 936	4,8
	116,4	1 328 140	846 294	-36,3	1 253 045	671 695	-46,4
GB20 15%RAP	152,9	84 158	117 146	39,2	82 650	171 815	107,9
	124,1	351 791	638 932	81,6	341 768	695 130	103,4
	114,9	1 027 737	1 194 073	16,2	980 180	1 163 653	18,7
	133,3	607 602	357 919	-41,1	607 602	431 230	-29,0
	145,3	76 374	177 689	132,7	76 375	242 179	217,1
GB20 25%RAP	122,4	241 937	842 364	248,2	243 191	1 042 202	328,6
	137,0	203 910	335 161	64,4	205 163	487 730	137,7
	129,7	577 019	523 175	-9,3	582 025	703 917	20,9
	156,8	53 227	111 906	110,2	64 309	197 545	207,2
	112,3	943 017	1 685 247	78,7	892 950	1 845 384	106,7
GB20 40%RAP	124,6	1 812 821	922 206	-49,1	2 385 837	1 464 947	-38,6
	133,2	1 028 208	536 223	-47,8	2 835 891	937 137	-67,0
	137,2	542 579	423 331	-22,0	985 665	771 284	-21,7
	153,4	214108	170024	-20,6	335 599	363 749	8,4
	160,3	296783	118927	-59,9	797 459	270 961	-66,0
	169,4	54043	76003	40,6	414 507	187 368	-54,8

Table-A IV-8 Comparison between Statistical predicted model versus measured N_f using the statistical fatigue parameters $k_1^{0/25}$. and $k_2^{0/25}$ and the $SF^{0/25}$ defined for the mixes combined up to 25% RAP mix

The mix	Imposed strain (µm/m)	$N_{f\text{-}50\%}$(cycles)		Relative error Er (%)	$N_{f\text{-}II/III}$(cycles)		Relative error Er (%)
		measured	General fatigue model		measured	General fatigue model	
GB20 0%RAP	145,3	161 375	181 649	12,6	206 478	189 821	-8,1
	134,8	692 216	330 939	-52,2	549 550	336 254	-38,8
	124,7	501 909	619 279	23,4	524 434	611 039	16,5
	132,6	314 163	379 141	20,7	314 163	382 786	21,8
	112,1	1 644 105	1 445 647	-12,1	1 639 096	1 370 925	-16,4
	107,9	1 874 412	1 972 015	5,2	1 874 412	1 843 109	-1,7
	112,1	902 680	1 453 922	61,1	827 584	1 378 404	66,6
	116,4	1 328140	1072 147	-19,3	1 253 045	1 031 053	-17,7
GB20 15%RAP	152,9	84 158	92019	9,3	82 650	98 341	19,0
	124,1	351 791	488 088	38,7	341 768	482 439	41,2
	114,9	1 027 737	902 841	-12,2	980 180	867 071	-11,5
	133,3	607 602	276 034	-54,6	607 602	280 216	-53,9
	145,3	76 374	138 624	81,5	76 375	145 334	90,3
GB20 25%RAP	122,4	241 937	455 799	88,4	243 191	449 150	84,7
	137,0	203 910	184 121	-9,7	205 163	189 298	-7,7
	129,7	577 019	285 312	-50,6	582 025	287 382	-50,6
	156,8	53 227	62 594	17,6	64 309	67 687	5,3
	112,3	943 017	901 546	-4,4	892 950	860 484	-3,6

Table-A IV-9 Comparison between the fatigue life values predicted from the basic and the general fatigue models according to the criteria $N_{f50\%}$ based on the structure level ($k_3 = k_2{}^{a}/2$): modelling up to 25%

The mix	Temp. – freq.	Alizé resulted strain µm/m (Pavement structure: Figure 7.12)	$N_{f50\%\text{-calculated}}$ (cycles)		
			Basic model (Eq. 7.1)	General fatigue model (Eq. 7.7)	Statistical model (model 3-Table 7.8)
			By considering the coefficients $k_1^{\%RAP}$ and $k_2^{\%RAP}$ established from $N_{f50\%}$	By considering the coefficients k_1^0, k_2^0, $k_4^{0/40}$, and universal value of $A^{0/25}$ and $SF^{0/25}$ established from $N_{f50\%}$	By considering the statistical coefficients $k_1^{0/25}$ and $k_2^{\%RAP}$ and $SF^{0/25}$ established from $N_{f50\%}$
GB20 0% RAP	40°C – 10 Hz	523,8	109 554	109 554	91 208
	40°C – 3 Hz	739,8	143 691	143 691	122 971
	25°C– 10 Hz	210,8	956 779	956 779	992 717
	25°C – 3 Hz	281,9	638 673	638 673	636 005
	10°C– 10 Hz	97,7	3 659 026	3 659 026	4 350 692
	10°C – 3 Hz	116,6	2 590 493	2 590 493	2 973 987
GB20 15% RAP	40°C – 10 Hz	737,5	62 736	22737	339 769
	40°C – 3 Hz	1097,5	22 384	7343	176 267
	25°C– 10 Hz	238,8	535 567	301589	1 710 151
	25°C – 3 Hz	323,2	324 413	159877	1 058 851
	10°C– 10 Hz	101,2	3 261 215	2479501	8 551 979
	10°C – 3 Hz	120	2 183 556	1577717	5 928 010
GB20 25% RAP	40°C – 10 Hz	523,3	317 081	52163	339 769
	40°C – 3 Hz	740,9	165 682	18327	176 267
	25°C– 10 Hz	188,8	1 567 982	846943	1 710 151
	25°C – 3 Hz	254,8	975 932	846943	1 058 851
	10°C– 10 Hz	84,8	7 704 143	10293747	8 551 979
	10°C – 3 Hz	100	5 361 770	5961637	5 928 010

a: In the case of the basic model, the slope of the fatigue line for each mix is varied and considered in the k_3 calculation (k_2 values that used were shown in Table 6.4. In the case of the general fatigue model the only slope value that was considered in the calculation was the slope of the mixture without RAP (k_2^0). and In the case of the statistical model, the determined statistical slope shown in Table 7.5 was taken into account in the calculation.

Table-A IV-10 Comparison between the estimated fatigue life values of the basic and the general fatigue models according to the criteria $N_{fII/III}$ based on the structure level ($k_3 = k_2/2$): (modelling up to 25%)

The mix	Temp. – freq.	Alizé resulted strain µm/m (Pavement structure: Figure 7.12)	$N_{fII/III\text{-calculated}}$ (cycles)		
			Basic model (Eq. 7.1)	General fatigue model (Eq. 7.7)	Statistical model (model 4–Table 7.8)
			By considering the coefficients $k_1^{\%RAP}$ and $k_2^{\%RAP}$ established from $N_{fII/III}$	By considering the coefficients k_1^0, k_2^0, $k_4^{0/25}$, and universal value of $A^{0/25}$ and the $SF^{0/25}$established from $N_{fII/III}$	the statistical coefficients $k_1^{0/25}$ and $k_2^{\%RAP}$and the $SF^{0/25}$ established from $N_{fII/III}$
GB20 0%RAP	40°C – 10 Hz	523,8	120 099	120 099	85 304
	40°C – 3 Hz	739,8	155 185	155 185	109 590
	25°C– 10 Hz	210,8	930 821	930 821	629 968
	25°C – 3 Hz	281,9	635 337	635 337	433 910
	10°C– 10 Hz	97,7	3 306 156	3 306 156	2 171 403
	10°C – 3 Hz	116,6	2 385 633	2 385 633	1 578 961
GB20 15%RAP	40°C – 10 Hz	737,5	66 077	141 834	149 417
	40°C – 3 Hz	1097,5	23 898	62 792	70 036
	25°C– 10 Hz	238,8	548 377	795 813	722 832
	25°C – 3 Hz	323,2	334 373	529 727	500 028
	10°C– 10 Hz	101,2	3 260 696	3 372 536	2 727 911
	10°C – 3 Hz	120	2 194 775	2 452 191	2 031 170
GB20 25%RAP	40°C – 10 Hz	523,3	339 130	649 794	815 519
	40°C – 3 Hz	740,9	187 219	349 754	470 708
	25°C– 10 Hz	188,8	1 464 668	3 067 237	3 156 141
	25°C – 3 Hz	254,8	948986	1 936 438	2 112 573
	10°C– 10 Hz	84,8	6 288 692	13 894 411	12 149 910
	10°C – 3 Hz	100	4 513 129	9 878 346	8 938 800

Table-A IV-11 Comparison between the estimated fatigue life values determined based on the structure level at 10°C – 10Hz and based on the material level determined at an equivalent deformation ε_t = 97,7 µm/m determined according to the $N_{f50\%}$ using the basic model (modelling up to 25%)

The mix	$N_{f50\%-calculated}$ *(cycles)*					
	Material level: (constant strain: ε_t)			**Structure level: (constant bituminous thickness)**		
	Basic model	**General predicted model**	**Statistical model**	**Basic model**	**General predicted model**	**Statistical model**
	By considering the coefficients $k_1^{\%RAP}$ and $k_2^{\%RAP}$ established from $N_{f50\%}$ (at strain = 97,7 µm/m	By considering the coefficients k_1^0, k_2^0, $k_4^{0/25}$, and universal value of $A^{0/25}$ established from $N_{f50\%}$ (at strain = 97,7 µm/m)	By considering the universal statistical fatigue coefficients $k_1^{0/25}$ and $k_2^{0/25}$ established from $N_{f50\%}$ (at strain = 97,7 µm/m	By considering the coefficients $k_1^{\%RAP}$ and $k_2^{\%RAP}$ established from $N_{f50\%}$ and used Alizé deformation resulted at 10°C – 10Hz (Table 7,10)	By considering the coefficients k_1^0, k_2^0, $k_4^{0/25}$, and universal value of $A^{0/25}$ established from $N_{f50\%}$ and used Alizé deformation resulted At 10°C – 10Hz (Table 7,10)	By considering the universal statistical fatigue coefficients $k_1^{0/25}$ and $k_2^{0/25}$ and the $SF^{0/25}$ established from $N_{f50\%}$ and used Alizé deformation resulted at 10°C – 10Hz (Table 7,10)
0 % RAP	3 659 026 (at strain = 97,7 µm/m)	3 659 026 (at strain = 97,7 µm/m)	4 350 692 (at strain = 97,7 µm/m	3 659 026 (at strain = 97,7 µm/m)	3 659 026 (at strain = 97,7 µm/m)	4 350 692 (at strain = 97,7 µm/m)
15% RAP	4 494 014 (at strain = 97,7 µm/m)	3 290 163 (at strain = 97,7 µm/m)	3 307 969 (at strain = 97,7 µm/m)	3 261 215 (at strain = 101,2 µm/m)	2 479 501 (at strain = 101,2 µm/m	2 496 387 (at strain = 101,2 µm/m)
25% RAP	2 513 446 (at strain = 97,7 µm/m	3 065 152 (at strain = 97,7 µm/m)	2 755 688 (at strain = 97,7 µm/m)	7 704 143 (at strain = 84,8 µm/m)	10 293 747 (at strain = 84,8 µm/m)	8 551 979 (at strain = 84,8 µm/m)

Table-A IV-12 Comparison between the estimated fatigue life values determined based on the structure level at 10°C – 10Hz and based on the material level determined at an equivalent deformation ε_t = 97,7 µm/m determined according to the $N_{fII/III}$ using the basic model (modelling up to 25%)

The mix	$N_{fII/III-calculated}$ *(cycles)*					
	Material level: (constant strain: ε_t)			**Structure level: (constant bituminous thickness)**		
	Basic model	**General predicted model**	**Statistical model**	**Basic model**	**General predicted model**	**Statistical model**
	By considering the coefficients $k_1^{\%RAP}$ and $k_2^{\%RAP}$ established from $N_{fII/III}$ (at strain = 97,7 µm/m)	By considering the coefficients k_1^0, k_2^0, $k_4^{0/25}$, and universal value of $A^{0/25}$ established from $N_{fII/III}$ (at strain = 97,7 µm/m)	By considering the universal statistical fatigue coefficients $k_1^{0/25}$, $k_2^{0/25}$ and the $SF^{0/25}$ established from $N_{fII/III}$ (at strain = 97,7 µm/m)	By considering the coefficients coefficients $k_1^{\%RAP}$ and $k_2^{\%RAP}$ established from $N_{fII/III}$ and used Alizé deformation resulted at 10°C – 10Hz (Table 7,10)	By considering the coefficients k_1^0, k_2^0, $k_4^{0/25}$, and universal value of $A^{0/25}$ established from $N_{fII/III}$ and used Alizé deformation resulted At 10°C – 10Hz (Table 7,10)	By considering the universal statistical fatigue coefficients $k_1^{0/25}$, $k_2^{0/25}$ and the $SF^{0/25}$ established from $N_{fII/III}$ and used Alizé deformation resulted at 10°C – 10Hz (Table 7,10)
0% RAP	3306156 (at strain = 97,7 µm/m	3306156 (at strain = 97,7 µm/m)	3 918 465 (at strain = 97,7 µm/m)	3306156 (at strain = 97,7 µm/m)	3 306 156 (at strain = 97,7 µm/m)	3 918 465 (at strain = 97,7 µm/m)
15% RAP	4474360 (at strain = 97,7 µm/m)	3 042 429 (at strain = 97,7 µm/m)	2 989 589 (at strain = 97,7 µm/m)	3260696 (at strain = 101,2 µm/m)	2 329 000 (at strain = 101,2 µm/m)	2 286 038 (at strain = 101,2 µm/m)
25% RAP	2255847 (at strain = 97,7 µm/m)	2 878 405 (at strain = 97,7 µm/m)	2 496 179 (at strain = 97,7 µm/m)	6288692 (at strain = 84,8 µm/m	9 037 775 (at strain = 84,8 µm/m)	7 346 719 (at strain = 84,8 µm/m)

LIST OF REFERENCES

Abdel-Hameed, H. M. 2006. « Evaluation of the Performance of Hot Mix Asphalt Concrete Mixtures with 40/50 and 60/70 Asphalt Grades ». Cairo, Cairo University.

Abdul-Rahman, Kefah Muhammad. 1985. « Recycling of deteriorated asphalt pavements ». 1355696. Saudi Arabia. King Fahd University of Petroleum and Minerals (Saudi Arabia), 152 p. <http://proquest.umi.com/pqdweb?did=747882021&Fmt=7&clientId=46962&RQT=309&VName=PQD>.

Abojaradeh, Mohammad. 2003. « Predictive fatigue models for arizona asphalt mixtures ». Arizona state.

Ahmad, J., M.Y.A. Rahman et K. Din. 2004. « Degradation and abrasion of Reclaimed Asphalt Pavement ». In International Journal of Engineering and Technology, Vol. 1, p. 139-149.

Al-Qadi, Imad L., Mostafa Elseifi et Samuel H. Carpenter. 2007. Reclaimed asphalt pavement a literature review. Research Report FHWA-ICT-07-001. Illinois Center for Transportation.

Anderson, D. A. 1987. « Guidlines for use of dust in hot mix asphalt concrete mixtures ». Association of Asphalt Paving Technologists, vol. 56, p. 492-516.

Anderson, D., Y.M.L. Hir, M.O. Marasteanu, J.P. Planche, D. Martin et G. Gautheir. 2001. « Physical properties of asphalt cement and development of performance related specifications ». Transportation Research Record, No. 1766, Washington, D.C.

Anderson, D., D. W. Christense et H. Bahia. 1991. « Physical properties of asphalt cement and the development of performance related specifications ». *Association of Asphalt Paving Technologists,* vol. 60, p. 437-475.

Artamendi, I., et H. Khalid. 2004. « Different approaches to depict fatigue of bituminous materials ». In *The 15th European conference of fracture, advanced fracture mechanics for life and fafety assessment* (August 11-13). Sttockholm, Sweden, Ashayer Soltani, M. A. 1998. « Comportement en fatigue des enrobés bitumineux ». Lyon. L'institut national des sciences appliquées, Thèse de doctorat en génie civil, 293 p.

Asphalt and Institute, 1981. Asphalt Institute. 1981. Asphalt hot mix recycling. MS-20. Lexington, KY, USA.: The Asphalt Institute manual series No. 20.

Asphalt Institute, 2003. Performance graded asphalt binder specification and testing. Superpave Series No. 1 (SP-1), 3rd Edition. Lexington, K Y.

Asphalt institute. cited in July 2014. « Individual Asphalt Binder Tests ». <http://www.asphaltinstitute.org/lab_services/individual-asphalt-binder-tests.dot>.

ASTM. 1998. *Annual Book of ASTM Standards*, 4.03. Coll. « Section 4, Construction ». Pennsylvania: Road and Paving Materials, American Society for Testing and Materials.Baaj. H, H. Di Benedetto et P. Chaverot. 2005. « Effect of binder characteristics on fatigue of as-phalt pavement using an intrinsic damage approach ». Road materials and pavement design, vol. 6, nº 2, p. 147-174.

Baaj, H. 2002. « Comportement a la fatigue des materiaux granulaire traites au liannt hydraulique ». ENTPE and INSA Lyon, 247 p.

Basueny, A., D. Perraton et A. Carter. 2014. « Laboratory study of the effect of RAP conditioning on the mechanical properties of hot mix asphalt containing RAP ». *Materials and structures,* vol. 47, p. 1425-1450.

Bell, Haley P. 2009. « Fatigue evaluation criteria for aged hot-mix asphalt surfaces ». 1470471, United States -- Mississippi. Mississippi State University. In ProQuest Dissertations & Theses (PQDT); ProQuest Dissertations & Theses A&I. <http://search.proquest.com/docview/304939493?accountid=27231 http://openurl.uquebec.ca:9003/ets?url_ver=Z39.88-2004&rft_val_fmt=info:ofi/fmt:kev:mtx:dissertation&genre=dissertations+%26+theses&sid=ProQ:ProQuest+Dissertations+%26+Theses+%28PQDT%29&atitle=&title=Fatigue+evaluation+criteria+for+aged+hot-mix+asphalt+surfaces&issn=&date=2009-01-01&volume=&issue=&spage=&au=Bell%2C+Haley+P.&isbn=9781109515756&jtitle=&btitle=>.

Berthier, J. 1982. Le recyclage en centrale des enrobés bitumineux: Note technique provisoire. Direction des routes, p.28.

Bonnaure, F. P., A. H. Huibers et A. Boonders. 1982. « A laboratory investigation of the influence of rest periods on the fatigue characteristics of bituminous mixes ». Association of Asphalt Paving Technologists, vol. 51, p. 104-128.

Brock, J. D., et J. L. Richmond. 2007b. *Milling and recycling*. Technical Paper T-127. <https://www.roadtec.com/images/uploads/productdocs/t127_techpaper_millingrecycling.pdf>.

Brown, E. R. et N.E. Murphy. 1994. Asphalt Content Determination by thei gnition Method. Alabama Department of Transportation Research Report 110B.

Brown, Elton Ray. 1983. « Evaluation of properties of recycled asphalt concrete hot mix ». Ph.D., Ann Arbor. Texas A&M University. 169-169 p. p. In ProQuest Dissertations & Theses Full Text. <http://search.proquest.com/docview/303307899?accountid=27231 http://openurl.uquebec.ca:9003/ets?url_ver=Z39.88-2004&rft_val_fmt=info:ofi/fmt:kev:mtx:dissertation&genre=dissertations+%26+theses&sid=ProQ:ProQuest+Dissertations+%26+Theses+Full+Text&atitle=&title=EVALUATION+OF+PROPERTIES+OF+RECYCLED+ASPHALT+CONCRETE+HOT+MIX&issn=&date=1983-01-01&volume=&issue=&spage=&au=Brown%2C+Elton+Ray&isbn=&jtitle=&btitle=&rft_id=info:eric/&rft_id=info:doi/>.

Burmister, D.M. 1943. « The theory of the stress and displacements in layered systems and applications of design of airport runway ». In *The Highway Research Board*. Vol. 23, p. 126-148. Carter, A. et M. Stoup-Gardiner. 2006. « Aging of Hot Mix Asphalt Specimens as Evaluated with an Indirect Tension Relaxation Test ». In Proceedings of the Fifty-First Annual Conference of the Canadian Technical Asphalt Association (CTAA) Charlottetown Prince Edward Island. Canada.

Carter, A. et M. Stroup-Gardiner. 2007. « Indirect Tension Relaxation Test to Evaluate the Effect of the Addition of RAP to HMA mixes ». Journal of materials in civil engineering. Asce american society of civil engineers, vol. 19, n° 3, p. 219-226.

Carter, A., M. Stroup-Gardiner et D. Perraton. 2006. « Aging of Hot Mix Asphalt Specimens as Evaluated with an Indirect Tension Relaxation Test ». In CTAA proceeding. Charlottetown (Canada).

Castedo-Franco, Luis Humberto. 1985. « Materials characterization and economic considerations of cold-mix recycled asphalt pavements (mix-design. Guidelines. Analyses. Bituminous, Indiana) ». 8606520. United states indiana, Purdue university, 348 p. <http://proquest.umi.com/pqdweb?did=752617521&fmt=7&clientid=46962&rqt=309&vname=pqd>.

Coenen, A., M.E. Kutay et H.U. Bahia. 2011. « Aggregate structure characterization of asphalt mixtures using 2-dimensional image analysis ». International journal of Road Materials and pavement Design.

Cooper, K.E.. et P.S, Pell. 1974. « The efffect of mix variables on the fatigue strength of bituminous materials ». LR 663, UK: Transport and Road Research Laboratory.

Daniel, J., Y. R. Kim et H. J. Lee. 1998. « Effects of aging on viscoelastic properties of asphalt-aggregate mixtures ». Transportation Research Record, vol. 1630, p. 21-27.

Daniel. J. S. et R. Y. Kim. 2001. « Laboratory evaluation of fatigue damage and healing of asphalt mixtures ». Journal of Materials in Civil Engineering, vol. 13, p. 434-440.

Daniel, J. S. et A. Lachance. 2003. « Reheological properties of asphalt mixtures containing recycled asphalt pavement ». In Transportation Research Board, TRB annual meeting CD-ROM.

Daniel, J.S., W. Bisirri et Y. K. Richard. 2004. « Fatigue evaluation of asphalt mixtures using dissipated energy and viscoelastic continuum damage approaches ». The Association of Asphalt Paving Technology (AAPT), vol. 7.

Daniel, J.S., et A. Lachance. 2005. « Mechanistic and volumetric properties of asphalt mixtures with RAP ». The Transportation Research Board 84th Annual meeting compendium of papers CD-ROM, TRB, National Research Council.

Deacon, JA., JS. Coplantz, AA Tayebali et CL Monismith. 1994. « Temperature considerations in asphalt-aggregate mixture analysis and design ». *Transportation Research Record*.

De la roche, Chantal. 1996. « Module de rigidité et comportement en fatigue des enrobés bitumineux ». Paris, Thèse de doctorat en matériaux, sols et structures, École Centrale Paris, 188 p. p.

Delaporte, B., H. Di Benedetto, P. Chaverot et G. Gauthier. 2007. « Linear viscoelastic properties of bituminous materials: from binders to mastics ». Association of Asphalt Paving Technologists, vol. 76, p. 488-494.

Di Benedetto, H., M.A. Ashayer Soltani et P. Chaverot. 1996. « Fatigue damage for bituminous mixtures: a pertinent approach ». Journal of the Association of Asphalt Paving Technologists (AAPT), vol. 65, p. 15.

Di Benedetto. H., et J.F. Corté (288 p.). 2004. Matériaux routiers bitumineux 1: description et propriétés des constituants. Lavoisier.

Di Benedetto. H., et C. De La Roche. 1998. State of the art on stiffness modulus and fatigue of bituminous mixtures. Rilem Rep. No. 17, Bituminous Binders and Mixtures. L Francken, ed., E&FN Spon. London.

Di Benedetto, H., C. De La Roche, H. Baaj, A. Pronk et R. Lundsrom. 2004. « fatigue of bituminous mixtures ». Materials and Structures, vol. 37, (April), p. 202-216.

Di Benedetto, H., M.N. Parti, L. Francken et C. De la Roche. 2001. « Stiffness testing for bituminous mixtures ». Materials and Structures, vol. 34, p. 66-70.

Doucet, Felix. et Bruno Auger. 2010. Complex modulus determination of asphalt mixes at the minstere des Transport du Quebec. Ministère des transports du Québec (MTQ).

Emery, J. J. 1993. « Asphalt concrete recycling in Canada ». Transportation Research Record, nº 1427, p. 38-46.

Etonray, B. 1983. « Evaluation of properties of recycled asphalt concretehot mix ». Texas A&M University., 169 pages; AAT 8329906 p.

Federation of Canadian Municipalities and National Research Council. 2005. *Reuse and recycling of road construction and maintenance materials*. ISBN 1–897094–86–8. <https://www.fcm.ca/Documents/reports/Infraguide/Reuse_and_Recycling_of_Road_Construction_and_Maintenance_Materials_EN.pdf>.

FHWA, Federal Highway Administration, U.S. department of transportation. 2011. « User guidelines for waste and byproduct materials in pavement construction ». <http://www.fhwa.dot.gov/publications/research/infrastructure/structures/97148/rap131.cfm>.

FHWA, Federal highway Administration. 1997. Pavement recycling guidelines for state and local governments. FHWA-SA-98-042. Washington, D.C.

FHWA, Federal Highway Administration. 1998. User guidelines for waste and by-product materials in pavement construction. FHWA-RD-97-148.

FHWA Superpave Mixture Expert Task grroup. 1997. « Guidlines for the design of superpave mixtures containg reclaimed asphalt pavement (RAP) ». <http://www.utexas.edu/research/superpave/articles/rap.html >.

Gandil, P. et P. Vesseron. 2001. Circulaire n° 2001-39 du 18 juin 2001 relative à la gestion des déchets du réseau routier national. Circulaire conjointe du Ministère de l'Aménagement du Territoire et de l'Environnement et du Ministère de l'Équipement. des Transports et du Logement, p.11.

Gannon, C.R., R.H. Wombles, C.A. Ramey, J.P. davis et Little W.V. 1980. « Recycling conventional and rubberized bituminous concrete pavements using recycling agents and virgin asphalt as modifiers (A laboratory and field study) ». In *Association of Asphalt Paving Technologists Proceedings (AAPT)*, p. 95-122. Louisville, Kentucky. Gaonach., M. 2012. « mesure in-situ de la teneur en eau avec sondes dans les matériaux recyclés traités à froid avec une émulsion de bitume ». Montreal. L'école de technologie supérieure.

Hajj, E. Y.. P.E. Sebaaly et R. Shrestha. 2007. A Laboratory evaluation of the use of recycled asphalt pavements in HMA mixtures Final report. Regional Transportation Commission

Harris, B.M. et K.D. Stuart. 1995. « Analysis of mineral fillers and mastics used in SMA ». the Association of Asphalt Paving Technologies, vol. 64, p. 54-87 p.

Howard, P. D., et D. A. Reed. 1989. « Microwave recycling of reclaimed asphalt pavement ». Public Works Journal Corporation, vol. 120, p. p. 53-55.

Huang, B., R. Kingery. Z. Zhang et G. Zuo. 2004. « Laboratory study of fatigue characteristics of HMA surface mixtures containing RAP ». In International symposium on long performing asphalt pavements (june 7-9), p. 501-22. Auburn. Ala.

Huet, C.. 1963. « Etude par une méthode d'impédance du comportement visco-élastique des matériaux ». Paris, Ph.D thesis. Faculté des Sciences de Paris.

Jaffee, Brian Ian. 2001. « Implementation of the SUPERPAVE(TM) level 1 mixture design system in The Cooper Union Asphalt Technology Laboratory by classifying an asphalt binder and compacting samples in the Gyratory Compactor ». United States -- New York. The Cooper Union for the Advancement of Science and Art 355 p. <http://search.proquest.com/docview/304693186?accountid=27231>.

Jeppson, M. R. 1986. « Microwave method and apparatus for heating loose paving materials ». n° 658122 <http://ip.com/patent/US4619550>.

John, R. Bukowski. Chair 1997. « Guidelines for the design of Superpave Mixtures containing Reclaimed Asphalt Pavement (RAP) ». In FHWA Superpave Mixtures Expert Task Group. <http://www.utexas.edu/research/superpave/articles/rap.html>.

Kallas, B.F. 1984. Flexible pavement mixture design using reclaimed asphalt concrete. FHWA/RD-84/088.

Kandhal, P. S., et Jr. F. Parker. 1998. Aggregate tests related to asphalt concrete performance in pavements. NCHRP Report 405. Washington, D.C.

Kandhal, P.S., S.S. Rao, Watson D.E. et B. Young. 1995. Performance of Recycled Hot-Mix Asphalt Mixtures in the State of Georgia. National Center for Asphalt Technology. NCAT Report 95-01.

Kennedy, T. W., W. O. Tam et M. Solaimanian. 1998. « Optimizing use of Reclaimed. Asphalt Pavement with the Superpave system». Asphalt Paving Technologists. vol. 67-98, p. 311-333.

Lachance, Aaron Marc. 2006a. « Properties of asphalt mixtures containing RAP ». 1439277. United States -- New Hampshire. University of New Hampshire, 163 p. p. In ProQuest Dissertations & Theses (PQDT); ProQuest Dissertations & Theses A&I. <http://search.proquest.com/docview/305279894?accountid=27231

http://openurl.uquebec.ca:9003/ets?url_ver=Z39.88-2004&rft_val_fmt=info:ofi/fmt:kev:mtx:dissertation&genre=dissertations+%26+theses&sid=ProQ:ProQuest+Dissertations+%26+Theses+%28PQDT%29&atitle=&title=Properties+of+asphalt+mixtures+containing+RAP&issn=&date=2006-01-01&volume=&issue=&spage=&au=Lachance%2C+Aaron+Marc&isbn=9780542973222&jtitle=&btitle=>.

Lamothe, S. 2014. « Endommagement d'un enrobé bitumineux partiellement saturé en eau ou en saumure soumis à des sollicitations cycliques de gel-dégel et mécaniques ». Montréal. École de technologie supérieure.

Langlois, P. 2006. Hot mix asphalt: LC method of mix design. Québec (Province): Ministère des transports. Laboratoire des chaussées. .

Laveissiere, D. 2002. « Modélisation de la remonte de fissure en fatigue dans les structures routières par endommagement et macro-fissuration- de l'expérimentation à l'outil de dimensionnement pour l'estimation de la durée de vie ». Limoges University.

Lavin, P. 2003. Asphalt pavements. a partical guide to design. production and maintenance for engineers and architects.

LCPC. 1994. Conception et dimensionnement des structures de chaussées. Coll. « Guide Technique, LCPC-SETRA, ». France. Lee, T., R.L. Terrell et J.P. Mahoney. 1983. « Measurement of mixing efficiency in pavement recycling ». Association of Asphalt Paving Technologists, vol. 52.

Li, X., T.R. Clyne et M. O. Marasteanu. 2004. Recycled asphalt pavement effects on binder and mixture Mn/RC-2005-02. Minnesota Department of Transportation. Research Services section. <http://www.lrrb.org/pdf/200502.pdf >.

Li, Xinjun, Mihai O. Marasteanu, Ronald Christopher Williams et Timothy R. Clyne. 2008. « Effect of Reclaimed Asphalt Pavement (Proportion and Type) and Binder Grade on Asphalt Mixtures ». Transportation Research Record: Journal of the Transportation Research Board, nº 2051, p. pp 90-97.

Lundstrom, R. 2002. « Rheological and fatigue characterization of asphalt concrete mixtures using unaxial testing ». Kungl Tekniska Hogskolan.

LTPP, Long-Term Pavement Performance Program. 1993. Distress Identification Manual for the Long-Term Pavement Performance Project. SHRP-P-338. Strategic Highway.

Luo, Z., E. Y. Chou et J. Yu. 2006. « Calibration of fatigue cracking model of flexible pavement using mechanistic-empirical based probabilistic method ». American Society of Civil Engineers (ASCE). p. 50-61.

McDaniel, R. S., H. Soleymani, R. Michael Anderson. P, Turner et R. Peterson. 2000. « Recommended use of Reclaimed Asphalt Pavement in the Superpave mix design method ». NCHRP Web. Document 30 (Project D9-12): Contractor's Final Report.

McDaniel, R. S. et R. Michael Anderson. 2001. Recommended use of Reclaimed Asphalt Pavement in the Superpave mix design method: Technician's Manual. Washington. D.C.: NCHRP REPORT 452.

McDaniel, R.S., A. Shah. G.A. Huber et V. Gallivan. 2007. « Investigation of properties of plant-produced RAP mixtures ». In Transportation Research Board 86th annual meeting (CD-ROM). Transportation Research Board, National Rsearch Council. Washington, D.C.

Meunier, Mathieu. 2012. « Élaboration d'un outil de prédiction du comportement de la chaussée à l'orniérage ». Thèse de doctorat en génie de la construction, Montréal, L'école de technologie supérieure.Moneron, P. et M. Measson. 2004. Etude sur le recyclage à 15% à chaud en centrale des matériaux bitumineux dans les graves bitune. Revue générale des routes et des aérodromes. (831), pp.10.

Myre, J. 1990. « Fatigue of asphalt pavements ». In Third international conference on bearing capacity of roads and airfields (July 3-5). Vol. 1-2, p. 703-714. Proceedings. Norwegian institute of technology, Trondheim, Norway: Tapir.

National Research Council of Canada. 2005. « reuse and recycling of road construction and maintenance materials ». <http://www.fcm.ca/Documents/reports/Infraguide/Reuse_and_Recycling_of_Road_Construction_and_Maintenance_Materials_EN.pdf>.

Navaro, J.C. 2011. « Cinétique de mélange des enrobés recyclés et influence sur les performances mécaniques ». Bordeaux (France), École Nationale Supérieure d'Arts et Métiers, 308 p. Newcomb., D., E. R. Brown et J. A. Epps. 2007. Quality Improvement Series 124: Designing HMA Mixtures with High RAP Content: A Practical Guide. National Asphalt Pavement Association, Lanham, MD.

Nguyen, Quang Tuan, H. Di Benedetto et Cédric Sauzéat. 2012. « Determination of Thermal Properties of Asphalt Mixtures as Another Output from Cyclic Tension-Compression Test ». *Journal of Road Materials and Pavement Design,* vol. 13, nº 1, p. 85-103.

Nguyen, M.L. 2009. «Étude de la fissuration et de la fatigue des enrobés bitumineux ». Lyon, L'Institut National des Sciences Appliquées de Lyon, 312 p.

Noël, F. 2011. « Personal communication with Touhara (2012) ».

Olard, F., C. Le Noan. D. Bonneau. S. Duperiet et C. Alvarez. 2008. Very high rate (50%) in hot mix and warm mix asphalts for sustainable road construction (may, 2008), 866. Paris: Revue generale des routes (RGRA).

Olard, F. et H. Di Benedetto. 2003. « General ‘‘2S2P1D’’ model and relation between the linear viscoelastic behaviours of bituminous binders and mixes ». Road materials and pavement design, vol. 4, nº 2/2003, p. 1-40.

Olard, F. et H. Di Benedetto. 2005. « The ‘‘DBN’’ model: a thermo-visco-elasto-plastic approach for pavement behaviour modeling ». Asphalt paving technology: Association of asphalt paving proceedings of the technical sessions, vol.74, Asphalt paving technology 2005, p.791-877, vol. 74, p. 791-877.

Paris, J., P. Pereira et L. Picado-Santos. 2002. « Variability of Laboratory Fatigue Life of Asphalt Mixes Using Four Point Bending Test Results ». IPJ, vol. 1, nº 2.

Pavement interactive. cited in December 2010. « Pavement » Pavement Types » HMA Pavement ». <http://www.pavementinteractive.org/article/hma-pavement/>.

Pavement interactive. cited in mai 2015. « Testing » Asphalt Tests » Binder Content ». <http://www.pavementinteractive.org/article/binder-content/>.

Pellinen, Terhi Kristiina. 2001. « Investigation of the use of dynamic modulus as an indicator of hot-mix asphalt peformance ». 3004132, United States -- Arizona. Arizona State University, 803 p. p. In ProQuest Dissertations & Theses (PQDT); ProQuest Dissertations & Theses A&I.
<http://search.proquest.com/docview/304686218?accountid=27231 http://openurl.uquebec.ca:9003/ets?url_ver=Z39.88-2004&rft_val_fmt=info:ofi/fmt:kev:mtx:dissertation&genre=dissertations+%26+theses&sid=ProQ:ProQuest+Dissertations+%26+Theses+%28PQDT%29&atitle=&title=Investigation+of+the+use+of+dynamic+modulus+as+an+indicator+of+hot-mix+asphalt+peformance&issn=&date=2001-01-01&volume=&issue=&spage=&au=Pellinen%2C+Terhi+Kristiina&isbn=9780493132181&jtitle=&btitle=>.

Perraton, D., H. Baaj. H. Di Benedetto et M. Paradis. 2003. « Évaluation de la résistance à la fatigue des enrobés bitumineux fondée sur l’évolution de l’endommagement du matériau en cours d'essai: aspects fondamentaux et application à l’enrobé à matrice de pierre ». Canadian Journal of Civil Engineering, vol. 30, nº 3, p. 902-913.

Perraton, D., H. Di benedetto et A. Carter. 2011. « Correspondances entre les coefficient des modeles de fatigue dans les methods mecanistiques-empiriques de dimensionnement de chaussees souples ». Canadian Journal of Civil Engineering, vol. 38, p. 1287-1299.

Peterson, R.L., H. R. Soleymani, M. Anderson et McDaniel R. S. 1999. « Recovery and testing of RAP binders from recycled asphalt pavement ». In Transportation Research Board Annual Meeting. Washington, DC.

Potyondy, Alexander Julius. 1996. « Recyling waste roofing material in hot mix asphalt pavement ». MM13629, Canada, Technical University of Nova Scotia (Canada), 148 p. <http://proquest.umi.com/pqdweb?did=740326111&Fmt=7&clientId=46962&RQT=309&VName=PQD>.

Pratheepan, Kandiah. 2008. « Use of reclaimed asphalt pavements (RAP) in airfield HMA pavements ». 1457012, United States -- Nevada. University of Nevada, Reno. In ProQuest Dissertations & Theses (PQDT); ProQuest Dissertations & Theses A&I. <http://search.proquest.com/docview/304532613?accountid=27231 http://openurl.uquebec.ca:9003/ets?url_ver=Z39.88-2004&rft_val_fmt=info:ofi/fmt:kev:mtx:dissertation&genre=dissertations+%26+theses&sid=ProQ:ProQuest+Dissertations+%26+Theses+%28PQDT%29&atitle=&title=Use+of+reclaimed+asphalt+pavements+%28RAP%29+in+airfield+HMA+pavements&issn=&date=2008-01-01&volume=&issue=&spage=&au=Pratheepan%2C+Kandiah&isbn=9780549741398&jtitle=&btitle=>.

Prithvi, S. K. et B. M. Rajib. 1997. Pavement Recycling Guidelines for State and Local Governments. Washington.

Prowell, B.D. et C.B. Carter. 2000. Evaluation of the effect on aggregate properties of samples extracted using the ignition furnace Interim Report Virginia Transportation Research Council.

Pumphrey, M. E. 2003. « Evaluation of performance graded asphalt binder equipement and testing protocol ». Morgantown, West Virginia, The college of engineering and mineral resources.

Racanel, C., et A. Burlacu. 2013. « The influence of asphalt mixtures components on asphalt mixtures behavior ». In *4th European conference of civil engineering (ECCIE' 13)*. Antalya, Turkey. Recycled Materials Resource Center. consulted on march 2014. « Reclaimed Asphalt Pavement - Material Description ». <http://rmrc.wisc.edu/ug-mat-reclaimed-asphalt-pavement/>.

Robert, F. L., P. S. Kandhal, E. R. Brown, D. Y. Lee et Th. W. Kennedy. 1996. Hot mix asphalt materials. mixture design, and construction. Second edition. Lanham. Maryland.

Roohi, N. S., L. Tashman et H. Bahia. 2012. « Internal structure characterization of asphalt mixtures for rutting performance using imaging analysis ». *Road Materials and Pavement Design,* vol. 13, nº S1 (June), p. 21-37.

Roohi, N., S., Pouya, P. Teymourpour et H. Bahia. 2013. « Effect of particle mobility on aggregate structure formation in asphalt mixtures ». *Road materials and pavement design,* vol. 14, nº S2, p. 16-34.

Sargious, M., et N. Mushule. 1991. « Behavior of Recycled Asphalt Pavement at Low Temperatures ». Canadian Journal of Civil Engineering, vol. 18, p. 428-435.

Sebaaly, H. K. 2007. « Evaluation of Nevada's Hot Mix Asphalt Mixtures Using Tire Rubber Modified Binder ». University of Nevada. Reno.

Sefimazgi, N. R., L. Tashman et H. Bahia. 2012. « Internal structure characterization of asphalt mixtures for rutting performance using imaging analysis ». Journal of the Association of Asphalt Paving Technologists (AAPT).

Setra-LCPC (266 p.). 1994. French design manual for pavement structures

Shah, A., R. S. McDaniel, G.A. Huber et V. L. Gallivan. 1998. « Investigation of Properties of Plant-Produced Reclaimed Asphalt Pavement Mixtures ». Transportation Research Record: Journal of the Transportation Research Board, nº 1998. p. 103-111.

SHRP-A404, 1994. Fatigue response of asphalt aggregate mixes. Strategic highway research program. National Research Council Shell. International Petroleum Company. 1978. Shell pavement design manual.

Shoenberger, J. E., R. S. Rollings et R. T. Graham. 1995. Physical properties of asphalt cement binder. Coll. « Properties of microwave recycled asphalt cement binders ». <http://books.google.ca/books?id=a2K1GReFqMgC&pg=PA199&lpg=PA199&dq=Shoenberger.physical+properties+of+asphalt+cement+binder.++properties+of+microwave+recycled+asphalt+binders&source=bl&ots=RYhnWXrlFI&sig=TVjESlfMOWV394w8M4OovAsVGfg&hl=en&ei=kwetTInuL861ngeUp_XhDA&sa=X&oi=book_result&ct=result&resnum=1&ved=0CBYQ6AEwAA#v=onepage&q=Shoenberger%2Cphysical%20properties%20of%20asphalt%20cement%20binder%2C%20%20properties%20of%20microwave%20recycled%20asphalt%20binders&f=false>.

Solaimanian, M., et M. Tahmoressi. 1996. « Variability Analysis of Hot-Mixed Asphalt Concrete Containing High Percent Reclaimed Asphalt. Pavements ». Presented at the 75th annual meeting of TransportationResearch Board, Transportation Research Record. NationalResearch Council, vol. 1543, p. 89-96.

Sondag, M. S., B. A. Chadbourn et A. Drescher. 2002. Investigation of Recycled Asphalt. Pavement (RAP) Mixtures. MN/RC – 2002-15. Department of civil engineering. University of Minnesota.

Souparth, N. 1998. Evaluation of Rutting Resistance Characteristics of Asphalt Binder containing Recycled Asphalt Pavement. Department of Civil & Environmental Engineering, University of Rhode Island. <http://personal.egr.uri.edu/jhwang/soupharath/soupharath.htm>.

Tam, K. K., P. Joseph et D. F. Lynch. 1992. « Five-Year Experience of Low-Temperature Performance of Recycled Hot Mix ». *Transportation Research Record, Transportation Research Board,* vol. 1362, p. 56-65.

Tapsoba, N., C. Sauzéat et H. Di Benedetto. 2013. « Analysis of Fatigue Test for Bituminous Mixtures ». Materials in civil engineering, vol. 25, p. 701-710.

Tayebali, A. A., B. Tsai et C. L. Monismith. 1994 stiffness of asphalt aggregate mixes. Report Number SHRP-A-388. Washington, D.C.: Stratgic Highway Research Program, National Research Council.

Tayebali, A.A., J.A. Deacon et C.L. Monismith. 1995. « Development and evaluation of surrogate fatigue models for SHRP A-003A a bridged mix design procedure ». Association of Asphalt Paving Technologists, vol. 64, p. 340-366.

Tayebali, A.A., J.S. Deacon, J.S. Coplantz et C.L. Monismith. 1993. « Modeling fatigue response of asphalt-aggregate mixtures ». Association of Asphalt Paving Technologists, vol. 62, p. 385-421.

Tayebali, A.A., G.M. Rowe et J.B. Sousa. 1992. « Fatigue response of asphalt-aggregate mixture ». The Association of Asphalt Paving Technologists 61: 333–360.

The Constructor, -Civil Engineering. cited in mai 2015. « Flexible pavement composition and structure ». <http://theconstructor.org/transportation/flexible-pavement-composition-and-structure/5499/>.

Thakur, Subhash Chandra. 2010. « Laboratory evaluation of characteristics of recycled asphalt pavement (RAP) in KENSAS ». KENSAS. Tremblay, D. 2001. « Influence des différents paramètres de formulation et optimisation des enrobés à matrice de pierre ». Montreal. École de Technologie Supérieure, 145 p.

Thompson, M. R. 1987. « Illi-pave base full-depth asphalt concrete pavement design procedure ». In Sixth international conference. structural design of asphalt pavements (July 13-17). Vol. 1, p. 13-22. university of Michigan, Ann Arbor, Michigan.

Thompson, Marshall R., et Samuel H. Carpenter. 2006. « Considering hot mix asphalt fatigue endurence limit in full depth mechanistic-mperical pavement design ». In International conference on Perptual pavement, Ohio.Walubita, L.F., A.E. Martin, C.J. Glover, R.L. Lytton et G.S. Cleveland. 2006. « Modeling the Fatigue Resistance of Hot-Mix Asphalt Concrete (HMAC) Mixtures Including the Effects of Aging ». In 10th International Conference on Asphalt Pavements (August 12 to 17). vol. 1, Quebec city, Canada.

Touhara, Radouen. 2012. « Étude de la résistance en fatigue des matériaux bitumineux. Mémoire de maîtrise électronique ». École de technologie supérieure.West, R. 2008. « Summary of NCAT Survey on RAP Management Practices and RAP Variability ». In presented to RAP ETG Meeting Phoenix, AZ <http://www.google.ca/#hl=en&source=hp&biw=1276&bih=839&q=Summary+of+NCAT%E2%80%99s+Survey+on+RAP+Management+Practices+and+RAP+Variability&aq=f&aqi=&aql=&oq=&fp=b391afe43845c36f>.

Tremblay, D. 2001. « Influence des différents paramètres de formulation et optimisation des enrobés à matrice de pierre ». Montreal, École de Technologie Supérieure, 145 p.

Walubita, L.F., A.E. Martin, C.J. Glover, R.L. Lytton et G.S. Cleveland. 2006. « Modeling the Fatigue Resistance of Hot-Mix Asphalt Concrete (HMAC) Mixtures Including the Effects of Aging ». In *10th International Conference on Asphalt Pavements* (August 12 to 17). vol. 1. Quebec city, Canada.

West, R. 2008. « Summary of NCAT Survey on RAP Management Practices and RAP Variability ». In *presented to RAP ETG Meeting Phoenix, AZ*. <http://www.google.ca/#hl=en&source=hp&biw=1276&bih=839&q=Summary+of+NCAT%E2%80%99s+Survey+on+RAP+Management+Practices+and+RAP+Variability&aq=f&aqi=&aql=&oq=&fp=b391afe43845c36f>.

Williams, M. L., R. F. Landel et J. D. Ferry. 1995. « The Temperature Dependence of Relaxation Mechanisms in Amorphous Polymers and Other Glass-forming Liquids ». Journal of the American Chemical Society, vol. 77, p 370.

Witczak, M., M. Mamlouk, M. Souliman et W. Zeiada. 2013. Validating an endurance limit for Hot-Mix Asphalt (HMA) Pavements: Laboratory Experiment and Algorithm Development. Project No. NCHRP 9-44 A. National Cooperative Highway Research Program <http://onlinepubs.trb.org/onlinepubs/nchrp/nchrp_rpt_762App1.pdf>.

Wu, J. 2006. Ageing of bituminous materials. first year Ph.D. Univeristy of Nottingham. United kingdom.

Xiao, Feipeng. 2006. « Development of fatigue predictive models of rubberized asphalt concrete (RAC) containing reclaimed asphalt pavement (RAP) mixtures ». 3239601, United States -- South Carolina. Clemson University, 212 p. In ProQuest Dissertations & Theses (PQDT); ProQuest Dissertations & Theses A&I. <http://search.proquest.com/docview/305353323?accountid=27231 http://openurl.uquebec.ca:9003/ets?url_ver=Z39.88-2004&rft_val_fmt=info:ofi/fmt:kev:mtx:dissertation&genre=dissertations+%26+theses&sid=ProQ:ProQuest+Dissertations+%26+Theses+%28PQDT%29&atitle=&title=Development+of+fatigue+predictive+models+of+rubberized+asphalt+concrete+%28RAC%29+containing+reclaimed+asphalt+pavement+%28RAP%29+mixtures&issn=&date=2006-01-01&volume=&issue=&spage=&au=Xiao%2C+Feipeng&isbn=9780542944802&jtitle=&btitle=>.

Yang, H. HUANG. 2004. Pavement analysis and design.

Young, J. Francis. 1998. The Science and technology of civil engineering materials. Coll. « Prentice-Hall international series in civil engineering and engineering mechanics ». Upper Saddle River, N.J.: Prentice-Hall, xiv, 384 p.

Standards

AASHTO. 1999. Standard specification for Superpave volumetric mix design AASHTO MP2-99, AASHTO Provisional Standards, Interim Edition, AASHTO, AASHTO Provisional Standards, Interim Edition, AASHTO, Washington, D.C.

AASHTO. 2000. Standard practice for mixture conditioning of hot mix asphalt (HMA), Short and Long-Term, AASHTO - PP2 – 2000, Washington (DC), AASHTO Provisional Standards, Interim Edition, AASHTO, Washington, D.C.

AASHTO. 2002. Standard Method of Test for Resistance to Degradation of Small-Size Coarse Aggregate by Abrasion and Impact in the Los Angeles Machine, AASHTO T 96-02 (Reapproved 2015), AASHTO Provisional Standards, Interim Edition, AASHTO, Washington, D.C.

AASHTO. 2004. Standard Method of Test for determining the percentage of fracture in Coarse Aggregate, AASHTO TP 61-02 (Reapproved 2004), AASHTO Provisional Standards, Interim Edition, AASHTO, Washington, D.C.

AASHTO. 2011. Standard Method of Test for Determining sieve analysis of fine and coarse aggregates, AASHTO T 27, AASHTO Provisional Standards, Interim Edition, AASHTO, Washington, D.C.

AASHTO. 2011. Standard Method of Test for un-compacted void content of fine aggregate, AASHTO T304-11, AASHTO Provisional Standards, Interim Edition, AASHTO, Washington, D.C.

AASHTO. 1998. Standard Method of Test determining the rheological properties of asphalt binder using a dynamic shear rheometer DSR, AASHTO TP5-1998**,** AASHTO Provisional Standards, Interim Edition, AASHTO, Washington, D.C.

AASHTO. 2008. Standard Method of Test for determining the flexural creep stiffness of asphalt binder using the Bending Beam Rheometer (BBR), AASHTO T 313-08, AASHTO Provisional Standards, Interim Edition, AASHTO, Washington, D.C.

AFNOR. 1999. Méthodes d'essai pour Bitumes et liants bitumeux:- Détermination de la pénétrabilité d'un liant bitumineux. Méthode Bille et Anneau, NF EN 1426, La Plaine Saint-Denis Cedex, France: Association Française de Normalisation.

AFNOR. 2000. Méthodes d'essai pour Bitumes et liants bitumeux:- Détermination de la température de ramollissement. Méthode Bille et Anneau, NF EN 1427, La Plaine Saint-Denis Cedex, France: Association Française de Normalisation.

AFNOR. 2007. Mélange bitumineux - Méthodes d'essai pour mélange hydrocarboné à chaud - Partie 33: confection d'éprouvettes au compacteur de plaque, NF EN 12697-33+A1, La Plaine Saint-Denis Cedex, France: Association Française de Normalisation.

AFNOR. 2007. Méthodes d'essai pour Mélanges bitumineux - Méthodes d'essai pour mélange hydrocarboné à chaud - Partie 35: malaxage en laboratoire, 12697-35+A1, La Plaine Saint-Denis Cedex, France: Association Française de Normalisation.

ASTM. 2001. Standard Test Method for determining the percentage of fractured particles in coarse aggregate, ASTM C131-01, West Conshohocken (PA): American Society for Testing and Materials.

ASTM. 2001. Standard Test Method for sieve analysis of Fine and coarse aggregates, ASTM C 136-01, West Conshohocken (PA): American Society for Testing and Materials.

ASTM. 2002. Standard Test Method for sand equivalent value of soils and fine aggregate, ASTM D2419 - 02, West Conshohocken (PA): American Society for Testing and Materials.

ASTM. 2004. Standard Test Method for Coarse aggregate for bituminous pavement mixtures, ASTM D 692-00 (Reapproved 2004), West Conshohocken (PA): American Society for Testing and Materials.

ASTM. 2006. Standard Test Method for Viscosity Determination of Asphalt at Elevated Temperatures Using a Rotational Viscometer, ASTM D4402 – 06, West Conshohocken (PA): American Society for Testing and Materials.

ASTM. 2006. Standard Test Methods for un-compacted void content of fine aggregate (as influenced by particle shape, Surface texture, and grading) ASTM C1252-06 (Withdrawn 2015), West Conshohocken (PA): American Society for Testing and Materials.

ASTM. 2006. Standard Test Method determining the percentage of fractured particles in coarse aggregate, ASTM D 5821-01 (Reapproved 2006), West Conshohocken (PA): American Society for Testing and Materials.

ASTM. 2007. Standard Test Method for fine aggregate for bituminous pavement mixtures, ASTM D 1073-07, West Conshohocken (PA): American Society for Testing and Materials.

ASTM. 2010. Standard Test Method for flat particles, elongated particles, or flat and elongated particles in coarse aggregate, ASTM D4791 – 10, West Conshohocken (PA): American Society for Testing and Materials.

ASTM. 2013. Standard Test Method for Penetration of Bituminous Materials, ASTM D5 / D5M – 13, West Conshohocken (PA): American Society for Testing and Materials.